

The University of Nottingham

UNITED KINGDOM · CHINA · MALAYSIA

Bacterial crowd control

AIP-based analogues and solonamides modulate staphylococcal virulence

Thesis submitted to the University of Nottingham for the degree of Doctor of Philosophy

Robert Hampson BSc (Hons)

September 2015

Acknowledgements

I would like to thank many people who have contributed to my life and work over the last four years which I have spent here in Nottingham. I am very grateful to both my supervisors, Dr. Weng Chan and Prof. Paul Williams, who have consistently provided professional help and advice throughout the course of my studies. This thesis would not exist without them. I would also like to thank the Medical Research Council for providing grant funding allowing me the privilege of being able to research here at the University of Nottingham.

My thanks go to Alan Cockayne, Daniel Dyer, Eric Pollitt, Chris Gordon, Fabio Rui, Victoria Steele, and Ewan Murray who have all aided me by performing assays, synthesising compounds, or offering guidance over the years. The *S. aureus* research group and my colleagues in C22 and C24 have also often provided invaluable support, help or guidance.

Finally, I'd also like to thank my family for cultivating my scientific interests throughout my life, encouraging me in my endeavours, and generally being there for me.

I'd also like to offer heartfelt thanks to Yumi for keeping me sane in these last few months.

Abstract

This thesis details research in three areas, in attempts to produce more effective inhibitors of the staphylococcal *agr* quorum sensing system. The non-ribosomal peptide synthase biosynthetic cluster responsible for the production of the aureusimines represents roughly 0.5% of the *S. aureus* genome. However, their function is yet to be elucidated. Research detailed herein develops a new reliable method for synthesis for these natural products. Efforts to discover the biological target or function of these compounds using affinity chromatography is reported. Further biological investigations revealed that the aureusimines are mild antagonists of the *agr* system. Weak inhibition of CCL-2 mediated chemotaxis of monocytes and staphylococcal biofilm formation is also observed. However, the main biological function of these natural pyrazinones is yet to be discovered.

The staphylococcal bioreporter assays were used to eludicdate the structure-activity relationship of a series of truncated AIP-based antagonists against the AgrC1 receptor. Promising inhibitors are then evaluated against AgrC2, AgrC3 and AgrC4. Several compounds were found to be potent low nanomolar inhibitors across all four *agr* groups. A bioreporter assay based on the mutant receptor A101T T104V AgrC1 in which (Ala^{5})AIP1 is an agonist was also used to evaluate the panel of compounds. This revealed that most of these truncated AIP-based compounds are agonists of the mutant receptor, similar to (Ala^{5})AIP1.

However, (Ala^2, Leu^4, Tfh^5)trAIP1 (**3.23**) effectively inhibited activation of this bioreporter by AIP1. Compound **3.23** was also a sub-nanomolar inhibitor of AgrC1 and a low nanomolar inhibitor in other *agr* groups. Compound **3.23** is the most potent AgrC1 inhibitor discovered to date and, furthermore, its effects are likely to be less susceptible to mutations within the AgrC receptor.

The depsipeptide natural products, solonamides, were synthesised using two uniquely different strategies. Development of a new synthetic strategy produced analogues with a high yield and diastereomeric excess in contrast with previous low yielding or non-stereoselective strategies. Their previously reported inhibition of the *agr* system was confirmed and fully quantified. Solonamide A and B inhibit activity in all four *agr* groups. Expression of toxic shock syndrome toxin-1 (TSST-1) and α-hemolysin were reduced in *Staphylococcus aureus* KH1187A. Schild analysis of data from *agr* bioreporters revealed that the inhibition is not competitive (as previously reported), but the solonamides act as negative allosteric modulators of both the AgrC1 and AgrC2 receptors, interacting with a new putative conserved allosteric binding site. Weak agonism at high concentrations was also discovered, which has not been previously observed. A panel of analogues was produced to assess the SAR with AgrC1. Modifications of the solonamide scaffold achieved mild improvements of physical characteristics and potency.

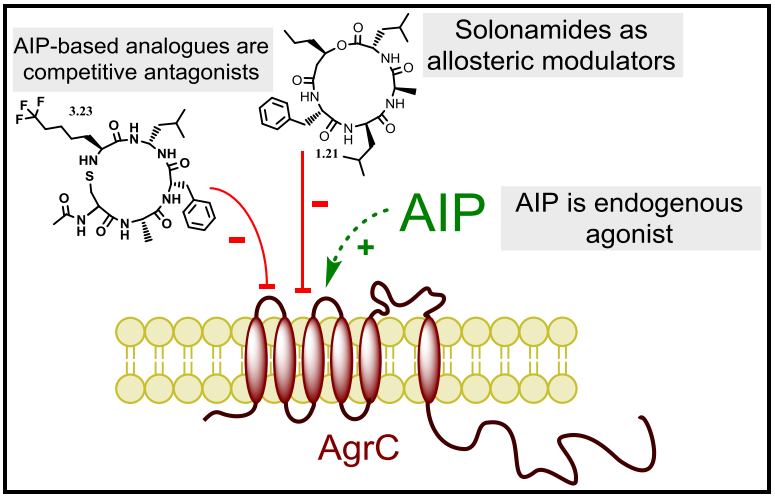


Figure 1: Illustration of inhibition by AIP-based analogues and the solonamides

Abbreviations

Standard one letter or three letter codes for DNA bases and natural amino acid residues are used throughout. A list of further abbreviations is below in alphabetical order:

2ClTrt	2-Chlorotrityl
3HDA	3-Hydroxydecanoic acid
3HHA	3-Hydroxyhexanioic acid
3HOA	3-Hydroxyoctanoic acid
5Me-3HHA	5-Methyl-3-hydroxyhexanoic acid
6FFF-3HHA	6,6,6-Trifluoro-3-hydroxy-hexanoic acid
Ac	Acetyl
agr	Accessory gene regulator
AIP	Autoinducing peptide
AOP	(7-Azabenzotriazol-1-yloxy)tris(di-methylamino)phosphonium hexafluorophosphate
Aus	Aureusimine
BHI	Brain heart infusion
Boc	*tert*-Butoxycarbonyl

BOP	(Benzotriazol-1-yloxy)tris(dimethylamino)phosphonium hexafluorophosphate
Bzl	Benzyl
CA-MRSA	Community acquired MRSA
Cbz	Carboxybenzyl
CCL-2	C-C motif ligand 2
CFU	Colony forming units
ChIP	Chemotaxis inhibitory protein
cLogP	Calculated LogP
COMU	(1-Cyano-2-ethoxy-2-oxoethylidenamino-oxy)dimethylamino-morpholino-carbenium hexafluorophosphate
COSY	Correlation spectroscopy
DCC	Dicyclohexylcarbodiimide
DCM	Dichloromethane
DIBAL-H	Diisobutylaluminium hydride
DIC	Diisopropylcarbodiimide
DIPEA	Diisopropylethylamine
DMAP	Dimethylaminopyridine
DMF	Dimethyl formamide
DMSO	Dimethylsulfoxide
DNA	Deoxyribonucleic acid
Eap	Extracellular adherance protein
EC_{50}	Concentration of an agonist at half the maximal activation
EDC	1-Ethyl-3-(3-dimethylaminopropyl)carbodiimide
epi	Epimer
Et2O	Diethylether
EtOAc	Ethyl acetate

EU	European Union
Fmoc	Fluorenylmethoxycarbonyl
Fur	Ferric uptake regulator
FY	Financial year
g	Grams
g	G-force
GBAP	Gelatinase biosynthesis-activatin pheromone
GFP	Green fluorescent protein
h	Hours
HAI	Healthcare associated infections
HATU	1-[Bis(dimethylamino)methylene]-1H-1,2,3-triazolo[4,5-b]pyridinium 3-oxide hexafluorophosphate
HBTU	*N*-[(1H-Benzotriazol-1-yl)(dimethylamino) methylene]-*N*-methylmethan-aminium hexafluorophosphate *N*-oxide
Hex	Hexane
HFIP	Hexafluoroisopropanol
HIV	Human immunodeficiency virus
HMPA	Hexamethylphosphorotriamide
HOAt	1-hydroxy-7-azabenzotriazole
HOBt	*N*-hydroxybenzotriazole
HOSu	*N*-hydroxysuccinimide
HPLC	High performance liquid chromatography
IBX	Iodoxybenzoic acid
IC_{50}	Concentration of an inhibitor at half the maximal activation
ICAM-1	Intercellular adhesion molecule-1
LipE	Lipophilic efficiency
m	Minutes

M	Molar
MeCN	Acetonitrile
MeOH	Methanol
MHC	Major histocompatibility complex
Mhs	*O*-Methylhomoserine
MIC	Minimum inhibitory concentration
min	Minutes
mL	Millilitres
mRNA	Messenger RNA
MRSA	Methicillin-resistant *S. aureus*
MS	Mass Spectrometry
MSCRAMM	Microbial surface components recognising adhesive matrix molecules
MSSA	Methicillin-susceptible *S. aureus*
*N*bz	*N*-benzylglycine
NHS	National Health Service
NHSN	National Healthcare Safety Network
*N*me	*N*-methylglycine
NMR	Nuclear magnetic resonance
*N*mse	*N*-methylsulfanylethylglycine
*N*msp	*N*-methylsulfanylpropylglycine
NOESY	Nuclear overhause effect spectroscopy
NRPS	Non ribosomal peptide synthase
*N*smp	(*S*)-*N*-(1-Methylpropyl)glycine
o/n	Overnight
^{o}C	Degrees centigrade
OD	Optical density

P	Partition coefficient between octanol and water
PBS	Phosphate buffered saline
PCR	Polymerase chain reaction
Pd/C	Palladium on activated carbon
PEGA	Polyethylene glycol-acrylamide co-polymer
Ph	Phenyl
PHE	Public Health England
PIA	Polysaccharin intercellular adhesin
ppm	Parts per million
PSM	Phenol soluble modulin
PVL	Panton-Valentine leukocidin
PyAOP	(7-Azabenzotriazol-1-yloxy)tris(pyrrolidino)phosphonium hexafluorophosphate
PyBOP	Benzotriazol-1-yl-oxytripyrrolidinophosphonium hexafluorophosphate
PyOxim	[Ethyl cyano(hydroxyimino)acetato-O^2]tri-1-pyrrolidinylphosphonium hexafluorophosphate
QS	Quorum sensing
RAP	RNAIII activating peptide
RIP	RNAIII inhibiting peptide
RLU	Relative light units
RNA	Ribonucleic Acid
RNS	Reactive nitrogen species
ROESY	Rotating-frame nuclear overhauser effect spectroscopy
ROS	Reactive oxygen species
rpm	Rotations per minute
RPMI	Roswell Park Memorial Institute
RT	Room temperature

SAR	Structure-activity relationship
SCV	Small colony variant
SDS-PAGE	Sodium dodecylsulfate - polyacrylamide gel electrophoresis
Sol	Solonamide
SPPS	Solid-phase peptide synthesis
TBAP	Tetrabutylammonium perruthenate
TBCR	Triazine based coupling reagent
TBTU	*O*-(Benzotriazol-1-yl)-1,1,3,3-tetramethyluronium tetrafluoroborate
tBu	tert-Butyl
TEA	Triethylamine
TEMPO	(2,2,6,6-Tetramethylpiperidin-1-yl)oxyl
TFA	Trifluoroactic acid
Tfb	2-Amino-4,4,4-trifluorobutanoic acid
Tfh	6,6,6-Trifluoro-2-aminohexanoic acid
Tfn	6,6,6-Trifluoronorleucine
THF	Tetrahydrofuran
TIPS	Triisopropylsilane
TOCSY	Total correlation spectroscopy
TPAP	Tetrapropylammonium perruthenate
tr	Truncated
TRAP	Target of RAP
TSB	Tryptic soy broth
TSST-1	Toxic Shock syndrome toxin 1
VRSA	Vancomycin-resistant S. aureus
Z	Carboxybenzyl

Contents

Acknowledgements i

Abstract ii

Abbreviations iv

Contents x

1 Introduction 1

1.1 Staphylococcus aureus *3*

1.1.1 Epidemiology - the scale of the problem 4

1.1.2 Pathology - the severity of infections 7

1.1.3 Antibiotic resistance 11

1.2 Virulence of S. aureus *19*

1.3 Quorum sensing *24*

1.4 Quorum sensing control of virulence in S. aureus *25*

1.4.1 The *Agr* system 25

1.4.2 The *Agr* groups of *S. aureus* 28

1.5 Analogous agr systems *34*

1.6 Agr and virulence inhibitors *42*

1.6.1 Targeting the action of RNAIII activating peptide 42

1.6.2 AIP-based analogues 42
1.6.3 Solonamides 44
1.6.4 Other inhibitors of AgrC 45
1.6.5 Aureusimines 48
1.7 Aims and objectives 49
1.7.1 Aureusimines 49
1.7.2 AIP-based analogues 53
1.7.3 Solonamides 55
2 Aureusimines 60
2.1 Introduction 62
2.2 Published synthesis of the aureusimines 67
2.3 Attempted synthesis of aureusimine A and B 68
2.4 Adapted oxidative approach for synthesis of aureusimine A and B 70
2.4.1 Alcohol to Aldehyde oxidations 70
2.4.2 Attempted oxidations 75
2.5 An O-Protected strategy 80
2.6 Do the aureusimines affect the agr system? 84
2.7 Affinity chromatography 87
2.7.1 Synthesis of required tethered-aureusimine analogues 88
2.7.2 Affinity chromatography protocol 93
2.8 Further biological evaluation of the aureusimines 97
2.8.1 Colony spreading 97
2.8.2 Persistence 98
2.8.3 Biofilm formation 100
2.8.4 CCL-2 mediated chemotaxis 103
2.9 Conclusions 106

2.10 Future Work *108*

3 Pharmacology of AIP analogues 109

3.1 Introduction *110*

3.1.1 Previous Research 111

3.1.2 Contemporary research 132

3.1.3 Contribution of this research 140

3.2 Results and discussion *141*

3.3 The Structure-Activity Relationship in AgrC *143*

3.3.1 AgrC1 144

3.3.2 Other *agr* groups 153

3.4 Activation of a mutant receptor (A101T T104V) *157*

3.4.1 Inhibition of the mutant receptor (A101T T104V) 159

3.5 Mode of inhibition of the AIP analogues *160*

3.5.1 Competitive inhibition assays 160

3.5.2 Interactions with a constitutively active receptor (S116K) 162

3.6 Activation of AgrC1 ..... *164*

3.7 Conclusion *166*

3.8 Ongoing and Future work *168*

4 Total synthesis of the solonamides 170

4.1 Introduction *171*

4.1.1 Solonamides 171

4.1.2 Contribution of this research 177

4.2 The synthetic strategy *178*

4.2.1 Retrosynthesis 178

4.2.2 Solid-Phase Peptide Synthesis 180

4.2.3 Resin selection and Cleavage 189

4.2.4 Cyclisation 190

4.3 Initial synthesis of solonamide A using 3-(RS)-hydroxyhexanoic acid 192

4.4 Synthetic strategy for the 3-(R)-hydroxy acids 194

4.5 Synthesis of 3-(R)-hydroxyhexanoic acid 195

4.5.1 Aziridine production 195

4.5.2 Triamine ligand formation 196

4.5.3 Ketene-Aldehyde cycloaddition 197

4.5.4 Hydrolysis reaction 198

4.6 Stereoselective synthesis of solonamide A and B 201

4.7 Synthesis of solonamide analogues 202

4.7.1 Epimerisation of the (ala^3)SolB 205

4.8 Conclusion 207

5 Developing an improved method for the synthesis of solonamides 210

5.1 Introduction 211

5.2 Alternative cleavage conditions 214

5.3 Effects of changing cyclisation reagents and conditions 215

5.4 Alternative cyclisation strategy 219

5.4.1 Alternative esterification reagents and conditions 220

5.4.2 Establishing the cyclisation 223

5.5 Conclusion 225

5.6 Future Work 227

6 Pharmacology of solonamide analogues 230

6.1 Introduction 231

6.2 Mode of binding 234

6.2.1 Competitive inhibition 234

6.2.2 Non-competitive inhibition 238

6.2.3 Irreversible inhibition 244

6.2.4 Uncompetitive inhibition 245

6.3 Pharmacological assessment of solonamide A, B and their epimers 246

6.3.1 Confirmation of inhibition and IC_{50}s 246

6.3.2 Schild analysis 249

6.3.3 Phenotypic studies 251

6.4 Synthetic programme 253

6.5 The Structure-Activity Relationship of solonamide analogues 258

6.5.1 3-hydroxy acid analogues 258

6.5.2 Alanine scan of SolB 259

6.5.3 Variation of Phe^2 residue 261

6.5.4 Second generation analogues 263

6.5.5 Phenotypic studies 264

6.5.6 Complete structure activity relationship data plus additional data from AgrC2 and AgrC3 reporters 265

6.6 Conclusions 268

6.7 Future Work 270

7 Conclusions and Future Work 271

7.1 Future work 277

7.1.1 Aureusimines 277

7.1.2 AIP-based analogues 278

7.1.3 Solonamides 280

8 Experimental 284

Bacterial strain list 284

General chemistry 284

8.1 Aureusimines 287

8.1.1 Literature synthesis of aureusimine A and B 287

8.1.2 Adapted oxidative synthesis of aureusimine A and B .. 289

8.1.3 Protected synthesis 292

8.1.4 Affinity chromatography - synthesis of tethered aureusimine 301

8.1.5 Biology 308

8.2 Pharmacology of AIP analogues 310

8.2.1 Bacterial strains and culture conditions 310

8.2.2 Construction of agrP3::lux bioreporter strains 311

8.2.3 AIP/AgrC bioluminescent reporter assay 311

8.2.4 Hemolysis assays and western blots 312

8.2.5 AgrC/AIP bioluminescent reporter assay graphs 312

8.3 Total synthesis of the solonamides 325

8.3.1 Standard UV Fmoc quantification 325

8.3.2 Synthesis of triamine ligand 325

8.3.3 Stereoselective synthesis of β-hydroxy acids 327

8.3.4 Derivatisation to determine ee 330

8.3.5 Preparation of Fmoc-Leu-2ClTrt Resin 336

8.3.6 Initial synthesis of solonamide depsipeptides 337

8.3.7 Stereoselective synthesis of solonamide depsipeptides 339

8.4 Developing an improved solonamide synthesis 342

8.4.1 Preparation of Fmoc-*D*-Ala-2ClTrt Resin 342

8.4.2 Stereoselective synthesis of solonamide depsipeptides 342

8.5 Pharmacology of the solonamides 350

8.5.1 Synthesis of solonamide analogues 350

8.5.2 Biological Assessment 370

8.5.3 Temperature dependant NMR 377

8.5.4 Stability testing 377

9 References 379

1 Introduction

The aim of the work outlined in this thesis is to develop more effective treatments for infection caused by *Staphylococcus aureus*, especially in light of the recent rise of antibiotic resistance. The research discussed herein aims to develop potential therapies which could be used to inhibit virulence expression by *S. aureus* thereby preventing the bacteria maintaining productive infections. This would then theoretically result in the natural resolution of the illness by the innate and adaptive immune systems.

In this chapter, the case for the development of new therapies against *S. aureus* is established. To this end, some background information on the bacteria is offered. The incidence, medical costs and economic expense of staphylococcal infection is then discussed, especially in healthcare settings. An outline of the pathology, potential clinical severity, and the spread of virulent and resistant strains into the community is then detailed. The rise in antibiotic resistance is then briefly discussed alongside the current strategies for addressing and overcoming bacterial resistance.

After establishing the case for the development of new therapies, the bacterial systems and mechanisms which are integral to establishing and maintaining *S. aureus* infections are outlined. The eventual strategy of this research is to target and inhibit these bacterial virulence strategies to render the bacteria defenseless against the host immune system. To this end, the

communal systems which the bacteria use to coordinate their virulence expression across bacterial communities are explored. These systems are commonly known as quorum sensing systems. This research exploits chemical agents in order to target these systems to disrupt or prevent the bacteria from becoming virulent. The *agr* quorum sensing system which is known to be a master regulator of *S. aureus* virulence is considered. The current knowledge of analogous *agr* systems in other bacterial species is then examined to ascertain whether any insights from *S. aureus* research could be used to develop therapies against other bacteria or if developments in these other bacterial species can contribute to this work in *S. aureus*.

Finally, previous and contemporary research which aims to develop potential therapies against staphylococcal virulence by targeting the *agr* quorum sensing system is discussed. In this last section, this research is set in the context of wider current scholarship and how this thesis aims to contribute to this exciting field is addressed.

1.1 *Staphylococcus aureus*



Figure 2: *Staphylococcus aureus* grown statically overnight at 37 ^{0}C on a Brain-Heart Infusion (BHI) agar plate.

Staphylococcus aureus (Figure 2), a facultative anaerobic gram positive bacterium,[1] commonly colonises human mucosa, skin and the *anterior nares* (the external part of the nose) with minimal impact on the host.[2] Even though *S. aureus* acts as a commensal bacteria, it can act as an opportunistic pathogen causing invasive infections, especially in older patients, patients who frequently visit hospital, or patients resident in care homes.[3] Other risk factors include recently undergoing surgery,[4] use of a central venous catheter, and previous use of more than two or more antibiotic drugs.[5] These infections can be serious and even fatal in some cases.[6] The ability of *S. aureus* to act as both a commensal and pathogenic bacteria is based upon a vast armamentarium of virulence factors tightly regulated and controlled in respect to the local bacterial population and environment.[7]

Recently, there has been considerable media attention focused on *S. aureus*, and especially the antibiotic resistant strains known as methicillin-resistant *S. aureus* (MRSA).[8] However, the true scale of the problem and the severity of these infections is often unclear in media coverage. In the following section, a

convincing case for further research to develop *S. aureus* treatments is established.

1.1.1 Epidemiology - the scale of the problem

In 2007, the European Centre for Disease Prevention and Control collaborated with the European Medicines Agency and the international network known as "Action on Antibiotic Resistance" to produce an in-depth analysis of the gap between the prevalence of antibiotic resistant infections in the EU and the research and development of new antimicrobial drugs.[9] The report estimated that across Europe in 2007 around 25,000 people died as a direct result of antibiotic resistant infections. As the total number of deaths in the 27 nations of the EU was around 5 million in 2007,[10] this represents roughly 0.5% of deaths across the entire EU. This seems to be a very high proportion of deaths caused by diseases which until recently were considered to be easily treatable. It was also estimated that an extra 2.5 million hospital days and €900 million were required to deal with these infections in medical facilities. Outpatient care costs represented a further €10 million, productivity losses from surviving patients' work absences amounted to a further €150 million, and finally the productivity losses from those patients who died as a result of one of these infections was estimated to be a further €450 million. These estimates produce a total cost of roughly €1.5 billion each year in treatments, hospital costs and societal impact in the EU alone. These estimates established a considerable economic case for further research into the monitoring, control, prevention and treatment of antibiotic resistant infections.

In support for a particular focus on *S. aureus*, the study confirmed that MRSA is the most common, single, multi-drug resistant bacterium in the EU.[9] Of the seven organisms which received attention in this report, there were two different classes of *S. aureus* further revealing the significance of this organism within the causative agents of antibiotic resistant infections. The two classes examined were the relatively widespread MRSA strains and the less common but more dangerous vancomycin resistant strains. The report found a reduction in the proportion of MRSA bacteraemia in relation to all *S. aureus* bacteraemia from a high of roughly 28% in 2004 (which was the highest of all those

organisms assessed) to roughly 22% in 2007.[9] It is believed that this reduction was due to national action plans which took place during this time period in member states, such as the United Kingdom, France and Slovenia. The proportion of vancomycin resistant bacteraemia was very low at less than 0.1% of all *S. aureus* bacteraemia. In fact, no vancomycin resistant isolates were reported across the EU member states, Norway and Iceland in 2007 showing that this kind of resistance is still, fortunately, very rare.[9]

However, these figures actually represent an underestimate of the situation in the EU. For example, only seven common organisms were examined of all possible resistant strains. Furthermore, the hospital costs were calculated based on the average cost of a single hospital day and did not account for the cost of special interventions such as intensive care or any particularly expensive antibiotic treatments which may have been prescribed. The figures also only accounted for confirmed bacteraemias thereby excluding conditions like the more common skin and soft tissue infections.

Public Health England (PHE) has also carried out enhanced screening for MRSA bacteraemia since October 2005. Bacteraemia is defined as the presence of bacteria in the blood, which is indicative of a very serious and life threatening infection. In the financial year(FY) 2007/8, there were 4,451 cases of MRSA bacteraemia in the NHS in England alone.[11] This represents a serious and life threatening MRSA case for roughly 0.04% or 4 of every 10,000 patients of each of the total long stay hospital admission patients in 2007 (roughly 12.3 million people stayed in hospital for more than 2 days in 2007).[12] These figures do not account for milder infections such as skin and soft tissue infections. Furthermore, cases in Northern Ireland, Scotland, and Wales would increase this number proportionally for the entire UK but the PHE did not report cases from these areas as they are outside its jurisdiction. In light of this situation, the government and the NHS decided on a programme to target *S. aureus* infections. Since this time, several measures have been taken to reduce the rates of MRSA infection in the NHS, including patient screening on admission and deep cleaning of wards where MRSA is discovered. These methods have successfully reduced the incidence of MRSA bacteraemia, consequently only 862 cases were

reported in the FY 2013/14.[11] However, the initially large reduction in infection rates of roughly 20% per annum have now slowed to roughly 5% per annum and this rate of decrease continues to slow.[11] It is possible that no further significant declines in incidence will be possible without new preventative strategies or treatments. Furthermore, by only measuring bacteraemia, these statistics include only very serious acute life threatening infections. More common and less serious MRSA infections are neglected, possibly hiding the true scale of the problem.

Since January 2011, PHE has also screened for methicillin-susceptible *S. aureus* (MSSA) bacteraemia in NHS acute trusts. Incidence has increased from 8,767 cases in FY 2011/12 to 9,290 cases in FY 2013/14 and this rate of annual increase seems to be continuing.[11] Even though MSSA bacteraemia has a better prognosis than MRSA bacteraemia (as many effective antibiotic therapies exist), any form of bacteraemia is still a very serious condition which can easily result in the death of the patient. As previously mentioned, these statistics are also likely to conceal the scale of the problem by only recording the incidence of bacteraemia and not the more common but less dangerous MSSA infections.

It is much harder to find reliable statistics for the worldwide incidence of MRSA and MSSA infections. In the USA, there is no compulsory national monitoring of MRSA infections. The Centre for Disease Control's National Healthcare Safety Network (NHSN) tracked data from over 13,000 facilities in 2013. The NHSN has produced a healthcare associated infections (HAI) report every year since 2008. However, only 2013 MRSA data is publically available in the HAI report. In 2013, 3,827 hospitals reported 9,471 cases of MRSA infection.[13] The American Hospital Association has 5,686 registered hospitals.[14] If the remaining non-reporting hospitals have a similar incidence to the reporting hospitals, this amounts to roughly 14,000 cases in American hospitals in 2013 alone. If there is a similar ratio of MSSA and MRSA infections in the US as were recorded in the NHS, this could mean there were roughly 140,000 cases of MSSA in the US in 2013 alone.

From these statistics, it is abundantly clear that many people across the world are seriously affected by *S. aureus* infections each year and, if resistance to an increasing number of antibiotics continues to spread (vancomycin-resistant *S. aureus* has been observed although only rarely to date)[15], the incidence and mortality due to *S. aureus* may well increase dramatically in future. This effectively demonstrates a very strong case for research into new therapies targeted at *S. aureus*, especially treatments that are effective against antibiotic resistant strains.

1.1.2 Pathology - the severity of infections

It is difficult to assess the severity of disease which a patient will suffer as the clinical presentation of *S. aureus* infection can vary widely. The bacteria can be responsible for various diseases ranging in severity from mild skin infections (such as impetigo[16] or cellulitis[17]) to more serious invasive (such as osteomyelitis,[18] bacteraemia,[19] or endocarditis[20]) and toxin-mediated (such as toxic shock syndrome,[21] food poisoning,[22] or scalded skin syndrome[21]) diseases.

Commonly, *S. aureus* infections are caused through inoculation of the patient's own commensal bacteria into a trauma site or open wound (for example, surgical incisions).[23] At this point, the vast majority of *S. aureus* infections cause fairly minor infections at the inoculation site or sometimes more serious abscesses which may require surgical drainage.[24] These kind of infections often complicate a patient's recovery from surgery increasing the risk of negative clinical outcomes and can cause unsightly scarring.[24] Occasionally, this is further complicated by the presence of methicillin-resistant *S. aureus* (MRSA) strains which cannot always be easily treated. In some patients, *S. aureus* infections can develop into more dangerous conditions. For example, if *S. aureus* is introduced to a HIV positive,[25] diabetic,[25, 26] substance abuse, chronic hepatitis C or cancer patient,[25] necrotising fasciitis can occasionally develop. The bacteria releases toxins and enzymes digesting the tissues in the skin leading to the colloquial name "flesh-eating bacteria" (Figure 3).



Figure 3: Left leg of patient with necrotising fasciitis caused by *S. aureus* [27]

S. aureus can also affect otherwise healthy individuals outside a healthcare setting. For example, the introduction of superabsorbant tampons in 1980 caused an epidemic of toxic shock syndrome amongst otherwise young healthy women.[28] The *S. aureus* bacteria colonised the nutrient rich tampons *in situ* releasing toxins and virulence factors. The illness was especially prevalent in women using one brand of tampon, 'Rely'. This used carboxymethylcellulose which acted as a "store" for the toxic shock syndrome toxin-1 (TSST-1), which was then released across the vaginal mucosa causing toxic shock syndrome, a condition which can often be life-threatening.[28]

Although to date most MRSA infections have been confined to healthcare settings, a strain which recently emerged in the USA, known as USA300, is a highly virulent community acquired MRSA. Outbreaks of serious USA300 infections have been reported in American football teams,[29] military units,[30] religious communities,[31] and adolescents,[32] as well as being observed among other young healthy individuals lacking the usual risk factors for staphylococcal infections. These outbreaks have been observed to be highly infectious often infecting 20-25% of a given close contact community, as well as being dangerous and highly virulent. The spread of MRSA outside of healthcare settings and the clear ability of the strain to easily infect close knit young healthy communities is both important and deeply worrying.[33]

By far the most common presentation of a community acquired MRSA infection is a skin or soft tissue infection, with over 90% of cases falling into this category.[34] Skin and soft tissue infections of this type range from moderate to severe and are often very painful, but even severe cases can be treated by simple surgical incision and drainage.[33] However, serious infections like necrotising fasciitis have also been reported.[25] Community acquired MRSA strains have also been known to cause more serious infections in bones, joints, the respiratory and urinary tracts, such as osteomyelitis, pneumonia, sepsis, and urinary tract infections.[33] Depending on the survey, these types of infections each account for between 1 and 4% of all community acquired MRSA infections.[33]

Since the rise of community acquired strains of MRSA, it has become evident that there are several factors which make these strains distinct from both MSSA and healthcare acquired MRSA strains. These factors are thought to be responsible for making these strains so successful at spreading in a community setting. Firstly, they generally possess different antibiotic resistance elements. Healthcare acquired MRSA strains generally have Type I, II, or III SCC*mec* resistance elements. However, community acquired strains generally possess Type IV or V SCC*mec* elements which possess considerably fewer base pairs and therefore encode for significantly shorter proteins.[35] Many researchers believe this is likely to present less of a fitness burden in an environment where antibiotics are less common (for example, in the community).[36]

Secondly, they are generally only resistant to methicillin and β-lactam antibiotics in comparison to the much larger spectrum of resistance observed in healthcare acquired MRSA strains.[33] However, non-multidrug resistant community acquired MRSA strains are sometimes also resistant to either ciprofloxacin or erythromicin. Furthermore, some strains have occasionally been found to be truly multi-drug resistant including resistance to mupirocin, clindamycin, and tetracycline as well as the drugs previously mentioned.[37] It could be that this reduced resistance profile in common community acquired MRSA strains again presents a reduced fitness burden allowing increased

infectivity or virulence thereby allowing the bacteria to spread more effectively in the community.

Thirdly, they are generally less resistant to any specific antibiotic. For example, a USA300 strain isolated from Los Angeles prisoners was found to display an MIC fifty times less compared to MRSA252, a typical UK healthcare acquired MRSA strain.[38] This reduced resistance may again be less of a fitness burden than the levels of resistance maintained by healthcare acquired strains of MRSA.

USA300 and other community acquired MRSA strains do not only differ in their antibiotic resistance profile. These strains also display increased virulence in comparison with healthcare acquired MRSA strains. Voyich *et al.* showed that MW2 and LAC (community acquired MRSA strains) display increased virulence in a mouse model in comparison with COL and MRSA252 strains.[39] Specifically, these results may be due to their increased survival rate inside neutrophils which is a key step in *S. aureus* infection.[39] Another possible source for the increased virulence of community acquired MRSA is their increased expression of virulence factors. These strains generally secrete higher amounts of phenol soluble modulins (PSM),[40] α toxin[40] and some strains also release Panton Valentine Leukocidin (PVL).[41] There are some indications that master regulators of virulence such as the *agr* quorum sensing system are more active in community acquired MRSA strains which may result in the increased levels of virulence factors observed.[38] This increase in virulence in comparison to healthcare acquired strains may increase the likelihood of productive infections in healthy community based individuals thereby contributing to the success of these strains outside of healthcare settings. It is important to note that, although community acquired MRSA does show an increased virulence in comparison with healthcare acquired strains, it is not more virulent than MSSA strains.[38] It is the unique combination of virulence and antibiotic resistance which makes them so dangerous.

Some researchers have suggested that the success of some community acquired strains may also partially rely on their increased fitness for

asymptomatic colonisation of hosts. A higher proportion of colonised hosts could then lead to an increased incidence of serious infections requiring treatment. Teams have found that *S. aureus* bacteraemia is often caused by the same strain which originally colonised the infected patient.[42] USA300 possesses an arginine catabolic mobile element which was likely acquired from *S. epidermidis*.[43] This element features both an arginine deaminase and an oligopeptide transport gene cluster. It is thought that these may contribute to an increased survival of USA300 in acidic environments, such as the human skin.[43, 44]

Although the individual clinical severity of a *S. aureus* infection can be difficult to predict, it is abundantly clear that *S. aureus* presents a high clinical burden due to: the common nature of *S. aureus* infections, its potential to produce very severe potentially fatal conditions even in healthy individuals, the difficulty of treatment due to the spread of antibiotic resistant strains, and the spread of highly virulent and resistant strains such as USA300 into the community. Therefore, considerable research into new therapies for staphylococcal infection is required to ameliorate the risks of increasing virulence, antibiotic resistance, and the spread of virulent and resistant strains into the community.

1.1.3 Antibiotic resistance

Since Fleming's discovery of penicillin in 1928 and Florey's subsequent clinical trials in 1941 ushered in the antibiotic era, humanity has been able to effectively treat bacterial infections which would previously have been fatal. Antibiotics are vital to modern medicine; crucial to routine treatments such as chemotherapy and any kind of invasive surgery. In recent years, the extensive use (and misuse) of antibiotics has contributed to the widespread rise of antibiotic resistance. vancomycin resistant *Enterococcus*,[45] extremely drug resistant tuberculosis,[46] clindamycin resistant *Clostridium difficile*,[47] MRSA,[48] and VRSA[49] are all severe and potentially fatal threats to human health. More strains and species are becoming resistant to antibiotics each year.[50] Surgeons are now sometimes reticent to perform routine surgeries due to the risk of antibiotic resistant bacterial infections. Finally, there are very few antibiotic

drugs in development to hedge against these risks of increasing virulence and antibiotic resistance in bacteria.[51] Research to understand the causes of resistance and its mechanisms may provide new therapies or strategies to overcome its continued spread.

1.1.3.1 The causes of resistance

Classical antibiotics function by interacting with specific bacterial molecular targets causing bacterial toxicity without causing significant harmful effects against the host. Bactericidal antibiotics kill the bacteria while bacteriostatic drugs simply prevent their growth and/or reproduction. Both of these classes produce an evolutionary selective pressure in the bacterial population. Any bacterium which is less susceptible to antibiotics will possess a significant competitive advantage within the bacterial community. Consequently, these bacteria and the genes promoting resistance are likely to spread through any population where antibiotics are consistently being used, such as in a hospital.

Evidence suggests that more careful and targeted use of antibiotics can reduce the rate of resistance in a hospital population. In the absence of the selective pressure generated by antibiotics, the bacteria generally regress over time slowly losing their resistant characteristics.[52] Therefore, if infections could be treated without the selective pressure generated by bactericidal and bacteriostatic antibiotics, it is possible that bacteria would not develop resistance and may even slowly revert back to their antibiotic susceptible forms. There are, currently, no treatments for bacterial infections which do not function by bactericidal or bacteriostatic mechanisms.

There is also only limited research on potential targets which do not function by significantly affecting bacterial viability. This is understandable as the resolution of an infection does ultimately require the death of the bacteria. A therapeutic intervention or strategy which allows the host to clear infections *via* the host adaptive and innate immune systems would be novel. For example, without the action of coagulase and clumping factor A, antibodies could effectively bind and opsonize the bacteria allowing phagocytosis. Also, without the ability to release hemolysins and siderophores, the bacteria will not be able

to sequester iron from host tissues eventually causing nutritional deficit and the eventual death of the bacteria. A lack of catalase, superoxide dismutase, and staphyloxanthin would make the bacteria much more vulnerable to the reactive oxygen species released by neutrophils effectively reducing the bacteria's ability to survive inside the host cells.

1.1.3.2 The mechanisms of resistance

There are two broad classes of antibiotic resistance. Firstly, some bacteria are naturally resistant to some types of antibiotic. For example, Gram negative bacteria, such as *Pseudomonas aeruginosa* have an extra phospholipid membrane outside their cell wall.[53] Antibiotics, such as vancomycin cannot pass through the outer membrane to their site of action at the bacterial cell wall and, therefore, do not affect the bacterium. This is called intrinsic antibiotic resistance. This kind of resistance is not generally attributed to *S. aureus*.

In addition to intrinsic resistance, bacteria can also develop antibiotic resistance through phenotypic adaptation to antibiotics or through evolution, this is called acquired resistance. Acquired antibiotic resistance is encoded by multiple genes, many of which are encoded on plasmids and can transfer between bacteria. This transmission commonly happens within the same and related species and occasionally can also occur with species less closely related. These genes encode for many different kinds of mechanisms of resistance. There are three main mechanisms which can cause acquired antibiotic resistance: reduction of intracellular concentration (this can be by promoting egress or by preventing ingress of the antibiotic), antibiotic target modification (by mutation or post-translational modification), and chemical inactivation of the antibiotic. Each of these mechanisms has been extensively reviewed in the last decade.[54]

1.1.3.3 Potential strategies for combating antibiotic resistance

Many strategies have been considered for effectively overcoming antibiotic resistance. One strategy with proven success is to produce drug compounds which block or are unaffected by the known mechanisms of antibiotic resistance. For example, β-lactam antibiotics, such as penicillin (**1.1**), which act

by inhibiting the transpeptidase enzyme thereby preventing cell wall biosynthesis, are neutralised by hydrolysis mediated by bacterial β-lactamase enzymes. Clavulanic acid (**1.2**) was developed as a suicide inhibitor of the β-lactamase enzymes.[55] When clavulanic acid binds the enzyme and undergoes hydrolysis, it forms a covalent bond with the β-lactamase effectively inactivating the enzyme (see Figure 4). By administering clavulanic acid alongside amoxicillin, many previously resistant bacteria expressing these enzymes became susceptible to amoxicillin once again.

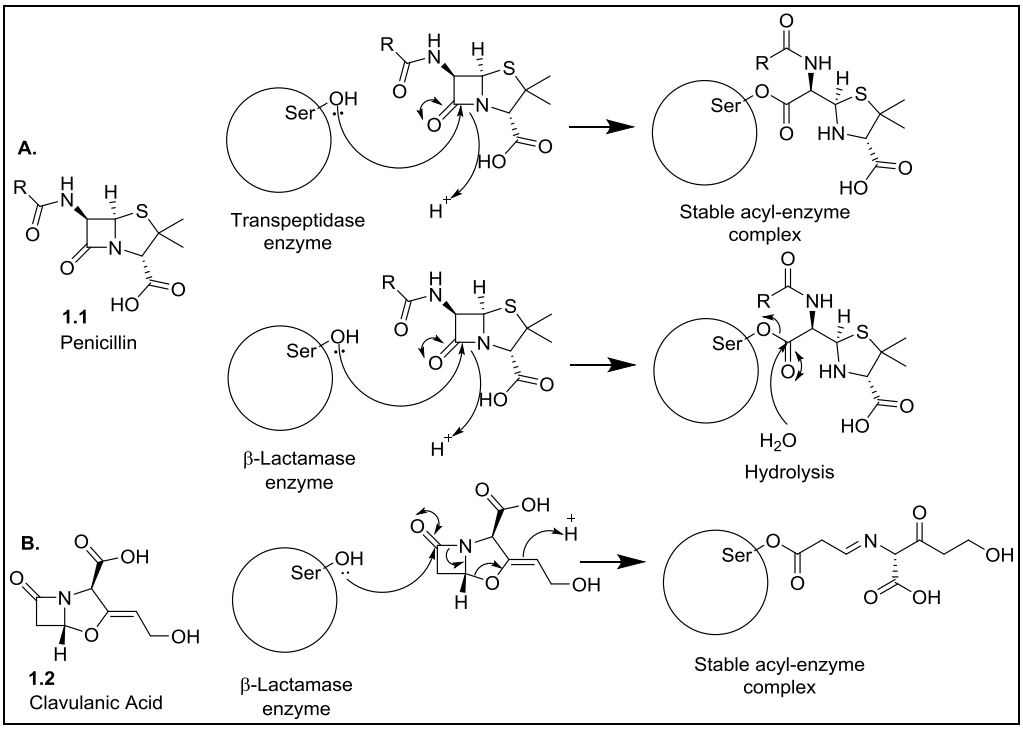


Figure 4: A diagram showing (**A**) the structure and mechanism of action of penicillin (**1.1**) resulting in a stable acyl-enzyme complex with a transpeptidase enzyme and hydrolysis by a β-lactamase enzyme and (**B**) the structure and mechanism of action of clavulanic acid (**1.2**) forming a stable acyl-enzyme complex with a β-lactamase enzyme, thus inactivated.

Some β-lactam antibiotics, for example, cephalosporins and carbapenems are less susceptible to β-lactamase enzymes due to their chemical structure.[56] However, over time bacteria can attain resistance through penicillin binding proteins with a reduced affinity for the drugs or by attaining new penicillin binding proteins which are insensitive to β-lactam based drugs.[57] Recently, inhibitor resistant β-lactamases and extended-spectrum β-lactamases which

can hydrolyse the modern more advanced antibiotics have begun to emerge in some bacterial species causing resistance to these newer compounds.[58]

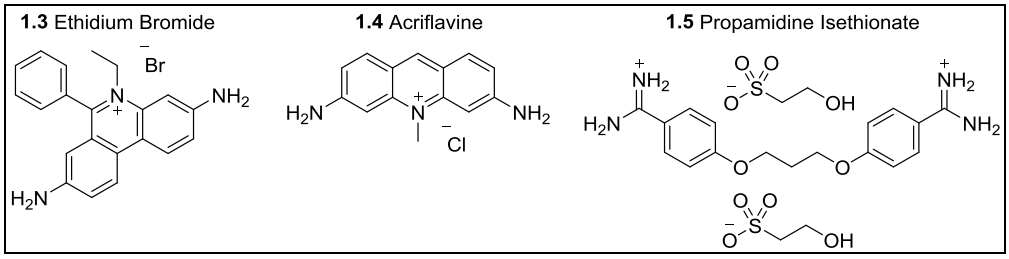


Figure 5: Examples of three antibacterial compounds which the QacA efflux pump removes from the cytoplasm of *S. aureus*

Some resistance mechanisms also cause resistance to multiple antibiotics simultaneously. For example, multidrug efflux pumps can remove a wide variety of drugs from the bacterial cytoplasm conferring multidrug resistance. These could theoretically represent promising targets for compounds designed to combat resistance and improve the effectiveness of existing antibiotics.

In *S. aureus*, the most well characterised drug efflux pumps are QacA, QacB and NorA.[59] QacA has been found to cause resistance against ethidium bromide (**1.3**), acriflavine (**1.4**), propamidine isethionate (**1.5**) and quaternary ammonium compounds (Figure 5).[60] The transporter substrates also include a wide range of dye compounds, diamidines, biguanidines, and guanyl hydrazones.[61] The *qacA* and *qacB* genes are very similar; only seven nucleotides differentiate the two genes.[62] Therefore, unsurprisingly, the substrate profiles are similar though not identical. QacB can remove monovalent cationic dyes while it cannot transport diamidines, biguanidines and divalent cationic drugs.[61] It is unknown whether QacA or QacB contribute to clinically relevant antibiotic resistance, however, there is a higher tendency for MRSA strains to possess these genes. Roughly 8% of MRSA isolates express these proteins while only 3.3% of MSSA isolates can produce them.[63] It does seem that cleaning with antiseptics like chlorhexidine provides strains possessing these efflux pumps with a selective advantage.[64] Resistance to chlorhexidine and benzethonium chloride has also been commonly observed in strains with these transporters.[65]

NorA is perhaps the most well characterised of the *S. aureus* efflux pumps. The *norA* gene was first observed in 1989 in a fluoroquinolone-resistant isolate

from a Japanese hospital.[66] The transporter can extrude many antibacterial agents, including some fluoroquinolones (notably norfloxacin **1.6**), rhodamine 6G (**1.7**), ethidium bromide (**1.3**), chloramphenicol (**1.8**), tetraphenylphosphonium bromide (**1.9**), puromycin (**1.10**) and acridine orange (**1.11**) (Figure 6).[67] This efflux pump may have originally evolved to extrude waste products and antimicrobials released by competing organisms.[59] This wide structurally permissive activity could conceivably confer resistance against new antibiotics before they have even been invented. The efflux pump is driven by proton motive force in a process known as the H^+:drug antiport mechanism (see Figure 7).[68] However, it is thought that resistance is driven by over expression of *norA* and not an increase in proton motive force or individual transporter activity.[69]

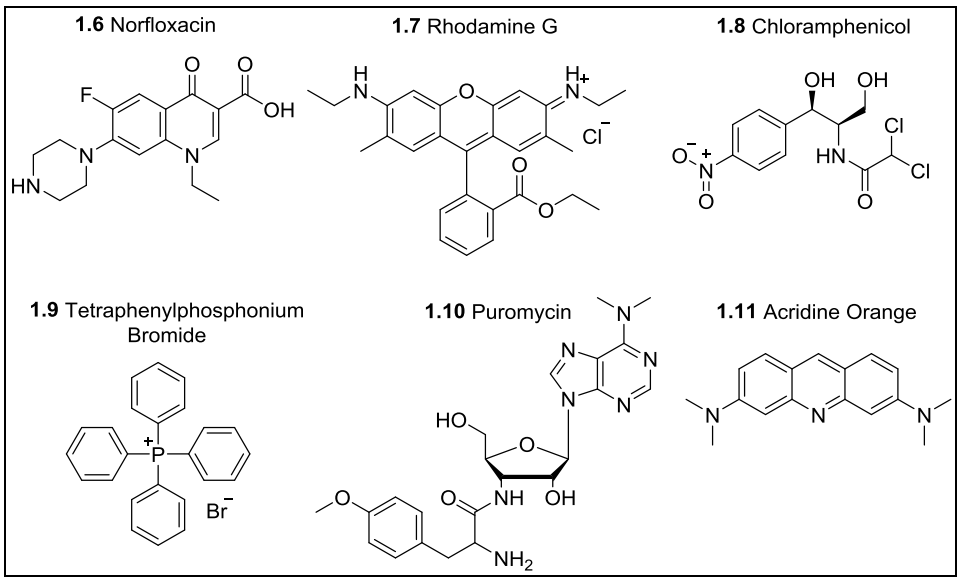


Figure 6: Examples of compounds which can be extruded by NorA

Inhibitors against the NorA efflux pump have been discovered.[59] CCCP and nigericin dissipate the proton motive force required to drive the efflux pump.[69] Reserpine also inhibits NorA by an unknown mechanism.[70] There are many other compounds which are also known to inhibit the NorA efflux pump including: kaempferol rhamnoside,[71] thiopyranopyridine moieties,[72] capsaicin,[73] chalcone,[74] ofloxacin based efflux pump inhibitors,[75] omeprazole derivatives,[76] isoflavones, flavones, pentaester, pterocarpan, epigallocatechin gallate, epicatechin gallate, neohesperidosides, orizabin XIX, orizabin IX, coumarin epoxide derivative, bergamottin epoxide derivative, piperidine

alkaloids and spinosan A.[77] However, many of these compounds and various other efflux inhibitors are known to cause toxicity problems at the high concentrations required for significant inhibition.[78] For this reason, there has not yet been any clinical use of efflux inhibitors against *S. aureus*.[78]

Another strategy which has been deployed in an attempt to limit antimicrobial resistance is known as 'antibiotic stewardship'. Antibiotic stewardship seeks to prevent the use of antibiotics where they are unnecessary or ineffective (such as viral infections like colds and flu) and to limit their use in milder conditions to patients with an increased risk profile. A normal healthy patient with a mild bacterial respiratory tract infection should not use antibiotics as their immune system can and will resolve the infection satisfactorily. However, if the patient was immunocompromised, for example, antibiotics should be used as their immune system is incapable of dealing with the infection.

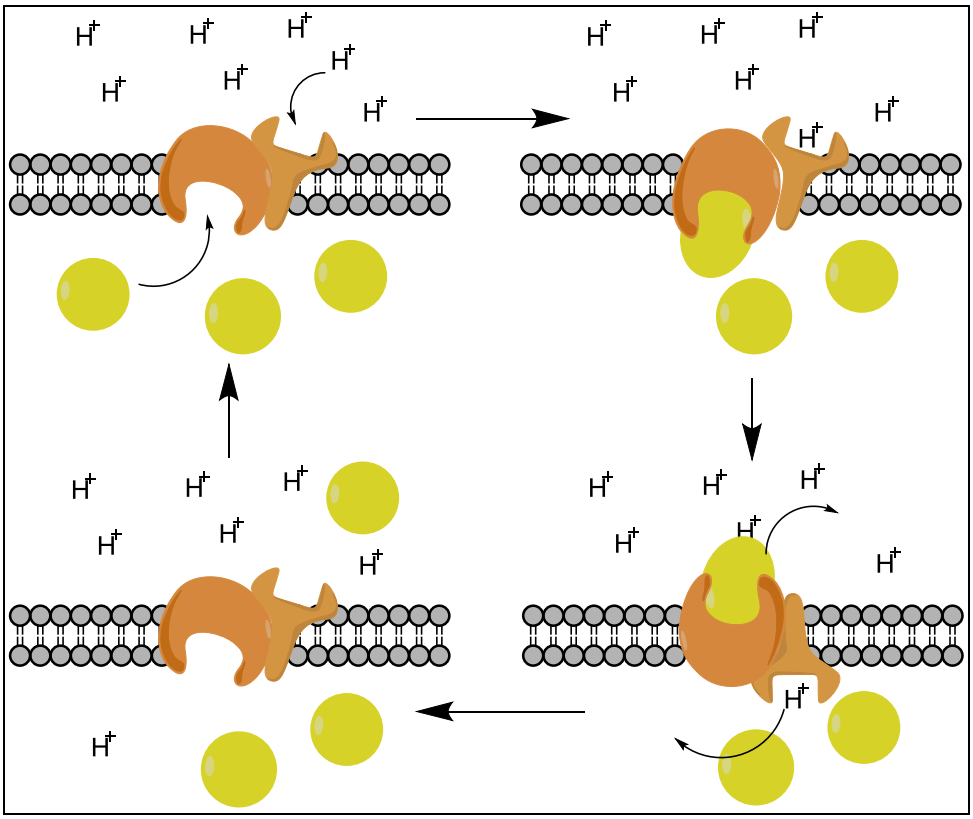


Figure 7: H^+:drug antiport mechanism used by the NorA efflux pump

Some antibiotic stewardship schemes in the UK have been quite successful. Research suggests that antimicrobial resistance decreased along with

improvement in long term adverse clinical outcomes without compromising short-term clinical outcomes.[79] However, this strategy has only managed to reduce resistance, it was not eliminated entirely in any setting. There are also no long term studies, these could be vital as the problem of antimicrobial resistance could return and continue to grow over decades as it has previously. Some scientists and politicians have also suggested that the widespread use of antibiotics in agriculture should be tightly regulated or even banned. Although these proposals sound plausible and they may have positive effects especially in the short term, there is currently no conclusive evidence to support the proposals.[80]

Finally, some more radical strategies have been suggested. Recently, extensive research has been carried out surrounding the idea of anti-virulence therapy. Instead of employing a bactericidal or bacteriostatic strategy, anti-virulence therapy inhibits the ability of a pathogen to establish and maintain an infection. Following the loss of these virulence mechanisms, the host immune system can more easily clear the quiescent bacteria. It is thought that this kind of strategy will produce only a minimal selective pressure as the new drugs would not directly kill or prevent the replication of the pathogen. The work outlined in this thesis focused on this type of new anti-virulence strategy, specifically the development of inhibitors of virulence expression in *S. aureus*.

1.2 Virulence of S. aureus

The ability of *S. aureus* to thrive as both a commensal and pathogenic bacteria is heavily reliant on highly regulated virulence factor expression systems throughout the infection pathway. These virulence factors perform a variety of vital functions, including immunoevasion, immunosuppression, colonisation (including cell attachment), and the acquisition of nutrients from the host (Table 1).

Table 1: Various virulence mechanisms of *S. aureus* and associated genes, virulence factors, and behaviours

Virulence mechanisms of *S. aureus*		
Targeting Neutrophils	**Preventing Immune Memory**	**Iron Sequestration**
Chemotaxis -Eap -ChIP	Superantigens -TSST-1 -Enterotoxins -Eap	Siderophores -Staphyloferrin -Aureochelin
Lysis -PSMs -Leukocidin A/B	B cell precursors -Protein A	Iron uptake systems -*Hts* -*Isd*
ROS & RNS -Catalase -Superoxide dismutase -Staphyloxanthin	**Immunoevasion**	**Mechanical Protection** -Formation of Biofilms
Antimicrobial peptides -Aureolysin -Staphylokinase	Avoiding Opsonization -Protein A -Clumping Factor A	**Persistence** -Formation of SCVs
	Phagocytosis Resistance -Coagulase	**Sequestration within epithelial cells**

Initial contact of the bacteria with host surfaces, e.g. the skin or mucosal surface is thought to trigger the initial upregulation of virulence genes.[81] In the host, exposure to bacterial products or tissue trauma stimulates local phagocytes and epithelial cells which, in turn, activate the immune system. *S. aureus* lipoproteins and peptidoglycans are detected by host pattern recognition systems.[82] Cellular detritus (RNA, DNA) released by necrotic tissue[83] and hyaluronan breakdown products,[84] indicating tissue injury and bacterial activity, respectively, are detected by toll-like receptors. These receptors act to increase local inflammation recruiting neutrophils and macrophages to the site of infection.

To survive and maintain this new infection, *S. aureus* must avoid opsonization by either antibodies or the complement system. Opsonization is a process where foreign particles are recognised by the immune system and are targeted for destruction by antibodies or the complement system, specifically the C3b protein.[85] Opsonized particles and bacteria are phagocytosed by macrophages or other immune cells, which recognise the antibodies or C3b coating with Fc or complement receptors.[86] Phagocytosis generally results in the death of the bacteria by digestion within a lysosome inside the phagocyte. Protein A, found in *S. aureus* cell wall and also released extracellularly, binds immunoglobulins inactivating them and thereby preventing opsonization.[87] Staphylococcal Clumping factor A is also produced which binds to complement regulator 1 protein and cleaves C3b helping to avoid recognition by the complement system.[88] Coagulase also converts fibrinogen to fibrin coating the bacteria and making it more resistant to both opsonization and phagocytosis.[89]

S. aureus can survive and shelter from the immune system within host cells such as endothelial, epithelial and even macrophage cells.[90] However, neutrophils represent a greater threat to the bacteria. There is an increased incidence of staphylococcal infections in patients with neutrophil dysfunctions as neutrophils are the most effective immune cells for clearing staphylococcal infections. Neutrophils act as highly effective phagocytes ingesting and destroying the bacteria quickly. *S. aureus* has several strategies to deal with the neutrophil challenge. It secretes extracellular adherance protein (Eap) and chemotaxis inhibitory protein (ChIP) which block neutrophil recognition of chemotaxis signals.[91] They also block neutrophil binding to ICAM-1.[92] ICAM-1 is vital for extravasation of the neutrophils from the bloodstream into the tissue and onwards to the site of infection. *S. aureus* also releases toxins which specifically kill neutrophils. Phenol soluble modulins (PSMs) cause neutrophil lysis and inflammation.[93] Similarly, staphylococcal leukocidin AB also forms pores in neutrophil membranes leading to cell lysis.[94]

Neutrophils which survive and arrive at the infection site release a battery of animicrobial substances. The reactive oxygen species (ROS), reactive nitrogen species (RNS), antimicrobial peptides, lysozyme, and proteases are all

released. *S. aureus* deploys antioxidant enzymes, such as catalase and superoxide dismutase and its pigment, staphyloxanthin, to neutralise the ROS and RNS.[95] Antimicrobial peptides are degraded by aureolysin[96] and neutralised by staphylokinase.[97] They are also less effective as *S. aureus* has a modified surface in comparison to most Gram positive bacteria. It has added *L*-Lysine to membrane lipids[98] and it uses *D*-Alanine in its teichoic acids, both of which make the neutrophilic antimicrobial peptides less effective.[99]

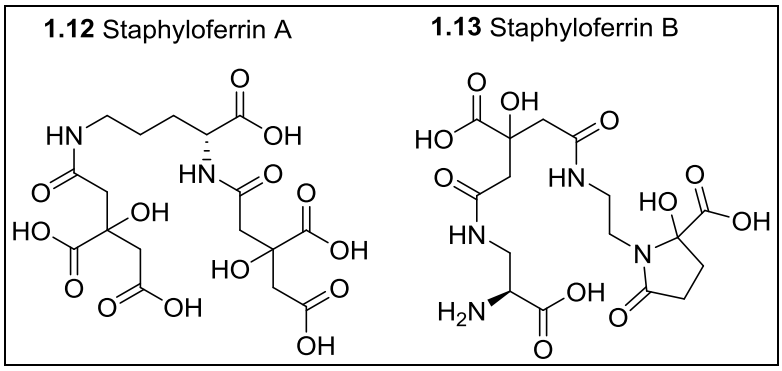


Figure 8: The fully characterised siderophores of *S. aureus* (aureochelin has not yet been characterised and its relevance has been called into question).[100]

Apart from evading the host immune system, *S. aureus* must also access vital nutrients from the host, especially iron. Hosts sequester iron inside cells with high-affinity serum proteins to prevent its use by pathogens in a system known as "nutritional immmunity".[101] The bacteria accesses the sequestered iron by releasing high affinity siderophores, such as staphyloferrin A (**1.12**), staphyloferrin B (**1.13**)[102] and aureochelin[103] (Figure 8). The iron acquisition genes, *hts* & *isd*, are also upregulated during iron starvation allowing the bacteria to capture heme and haptoglobin on its cell surface. They are subsequently transferred across the membrane for oxidative degradation and use inside the cell.[104] Hemolysins are also released which lyse erythrocytes releasing the iron-rich contents for sequestration by staphylococcal siderophores.[105]

Within a week to ten days of infection, the host is likely to mount an adaptive immune response to eliminate the infection and produce an immune memory which normally prevents reinfection. However, *S. aureus* seems to be able to repeatedly infect patients throughout their lives. This evasion of the

adaptive immune response is poorly understood. Some studies have suggested that staphylococcal superantigens, such as TSST-1, Eap (an MHC-II class analogue) and enterotoxins may play a role in corrupting the immune response, possibly by targeting T-cell activation pathways as a means to prevent the development of a long term immune memory.[106] Protein A has also been implicated in reducing B-cell precursor cell numbers which could be implicated in the poor generation of immune memory.[107]

S. aureus virulence strategies also include the formation of biofilms to mechanically protect against antibiotics and the host immune system.[95] The biofilm acts as a chemical barrier around an infection slowing or eliminating threats before they can reach the bacteria. The bacteria can also become persistent forming small colony variants (SCVs) which relapse into a very robust metabolically quiescent state during challenging conditions. The SCVs can then reemerge once conditions are friendlier, thereby contributing to ongoing chronic repetitive infections.[108]

1.2.1.1 Could anti-virulence be a new therapeutic strategy?

The virulence strategies described above are vital to the survival of the bacteria inside the host. By disrupting the tightly controlled expression of virulence factors, it may be possible to resolve staphylococcal infections without directly killing the bacteria.

Disrupting the function of virulence factors has already seen some success. For example, human antibody raised against α-hemolysin has been shown to cause a reduction in infectivity and potential therapeutic potential.[109] Inhibitors of the biosynthesis of staphyloferrin have been shown to reduce bacterial growth.[110] Furthermore, mouse anti-Protein A antibodies protected neonatal mice from staphylococcal infection.[111] Recently, a silkworm model showed reduced infectivity of gene-disrupted mutants, when mutations affected clumping factor B, fibronectin binding protein B or sortase A.[7] This model also showed attenuated virulence when global regulators of virulence such as *agr*, *arlS* and *saeS* were mutated.[7]

Even though success has been seen with inhibiting or mutating individual virulence factors, it is likely that disrupting multiple virulence factors could have more significant therapeutic potential. There are several global regulators of virulence in *S. aureus*. For example: *arlS, saeS, sarA,* and *agr* all regulate large networks of virulence factors. This makes them attractive targets for a putative anti-virulence therapy.

1.3 Quorum sensing

Many bacterial species use chemical signals to monitor their local population density, this is called quorum sensing (QS).[112] Behaviours controlled by QS systems include bioluminescence,[113] swarming,[114] stress response,[115] and biofilm formation,[116, 117] In pathogenic bacteria, virulence is often controlled by QS systems.[118-120] The specific molecules and receptors often vary, but the basic function of the system remains similar.[121] The QS system releases a chemical signal, generally called an autoinducer. At low population densities, the signal diffuses away without any effect. However, above a certain threshold, the secreted autoinducer reaches a concentration high enough to activate the receptors of the QS system.[122] This causes the production and release of virulence factors.[120]

When population density is low, the bacteria act as commensal organisms causing no trouble for the host. However, in the same way that large dense crowds can reinforce individual aggression eventually leading to riots, high population densities of bacteria cause the release of a battery of virulence factors which mount a coordinated attack on the host immune system. In this situation, the QS signals act to continually reinforce the aggressive phenotype of the bacterial 'crowd'. It may be possible, that by eliminating or reducing these 'crowd' signals the bacteria could be returned to a quiescent state and pathogenic infections could be prevented or resolved.[119]

1.4 Quorum sensing control of virulence in S. aureus

In *S. aureus*, one of the most well characterised regulators of virulence is the accessory gene regulator (*agr*) QS system. It is known to regulate a multitude of important virulence factors.

1.4.1 The *Agr* system

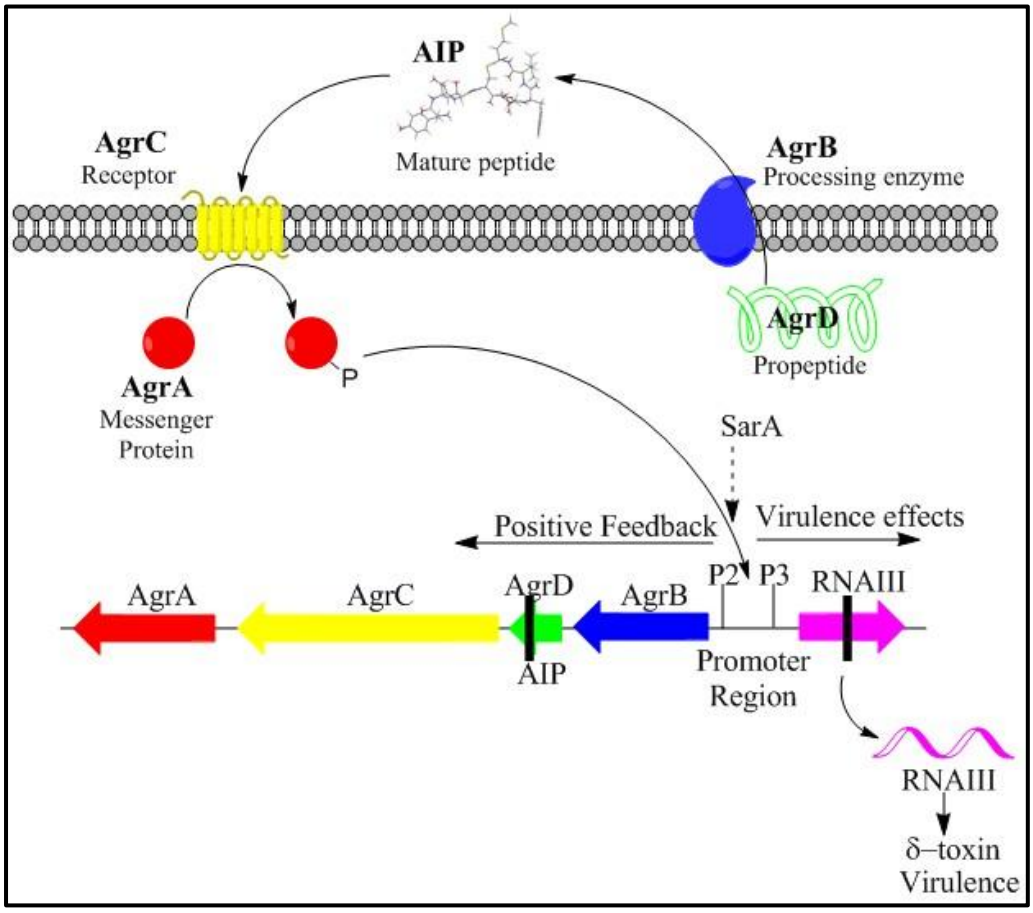


Figure 9: Schematic of the *agr* system

The *agr* system is a two-component signal transduction system. The operon consists of two divergent promoters, P2 and P3, a polycistronic four protein coding sequence, *agrBCDA* and a downstream effector, *rnaIII* (Figure 9). Initially, AgrB cleaves and processes the propeptide AgrD in the cell membrane, producing the mature autoinducer peptide (AIP). The macrocyclic thiolactone peptide is then released outside the bacterium.[123] When the concentration of the cognate AIP ligand reaches a threshold concentration (EC_{50}s range from 10-30 nM)[124], activation of AgrC (a transmembrane histidine kinase) causes autophosphorylation which consequently causes phosphorylation of AgrA.[125]

Phosphorylated AgrA then interacts with the P2 and P3 promoter sequences, upregulating transcription[126, 127] (possibly with the help of SarA[128]). This concurrently produces a positive feedback loop in the QS system as well as causing transcription of RNAIII. RNAIII causes downstream virulence effects (production of exotoxins, colonisation factors, hemolytic enzymes, etc.[81]) and, because the *hld* gene is embedded within *rnaIII*, it is also directly translated to δ-toxin.

1.4.1.1 Virulence factors regulated by the Agr system

The *agr* QS system, alongside *sarA*, *rot* and *saeS*, is known to be one of the master regulators of *S. aureus* virulence. It directly upregulates the production of its own *agr* system proteins as well as RNAIII and δ-toxin. RNAIII acts as a downstream RNA effector molecule which upregulates multiple toxins, secreted enzymes, surface factors, immunomodulatory proteins and regulatory substances, while downregulating some surface proteins, secreted enzymes and regulators (see Table 2). Activated AgrA separately upregulates the Phenol-Soluble Modulins (PSMs) and AgrA also exerts control over the metabolism of the bacteria, downregulating carbohydrate and amino acid metabolism, while reducing the biosynthesis of staphyloxanthin.[129]

Table 2: *agr*-regulated genes

Gene	Product	Reference
Directly upregulated		
agrBCDA	AgrB, C, D, & A	130
RNAIII	RNAIII & δ-toxin	131
Upregulated downstream		
-Toxins		
seb	Staphylococcal enterotoxin B	132
sec	Staphylococcal enterotoxin C	133
sed	Staphylococcal enterotoxin D	132
etaAB	Exfoliative toxins	134
tst	TSST-1	135
lukD/E	Leukocidin	136
lukG/H	Leukocidin	
pvl (or lukS/F)	Panton-Valentine Leukocidin	136
hla	α -Hemolysin	135
hlb	β -Hemolysin	135
hlgBC	γ -Hemolysin	136
hld	δ-toxin	135
-Secreted Enzymes		
sak	Staphylokinase	135
geh	Glycerol ester hydrolase	
ureA-G	Urease	
plc	PI-Phospholipase C	137
fme	Fatty acid modifying enzyme	138
splA-F	Spl proteases	139
lip	Lipase	
aur	Aureolysin	140
ssp	Staphylococcal serine proteases	140
scp	Staphylococcal cysteine proteases	140
bsaA	Glutathione Peroxidase	141
-Immunomodulation		
psmα1-4	Phenol Soluble Modulins PSMα1-4	142
psmβ1-2	PSMβ1-2	142
scn	Staphylococcal Complement Inhibitor	143
eap	Extracellular adherence protein	144
(called map)	(also called MHC-II analogous protein)	144
-Regulators		
arcR	Transcriptional regulator	
rsaE	RsaE sRNA	145

Table 1 continues on the next page...

Table 1 continues...

Gene	Product	Reference
-Surface factors		
clfA & clfB	Clumping factor A & B	146
cap5	Polysaccharide capsule 5	147
cap8	Polysaccharide capsule 8	148
Downregulated downstream		
-Surface proteins		
spa	Protein A	135
fnbA/B	Fibronectin binding protein A/B	149
coa	Coagulase	150
-Secreted enzymes		
ssl5	Staphylococcal superantigen like protein 5	151
ssl8	Staphylococcal superantigen like protein 8	151
-Regulators		
rot	Rot transcription factor	152

The *agr* quorum sensing system has a significant role in regulating all of the virulence strategies mentioned previously. It regulates the bacterial response to opsonization, the neutrophil challenge and the nutritional immunity of the host. It also regulates the superantigen toxins and biofilm formation. Given the ubiquitous nature of its virulence regulation, it represents a very attractive target for the development of an anti-virulence therapy.

1.4.2 The *Agr* groups of *S. aureus*

S. aureus has evolved four distinct *agr* groups. Each group has evolved with a different AIP cognate ligand and AgrC receptor. However, the groups are broadly similar and the *agr* system still operates in the same way. In the literature, these are referred to as *agr-I*, *agr-II*, *agr-III*, and *agr-IV*.

There are differing reports regarding the frequency of each of the *agr* groups. One study[153] which analysed 1,100 MRSA cases in Minnesota hospitals found that *agr-III* strains cause the vast majority of community acquired MRSA cases while *agr-II* strains cause the most of healthcare acquired MRSA cases. However, although this study nominally analysed 1100 isolates, many of the

isolates were identical. Five clonal groups represented 96% of all isolates and the limited geographical coverage also reduced the diversity of the samples.[153]

A study in focused on German and eastern european epidemic strains found that most MRSA strains are *agr-I* and only one *agr-II* strain was found in the study.[154] Another study examined a geographically diverse panel of 200 SCC*mec* type IV community acquired strains and 50 SCC*mec* type II healthcare acquired MRSA strains. They found that the community acquired strains were typically USA300 strains with *agr-I*, while healthcare acquired strains were typically USA100 strains with *agr-II*.[155] However, this study is also flawed as *agr* type could be correlated to SCC*mec* type and each of the *agr* types could have a different prevalence in healthcare and community settings.

Van Leeuwen *et al.* produced a widely cited study in 2000 which analysed 192 geographically and epidemiologically isolated.[156] They found that all of the strains studied could be identified as one of *agr-I*, *agr-II*, or *agr-III*. The vast majority of strains (92.2%) were *agr-I* type strains. They also found similar results when they examined strains which colonised healthy individuals. Given there were a large number of isolates studied which were genetically, epidemiologically and geographically unrelated, this study is likely to give the most reliable picture of *agr* groups worldwide. However, as other studies have found, local areas often do not follow a similar trend to the worldwide prevalence of each group. Also, as 15 years have passed since this study, it is possible that the worldwide spread of *agr* groups may have changed in the intervening time. One of the few areas of consensus among these studies is the rarity of *agr-IV* which was not discovered until well after the other three *agr* groups.[157]

1.4.2.1 How do the groups differ?

The *agrBDCA* operon possesses a "hypervariable region" consisting of the 3' end of *agrB*, *agrD*, and the 5' end of *agrC*.[158] In this region, the nucleotide sequence has changed over time establishing four different *agr* groups. The first 34 amino acids at the *N*-terminal of AgrB are completely conserved across the four *agr* groups. However, the *C*-terminal shows significant variability. Variation

in *agrD* is most notable for producing the divergent AIP signal molecules. The *C*-terminal kinase domain of AgrC is almost completely conserved. However, the *N*-terminal sensor domain shows substantial variation which is significant in allowing the AgrC receptor exquisite sensitivity to structurally different AIP signal molecules.[158]

This variation in the *agrBDCA* operon has led to classification of the four different *agr* groups. Each of these individual systems produce a different AIP ligand (called AIP1, 2, 3, and 4) and senses the concentration of these ligands with a different AgrC receptor (called AgrC1, 2, 3, and 4). For many years, only three *agr* groups were known,[159] but more recently a fourth group has also been discovered.[157] This final group is quite rare and only differs very slightly from *agr*-I. These two groups can also stimulate receptors from the other group (AIP1 can activate AgrC4 and AIP4 can stimulate AgrC1).

1.4.2.1.1 AIP signal molecules

The *agr* system responds to the extracellular concentration of its cognate AIP signal molecule. Each signal molecule is derived from the central region of AgrD *via* AgrB and signal peptidase dependent mechanisms.[160] The cognate AIP ligand contains between seven and nine amino acids. They contain a macrocyclic region with five amino acid residues and a tail region with two to four residues. A thiolactone bond between a conserved central cysteine residue and the C-terminal of the linear peptide forms the five-residue macrocycle. The primary sequence of each AIP signal molecule differs in each group (Figure 10 and Table 3).

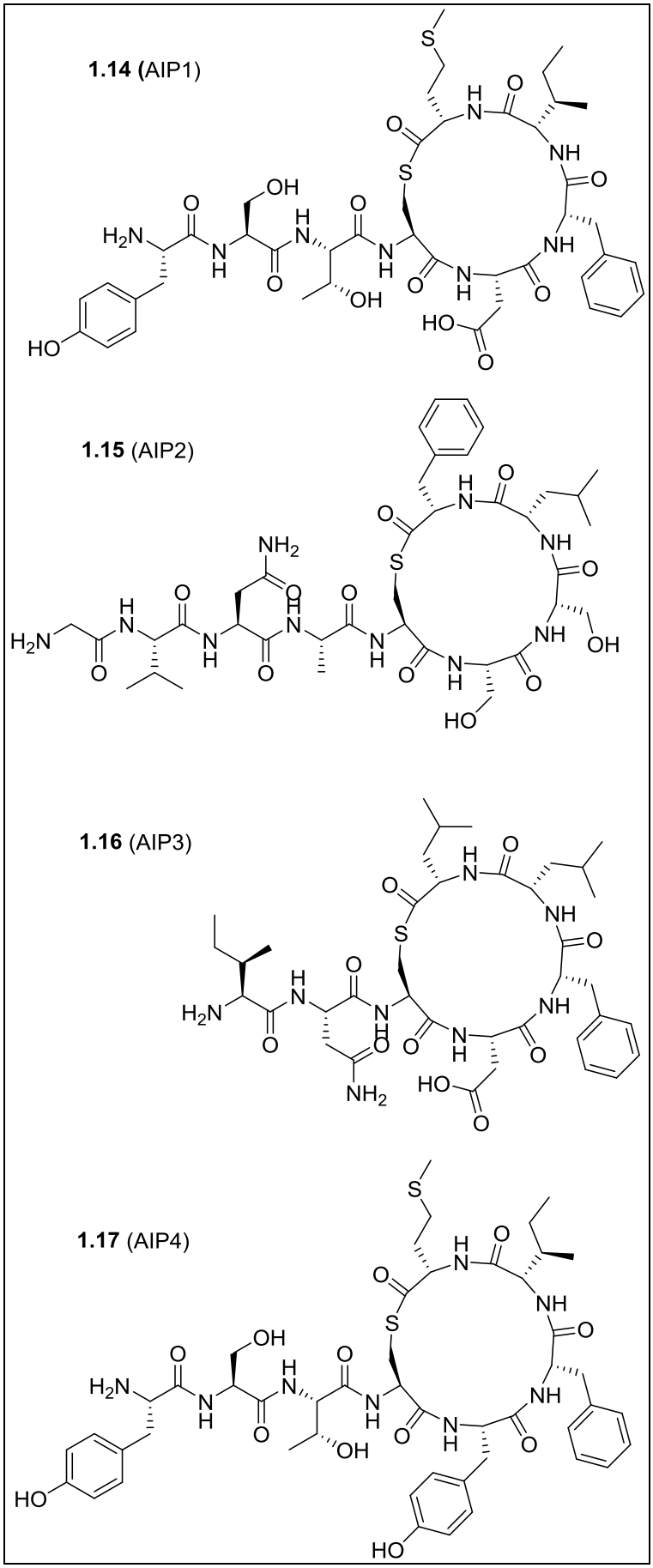


Figure 10: Structures of endogenous AIP cyclic thiolactone peptide ligands

Table 3: Primary sequence of each AIP signal peptide (*-* marks side chain to C-terminal thiolactone bond)

Signal peptide	Compound Number	Structure
AIP1	**1.14**	Tyr-Ser-Thr-Cys*-Asp-Phe-Ile-Met*
AIP2	**1.15**	Gly-Val-Asn-Ala-Cys*-Ser-Ser-Leu-Phe*
AIP3	**1.16**	Ile-Asn-Cys*-Asp-Phe-Leu-Leu*
AIP4	**1.17**	Tyr-Ser-Thr-Cys*-Tyr-Phe-Ile-Met*

The methionine in position eight of both AIP1 and AIP4 is susceptible to oxidation by ROS and RNS generated by the host immune response. The oxidised AIP molecules are unable to activate their cognate receptor.[161] It is unknown whether this is a mechanism which the bacteria has evolved to naturally turn over the signal molecule or whether it is a specific strategy by the host to reduce the virulence of the infection.

1.4.2.1.2 *agr* interference

Interestingly, the AIP signal molecules of one group often inhibit other *agr* types. This has been referred to as "*agr* interference".[159] The potency of this cross-group inhibition is surprising. Each of the three AIP groups bind other AgrC receptors with low nanomolar IC_{50} values (Table 4) except for *agr-I* and *agr-IV* which cross-activate.[124, 162] The biological role of *agr* interference is not clear. It could simply be due to the chemical similarity of the signal molecules, though some have argued that cross-group inhibition gives the producing strain a competitive advantage.[163] The interference effect has been used to reduce virulence of *S. aureus* in animal models demonstrating the potential of AgrC inhibition as an anti-virulence therapy.[164]

Table 4: IC_{50} values (nM) for each AIP ligand at every AgrC receptor determined using *S. aureus* fluorescent reporter strains[165]

Signal Molecule	AgrC1	AgrC2	AgrC3	AgrC4
AIP1 (1.14)	-	8.0	0.5	-
AIP2 (1.15)	1.6	-	0.5	0.4
AIP3 (1.16)	5.1	5.6	-	8.5
AIP4 (1.17)	-	0.4	0.5	-

1.4.2.1.3 AgrC receptor

The concentration of the AIP signal molecules is monitored by a two-component histidine kinase system consisting of the receptor histidine kinase, AgrC, and the response regulator, AgrA. AgrC acts as a homogenous dimer.[125, 166]

Binding of a cognate AIP ligand to the AgrC dimer can result in autophosphorylation of both kinase domains and activation of AgrA by phosphorylation.[125] Recently, Wang *et al.*[166] proposed a helical linker between the sensor and kinase domains exercises rheostat-like control over the dimer activation, rotation of this linker in either direction causes the receptor to be more or less active Binding of agonists can cause the rotation of the linker allowing phosphorylation of the kinase domain.[166]

AIP binding occurs outside the membrane at the AgrC sensor domain. The sensor consists of three extracellular loops and six transmembrane domains (Figure 11).[126] The *N*-terminal of the sensor domain is more variable and it is thought to be the site of AIP recognition. Recognition is believed to occur at loops 1 and 2, loop 1 is thought to interact with the tail region while loop 2 binds the macrocyclic ring.[167] Amino acid substitutions in these loops can change the AIP binding properties of the receptor, even changing its specificity.[125, 168] Transmembrane domain 5 and 6 and loop 3 are more conserved and are thought to be involved in signal transmission to the kinase domain *via* the helical linker.[169]

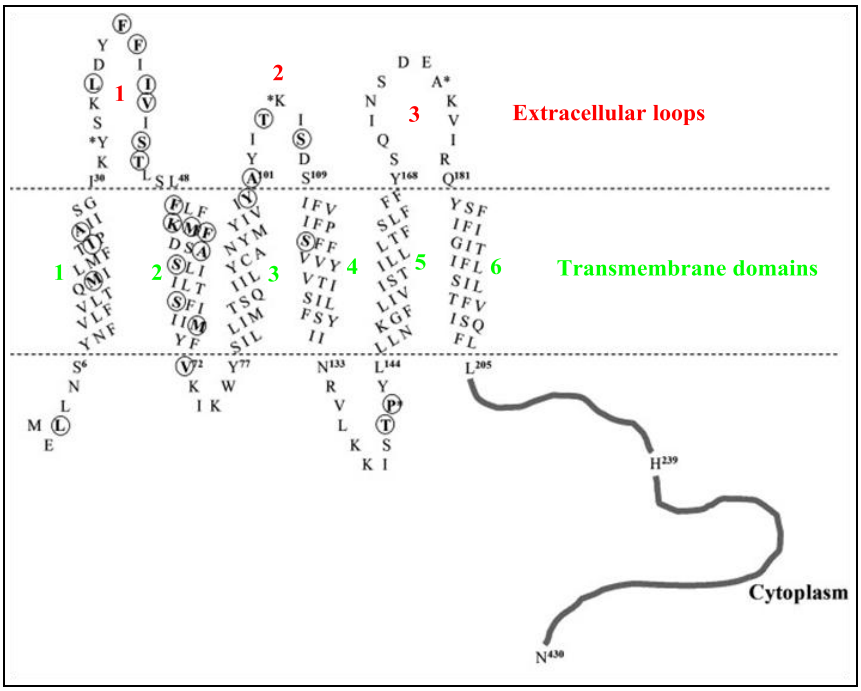


Figure 11: Predicted transmembrane topology of the *S. aureus* AgrC1 protein[167]

1.5 *Analogous* agr *systems*

There are many bacteria which possess systems analogous to the *agr* system of *S aureus*. Consideration of the function of these systems and analysis of previous research aimed at inhibiting them may unveil useful insights which can be redeployed in the development of inhibitors of the *S. aureus agr* system.

1.5.1.1 Staphylococcal species

Many staphylococcal species possess analogous *agr* systems. Of all the species with these systems, *S. epidermidis* is generally considered to be the most clinically relevant nosocomial pathogen. [170] This is partly because of its ubiquitous presence on the human skin and mucous membranes. However, unlike *S. aureus*, *S. epidermidis* rarely causes invasive infections. It is more well known for its ability to colonise medical devices and form tenacious biofilms. The *agr* system of *S. epidermidis* is very similar to the *agr* system of *S. aureus*. There are some notable differences, however, for example, the system also upregulates many adhesin proteins (including polysaccharide intercellular adhesin)[170] alongside the virulence upregulation observed in the *S. aureus* system. There is also more significant regulation of metabolic proteins by the *agr* system of *S. epidermidis* suggesting that the system may be geared towards preparing the bacteria for a sessile lifestyle in a biofilm phenotype.[171] Interestingly, *agr* also promotes biofilm remodelling, maturation and dissemination through the upregulation of PSMβ.[172]

Currently, there are two main strategies known to inhibit the *agr* system. The first exploits the similarities between the *S. aureus* and *S. epidermidis agr* systems. The *S. aureus* native AIP4 ligand inhibits the *agr* system of *S. epidermidis* and some compounds developed to target *S. aureus* have also been found to inhibit the *agr* system of *S. epidermidis*.[173] Secondly, a small peptide known as RNAIII inhibiting peptide, which is also thought to inhibit *S. aureus,* may inhibit the *agr* system of *S. epidermidis*.[174] However this is a controversial area and the details of this inhibition will be expanded in Section 1.6.1.

S. lugdunensis is also a commensal skin bacterium commonly colonising humans with no recognisable symptoms. However, similarly to *S. aureus*, it can also act as an opportunistic, highly virulent, invasive pathogen. The bacteria also secretes a host of virulence factors similar to those found in *S. aureus* and an analogous *agr* system which produces an AIP compound is known to be present in the bacterium.[158, 175] However, even though a δ-hemolysin is secreted,[176] there does not seem to be a gene homologous to *hld* embedded in the *rnaIII* gene.[177] Also, because of the lack of animal models specific to this species at present, it is unknown whether the *agr* system is clinically relevant.[178]

The situation is somewhat similar in *S. saprophyticus,* an AIP secreting *agr* system is known to be present, however it also lacks a homologous *hld* gene.[179] There are also no animal models for the evaluation of the clinical importance of the *agr* locus in *S. saprophyticus*. The lack of knowledge of the clinical relevance in *agr* in these species has meant that no considerable work has been executed to develop effective *agr* inhibitors.

The *S. intermedius* group, which actually contains three recently defined sub-species, is similar to *S. aureus* and other staphylococcal strains previously mentioned in that it is both a successful commensal bacterium as well as being an opportunistic and invasive pathogen in each of the sub-species' respective hosts. *S. pseudintermedius* is one of the sub-species which is known as an intestinal commensal bacterium in dogs. This species can cause productive infections in the host.[180] It is interesting as the resident *agr* system produces a unique AIP molecule (**1.18**) which uses a lactone instead of the normal thiolactone observed in other staphylococcal species (Figure 12). This depsipeptide molecule uses a central serine residue to form the essential cyclic structure.[181] Replacing this central serine with a cysteine (as observed in other staphylococcal species) actually reduces RNAIII levels in the bacteria demonstrating that the lactone moiety is important for quorum sensing functioning in this bacteria.[181]

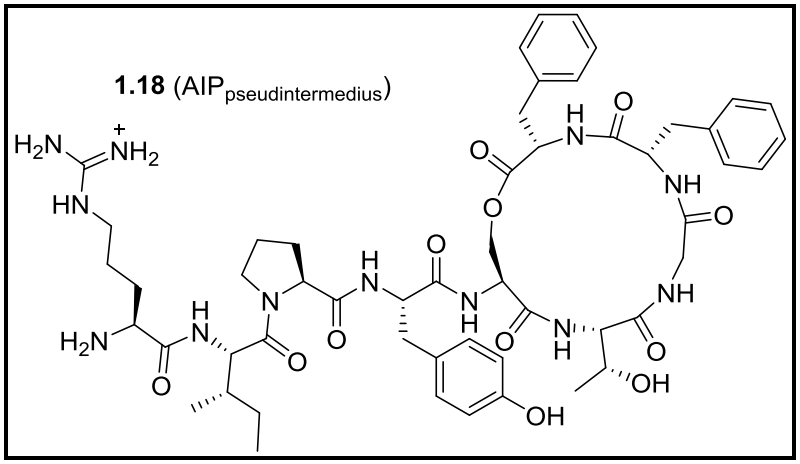


Figure 12: Endogenous AIP ligand of *S. pseudintermedius*

1.5.1.2 Clostridial species

Many *Clostridium* species secrete some of the most toxic substances known to man. For example, *C. botulinum* releases the extremely potent neurotoxin widely known as botox (botulinum toxin) which is the causative agent of botulism. Many clostridial species are also known to possess *agr* analogue systems including the problematic *C. difficile*.[182] However, the role of *agr* in virulence in many clostridial species has not yet been determined. Common pathogenic clostridial species are often naturally physiologically resistant to antibiotics. They can also be problematic because of the reduced rate of growth of many species, their obligate anaerobic existence, and the formation of endospores which are highly resistant to heat, oxidation, radiation, desiccation and many of the usual chemical means of bacterial control. Given this difficulty, the role of quorum sensing in the virulence and metabolism of these common pathogenic species has received considerable attention. It is now known that the *agr* system is vital for control of toxigenesis and sporulation in *C. botulinum*.[183] *C. botulinum* is also now known to have two different *agrBD* homologues, which produce two divergent AIP molecules; these two signal systems regulate toxigenesis and sporulation separately.[183] The cognate receptors for these two divergent signals have not yet been studied. The divergent signals and lack of understanding of the cognate receptors is not conducive to the development of *agr* inhibitors, and consequently no significant work has been undertaken in this area.

C. perfringens causes food poisoning, however, it is more well known as the most common causative agent for gas gangrene. Anaerobic conditions in deep trauma sites (such as surgical incisions or battlefield injuries) can give rise to conditions necessary for infection and growth of this bacterium. As the endospores of *C. perfringens* germinate within a deep wound, they release proteases and exotoxins digesting the host tissue. The nutrients generated by the damaged tissue then rapidly accelerate bacterial growth. An *agrBD* homologue is known to regulate toxin production in *C. perfringens*.[184-187] Deletion of *agrB* results in a reduction in both Epsilon-toxin and Beta2-toxin production,[186, 187] it also reduces toxicity and colitis in an *in vivo* rabbit model.[188] In some cases, regulation of genes located on plasmids has been observed which is unprecedented in previous *agr* system research.[184] Although *virRS* regulation of several toxins and virulence factors in response to the *agrBD* quorum sensing signal molecule has been seen in some strains,[185, 186, 189] full details of the true cognate receptor and mechanisms for the consequent regulation of virulence in *C. perfringens* are not well understood. However, some initial research has found that 5-mer cyclic peptides activate the system while 6-mer peptides have the ability to inhibit quorum sensing mediated virulence.[190] The non-cyclic linear 5-mer peptides were still able to activate the system which is dissimilar to research in other *agr* systems.

C. difficile is a common and problematic cause of nosocomial infections. Following antibiotic therapy, the gut microbiota is disturbed and this can often allow *C. difficile* to flourish in the absence of the normal competition for gut micronutrients. The bacteria produces significant amounts of toxin A and B which causes severe diarrhoea, a hallmark symptom of the infection. *C. difficile* has been known to possess a full homologous *agrBDCA* operon for some time alongside a second copy of *agrBD*.[183] However, recently it has been proven that the bacteria uses the homologous *agr* system to regulate the production of these toxins *via* a quorum sensing mechanism using a small cyclic thiolactone signal peptide similar to the AIP compounds seen in *S. aureus*.[191] Unfortunately, information on the structure of the signal peptide, its cognate receptor, or the mechanisms of toxin upregulation are still lacking.

1.5.1.3 *Enterococcus faecalis*

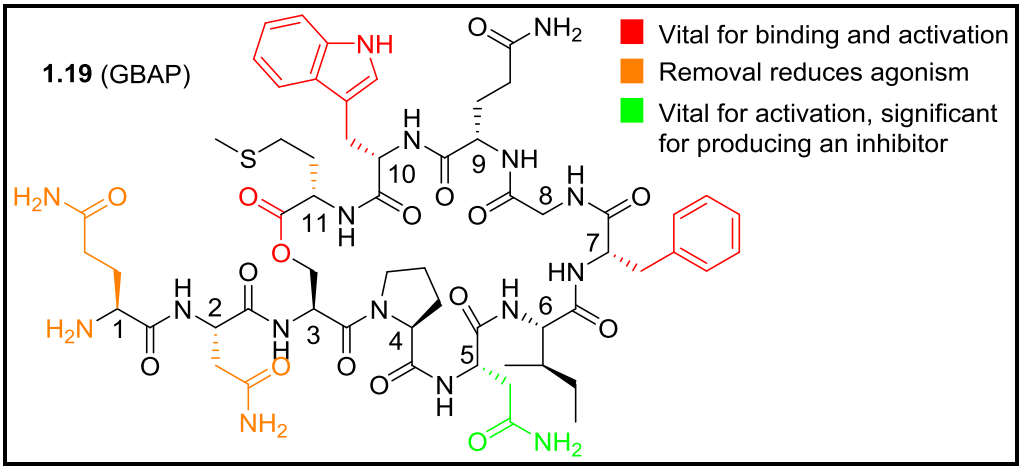


Figure 13: Endogenous GBAP ligand of FsrC receptor in *E. faecalis* highlighting some structures important to the structure activity relationship

E. faecalis is probably the best studied *agr*-like quorum sensing system apart from *S. aureus*. Vancomycin-resistant strains are of increasing importance as an emergent cause of nosocomial infections. It is also a fairly common cause of infections in the seminal and urinary tracts including nephritis, urethritis, and prostatitis. Systemic bacteraemia and endocarditis have been observed caused by the progression of the infection *via* the kidneys. The virulence factors of *E. faecalis* comprised of numerous proteases, adhesins and biofilm components. A gelatinase and serine protease are particularly important in aiding the bacteria to invade host tissues.[192, 193] The *fsr* operon regulates the production of both these proteins, it also downregulates biofilm components, and alters metabolic activity.[194] FsrD is cleaved, cyclised and released extracellularly by FsrB to produce the GBAP signal peptide (**1.19**, Figure 13).[195, 196] This GBAP signal peptide is unlike AIP as it has 9 amino acid residues in a lactone ring arrangement formed with a central serine residue. The organisation of the *fsr* operon also differs as the sequence for *fsrD* lies entirely within the sequence for *fsrB* but in a different reading frame.[197] In contrast, *fsrA* and *C* are highly homologous to *agrA* and *agrC*. The target for FsrA is also adjacent to the *fsr* operon similar to the proximity of the *rnaIII* gene in the *agr* system.[195] Deletion or inhibition of the *fsr* operon results in a stress-response phenotype,[198] reduces tissue damage in a rabbit endopthalmitis model[193] and it enhances murine survival in a peritonitis model.[195]

Extensive work has been undertaken to attempt the development of a GBAP-based inhibitor of the *fsr* system in *E. faecalis*. Initial structure activity relationship data showed that linear GBAP analogues are completely ineffective and do not activate the system. Using a *D*-methionine or *N*-acetylating the compound also showed reductions in activity.[199] An alanine scan was later performed which revealed that the two tail residue side chains were not necessarily required for recognition by the receptor, however side chain replacement of the residues of the macrocyclic residue reduced activity. Specifically, Phe^{7} and Trp^{10} were found to be vital for binding and activation. NMR studies revealed that Trp^{10} oriented itself within the hairpin structure of the macrocycle providing significant stability while Phe^{7} is oriented away from the body of the molecule. It is thought that its presence and orientation could be very important for receptor binding, recognition or activation.[200]

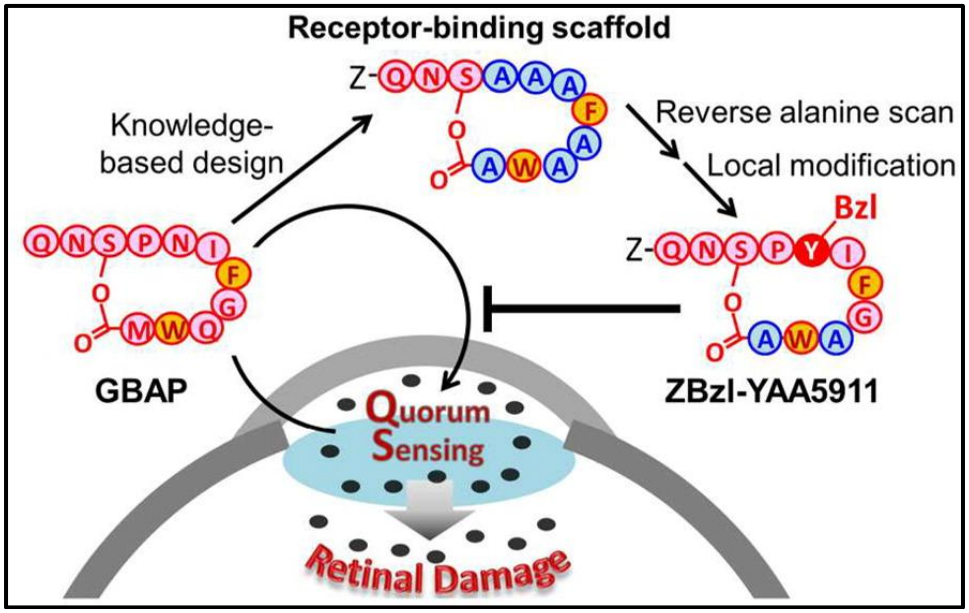


Figure 14: Figure from Nakayama *et al*. illustrating rational inhibitor design based on the original GBAP ligand.[201] Phe^{7} and Trp^{10} are retained, a reverse alanine scan is performed, and Asn^{5} is modified to produce a nanomolar inhibitor of the *fsr* system.

Recently, a systematic search for a potent inhibitor was performed using a technique known as reverse alanine scanning. All non-vital side chains were converted to alanine (Phe^{7} and Trp^{10} were retained) producing a weak inhibitor of the receptor (see Figure 14). Each residue of this compound was then reverted in turn to its original residue, each of these new compounds were tested for inhibitory potency, and the structure of the most potent inhibitor was

identified. Each amino acid residue of this new inhibitor was then reverted in turn again, the new compounds were again tested for inhibitory potency, and the structure of the strongest inhibitor was taken forward into another round of this process. This process was repeated until the most potent inhibitor was found. Using this technique, an inhibitor with an IC_{50} of 8.7 μM was developed with alanine residues at position 5, 9, and 11 while positions 4, 6, 7, 8, and 10 contained the original GBAP residues.[201]

This was a very elegant and well executed study. Alanine scanning has already been used in *S. aureus*, however, the reverse alanine scanning strategy has not yet been attempted. This could be an interesting avenue of research for rational design of AgrC inhibitors.

1.5.1.4 Listerial species

Listeria monocytogenes is the causative agent of listeriosis, a food-bourne infection which can cause severe illness in patients with other risk factors. This bacteria has the ability to form biofilms on many abiotic surfaces, such as plastic and stainless steel, which act as a source of contamination for many different foodstuffs. Many virulence factors are present, including listeriolysin O, hemolysin, phospholipase and many cell-surface proteins which promote actin polymerisation and phocytosis. This bacterium also has the ability to breach the phagosome and then deploy actin tails which propel the cell through the cytosol and into a neighbouring cell thereby evading the host immune system. *L. monocytogenes* possesses a complete *agrBDCA* operon which regulates the expression of adhesion factors, internalins, and biofilm maintenance.[202, 203] However, it lacks an *rnaIII* gene and AgrA interacts directly with promoter regions producing the downstream virulence effects.[202] The regulation of virulence by *agr* seems to be growth dependent; a murine model showed reduced virulence by mid-exponential phase *ΔagrA* strains.[204] However, a similar strain grown to stationary phase showed no effect on virulence.[205] *In vitro* invasion assays also showed no difference in the ability of the bacteria to thrive intracellularly.[204, 205] Most *L. monocytogenes* isolates are *agr*$^{+}$ suggesting it plays an important part in the bacterial life cycle, even if it is not necessary for human infection.[206] It may be that anti-*agr* compounds could be used to limit

the spread of the bacteria in food processing environments. However, to date, no compounds have been developed targeting the *agr* system in *L. monocytogenes*.

1.6 Agr and virulence inhibitors

1.6.1 Targeting the action of RNAIII activating peptide

A second quorum sensing system in *S. aureus* has been previously proposed and extensively researched.[174, 207] However, there is considerable controversy in the literature with several groups publishing contradictory findings.[208] RNAIII production was thought to be independently stimulated by the action of RNAIII activating peptide (RAP) at TRAP (target of RAP). A compound known as RNAIII inhibiting peptide (RIP) was also thought to inhibit the action of RNAIII thereby reducing virulence of the bacteria. One of the original researchers recently found that the results which led to the original team to hypothesise the existence of the *traP* gene were caused by a nonsense mutation in *agrA*.[209] However, some studies have still found RIP to be effective in improving host survival and response to *S. aureus* infection.[210] An anti-TRAP antibody has also been shown to protect against *S. aureus*.[211] Furthermore, structure-based virtual screening using the RIP pharmacophore produced the effective inhibitor of virulence, hamamelitannin (a witch hazel natural product derivative).[212] Currently, the presence of RAP, TRAP, and RIP in *S. aureus* is highly disputed and these inhibitors may function by an unknown mechanism.

1.6.2 AIP-based analogues

The discovery that the administration of AIP2 could prevent *agr-I* S. *aureus* infections in mice[162] led to considerable research to develop cross-group inhibitors based on the endogenous AIP1 (**1.14**) and AIP2 (**1.15**) ligands. Early studies found that small changes to the AIP ligands commonly eliminated their agonistic activity converting them to antagonists.[157, 159] Although small changes to the native ligands generally caused inhibitory activity, oxidation of the methionine of AIP1, which seems to happen naturally in media over time, caused the molecule to lose all activity in group 1, both activating and inhibitory (see Figure 15 in red).[157] It may be that this is intended for natural turnover of the AIP1 ligand over time. Synthetic conversion of this methionine to norleucine (which replaces the sulfur atom with a methylene group) showed a dramatic loss of activity. However, *D*-amino acid scanning of AIP1, which generally

resulted in loss of activity, showed that *D*-methionine possessed a similar activity to the parent AIP1 molecule (a similar result was seen in the *D*-phenylalanine analog). It seems that the presence of a non-oxidised sulfur in either stereoconfiguration is important for activity at AgrC1.[157] The team continued to perform an alanine scan, replacement of the tail serine residue with alanine produced an agonist more potent than AIP1 (see Figure 15 in orange). A potent AgrC1 inhibitor was also produced by replacing the macrocycle's aspartate residue with alanine (see Figure 15 in blue). Replacing the sulfur of the thiolactone bond with nitrogen, thereby producing a more stable lactam structure, produced a molecule which maintained agonistic activity at AgrC1 at high concentrations indicating that a previously hypothesised trans-acylation of AgrC was unlikely to be necessary for activation of the receptor (see Figure 15 in green).[157]

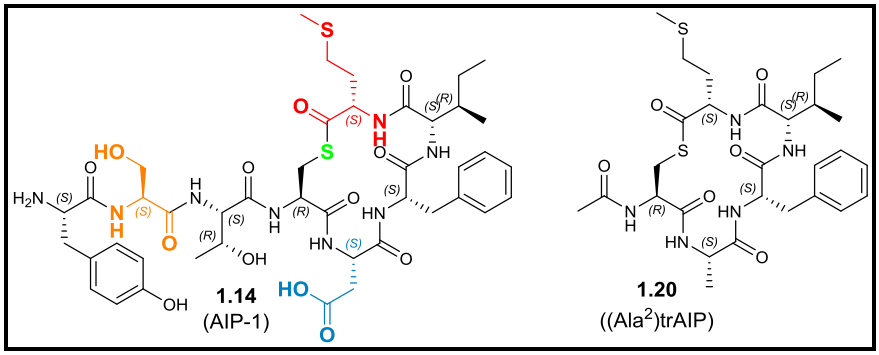


Figure 15: The structure of native AIP1 & AIP2 with potent truncated analogue **1.20**. Significant residues are highlighted.

Early analysis of the influence of the tail and macrocyclic region of AIP1 on AgrC binding showed that both the tail and macrocycle are required for full activation. The AIP1 macrocycle lacking a tail region can cause partial agonism of AgrC1 but when the aspartate residue is converted to alanine the compound is a potent nanomolar inhibitor (**1.20** - see Figure 15).[124] The group also proved that macrocycles without the tail region can act as potent cross-group inhibitors.[213] There has been a large number of further studies into the structure activity relationship of AIP1 and AIP2; they are discussed in more depth in Chapter 3.

1.6.3 Solonamides

During a global research expedition, a panel of more than 500 strains of marine bacteria were collected. Each of these strains was screened for their ability to interfere with the *agr* QS system in *S. aureus*. Positive results were reported when strains enhanced the expression of *spa* (Protein A) while concurrently reducing the expression of *hla* (α-hemolysin) and *rnaIII* (RNAIII) with minimal growth effects on the bacteria. A newly discovered strain of *Photobacterium halotolerans* was found to interfere with the *agr* system. Fractionation of the crude extract and testing of the isolated compounds revealed that the activity was due to two novel cyclic depsipeptides, solonamide A and B (SolA-**1.21** & SolB-**1.22**, Figure 16). The structure of these compounds was elucidated using high resolution mass spectroscopic and NMR techniques. Northern blots further confirmed the effects on RNA levels of *spa*, *hla*, and *rnaIII*.[214]

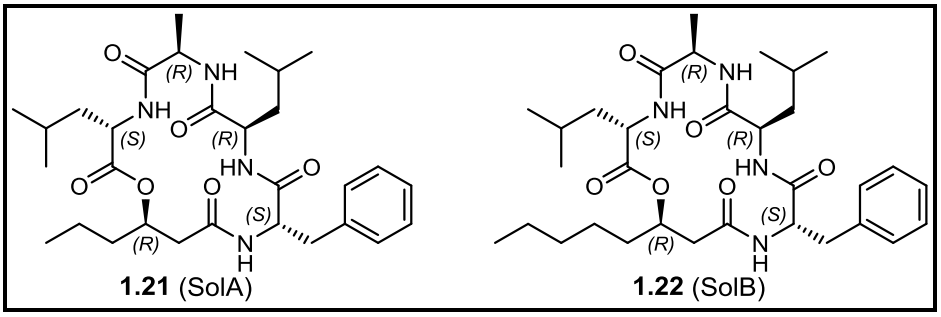


Figure 16: Structure of SolA and SolB

The solonamides were shown to reduce transcription at the P3 promoter of the *agr* system demonstrated by using P3::*lux* reporter strains representing all of the *agr* subtypes in a zone of inhibition assay. However, reporters with constitutively active AgrC receptors (R238H-AgrC[215]) were not affected. Therefore, the solonamides are thought to act on the AgrC receptor of the QS system. The solonamides were also shown to inhibit hemolysis and the expression of *psmα* and *agrA*. The team also demonstrated that PSM expression and neutrophil killing were reduced in bacteria treated with the solonamides.[216] A more detailed discussion of existing research on the solonamides can be found in chapter 4.

1.6.4 Other inhibitors of AgrC

Other compounds and strategies aiming to inhibit the *agr* system have previously been explored. Mice were used to raise antibodies against an AIP4-based immunogenic compound. The monoclonal antibody, AP4-24H11, which was produced eliminated hemolytic activity of bacterial supernatant, reduced expression of α-hemolysin and increased expression of protein A in *agr*-IV strain RN4850 without eliciting any effects from other *agr* group strains. This shows that the antibody is highly selective which is interesting as AIP4 only differs from AIP1 by one residue (Asp to Tyr). It also suppressed *S. aureus* pathogenicity in a mouse model of abscess formation and provided complete protection against a *S. aureus* challenge which is usually lethal.[217]

Further work yielded a crystal structure of the antibody bound to AIP4.[218] A key Glu^{H95} was observed to provide much of the binding specificity by forming hydrogen bonds with each of the four amide nitrogens in the AIP4 macrocycle. The structure also reflected many features of binding models proposed for AgrC-AIP interactions and as such could provide a model for recognition of the native ligand by the receptor.[218] Further work could generate cross-reactive antibodies or antibody mixtures which it would be possible to use as active or passive immunotherapy to modulate infection by *S. aureus*.

Some small molecules have also been discovered which inhibit the *agr* system. While screening for inhibitors of the *agr*-like QS system of *Enterococcus faecalis*, a compound which inhibits the biosynthesis of the cyclic peptide signal molecules was discovered. The molecule, named ambuic acid (**1.23**, Figure 17), was found to inhibit the proteolytic processing of FsrD (the AgrD analogue) by FsrB (the AgrB analogue). When the compound was tested with *S. aureus*, *agr* bioreporters were inhibited, AIP1 in the supernatant was eliminated and hemolytic activity was reduced. Unfortunately, the inhibition caused by this compound was not "substantial or sustainable" and more work is required to produce more potent inhibitors before this scaffold could be used as an anti-virulence therapy.[219]

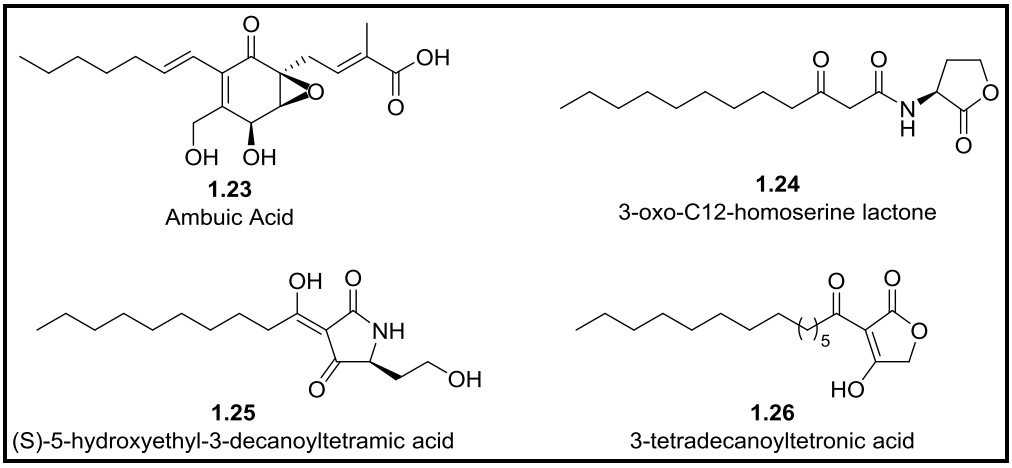


Figure 17: Other small molecule *agr* inhibitors

Many Gram negative bacteria deploy *N*-acylhomoserine lactones to mediate QS systems. Some of these compounds derived from *Pseudomonas aeruginosa* are known to inhibit *agr* mediated QS and growth in *S. aureus*. The 3-oxo-C12-homoserine lactone (**1.24**, Figure 17) seems to interact with the staphylococcal membrane at sub-growth inhibitory concentrations *via* an unknown mechanism thereby reducing *agr* and *sar* expression.[220] Under alkaline conditions, the 3-oxo-C12-homoserine lactone undergoes an intramolecular rearrangement to afford (*S*)-5-hydroxyethyl-3-decanoyltetramic acid (**1.25**, Figure 17) which has antibacterial properties against Gram positive organisms including *S. aureus*.[221] These antibacterial properties also seem to be a consequence of disruption of membrane potential and pH gradient.[222] Therefore, Murray *et al.* synthesised a series of 3-oxo-C12-homoserine lactones, and related tetramic and tetronic acids to examine their potential as antibiotics or antivirulence compounds. The most active compound (**1.26**, Figure 17) reduced human nasal cell colonisation and arthritis in mouse models below the minimum inhibitory concentration (MIC) without displaying any obvious toxicity. It also appeared to act as a negative allosteric modulator unlike previously discovered inhibitors. However, with an *agr* IC_{50} of 3 μM and MIC of 25 μM, there is only a small therapeutic window between acting as an anti-virulence compound or a traditional antibiotic.[223]

Very recently, Desouky *et al.* used culture extract from actinomyecetes to screen for compounds with activity against the *E. faecalis fsr* system or the *S. aureus agr* system.[224] Three compounds, which are previously known for either

tachykinin or endothelin inhibition, were discovered to possess anti-virulence activity in both *E. faecalis* and *S. aureus* (see Figure 18). Furthermore, one of the compounds also seems to be an inhibitor of the *Clostridium perfringens* virulence system, VisSR. One of these compounds was assessed *in vitro* using a human corneal cell assay, *S. aureus* showed a significantly reduced toxicity in this *ex vivo* assay. These new compounds raise the exciting prospect of a possible cross-species virulence inhibitor, not just a simple cross-group inhibitor of *agr* mediated virulence within *S. aureus*. However, at this stage, the compounds have low potency (Table 5) and require considerable research and optimisation before they will be able to reach their full potential.

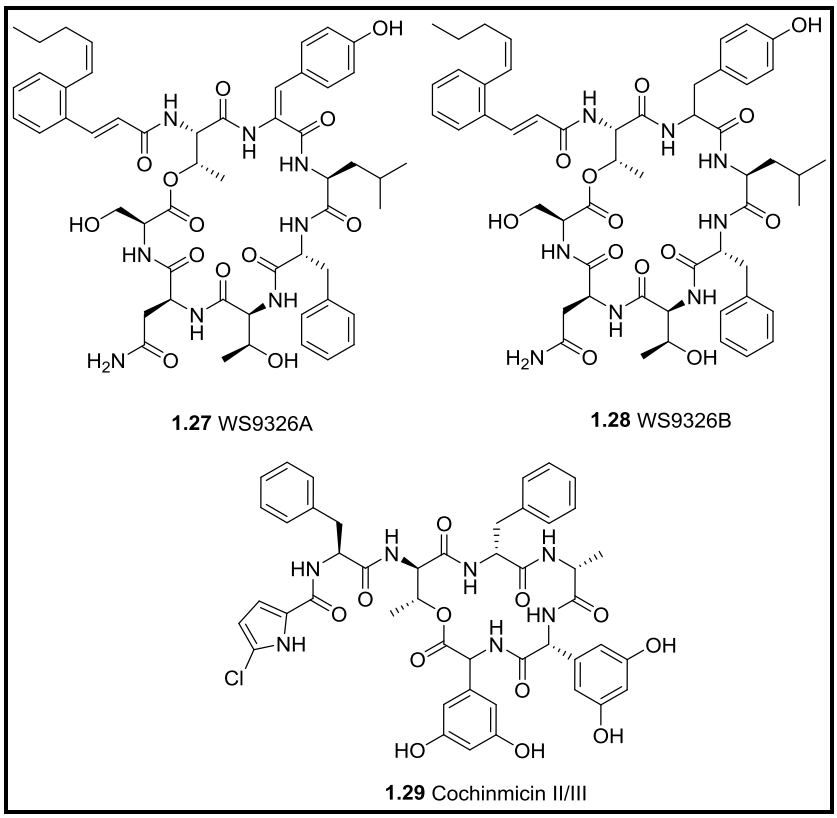


Figure 18: Compounds discovered by Desouky *et al.* which inhibit *E. faecalis*, *C. perfringens*, and *S. aureus*.[224]

Table 5: Inhibitory properties of WS9326A, WS9326B, and Cochinmicin II/III. All values in μM.

	agr	*fsr*	VirSR
WS9326A	2.7	19	0.88
WS9326B	2.1	23	<10
Cochinmicin II/III	0.2	Not tested	Not tested

Furthermore, these compounds have not yet been fully evaluated and a total synthesis of each compound will need to be developed before their potential can be fully assessed.

1.6.5 Aureusimines

In 2010, Wyatt *et al.* discovered two new nonribosomal peptide secondary metabolites (known as aureusimine A, **1.30**, and B, **1.31**) secreted at high concentrations into the extracellular fluid by *S. aureus*.[225] Upon investigation, they discovered that these small molecules do not act as antibiotics but instead regulate the virulence of *S. aureus* and that they are actually necessary for the bacteria to establish infections. Mouse models showed that *S. aureus* strains which could not biosynthesise the aureusimines displayed attenuated virulence and were easily cleared from major organ systems.[225] The team proposed that by investigating the mechanism of virulence control exerted by the aureusimines, it may be possible to design improved anti-virulence compounds.[225] These new compounds and the current state of research are extensively discussed in chapter 2.

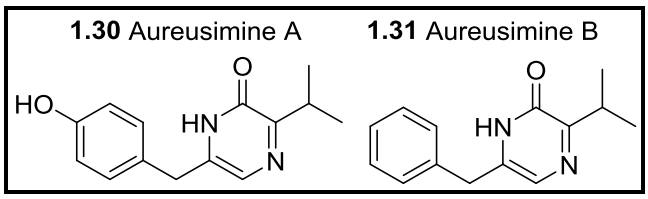


Figure 19: Chemical structure of the aureusimines

1.7 Aims and objectives

The aim of this research is to design and synthesise compounds which could be used as a successful anti-virulence therapy against *S. aureus*. In pursuit of this aim, three main areas were chosen to be explored:

1. Research into establishing a reliable and facile synthesis of the aureusimines and then investigating the function of these compounds in the virulence of *S. aureus*.
2. Pharmacological evaluation of a series of AIP-based inhibitors to develop and build upon previous structure activity relationship studies.
3. Synthesis and pharmacological evaluation of the natural product solonamides followed by an analysis of their structure activity relationship in the hope of producing more potent compounds

The techniques and strategies which will be used to explore these areas are now briefly detailed in the relevant sections below.

1.7.1 Aureusimines

Firstly, to investigate the function of the aureusimines, a facile, robust, and selective synthesis is required. To develop more complex assays and experiments which use modern chemical biology methods requires a sensitive and selective procedure for the production of various aureusimine analogues.

The current synthesis detailed in the literature was reported to have a good yield.[226] However, it utilises a diisobutylaluminium hydride (DIBAL-H) reduction of a dipeptide ester (**1.32**) to produce a dipeptide aldehyde intermediate (**1.33**) (see Figure 20). This DIBAL-H reagent is likely to be unsuitable for several reasons. On aqueous work up, several potential problems are often reported. When quenching the reaction, the tetrahedral intermediate theoretically reacts to form the desired aldehyde.[227] However, the tetrahedral intermediate is unstable at high temperatures and decomposes to an alcohol side product. As this reaction is exothermic, maintaining the low temperature

required can be quite challenging. Some procedures have been reported to avoid these problems,[228, 229] however partial reduction and over reduction still occur often though this could be due to solvent selection.[227] Furthermore, precipitating aluminium salts can cause stable emulsions during aqueous work up. Though again some protocols have been reported to avoid this problem.[229] As this reaction has been reported, the procedure will be attempted during the course of this research (this is discussed in Section 2.3). However, it is likely that a replacement reaction will be required to establish a more robust synthesis for production of aureusimine analogues.

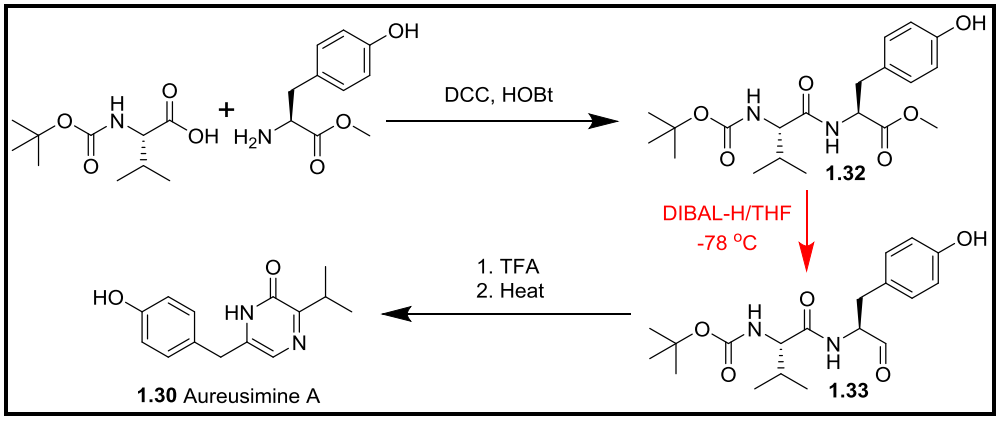


Figure 20: Scheme showing the reported literature synthesis of aureusimine A.[225] The step which is expected to be problematic is highlighted in red.

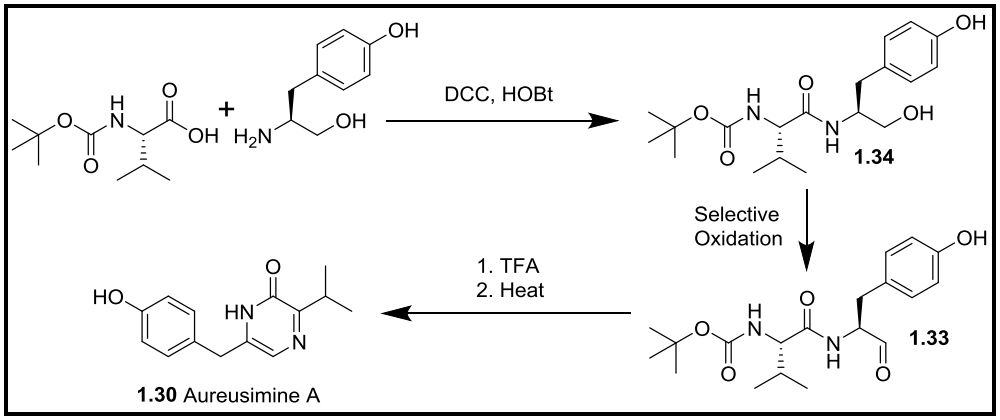


Figure 21: The proposed synthesis of aureusimine A (**1.30**)

An alternative synthetic strategy will be developed which replaces the ester reduction step with the oxidation of an alcohol (Figure 21). There are many mild and selective reactions designed to oxidise an alcohol to an aldehyde without over oxidation. These reactions will be assessed and attempted should the DIBAL-H reduction fail to reliably produce the desired product. Preliminary

analysis suggests that the Swern reaction or an oxidation using IBX may be the most promising routes for this functional group interconversion (this is discussed in Section 2.4.1).

As a selective and sensitive synthetic method is required, it may be necessary to protect the free phenol functionality of the tyrosinol to synthesise aureusimine analogues. Should this become necessary, previous work in our lab produced a sensitive and reliable synthesis of amino alcohols from their parent amino acids, this procedure would be employed to produce the required protected tyrosinol (see Figure 22).

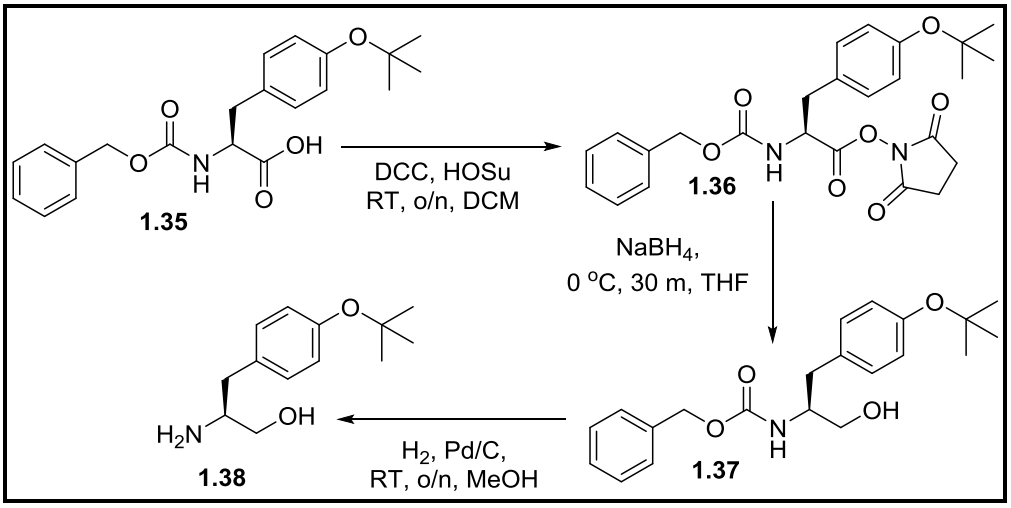


Figure 22: A proposed synthetic strategy for the production of protected tyrosinol analogues adapted from Detzer *et al.*[230]

Initially, the natural aureusimine molecules will be synthesised. As the aureusimines were reported as virulence regulators,[225] it is likely that they interact with the *agr* system in some way. Therefore, using previously developed bioreporter assays,[231] their activity in the *agr* quorum sensing system will be assessed. The results of this experiment will then inform further investigations.

Once a robust selective synthesis has been established, analogues of the aureusimines will be produced in order to perform affinity chromatography experiments and to establish the biomolecular target of these small molecules. Initial assessment suggests that two sites are promising for the addition of long

molecular tethers to attach the aureusimines to a polymer support in preparation for this experiment (see Figure 23).

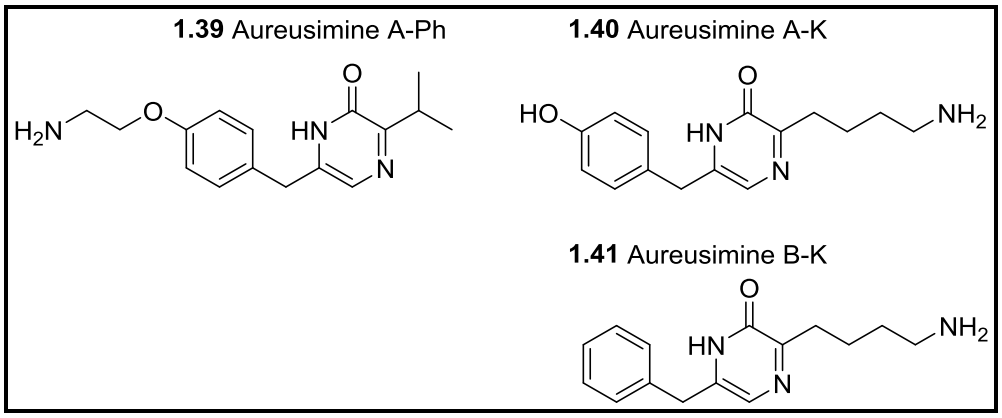


Figure 23: Aureusimine analogues with additional tether regions for affinity chromatography experiments

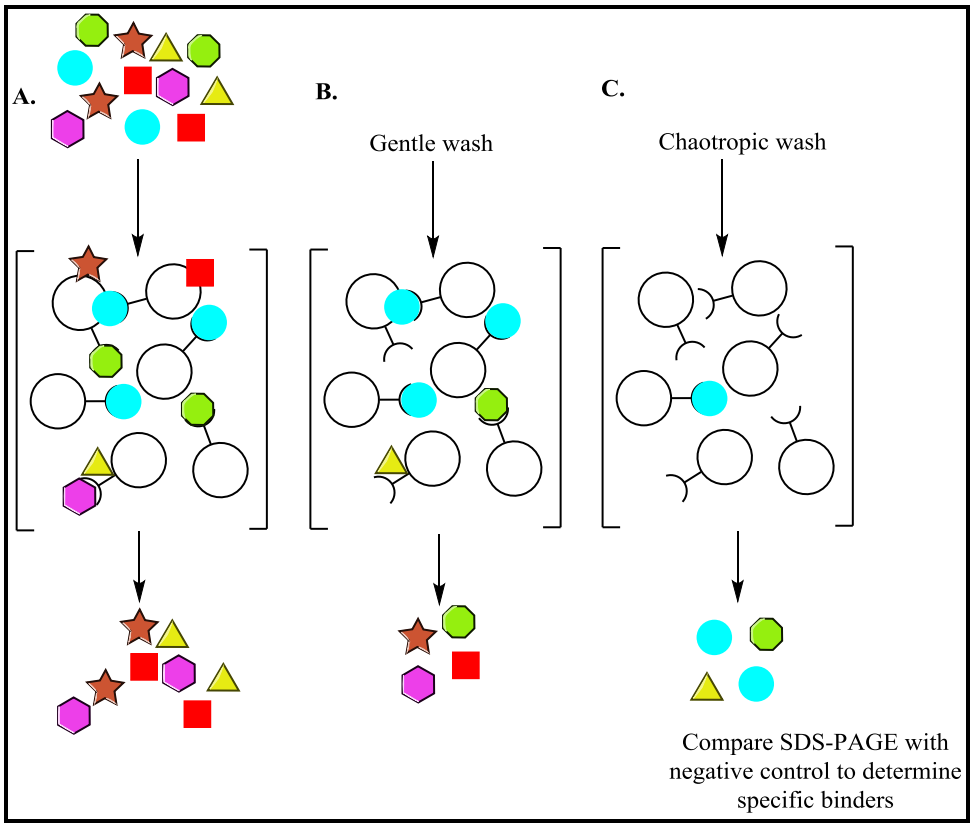


Figure 24: Schematic representing affinity chromatography. **A.** Resin is suspended in complex mixture. The mixture is then poured off and the resin washed with saline. **B.** The resin is then gently washed with either high salt or non-neutral pH wash to remove non-specific binders. **C.** A chaotropic salt is used to remove all proteins and the resulting wash is concentrated and run on an SDS-PAGE gel. Comparisons with control allow the identification of specific binders.

Affinity chromatography is a technique used to identify targets which specifically bind to a given compound (Figure 24).[232] Initially, the ligand-

tethered resin is mixed with cell culture lysate. At this point many specific and non-specific binders will adhere to the resin and the tethered aureusimine analogues. The cell lysate is then removed and mild washes remove most of the non-specific binding proteins. Finally, a chaotropic or particularly harsh wash is used to remove the remaining non-specific binders and any specific binders. An SDS-PAGE gel of this mixture is then compared with a control resin. Any bands which are unique to the aureusimine resins are likely to represent proteins which specifically bind to these compounds.[233]

1.7.2 AIP-based analogues

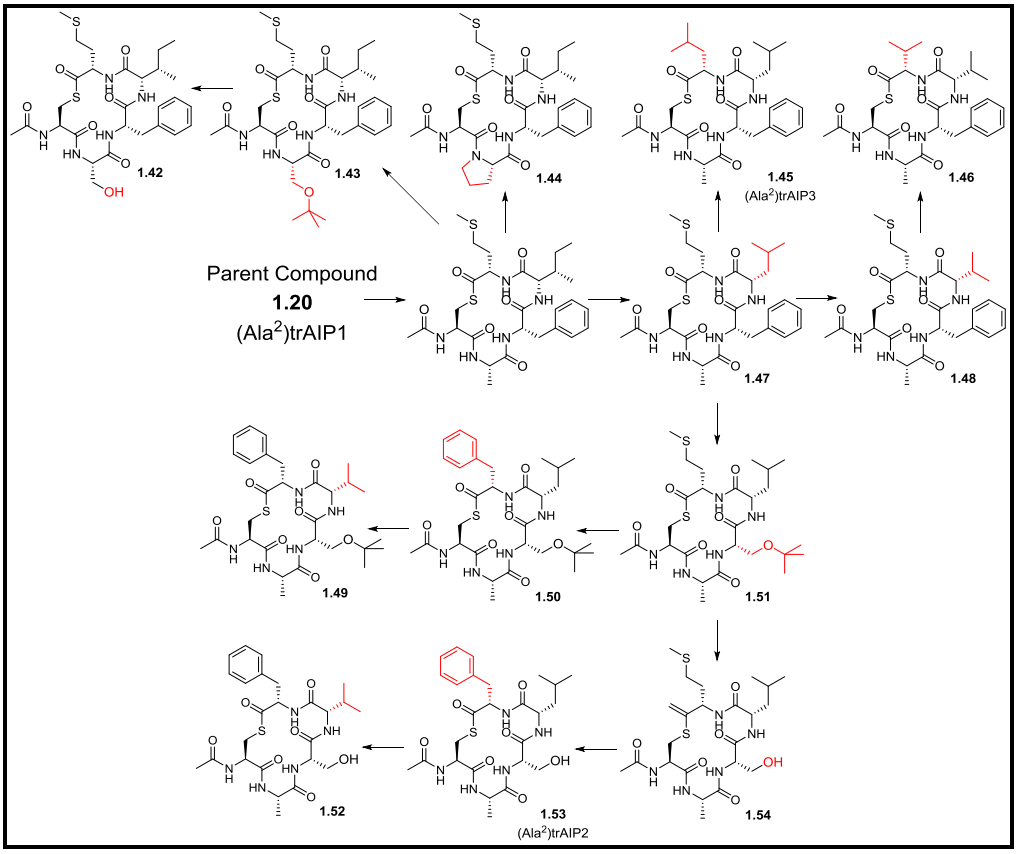


Figure 25: A compound tree showing the first series of AIP-based analogues and their relationship to (Ala[2])trAIP1 (**1.20**). Each structural change from the previous compound in the tree is highlighted in red.

A series of AIP analogues were previously synthesised by Dr. F. Rui and Dr. C. Gordon. Each of the endogenous ligands, AIP1 (**1.14**), AIP2 (**1.15**), and AIP3 (**1.16**), are known to be potent cross group inhibitors[162] and removing the tail region of these ligands is known to produce weak self inhibitors while maintaining potent cross group inhibition.[213] Furthermore, mutation of the aspartate residue in truncated AIP1 is known to produce a potent pan-group

inhibitor.[157] Therefore, a series of analogues based on this known potent pan-group inhibitor (Ala[2])trAIP1 (**1.20**) was produced. Individual amino acid residues were replaced with physicochemically related residues, e.g. leucine with isoleucine, as well as distinctly different amino acid residues, e.g. alanine was replaced with serine and proline. All of the analogues in this series were synthesised without a tail region in an effort to produce potent pan-group inhibitors (see Figure 25).

A further series of peptoid analogues (Figure 25) were synthesised to fully assess the importance of the orientation of the amide bonds and the steric position of the amino acid side groups. Therefore, it will be interesting to know which peptide modifications are tolerated by the receptor.

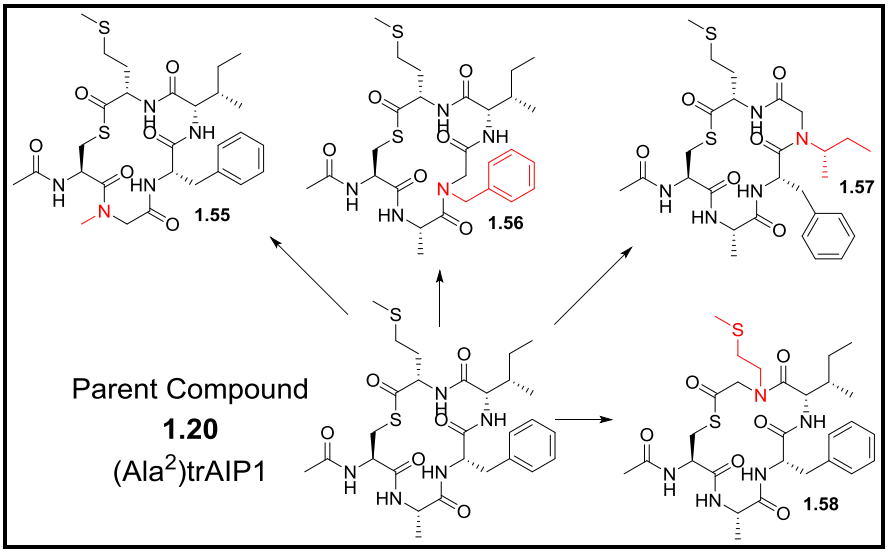


Figure 26: A compound tree showing the series of peptoid compounds. Each structural change from the previous compound in the tree is highlighted in red.

All of these analogues will be fully assessed and evaluated pharmacologically against AgrC1 using a previously reported *P3::lux* based bioreporter assay.[231] The most promising and interesting compounds will then be assessed using AgrC2, AgrC3 and AgrC4 bioreporters. The results of these assays will be used to inform the synthesis of a second generation of AIP analogues in an attempt to provide both deeper understanding of the complex structure activity relationship of these macrocyles and to produce a more potent and "drug-like" pan group inhibitor.

Previous work in this group created a new a*gr* group by forced evolution.[167, 231] This group is activated by the known cross group AgrC inhibitor (Ala^5)AIP1 (**1.59**, Figure 27). As only two mutations were required to create this new *agr* group, it is possible that the bacteria could evolve in this manner. Therefore, each of the promising compounds will also be tested in the above *agr* group bioreporter.

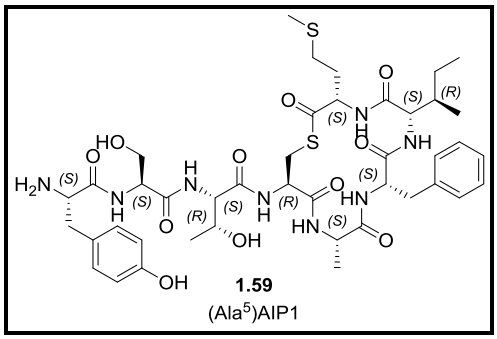


Figure 27: Structure of the known cross group inhibitor, (Ala^5)AIP1 (**1.59**).

Finally, the binding mode and interactions of these compounds will be assessed using constitutively active receptors. This will determine if any of the inhibitors act as neutral antagonists or inverse agonists. Competition assays will also be performed to confirm the compounds competitive inhibition mechanism.

1.7.3 Solonamides

When this research began, there was no published synthesis of the solonamide compounds. Preliminary assays showed that the molecules reduced *hla* and *rnaIII* expression while concurrently increasing *spa* expression.[214] This strongly indicated that they could be *agr* system inhibitors. It was tentatively suggested by the original researchers that they act as AgrC inhibitors based on their structural similarity. Therefore, this research initially set out to establish a synthesis and unambiguously prove that the solonamides inhibit the AgrC receptor.

Initial retrosynthetic analysis of solonamide A (**1.21**) revealed an important 3-(*R*)-hydroxyhexanoic acid (**1.60**) constituent which was not commercially available (Figure 28). All of the other building blocks were amino acids which could be purchased with a variety of protecting groups suitable for various

synthetic strategies. Given that a racemic mixture of 3-hydroxyhexanoic acid (**1.60**) was available, an initial synthesis of the solonamides would be piloted using this commercial mixture. This would allow confirmation of the action of the solonamides and optimisation of the synthesis before further research to develop a fully stereoselective total synthesis of both of the solonamide natural products.

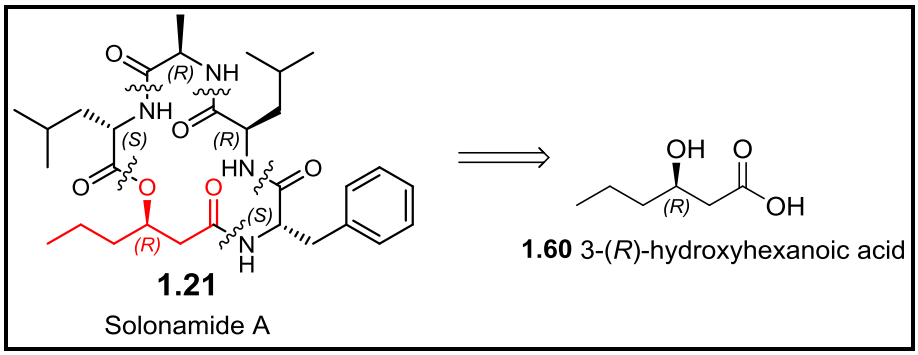


Figure 28: Retrosynthetic analysis of solonamide A (**1.21**) reveals a key 3-(*R*)-hydroxyhexanoic acid moiety.

When designing the synthesis of a macrocycle, a key step is deciding where the macrocyclisation reaction will occur. Macrocyclisation at the lactone position would eventually allow the easy incorporation of multiple 3-hydroxy acid residues to investigate the role of this unusual moiety. The Steglich esterification has been used many times to produce macrocyclic lactones and offered a promising strategy for cyclisation of the solonamides at the desired position.[234] Therefore, the initially adopted synthetic strategy was to use solid phase peptide synthesis techniques producing the four residue linear peptide on a 2-chlorotrityl resin (**1.61**). This would be followed by an optimised peptide coupling of the 3-hydroxyhexanoic acid (**1.60**) intended to avoid polymerisation *via* the nucleophilic hydroxy group while producing the final linear peptide chain on the resin (**1.62**). Resin cleavage with TFA in DCM would then furnish the linear peptide (**1.63**) which would be cyclised using the Steglich esterification to produce the desired product, Solonamide A (**1.21**, see Figure 29), and a related epimer, epiSolonamide A (epiSolA, **1.65**).

However, as the macrocyclisation stage is often the most problematic, it was predicted that a change in the site of cyclisation may be required. Assessment of the two cyclic depsipeptide natural products and our initial synthetic strategy

revealed that the most sensible site for an alternative cyclisation strategy was between *D*Ala[4] and Leu[5]. Using this position would only necessitate special coupling conditions for one amino acid residue (Leu[5]) before resin cleavage and cyclisation of the linear peptide chain thus making it an optimal alternative cyclisation site should problems with the Steglich macrolactonisation arise.

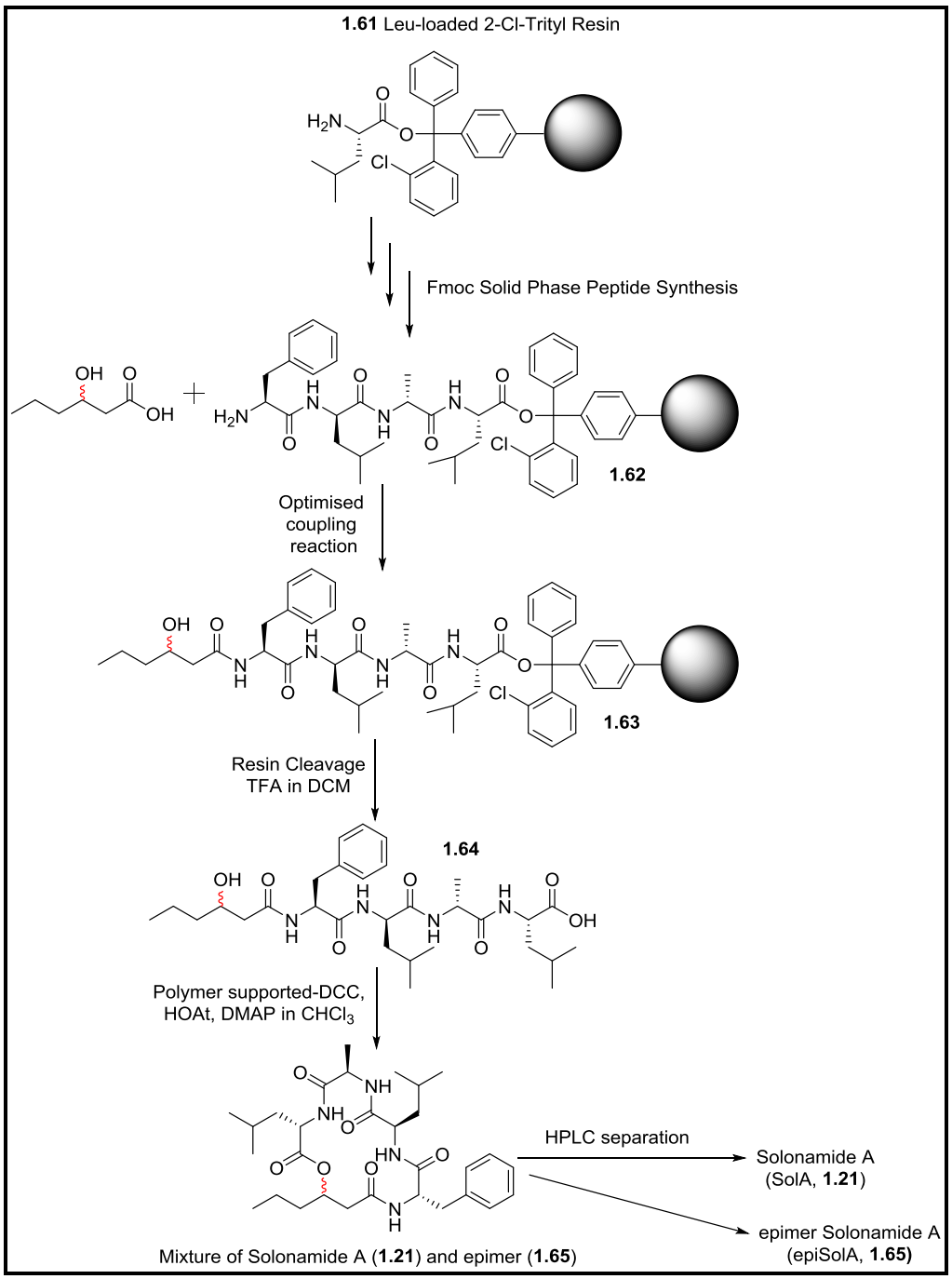


Figure 29: Initial synthetic strategy for the pilot synthesis of solonamide A (**1.21**)

Once an initial synthesis has been developed and the activity of the solonamides has been confirmed in a *P3::lux* bioreporter assay, development of

a stereoselective synthesis of the 3-(*R*)-hydroxyhexanoic acid (**1.60**) and consequently SolA (**1.21**) will begin. Previous research suggested that stereoselective production of chiral 4-substituted oxetan-2-ones was possible using a ketene-aldehyde cycloaddition (Figure 30).[235] These moieties would easily undergo hydrolysis forming the required 3-(*R*)-hydroxy acid compounds.

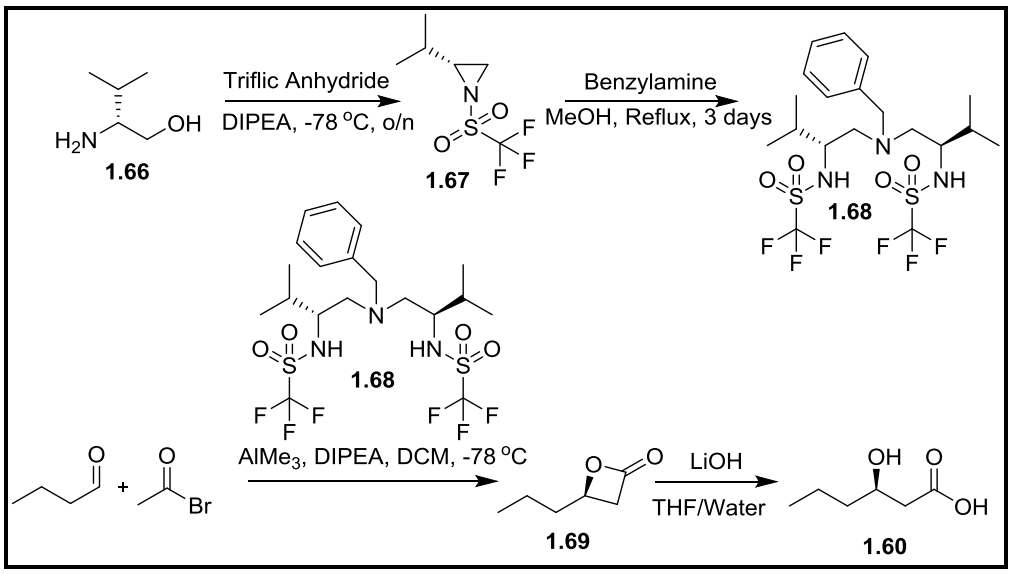


Figure 30: Proposed synthesis of 3-(*R*)-hydroxyhexanoic acid (**1.60**) adapted from Nelson *et al.*[235]

Once synthetic 3-hydroxy acids are in hand, they will be deployed in the total synthesis of SolA (**1.21**) that was initially developed in this research. By completing a stereoselective synthesis, the configuration of the solonamides would be unambiguously confirmed by matching the NMR data of the natural product with the synthetic compound.

Full assessment of the mode of action would follow. It is expected that the solonamides inhibit the AgrC receptor.[214] If this proves to be the case, then a full pharmacological assessment of their mode of binding will be performed in the AgrC1 bioreporter. The solonamides will then be assessed in the three most clinically relevant *agr* groups (*agr-I*, *agr-II*, and *agr-III*).[156]

Once the solonamides have been fully assessed pharmacologically, the structure activity relationship (SAR) of these compounds will be examined against AgrC1. Initially, an alanine scan will highlight important residues and guide further studies (Figure 31). A significant residue will be selected for

alteration, alongside variation of the 3-(*R*)-hydroxy acid moiety. IC_{50} data gained from all these compounds will then be used to generate a further generation of solonamide analogues in an effort to improve the potency and physical characteristics of the compound.

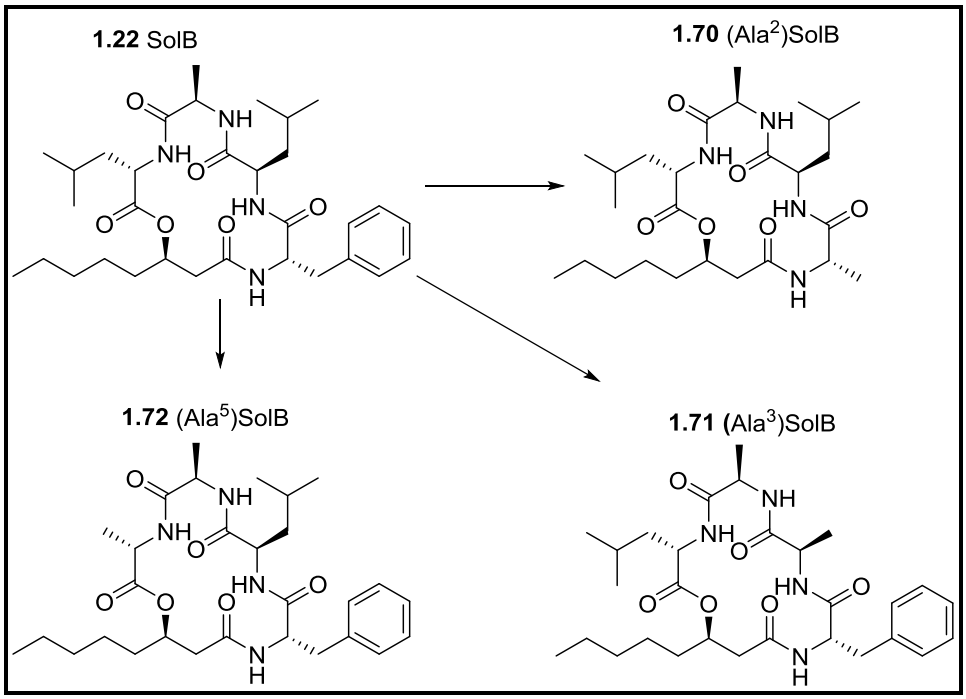


Figure 31: A compound tree of an alanine scan of SolB (**1.22**)

2 Aureusimines

This chapter details investigations into the new putative *S. aureus* virulence master regulators known as the aureusimines.

Initially, the current state of knowledge in regard to the aureusimines including their biosynthesis, function and genetics is outlined. The synthesis previously used for investigating the aureusimines is also detailed. This literature method uses a DIBAL-H reduction of an ester (**1.32**) to the required dipeptide aldehyde (**1.33**) before cyclisation to the required product, aureusimine A (**1.30**). Attempts to apply the reported procedure are reported along with the reasons for its failure. Consequently, attempts to synthesise the aureusimine A (**1.30**) by oxidising a dipeptide alcohol (**1.34**) are discussed. Various oxidations were attempted to produce the required dipeptide aldehyde intermediate(**1.33**). The difficulties which were found to be insuperable are reported and, finally, a successful synthesis of the aureusimine products is discussed using a protected dipeptide alcohol (**1.38**) followed by an oxidation to the vital protected dipeptide aldehyde intermediate, which is then successfully cyclised to yield the required products.

Experiments analysing the effects of the aureusimines on *agr* regulated virulence are outlined. Then an outline of further biological investigations into the function of these non-ribosomal peptide secondary metabolites is offered. Initially, the results of affinity chromatography experiments are reported and

discussed. Subsequent biological assays are then reported including the aureusimines effects on bacterial swarming, persistence, biofilm production and CCL-2 mediated chemotaxis.

2.1 Introduction

The non-ribosomal peptides represent a large number of bacterial secondary metabolites. These compounds are produced by non-ribosomal peptide synthetase (NRPS) systems which primarily utilise a variety of amino acids as building blocks. The amino acids are chemically bonded together and then altered by the NRPS to afford the final product. Soil-dwelling bacteria are known to deploy them for intercellular communication and as chemical weapons.[236] In fact, many of the naturally occuring antibiotics are the most well known of the non-ribosomal peptides. For example, penicillin (**1.1**) is produced from cysteine, valine, and α-aminoadipic acid by an NRPS enzyme (see Figure 32).[237]

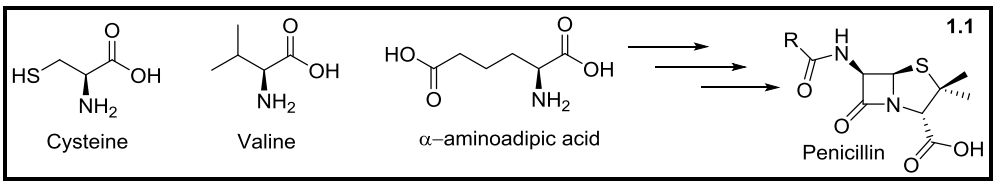


Figure 32: Building blocks and general structure of the penicillins.

NRPS systems use various domains to process each amino acid or to add further amino acids to the growing peptide chain (Figure 33). Many of the common domains have been well characterised. For example, adenylation (A) domains use adenosine monophosphate esters of various amino acids, and deliver them to thiolation (T) domains.[238] T domains have previously undergone post-translational modification adding a phosphopantetheine moiety, in order to tether the amino acid transferred from the A domain to the enzyme. Condensation (C) domains can then mediate reactions on the T domain-tethered amino acid, adding a further amino acid and producing a growing peptide chain. Reductase (Re) domains at the C terminus of the NRPS can release the peptide chain as a peptide aldehyde or alcohol that often undergoes intramolecular cyclisation (spontaneously) upon release. Alternatively, thioesterase domains at the C-terminus of the NRPS can release the non-ribosomal peptide as a cyclic thiolactone.

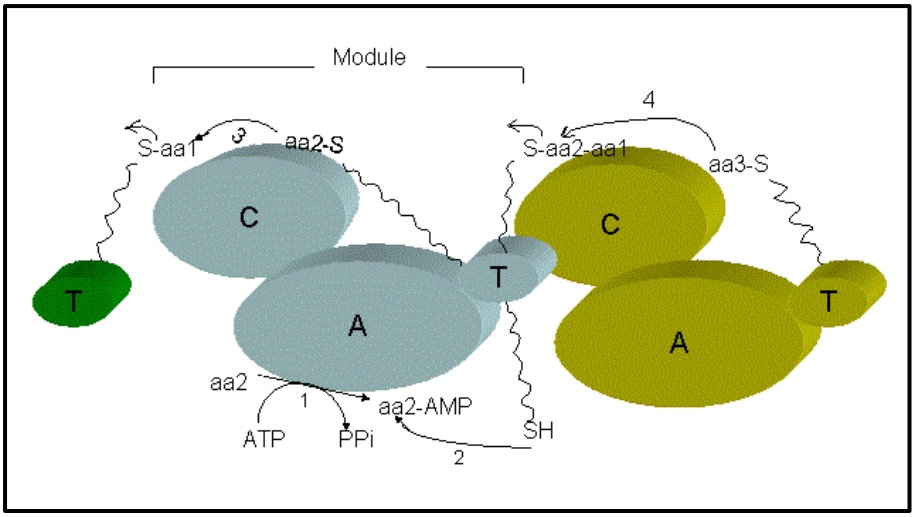


Figure 33: Schematic of a NRPS system. **1.** Amino acid adenylation by A domain leading to **2.** thioester formation which loads the amino acid onto the phosphopantethiene of the second thiolation domain. **3.** amide bond formation by upstream condensation domain which moves the first amino acid from the first thiolation domain forming a dipeptide on the second thiolation domain. **4.** amide bond formation by downstream condensation domain (the second thiolation domain releases the tripeptide to the third thiolation domain which in turn passes the growing peptide upstream).

Genomic sequencing of bacterial species has allowed researchers to rationally search for NRPS gene clusters. This is possible because NRPS systems are generally consistent and predictable, several common domains have been fully characterised with complete structural assignments. Moreover, the rules governing assembly of the non ribosomal peptide on the NRPS enzyme seemed to be conserved across most NRPS systems. Genome scanning for NRPS gene clusters and the subsequent prediction of the non-ribosomal peptide compounds produced by the cluster has become known as secondary metabolite genome mining.[239]

Using the genome mining approach, Wyatt *et al.* analysed over 50 different *S. aureus* strains to identify a highly conserved (97% identical and 97% similar) NRPS gene cluster now known as *ausA* (Figure 34A).[225] This NRPS cluster is quite large, accounting for approximately 0.25% of the staphylococcal genome. Orthologs are also present in other pathogenic staphylococcal strains but are absent from non-pathogenic *Staphylococcus* species and other gram-positive organisms. The NRPS enzyme, AusA, contains 2389 amino acids and is split into two modules each containing a single A domain for valine and tyrosine respectively. The C terminus contains a Re domain and releases the dipeptide as

an aldehyde. It was thought that nucleophilic attack of the free amine was likely to produce a cyclic imine (Figure 34B). HPLC analysis of organic extracts of *S. aureus* culture broths followed by mass spectrometric analysis revealed two related compounds differing by 16 mass units in a 3:1 ratio. Both one-dimensional and two-dimensional NMR experiments revealed the structures of both of the metabolites. The most abundant metabolite was a valine-tyrosine dipeptide with a pyrazinone core which is now called aureusimine A. The second metabolite, aureusimine B, was consistent with a similar valine-phenylalanine dipeptide with a pyrazinone core (Figure 34C).

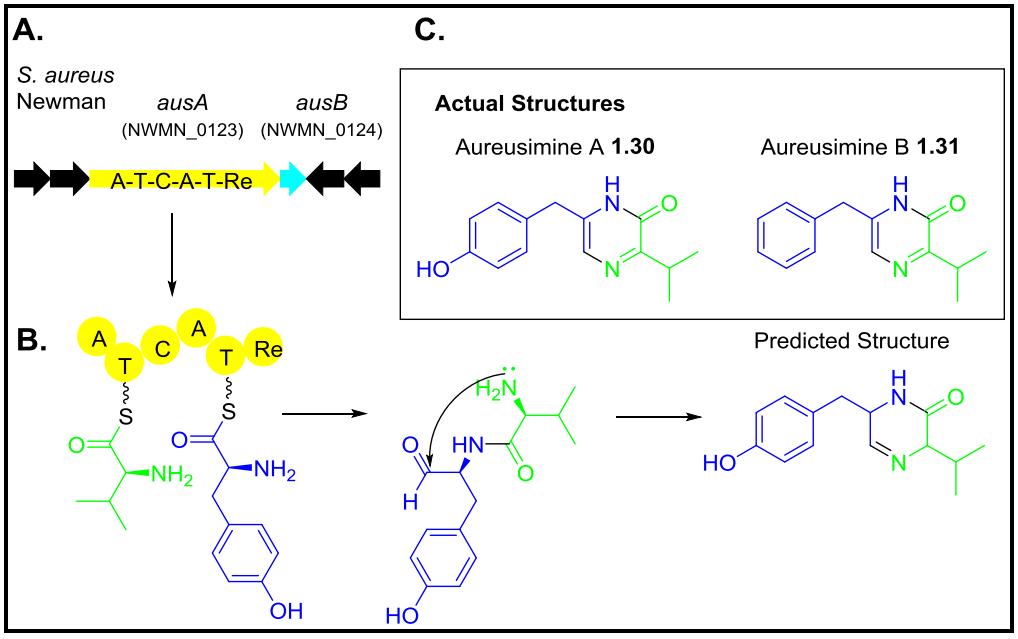


Figure 34: A schematic showing: **A.** the aureusimine biosynthesis gene cluster, **B.** the biosynthesis of aureusimine A, and **C.** the structure of both aureusimine A and B.

The structure of this secondary metabolite, aureusimine B matched a previously identified secondary metabolite known as phevalin from *Steptomyces.* sp. SC433 which was examined as a potential calpain inhibitor.[240] It is common for the A domains of NRPS enzymes to slightly lack substrate specificity, occasionally incorporating more than one amino acid into a non-ribosomal peptide product. This is consistent with incorporation of either tyrosine and phenylalanine into this non-ribosomal peptide product to produce aureusimine A and B, respectively.

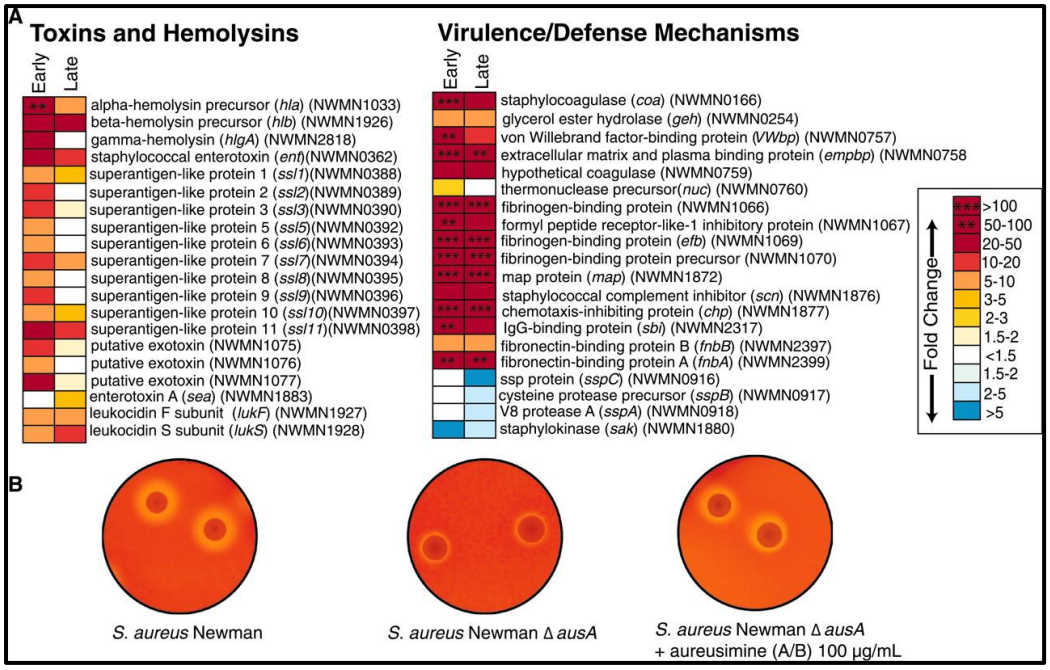


Figure 35: Diagram from Wyatt *et al.*[225] showing **A.** differential expression of various virulence genes caused by the presence of the aureusimines and **B.** reduction in hemolysis caused by the absence of the aureusimines in a isogenic *ΔausA* strain and reconstitution of the mutant's hemolysis activity caused by exogenous addition of the aureusimines.

Moreover, a mutant *ΔausA* strain which produced no aureusimine A or B confirmed that *ausA* is responsible for the synthesis of these secondary metabolites. The deletion strain actually grew better than the wild type parent strain indicating that the aureusimines are not required for growth of the bacteria. Global microarray analysis of both Newman wild type and Newman Δ*ausA* revealed that transcription of metabolic genes was largely unchanged in each strain, corroborating the findings of the previous growth studies. However, a large number of virulence associated genes were upregulated by the aureusimines. For example, chemotaxis inhibitory protein (ChIP) was upregulated by nearly 150 fold. Cultivation of the two strains on blood agar revealed that Newman Δ*ausA* lacked the ability to lyse red blood cells indicating a reduction in production of hemolysins. Exogenous addition of aureusimines A and B restored the lytic activity of the Newman Δ*ausA* strains.

Murine infection models showed that the wild type Newman strain was able to establish productive infection, indicated by a 22% loss of body weight over four days. Meanwhile, the isogenic *ΔausA* strain only reduced bodyweight by 7%. When the organs of each mouse were harvested four days post infection, a

high bacterial load was found in the mice infected with the wild type strain while those infected with the isogenic strain showed a significant reduction in every organ except the kidneys. Moreover, no bacterial colonies at all could be recovered from the hearts of mice infected with the Newman *ΔausA* strain.

The data collected by Wyatt *et al.* strongly suggests that the aureusimines are involved in virulence regulation in *S. aureus*, possibly acting *via* a quorum sensing mechanism.[225]

2.2 Published synthesis of the aureusimines

A synthetic route to the aureusimines was previously reported by Zeng *et al.* during investigations into their potential activity as calpain inhibitors.[226] Boc-protected valine and phenylalanine methyl ester were coupled using DCC and HOBt in DCM/DMF forming the dipeptide **2.1** with a very high 95% yield. The C-terminal methyl ester was then reduced to the aldehyde **2.2** using DIBAL-H in THF with a high 76% yield. Finally, the Boc-protecting group was removed using TFA and the mixture was heated to complete the cyclisation affording the final product, aureusimine B (**1.31**), with a good 65% yield (Figure 36).

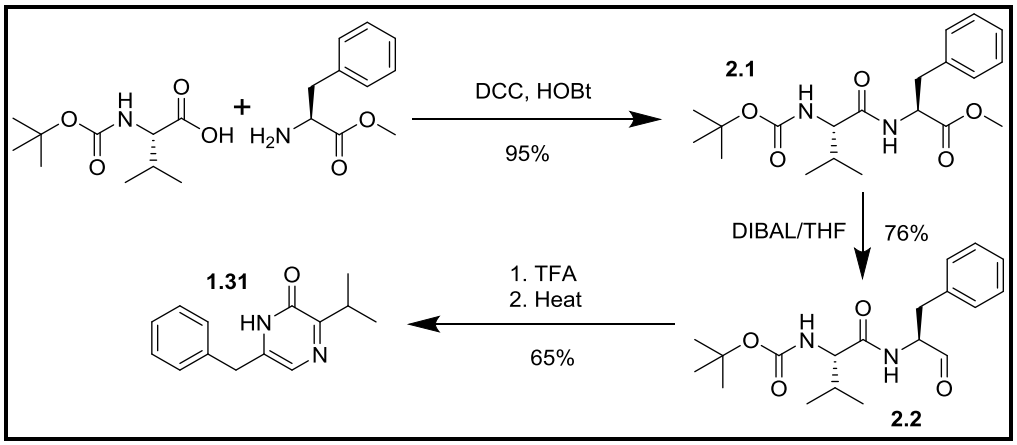


Figure 36: Synthesis of aureusimine B designed by Zeng *et al.*[226]

Thus, the above synthetic route was evaluated as an approach to obtain both aureusimine A and B, as well as analogues thereof, for future biological assays.

2.3 Attempted synthesis of aureusimine A and B

The coupling of Boc-protected valine and *DL*-tyrosine methyl ester to produce the dipeptide **1.32** proceeded without problems, in a yield similar to that reported in the literature.[226] However, the DIBAL-H mediated reduction of the dipeptide methyl ester **1.32** to the dipeptide aldehyde **1.33** was found to be inefficient (Figure 37). Full chemical transformation of the starting material was never achieved and the products were challenging to separate using column chromatography. Several synthetic attempts showed conversion of the starting material ranged from negligible to 52% with an average of 12% (as measured by analysis of NMR signals of the methyl ester and aldehyde groups at δ3.57 and 9.60 ppm, respectively). Aqueous work-up was also complicated as the aluminium salts generated by the DIBAL-H reagent formed stubborn emulsions making the work up time consuming and challenging.

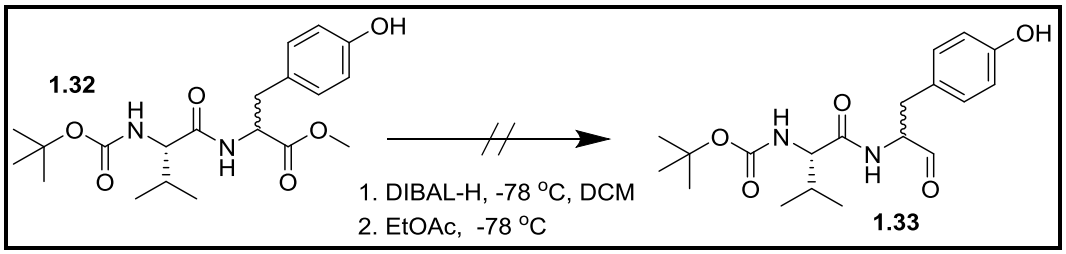


Figure 37: Unsuccessful DIBAL-H reduction of dipeptide methyl ester **1.32** to dipeptide aldehyde **1.33**

In the literature, Zeng *et al.* did not attempt to produce a phenolic version of their target compound, aureusimine A (**1.30** then known as tyrvalin).[226] Hence, it was postulated that the phenol moiety could be responsible for the disappointing results of the DIBAL-H reduction; the phenol group could be inactivating the DIBAL-H by ligand exchange. DIBAL-H is the most common reagent used for selective reduction of esters to aldehydes. Lithium aluminium hydride has been used in some cases where selectivity is less important and other sensitive groups are not present. However, $LiAlH_4$ is a much stronger reducing agent and it is prone to causing side reactions with sensitive functional groups. This reagent also functions *via* a similar mechanism to DIBAL-H and could therefore fail in a similar manner. To avoid this complication, an

alternative approach was investigated, in which a dipeptide alcohol would be oxidised to afford the desired aldehyde.

2.4 Adapted oxidative approach for synthesis of aureusimine A and B

There are many reliable and widely reported reactions available for the oxidation of alcohols to aldehydes which could be exploited.

2.4.1 Alcohol to Aldehyde oxidations

The most commonly used oxidations broadly fall into a few significant categories.

2.4.1.1 Chromium based reagents

Chromium based reagents, such as Jones (**2.3**),[241] Collins (**2.4**),[242] Cornforth (**2.5**),[243] and Corey (**2.6**)[244] reagents, were widely used before the 1990s (Figure 38). However, more recently the toxic nature of the waste products and the discovery of easier, more reliable and ecologically friendly alternatives has led to these reactions falling out of favour. Manganese dioxide has been used and functions similarly to chromium based reagents, however, it also suffers from similar problems with toxic waste products.[245]

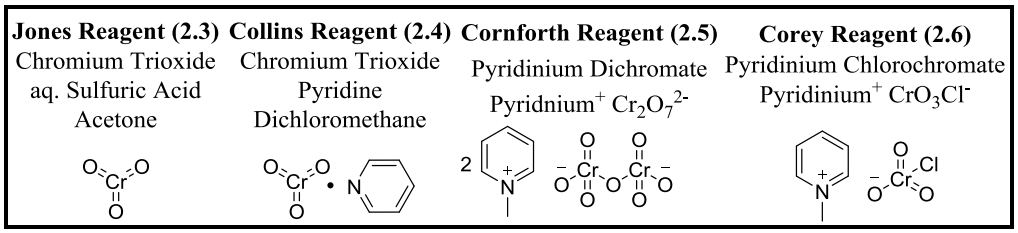


Figure 38: Diagram of the chromium based oxidation reagents

2.4.1.2 Oxoammonium-catalysed oxidations

Oxoammonium-catalysed oxidations use TEMPO (**2.7**) in catalytic amounts with additional sodium hypochlorite or another secondary oxidising agent. The TEMPO is oxidised to the active oxoammonium salt (**2.8**) and then it oxidises the alcohol (**1.34**) to the required aldehyde product (**1.33**). The sodium hypochlorite re-oxidises the spent TEMPO reagent (**2.9**) *in situ* allowing the redox reaction to continue to produce additional aldehyde product (Figure 39). TEMPO side products are also known to inhibit the over-oxidation of aldehydes to carboxylic acid by atmospheric oxygen allowing this reaction to be performed open to the atmosphere.[246] Unfortunately, these reagents can oxidise

phenols generating free radicals and undesirable side products (**2.10**) making them incompatible with our synthetic strategy (Figure 40[247]).

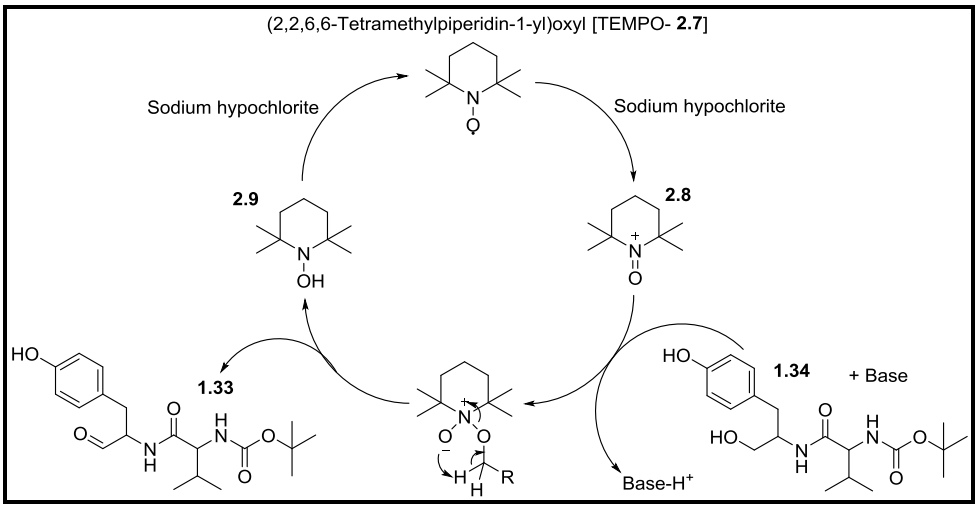


Figure 39: Diagrammatic representation of the TEMPO (**2.7**) mediated oxidation of dipeptide alcohol **1.34** to dipeptide aldehyde **1.33**.

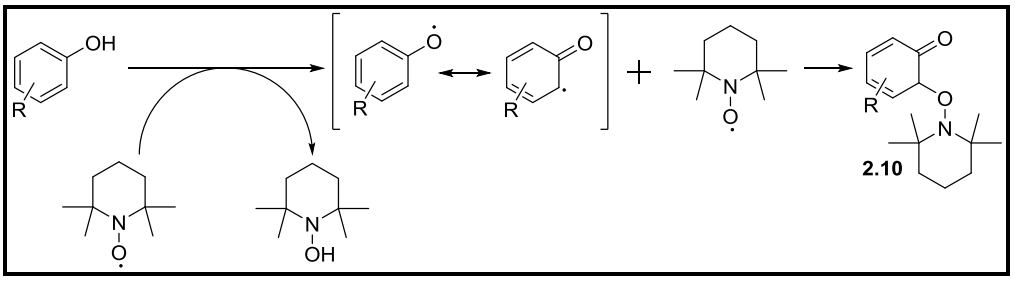


Figure 40: The formation of undesired side products when using TEMPO-mediated oxidations with free phenols

2.4.1.3 Ley oxidation

The Ley oxidation uses catalytic amounts of TPAP (**2.11**) or TBAP with excess *N*-methylmorpholine *N*-oxide (**2.12**). The TPAP (**2.11**) oxidises the alcohol to an aldehyde before the *N*-methylmorpholine *N*-oxide (**2.12**) reoxidises the spent TPAP allowing the redox reaction to continue to produce additional aldehyde. The presence of water in this reaction can poison the catalyst slowing the reaction considerably and can also lead to the over-oxidation of the aldehyde products to carboxylic acids.[248] As *N*-methylmorpholine *N*-oxide is often added as a hydrate, this can be problematic. Molecular sieves are often added to overcome this problem. TPAP uses a rare earth metal, ruthenium, which makes it expensive so it is generally only used for challenging alcohols especially those which are very sterically hindered.

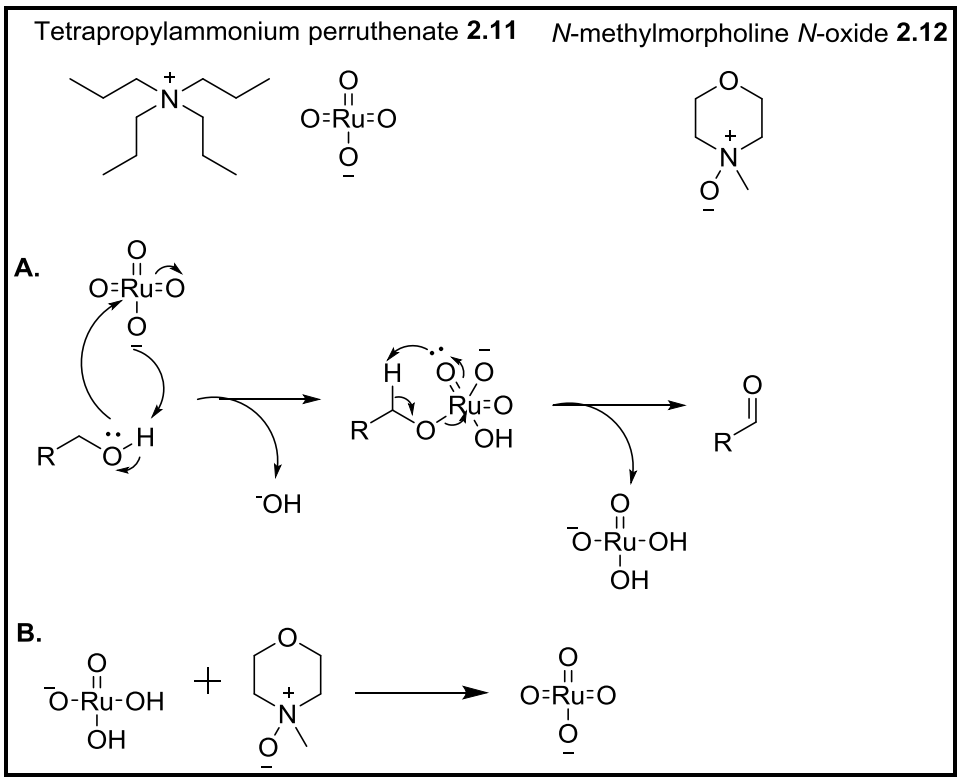


Figure 41: Ley oxidation of a primary alcohol to an aldehyde showing **A.** the perruthenate catalyst **2.11** oxidising a primary alcohol to an aldehyde and **B.** *N*-methylmorpholine *N*-oxide (**2.12**) regeneration of the catalyst.

2.4.1.4 Activated DMSO

The activated DMSO oxidative strategies use various compounds such as oxalyl chloride (**2.13**) to convert DMSO to an active sulfonium species (for example, **2.14**) *in situ* (see Figure 42). Reaction with an alcohol then leads to the production of an alkoxydimethylsulfonium salt (**2.15**). A base removes a methyl proton forming a sulfur ylide (**2.16**) which consequently decomposes *via* an intramolecular elimination producing both dimethyl sulfide (with a particularly nauseating odour) and the desired aldehyde product (**1.33**). Activated DMSO strategies have been successfully employed previously in the presence of a phenol moiety where other oxidants (including MnO_2, TPAP, Dess-Martin periodane, and Collins reagent) produced complex mixtures.[249] Thus, this is a promising strategy for initial pilot experiments aiming to produce the desired dipeptide aldehyde **1.33**. Both the reaction protocol and work-up are straightforward, the only challenges are the requirement that the reaction is executed under an anhydrous, inert atmosphere and at low temperature. Furthermore, there are many techniques which can be used to generate the

active sulfonium species, so if one method proves to be incompatible, other methods can easily be attempted.

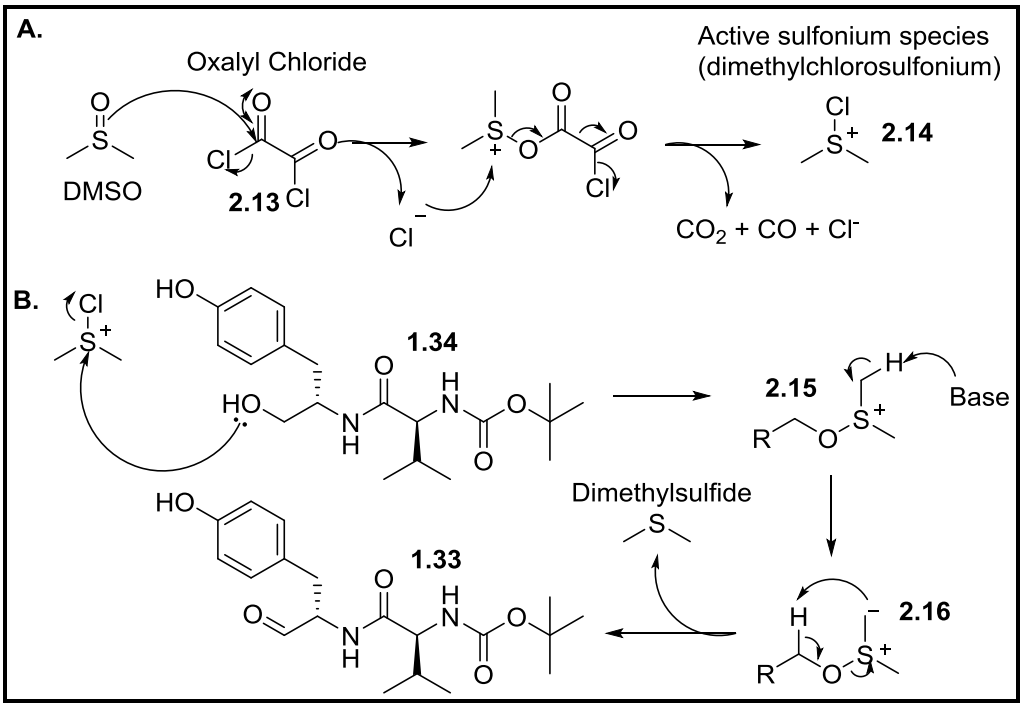


Figure 42: **A.** A mechanism for the production of an active sulfonium species (**2.14**) using oxalyl chloride (**2.13**) and **B.** the mechanism for the oxidation of dipeptide alcohol **1.34** to dipeptide aldehyde **1.33** using the active sulfonium species **2.14**.

2.4.1.5 Hypervalent iodine

Finally, there are hypervalent iodine reagents, such as Dess-Martin periodane (**2.17**) and IBX (**2.18**) to mediate oxidation reactions.

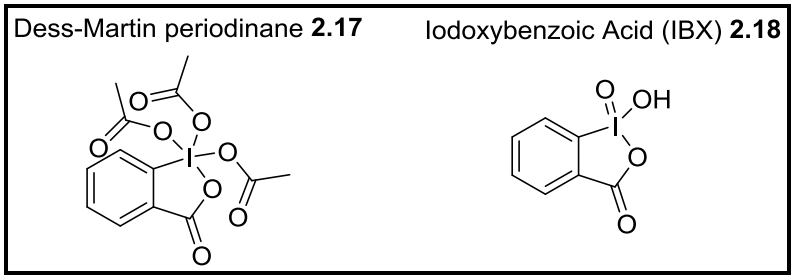


Figure 43: Structure of Dess-Martin periodinane (**2.17**) and IBX (**2.18**)

Dess-Martin periodinane (**2.17**) effectively oxidises alcohols at room temperature, producing acetic acid as the byproduct (Figure 44). The periodinane byproduct (**2.19**) can be removed by treating with sodium thiosulfate forming 2-iodobenzoic acid (**2.20**) or by hydrolysis with NaOH to *o*-iodosobenzoic acid (**2.21**), both of which can then be removed by an aqueous

wash with sodium bicarbonate (see Figure 45). If necessary, these byproducts can be recycled to produce further Dess-Martin periodinane (**2.17**).

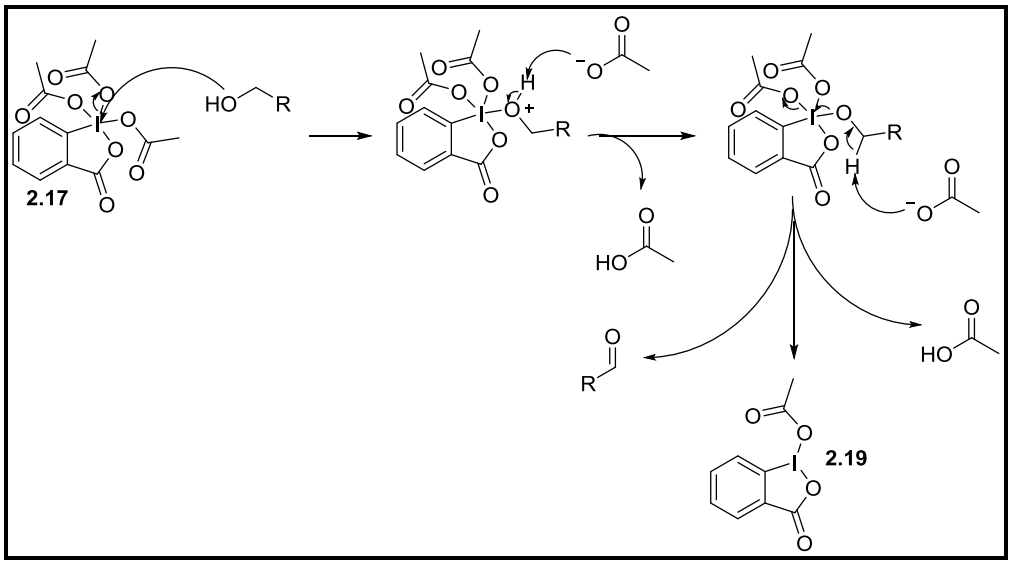


Figure 44: Mechanism of a Dess-Martin periodinane oxidation of a primary alcohol to an aldehyde producing a periodinane side product **2.17**

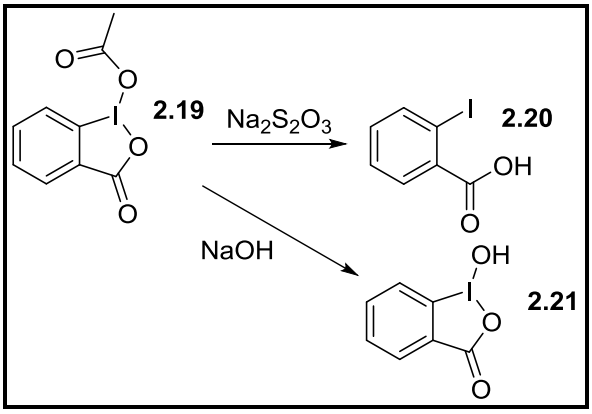


Figure 45: Treatment of the periodinane side product (**2.19**) of the Dess Martin oxidation producing 2-iodobenzoic acid (**2.20**) or *o*-iodosobenzoic acid (**2.21**) which can be removed using an aqueous sodium bicarbonate wash

It should be noted that Dess-Martin periodinane (**2.17**) has been reported as an explosive compound. Pure Dess-Martin periodinane (**2.17**) is refractory to explosion, however impurities can often make an explosive mixture. Successful alcohol oxidations of aldehydes using Dess-Martin periodinane (**2.17**) have been reported in the presence of free phenols.[250] Dess-Martin periodinane (**2.17**) is sensitive to moisture although a carefully measured amount of water produces a faster oxidising agent.[251] Therefore, the oxidation is best performed in dry solvent under an inert atmosphere.

Recently, a precursor compound used in the production of Dess-Martin periodinane called *o*-iodoxybenzoic acid (IBX, **2.18**) has been used for the oxidations of alcohols to aldehydes. The protocol is to mix IBX (**2.18**) with the alcohol as a solid suspension in ethyl acetate or 1,2-dichloroethane with a small amount of DMSO (this is thought to aid in solubility) and heating to accelerate the reaction.[252] As the IBX byproducts (**2.21**) are also insoluble, reaction work up is a simple filtration and solvent evaporation. Furthermore, this reaction can be executed in an open vessel as it is insensitive to both moisture and air. Unfortunately, this compound has been observed to be explosive in a similar way to Dess-Martin periodinane. Given that the IBX-mediated oxidation is selective, easy to use, and operates similarly to Dess-Martin periodinane, this reagent was evaluated alongside the activated DMSO strategy for the production of the required dipeptide aldehyde **1.33**.

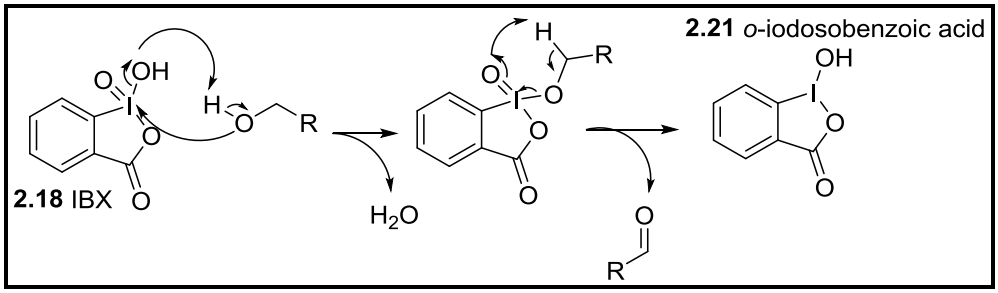


Figure 46: Mechanism of IBX (**2.16**) oxidation of a primary alcohol to an aldehyde producing *o*-iodosobenzoic acid (**2.19**)

2.4.2 Attempted oxidations

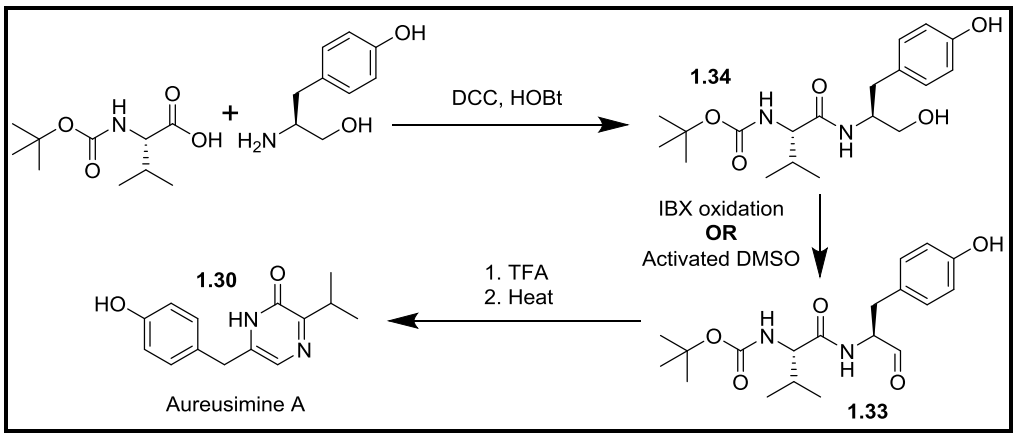


Figure 47: Proposed synthetic strategy for the production of aureusimine A

Having decided to evaluate activated DMSO and IBX oxidation strategies (see Figure 47), the dipeptide alcohol **1.34** was produced in a similar manner to

the previous synthesis of the dipeptide ester **1.32**. Thus, tyrosinol was coupled to Boc-valine using DCC and HOBt to afford the dipeptide alcohol **1.34** in a good 86% yield (Figure 48).

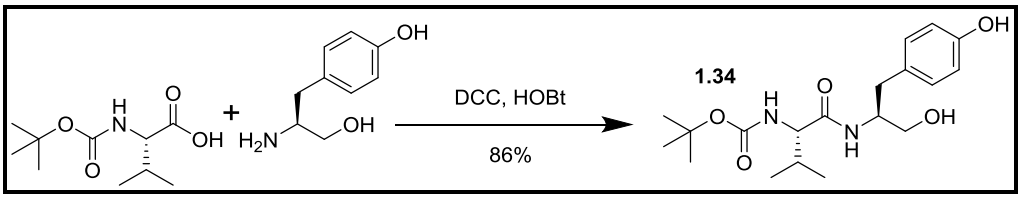


Figure 48: Coupling of tyrosinol to Boc-valine

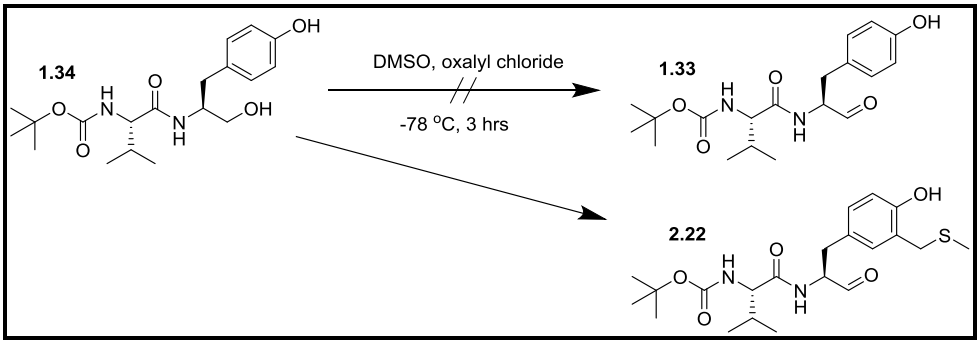


Figure 49: Swern oxidation produces an undesired meththiomethyl ether side product **2.20**[253]

The most common method for activation of DMSO is known as the Swern oxidation (Figure 50). Thus, DMSO is mixed with oxalyl chloride (**2.13**) at -78 ^{0}C in DCM for 10 minutes to produce the activated dimethylsulfonium species (**2.14**) before the alcohol is added. After stirring for one hour, base is added and the mixture is stirred for a further three hours maintained at -78 ^{0}C. The reaction then undergoes an aqueous work up to produce the desired aldehyde product. However, when this protocol was attempted using the dipeptide alcohol **1.34**, mass spectroscopy did not reveal the presence of any of the desired aldehyde product **1.33**. A complex mixture was produced, the main product had a mass of 425 corresponding to a meththiomethyl ether side product **2.22** (Figure 49), in which the phenolic moiety also participated as a substrate.[253, 254]

A common side reaction of activated DMSO oxidations especially under Swern conditions can cause the production of meththiomethyl ether side products (**2.22**). This can be caused by the degradation of the active dimethylsulfonium species (**2.14**) to a highly reactive

methyl(methylene)sulfonium species (**2.23**), however, this only happens very slowly at low temperatures so is unlikely in this case. In this side reaction, it is anticipated that the dimethylsulfonium reacted with the phenol and formed the intermediate ylide (**2.16**). However, since an α proton is not present, effectively blocking the rearrangement to an aldehyde or ketone product, the ylide can rearrange to a meththiomethyl ether product (**2.22**) *via* a Pummerer-like rearrangement (see Figure 51).

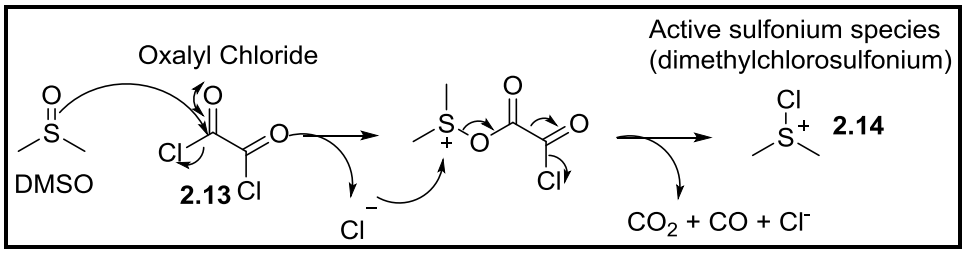


Figure 50: The production of an active sulfonium species (**2.14**) using oxalyl chloride (**2.13**).

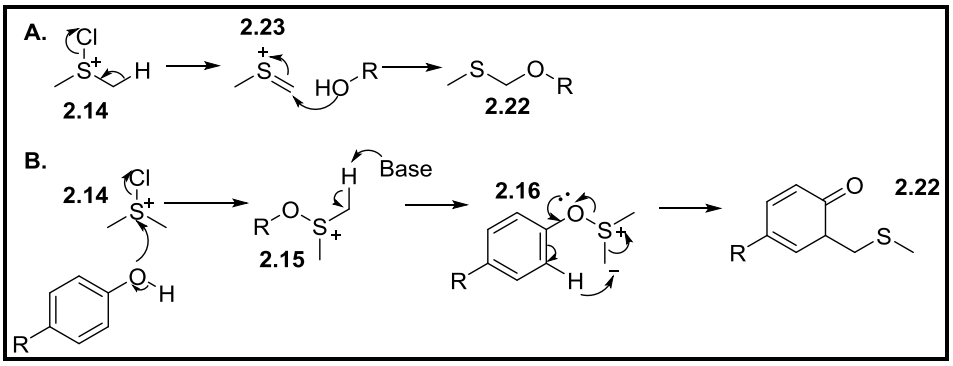


Figure 51: Potential mechanisms for the formation of meththiomethyl ether side product **2.22** by **A.** decomposition of active dimethylsulfonium species (**2.14**) to a highly reactive methyl(methylene)sulfonium species (**2.23**) and **B.** Pummerer-like rearrangement of sulfur ylide (**2.16**)[255]

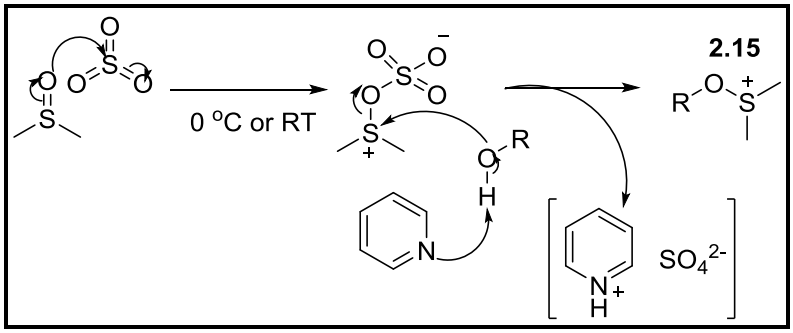


Figure 52: Scheme showing the mechanism of the formation of the alkoxydimethylsulfonium salt **2.13** using Parikh-Doering conditions

Some reports suggested that Parikh-Doering conditions are less likely to form meththiomethyl ether side products (see Figure 52).[256] However, later

attempts at this adapted oxidation in the presence of a free phenol still produced the same meththiomethyl ether side product **2.22**.

Next, an IBX-mediated oxidation was attempted for the production of the dipeptide aldehyde **1.33**. Thus, dipeptide alcohol **1.34** was refluxed in EtOAc with five equivalents of IBX as a solid suspension for six hours in accordance with literature procedures.[252] Mass spectroscopic analysis of the final reaction mixture did not reveal any of the dipeptide aldehyde product. The starting material was present alongside a product which corresponded to the *o*-quinone **2.24**.

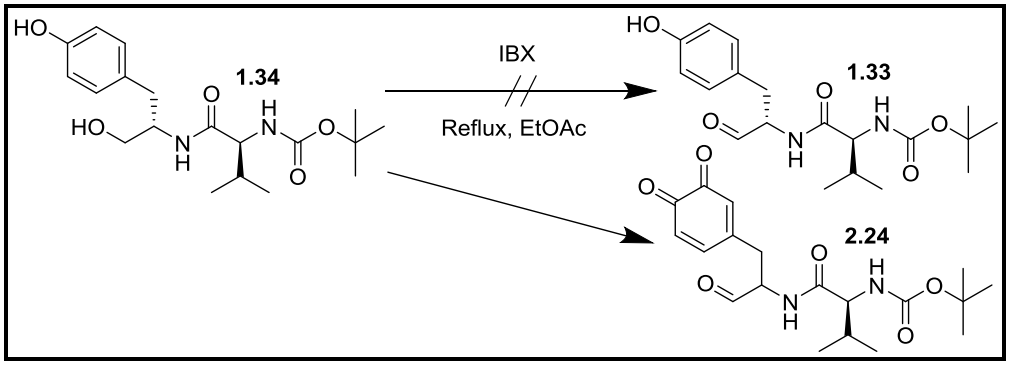


Figure 53: Scheme showing the conversion of dipeptide alcohol **1.34** to the *o*-quinone product **2.24**

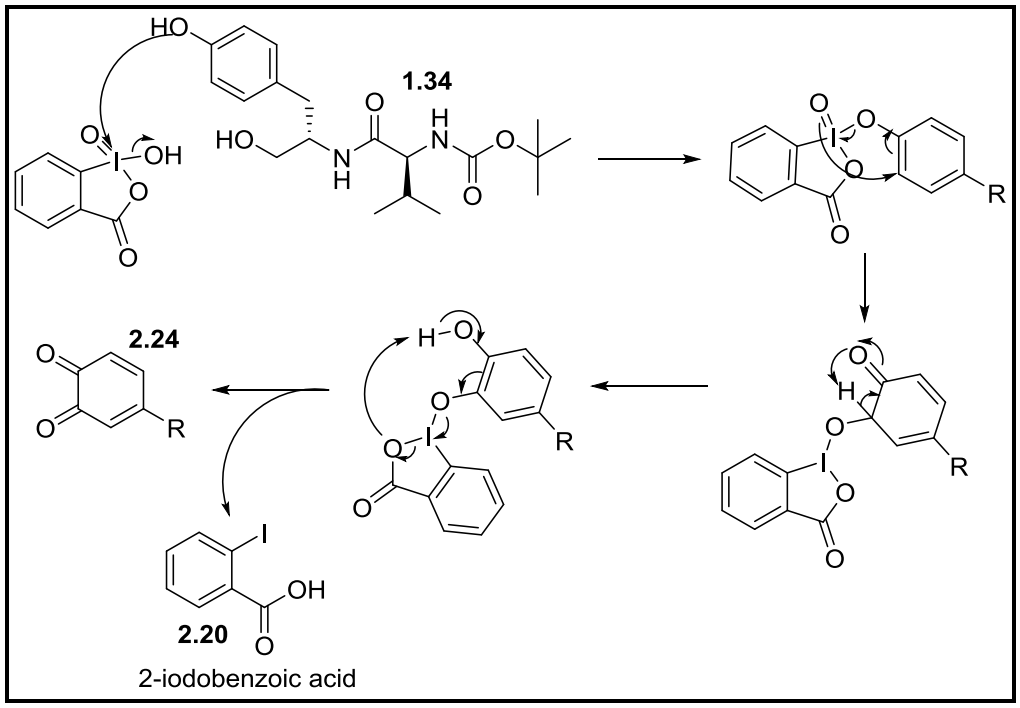


Figure 54: Proposed mechanism of IBX-mediated formation of *o*-quinone side product **2.24**. Modified from Magdziak *et al.*[257]

A review of the literature revealed that IBX can occasionally oxidise phenols to *o*-quinone moieties (Figure 54).[257] The authors suggested that the phenol could react with the hypervalent iodine, resulting in an oxidation reaction producing the *o*-quinone. In summary, although this was an interesting observation, unfortunately the product obtained was not useful.

2.5 An O-Protected strategy

Given the failure of these oxidation reactions to produce the required dipeptide aldehyde **1.33** due to the free phenol functionality, it was decided to *O*-protect the tyrosine before performing the dipeptide coupling to produce the dipeptide alcohol. As no protected tyrosinol was commercially available, the required amino alcohol **1.38** was obtained from a protected amino acid. The most facile protecting group for the phenol functionality of the tyrosine would be tBu, as this group would readily be removed by TFA at the same time as the Boc-protecting group of valine prior to the final cyclisation step. Protection of the tyrosine free amine was also necessary for the amino alcohol synthesis as we could avoid any potential interference by the reactive free amine while attempting to reduce the carboxylic acid to an alcohol.

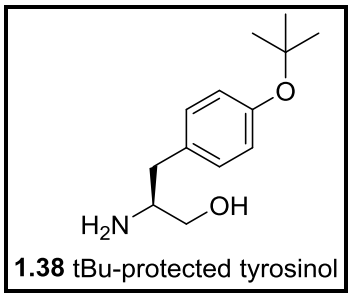


Figure 55: Structure of the desired tBu-protected tyrosinol amino alcohol **1.38**

2.5.1.1 Protected tyrosinol synthesis

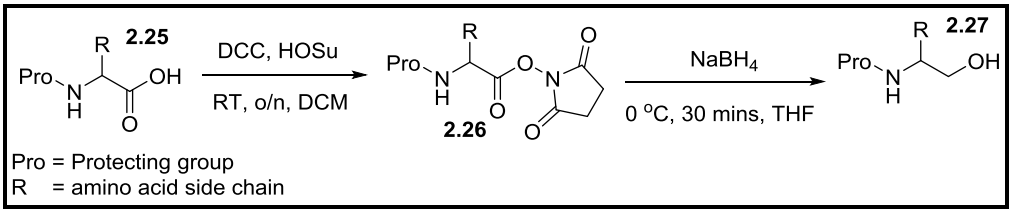


Figure 56: Scheme showing the general method for the production of amino alcohols developed by Detzer *et al.*[230]

Previous research in Chan's group developed a convenient facile synthesis of amino alcohols from amino acids. The strategy involved the activation of the carboxylic acid moiety of an amino acid (**2.25**) using *N*-hydroxysuccinimide (HOSu) followed by a gentle and selective reduction with sodium borohydride to produce the desired amino alcohol (**2.27**, Figure 56). This synthesis was

adapted to suit tyrosine and the required protecting group strategy (Figure 57).[230]

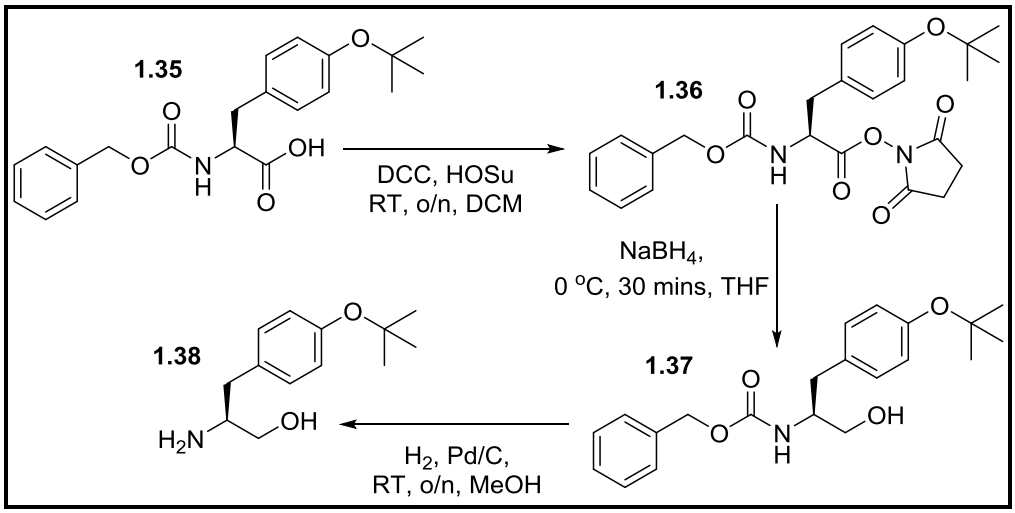


Figure 57: Synthesis of tBu-protected tyrosinol adapted from Detzer's protocol.[230]

This synthesis proceeded very smoothly without any significant problems. Thus, the succinimido ester **1.36** was produced in an excellent 94% crude yield and immediately used in the sodium borohydride reduction. This reduction produced **1.37** in an excellent yield of 95%. Finally, the deprotection produced high purity final product **1.38** in a yield of 91%. Overall, a very satisfying cumulative yield of 81% over three reaction steps was achieved, which further supports the ease, reproducibility and applicability of Detzer's method.[230]

2.5.1.2 Successful aureusimine synthesis

During the development of the synthesis of tBu-protected tyrosinol **1.38**, a synthesis for aureusimine B (**1.31**), which lacks the problematic phenol moiety of aureusimine A was also developed. Phenylalaninol (**2.28**) was commercially available which allowed the optimisation of the synthetic strategy without the need to use valuable tBu-protected tyrosinol (**1.38**). Hence, the initial strategy was identical to the strategy which was originally adopted for the production of aureusimine B before the insurmountable difficulties with the unprotected phenol group were discovered (see Figure 58).

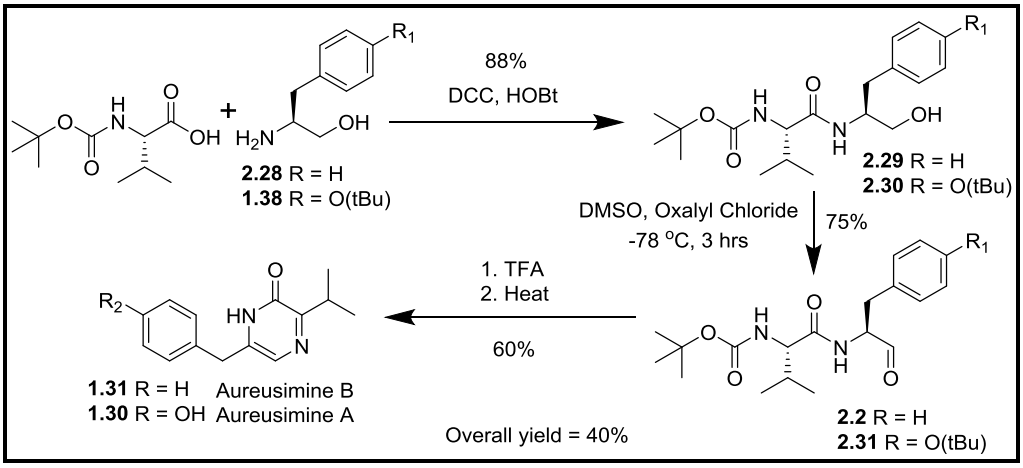


Figure 58: Scheme showing the synthetic strategy for the production of aureusimine B (**1.31**)

The coupling of Boc-valine and phenylalaninol using DCC and HOBt proceeded without any problems (88% yield). A pilot reaction employing the previous protocol for IBX-mediated oxidation of alcohols to aldehydes did not achieve complete oxidation. The reaction produced a mixture of the starting material and product which was difficult to separate. It is possible that the IBX reagent had degraded in storage and a fresh IBX preparation may have produced complete oxidation. However, NMR analysis revealed that there were also some IBX type impurities and some evidence of an undesirable racemisation of the phenylalaninol residue. This makes it unsuitable for use in this synthesis.

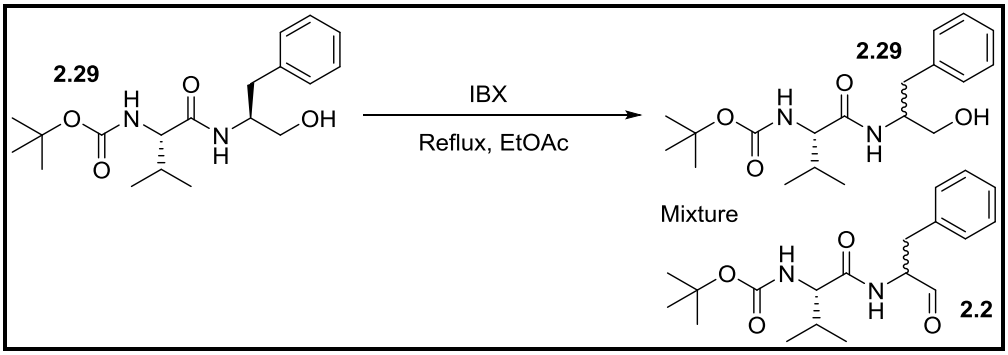


Figure 59: Result of the IBX-mediated oxidation of dipeptide alcohol **2.29**

Fortunately, when the dipeptide alcohol **2.29** was subjected to the previously employed Swern oxidation protocol, it fully converted the starting material to the desired aldehyde **2.2** with a good yield of 75% (Figure 60). Deprotection using TFA in DCM followed by cyclisation proceeded smoothly as reported in the original paper[226] to successfully produce aureusimine B (**1.31**).

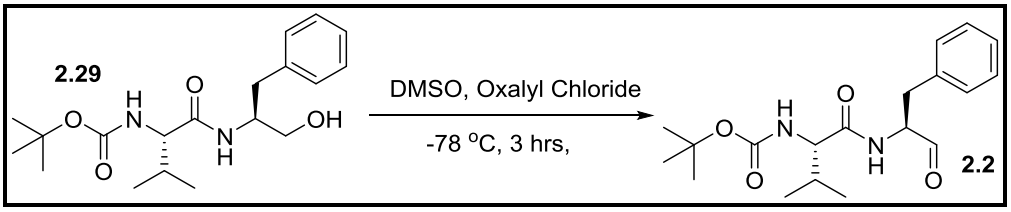


Figure 60: Scheme showing the successful Swern oxidation of dipeptide alcohol **2.29** to dipeptide aldehyde **2.2**

The synthesis of aureusimine A (**1.30**) was then attempted. The previously synthesised tBu-protected tyrosinol (**1.38**) was coupled with Boc-valine with an excellent 91% yield. The dipeptide alcohol (**2.30**) was then smoothly oxidised to the dipeptide aldehyde (**2.31**) without any problems using the Swern oxidation with a good yield of 84%. Deprotection of the Boc and tBu groups by TFA followed by cyclisation produced the final product aureusimine A (**1.30**, Figure 61).

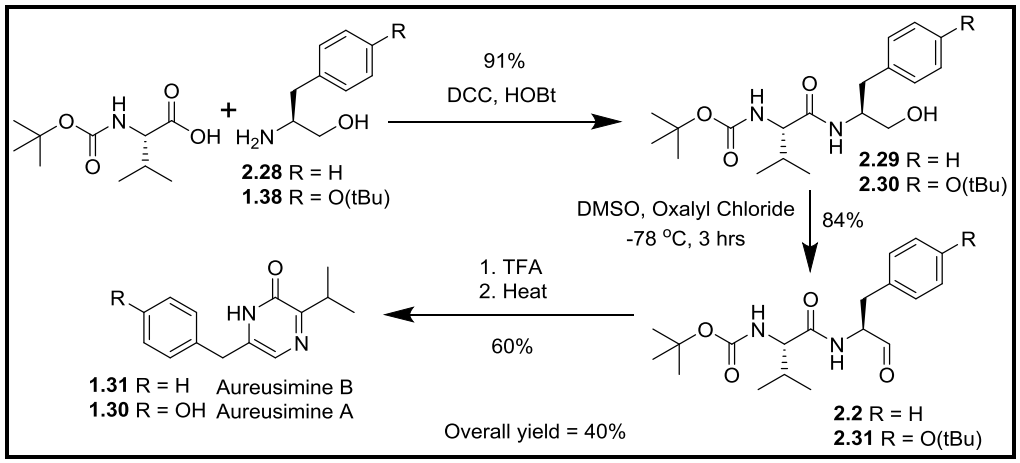


Figure 61: Total synthesis of both aureusimine A (**1.30**) and aureusimine B (**1.31**)

2.6 Do the aureusimines affect the agr system?

Wyatt *et al.* originally discovered that the aureusimines controlled the expression of many virulence genes.[225] Apparently, many of these virulence genes are associated with the *agr* system. Thus, the observed virulence effects could be the result of the aureusimines interacting with the *agr* system. To test the hypothesis, the synthesised aureusimines A (**1.30**) and B (**1.31**) were evaluated for activity in the *agr* system using a luciferase based bioreporter previously generated by Jensen *et al.* (see Figure 62).[167]

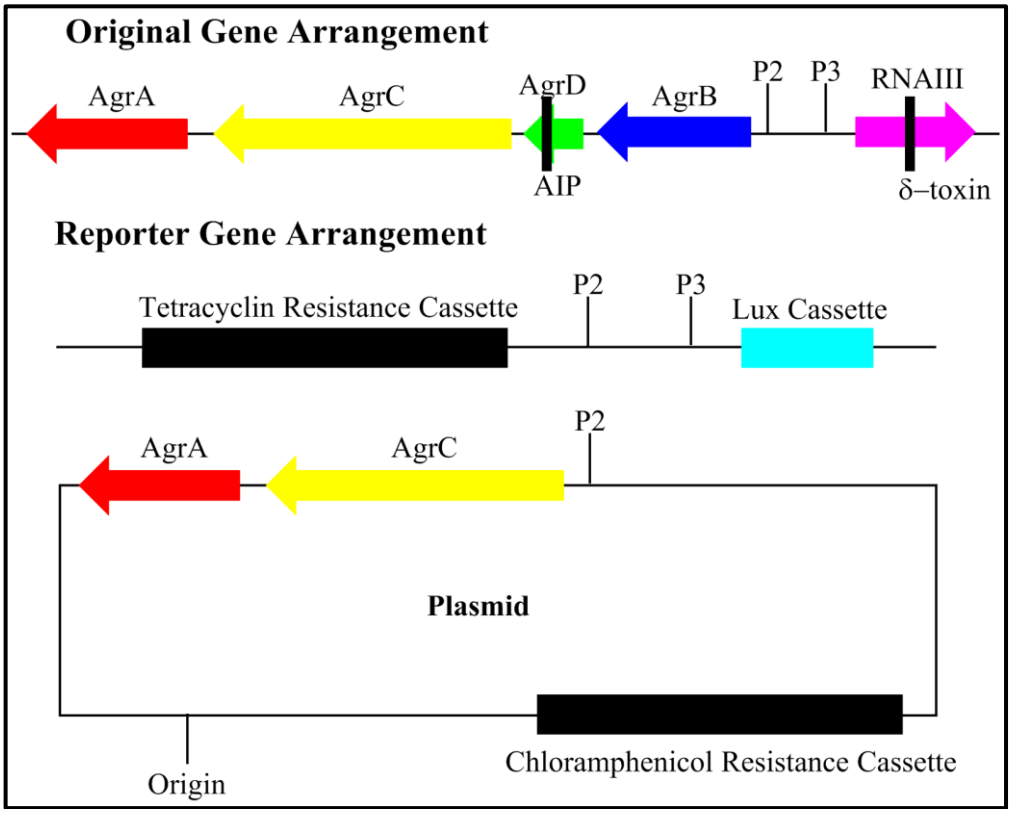


Figure 62: Schematic representation of luciferase based *agr* bioreporter created by Jensen *et al.*[167]

In this bioengineered strain, the original *agr* cassette was replaced by a tetracycline resistance cassette, effectively eliminating the entire quorum sensing system. The *rnaIII* gene under the P3 promoter has also been replaced by a *lux* cassette. This *lux* cassette, when P3 is activated, produces luminescence which can be detected by plate readers such as a TECAN multimode plate reader. This can be used as a proxy measure for P3 activity (which would cause virulence effects in the wild type bacteria). A plasmid which contains *agrC* and

agrA under the control of the original P2 promoter is then introduced into the bacteria, allowing the strain to detect and respond to exogenous AIPs while being unable to produce its own endogenous AIP ligand. Any signal now detected by the bioreporter AgrC receptors causing P3 activation and subsequent light production must be caused by exogenous AIPs. Thus, adding AIP into the growth medium causes the activation of AgrC and consequently P2 and P3 *via* AgrA, which finally results in the production of luminescence. Test compounds can then be added to the medium to determine their effect on the *agr* system.

In the presence of a defined concentration of the agonist AIP1 (**1.14**, 100 nM), a reduced level of luminescence demonstrates an inhibition of *agr*. In contrast, in an activation assay, the addition of the test compound can result in a positive outcome. However, no change in luminescence demonstrates that the compound has no agonistic effect on the reporter system.

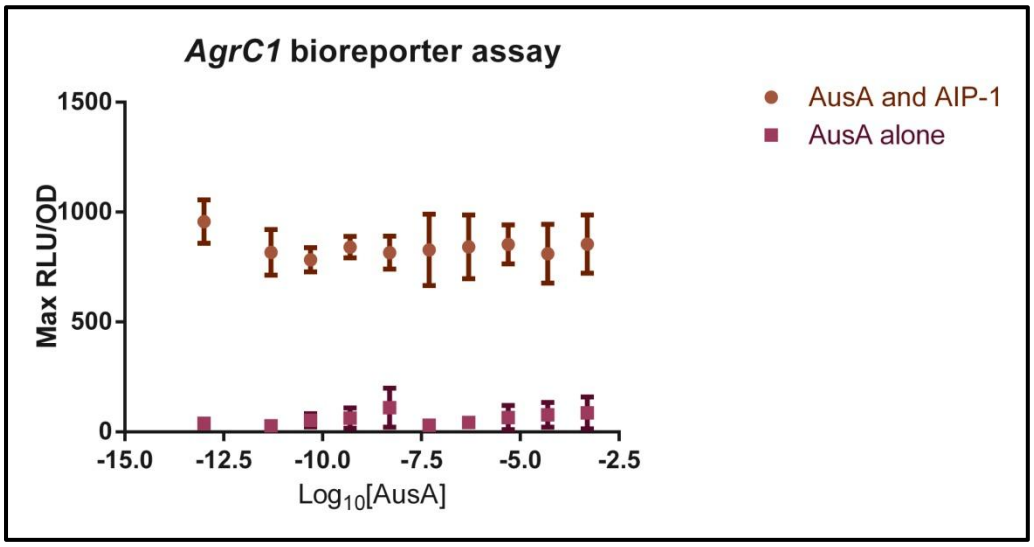


Figure 63: Effects of aureusimine A (**1.30** - concentration in M) on the AgrC1 bioreporter assay (inactive and activated by 100 nM AIP1).

As the aureusimines were previously observed to increase the expression of virulence factors,[225] it is reasonable to expect an activation of the *agr* system. However, when the aureusimines A (**1.30**) or B (**1.31**) were added to the AgrC1 bioreporter assay alone, no activation of the *agr* system was observed. Furthermore, when aureusimine B was added to the assay at millimolar

concentrations, it actually inhibited the *agr* system (see Figure 63 and Figure 64).

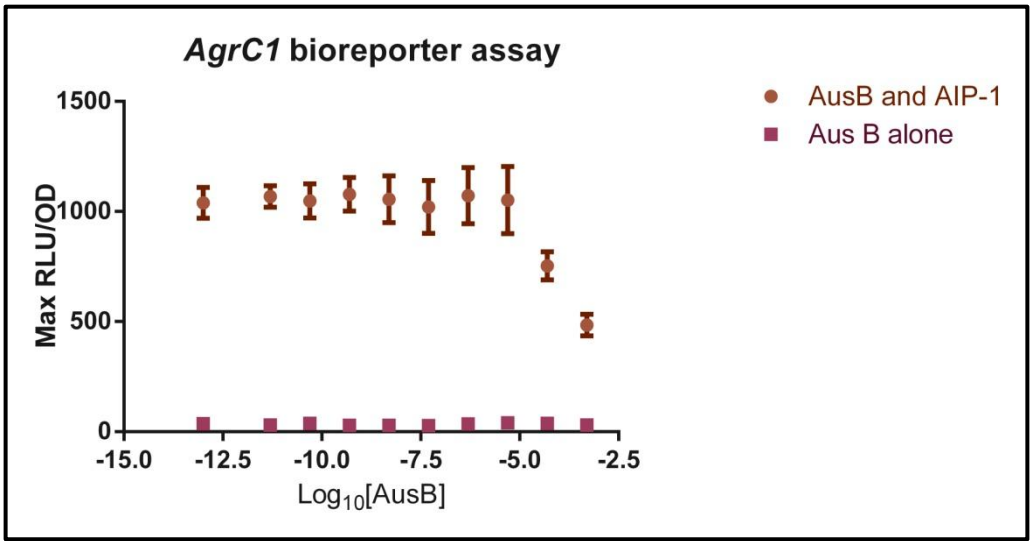


Figure 64: Effects of aureusimine B (**1.31**, concentration in M) on the AgrC1 bioreporter assay.

Sun *et al.* recently published further research into the mechanisms and effects of the aureusimines.[258] They found that the virulence effects originally observed by Wyatt *et al.* had been caused by an unintended mutation in the *saeS* operon. This was further verified using a mRNA microarray and monitoring the expression of common virulence markers. Consequently, the aureusimines were relegated from putative virulence regulators to non-ribosomal peptides secreted at high concentration with an unknown function. Thus, the observed lack of biological activity reported here further supports the recent findings reported by Sun *et al.*[258]

2.7 Affinity chromatography

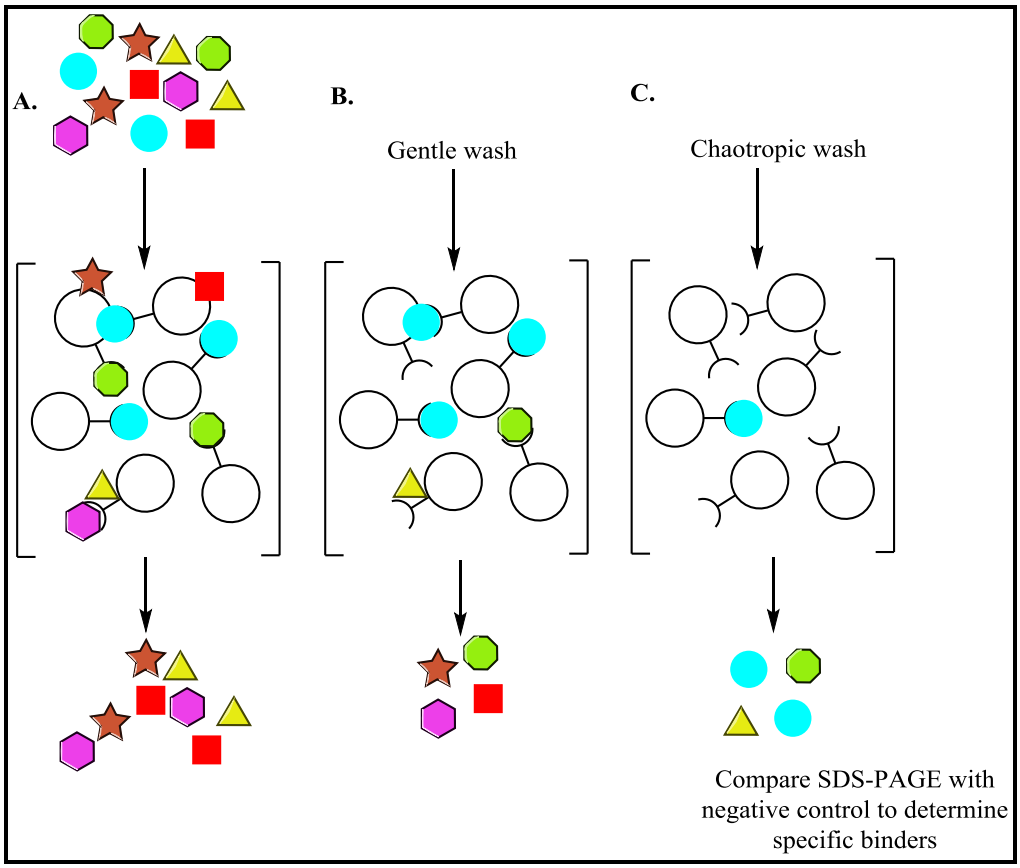


Figure 65: Schematic representing affinity chromatography. **A.** Resin is soaked in complex mixture. The mixture is then poured off and the resin washed with saline. **B.** The resin is then gently washed with either high salt or non-neutral pH wash to remove non-specific binders. **C.** A chaotropic salt is used to remove all proteins and the resulting wash is concentrated and run on an SDS-PAGE gel. Comparisons with control allow the identification of specific binders.

As the aureusimines are no longer putative virulence regulators, various strategies were considered to elucidate their biological function. Affinity chromatography is a promising strategy to investigate the aureusimines interactions with bacterial target(s). This technique has been used to identify proteins with high affinity binding to a compound of interest. Thus, the compound is tethered to a resin or polymer support designed to have low non-specific binding to protein mixtures. A complex mixture of proteins such as cell lysate is then mixed with the functionalised resin. Theoretically, high affinity binders and some low affinity binders all interact with the functionalised resin. A series of gentle washes can then largely remove low affinity non-specific binders. A stronger chaotropic wash should then disengage remaining bound

proteins from the functionalised resin. This wash is concentrated and an SDS-PAGE gel with Coomassie staining should visualise the previously resin-bound protein. Comparison with a control resin, which is unmodified allows identification of binders which are specific to the compound of interest (see Figure 65).

2.7.1 Synthesis of required tethered-aureusimine analogues

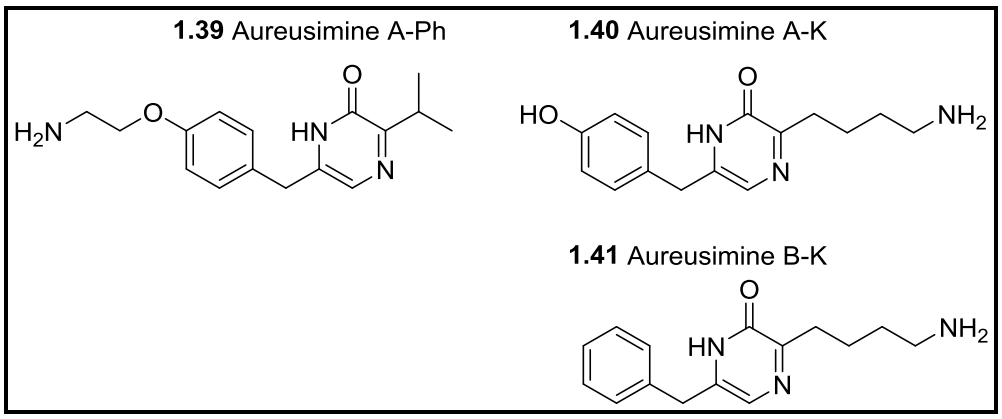


Figure 66: Aureusimine analogues with additional tether regions for affinity chromatography experiments

Thus, in order to produce aureusimine analogues with the required tether functionalities, two positions of interest were identified, in which functionalised carbon chains could be incorporated into the compound to act as a tether. The existing synthetic strategy for the aureusimines would allow a simple exchange of the valine residue for a protected lysine residue which would eventually produce analogues **1.40** and **1.41**. Alternatively, the reactivity of the phenol in the synthetic aureusimine A (**1.30**) could allow the specific functionalisation of the phenol moiety, thus permitting the installation of a chemical tether which would eventually produce analogue **1.39** (see Figure 66). It could also be possible to use the previous synthesis of the protected tyrosinol residue (**1.38**) to accomplish the same goal. It was hoped that by producing these three analogues, including tethers at two distal points in the compound and both phenolic and non-phenolic analogues, that all potential binding targets could be assessed in the eventual affinity chromatography experiments.

Initial assessment of aureusimine A (**1.30**) suggested that, by employing a Williamson ether synthesis, it may be possible to incorporate a carbon linker at

the free phenol position to produce the Boc-protected analogue **2.32**. This could easily be deprotected to produce the required analogue **1.39** (see Figure 67).

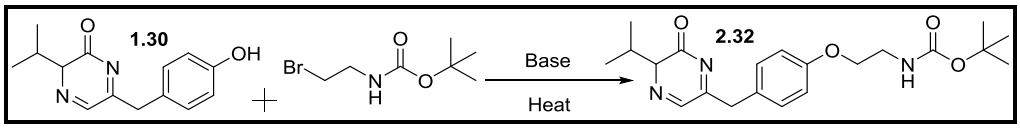


Figure 67: Planned Williamson ether synthesis producing protected analogue **2.32**

However, when this reaction was attempted, a mixture containing three significant compounds was produced. Mass spectroscopic analysis showed that these three compounds were consistent with the starting material (**1.30**), the expected product (**2.32**), and an unexpected product which corresponded to a compound which had undergone a dual addition (**2.33**, Figure 68). It is hypothesised that the enolic form of the pyrazinone moiety nucleophilically displace the bromine atom of the linker molecule, thereby producing this dual addition product **2.33**.

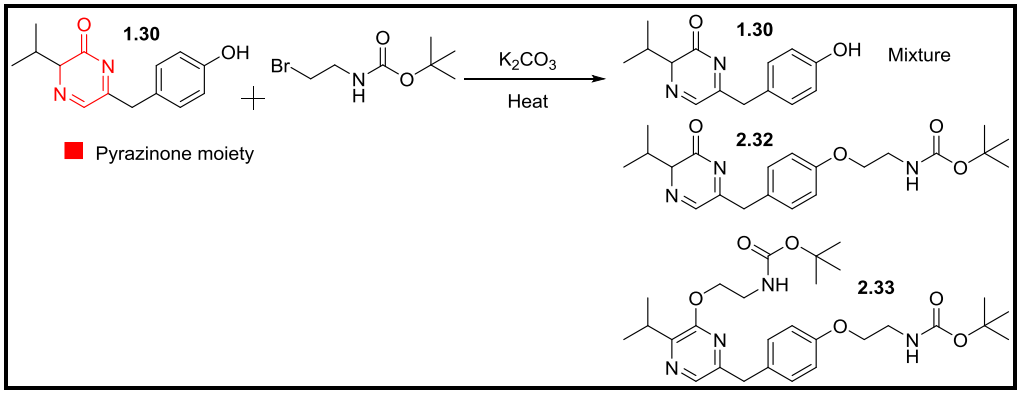


Figure 68: Scheme showing the result of the Williamson ether synthesis.

Since the pyrazinone moiety was causing problems for the facile synthesis of the desired product **2.32**, a similar reaction with Cbz-protected tyrosine (**2.34**) was then attempted (Figure 69). This strategy was considered to be more promising as the pyrazinone structure of aureusimine A (**1.30**) was absent. However, when this reaction was attempted in DMF with sodium hydride as a base, a mixture of the starting material (**2.34**) and the desired product (**2.35**) was produced. Furthermore, this mixture could not be isolated from the DMF in a good yield. As the first step of a seven step synthesis, a very low yielding reaction and a complicated purification of this mixture were highly undesirable.

Therefore, other bases and solvents were evaluated for the production of this early intermediate (**2.35**).

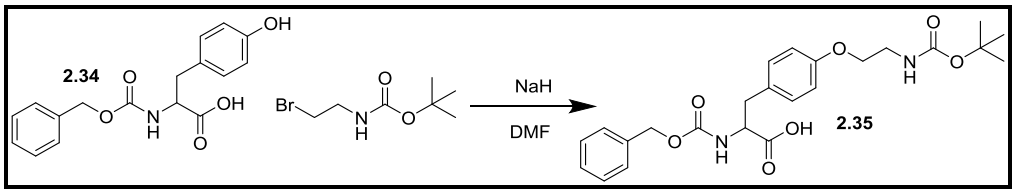


Figure 69: Attempted Williamson ether synthesis reaction

Use of potassium carbonate in acetonitrile heated at 50 °C produced reduced amounts of the desired product **2.35**. It was thought that the reduction in yield was due to a reduced solubility of the base. It is also possible that sodium hydride produces a better yield in this reaction because it is a stronger base. Although the work up was simplified using this protocol, such a low yielding reaction was still undesirable.

As solubility and base strength could have affected the success of the previous protocol, an organic base was evaluated. Triethylamine in THF heated to 80 °C overnight produced the desired product, however, acidic work up partially removed the Boc-protecting group even though only mild aqueous acids were used. Using the same reaction protocol with a modified acidic work up, where pH4 citrate buffer was used as a single aqueous wash, isolation of the crude product **2.35** was accomplished in an acceptable yield. However, NMR analysis revealed the presence of significant residual triethylamine. As this synthesis was proving to be more challenging than originally expected, this crude product was reserved for potential future use while the alternative analogues **1.40** and **1.41** were synthesised.

Synthesis of the Cbz-protected analogue **2.41** proved to be less problematic. Thus, *N*-Cbz *N*-Boc lysine (**2.36**) was successfully coupled to phenylalaninol (**2.28**) in a 79% yield using the previous protocol. A Swern oxidation also proceeded well with an 87% yield. Deprotection and cyclisation afforded the Cbz-protected analogue **2.41** in a 59% yield.

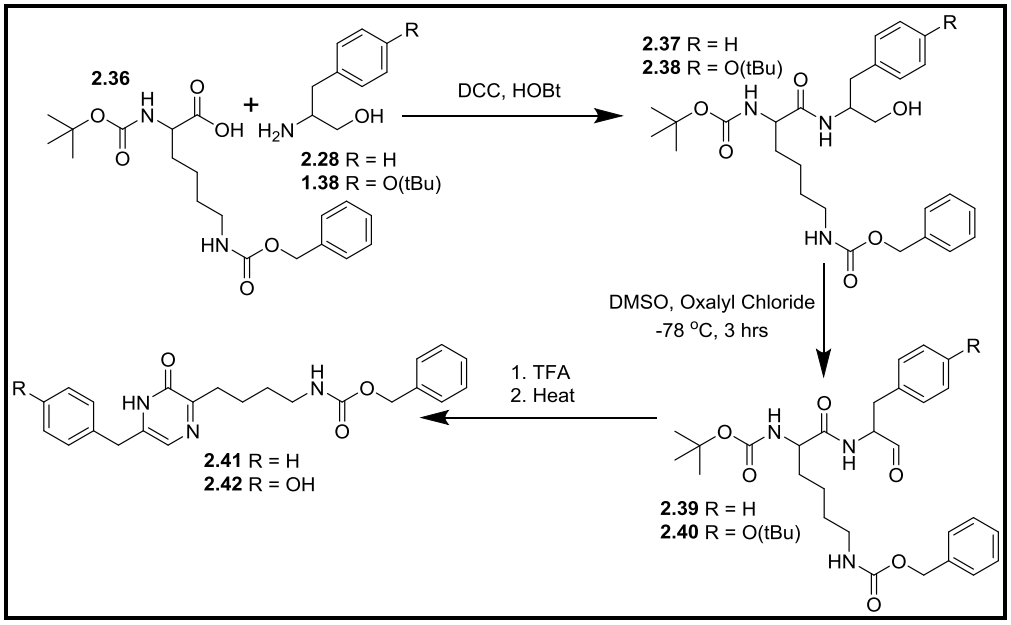


Figure 70: Scheme showing the synthesis of Cbz-protected aureusimine analogues **2.41** and **2.42** using previously discussed methods.

However, attempts to cleanly remove the Cbz-protecting group using hydrogenation were problematic. Although the hydrogenation reaction using palladium-on-carbon in a hydrogen atmosphere produced a relatively pure product, mass spectroscopic analysis showed that it was 4 mass units heavier than expected. This corresponds to the hydrogenation of two π bonds in the required product, it is possible that the π bonds of the pyrazinone core are vulnerable to hydrogenation thereby producing the undesired product (**2.43**, Figure 71). Multiple attempts using different solvents in acidic and neutral conditions were attempted; however, the required product (**1.41**) could not be produced by this method.

Apparently, the Cbz-protecting group of **2.41** could be selectively removed by employing strong acids, 4 M hydrochloric acid in anhydrous dioxane and triflouroacetic acid (TFA) had both previously found success.[259] Therefore, three parallel reactions were performed using aqueous 4 M hydrochloric acid, 4 M hydrochloric acid in anhydrous dioxane, and 50% TFA in DCM. These reactions were all left overnight. The aqueous hydrochloric acid only showed trace amounts of the required product **1.41** by mass spectroscopy. The 4 M hydrochloric acid in anhydrous dioxane reaction formed fine crystals as the reaction progress. When the solvent was evaporated these crystals redissovled,

however, on trituration with diethyl ether gave the required crystals, which were collected by filtration. Both 4 M hydrochloric acid in anhydrous dioxane and TFA in DCM showed a single pure product when analysed by thin layer chromatography. However, mass spectroscopic analysis showed two peaks; one which corresponded to the expected product **1.41** and a similar peak which was 16 mass units less than the expected product.

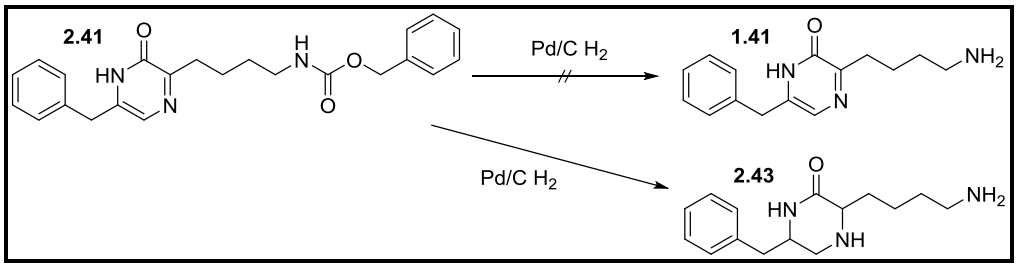


Figure 71: Scheme showing the use of catalytic hydrogenation treatment of **2.41**

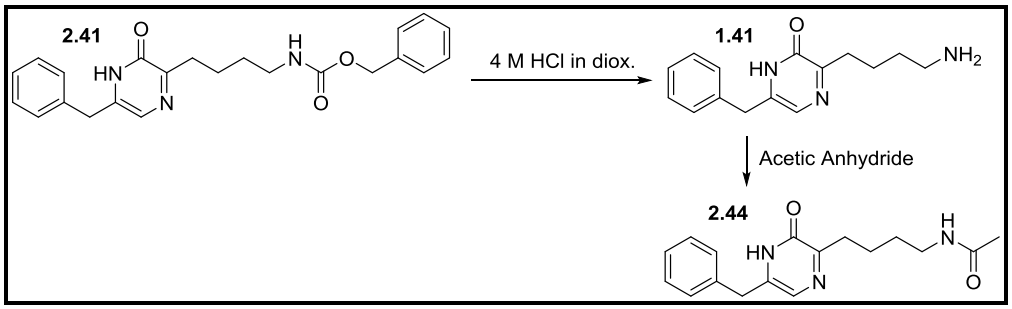


Figure 72: Scheme showing successful synthesis of required aureusimine analogue **1.37**

Given all evidence available indicated that the crystalline product was a pure single compound, it was considered that this separate peak may represent a fragmentation phenomenon. To confirm this hypothesis, a small amount of the product was acetylated with acetic anhydride. Mass spectroscopic analysis then revealed a single pure product **2.44** with the expected atomic mass thereby confirming the successful synthesis of the required analogue **1.41** (Figure 72). Both the tyrosine (**1.40**) and phenylalanine (**1.41**) analogues were successfully produced *via* this route.

With the required aureusimine analogues **1.40** and **1.41** in hand, Affigel-10 (**2.45**) was selected as a useful bare affinity resin. Initially, compound **1.41** was successfully loaded on to the resin producing loaded resin **2.46** with an estimated 83% loading using the manufacturer's instructions (Figure 73).

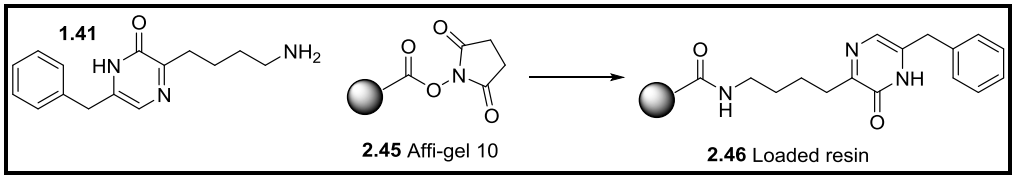


Figure 73: Condensation reaction of Affi-gel 10 resin (**2.45**) with aureusimine analogue **1.41** to produce the loaded resin **2.46**

2.7.2 Affinity chromatography protocol

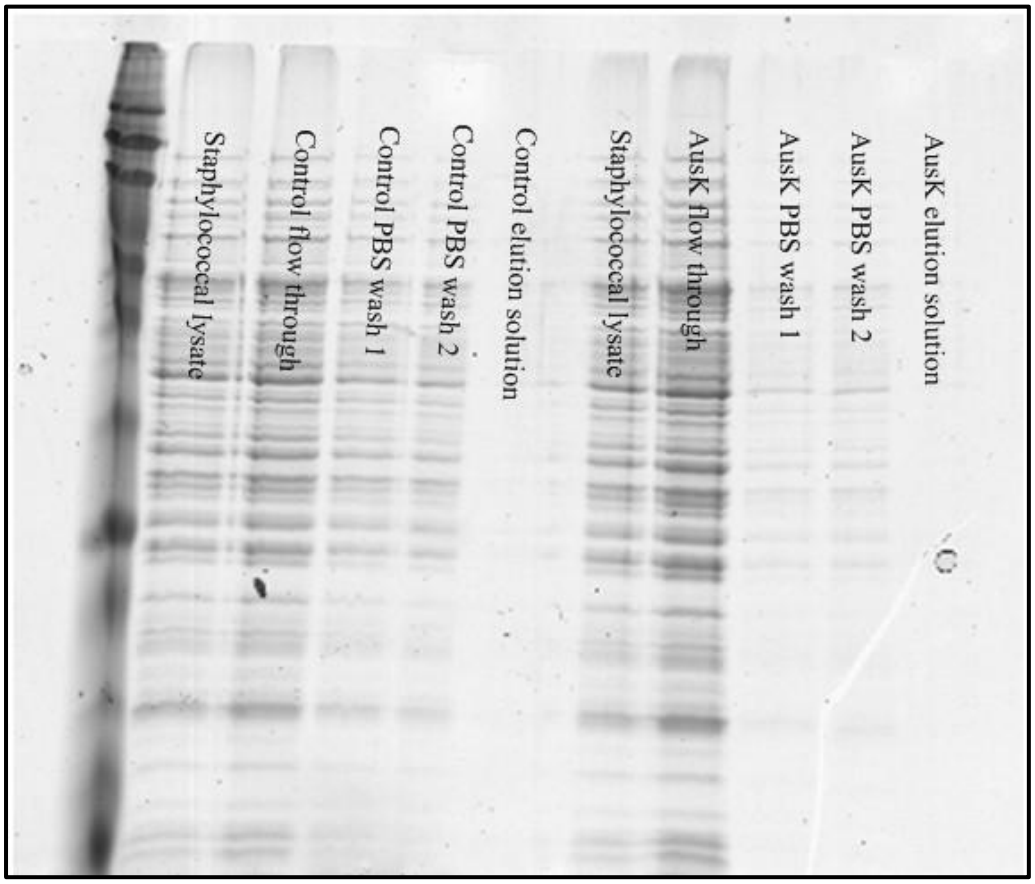


Figure 74: Coomassie stained SDS-PAGE gel of each relevant fraction from initial affinity chromatography experiment

Initially, a protocol by Dehbi *et al.* was evaluated with the functionalised resin (**2.46**).[260] The resin was bathed in PBS with 0.2% sodium azide for storage. Meanwhile, the bacteria were prepared by growing a single culture of a *ΔAusA* mutant strain and the corresponding wild type strain in 5 mL BHI each overnight. 2 mL of each of these cultures were pelleted and resuspended in PBS. These were then used to inoculate two flasks of 500 mL BHI. These were grown at 37 °C to an optical density of 2.6. 400 mL of each culture was removed and centrifuged at 4200 rpm for 5 min and the pellets were stored at -20 °C. A protease inhibitor cocktail was prepared in 10 mL PBS (Roche cOmplete ULTRA

tablets) and 5 mL was added to each pellet followed by lysostaphin stock for a final concentration of 60 μg/mL. A further 5 mL of PBS was added before the pellets were incubated at 37 °C with agitation at 200 rpm. Finally, this lysate mixture was spun at 10,000 g for 15 min at 4 °C to remove cell wall fragments and solid cellular detritus. The supernatant was incubated with the resin at 4 °C for 1.5 h then it was drained and two further PBS washes followed. The resin was then washed with 1 M NaCl solution. Elution of specific binders was accomplished with 1 M propanoic acid dissolved in 10% dioxane and water. The elution solution was then neutralised and concentrated before being run on an SDS-PAGE gel. Unfortunately, all of the protein had been removed in previous washes so no binders at all could be observed in the elution solution (see Figure 74).

In a second attempt, the bacteria was grown for 4 h and 300 mL of culture was centrifuged at 4200 rpm for 5 min. The pellet was lysed in PBS with lysostaphin and protease inhibitors as before. This lysate mixture was centrifuged at 10,000 rpm for 15 min at 4 °C. The supernatant fraction representing intracellular proteins was incubated with the resin for 1 h and 16 h in eppendorf tubes. Separately, the pellet representing the cell wall fraction and other solid cellular detritus was incubated with Triton for 4 or 16 h to solubilise the proteins and then with the resin for a further 4 or 16 h in eppendorf tubes. After incubation, each tube was centrifuged and the supernatant was removed and stored at 4 °C for later analysis. The resin was washed twice with a buffer containing Tris.HCl (50 mM), NaCl (1 M), CHAPS (0.125 mM), EDTA (0.25 mM) adjusted to pH8. Each time the resin was mixed with the washing buffer and then centrifuged, the supernatant was removed and stored at 4 °C for later analysis. The resin was washed a further four times with buffers of reducing ionic strength. Finally, each of the washed resins were split into two equal portions and suspended in SDS-PAGE sample buffer and heated to 100 °C for 5 mins and 37 °C for 30 mins respectively to remove all remaining proteins and these samples were analysed on an SDS-PAGE gel alongside the supernatant samples retained from the washing procedure. This protocol with both a milder washing procedure and harsher conditions for

removal of the remaining protein on the resin comprehensively improved the results of the experiment (see Figure 75).

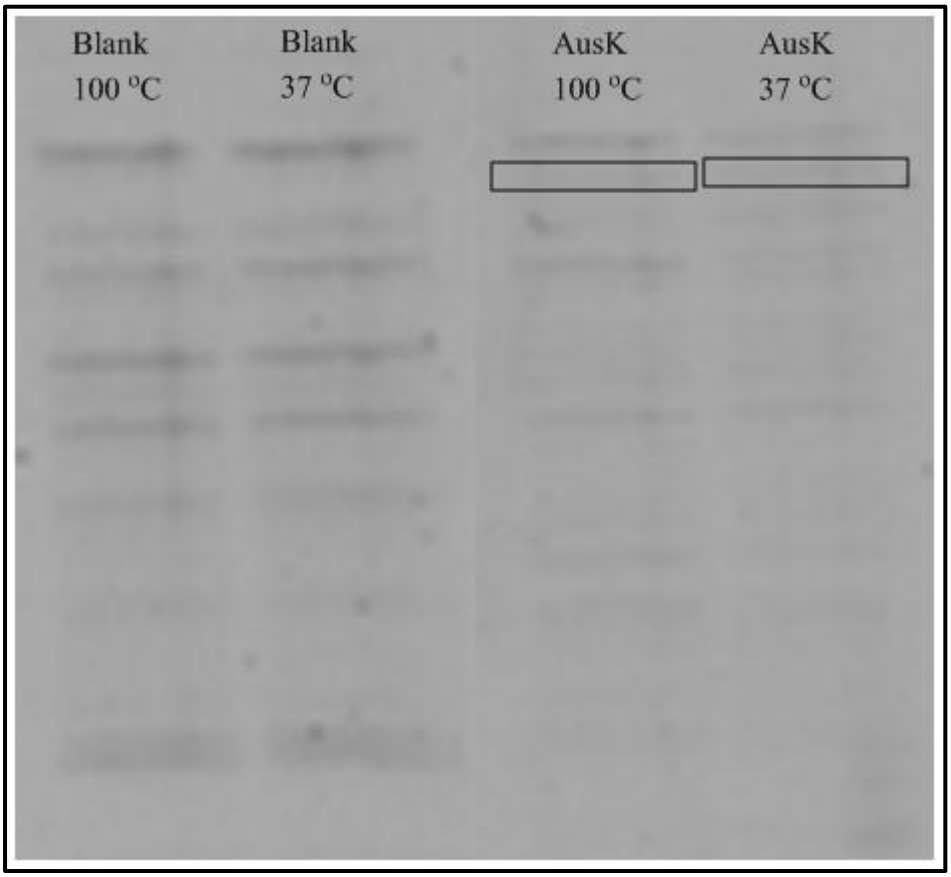


Figure 75: Coomassie stained SDS-PAGE gel of resin fractions from second affinity chromatography experiment. Rectangles highlight unique band eluted from functionalised resin **2.46**

A single unique band was identified which was enriched by the aureusimine functionalised resin **2.46** and not the control resin. This band was excised and sent for analysis by trypsin digestion and mass spectroscopic techniques at PNACL, University of Leicester. This analysis showed that the protein responsible for the band was elongation factor G.

In many studies, ribosomal proteins like elongation factor G, due to their abundance, are considered to be the most likely false positive.[261] Others consider them to be a positive result if the protein band could also be seen in a second repeat experiment.[261] Although repeating this experiment did reproduce these results, it was only observed as a very small enriched band of elongation factor G. Since ribosomal proteins are ubiquitous and highly abundant, a strong specific binder should result in a much stronger band. This suggests that the

observed results could be caused by a weak specific interaction of elongation factor G with the aureusimine functionalised resin **2.46**. Thus, it is unlikely that elongation factor G represents the aureusimines true molecular target.

Finally, in the absence of a detailed structure activity relationship of the aureusimines, it is unclear if the location of the tether on resin **2.46** prevented the effective binding of the true molecular target. As no encouraging results were observed and the likelihood of success in this endeavour was low, the affinity chromatography programme was terminated at this juncture.

2.8 Further biological evaluation of the aureusimines

Although the affinity chromatography programme had been terminated, investigations utilising other biological assays continued. Thus, the synthetic aureusimines A (**1.30**) and B (**1.31**), and a *ΔAusA* mutant strain (kindly provided by Prof. Schneewind and Missiakas) were used in further biological evaluation of the aureusimines. The *ΔAusA* strain provided had been previously validated and was confirmed to have a fully functional *saeS* system,[262] in contrast to the *ΔAusA* deletion strain (lacking a functional *saeS* system) which produced the misleading results of Wyatt *et al*.[225]

2.8.1 Colony spreading

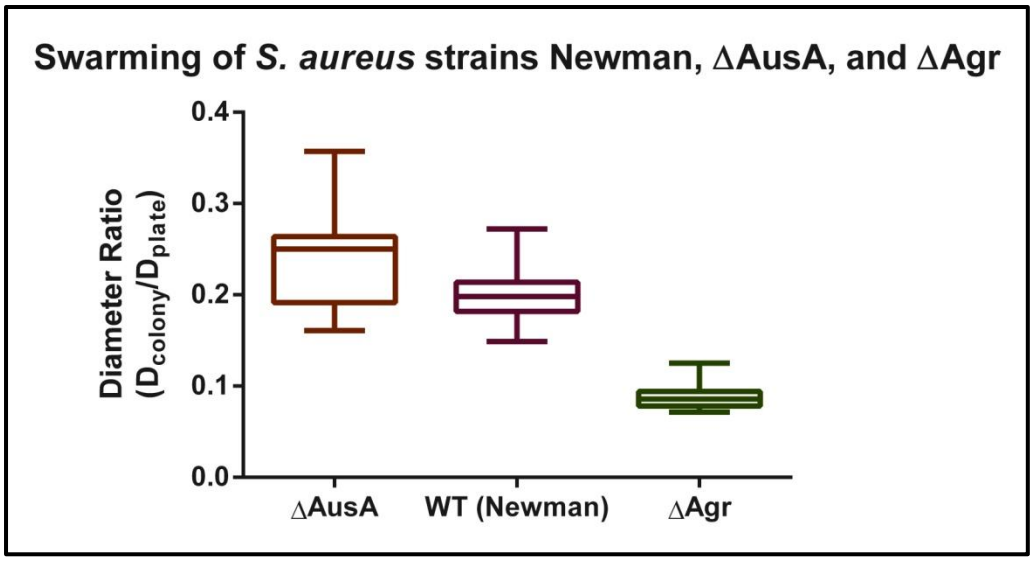


Figure 76: Swarming of *S. aureus* strains

Although *S. aureus* was originally believed to be non-motile, it has recently been shown that it does have the ability to spread over wet surfaces.[263] It has been hypothesised that this phenomenon is responsible for the ability of *S. aureus* to rapidly colonise healthcare devices, wounds and food. Even more recently, it has been shown that the *agr* system and specifically the *agr*-regulated phenol soluble modulins (PSMs) are required for the bacteria to exhibit this behaviour.[264] As the aureusimines are secreted at high concentrations into the extracellular medium, these compounds could affect the spreading phenomenon. However, when the *ΔAusA* deletion strain was evaluated in a spreading assay on agar plates, no significant change in colony

spreading was observed in comparison to the wild type Newman strain (Figure 76). In contrast, as a control experiment, the *Δagr* strain showed the expected reduction in spreading due to the role of *agr* in controlling the production of the PSMs.[265]

2.8.2 Persistence

S. aureus often causes recurrent infections. Even in infections which are highly susceptible to penicillin G, treatment must be specially extended for *S. aureus* infections and complete eradication of the organisms is not guaranteed.[266] For example, Procter *et al.* reported a patient with a *S. aureus* infection; a hemotoma following an ankle sprain had triggered a recurrence of an infection which he had previously suffered as a result of shrapnel injury during World War II. The infection had theoretically been effectively treated with penicillin G over forty years beforehand.[267] These kind of cases raise questions about how the bacteria survived the original antibiotic therapy especially as the infective strain was susceptible to as little as 0.01 μg/mL of penicillin G.[267] Further questions such as what triggers the bacterial reactivation are also interesting. In part, this phenomenon is thought to be due to the ability of *S. aureus* ability to form small colony variants (SCVs).[268] SCVs are part of the regular staphylococcal growth cycle, they can be either highly dynamic or stable, and they can have a selective advantage in harsh environments.[269] SCVs are characterised by slow growth, both virulence and metabolic associated genes are downregulated, whilst both the biofilm and persistence associated genes are upregulated.[269] SCVs have also been documented to exhibit increased resistance to trimethoprim-sulfamethoxazole,[270] aminoglycosides,[271] fusidic acid,[272] fluorquinolones,[273] and even to some antiseptics such as triclosan.[274] This antibiotic resistance twinned with low virulence and metabolic inactivity make this phenotype optimal for persistence within the host. The mechanisms which cause this phenotype have been discovered for some SCV sub-types, such as menadione,[275] hemin,[276] and thymidine[277] dependent SCVs and those with a defective stress response.[269] However, not all SCVs can be explained by these mechanisms and the mechanisms for the reversion of the SCV phenotype to an infective phenotype

are less well understood. Thus, it was considered that the aureusimines could constitute a communal signal which converts bacteria into SCVs or possibly reverts these variants back to an "ordinary" phenotype.

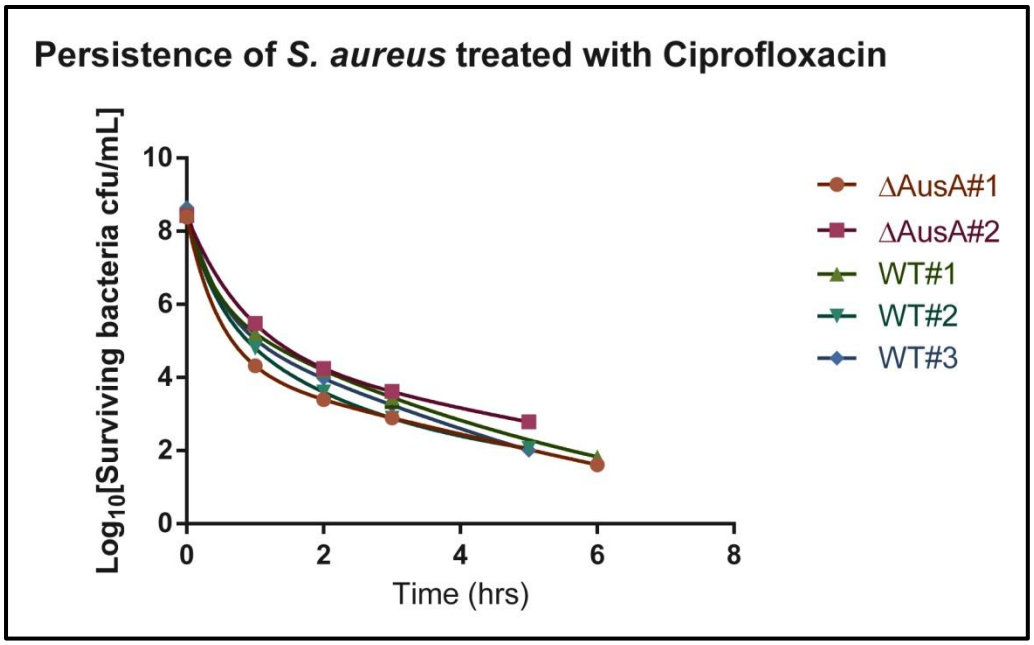


Figure 77: Graph showing the persistence of *S. aureus* strains when treated with ciprofloxacin

When *S. aureus* biofilms are treated with ciprofloxacin, these SCVs can be observed as persister cells.[278] Persister cells are defined as bacteria which survive antibiotic treatment and can then go on to form viable colonies after the end of the treatment (generally measured as colony forming units or CFUs).[279] A *ΔAusA* strain and a Newman wildtype strain were treated with ciprofloxacin (see Figure 77). As expected, both strains showed a significant initial drop in colony forming units in the first 1 to 2 h as the antibiotic successfully eliminated the regular cells in the population. A remaining resistant population of persistent bacteria were also observed in both strains over the following 4 h. However, no significant difference in the number of persister cells was observed at any time between the two strains. This indicates that the aureusimines are unlikely to affect the persistence phenomenon in either a positive or negative way. However, it is possible that expression of *ausA* only occurs in specific circumstances or environments, if this is the case it is difficult to assess the effect of *ausA* on the persistence phenomenon as the assay may not reproduce the required conditions for *ausA* expression.

2.8.3 Biofilm formation

S. aureus readily forms biofilms. This is a phenotypic adaptation which allows both defense against antibiotics and the host immune system and can lead to chronic or persistent infections.[280] This has been seen to be especially important in several significant pathologies, such as native valve endocarditis, otitis media, cystic fibrosis pneumonia and infections associated with implanted biomaterials.[281] Biofilms forming on implanted medical devices can be especially problematic.[282] Biomaterials are rapidly coated with host-derived extracellular matrix proteins upon insertion. Some of these proteins can then act as bacterial attachment sites and play an important role in the early stages of biofilm formation. Staphylococcal binding to these extracellular matrix proteins is mediated by the "microbial surface components recognising adhesive matrix molecules" (MSCRAMMs).[283] Following the attachment to a medical device surface, the biofilm forms *via* cell accumulation mechanisms[281] and the bacteria forms a protective slime known as glycocalyx.[284] This glycocalyx is composed of polysaccharides, DNA, and proteins.[117]

There are many different mechanisms and external factors which cause the attachment and accumulation of bacteria, eventually leading to formation of a biofilm. Currently, the most understood system controlling the formation of biofilms is the *ica* operon.[285] This operon controls the production of an important extracellular polysaccharide adhesin known as polymeric *N*-acetyl-glucosamine (PNAG)[286] or alternatively polysaccharin intercellular adhesin (PIA).[287] Expression of the *ica* operon is tightly controlled in *in vitro* conditions[288] but is upregulated in an infective phenotype.[289] It has been reported that *icaR* encodes a transcriptional repressor which plays an important role in the overall regulation of the *ica* operon especially in response to environmental cues.[290] Other loci have been reported to regulate the *ica* operon including: SigB, TcaR, SarA, SrrAB, CcpA, PurR, SarX, and Rbf.[291] A Mu transposon insertion library produced multiple biofilm-impaired phenotypes. Most of the insertion sites outside of the *ica* operon were still associated with decreased PIA production, indicating that regulators of PIA production other than *ica* are likely to play an important role in biofilm formation.[292]

There are many *ica*-independent mechanisms of biofilm formation. For example, the *agr* system significantly effects biofilm formation. However, in different circumstances, different effects are observed. It can decrease[293] or increase[294] or even have no effect on biofilm formation.[295] The downstream effector of the *agr* system, RNAIII, appears to regulate both cell accumulation and biofilm formation.[296] It is believed that these divergent effects on biofilm formation are caused by the responsiveness of *agr* to external conditions.[297] In fact, environmental conditions are very important for biofilm formation. For example, biofilm formation is upregulated in iron-limited conditions *in vitro*.[298] This upregulation seems to be controlled in tandem by the *fur (ferric uptake regulator)*, *sae*, *agr*, and to a lesser extent the *sar* operons with a requirement for both the known virulence factors, Eap and Emp .[299] The same study showed that the *ica* operon is vital for the production of both Eap and Emp and, ultimately, the formation of biofilms in these iron-limited conditions.[299] As the bacteria is highly adapted to survive inside a host where the availability of iron is limited, it is possible that the bacteria use this as an environmental cue to indicate their presence *in vivo*. This would explain the close relationships observed between virulence regulators such as *agr*, *sae*, and *sar* and the *fur* operon. Glucose levels can also significantly affect biofilm formation. Unlike iron regulation and many other environmental regulators, glucose regulation appears to be independent of the *icaR* repressor[290] although it does upregulate the *ica* operon and PIA production *via* interaction with the *gbaAB* operon.[291] These effects are also associated with CcpA regulation which is a gene normally controlling the metabolism.[300] It seems likely that these systems are required to ascertain the presence of nutrients which are required for the formation of the glycocalyx during biofilm formation.

As the aureusimines are secreted at high concentrations outside the cell, it was reasonable to consider that the aureusimines could affect biofilm formation in *S. aureus*. It is possible that they could act as a kind of quorum sensing signal to either form or dissolve a biofilm. Alternatively, they could play a structural role in biofilm formation. Therefore, a biological assessment of the ability of

both the *ΔAusA* strain and the wild type Newman strain to form biofilms was executed.

As previously discussed, biofilms are upregulated in *S. aureus* in various environmental conditions. Given that iron depletion and glucose supplementation increase biofilm formation by different mechanisms, it was decided that both of these conditions would be utilised in the biological evaluation. Iron starvation alongside similar nutritional stress was established using iron-depleted RPMI medium for the formation of biofilms. Meanwhile, TSB complemented with glucose was also used to cause biofilm formation *via* a *gbaAB*-mediated mechanism. The ability of both a wild type Newman strain and a *ΔAusA* strain to form biofilms was compared in both of these conditions. Exogenous aureusimines (**1.30** and **1.31**) were also added to the media to fully assess their effects.

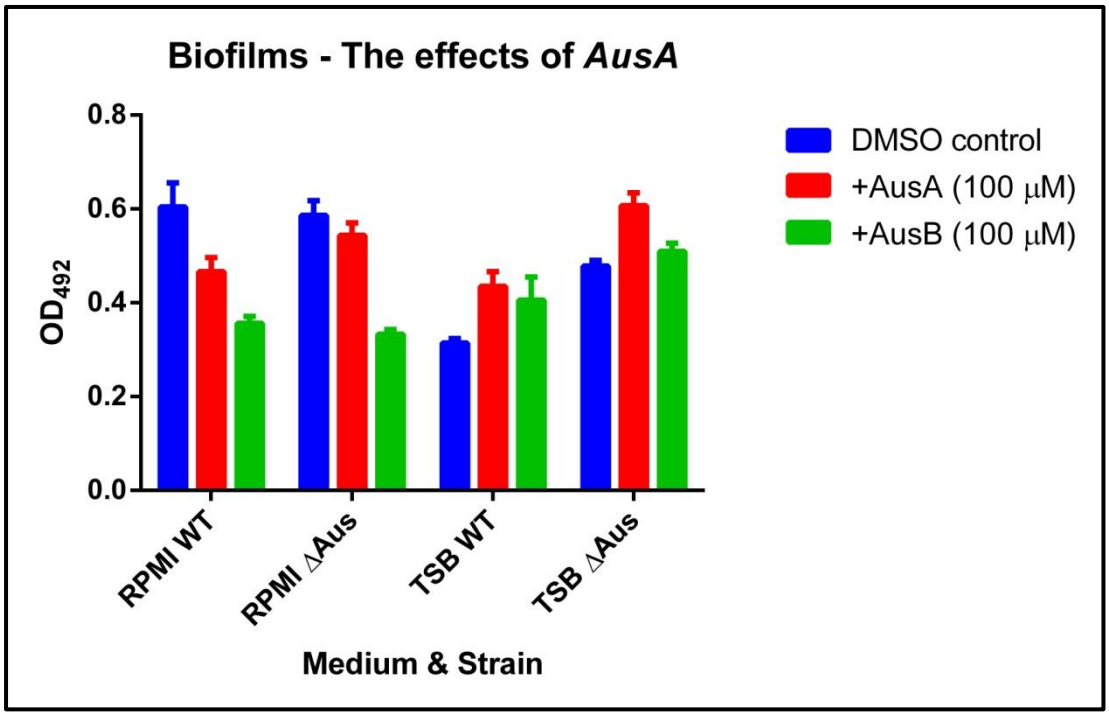


Figure 78: Differences in biofilm formation between *AusA* knockout strains and wild type parent strains with exogenous aureusimine A or B, in iron-depleted RPMI and 2% glucose supplemented TSB media.

In iron deprived conditions, the addition of aureusimine B (**1.31**) significantly reduced the ability of both strains to form biofilms (Figure 78). However, aureusimine A (**1.30**) only reduced biofilm formation in the wild type strain. As there was no equivalent reduction in the glucose supplemented

conditions, we consider that there must be a unique mechanism affecting only the biofilms formed in iron-deprived conditions. However, although there was a significant reduction in the amount of biofilm formation, a considerable biofilm was still formed by both strains. Also, there was no significant difference between the *ΔAusA* deletion strain and the wild type bacteria in these iron-deprived conditions. Therefore, although aureusimine B seems to affect biofilm formation at high concentrations in iron-deprived conditions, it is not likely that the primary target or function of the aureusimines is the control of biofilm formation in these conditions.

In glucose supplemented conditions, the *ΔAusA* deletion strain produced slightly improved biofilms in comparison to the wild type strain. It is possible that this effect is caused by the lack of aureusimine production in the *ΔAusA* deletion strain. Without this metabolic burden, the metabolically regulated mechanism could naturally upregulate biofilm formation. However, this is unlikely to be the main function of *ausA*.

2.8.4 CCL-2 mediated chemotaxis

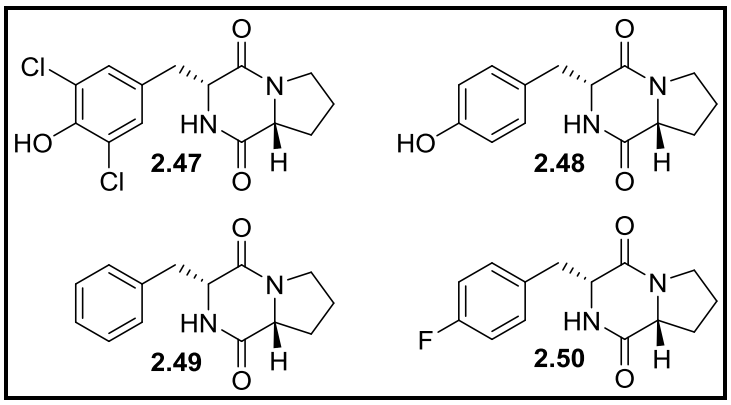


Figure 79: Inhibitors of CCL-2 mediated chemotaxis.

Monocyte chemotactic protein-1 (CCL-2) plays an important role in recruiting monocytes to sites of infection. It is a chemokine ligand, 8.6 kDa with 76 amino acid residues. CCL-2 activates monocytes and promotes chemotaxis through the action of a seven transmembrane spanning G-protein-coupled receptor, CCR-2B.[301] A biological screen was previously used to identify inhibitors of CCL-2 mediated chemotaxis in fungal fermentation extracts. A DCM extract from a *Leptoxyphium sp.* fungus showed promising activity and the

following bioactivity-guided fractionation revealed a diketopiperazine compound **2.47** which effectively inhibited CCL-2 mediated chemotaxis (see Figure 79).[302]

Further assays revealed that the related dikeopiperazine molecule **2.48** was 10- to 20-fold less active than the parent compound **2.47**,[302] indicating that the chlorination of the aromatic ring in the original compound **2.47** was important but not vital for activity. It should also be noted that neither compound affected monocyte survival *in vitro*.[302] Radioligand-binding assays revealed that these compounds are not high affinity binders of CCR-2B.[302]

Following the discovery of these compounds, Salecki *et al.* synthesised and assessed two compounds **2.49** and **2.50** for activity against CCL-2 mediated chemotaxis.[303] They found that these compounds were also effective inhibitors in trans-endothelial assays and in flow based adhesion assays. Furthermore, they found that the inhibition was specific to CCL-2 and no inhibition was observed for the similar chemokines CCL-5 or CCL-7. Initial experiments attempting to elucidate the mechanism of this activity were also performed. Signalling *via* ERK1/2 was observed to be inhibited by these compounds in cells responding to stimulation by CCL-2.[303] It is therefore possible that these compounds exert their chemotactic inhibitory activity by inhibiting ERK1/2 signalling in monocytes.

As aureusimine A (**1.30**) and B (**1.31**) are structurally similar to the newly discovered inhibitors of CCL-2-mediated chemotaxis, it was considered that they may inhibit monocycte chemotaxis. This phenomenon would be very beneficial to the bacteria and could represent a new type of virulence factor produced by *S. aureus*. The team who tested the original cyclic peptides at Newcastle University kindly agreed to perform the chemotaxis assays using the synthetic aureusimine A and B.

Aureusimine B did cause roughly a 40% reduction in monocyte chemotaxis *in vitro* (Figure 80). This was comparable to the 60% caused by the cyclic dipeptides which were initially investigated.[302] However, the experiment was performed at high concentrations (100 μM) and it is unlikely that the

concentration of aureusimine B would ever reach such a high concentration *in vivo*. Also, aureusimine B only represents around 25% of the aureusimines produced by *ausA* and no effect on chemotaxis was observed by aureusimine A. Therefore, it seems unlikely that these compounds are released for the purposes of affecting monocyte chemotaxis in this manner.

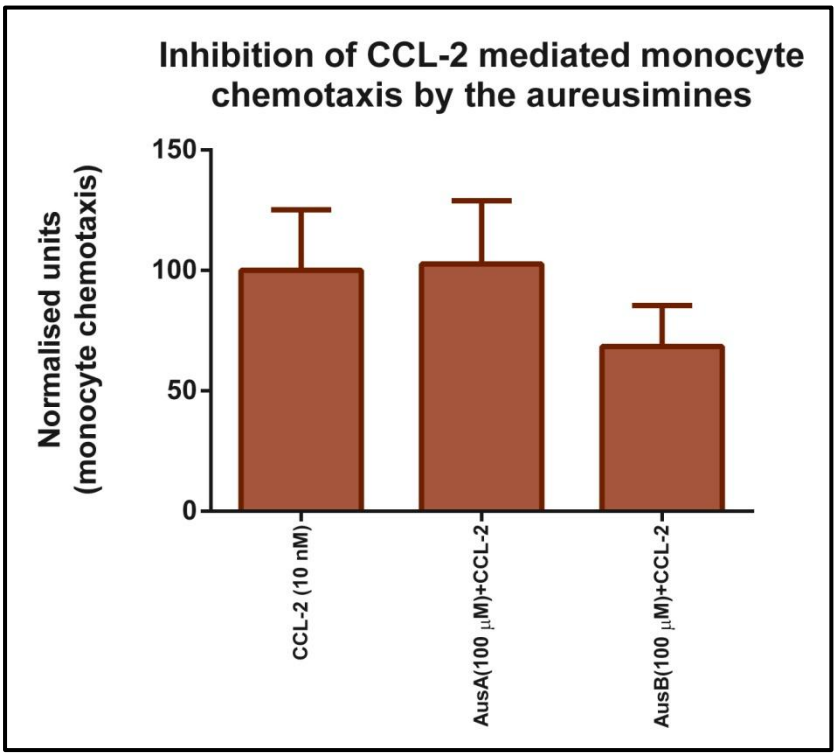


Figure 80: A graph showing the chemotaxis of monocytes due to CCL-2 in the presence of aureusimine A & B

2.9 Conclusions

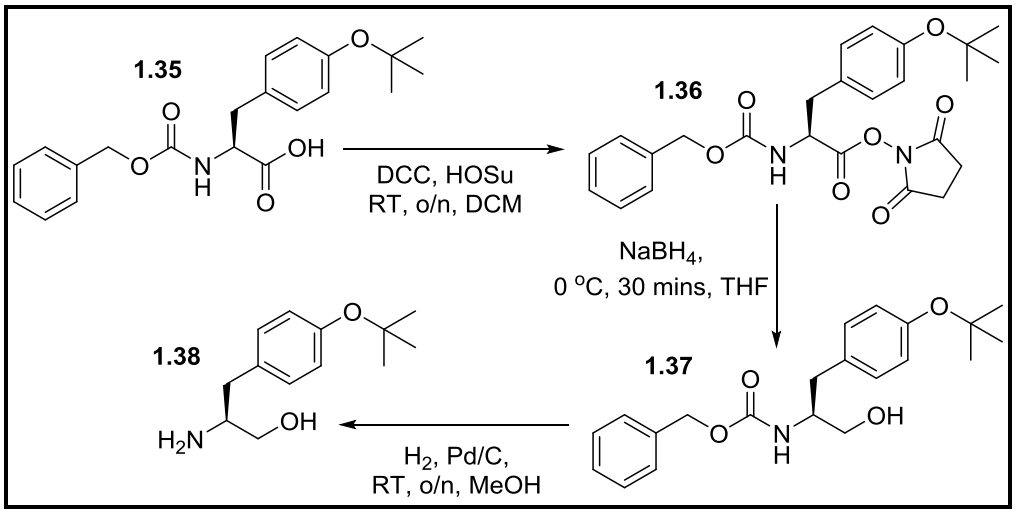


Figure 81: Synthesis of tBu-protected tyrosinol adapted from Detzer's protocol.[230]

The initial promise of the aureusimines as putative master regulators of *S aureus* virulence has proved to be incorrect. However, 0.25% of the staphylococcal genome is still dedicated to producing these compounds. This indicates that they are still likely to have a vital function for the survival or reproductive success of *S. aureus*. In light of this, the facile synthesis reported in this thesis for the production of the aureusimines could prove to be highly useful in further research.

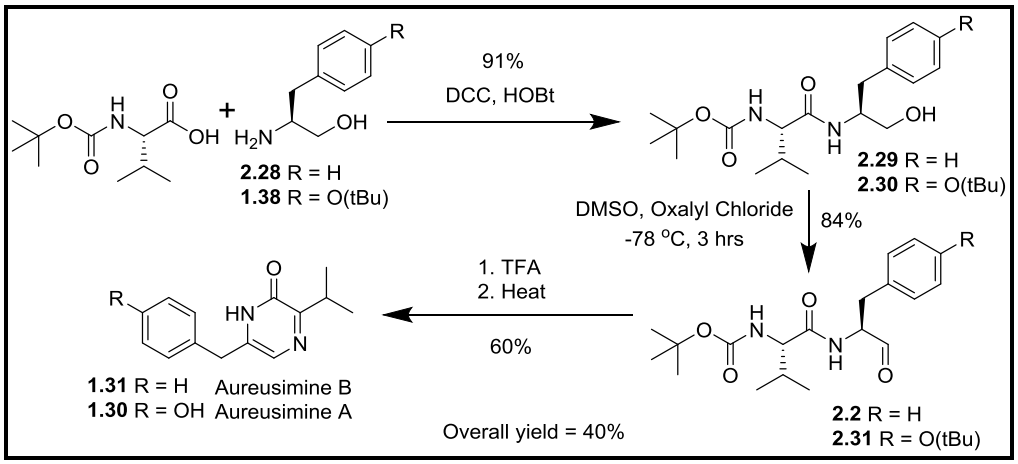


Figure 82: Total synthesis of both aureusimine A (**1.30**) and aureusimine B (**1.31**)

Utilising the amino alcohol synthesis pioneered by Detzer[230] allowed the synthesis of the required protected tyrosinol **1.38** (see Figure 81). Furthermore, it also allowed the synthesis of a tethered tyrosinol analogue **2.35** for the potential inclusion in a tethered aureusimine analogue. This simple

synthesis can easily be employed for the production of building blocks for use in the aureusimine synthesis developed in this research. Thus, allowing the synthesis of other phenolic and non-phenolic analogues of the aureusimines.

The reliable aureusimine synthesis which was pioneered in this research used a simple peptide coupling reaction to produce a dipeptide alcohol (**2.29**/**2.30**). It then avoided the unreliable DIBAL-H reduction of a dipeptide methyl ester and replaced it with a reliable Swern oxidation of a dipeptide alcohol (**2.29**/**2.30**) to produce a dipeptide aldehyde (**2.2**/**2.31**). A simple deprotection and cyclisation step then produced the required aureusimine compounds (**1.30**/**1.31**) with an impressive cumulative yield of roughly 40% over three steps. Further analogues were also successfully synthesised with similarly high yields demonstrating the flexibility of the synthesis. The pyrazin-2-one moiety is a common biological structure with known activities and there are limited synthetic routes currently available.[304] This synthesis could therefore also be useful in the production of other useful compounds with diverse biological activities.

Although the main biological function of the aureusimines was not discovered, several potential functions have been eliminated. Furthermore, this research found that aureusimine A (**1.31**) does have weak effects on CCL-2-mediated monocyte chemotaxis. Furthermore, aureusimine A (**1.30**) mildly affects staphylococcal biofilm formation in iron-deprived conditions. Optimisation of these molecules could eventually lead to: further understanding of these complex processes, compounds which prevent inflammation caused by monocyte ingress, or compounds which effectively eradicate problematic biofilm formation on medical devices.

2.10 Future Work

To ascertain the function of the aureusimines, further affinity chromatography experiments should be attempted. Tethers attached in multiple molecular locations and experiments using both bacterial cell and host tissue lysate could discover a molecular target for the aureusimines. However, these experiments may not uncover potential molecular targets especially if the target is of low natural abundance. It may be necessary to use more advanced affinity chromatography techniques. For example, click chemistry could be deployed for the design of various aureusimine molecular warheads which would interact with potential targets freely *in vivo* before being separated from tissue lysate by a click reaction with a functionalised resin followed by filtration.[305]

Given that the clarification by Wyatt *et al*.[225] showed that deletion of the gene responsible for the biosynthesis of the aureusimines actually mildly affects the expression of metabolic genes, metabolomics based investigations[306] may possibly elucidate the effect that these molecules have on the metabolism of *S. aureus*.

Finally, although the function of the aureusimines remains a mystery, the synthetic route outlined in this thesis could be used to efficiently produce many analogues of the privileged pyrazin-2-one moiety, especially those with amino acid based side-groups at the 3 or 6 position. This could easily be deployed in the total synthesis of natural products or for the production of compounds in biological research or medicinal chemistry programmes where applicable.

3 Pharmacology of AIP analogues

In this chapter, a detailed pharmacological assessment of a focused library of truncated AIP-derived macrocycles, synthesised by Dr. C. Gordon and Dr. F. Rui, are reported. Bacterial *agr* bioreporter strains are used to generate IC_{50} data which is interpreted to produce an analysis of the structure activity relationships (SAR) with various AgrC receptors.

Initially, some recent SAR studies in the field of AgrC inhibition by AIP analogues are outlined. This background literature analysis then informs the synthetic programme which is explored in some detail. The biological tools which are used to elucidate the SAR in all four AgrC receptors are explained and then the value of a further mutant bioreporter is discussed.

IC_{50} data against AgrC1 is reported and the SAR is discussed. Furthermore, IC_{50} data is reported for the other three natural receptors and the mutant receptor and interesting observations, relationships and effects are analysed. The mode of binding of the AIP analogues is assessed using the above bioreporters and a partial constitutively active bioreporter.

3.1 Introduction

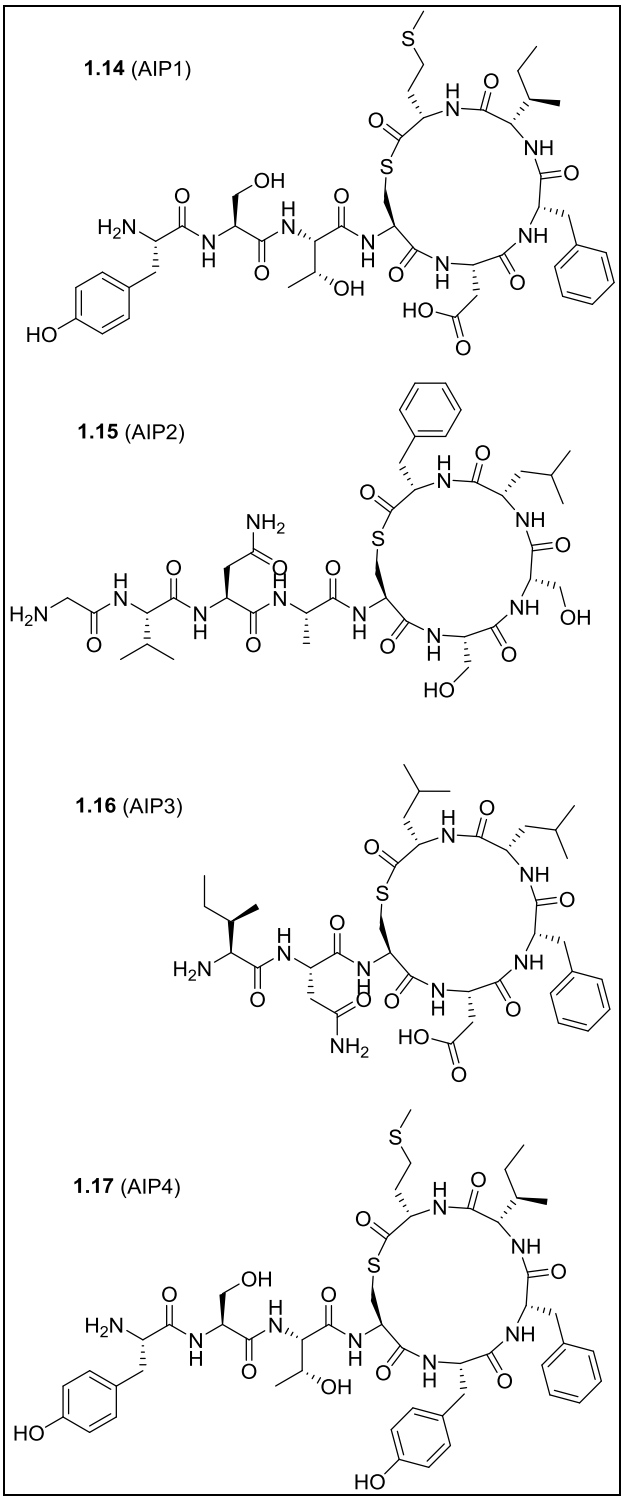


Figure 83: Structures of endogenous AIP cyclic thiolactone peptide ligands.

Ever since Mayville *et al.* discovered that the administration of AIP2 (**1.15**) protects mice from infection with *agr*-I strains of *S. aureus,* there has been considerable interest in developing inhibitors of the *agr* system based on

derivatives of endogenous AIP ligands (see Figure 83).[162] Several SAR studies have been performed contributing to a well developed understanding of the basic features and interactions of AIP1 (**1.14**) and AIP2 (**1.15**) with cognate AgrC receptors. In this section, previous studies will be examined and key findings are highlighted.

3.1.1 Previous Research

3.1.1.1 Mayville's study[162]

This study pioneered a new synthesis of the AIP macrocylic lactone structure using a solid-phase intramolecular trans-esterification strategy. By using a 3-mercaptopropionyl PEGA resin (**3.1**), the linear peptide could be assembled using standard solid phase peptide synthesis conditions. Once the sequence was completed (**3.2**) and deprotected (**3.3**), the resin was swelled in water allowing a chemoselective trans-esterification reaction with concurrent release of the peptide from the 3-mercaptopropionyl PEGA resin to afford the desired macrocyclic products (such as AIP1 **1.14** and AIP2 **1.15**, see Figure 84). With these synthetic peptides in hand, the team deployed a P3/β-lactamase fusion assay for both *agr-I* and *agr-II*, to report EC_{50} figures for the respective native ligands (AgrC1/AIP1 EC_{50} = 10.2 nM; AgrC2/AIP2 EC_{50} = 3.6 nM) and IC_{50} data for the cross group inhibition effects (AgrC1/AIP2 IC_{50} = 3.4 nM; AgrC2/AIP1 IC_{50} = 2.9 nM).

The new synthesis allowed the production of further analogues to begin the examination of the SAR of AIP-based compounds with AgrC1 and AgrC2. Initially, the team examined the interaction of AIP3 (**1.16**) with the two receptors; they found that AIP3 (**1.16**) was equally potent as an inhibitor at both AgrC1 and AgrC2 (AgrC1/AIP3 IC_{50} = 3.1 nM; AgrC2/AIP3 IC_{50} = 3.2 nM).

They then assessed the importance of the macrocyclic thiolactone structure. The specific importance of the thiolactone structure was examined by the production and testing of analogues possessing a lactam and lactone macrocyclic structure by substituting the central cysteine (C) residue of AIP2 (**1.15**) with diaminopimelic acid (X) and serine (S) respectively. These analogues proved to be potent inhibitors of AgrC1 (AgrC1/C5X-AIP2 IC_{50} = 7.9

nM; AgrC1/C5S-AIP2 IC_{50} < 1 nM) but had no effect on AgrC2. The team concluded that the thiolactone structure was vital for activation but not for inhibition and they proposed that this may be because a thiol ester acylation may be necessary for the activation of AgrC. They went on to address the importance of the macrocyclic arrangement by producing and testing a linear thiol ester analogue and the linear carboxylate, neither compound was observed to interact with the *agr* system even at high micromolar concentrations. This suggests that the macrocyclic structure is indispensible for AgrC binding.

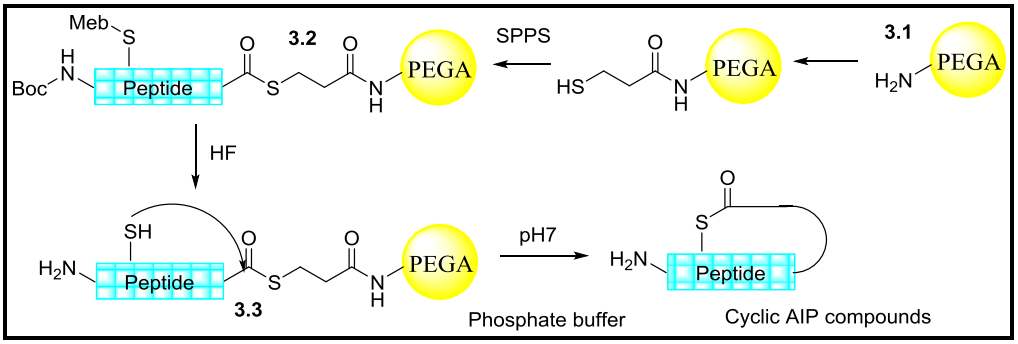


Figure 84: Chemical synthesis of AIP via a solid-phase intramolecular trans-esterification strategy. A fully deprotected peptide on a solid support is prepared *via* a reactive thiol ester bond. Swelling the peptidyl resin material in an aqueous buffer leads to a chemoselective *S*-acyl migration and concomitant release of the peptide.

Having addressed the importance of the macrocyclic thiolactone arrangement, the team systematically assessed the importance of each amino acid residue of AIP2 by performing an alanine scan. The results of the scan are visually displayed in Figure 85.

Activation of AgrC2 requires the presence of Asn^3, Leu^8, and Phe^9 while inhibition of AgrC1 only requires Leu^8 and Phe^9 which both reside in the macrocycle. It is interesting that Asn^3 is required for activation but its replacement actually improves the inhibitory activity of the compound. This suggests that Asn^3 is likely to be unimportant for recognition or binding to the receptor but has an important part to play in the activation mechanism of the receptor. In contrast, Leu^8 and Phe^9 are required for both inhibition and activation and are therefore likely to be important for receptor recognition or

binding. It is interesting that the only residues required for inhibitory activity are present in the macrocycle.

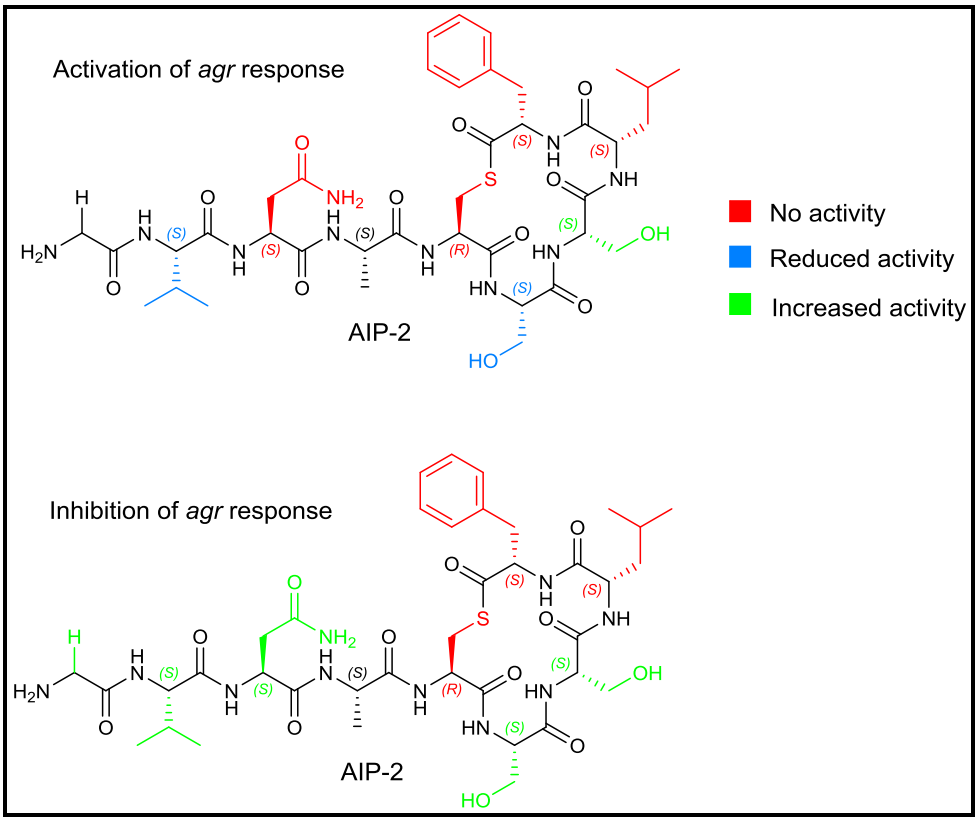


Figure 85: The results of the Mayville *et al.* alanine scan of AIP2. The EC_{50} values (activation, AgrC2) were as follows: Ala^1 = 3.2 ± 2.2 nM; Ala^2 = 73.7 ± 1.9 nM; Ala^3 = no activity; Ala^6 = 33.6 ± 1.5 nM; Ala^7 < 1 nM; Ala^8 = no activity; Ala^9 = no activity. The IC_{50} values (inhibition, AgrC1) were as follows: Ala^1 < 1 nM; Ala^2 < 1 nM; Ala^3 < 1 nM; Ala^6 ≪ 1 nM; Ala^7 < 1 nM; Ala^8 = no activity; Ala^9 = no activity. None of the peptides activated AgrC1 or inhibited at AgrC2.

These observations led the team to propose a binding model for the AIP/AgrC interaction. They proposed that for the AgrC receptor to be activated, the macrocycle must bind the receptor and then precise interactions with the tail residue, Asn^3, positions the thiolactone bond for a trans-acylation with a nucleophilic group in the receptor. In contrast, inhibition is caused by recognition of the macrocycle (especially of Leu^8 and Phe^9) without the precise positioning provided by the Asn^3 tail residue, thereby not leading to the trans-acylation of the receptor. However, this macrocyclic binding is still strong enough to cause competitive inhibition with the endogenous ligand. The proposed receptor acylation pathway was later refuted.[157]

3.1.1.2 Lyon's first study[213]

Lyon *et al.* created the first non-chromosomal bioreporter for the *agrCA* response. They produced a plasmid with *agrCA* under the control of the P2 promoter and β-lactamase under the P3 promoter and transformed into an *agr*-null *S. aureus* strains. This allowed more precise measurement of EC_{50} and IC_{50} because exogenous activator is added to the assay to stimulate the β-lactamase activity instead of relying on production of native AIP by the reporter strain. The quantity of AIP is therefore more precise. The team chose 100 nM as sufficient to produce full activation of the receptor without oversaturation.

Once they had prepared this reporter, they reasoned that as the macrocyclic residues of AIP2 (**1.15**) seemed to be sufficient for receptor binding and the tail residues seemed to be both unnecessary for binding and vital to agonism, an AIP2 analogue with a truncated tail region could therefore act as a cross-group inhibitor (**3.4**, Figure 86). In fact, this analogue is a potent inhibitor of AgrC1 (IC_{50} = 272 nM), AgrC2 (IC_{50} = 209 nM), AgrC3 (IC_{50} = 10 nM), and AgrC4 (IC_{50} = 188 nM). This was a very exciting result as this was the first pan-group *agr* inhibitor which was discovered and this revealed the potential of anti-virulence therapies targeted at the *agr* system of *S. aureus*. The team then also tested this compound for inhibition in other staphylococcal strains finding a weak inhibition in *S. epidermidis* and quite strong inhibition in *S. warnerii*. In light of this, there also seems to be potential for the development of potent cross-species *agr* inhibitiors.

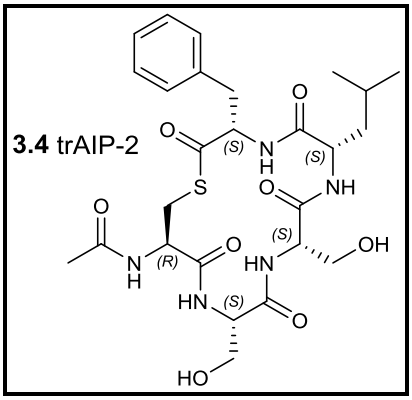


Figure 86: The first pan-group inhibitor of *agr* truncated AIP2 (**3.4**)

3.1.1.3 McDowell's study[157]

McDowell *et al.* focused on AIP1 (**1.14**) as the parent compound for the examination of the AgrC1 SAR and the development of AgrC inhibitors. Initially, while trying to isolate AIP1 (**1.14**) from spent medium, they noticed that the medium contained two related HPLC peaks. Analysis revealed that one of these peaks was the expected native AIP1 (**1.14**), the other peak was an oxidation product of AIP1. The methionine residue, under certain conditions, is readily oxidised to a methionyl sulfoxide (Figure 87). This was confirmed by the observation that this compound could be chemically reduced to afford AIP1 (**1.14**). The team tested this compound revealing that it neither activates nor inhibits the AgrC1 receptor. They proposed that this phenomenon could be a mechanism by which the quorum sensing signal is modulated over time. Replacements of the methionine residue with norleucine, serine, glutamic acid, lysine, and proline all failed to inhibit or activate the AgrC1 receptor highlighting the importance of this methionine residue to the activity of the ligand.

The team also performed a *D*-amino acid scan (Figure 87). Interestingly, replacing methionine with *D*-methionine produced a compound which maintained agonist activity. Therefore, it appears that it is the mere presence of the methionine residue and not its stereoconfiguration which is important for activity. The only other residue which maintained agonism when replaced with a *D*-residue was phenylalanine. When serine and cysteine residues were exchanged, the resulting compounds were mild inhibitors.

These results show the stereoconfiguration of both methionine and phenylalanine are unimportant for both receptor binding and the mechanism of receptor activation. The configuration of serine and cysteine seems to be unimportant for binding the receptor, however, their stereoconfiguration does seem to be important for receptor activation. The stereoconfiguration of all the other residues may be important for binding; direct replacement with a *D*-amino acid residue resulted in near complete loss of activity.

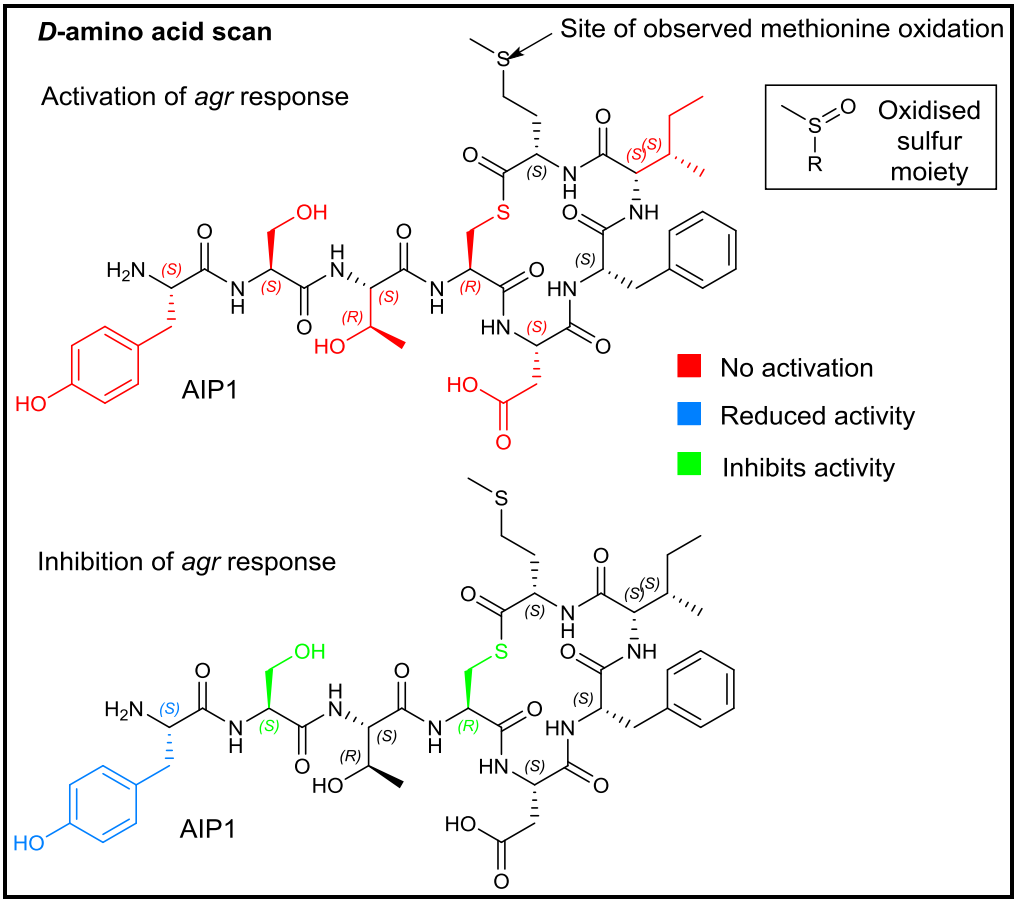


Figure 87: Results of McDowell *et al.* *D*-amino acid scan. EC_{50} and IC_{50} curves were obtained using an *agr*-I reporter.

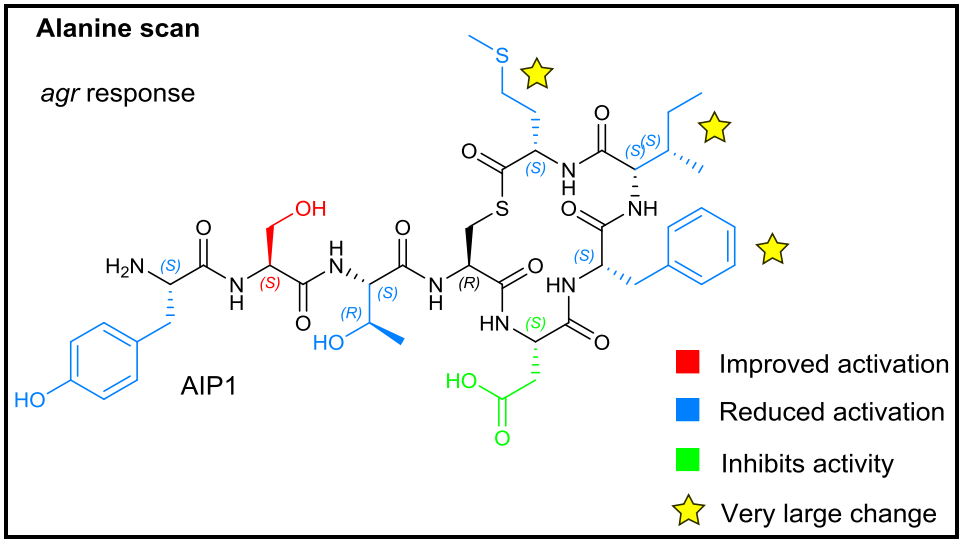


Figure 88: Activity of alanine scan analogues against an *agr*-I reporter in comparison with AIP1 (EC_{50} = 19 nM). (Ala^2)AIP1 was an improved agonist (EC_{50} = 9 nM) (Ala^5)AIP1 was a potent antagonist (IC_{50} = 33 nM).

Following the *D*-amino acid scan, an alanine scan was also performed (see Figure 88). The importance of the serine residue for activation of the receptor was further confirmed. Similarly to the *D*-amino acid scan, the alanine scan

found that alteration of this residue changed the characteristics of the receptor activation. When converting the residue to *D*-serine, an inhibitor was produced; when this serine residue was converted to alanine, an improved agonist was produced. The serine residue of AIP1 is the same distance from the macrocycle/central cysteine residue as the significant Asn[3] residue of AIP2 (**1.15**) which Mayville *et al.* found to be vital to the activation of the receptor. It is possible that the importance of these residues is analogous in both receptors especially as both residues are of similar polarity and steric size.

It is interesting that conversion of the aspartate residue produces a self inhibitor. The analogous serine residue in AIP2 (**1.15**) when exchanged with alanine in the Mayville *et al.* study produced a potent cross-group inhibitor. However, in contrast, that compound was also reported to be a self activator.[162]

The team noted that changes to residues in the macrocycle produced very large reductions in agonist potency, whereas residues in the tail only produced mild changes in activity. This observation, twinned the previous success of the truncated AIP2 (**3.4**) analogue in the Lyon *et al.* study, led to the production of a truncated AIP1 analogue (**3.5**, Figure 89). Whereas the truncated AIP2 was a self activator and a cross-group inhibitor; the truncated AIP1 is a weak self inhibitor and a cross-group inhibitor.

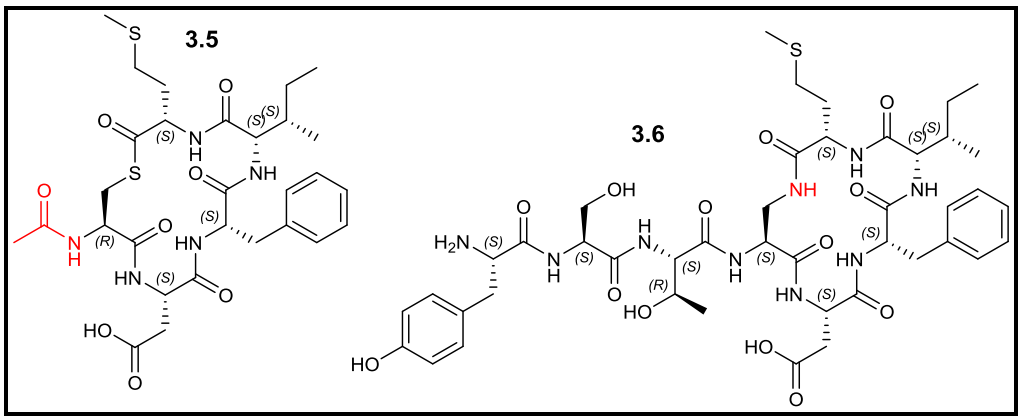


Figure 89: truncated AIP1 (**3.5**) and the lactam analogue of AIP1 (**3.6**)

Finally, McDowell *et al.* produced a lactam AIP1 analogue (**3.6**). In contrast to the AIP2 lactam analogue previously examined, the AIP1 lactam analogue could activate the AgrC1 receptor. This successfully refuted the proposal that an

S-acylation is required for receptor activation, as the lactam moiety cannot react in this manner.

During this research programme, the team also identified the most recent *agr* group, *agr-IV*. AIP4 (**1.17**) differs from AIP1 (**1.14**) only at position 5 where a tyrosine instead of an aspartic acid residue is present. AIP1 was shown to inhibit virulence of putative *agr-IV* strains while *agr-IV* supernatant (containing AIP4) effectively inhibited the activity of other *agr* groups.

3.1.1.4 Lyon's second study[307]

In a second study by Lyon *et al.*, the team focused on the ligand interaction with the receptor. They aimed to discover both the group specificity determinant of the receptor and the mode of ligand binding.

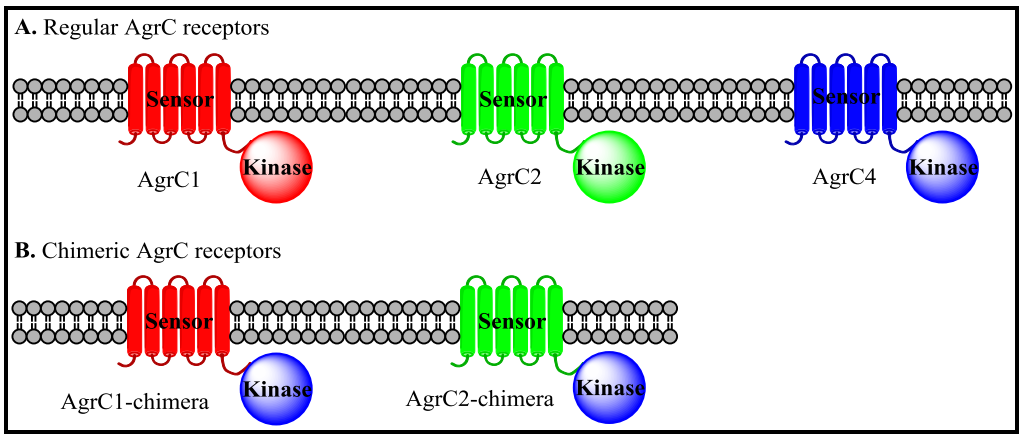


Figure 90: Diagram of **A.** the regular AgrC1, AgrC2, and AgrC4 histidine kinase receptors and **B.** the chimeric AgrC receptors

To identify the group specificity determinant the group created chimeric receptors, the sequence for N-terminal sensor domains from *agrC1* and *agrC2* were fused to the histidine kinase domain of *agrC4* (see Figure 90). Activation and inhibition curves were attained with the addition of culture supernatants and synthetic AIP. The results for receptors with an AgrC1 N-terminal sensor domain were identical to the wild type AgrC1 receptor and the receptors with an AgrC2 N-terminal sensor domain produced results identical to wild type AgrC2 receptors. This data proves that the group specificity determinant resides in the N-terminal sensor domain of the AgrC receptors.[307]

The team then moved on to analyse the mode of AIP binding. Initially, they used a bacterial bioreporter assay to determine activity; they used 1 μM AIP1 (**1.14**) to activate the receptor and then determined that washing the bacteria could significantly reduce activity, however, it was never eliminated. This supported previous findings by McDowell *et al.* that suggested acylation of AgrC is not required for activation since as a thiol ester formation would cause irreversible activation which could not be affected by washing. However, it was not conclusive as there was still the possibility that bound receptors could be recycled with newly produced receptors requiring a constant extracellular concentration of AIP1 (**1.14**) for activation. Similar results were found using AgrC2 reporters and for trAIP2 (**3.4**) inhibition. The team went on to pretreat the reporter strains with antagonist or buffer followed by washing and a later addition of activator. Both produced very similar results indicating that inhibition by these compounds is reversible.

Agonist dose-response curves were generated for increasing antagonist concentrations. The curves shifted in a parallel right hand manner with no effect on the maximum response to the agonist. Pharmacological analysis revealed Schild slopes which were considerably lower than 1 which is normally observed in simple competitive antagonism. It is possible that this may be due to the receptors interaction as a dimer (most receptor histidine kinases form dimers).

3.1.1.5 Lyon's third study[124]

This study was focused on developing the SAR especially examining the functions of the tail and macrocyclic regions and key determinant residues in each of the *agr* groups.

Initially, the team analysed the dynamic structure of AIP2 and related compounds using two dimensional ^{1}H NMR. Chemical shift differences between the backbone amide protons of AIP2 (**1.15**) and those of truncated AIP2 (**3.4**) and alanine substituted AIP2 analogues were assessed. Alanine substitution at any position slightly affects the shift of the surrounding proton signals without affecting distal parts of the amide backbone, thus suggesting that the side chains

of amino acid residues in the AIP2 macrocyclic region do not affect the macrostructure of the tail region and *vice versa*. Furthermore, truncated AIP2 (**3.4**) showed no significant differences in amide chemical shift supporting the structural independence of the tail and macrocyclic regions. Experiments with the AIP2 lactam analogue (**3.6**) revealed several significant amide, α, and β proton shift differences within the macrocycle with no significant alterations to the signals of the tail region. This further supports the structural independence of the two regions and the large differences may explain the significant drop in agonist activity between AIP2 (**1.15**) and its lactam analogue (**3.6**). Similar results were obtained in AIP1 (**1.14**) and AIP4 (**1.17**) reinforcing the idea that each region is structurally independent in each AIP ligand.

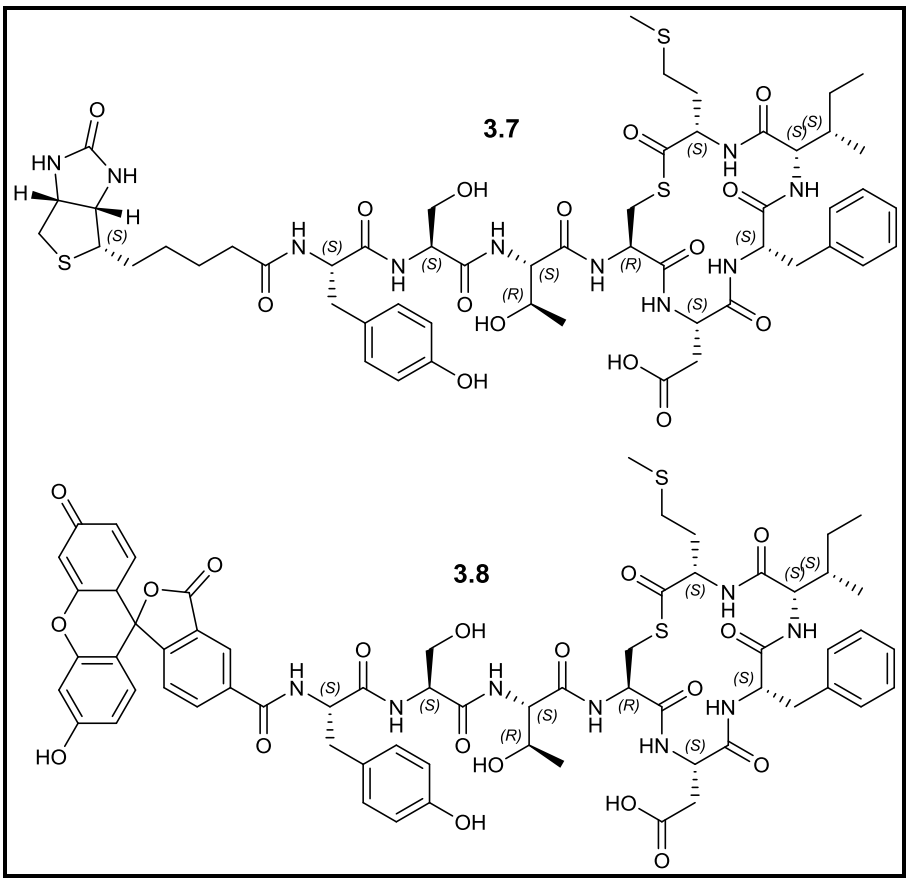


Figure 91: Biotinylated AIP1 (**3.7**) and fluorescein AIP1 (**3.8**)

The team then moved on to examine the function of the N-terminus of AIP1 (**1.14**). Acetylation of the free amine did not significantly affect the function of AIP1 (**1.14**) in any experiment attempted. Furthermore, addition of bulky biotin (**3.7**) and fluorescein (**3.8**) groups (see Figure 91) did not dramatically affect

the function of AIP1 suggesting the N-terminus is in a particularly spacious area of the receptor recognition site or, more likely, that it is solvent exposed.

Examination of the function of the methionine residue was performed using hydrophobic residue replacements, similarly to McDowell *et al*.[157] Replacement with leucine and isoleucine did not produce dramatic differences in the functioning of the AIP1 ligand suggesting that the methionine thioether moiety is not necessary for function. This is in contrast to the previous findings of McDowell *et al.* who used norleucine (among other residues) to show that the methionine and the thioether moiety in particular were necessary for AIP1 function.

As the tail length of each native AIP ligand varies and the structure of AIP3 (**1.16**) was previously unconfirmed, the team decided to examine the effects of tail length in AIP3 using the primary DNA sequence to guide their synthetic programme. Initial testing of a synthetic octapeptide did not show *agr-III* activation. The nonapeptide also proved to be an inhibitor of an *agr-III* bioreporter, while the heptapeptide was an agonist. This peptide also could not demonstrate any inhibitory or additive effects when used in tandem with culture supernatant from an *agr-III* strain. It also mimics the behaviour of *agr-III* supernatant in the other *agr* groups. Thus, this confirms that the heptapeptide is the native AIP3 ligand. Interestingly, this data does show the importance of the N-terminus residues, since addition of a single amino acid can abolish activity.

The team synthesised and tested AIP4 in all other *agr* groups. They found that it activated AgrC4 and inhibited AgrC2 and 3 as expected. However, they found that it is an agonist of AgrC1. This is in contrast to McDowell *et al.*[157] who reported that it inhibited AgrC1.

As AIP1 (**1.14**) and AIP4 (**1.17**) differ at only one residue, the team varied this residue to assess effects on group 1 and 4 specificity. The Tyr^5 residue of AIP4 (**1.17**) was modified to phenylalanine without dramatic changes to agonism of AgrC1 or AgrC4, there was also no effect on antagonistic activity against AgrC2 or AgrC3.

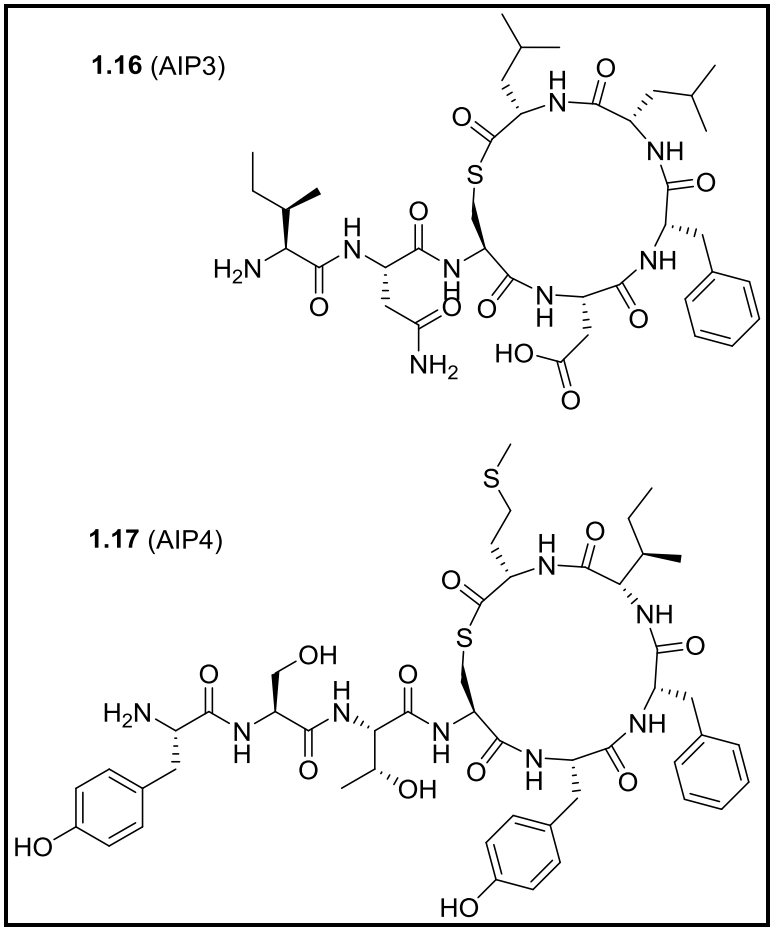


Figure 92: Proven heptapeptide AIP3 structure (**1.16**) and AIP4 (**1.17**)

When switching the Asp^5 residue of AIP1 (**1.14**) for an asparagine residue, activation of group 1 and inhibition of AgrC2 remained similar to AIP1 (**1.14**). This showed that the negative charge of the aspartate was also unnecessary for activity and only a polar residue at this position is required for activity. However, this compound was converted into an antagonist of AgrC4 and an agonist of AgrC3. This represented the first case of conversion of a previous antagonist compound into an agonist in the *agr* system.

Given that the key determinant of AIP2 (**1.15**) activity is the exocyclic Asn^3 residue and removal of the tail creates an antagonist and as the key determinant of AIP1 activity is the Asp^5 endocyclic residue, the team reasoned that tail removal could produce a compound which maintained agonism in AgrC1. A truncated AIP1 peptide (**3.5**) did indeed activate AgrC1 weakly at high concentrations. It also acted as a competitive inhibitor in the presence of AIP1, activation was reduced significantly with an IC_{50} similar to its EC_{50}. This, by definition, makes the compound a partial agonist. The compound possessed no

activity in AgrC4 and only weakly inhibited AgrC3. These data suggest that the tail region does contribute to effective binding in these three systems. Interestingly, the potency of inhibition against AgrC2 was maintained, seemingly indicating that the tail is unnecessary for binding but vital for activation.

The team also tested a (Ala^2)trAIP1 (**1.20**) to ascertain whether mutation of the aspartate residue converted the agonist to an antagonist as previously observed in the full length AIP1 (**1.14**). This compound did not activate AgrC1 and was a potent pan-group inhibitor reinforcing the importance of this residue.

Finally, the team used chimeric AIP analogues containing a tail region from one group AIP ligand and a macrocycle from another to analyse the group specificity determinant within the AIP ligands. Abbreviations for these compounds will be AIPX/Y where X is the tail number and Y is the macrocycle number. AIP2/1 (**3.9**) inhibited the AgrC2 receptor showing that by adding the macrocycle of AIP1 to the AIP2 tail region, the AIP2 tail orientation must have been altered preventing activation even though the key activation determinant residue of AgrC2, asparagine, is still present in the tail region. The key activation determinant reside for AgrC1, aspartate, is also present, however, AIP2/1 (**3.9**) also inhibited the AgrC1 receptor suggesting that the AIP2 tail region eliminates the compound agonistic ability. This chimeric peptide also inhibits at AgrC3 and AgrC4. The reverse chimera, AIP1/2 (**3.10**), is a pan-group inhibitor. The IC_{50} data suggest that the AIP1 tail addition increases affinity for AgrC1, AgrC3, and AgrC4 without affecting the affinity for AgrC2. Furthermore, NMR studies confirmed again the structural independence of the two regions by showing that chemical shift differences were small to insignificant when comparing the chimeric analogues with the parent compounds.

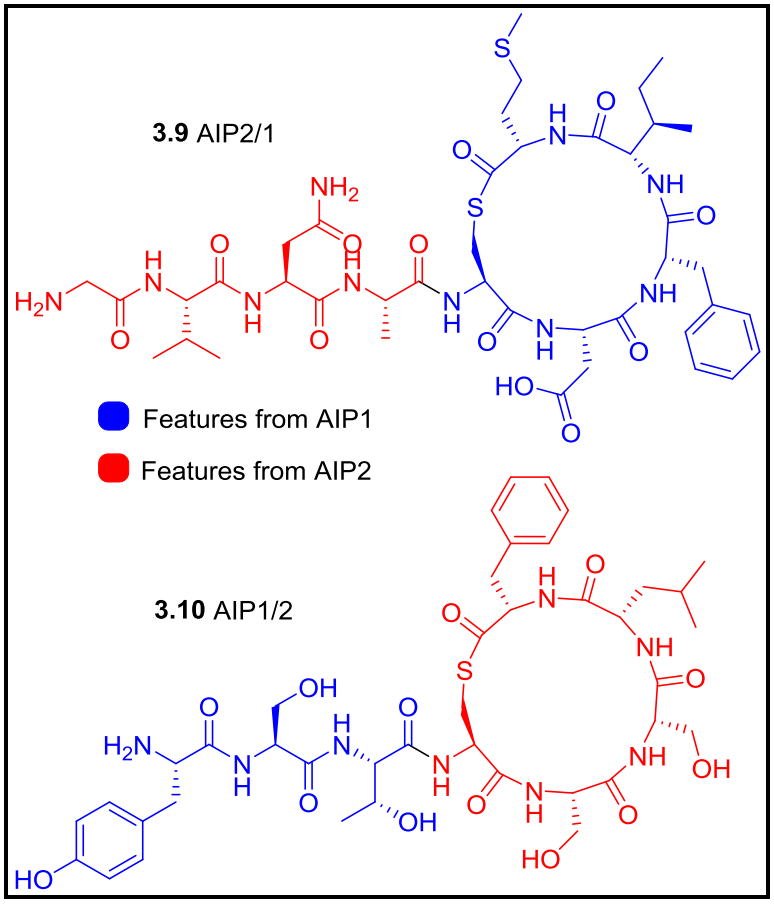


Figure 93: Diagram of chimeric AIP compounds AIP2/1 (**3.9**) and AIP1/2 (**3.10**)

3.1.1.6 Scott *et al.* study[308]

This study piloted a new strategy for the synthesis of AIP analogues. Briefly, instead of synthesising the linear peptide, cleaving the peptide from the resin, selectively deprotecting the cysteine, then cyclising as in previous strategies; the team synthesised the linear peptide on the resin, selectively deprotected the cysteine, formed the thioester bond with the C-terminal amino acid residue, cleaved the peptide from the resin, and then cyclised *via* the formation of an amide bond. Theoretically, cyclisation via an amide is more favourable than cyclisation *via* a thioester. Furthermore, this would allow a facile method for varying the C-terminal residue of AIP analogues. This would be especially useful as this residue had previously been seen to be important for AIP activity.

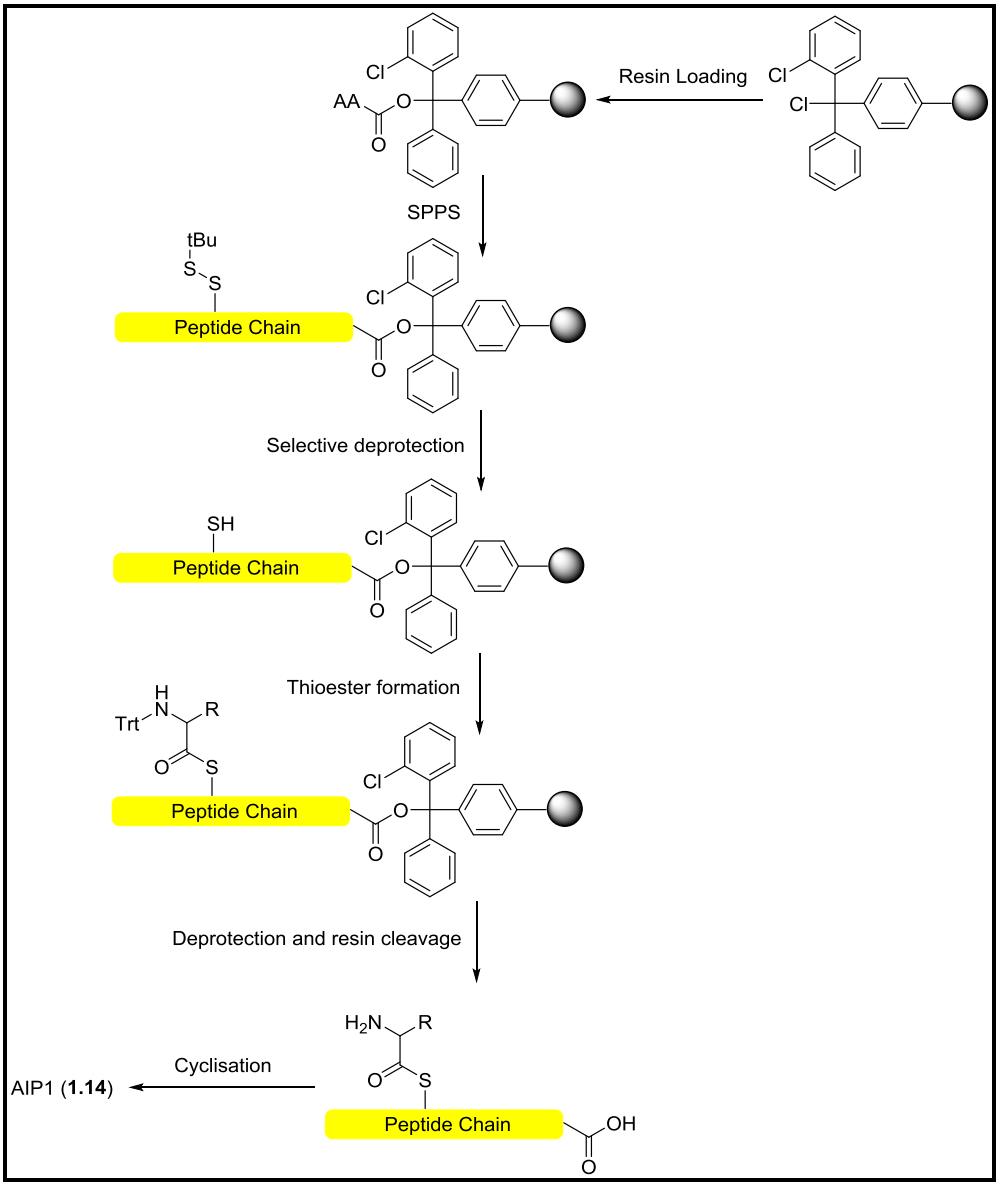


Figure 94: Scheme showing the branched synthetic strategy of Scott *et al.*[308]

Following the development of the synthesis, the team synthesised three analogues. The first added a further methylene group to the Ala[5] modification which had previously been observed to be a potent cross group inhibitor. Surprisingly, addition of a single methylene group reduced antagonist potency fairly significantly. The team believed that the steric bulk of the side chain could negatively affect the interaction with the receptor.

Further analogues were synthesised by replacing the N-terminal tyrosine with a photoactivatable biaryl ketone group which could be useful for labeling and mapping the AgrC recognition site. These analogues acted as inhibitors of both AgrC1 and AgrC2 which would make them useful functional probes.

3.1.1.7 George *et al.* study[309]

This work aimed to discover a minimal AIP inhibitory pharmacophore based on the previously analysed trAIP2 (**3.4**) structure. The team aimed to systematically perturb every structure possible to address its importance to inhibitory activity.

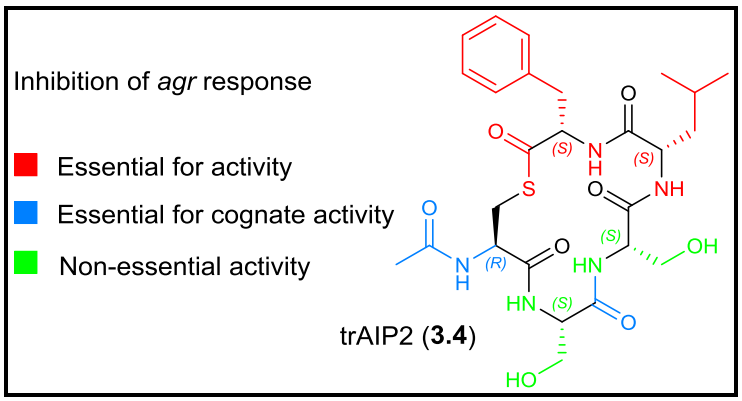


Figure 95: trAIP2 colour coded to highlight structures found to be required for cognate (AgrC2) and non-cognate inhibition. Adapted from George *et al.*[309]

Previous studies suggested the requirement of both phenylalanine and leucine residues, however, the two serine residues seemed to be unnecessary. Therefore, the team individually exchanged each serine with glycine and also produced an analogue where both serine residues were replaced with glycines. The team also synthesised a series of *N*-methylated analogues to investigate the function of the amide backbone. To see if alterations to side groups and the amide backbone could be combined, they also syntheised an analogue where both serine residues were replaced by a simple alkyl linker of the same length. A truncated AIP2 lactam analogue and an analogue lacking the acetylated α-amino group of cysteine were also synthesised.

In general, each compound had a reduced antagonistic activity against AgrC2 in comparison to the activity against other AgrC receptors. For less potent analogues, this difference increases dramatically.

Serine modifications were well tolerated. Replacement with glycine resulted in less than five-fold reductions in activity and some compounds actually increased in potency in some groups. Generally, *N*-methylation of the serine residues was also well tolerated. However, *N*-methylation of either leucine or

phenylalanine residues resulted in complete loss of activity. This could be indicative of stabilising hydrogen bonds at these positions as *N*-methylation prevents the formation of amide hydrogen bonds.

The lactam and methylene linker analogues both inhibited each group but with a significantly less potent IC_{50}. Although the thiolactone structure is therefore not required for inhibition in the truncated analogues, the lactam structure is not well tolerated. The methylene linker analogues loss of activity cannot be explained simply by the lack of side chains as the glycine analogues maintained potency much better. It is likely that the loss of an amide bond and greater structural constraints due to the methylene linker are responsible. The loss of the acetylated amine of cysteine resulted in a dramatic loss of inhibitory activity demonstrating the importance of this group.

Furthermore, the team used NMR studies in order to correlate changes in chemical shift with observed activity in each analogue. They could see no clear trend between chemical shift and potency. Three of the peptides produced double the number of expected resonance signals. ROESY ^{1}H-NMR studies revealed this is caused by cis-trans isomerism at the amide bond between Ser^{2} and *N*-methyl-Ser^{3}. As *N*-methylation is known to increase the incidence of cis-trans amide bond isomerism, this was unsurprising and the multiple resonance signals in the other analogues were assumed to be caused by the same phenomenon.

3.1.1.8 Geisinger *et al.* study[215]

Geisinger *et al.* examined both AgrC1 and AgrC2 to try to elucidate the interaction of the ligands with the receptor, the mechanisms of the receptor activation, and the sensor domain activation determinants.

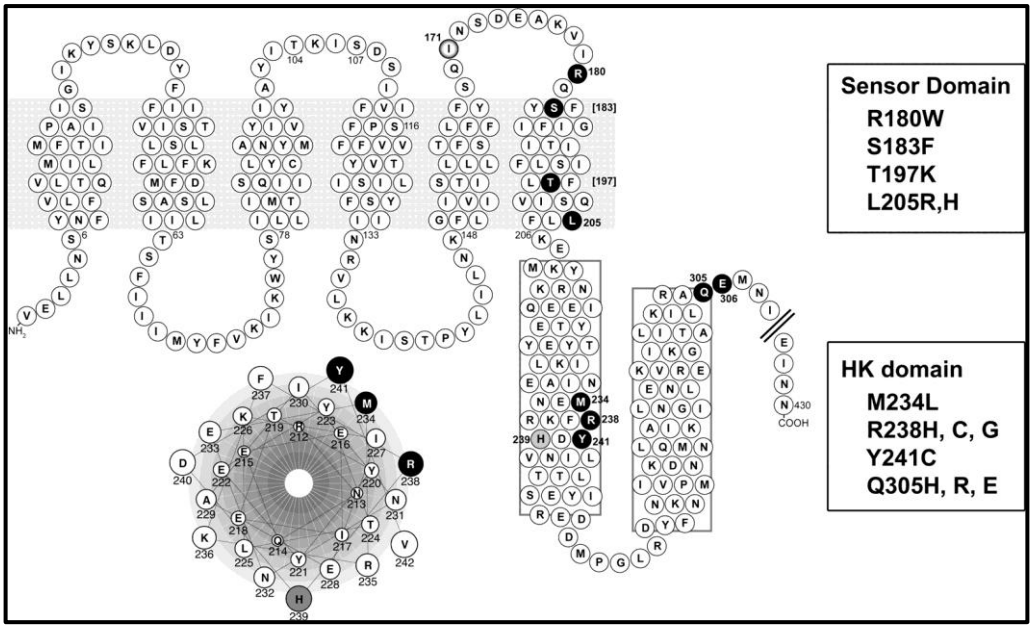


Figure 96: Map of significant mutations in the AgrC1 receptor from Geisinger *et al*.[215]

First, using error-prone PCR, they created a library of constitutively active mutants of AgrC1. Several key residues were identified. Four key alterations are present in the histidine kinase domain; they are M234L, R238H/C/G, Y241C in the dimerisation histidine phosphotransfer subdomain and Q305H/R/E in the junction between the dimerisation histidine phosphotransfer and catalytic ATP-binding domains. One residue is present in the interface between the sensor and histidine kinase domains, L205R/H. Three key residues are also present in the sensor domain, R180W, S183F, and T197K. The constitutive activity of receptors containing mutations in the histidine kinase domain were not generally affected by the addition of exogenous AIP ligand. In contrast, constitutive receptors containing alterations in the sensor domain were affected by the addition of exogenous ligand. AIP1 further agonised the receptor whilst AIP2 antagonised the constitutive activity. AIP3, AIP4 and (Ala^5)AIP1 did not affect the mutated receptors. By definition, a compound which inhibits a constitutively active version of a receptor is an inverse agonist. Further experiments revealed that AIP3, AIP4, and (Ala^5)AIP1 could prevent the inverse agonistic activity of AIP2, thereby demonstrating they do in fact bind the receptor. By definition, a compound which binds but does not antagonise a constitutively active version of a receptor is a neutral antagonist.

The roles of the significant residues residing in the histidine kinase domain were also determined. Specifically, R238 resides next to H239 which is the histidine responsible for transferring phosphate to AgrA. Further mutations were tested including replacement with the negatively charged glutamic acid and the positively charged lysine. R238E is a constitutively active receptor unaffected by AIP ligand interactions at the sensor domain; R238K is a weakly constitutively active receptor which is strongly activated by the cognate ligand and strongly inhibited by inverse agonists. This indicates that it is not simply a positive charge required at this position for regulation of agonism but specifically arginine with its specific hydrogen bonding properties and delocalised positive charge.

Furthermore, the team analysed the sensor domain determinants of agonism. They selected for AgrC1 mutants which are activated by AIP3 (**1.16**) and found L62I I171K-AgrC1. Further research suggested that I171K was the modification causing this cross group agonism. AgrC1 I171K was activated by AIP3 (**1.16**) , AIP1 (**1.14**), AIP4 (**1.17**), (Ala^5)AIP1 (**1.55**) and AIP from *S. caprae*. This receptor was also unaffected by AIP2 (**1.15**), and AIP from both *S. epidermidis* and *S. simulans*. Furthermore, AIP2 (**1.15**) and AIP from both *S. epidermidis* and *S. simulans* could not inhibit the activation caused by the other ligands thereby indicating they can no longer bind the recognition site of the receptor. This highlights the importance of I171 to the recognition site of the receptor.

3.1.1.9 Cisar *et al.* study[125]

The aim of this study was to elucidate the signal transduction mechanism of AgrC as a model class 10 histidine protein kinase receptor. AgrC possesses many of the properties of this class of receptor; specifically, it has a polytopic transmembrane sensor domain and an arginine adjacent to the active histidine residue alongside other common markers.

Initially, the team demonstrated the expected formation of AgrC receptor dimers using coimmunoprecipitation techniques. Strains lacking the *agr* locus were transformed with plasmids containing *agrC-ha* and another containing

agrC-gfp. The AgrC-GFP and AgrC-HA were proved to be active using the previously discussed β-lactamase bioreporter strains. These tagged proteins coprecipitated both in the presence of AIP and when AIP was not present. This indicates that the receptors are pre-formed dimers and do not form dimers in response to the action of the AIP ligand.

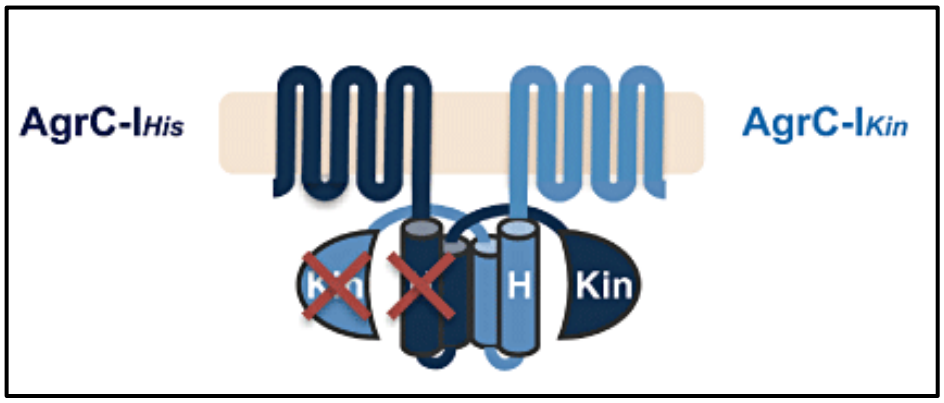


Figure 97: Illustration of AgrC1 dimer structure and subsequent inactivations from Cisar *et al.*[125]

Typically, histidine protein kinase dimers have two independent sensor domains. However, the histidine subdomain is required to interact with the dimeric partner kinase subdomain to form a functional histidine kinase domain (see Figure 97). Using a *Δagr* strain, the team could transform two plasmids into the bacteria creating a new bioreporter strain with a different receptor dimer structure each time. Each plasmid contained the sequence for a single copy of the receptor dimer. A small proportion of the protein expressed by these plasmids would form homodimers, however, the majority would form heterodimers.

3.1.1.10 Summary of Previous research

In summary, the following were established with regards to the AIP/AgrC interaction:

- There are four *agr* groups with four distinct AgrC receptors and four distinct AIP ligands
- Receptors contain N-terminal sensor domain and C-terminal histidine kinase domain
- AgrC receptors are preformed dimers
- Dimers transduce signal symmetrically across the dimer surface
- Native ligands are intra-group agonists and inter-group antagonists
- Observed inhibition and activation is generally competitive and reversible
- The tail and macrocycle regions are structurally independent
- Changes to thiolactone can preserve inter-group inhibition, however, they dramatically reduce intra-group agonism
- AIP1 (**1.14**) is an inverse agonist against AgrC2, AIP2 (**1.15**) is an inverse agonist against AgrC1, others are neutral antagonists
- In AIP1 (**1.14**) , Asp^5 is an important activity determinant
- Phe^6, Ile^7, and Met^8 also seem to be important for binding in AIP1 (**1.14**)
- N-terminal could be solvent exposed in AIP1 (**1.14**) as bulky groups can be incorporated here without affecting activity
- In AIP2 (**1.15**) , Asn^3 is an important activity determinant
- Leu^8, and Phe^9 seem to be important for binding in AIP2 (**1.15**)
- Ser^6, and Ser^7 seem to be unnecessary for activity of AIP2 (**1.15**)
- Truncated tailless analogues are often potent inter-group inhibitors
- α-Amino acetyl moiety is required for activity of trAIP2 (**3.4**)

Having reviewed the existing literature, there are still some questions which are yet to be answered. It was surprising to realise that a systematic peptoid or *N*-methyl scan of the potent pan-group inhibitor, (Ala^2)trAIP1 (**1.20**) had not yet been performed. Given that the importance of amide bond configurations to

the overall configuration of cyclic peptides was known three decades ago[310] and that *N*-methyl or peptoid modifications are often used to improve the drug-like properties of a compound or alter its configuration,[311] this was considered to be a neglected line of investigation.

It was also noted that there is considerable knowledge of the SAR for each of the native ligands and closely related analogues. However, there is limited data on compounds which are structurally similar to multiple endogenous ligands; analogues which, structurally speaking, lie between the four known AIP ligands. As modified versions of each AIP ligand are generally potent inter-group antagonists while being weak intra-group antagonists or even weak agonists, it was sensible to consider that compounds with structural features from multiple ligands may be improved pan-group inhibitors.

Finally, it has been reported that isoleucine and valine residues in AIP1-4 can have strong effects on the conformation of the amide backbone due to the steric interactions caused by the β-branched structure.[311] To some extent, threonine's hydroxyl group has been reported to have a similar effect.[311] Therefore, as previous work had identified a potent inhibitor, truncated (Ala^5)AIP1 (**1.20**), which contains isoleucine, examination of the effects of exchange with both valine and leucine could reveal the effects of this β-branched structure. This is especially interesting as both AIP1 (**1.14**) and AIP4 (**1.17**) contain an isoleucine while AIP2 (**1.15**) and AIP3 (**1.16**) both contain a leucine at this position. It was considered that the conformational effects of leucine/isoleucine may be causing inter-group variability in the AIP ligands.

3.1.2 Contemporary research

As this research programme was conducted, several relevant studies were also published extending the knowledge of the AgrC/AIP structure activity relationships further.

3.1.2.1 Tal-Gan *et al.* studies[312-314]

Initially, Tal Gan *et al.* synthesised a panel of analogues to fully characterise and assess the SAR of AIP3 with the AgrC receptors.[312] To begin, the team performed a systematic alanine and *D*-amino acid scan to reveal significant

residues and stereocentres to inform the design of later compounds. This systematic study revealed two different trends in the SAR. Firstly, the trend for inhibition of AgrC1, AgrC2, and AgrC4 is discussed (see Figure 98), followed by the trend for interaction at AgrC3 (see Figure 99).

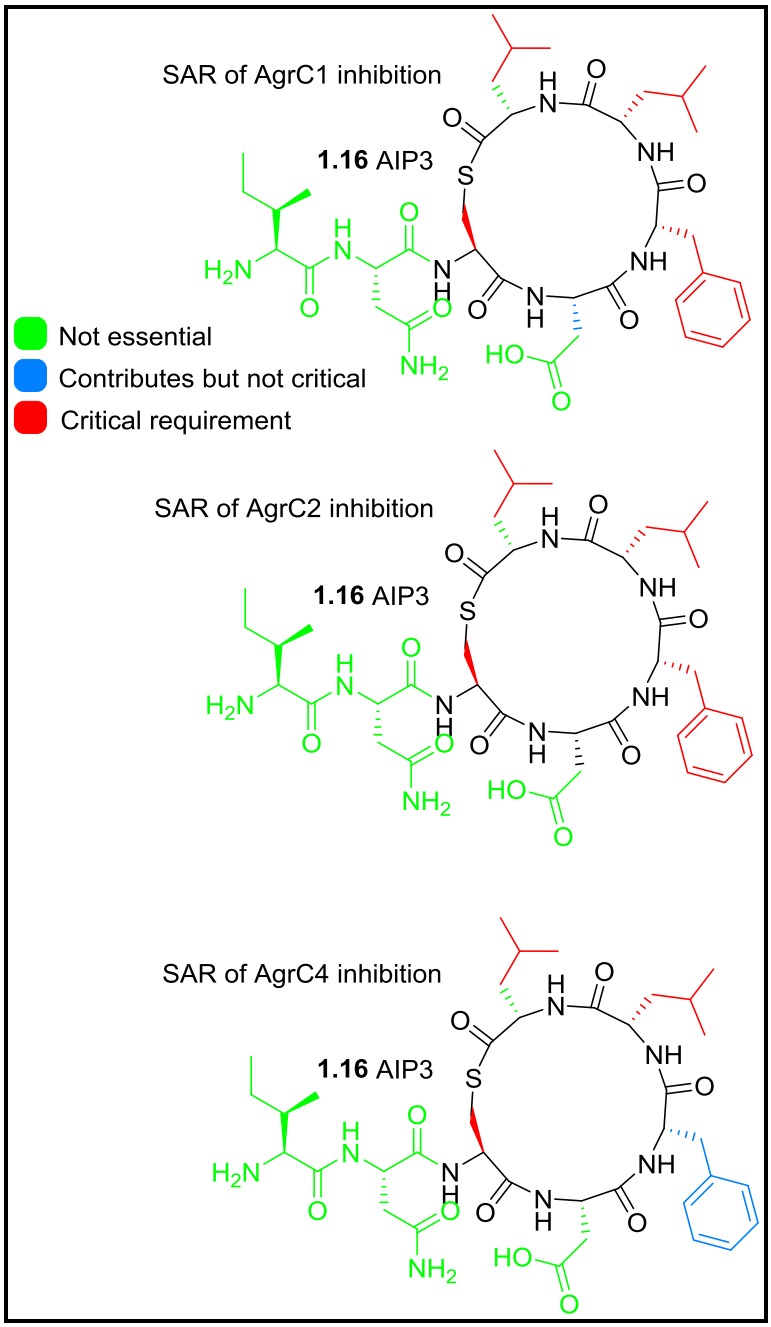


Figure 98: Diagram illustrating the SAR of intergroup inhibition by AIP3 (**1.16**)

Similarly to studies using AIP1 (**1.14**) and AIP2 (**1.15**), mutations of the tail residues resulted in analogues with similar cross group inhibition properties. Alanine substitution of Phe^5, Leu^6, or Leu^7 resulted in a dramatic loss of inhibition in each AgrC receptor. *D*-amino acid substitution of Phe^5 or Leu^6 was

also not well tolerated. In fact, (*D*-phe[5])AIP3 and (*D*-leu[6])AIP3 both seemed to activate the AgrC2 receptor. However, *D*-amino acid substitution of Leu[7] showed inhibitory activity in AgrC1, AgrC2 and AgrC4, indicating that stereoconfiguration may not be as important for binding at this position. This is similar to observations by McDowell *et al.* who found these corresponding spatial positions to be important in AIP2 but stereoconfiguration to be less important.[157]

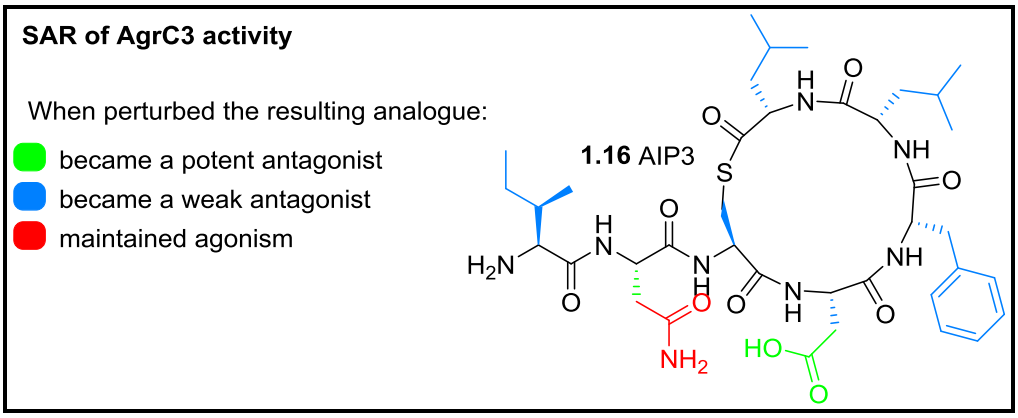


Figure 99: Diagram showing the SAR of AIP3 at AgrC3.

Cys[3] and Asp[4] were found to significantly contribute to receptor inhibition; (*D*-cys[3])AIP3 was 20 fold less active than AIP3 and (*D*-asp[3])AIP3 was 28-fold less active indicating that the stereoconfiguration of these residues is important for receptor binding. Most interestingly, replacement of Asp[3] to alanine produced an improvement in potency of roughly 10-fold in antagonism of AgrC1, AgrC2 and AgrC4. This is a 5- to 24-fold improvement over the corresponding modification in truncated AIP1 and further highlights the importance of this position for producing cross-group inhibitors.

This panel of analogues was also used to produce data on the structure activity relationship of AIP3 agonism at AgrC3. The exocyclic Ile[1] tail residue is important for activation, modification to either the *D* isomer or alanine converted AIP3 to a weak antagonist. Modifying the other tail amino acid, Asn[2], to a *D*-residue converted AIP3 to a strong antagonist while using an alanine maintained agonistic activity. This shows, as previously observed in AIP1 and AIP2, that the tail is important for activation of the cognate AgrC receptor.

Examining the macrocyclic residues, Phe[5] and Leu[6] were again shown to be important, this time for maintaining agonistic activity. Either modification resulted in weak AgrC3 inhibitors. Furthermore, the stereochemistry of Leu[7] did not seem to be important as the (*D*-leu[7])AIP3 analogue maintained agonistic activity, however, the alanine analogue was a weak antagonist. The activation trends were similar to the inhibition trends seen for Phe[5], Leu[6], and Leu[7] supporting the importance of the presence of all three residues but with the stereoconfiguration of Leu[7] not being as important.

The SAR trends for the initial alanine and *D*-amino acid scan analogues were confirmed using a hemolysis assay which verified the activity of the compounds *in vitro*. After their structure activity trends had been confirmed, the team used the data to design a second generation of AIP3 based analogues. The second series included analogues with multiple alanine analogues, alternate aromatic analogues in place of Phe[5], and both truncated and elongated tail regions.

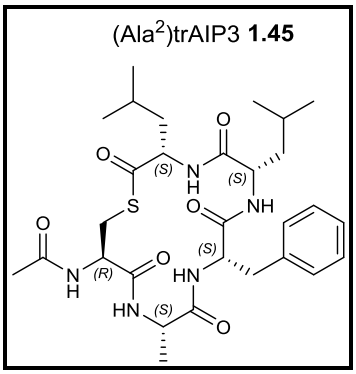


Figure 100: Structure of potent analogue (Ala[2])trAIP3 (**1.45**)

Specifically, the truncated analogue trAIP3 was found to be a weak self-inhibitor, similar to findings with trAIP1 (**3.5**) and trAIP4 but in contrast to trAIP2 (**3.4**). The truncated analogue showed similar inhibitory activity in AgrC2 and AgrC4 with only a mild loss of inhibition at AgrC1. This suggests that the tail is not important in the production of cross-group *agr* inhibitors. When (Ala[4])AIP3 was truncated it produced a potent cross group inhibitor which has an IC_{50} of less than 1 nM (Figure 100). This analogue is a potent, structurally streamlined, pan group inhibitor of AgrC and represents a very promising scaffold for further optimisation and development.

To enrich the understanding of the three dimensional structure of each native AIP ligand and relevant analogues of AIP3, solution structures were established using NMR studies.[313] This study wanted to generate a mechanistic understanding of AgrC binding and inhibition. However, it is likely that, upon receptor binding, ligand conformation changes and adopts a more stable bound configuration. Furthermore, the solution conditions used (30% MeCN pH 3.65) were not similar to the native conditions. Finally, the team proposed calculated structures for each compound analysed. This is an oversimplification of macrocyclic peptides which are dynamic and able to access different conformations. Nevertheless, the findings of Tal Gan *et al.* could be correlated to their previous biological findings and could therefore represent some reflection of the conformational reality.

To produce a three dimensional structure, the team used COSY and TOCSY spectra to fully assign NMR signals of each molecule and then used ROESY spectra to find ROE signals between individual protons. Using the ROE data, a series of interproton distance restraints was created with a possible 20% distance error applied. The structure was then minimised using torsion angle molecular dynamics and internal variable dynamics.

A variety of analogues were subjected to NMR analysis including all four native AIP ligands and a range of AIP3 analogue representing a range of different activities and potencies in AgrC3 and other AgrC receptors. Significantly, both (Ala^4)AIP3 and its truncated analogue **1.45** were included in the panel. Analysis of AIP3 and (Ala^4)AIP3 revealed significant differences in conformation. AIP3 possess three extruding hydrophobic residues, Phe^5, Leu^6, and Leu^7 forming a structure which the team named a "hydrophobic knob" (Figure 101); it appears that the Asp^4 side chain forces both the tail and phenylalanine side chain away from the core of the macrocycle to correctly form this hydrophobic structure. However, in (Ala^2)trAIP3 (**1.45**), both Phe^5 and Ile^1 from the tail region are oriented back towards the macrocycle preventing the correct formation of this "knob". It still seems to possess a smaller knob which allows receptor binding but the team believe that the incorrect positioning of Ile^1 then prevents activation of the receptor.

Moreover, trAIP3 appeared not to possess a regular "hydrophobic knob" region, which could explain its weaker inhibitory properties. Meanwhile (Ala[2])trAIP3 (**1.45**) possessed a similar hydrophobic knob to the parent compound allowing better binding and therefore more potent inhibition of AgrC3.

Interestingly, when the determined structure of AIP4, which is closely related to AIP1, was overlaid with an X-ray diffraction crystal structure of AIP4 bound to a quorum quenching antibody, the team believed it showed a moderate to good overlap (Figure 102).[218]

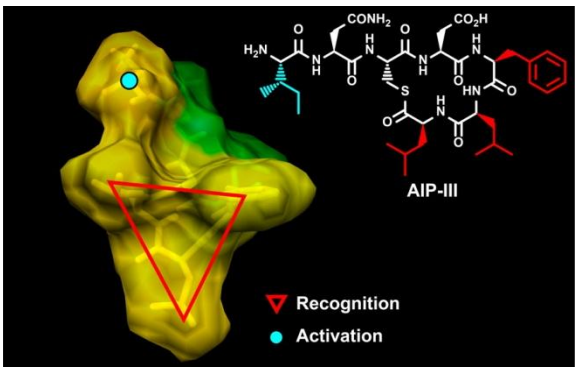


Figure 101: The "hydrophobic knob" of AIP3 and its activation point from Tal-Gan *et al.*[313]

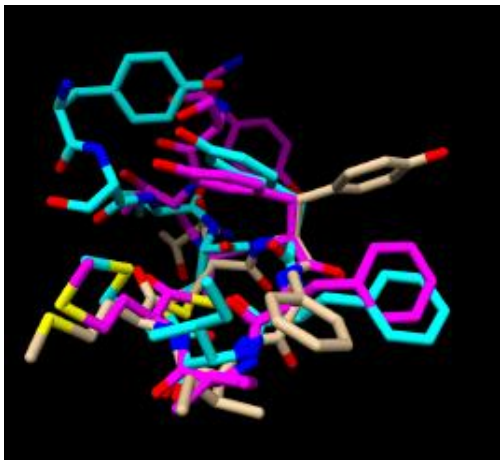


Figure 102: Image from Tal-Gan *et al.* supporting information[313] showing their two calculated conformations for AIP4 in cyan and magenta and a further X-ray diffraction crystal structure from Kirchdoerfer *et al.*[218]

Finally, following their NMR studies, Tal Gan *et al.* published a further study which detailed a peptoid and *N*-methyl scan of AIP3. They considered both the activity of the compounds against AgrC3 and other non-cognate receptors,

AgrC1, AgrC2, and AgrC4. Focusing on the inhibitory activities, *N*-methylation of Ile[1] caused less potent inhibition of non-cognate receptors.

Furthermore, *N*-Me modifications to Cys[3] or Asp[4] and using a peptoid version of Asp[4] produced mild reductions in inhibition of non-cognate AgrC receptors. Phe[5] modification to an *N*-Me or peptoid residue produced no change or even mild improvement in non-cognate receptor inhibiton. Previous work suggested that Phe[5] is very important for binding, however, it appears that its relative position and its amide bond are less important for activity. The amide bonds of Leu[6] and Leu[7] were shown to be vital to inhibition by both forms of modification.

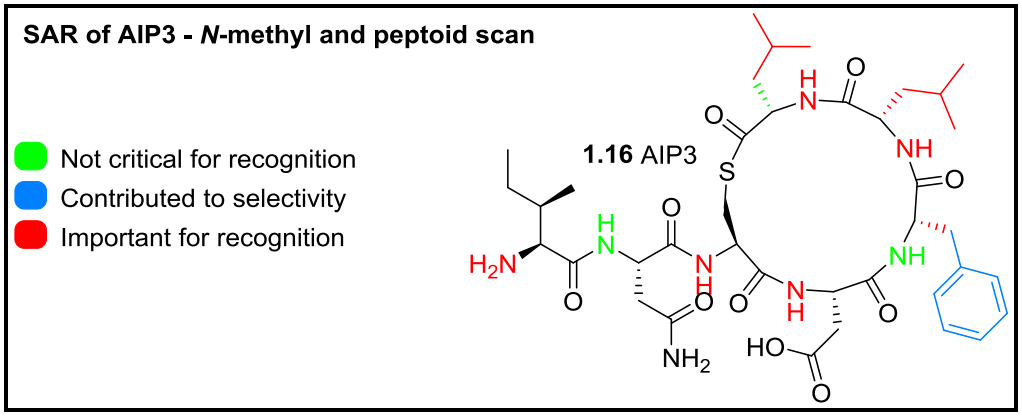


Figure 103: Illustration of the SAR of AIP3 adapted from Tal-Gan *et al.*[314]

This study produced several selective inhibitors, of which few were previously known. Four AgrC3 selective inhibitors, one AgrC2 selective inhibitor, and one AgrC4 selective inhibitor were discovered. Given the high similarity between group 1 and group 4 ligands and receptors, a selective inhibitor highlights how very small changes in the macrocyclic structure can affect interactions with *agr* receptors.

3.1.2.2 Johnson *et al.* study[315]

Finally, the most recent study assessed the effects of altering ring size on the interactions of AIP1 with AgrC1 and AgrC2. EC_{50} in AgrC1 and IC_{50}s in both AgrC1 and AgrC2 were found using a previously discussed cell based β-lactamase assay. Binding affinity was also assessed using a system with AgrC1 receptors embedded in nanodiscs which was pioneered by Wang *et al.*[166] Previous use of this system helped them to reveal that sensor domain activation

is transmitted to the histidine kinase domain by the rotation of an α-helix between the membrane bound and cytoplasmic domains of the receptor.

The team discovered that changing the size of the macrocycle in AIP1 is not well tolerated for activation of the AgrC1 receptor. Deletion of amino acids or proline substitution results in inactive analogues. Even more minor alterations like methylene insertions produce inactive analogues in most positions. The only exception is the second endocyclic Asp^5 position which can tolerate a methlyene insertions. NMR studies suggest that this is because the overall conformation is more resistant to ring expansion at this location. Cross-group inhibition was more tolerant of changes. Interestingly, an *L*-homocysteine analogue was well tolerated whereas a *L*-β-homo-methionine was not tolerated. This seems to indicate that the distance between the thioester linkage and methionine residue is important for inhibitory activity. Unexpectedly, when *L*-β-homo-alanine was incorporated into the potent cross group inhibitor, (Ala^5)AIP1 (**1.59**), it reverted to an agonist. This could be caused by this residue penetrating deeper into a binding pocket than the alanine present in the inhibitor to regenerate the agonism of the AIP1 parent compound.

3.1.2.3 Summary of contemporary research

To date, four structural features are accepted requirements for activation of a cognate receptor based on both SAR data and NMR studies. These four features are: the tri-residue "hydrophobic knob" on the C-terminus of the peptide, the second endocyclic position must have some steric bulk, the thiolactone bond must be appropriately adjacent to the "hydrophobic knob", and a tail or other anchor point must also be present for activation. Although the details for activation in each group vary, these four criteria seem to be necessary for agonism. For antagonism, the only requirement seems to be a structurally similar "hydrophobic knob" region. No studies have been able to accurately assess the binding state of the peptide ligands so it is possible that the solution-phase NMR studies do not truly represent the reality of the receptor-ligand binding interaction.

3.1.3 Contribution of this research

In the study reported herein, the aim is to discover more potent pan-group inhibitors of AgrC. To do this, the SAR of (Ala^2)trAIP1 (**1.20**), the most potent known inhibitor, with AgrC1 was explored.

A peptoid scan would be performed as it was surprising to learn that the potent inhibitor (Ala^2)trAIP (**1.20**) had not previously been assessed in this way. Peptoids are typically less susceptible to proteases and can be more stable *in vivo*, possibly improving the half life of the compound.

3.2 Results and discussion

The most potent known inhibitor of AgrC1 and AgrC2 at the beginning of the project was a truncated and *N*-acetylated AIP-1 compound, in which the aspartic acid was replaced with an alanine residue ((Ala^2)trAIP1 **1.20**).[124] Using a systematic strategy, an array of compounds was synthesised in the hope that some of the compounds would prove to be more potent, stable, cross-group inhibitors of the *agr* systems of *S. aureus*. In an iterative approach, initial SAR data would be used to guide further inhibitor design efforts.

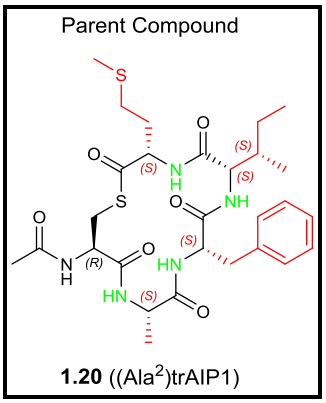


Figure 104: Schematic showing original (Ala^2)trAIP1 parent compound (**1.20**) with residues to be replaced highlighted in red. Amide nitrogens to be used in peptoid scan also highlighted in green.

A series of peptoid analogues was also synthesised, in which the amino acid side-chain groups are located on the α-nitrogen instead of their usual α-carbon position. Peptoids are generally less prone to digestion by proteases and are therefore often more stable *in vivo*.[316] However, by placing the side chain on the nitrogen atom of the amide bond, the orientation of the amide bond can be altered significantly and the hydrogen bonding pattern of the compound can be seriously disrupted.[316] This, in turn, can disrupt the binding of the ligand to the receptor which may make these analogues less potent than the parent compound. By synthesising and testing a series of peptoids, it was hoped that amide bonds which are important for activity would be discovered as well as finding positions where peptoid moieties can be tolerated in the truncated AIP analogues.

Previous work in Chan's group has produced a bacterial strain containing a new *agr* group which was strongly activated by the commonly used inhibitor (Ala[5])AIP1 (**1.59**).[167] As only two residues in AgrC1 were altered in the production of this strain, it is possible that *S. aureus* could mutate and evolve *via* this route effectively evolving "resistance" to any potential AIP based therapies. Hence, it was considered highly valuable to assess the activities of the panel of compounds against this new, more challenging *agr* system alongside the four classical wild type *agr* groups.

Further work in Chan's group also created partially constitutive AgrC receptors (unreported data). Assessment of the impact of the compounds on these receptors was considered worthwhile so that the mode of inhibition could be elucidated. For example, do these compounds promote the off-state of the receptor acting as inverse agonists or do they simply occupy the receptor site preventing binding of the endogenous ligand thereby acting as simple neutral antagonists? It was hoped that this knowledge would result in an improved understanding of the binding of the AIP analogues.

3.3 The Structure-Activity Relationship in AgrC

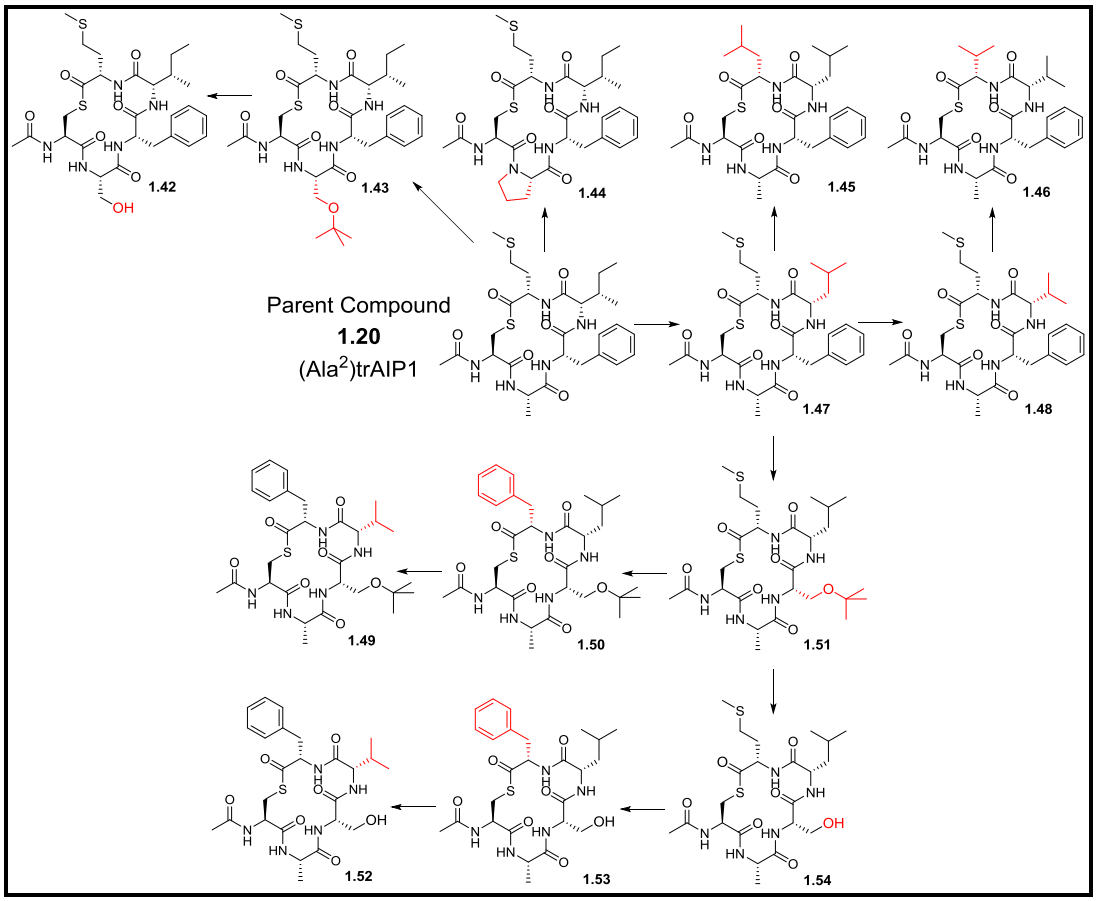


Figure 105: Schematic showing the relationships, i.e. structural evolution, of compounds synthesised in the initial AIP analogue series. Single changes from previous compound in tree are highlighted in red.

In designing the series of AIP analogues for testing, individual amino acids were systematically replaced with physicochemically related residues, e.g. leucine with isoleucine, as well as distinctly different amino acid residues. For example, alanine was replaced with serine (**1.42**) and proline (**1.44**) while isoleucine was exchanged for both leucine (**1.47**) and valine (**1.48**). Given that the synthesis of serine analogues required the purification of a *tert*-butyl protected intermediate, these compounds were also tested for biological activity (**1.43**, **1.49**, **1.50**, and **1.51**). Other analogues synthesised included the installation of phenylalanine for serine (**1.54**) and methionine for phenylalanine (**1.53**), valine (**1.46**), and leucine (**1.45**) (see Figure 105). After testing this initial series of compounds in our bioassay, a further series of analogues was also synthesised to determine IC_{50} values.

The importance of *N*-acetylation of the *N*-terminal amine was also investigated by producing two non-acetylated analogues of known inhibitory AIP analogues.

3.3.1 AgrC1

To assess the inhibitory properties of the library of synthetic AIP analogues, the *agr-I lux*-based reporter assay previously discussed in Section 2.6 was used. A range of inhibitor concentrations was employed, in the presence of AIP1 (100 nM) acting as the activator. Each data point was obtained in triplicate to produce an IC_{50} curve in Prism. Triplicate IC_{50} curves were then obtained calculating the mean and standard deviation from the experimental IC_{50} values. Results are listed in Table 6.

Table 6: Competitive inhibition of native AgrC1 (IC_{50} in nM, n = 3) determined using a staphylococcal *lux*-based reporter. The final AIP-1 concentration is 100 nM. Changes from the parent compound are highlighted in red.

Alteration from (Ala²)trAIP1	#	Macrocyclic peptides	clogP	IC_{50}(AgrC1)
(Ala⁵)AIP1	**1.59**	H-Tyr-Ser-Thr-Cys*-Ala-Phe-Ile-Met*	-	1.3 ± 0.4
AIP2	**1.15**	H-Gly-Val-Asn-Ala-Cys*-Ser-Ser-Leu-Phe*	-	47.0 ± 6.8
Parent and related compounds				
(Ala²)trAIP1 (parent)	**1.20**	Ac-Cys¹*-Ala²-Phe³-Ile⁴-Met⁵*	2.89	5.0 ± 1.4
M5*M*	**3.11**	Ac-Cys¹*-Ala²-Phe³-Ile⁴-*D-Met*⁵*	2.89	> 100
deacetylated	**3.12**	H- Cys¹*-Ala²-Phe³-Ile⁴-Met⁵*	2.80	>5000
Alanine 2 position				
A2P	**1.44**	Ac-Cys¹*-Pro²-Phe³-Ile⁴-Met⁵*	3.43	> 5000
A2S(tBu)	**1.43**	Ac-Cys¹*-Ser(tBu)²-Phe³-Ile⁴-Met⁵*	3.73	12.5 ± 0.6
A2S	**1.42**	Ac-Cys¹*-Ser²-Phe³-Ile⁴-Met⁵*	1.87	38.2 ± 7.4
Isoleucine 4 position				
I4V	**1.48**	Ac-Cys¹*-Ala²-Phe³-Val⁴- Met⁵*	2.37	35.3 ± 2.4
I4V M5V	**1.46**	Ac-Cys¹*-Ala²-Phe³-Val⁴-Val⁵*	3.15	> 300
I4L	**1.47**	Ac-Cys¹*-Ala²-Phe³-Leu⁴-Met⁵*	2.89	3.3 ± 0.0
I4L M5L	**1.45**	Ac-Cys¹*-Ala²-Phe³-Leu⁴-Leu⁵*	4.20	1.6 ± 0.8
deacetylated I4L M5L	**3.13**	H-Cys¹*-Ala²-Phe³-Leu⁴-Leu⁵*	4.11	682.2 ± 51.4
I4L M5V	**3.14**	Ac-Cys¹*-Ala²-Phe³-Leu⁴-Val⁵*	3.67	17.6 ± 7.4
Phenylalanine 3 position				
I4L	**1.47**	Ac-Cys¹*-Ala²-Phe³-Leu⁴-Met⁵*	2.89	3.3 ± 0.0
F3S(tBu) I4L	**1.51**	Ac-Cys¹*-Ala²-Ser(tBu)³-Leu⁴-Met⁵*	2.31	>2000
F3S I4L	**1.54**	Ac-Cys¹*-Ala²-Ser³-Leu⁴-Met⁵*	1.38	83.8 ± 18.3
F3S(tBu) I4L M5F	**1.50**	Ac-Cys¹*-Ala²-Ser(tBu)³-Leu⁴-Phe⁵*	3.58	>500
F3S I4L M5F	**1.53**	Ac-Cys¹*-Ala²-Ser³-Leu⁴-Phe⁵*	1.73	59.9 ± 5.6
F3S(tBu) I4V M5F	**1.49**	Ac-Cys¹*-Ala²-Ser(tBu)³-Val⁴-Phe⁵*	3.05	>1000
F3S I4V M5F	**1.52**	Ac-Cys¹*-Ala²-Ser³-Val⁴-Phe⁵*	1.20	>1000
Peptoid scan				
M5pM	**1.58**	Ac-Cys¹*-Ala²-Phe³-Ile⁴-Nmsp⁵*	3.94	> 300
M5Nmse	**3.15**	Ac-Cys¹*-Ala²-Phe³-Ile⁴- Nmse*	4.15	> 300
I4pI	**1.57**	Ac-Cys¹*-Ala²-Phe³-Nsmp⁴-Met⁵*	3.03	> 300
F3pF	**1.56**	Ac-Cys¹*-Ala²-Nbz³-Ile⁴-Met⁵*	3.25	44.5 ± 17.4
F3pF M5L	**3.16**	Ac-Cys¹*-Ala²-Nbz³-Ile⁴-Leu⁵*	4.56	64.2 ± 14.4
F3pF I4L M5L	**3.17**	Ac-Cys¹*-Ala²-Nbz³-Leu⁴-Leu⁵*	4.56	112.7 ± 11.4
F3pF I4L M5Nva	**3.18**	Ac-Cys¹*-Ala²-Nbz³-Leu⁴-Nva⁵*	4.16	>300
A2pA	**1.55**	Ac-Cys¹*-Nme²-Phe³-Ile⁴-Met⁵*	3.07	> 300

Table 4 continues over the page...

Table 4 continued				
Second generation compounds based on AIP84				
I4L	**1.47**	Ac-Cys[1]*-Ala[2]-Phe[3]-Leu[4]-Met[5]*	2.89	3.3 ± 0.0
I4L M5L	**1.45**	Ac-Cys[1]*-Ala[2]-Phe[3]-Leu[4]-Leu[5]*	4.20	1.6 ± 0.8
I4L M5Nle	**3.19**	Ac-Cys[1]*-Ala[2]-Phe[3]-Leu[4]-Nle[5]*	4.33	5.9 ± 1.7
I4L M5Nva	**3.20**	Ac-Cys[1]*-Ala[2]-Phe[3]-Leu[4]-Nva[5]*	3.80	5.8 ± 1.7
I4L M5Mhs	**3.21**	Ac-Cys[1]*-Ala[2]-Phe[3]-Leu[4]-Mhs[5]*	2.00	21.5 ± 2.2
I4L M5Tfn	**3.22**	Ac-Cys[1]*-Ala[2]-Phe[3]-Leu[4]-Tfn[5]*	3.70	3.9 ± 1.8
I4L M5(*S*)Tfn	**3.23**	Ac-Cys[1]*-Ala[2]-Phe[3]-Leu[4]-*S*-Tfn[5]*	3.70	0.9 ± 0.1
I4L M5Tfb	**3.24**	Ac-Cys[1]*-Ala[2]-Phe[3]-Leu[4]-Tfb[5]*	2.99	43.1 ± 4.0
I4L M5(*S*)Tfb	**3.25**	Ac-Cys[1]*-Ala[2]-Phe[3]-Leu[4]-*S*-Tfb[5]*	2.99	17.8 ± 10.4

Mhs = *O*-Methylhomoserine; *Tfn* = *RS*-6,6,6-trifluoronorleucine; *Tfb* = *RS*-2-amino-4,4,4-trifluorobutanoic acid; *N*mse = *N*-methylsulfanylethylglycine; *N*msp = *N*-methylsulfanylpropylglycine; *N*smp = (*S*)-*N*-(1-methylpropyl)glycine; *N*bz = *N*-benzylglycine; *N*me = *N*-methylglycine. *-* Side-chain-to-tail thiolactone

3.3.1.1 Importance of *N*-terminal acetylation

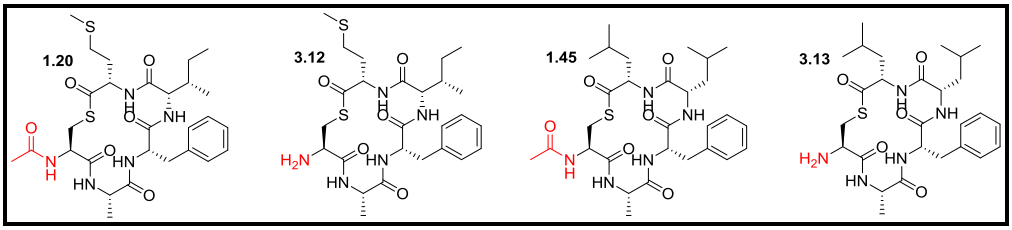


Figure 106: Diagram of non-acetylated analogues **3.12** and **3.13** with their parent compounds **1.20** and **1.45**

In the first instance, the importance of *N*-acetylation was considered. Both compounds, **3.12** and **3.13**, which possess exposed free amine functionalities displayed considerably reduced activity when compared with their *N*-acetylated counterparts. Specifically, compound **3.12** is at least 1000 times less potent than compound **1.20**, while the potency of compound **3.13** was reduced by roughly 500 times in comparison with **1.45**. This demonstrates that *N*-acetylation is vital to the activity of these truncated AIP analogues. This finding is commensurate with the findings of George *et al*. who found that the *N*-acetyl α-amino functionality is required for activity of trAIP2 (**3.4**) as an inhibitor. The reason for the importance of the *N*-acetyl group is unclear. It is possible that the acetyl group is only required to conceal the positive charge which a free amine may display (depending on the pK_a of the amine group) at physiological pH. Alternatively, the sp^2 amide functionality or the simple steric bulk of the acetyl group could be important for inhibition.

3.3.1.2 Varying Ala^2 position

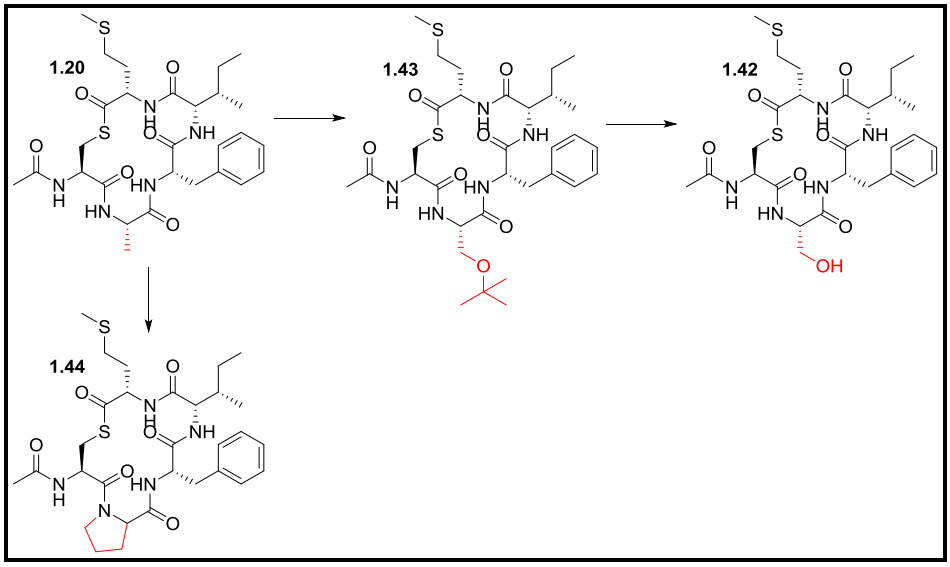


Figure 107: Diagram showing variation of the Ala^2 position

Replacement of the alanine residue at position-2 to serine (**1.42**) and proline (**1.44**) resulted in the complete loss of activity. Proline (**1.44**) was remarkably ineffective, producing a compound at least 1000 times less potent that the parent compound (**1.20**). Proline replacement can significantly alter the orientation of the amide bond and prevents hydrogen bonding at the amide nitrogen. In a small cyclic molecule, these kind of effects are likely to considerably change the shape of the macrocycle thus the loss in activity unsurprising.

The serine replacement proved to be better accommodated, reducing activity by roughly two-fold when *tert*-butyl protected (**1.43**) and roughly 8-fold when deprotected (**1.42**). Previously, Scott *et al.* found that adding a single methylene group to the alanine residue reduced inhibitory activity of the compound by six-fold.[308] It is interesting that when a hydroxy-methylene side-chain is present instead of an ethyl side-chain, inhibition is relatively well maintained. Considering that these groups have a broadly similar steric bulk, the polarity of the hydroxyl functionality might be important in maintaining activity. However, trAIP1 (**3.5**) containing a polar aspartate residue at this position was reported to be a mild agonist by Lyon *et al.*[124] It could be that a negative charge at this position is necessary for activation of AgrC1 while serine, which is not charged, can only inhibit the receptor. Furthermore, the

tBu-protected analogue **1.43**, with increased steric bulk resulted in partially decreased activity. It is possible that the oxygen atom is involved in a hydrogen bond with the receptor stabilising ligand binding.

3.3.1.3 Varying Ile[4] position

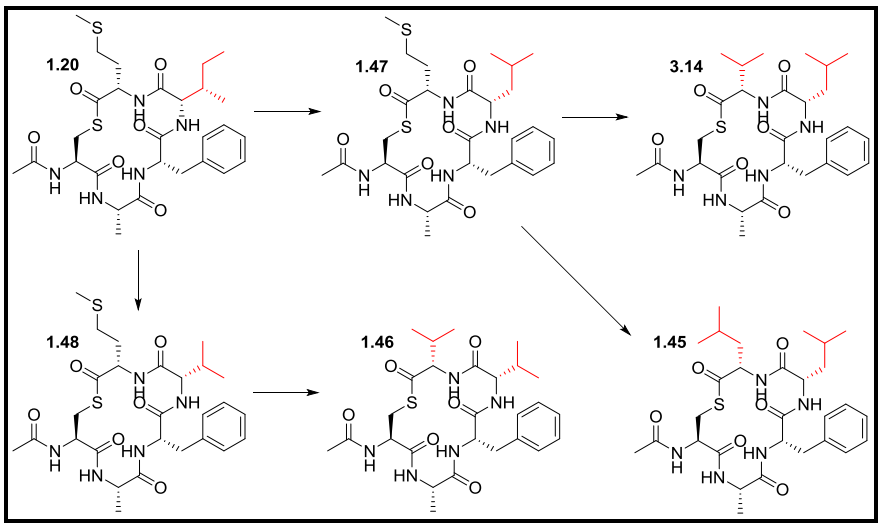


Figure 108: Diagram showing the variation of the Ile[4] position

The isoleucine at position 4 of the parent compound **1.20** proved to be an interesting place for residue replacements. Valine contains a β-branched structure, which is similar to isoleucine, however it an additional terminal methyl group. By substituting isoleucine for valine, the IC_{50} was increased roughly 7-fold (**1.48**). Significantly, when isoleucine is replaced with leucine (**1.47**), which does not contain a β-branched structure, inhibitory potency was improved 1.5-fold, compared to **1.20**. Clearly, the presence of an extra terminal methyl group allows positive bonding interactions with the receptor explaining the increased inhibitory potency of isoleucine and leucine at this position. In contrast, β-branching has previously been thought to effect the conformation of the amide backbone of various macrocyclic peptides explaining the reduced potency of **1.20** and **1.48** in comparison with **1.47**.[311] Furthermore, isoleucine and leucine maintain the same lipophilicity and the variance in the analogues inhibitory activity presents a challenge to the hypothesis by Tal Gan *et al.* that a C-terminal hydrophobic knob is responsible for inhibition. As we see in this case, the reality seems to be more complicated than relying on simple lipophilicity.

Exchanging the methionine at position-5 with valine while maintaining the previous valine (**1.46**) or leucine (**3.14**) modification at position 4 produced further reductions in inhibitory potency. As valine is a hydrophobic residue, this further emphasises that the SAR of this macrocycle relies on more than just lipophilicity. In fact, deploying leucine at this position (**1.45**) produced potency improvements. This strategy produced our strongest inhibitor to date with an IC_{50} of 1.6 nM, roughly three-fold more potent than the parent compound **1.20**. The potency of this compound was later confirmed by Tal Gan *et al.* as it actually displayed a picomolar activity in their hands.[312] Interestingly, the increase in lipophilicity of compound **1.45** did actually reduced the lipophilic efficiency. Nevertheless, since modifications to this position resulted in an increased inhibitory potency, it was considered that variants at the 5-position in the presence of leucine at the 4-position would yield more potent, high quality compounds. This eventually led to the synthesis of the second generation series of AIP analogues (**3.19** - **3.25**).

3.3.1.4 Varying Phe^3 position

As substitution of the position-4 isoleucine with leucine (**1.47**) had been so successful, the analogues which contained the variation of the position-3 residue were synthesised with leucine at positon-4. Thus, replacement of the phenylalanine residue with *tert*-Butyl protected serine produced compounds displaying no significant activity (**1.51**, **1.50**, and **1.49**) in every case. Although this protected residue has a similar lipophilic profile, the planar aromatic properties of the phenylalanine side-chain are likely to be better suited to the receptor environment, e.g. necessary for π-π interactions.

When a serine residue was present in the 3-position (**1.54**), the compound displayed a reduced potency (by roughly 25-times). This is a further challenge to the "hydrophobic knob" hypothesis as serine is a very polar residue replacing one of the key hydrophobic residues of the putative "hydrophobic knob". As the compound is still an effective nanomolar inhibitor, it is considered that the "hydrophobic knob" hypothesis is a simplification of the true SAR of these ligands. Lipophilicity is obviously important for receptor binding as the SAR data shows a preference for hydrophobic residues (Figure 109). However, this

seems to be a more general correlation than relating to specific key residues. Only deacetylation and peptoid modifications make a significant deviation from the general correlation.

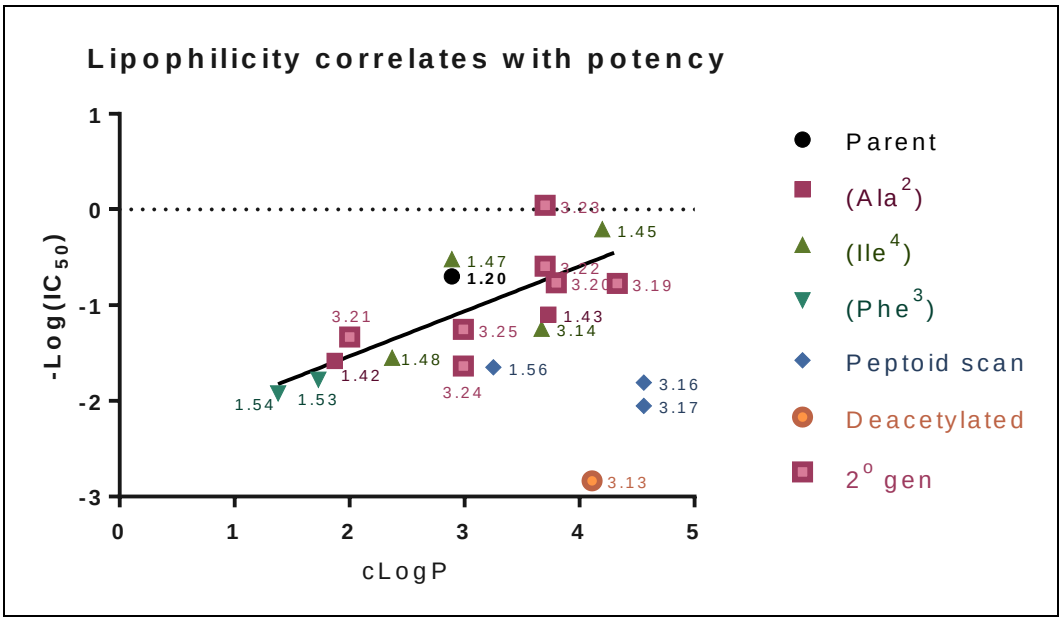


Figure 109: An increase in lipophilicity (cLogP) generally improves the IC_{50}

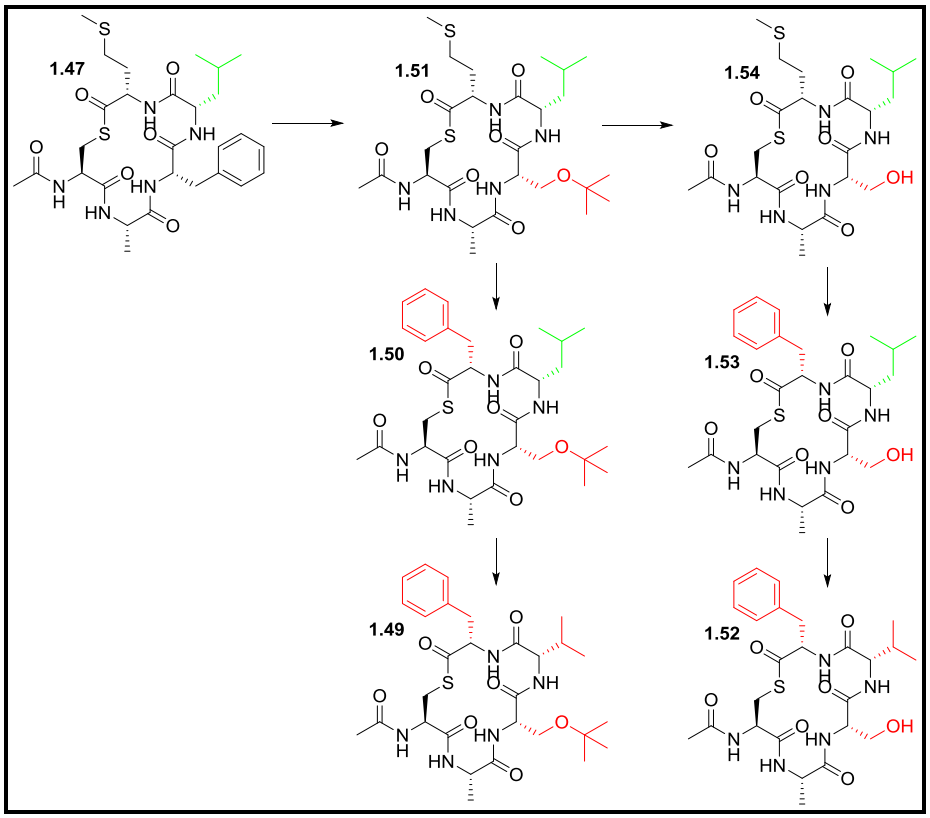


Figure 110: Diagram showing variation of the Phe[3] position

Although a more polar compound could be more desirable, we considered the loss of potency to be an unacceptable outcome. Although the later exchange

of the position-5 methionine for phenylalanine (**1.53**) did marginally increase activity, the improvement was not significant enough to pursue this modification strategy further. Similar exchanges were performed in the presence of valine at the 4-position and these confirmed the negative effects of valine in this position, since neither compound **1.49** nor **1.52** showed any measurable activity.

3.3.1.5 Peptoid scan

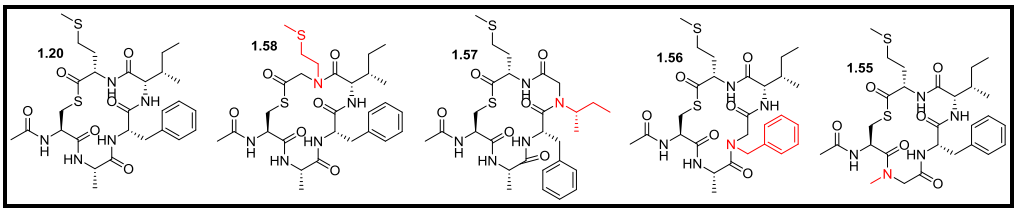


Figure 111: Diagram showing peptoid scan compounds

Following the examination of the effects of amino acid residue replacement on the activity of the AIP analogues, the feasibility of introducing peptoid residues in the AIP-based inhibitors was then assessed. This would be beneficial as peptoids are generally less susceptible to protease breakdown, giving a potential drug a longer half life and an improved dosage regimen. However, installation of peptoid residues in position 2, 4, and 5 (**1.55**, **1.57**, **1.58**) resulted in dramatic loss of inhibitory activity. This could be because the side-chain groups on the amide nitrogen disrupt stabilising intramolecular interactions, alter the orientation of the amide bond, or the slight change in steric configuration reduces the affinity of the ligand for the receptor. In contrast, replacing the position-3 phenylalanine with a peptoid residue produced an effective inhibitor (**1.56**). This is likely to indicate that the chemical characteristics and orientation of the amide remain similar to the parent compound **1.20**. With this in hand, the Nbz peptoid residue fixed at position-3, replacement of isoleucine at position-4 with leucine (**3.16**) or replacement of methionine at position-5 with leucine (**3.17**) did not afford increases in inhibitory potency. It is likely that the interplay between each of these alterations in the complex environment of the macrocycle changes the response to each individual modification when applied in the presence of other

modifications. Nevertheless, potency is broadly maintained with a loss of 1.5- to 2.5- fold of inhibitory activity.

3.3.1.6 Second Generation Analogues - Variation of Position 5

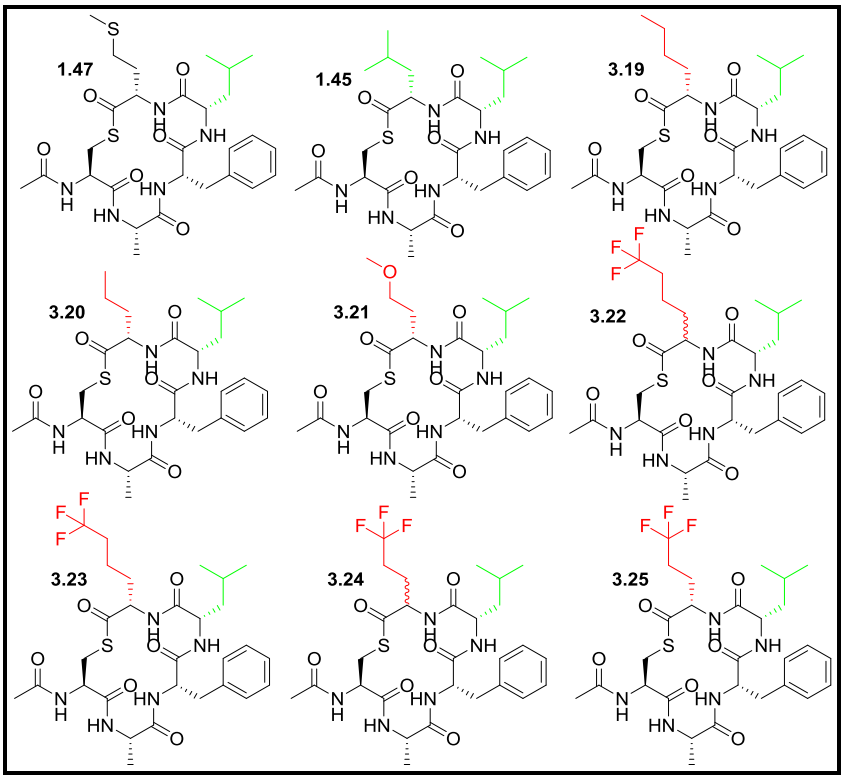


Figure 112: Diagram showing variation of Met[5] in the presence of a Leu[4] modification

In light of the potency gained from the installation of leucine at positions-4 and 5 (**1.47** and **1.45**), further analogues were produced which varied at the position-5, with leucine fixed at position-4. This was a strategy intended to increase the potency while maintaining the LipE. Even though McDowell *et al.* had previously varied this position in AIP1 producing a series of inactive analogues, the difference between the activity profile of the parent AIP1 and the truncated analogues at this position was interesting enough in itself to investigate.[157] In the case of the truncated analogues, variation of position-5 in the presence of leucine residue at position 4 produced a series of impressively potent analogues. Incorporation of an *O*-methylhomoserine analogue (**3.21**) slightly reduced the activity, this demonstrates that the sulfur is somewhat unique in its ability to maintain potent inhibition and a different heteroatom at this position cannot maintain the same potent activity profile. Furthermore, the inhibitory activity of the relatively polar *O*-methylhomoserine in the putative

"hydrophobic knob" region challenges the assertions of Tal Gan *et al.*[312] The incorporation of a norleucine residue (**3.19**) effectively replaced the sulfur atom with a methylene group; this analogue only possessed a slightly reduced inhibitory potency along with the norvaline analogue (**3.20**).

In light of the loss of activity in both the linear alkyl chain residues and the *O*-methylhomoserine exchange, it was postulated that the loss of activity could be due to the lack of polarity in the linear residues and the presence of electron lone pairs in *O*-methylhomoserine. Non-natural residues containing a terminal trifluoromethyl group were designed to be incorporated at this position. It was hoped these would mimic the electronic properties of the methionine sulfur while maintaining the lipophilic properties of the residue. The 5,5,5-trifluoronorvaline analogue (**3.25**) was less potent than hoped, however the 6,6,6-trifluoronorleucine modification (**3.23**) produced a sub-nanomolar inhibitor with an impressive LipE. Furthermore, incorporation of non-natural amino acids may make this compound more resistant to proteases, in a manner similar to the previously attempted peptoid modifications. With this impressively potent new analogue in hand, the compounds were tested in the other *agr* system bioreporters.

3.3.2 Other *agr* groups

Having developed an extensive SAR against the AgrC1 receptor, it was considered that it was necessary to test the most potent compounds in the other *agr* groups. If an anti-virulence therapy could function therapeutically, it would be hugely beneficial for the compound to work against all *agr* groups. If the therapy did not function across all the staphylococcal groups, then genotyping of the infective strain would be required before this kind of treatment could be prescribed. At present, this would be a prohibitively onerous task, therefore the case for designing a pan-group inhibitor from the outset is clear.

A subset of potent and interesting compounds were selected for testing in the other *agr* group bioreporters. The subset consisted of the parent compound **1.20**, both fluorinated analogues (**3.23** and **3.25**), two active peptoids (**1.56**

and **3.17**), both the non-acetylated compounds (**3.12** and **3.13**), and two of our other most potent analogues (**1.45** and **3.20**, Table 7). It was hoped that this variety of compounds and alterations would suitably reveal SAR details in the other AgrC receptor sub-types.

Table 7: Comparing the competitive inhibition of AgrC1, AgrC2, AgrC3, and AgrC4 (IC_{50} in nM, n = 3) determined using staphylococcal lux-based reporters. The concentrations of the agonists used, AIP-1, AIP-2, AIP-3, and AIP-4, were 100, 100, 400, and 100 nM, respectively. *-* Side-chain-to-tail thiolactone

	Macrocyclic peptides	IC_{50} (AgrC1)	IC_{50} (AgrC2)	IC_{50} (AgrC3)	IC_{50} (AgrC4)
AIP1		-	55.8 ± 11.4	20.7 ± 3.8	-
(Ala^5)AIP1		1.3 ± 0.4	60.9 ± 9.8	0.6 ± 0.1	1.7 ± 1.0
AIP2		47.0 ± 6.8			
1.20	Ac-Cys*-Ala-Phe-Ile-Met*	5.0 ± 1.4	70.3 ± 4.1	2.7 ± 0.8	6.2 ± 1.5
1.45	Ac-Cys*-Ala-Phe-Leu-Leu*	1.6 ± 0.8	76.3 ± 3.3	1.5 ± 0.1	1.4 ± 0.2
3.20	Ac-Cys*-Ala-Phe-Leu-Nva*	5.8 ± 1.7	68.3 ± 15.5	2.7 ± 0.8	1.6 ± 0.9
3.22	Ac-Cys*-Ala-Phe-Leu-Tfn*	3.9 ± 1.8	73.0 ± 4.8	0.9 ± 0.1	-
3.23	Ac-Cys*-Ala-Phe-Leu-(S)-Tfn*	0.9 ± 0.1	45.7 ± 5.5	1.5 ± 0.2	1.7 ± 0.5
3.24	Ac-Cys*-Ala-Phe-Leu-Tfb*	43.1 ± 4.0	590.4 ± 114.7	7.8 ± 0.2	-
3.25	Ac-Cys*-Ala-Phe-Leu-(S)-Tfb*	17.8 ± 10.4	137.0 ± 58.7	1.0 ± 0.8	1.8 ± 0.8
3.13	H-Cys*-Ala-Phe-Leu-Leu*	682.2 ± 51.4	>2000	>500	113.4 ± 48.7
3.12	H-Cys*-Ala-Phe-Ile-Met*	>5000	>2000	>500	181.2±121.9
1.56	Ac-Cys*-Ala-Nbz-Ile-Met*	44.5 ± 17.4	> 5000	7.5 ± 2.2	15.5 ± 3.4
3.17	Ac-Cys*-Ala-Nbz-Leu-Leu*	112.7 ± 11.4	538.5 ± 102.4	2.5 ± 0.7	2.0 ± 0.3

Tfn = *RS*-6,6,6-trifluoronorleucine; *Tfb* = *RS*-2-amino-4,4,4-trifluorobutanoic acid; *N*bz = *N*-benzylglycine.

On first inspection of the results, it appears that AgrC2 is less susceptible to inhibition by these analogues, while AgrC3 and AgrC4 seem to be at least equally susceptible and often more susceptible than AgrC1. Also, patterns previously observed in the SAR for AgrC1 seem to be applicable to the other receptors. For example, the non-acetylated compounds and peptoids are less active than their parent compounds in each of the four receptors.

3.3.2.1 The effect of acetyl group absence

The free amine group in the non-acetylated analogues (**3.12** and **3.13**), which dramatically reduced activity in AgrC1, produces a complete loss of activity in both AgrC2 and AgrC3, but they were active in AgrC4.

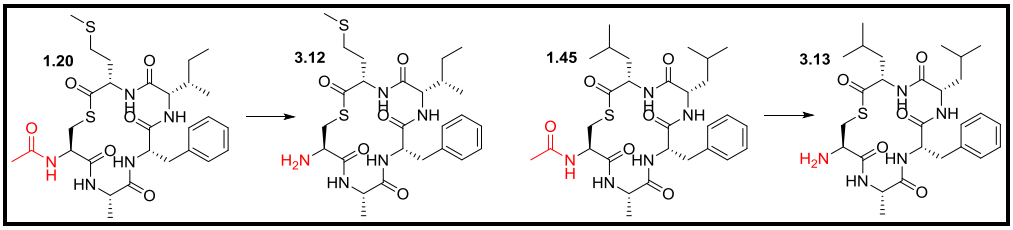


Figure 113: Diagram of non-acetylated analogues **3.12** and **3.13** with their parent compounds **1.20** and **1.45**

3.3.2.2 Peptoid analogues

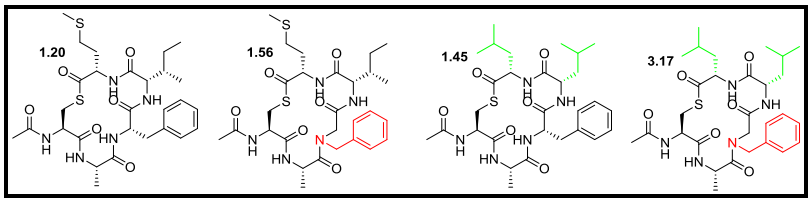


Figure 114: Diagram showing peptoid scan compounds

In AgrC1, the phenylalanine peptoid analogues **1.56** and **3.17** cause a dramatic loss of activity by roughly 10-times and 100-times, respectively. In AgrC2, similarly precipitous reductions of potency were observed. However, in AgrC3 and AgrC4, these compounds act as impressive inhibitors. In fact, compound **3.17** acts as an effective inhibitor in all groups tested and could represent a viable peptoid modification to improve overall stability of the molecule and especially its resistance to proteases.

3.3.2.3 Varying Position-4

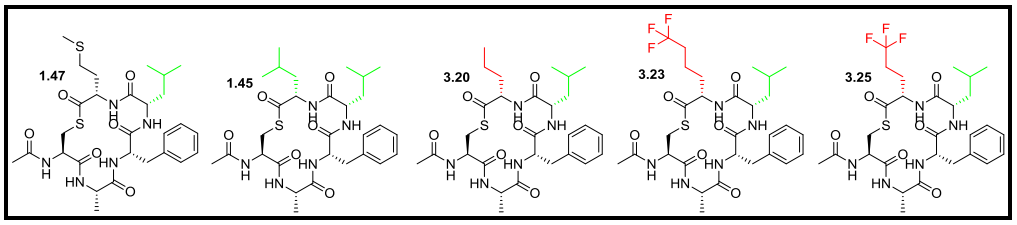


Figure 115: Diagram showing variation of Met[5] in the presence of a Leu[4] modification

The double leucine modified analogue (**1.45**), being one of the most potent compounds against AgrC1, is also a potent inhibitor of AgrC2, AgrC3 and AgrC4. This highlights the effectiveness of these leucine modifications in each group and is in keeping with the findings of Tal Gan *et al.* who also found it to be a potent pan-group inhibitor.[312] Moreover, the most potent inhibitor (**3.23**) was an improved inhibitor of both AgrC1 and AgrC2, and had an equivalent potency against AgrC3 and AgrC4. The parent compound (**1.20**) and the norvaline modified compound (**3.20**) are also potent cross-group inhibitors. This was

very encouraging as all four compounds could be seen as potential anti-virulence therapies in *S. aureus*.

3.4 Activation of a mutant receptor (A101T T104V)

Table 8: Interaction of the AIP analogues with the mutant (A101T,T104V)-AgrC1 receptor (IC_{50} and EC_{50} in nM, *n* =3) determined using staphylococcal *lux*-based reporter. The concentration of the agonist, AIP-1, in IC_{50} experiments was 100 nM. *-* Side-chain-to-tail thiolactone

	Macrocyclic peptides	EC_{50} and/or IC_{50} (A101T,T104V-AgrC1)
AIP1	-	13.2 ± 1.8[1]
(Ala[5])AIP1	-	6.4 ± 1.1[1]
1.20	Ac-Cys*-Ala-Phe-Ile-Met*	33.9 ± 11.7[2]
1.45	Ac-Cys*-Ala-Phe-Leu-Leu*	13.0 ± 1.6[2]
3.20	Ac-Cys*-Ala-Phe-Leu-Nva*	14.7 ± 7.0[2]
3.22	Ac-Cys*-Ala-Phe-Leu-*Tfn**	7.4 ± 1.1 73.4 ± 7.7[3]
3.23	Ac-Cys*-Ala-Phe-Leu-(*S*)-*Tfn**	2.4 ± 0.3 80.9 ± 5.4[3]
3.24	Ac-Cys*-Ala-Phe-Leu-*Tfb**	56.2 ± 13.6[2]
3.25	Ac-Cys*-Ala-Phe-Leu-(*S*)-*Tfb**	49.0± 5.6[2]
3.13	H-Cys*-Ala-Phe-Leu-Leu*	>2000 >2000
3.12	H-Cys*-Ala-Phe-Ile-Met*	>2000 >2000
1.56	Ac-Cys*-Ala-*N*bz-Ile-Met*	153.3 ± 30.0[2]
3.17	Ac-Cys*-Ala-*N*bz-Leu-Leu*	57.1 ± 6.6[2]

Tfn = *RS*-6,6,6-trifluoronorleucine; *Tfb* = *RS*-2-amino-4,4,4-trifluorobutanoic acid; *N*bz = *N*-benzylglycine.

[1]Strong activators of the mutant reporter [2]Inhibition observed, however, activation (roughly 40-60% magnitude of AIP1) prevented attainment of a meaningful IC_{50} value [3]Predominantly behaves as an inhibitor with only a very small activation (roughly 5% of max AIP1 agonism) in the mutant reporter.

Previous work in Chan's group which analysed the function of various residues present in AgrC1, produced a receptor which was not antagonised by the common inhibitor, (Ala[5])AIP1 (**1.59**). The new receptor contains only two changes: A101T and T104V. These changes actually resulted in the (Ala[5])AIP1 (**1.59**) being a potent agonist of this new AgrC receptor. As only two receptor residues and a single ligand residue had been altered, it was considered that it could be possible with only a very slight selective pressure for this receptor-ligand pair to spontaneously evolve as a new *agr* group. This could be especially likely if our new putative anti-virulence compounds became widely used. Therefore, the subset of analogues previously tested in AgrC1-4 were also tested in a bioreporter containing this new receptor (Table 8 and Figure 116).

The activation by (Ala^5)AIP1 (**1.59**) previously observed was again confirmed with a similar EC_{50} to the original data. AIP1 (**1.14**) was also confirmed as an effective agonist as previously reported with both AIP1 (**1.14**) and AIP4 (**1.17**) in the original data. [231]

The series of truncated AIP analogues are all partial agonists of the mutant receptor. However, they did not activate the system to the same extent as (Ala^5)AIP1 (**1.59**) or AIP1 (**1.14**). Most of the compounds activated the bioreporter to roughly 40-60% of the maximal activation of AIP1 (**1.14**). This effectively prevented the attainment of meaningful IC_{50} figures as, although the compounds slightly reduced activation by AIP1 (**1.14**), significant activity caused by the truncated analogues remained at high concentrations. However, the two trifluoromethyl compounds (**3.23** and **3.25**) only caused a small activation (less than 5%) of the mutant receptor (Figure 116). At high concentrations, they effectively reduced activity caused by AIP1 (**1.14**) to near basal levels. This allowed us to attain IC_{50} figures which showed that these molecules were effective low nanomolar inhibitors even in this new putatively resistant *agr* group.

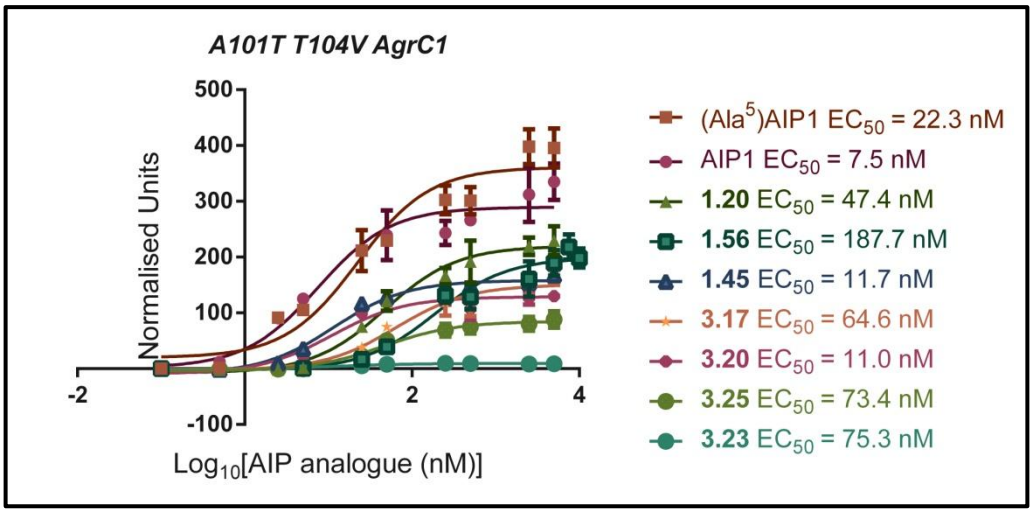


Figure 116: Graph showing activation of the mutant receptor by each truncated AIP-analogue in the absence of any agonist.

Interestingly, the peptoid compound **1.56** possessed a similar maximal activation to its non-peptoid counterpart **1.20**. However, the dose-response curve was right shifted demonstrating a reduction in receptor affinity. This observation also held true for the peptoid compound **3.17** and its non-peptoid

counterpart **1.45**. The presence or absence of peptoid residues could have little effect on the compounds ability to agonise or antagonise the receptor. However, the affinity of the compounds seem to be dramatically reduced by the presence of peptoid residues.

3.4.1 Inhibition of the mutant receptor (A101T T104V)

IC_{50} data could only be attained for compound **3.23**. Most compounds produced significant agonism in the mutant receptor preventing the attainment of IC_{50} values, however, compound **3.23** was a partial agonist which caused less than 5% of the agonism of AIP1. This mild activity allowed effective competitive inhibition in the presence of AIP1 (100 nM). The IC_{50} of 2.4 nM is exceptionally potent and it is considered that development of this compound could produce further analogues with inhibitory activity in this new *agr* group. This data also supports the superiority of compound **3.23** over the previously reported leucine analogue (**1.45**) of Tal Gan *et al.*[312]

3.5 Mode of inhibition of the AIP analogues

Having established that several of these compounds are potent cross-group inhibitors and that one of them is an effective inhibitor of the newly created mutant strain, further work to understand the mechanism of inhibition of the compounds was performed. Initially, experiments to confirm that the new analogues remain competitive inhibitors was executed.

3.5.1 Competitive inhibition assays

Competitive inhibition is defined by Tomlinson as "the mutually exclusive binding of two compounds to a common site on a receptor."[317] In this case, a constant concentration of an inhibitor increases the EC_{50} of the agonist without affecting the maximal activation. Increasing the concentration of the inhibitor should further increase the EC_{50} without any saturation of this effect because of the direct competition for the active site between the two compounds. The maximal activation should also always remain constant as there is no means for the inhibitor compound to potentiate or reduce the agonist's effect.

In the case of non-competitive and uncompetitive inhibition, the decrease of EC_{50} is saturable as all receptors can be occupied by the inhibitor, irrespective of the concentration of the agonist. A hallmark of allosteric inhibition is the possibility that the maximal activation can be reduced as binding to an allosteric site can cause potentiation or reduction in the agonist's effect.

The testing of AIP2 (**1.15**) and AIP3 (**1.16**) showed that they act as competitive inhibitors as expected. Further testing of the truncated analogues **1.20**, **1.45**, and **3.23** also showed a competitive mode of inhibition (see Figure 117). This is indicative that the series of analogues all function *via* a competitive mode of inhibition.

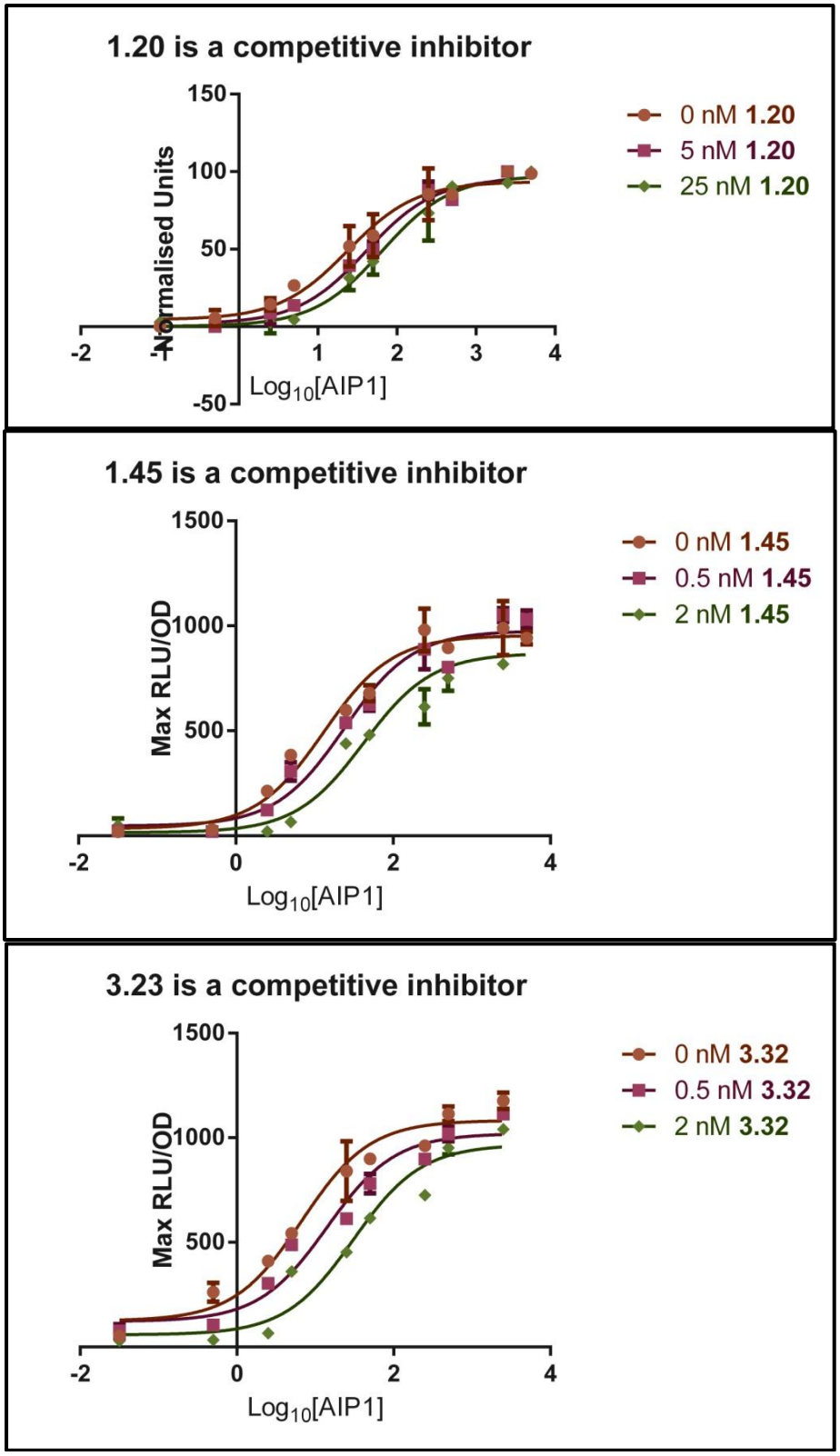


Figure 117: Graphs showing competitive inhibition by truncated AIP analogues

3.5.2 Interactions with a constitutively active receptor (S116K)

As it had been confirmed that the truncated AIP analogues were binding competitively at the receptor binding site, the only remaining question was whether the compounds acted as neutral antagonists or inverse agonists. Neutral antagonists have no effect on the activation state of the receptor, whereas inverse agonists actively promote the "off-state" of the receptor on binding the recognition site. However, these effects cannot be observed in the regular AgrC1 receptor as its basal activity is too low to observe any drop in activity which could be caused by an inverse agonist. Previous work in Chan's group created a receptor with a single residue exchange, S116K, creating a receptor which is partially constitutively active. The corresponding reporter displays roughly a 5-10% signal in comparison to the regular AgrC1 reporter when activate with 100 nM AIP1.

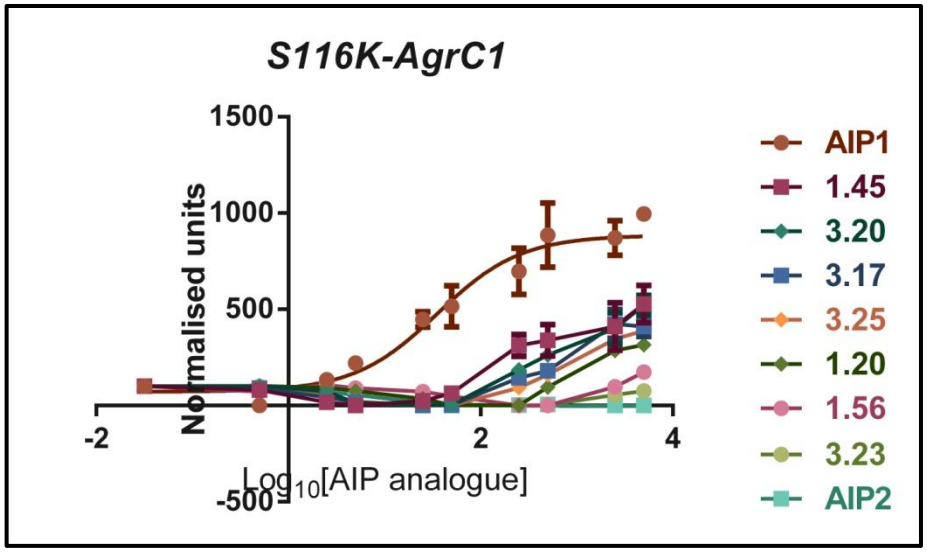


Figure 118: Graph showing truncated AIP analogues interaction with the mutant partially constitutive receptor S116K-AgrC1.

This reporter was used to determine how the truncated AIP analogues interact with the receptor. Interestingly, each of the compounds displayed an initial reduction in activity at low concentrations suggesting they act as inverse agonists. As these concentrations were commensurate with the IC_{50} values recorded in AgrC1-4, it is likely that these inhibitory effects also have an inverse agonist character. However, at higher concentrations, the compounds also acted as agonists. This cannot be caused by a single binding site-ligand interaction. This must indicate a multi-site model for the interaction of these compounds

with the receptor. As recent work has proved that these receptors act as dimers,[125, 166] it is possible that single or double binding to the two available recognition sites of the dimer causes these divergent effects. However, this is in contrast to previous research which found that AgrC signalling is symmetric with both recognition sites equally able to activate the histidine kinase domain.[125] It is also possible that the compounds are interacting with a previously unknown new binding site on the AgrC receptor accounting for the agonistic effects at higher concentrations.

3.6 Activation of AgrC1

As activation of both mutant receptors by the sub-set of analogues had been observed, it was decided to affirm that they did not also agonise the wild type AgrC1 receptor. Incubating the bioreporter strain with high concentrations of each compound with a control in BHI medium revealed that (Ala^5)AIP1 (**1.59**) significantly agonises the receptor. This agonism was significant enough to quantify the EC_{50} of 93.7 nM. Compounds **1.20**, **1.42**, and **1.43** also possess the ability to slightly activate the AgrC1 receptor with a much less significant magnitude. However, this is the first time that macrocycles lacking a tail region have been observed to activate the AgrC1 receptor at any magnitude.

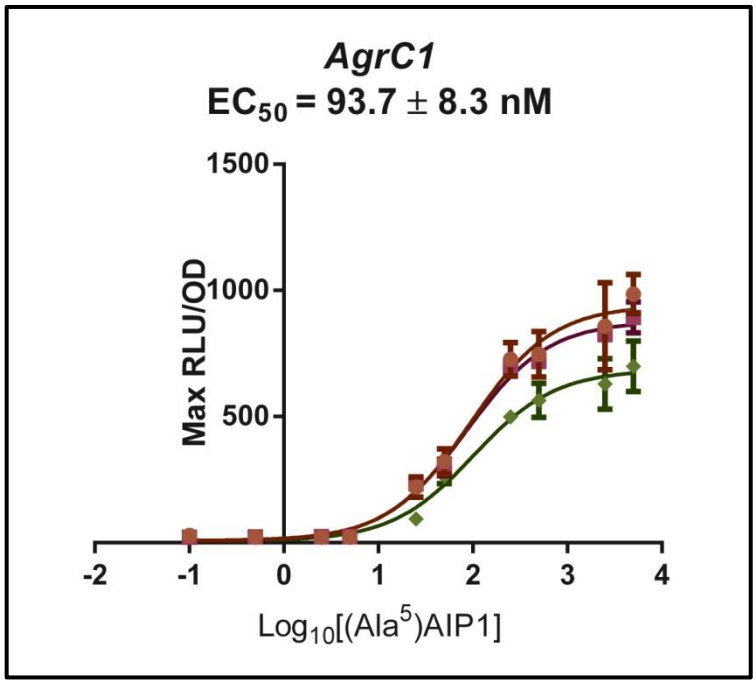


Figure 119: A graph showing activation curves (triplicate) of previously reported inhibitor, (Ala^5)AIP1 (**1.59**)

Further experimentation within our group does showed that, even at high concentrations, (Ala^5)AIP1 (**1.59**) does effectively eliminate the production of virulence factors such as α-hemolysin. This has also recently been observed elsewhere, Johnson *et al.* proposed a two site binding model with initial single binding by (Ala^5)AIP1 at a high affinity binding site producing the familiar competitive inhibition while a second binding at a low affinity binding site produces an auto-phosphorylation of the receptor.[315] They believed that this

effect was physiologically irrelevant and was an artifact of the nanodisc system which they were using to generate their results. However, in our assay, for a signal to be produced, P3 must be activated to produce the *lux* signal.

It is possible that in the wild type bacteria, the bound receptor or (Ala^5)AIP1 (**1.59**) could inhibit the later effects of the transcribed RNAIII thereby preventing the production of virulence factors. This does not seem to be likely, however, the *lux* system is active in our reporter while there is definitely no production of virulence factors in wild type strains. Therefore, (Ala^5)AIP1 (**1.59**) must activate P3 at high concentrations without causing the subsequent production of virulence factors. How this effect occurs and why (Ala^5)AIP1 (**1.59**) causes this effect is unknown.

3.7 Conclusion

A focused library of analogues (previously synthesised by Dr. C. Gordon and Dr. F. Rui) based on the known potent pan-group inhibitor, (Ala^2)trAIP1 (**1.20**), were tested in bioreporter assays to fully characterise and quantify their inhibitory effects. IC_{50} values were experimentally determined against AgrC1 to evaluate the SAR. Replacement of the isoleucine residue at position-4 with a leucine produced compound **1.47** which was an impressively potent inhibitor. Further replacement of methionine at position-5 with leucine fixed at position-4 produced further improvements in inhibitory activity (**1.45**). The most potent inhibitor of AgrC1 discovered to date was produced by replacing the position-5 methionine with a 6,6,6-trifluoronorleucine residue in the presence of a leucine at position-4. This compound actually possessed a sub-nanomolar IC_{50}. Further testing of a sub-set of these analogues in other *agr* group bioreporters revealed several compounds are effective pan-group inhibitors including the most potent compound in AgrC1, **3.23**.

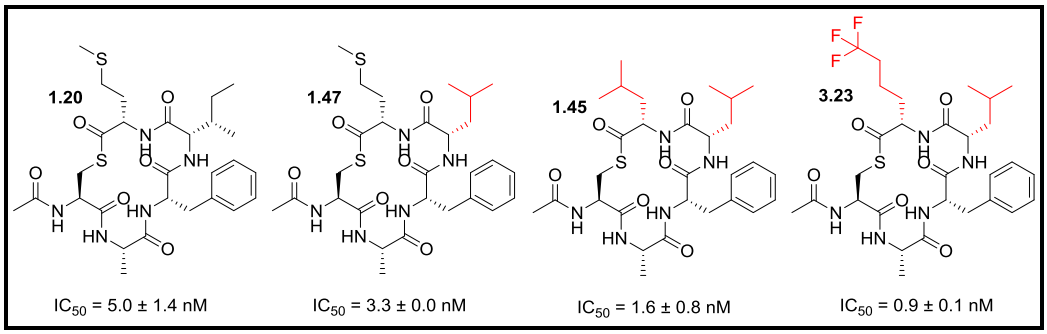


Figure 120: Iterative development of compound **3.23**, the most potent inhibitor of AgrC1 discovered to date.

A series of peptoid analogues were also assessed where the amino acid side-chains were systematically transferred to the α-nitrogen instead of the usual α-carbon position. Introducing these peptoid modifications at position-2 (**1.55**), 4 (**1.57**), and 5 (**1.58**) was not well tolerated. However, exchanging phenylalanine for the equivalent peptoid residue at position-3 (**1.56**) did produce a potent inhibitor suggesting this amide bond is less important for inhibitory activity of AgrC1.

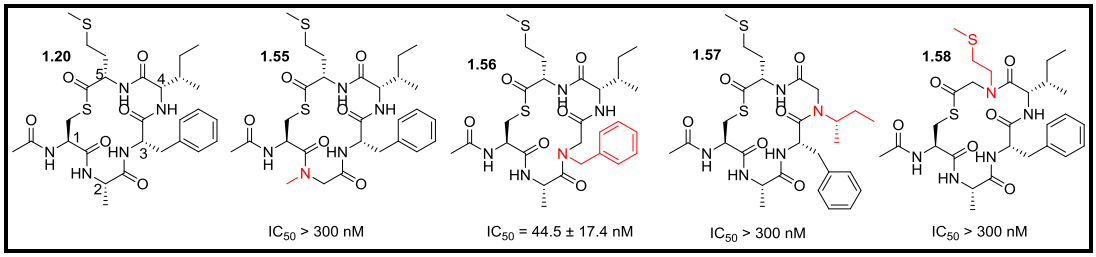


Figure 121: Results of the peptoid scan of the known potent pan-group inhibitor, (Ala[2])trAIP1 (**1.20**)

A receptor which is agonised by the known potent pan-group inhibitor (Ala[5])AIP1 was previously developed *via* forced evolution. A bioreporter strain incorporating this new AgrC receptor was agonised by the majority of the AIP-based analogues tested. However, a single effective inhibitor compound (with only very mild agonistic activity) was discovered. This sole effective inhibitor was the previously mentioned, potent, pan-group inhibitor compound **3.23**. Its impressive inhibitory potency was also maintained in this assay with an IC_{50} of 2.4 nM.

A further mutant bioreporter with a partially constitutively active receptor was also utilised. The truncated AIP analogues inhibited this system at concentrations similar to the IC_{50} values recorded in AgrC1-4. At these concentrations, the analogues act as inverse agonists. However, at high concentrations, the compounds also activated the bioreporter strain. It is likely that this high concentration agonistic effect is caused by an interaction with a previously uncharacterised binding site or dimer effect. Again, the 6,6,6-trifluoronorleucine analogue **3.23** only caused minimal agonism of this receptor further emphasising the robust inhibitory activity of this analogue.

This analogue is very exciting as, to the best of our knowledge, it is the most potent inhibitor of AgrC1 yet discovered. It also potently inhibits in all three of the other *agr* groups making it a pan-group inhibitor. Encouragingly, this compound is still effective against a reporter which was designed to be resistant to (Ala[5])AIP1 (**1.59**) *via* forced evolution. Finally, it also seems to inhibit a partially constitutive receptor showing it is likely to act as an inverse agonist and not a simple neutral antagonist.

3.8 Ongoing and Future work

This SAR study has been part of a larger group project investigating the potential of truncated AIP analogues as a potential anti-virulence therapy. The SAR revealed some unpredictable developments when multiple modifications were sequentially applied to the parent molecule. This is explained by the dynamic nature of the macrocyclic peptide compound. Multiple modifications can change the overall configuration of each analogue. However, rational drug design requires the combination of multiple successful modifications to gradually improve the potency and physical characteristics of the lead compound. In this project, combining successful modifications did not reliably produce more successful compounds. This means alternative rationales must be used to explain the results and develop improved compounds.

Other members of this laboratory have been undertaking NOESY ^{1}H-NMR studies twinned with computer modeling to try to understand how each modification effects the overall configuration of the macrocycle. The NOESY ^{1}H-NMR gives details on the average distance between individual protons and can be used to gain information on the orientation of the amide bonds of the peptide backbone. This information can then be input into computer modeling software as structural constraint figures and the model subsequently predicts a multitude of accessible conformations of the analogue in question. This large number of accessible configurations can then be presented graphically using bond angles. Initial results suggest that the 6,6,6-trifluoronorleucine analogue **3.23** is exceptional because it produces a more constrained macrocyclic ring which cannot access as many possible conformations as other analogues.

Temperature-dependent NMR studies have also suggested that the peptoid substitution of phenylalanine (**1.56**) is well tolerated because the phenylalanine amide is not involved in intramolecular hydrogen bonding. Other amide bonds of the macrocycle are involved in hydrogen bonding. These NMR studies are ongoing to try and discover how the 6,6,6-trifluoronorleucine residue constrains the ring and how alternative modifications could be deployed to recreate this effect complementing the existing structure and improving the

compound's efficacy. Some suggestions include methylation of the cysteine amide to constrain the configuration of the cysteine, an α-methylalanine analogue could also constrain the configuration of the amide bond on either side of the alanine residue. However, it could be that the conformations to which the macrocyclic ring is constrained is also important which may make these modifications less successful then desired.

As a potent pan-group inhibitor **3.23** has now been developed and reduction of the production of virulence factors by wild type bacteria from multiple *agr* groups has also been confirmed. The next stage of assessment will be toxicity testing to assure that these compounds do not possess unexpected toxic effects in various mammalian cell lines. Once this and the stability of the compound *in vivo* is confirmed, it is hoped that testing of some of these compounds in a murine infection model will confirm their *in vivo* efficacy.

4 Total synthesis of the solonamides

The current state of knowledge on the solonamides is outlined, which includes the initial discovery of the solonamides and early biological testing. A recent synthetic paper by Kitir *et al*. is also discussed.[318]

Following this background information, a synthetic strategy for production of the solonamides is then formulated. Each of the main areas of the synthetic strategy are then discussed in more detail to inform later discussion including solid phase peptide synthesis, resin cleavage strategies and macrolactonisation reactions. The synthesis development process is then outlined including the eventual successful solonamide synthesis using commercially available chemical reagents/building blocks. Following the successful execution of the initial solonamide synthesis, an adapted synthesis used to produce the key building block, 3-(*R*)-hydroxyhexanoic acid (**1.60**) is detailed. The results of incorporating this optically enriched building block into the original synthesis are reported. Finally, limitations of this synthetic strategy are discussed and future work required to overcome these limitations are detailed.

4.1 Introduction

As knowledge of the therapeutic potential of anti-virulence compounds has spread, more research groups have been testing compounds in anti-virulence assays. The *agr* system is one of the most well known virulence regulators in *S. aureus* and as such has attracted significant attention in this field. This has led to the discovery of compounds from natural sources and high throughput screening which inhibit the *agr* system.

4.1.1 Solonamides

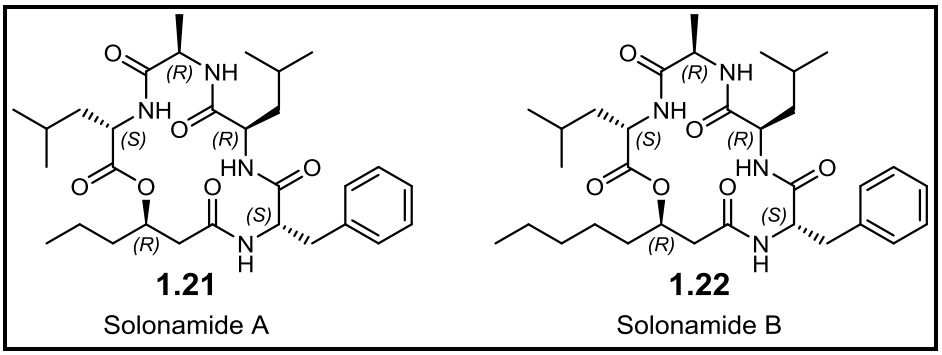


Figure 122: Structure of solonamide A and solonamide B

A global research expedition (Galathea III) discovered more than 500 bacterial strains capable of inhibiting the growth of various pathogenic bacteria. This bacterial library was later screened for their activity against the *agr* quorum sensing system using a gene reporter fusion bioassay.[319] In this context, the extract of a *Photobacterium halotolerans* strain demonstrated an increase in the expression of *spa* while concurrently reducing the expression of *hla* and *rnaIII*. The active compounds were purified, characterised and identified as solonamide A (**1.21**) & B (**1.22**, Figure 122).[319] The amino acid composition was confirmed using NMR techniques. Then acid hydrolysis followed by derivatisation with Marfey's reagent revealed the absolute configurations of each amino acid residue. Analysis of the NMR data also confirmed the presence of an unusual 3-hydroxy acid residue; Mosher's esters were created to establish that the unique residue in both solonamide A and B were of the *R* configuration.[319]

4.1.1.1 Previous Research

Following the discovery of the solonamides, studies to determine their affects on the mRNA levels of virulence related genes in *S. aureus* strain 8325-4 and the hyper-virulent CA-MRSA strain USA300 by Northern blot analysis were performed.[214] This confirmed that expression of *hla* and *rnaIII* was reduced by solonamide B (**1.22** with a particularly noticeable effect in USA300) and that the expression of *spa* was also increased. Solonamide A (**1.21**) did not affect *hla* or *rnaIII* noticeably though it did manage to increase *spa* expression.

The solonamides are structurally similar to the native AIP ligands of the *agr* system. Previous research on the AIP ligands found that lactam and lactone analogues often inhibit AgrC by competitive inhibition.[124, 157] Recent research has also shown that hydrophobic residues are very important in inhibition of AgrC, especially at the C-terminal of the macrocyclic domain.[162, 312] Both solonamides contain a lactone structure and the hydrophobic phenylalanine and leucine residues similar to other known inhibitors of AgrC. Therefore, it is hypothesised that the solonamides are likely to be competitive inhibitors of the AgrC receptor. As the presence of staphylococci in the deep marine environment of these bacteria is unlikely, it seems improbable that the solonamides are intended for *agr* inhibition. It is possible that they may be targeting other Gram positive marine bacteria with *agr* homologues, however, very little is known about quorum sensing in marine bacteria and so this cannot be confirmed. It is also possible that they are part of the bacterial strains own quorum sensing system, however, no structurally similar compounds have been discovered in Gram negative strains and the solonamides or homologous compounds were not found in other strains of bacteria from this species making this seem unlikely.

Following on from the first study, the team moved on to examine: the effects of the solonamides on virulence protein expression, their mechanism of action, and their effects on the toxicity of *S. aureus in vitro* against human neutrophils and rabbit erythrocytes.[216] Initially, they used a reporter strain containing the R238H mutation which makes the AgrC1 receptor constitutively active and non-responsive to AIP1 (**1.14**). The solonamide compounds had no effect on this

system. In a control reporter system with a functional AgrC receptor, the team observed dose-dependency indicating that the solonamides may act as competitive antagonists.

Using 5 μg/mL (e.g. 8.5 μM)of solonamide B (**1.22**), the team showed that increasing amounts of AIP-containing supernatant could reduce the inhibition caused by solonamide B (**1.22**) in a β-lactamase assay; they believed that this indicated a competitive mode of action.[214]

The team went on to use *S. aureus P3::lux* reporter assays to show that solonamide B also inhibits AgrC2, AgrC3, and AgrC4.[216] They also used hemolysis assays with rabbit erythrocytes to prove that bacterial hemolysin production was reduced by the solonamides.[216] Finally, they showed that the production of phenol soluble modulins was reduced and consequently *S. aureus* caused reduced toxicity to human neutrophils when cultivated *in vitro*.[216]

Very recently, following the successful validation of the solonamides as *agr* system inhibitors, attempts have been made to synthesise these compounds.[318] It was hoped that this would enable more comprehensive studies of their action and confirmation of the initial structural assignment of the compounds. Initially, Kitir *et al.* used a strategy (Figure 123) requiring the initial synthesis of two building blocks (**4.1** and **4.2**).[318] Standard solid phase peptide synthesis techniques were used to produce 2'-chlorotrityl-resin bound H-*L*-Phe-*D*-Leu-*D*-Ala (**4.1**). The carboxylate of (±)-β-hydroxyoctanoic acid was selectively benzyl-protected and Boc-*L*-Leu-OH was coupled to the hydroxy group using diisopropylcarbodiimide (DIC) and dimethylaminopyridine (DMAP), followed by catalytic hydrogenation afforded the racemic building block **4.2** in 36% yield over three steps. Building block **4.2** was coupled to resin **4.1** to produce **4.3**. Boc-deprotection and resin cleavage with triflouroacetic acid produced the linear peptide **4.4**. Cyclisation with HATU, diisopropylethylamine (DIPEA) and dimethylformamide (DMF) over 16 hours produced solonamide B (SolB, **1.22**) and diastereomer epimer-solonamide B (epiSolB, **4.5**).

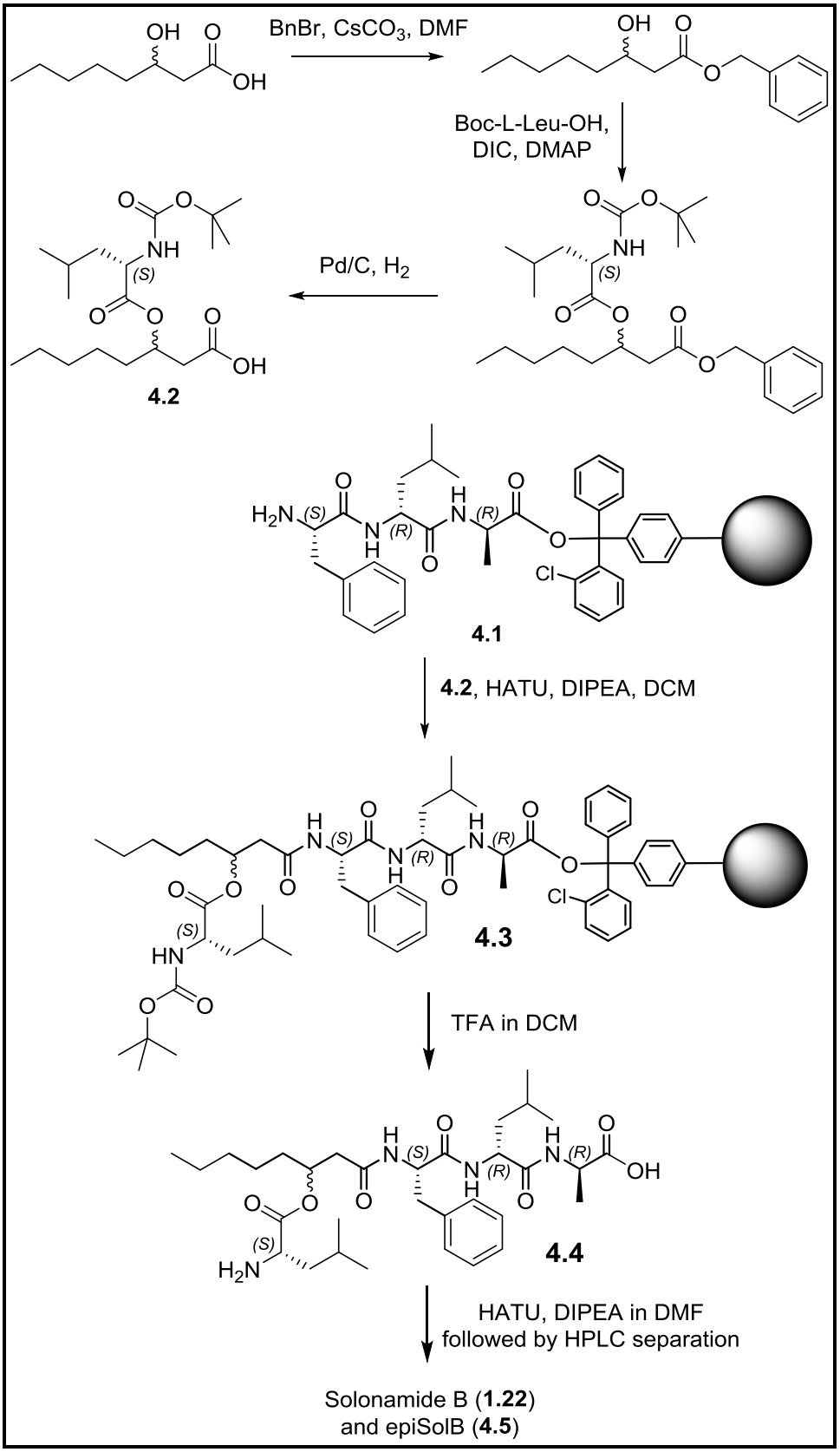


Figure 123: Kitir *et al.*'s initial strategy for synthesis of the solonamides[318]

Having successfully produced the diastereomers, the team moved forward to attempt a stereoselective synthesis of both SolA (**1.21**) and SolB (**1.22**). First,

they synthesised enantiomerically pure 3-hydroxy acids (Figure 124). However, when they employed these 3-hydroxy acids in their original solonamide synthesis they achieved a yield of only 2% of SolB (**1.22**) and observed multiple significant unidentified byproducts. They believed these byproducts could be caused by difficulties during the previous couplings or side reactions during cleavage.

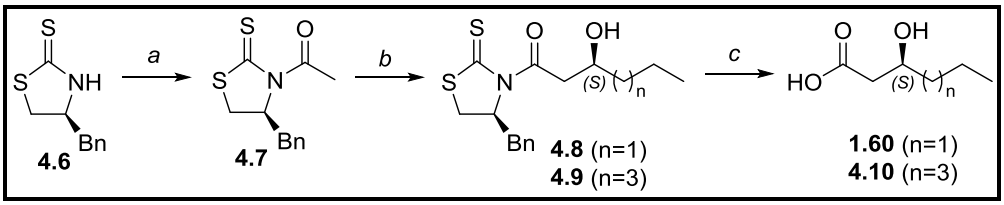


Figure 124: Stereoselective synthesis of 3-hydroxy acids Hha (**1.56**) and Hoa (**4.11**). *Reagents and Conditions:* (a) AcCl, DMAP, NEt_3, DCM; (b) butanal or hexanal, $TiCl_4$, DIPEA, DCM; (c) LiOH, THF.[318]

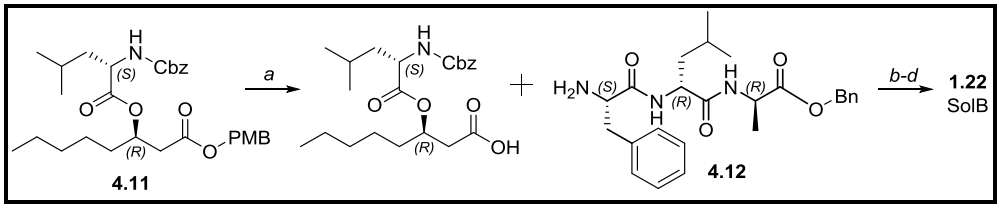


Figure 125: Alternative stereoselective synthesis of SolB (**1.22**). *Reagents and conditions*: (a) TFA, Et_3SiH in DCM; (b) PyBOP, DIPEA, DMF; (c) Pd/C, H_2, EtOH; (d) HATU, DIPEA, DMF.

The team then deployed a new solution-phase only synthesis in the hope that this would enhance the coupling efficiencies while avoiding the need for resin cleavage (see Figure 125). A different protecting group strategy was applied producing dimer **4.11** from 3-(*R*)-hydroxyoctanoic acid (**4.10**). This dimer was deprotected in acidic conditions in preparation for coupling to the trimer (**4.12**). A selection of coupling reagents were tested for the coupling to produce the protected pentapeptide; the PyBOP reagent gave the product with the best purity. The crude linear peptide was then deprotected *via* catalytic hydrogenation ready for the macrocyclisation. The macrolactamisation was achieved with HATU and DIPEA in DMF. Unfortunately, on purification by HPLC, only a 1% yield was achieved and now four diastereomers were present. Both SolB (**1.22**) and epiSolB (**4.5**) with two further isomers indicating epimerisation at another location. Finally, the team tested their synthetic

solonamides which displayed similar activity to samples isolated from bacterial culture thereby confirming the originally assigned structure.[318]

To date, all attempts in the stereoselective synthesis of the solonamides have resulted in a final purified yield of 2% or less. The activity of the solonamides also remains to be quantified. Little is known about how the solonamides interact with the AgrC receptor and the SAR remains a mystery.

4.1.1.2 Solonamide research summary

Research into the compounds known as the solonamides is in its infancy. To date only three publications are available examining their activity, structure, and synthesis. In light of this, many questions remain to be answered.

Currently, it is known that:

- the solonamides are produced by a marine bacterium (*P. halotolerans*) for unknown reasons.
- the structure and configuration of the solonamides has been predicted using a combination of mass spectrometric, NMR, Marfey's, and Mosher's techniques.
- they contain a non-amino acid 3-(*R*)-hydroxyhexanoic (**1.60**) and octanoic acid (**4.10**) moiety.
- the solonamides reduce the expression of *hla*, *rnaIII* and increase the expression of *spa*.
- they also reduce the production of PSMs.
- the solonamides reduce *S. aureus* toxicity against human neutrophils and rabbit erythrocytes.
- A mixture of SolB (**1.22**) and epiSolB (**4.5**) has been produced with a cumulative yield of less than 5%.
- An attempted stereoselective synthesis produced SolB (**1.22**) in yields lower than or equal to 2%, and an intractable of unidentified side products was also produced.
- Further attempts at stereoselective synthesis produced mixtures of four isomers of SolB (**1.22**)

4.1.2 Contribution of this research

Previously developed syntheses of the solonamides are either low yielding or non-stereoselective. The research reported herein aimed to develop a reliable, high yielding, stereoselective synthesis of the solonamides. This synthesis can then be used to produce sufficient quantities of each solonamide compound to establish their IC_{50} values using *P3::lux* bioreporter assays in all four *agr* groups. This data will allow direct comparison with previously discovered *agr* inhibitors to accurately assess the potency of these newly discovered natural products. Furthermore, competition assays with synthetic AIP ligands will allow the unambiguous determination of the mode of binding of the solonamides using Schild analysis.

Once this knowledge has been established, further analogues of the solonamide compounds will be synthesised and tested to assess the SAR with AgrC1. Some analogues will also be assessed in AgrC2 and AgrC3.

4.2 The synthetic strategy

4.2.1 Retrosynthesis

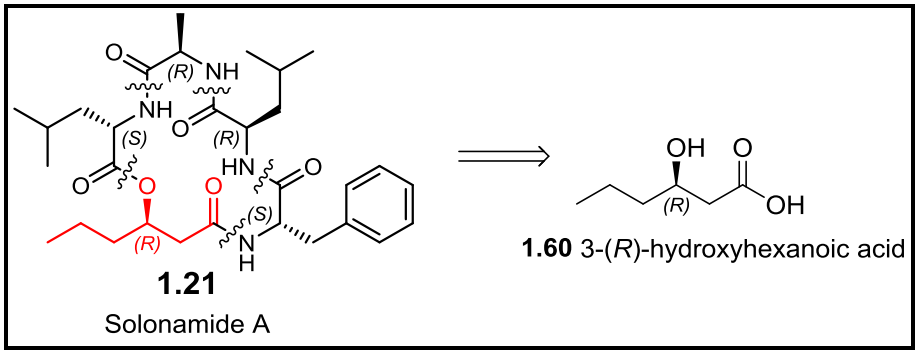


Figure 126: Retrosynthetic analysis of solonamide A (**1.21**) reveals a key 3-(*R*)-hydroxyhexanoic acid moiety.

Initial retrosynthetic analysis of SolA (**1.21**) showed that an unusual 3-(*R*)-hydroxyhexanoic acid moiety (**1.60**) would be required for the stereoselective synthesis of the compound (**1.21**). The other four constituents were all amino acids which are commercially available with different protecting group options to suit various synthetic strategies. At the time, the activity of the solonamides was yet to be confirmed, therefore it was sensible to initially develop a simple non-stereoselective synthesis to confirm the activity of these natural products against AgrC before proceeding to a stereoselective synthesis. For this purpose, a commercially available racemic 3-(*RS*)-hydroxyhexanoic acid would be suitable.

The four amino acid linear peptide structure could be easily synthesised using standard Fmoc-solid phase peptide synthesis (SPPS) strategy (discussed in Section 4.2.2). When considering how to incorporate the 3-hydroxyhexanoic acid moiety, the instability of ester bonds in basic conditions was a concern. Standard Fmoc-based SPPS requires piperidine deprotection after the addition of each new amino acid residue and therefore envisaged not to be compatible with maintaining an ester bond. Thus, it was decided that the four amino acid linear peptide would be assembled on the resin (**1.62**) before an adapted peptide coupling protocol would install the 3-hydroxyhexanoic acid residue. Given that the hydroxy moiety is nucleophilic, it was considered that it could potentially react with an active ester of the 3-hydroxyhexanoic acid causing

polymerisation (see Figure 127). In response to this problem, mild coupling conditions would be evaluated to produce the linear peptide (**1.63**). If necessary, the hydroxy group could be protected to avoid this polymerisation problem.

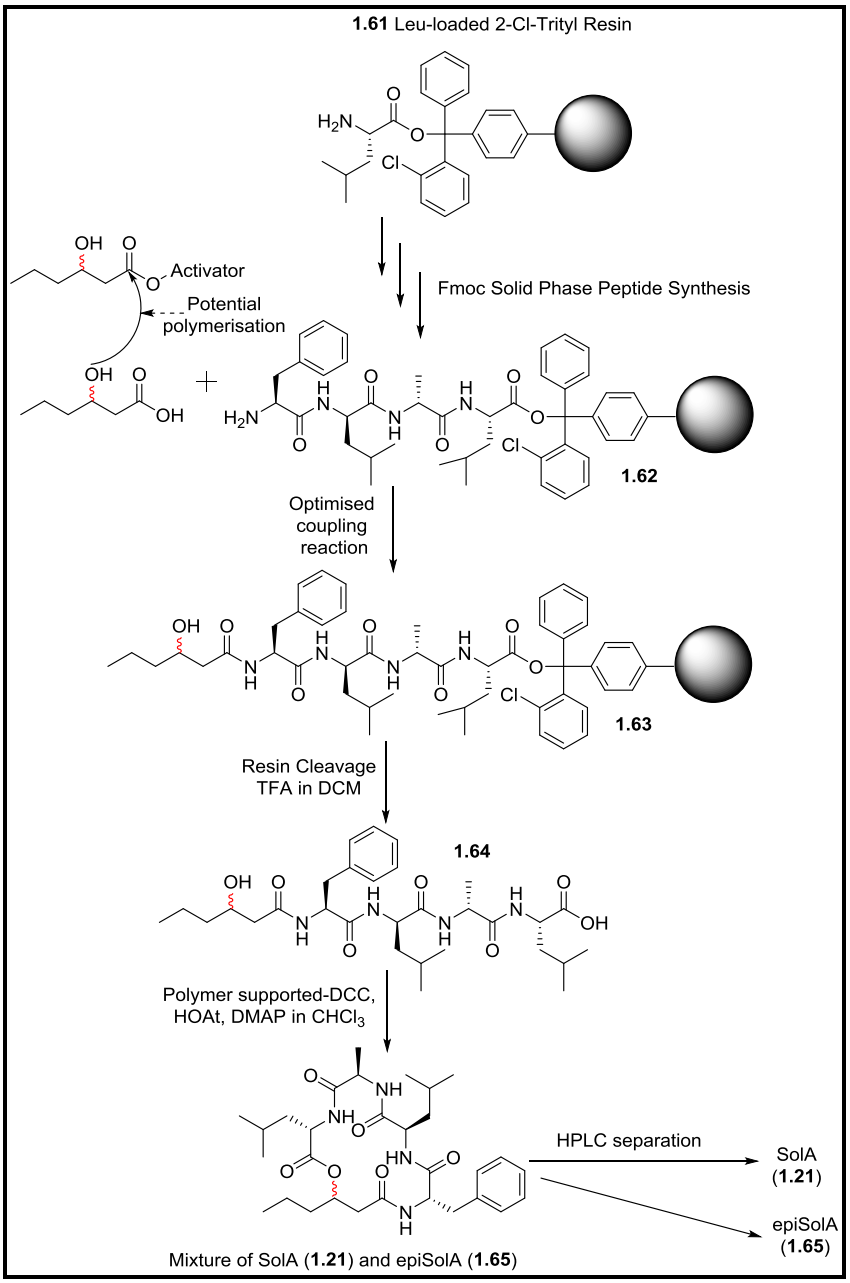


Figure 127: Initial synthetic strategy for the pilot synthesis of solonamide A (**1.21**)

Once the linear peptide with the 3-hydroxyhexanoic acid residue was assembled, it could be cleaved from the resin to produce the free linear peptide **1.64**. There are several methods available for the formation of ester bonds which could be used for the macrolactonisation of this linear product. Initially,

the Steglich esterification[320] was a promising strategy for the cyclisation to produce SolA (**1.21**) and its epimer, epiSolA (**1.65**). HPLC could then be used to isolate each of these diastereomers which would then be tested in *agr* bioassays to confirm the previously reported activity. It was hoped that it would be possible to use this assembly strategy in the eventual stereoselective synthesis of the solonamides, after developing a method to produce 3-(*R*)-hydroxy acid moieties.

This strategy has four main areas: solid-phase peptide synthesis of the initial four amino acid chain, attachment of the 3-hydroxy acid moiety to the peptide, resin cleavage, and macrolactonisation. These areas will be outlined and discussed below.

4.2.2 Solid-Phase Peptide Synthesis

Bruce Merrifield pioneered the solid-phase synthesis of peptides in 1963.[321] Peptide chemistry, which had largely been performed in solution previously, was revolutionised. The tedious and demanding steps of purification between each solution-phase coupling were no longer necessary. This strategy also allowed the development of automation for the synthesis of peptides and proteins which is commonly seen today. Nevertheless, solution-phase methods are still occasionally used for the production of very long sequences by native chemical ligation.[322]

4.2.2.1 Principles

Peptide synthesis involves a multitude of repetitive steps and this makes the incorporation of a polymer/solid support invaluable. Solutions with large excesses of reactants in high concentrations can drive coupling reactions to completion. The excess reagents can then easily be removed by filtration and further washes while the growing peptide chain remains attached to the solid phase resin. Furthermore, all synthetic steps can be performed in a single reaction vessel thereby reducing loss during material transfer.

The general principles of SPPS are illustrated in Figure 128. Initially, an *N*-protected amino acid residue is loaded onto a resin containing a reactive linker. This is generally a hydroxy, chloro, or amino functionality which forms an ester

or amide link to the resin. Cleavage will eventually result in the release of a carboxylic acid or amide moiety at the C-terminus of the peptide. The temporary α-amine protecting group is removed, and a further activated amino acid residue is coupled to the exposed amine. This process is repeated, thus forming a peptide in a C-to-N direction. Side-chain protection should be stable during *N*-deprotection, coupling, and washing of the peptidyl resin. Eventually, the linear peptide chain is concurrently side-chain deprotected and released from the solid support under specific cleavage conditions.

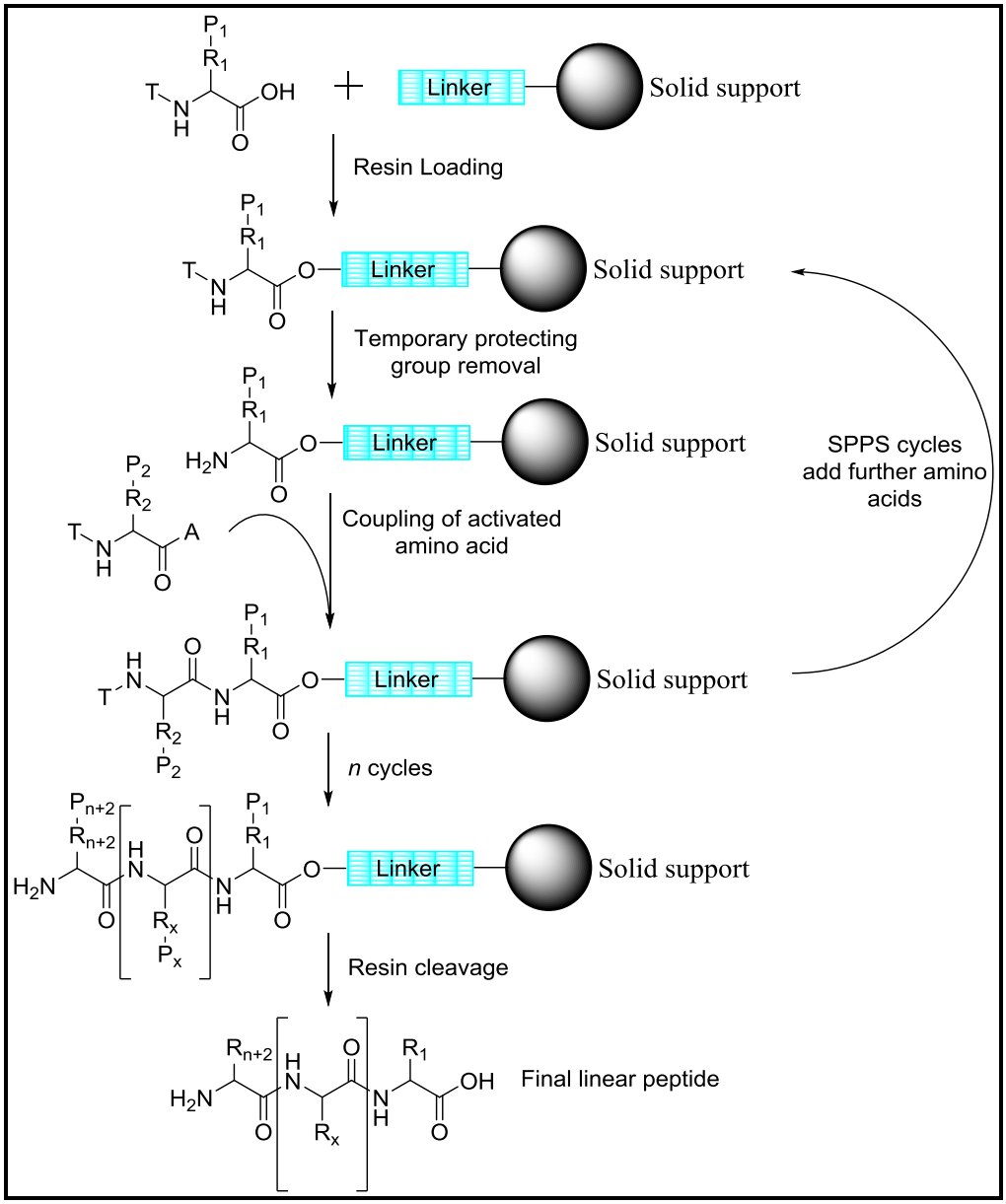


Figure 128: Principles of solid phase peptide synthesis (SPPS).

4.2.2.2 Strategies

There are two common protocols (and associated protecting group strategies) for solid phase peptide synthesis. The original method used by Merrifield *et al.*[321] was a Boc/Bzl strategy. In this strategy, the *N*-terminal is protected using a *tert*-butoxycarbonyl protecting group, also commonly known as a Boc group. Deprotection of the α-amino group is easily accomplished using an anhydrous acid; trifluoroacetic acid (TFA) is commonly used. In this strategy, side chains are often protected using benzyl or benzyl-based groups which are stable in the acidic α-amino group deprotection conditions. Subsequently, cleavage from the resin along with complete side-chain deprotection is achieved using anhydrous hydrogen fluoride *via* acidolytic cleavage.[323] A very recent review by Muttenthaler *et al.* has outlined the safest and most reliable protocols for HF-mediated resin cleavage.[324]

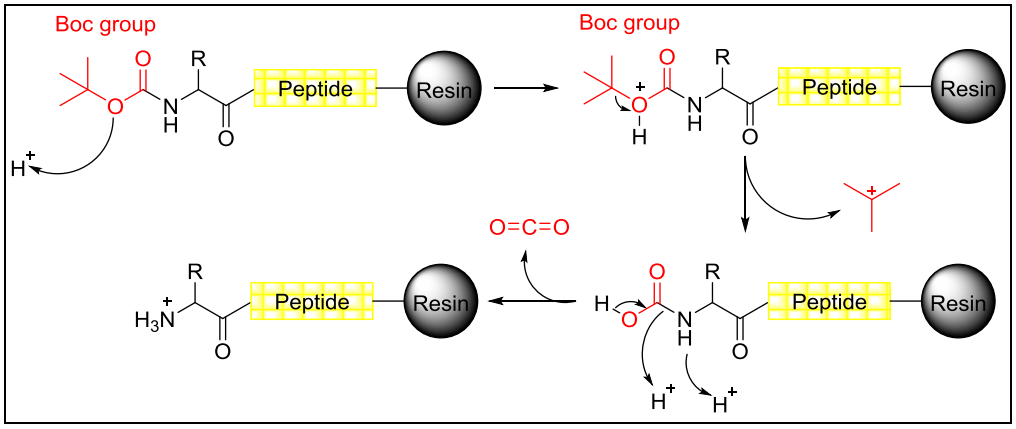


Figure 129: Boc deprotection mechanism

Unfortunately, HF is highly toxic and a special polytetrafluoroethylene-lined apparatus is required to prevent corrosion. Furthermore, the strongly acidic conditions can cause deleterious changes in peptides containing some vulnerable amino acid sequences.[325] Therefore, in response to these potential problems, a new strategy was developed. This strategy is known as the Fmoc/tBu strategy. It deploys 9-fluorenylmethyloxycarbonyl (Fmoc) as the α-amino protecting group. The protecting group is removed under mild basic conditions, usually piperidine (20-50%) in DMF.[325] Another benefit of this method is that basic deprotection forms a neutral amine product. Hence, no neutralisation step is required unlike the previous Boc deprotection performed in acid. Although, *in situ* protocols for neutralisation in Boc-SPPS are now

available.[326] There are also some benefits to Boc-SPPS. For example, the positive charge generated can help to prevent aggregation of the growing peptide chains due to electrostatic repulsion forces and, therefore, some researchers still use this method for sequences which are very prone to problematic aggregation[327] or for sequences vulnerable to the basic conditions of Fmoc deprotection.[322]

Release of the assembled peptide chain in Fmoc-SPPS is typically performed in mildly acidic conditions making the method less hazardous and less likely to degrade the required products.[328]

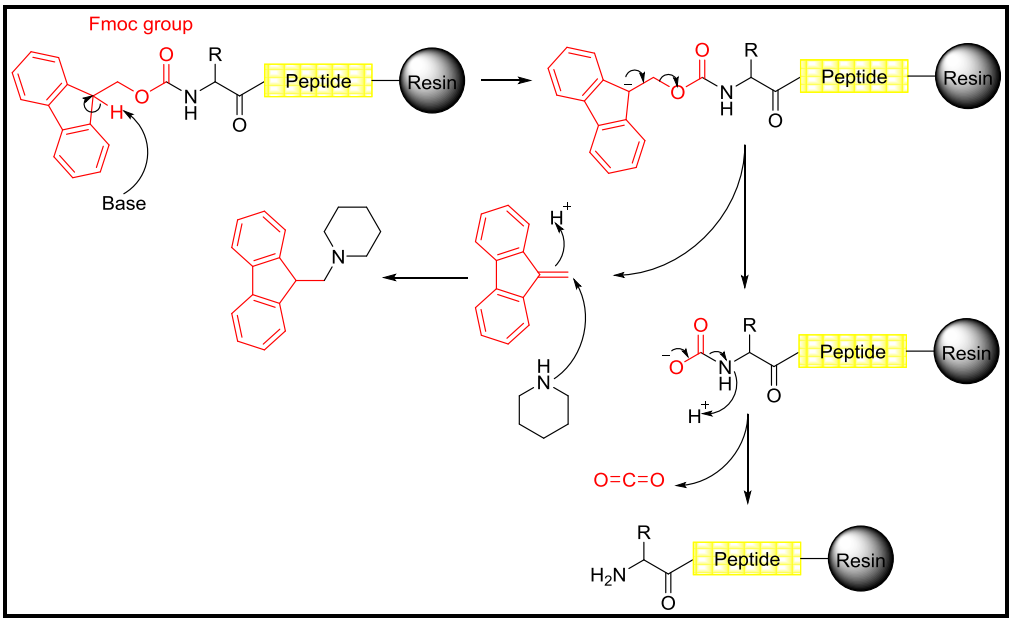


Figure 130: Fmoc deprotection mechanism

Generally, Fmoc strategies are preferred over Boc due to the ease of deprotection and cleavage. Furthermore, if necessary, systems using orthogonal *N*-terminal protection, side group protection and resin cleavage can be designed, sometimes even individual resins are deprotected while the linear peptide is still attached to the resin. This wide range of available protecting group strategies is often a major benefit to the Fmoc strategy. However, depending on the peptide sequence, orthogonality is sometimes easier to achieve in Boc-SPPS. Finally, the liberated fluorenyl group is also a chromophore and deprotection can easily be detected by UV monitoring of the run-off. This is a further benefit which is often used in the production of automated peptide synthesisers.

4.2.2.3 Coupling Agents

The easiest way to incorporate *N*-protected amino acids into the growing peptide chain is the *in situ* activation of the carboxylic acid functionality. A large excess of the activated amino acid can be used in comparison to the number of reactive sites available, forcing the reaction to completion. There are primarily three common and well established mechanisms used when designing these coupling agents: phosphonium-based, aminium/uronium-based and carbodiimide-based mechanisms. The numbers of different reagents in each of these categories is large. There are extensive reviews which document many of the various available reagents.[329]

4.2.2.3.1 Phosphonium based reagents

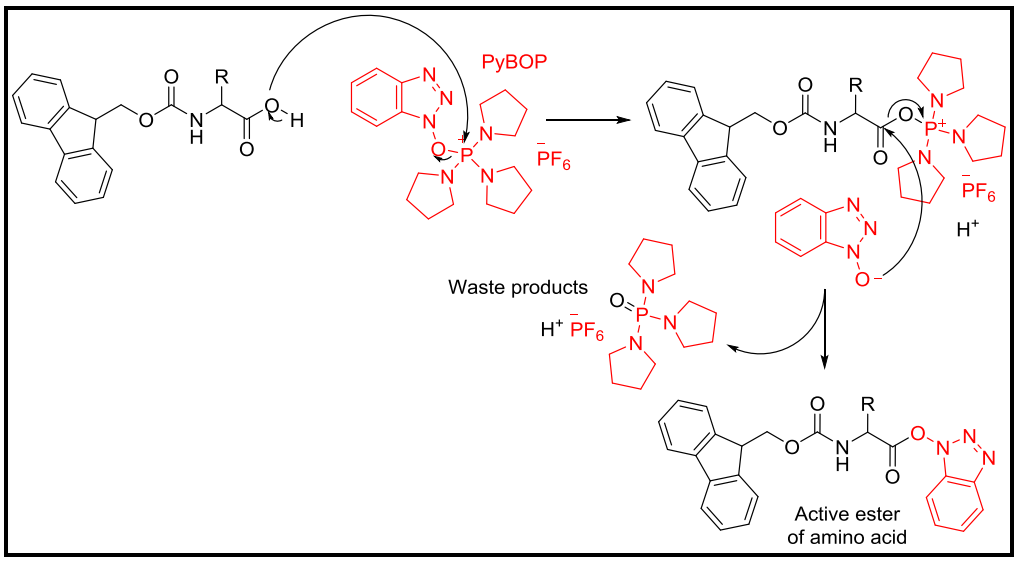


Figure 131: Mechanism for the formation of active esters by phosphonium-based reagents.

There are a multitude of different varieties of phosphonium-based reagents. Of the phosphonium-based coupling reagents, (benzotriazol-1-yloxy)tris(dimethylamino)phosphonium hexafluorophosphate (BOP, **4.13**) is easy to use and allows fast coupling. However, a side product hexamethylphosphorotriamide (HMPA, **4.14**) is known to be a human carcinogen. To avoid this product, benzotriazol-1-yl-oxytripyrrolidinophosphonium hexafluorophosphate (PyBOP, **4.15**) was developed. The more recently introduced (7-azabenzotriazol-1-yloxy)tris(dimethylamino)phosphonium hexafluorophosphate (AOP, **4.16**) and (7-azabenzotriazol-1-yloxy)tris(pyrrolidino)phosphonium hexafluorophosphate

(PyAOP, **4.17**) are slightly more efficient than BOP (**4.13**) and PyBOP (**4.15**). This is due to the HOAt-based active ester which is formed.[330]

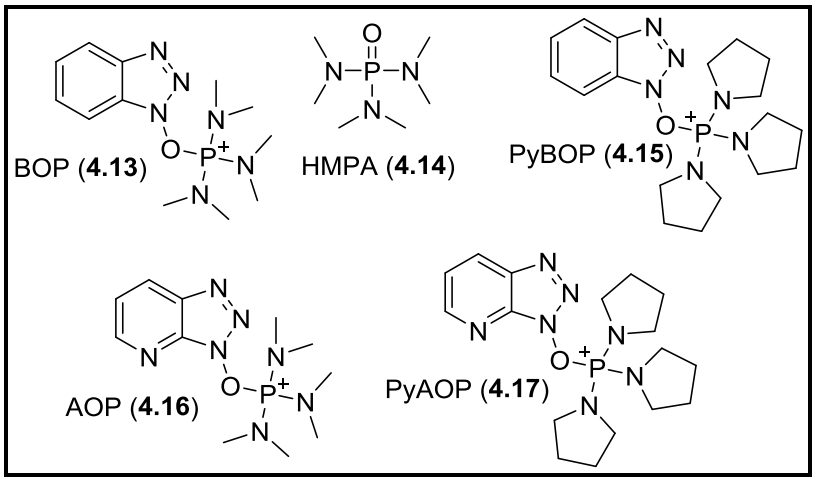


Figure 132: Examples of phosphonium-based coupling agents and carcinogenic waste product HMPA (**4.14**)

4.2.2.3.2 Aminium/Uronium-based reagents

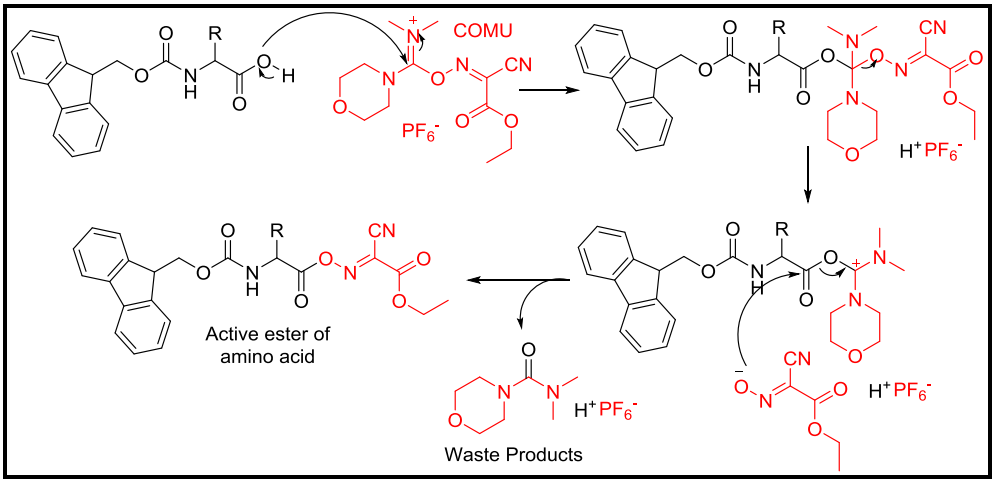


Figure 133: Mechanism for the formation of active esters by uronium-based reagents.

Similarly to phosphonium-based reagents, there are also a range of uronium-based reagents. *O*-(benzotriazol-1-yl)-1,1,3,3-tetramethyluronium tetrafluoroborate (TBTU, **4.18**) or *N*-[(1H-benzotriazol-1-yl)(dimethylamino) methylene]-*N*-methylmethan-aminium hexafluorophosphate *N*-oxide (HBTU - **4.19**) are commonly used.

Uronium-based reagents function in a manner similar to their phosphonium counterparts. However, they can irreversibly react with the N-terminal amino moiety of the peptide in a side-reaction which forms permanent tetramethylguanidinium groups thereby preventing further progress of the

peptide synthesis.[331] This side reaction can easily be avoided by generating the active ester before adding the mixture to the peptidyl resin.

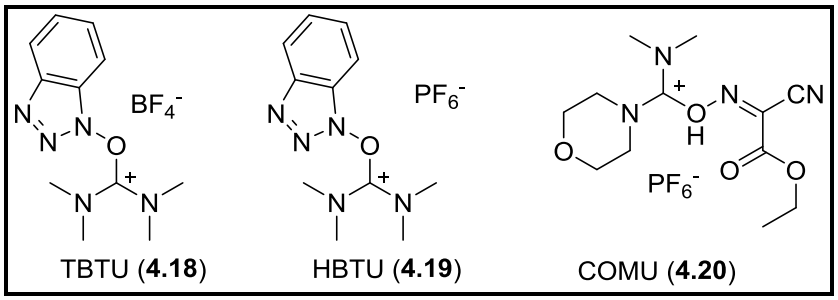


Figure 134: Examples of uronium-based coupling agents

A more modern reagent known as (1-cyano-2-ethoxy-2-oxoethylidenamino-oxy)dimethylamino-morpholino-carbenium hexafluorophosphate (COMU, **4.20**) uses the oxyma moiety to form the active ester which has been shown to reduce side reactions and racemisation during peptide synthesis.[332]

4.2.2.3.3 Carbodiimide-based reagents

Carbodiimides are the oldest group of coupling reagents and were used in the original Merrifield protocol.[321] Although it is possible to use carbodiimide reagents such as DCC (**4.21**) alone to form amide bonds, the formation of the reactive *O*-acylisourea (**4.22**) can then lead to a rearrangement producing a stable side product, an *N*-acylurea (**4.23**).[333] Therefore, in contrast to both uronium and phosphonium based agents which generally include the moieties which will eventually form the active ester, carbodiimides require the addition of an auxiliary reagent, such as HOBt or HOAt. The active ester can then rapidly form from the *O*-acylisourea (**4.22**), avoiding production of the side product (**4.23**).

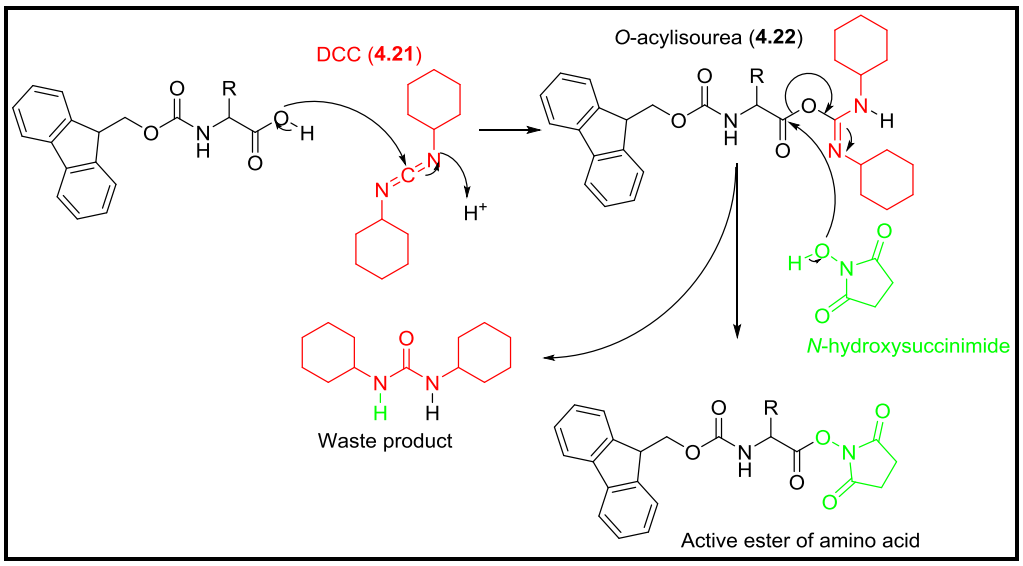


Figure 135: Mechanism for the formation of active esters by carbodiimide-based reagents.

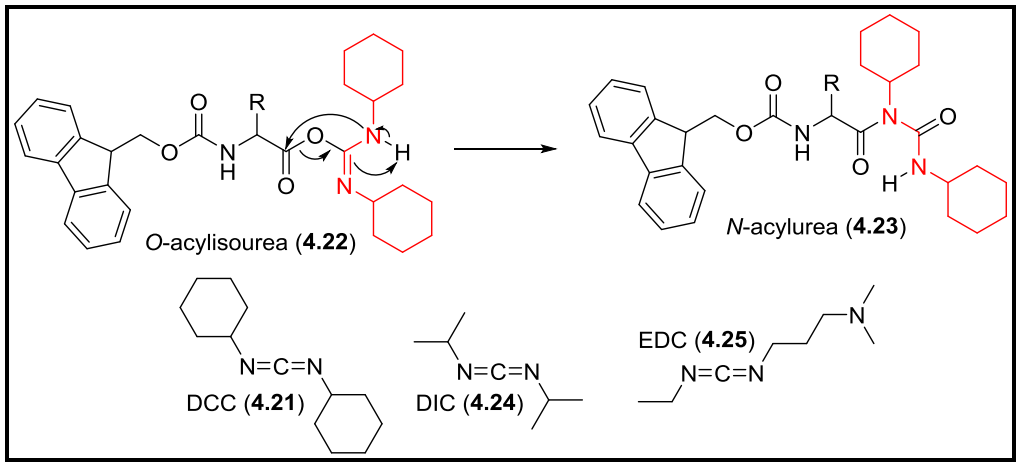


Figure 136: Formation of *N*-acylurea (**4.23**) side product and examples of common carbodiimide reagents

Often, it is the nature of the "active ester"[334] and not the phosphonium/uronium/carbodiimide component of the reagent which determines coupling efficiencies.[329] There are many different reagents used to form these active esters. The hydroxybenzotriazole (HOBt, **4.26**) is commonly used. An aza variant of HOBt (**4.26**) known as HOAt (**4.27**) has been seen to increase the coupling efficiency in comparison with HOBt.[335] This is due to a strategically located nitrogen atom which can interact during the reaction, stabilising the transition state (see Figure 137).

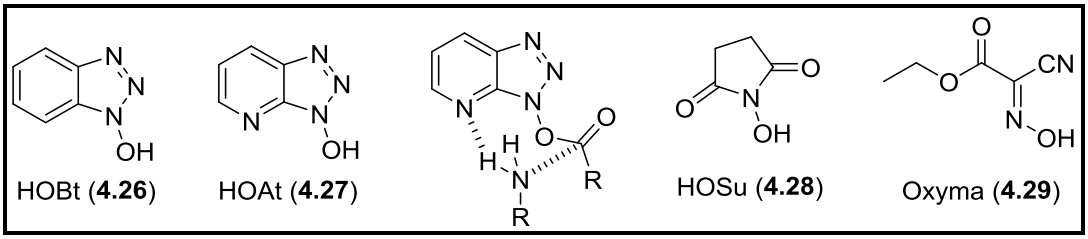


Figure 137: Structures of HOBt (**4.26**), HOAt (**4.27**), HOSu (**4.28**) and Oxyma (**4.29**) and the stabilising effects of HOAt

N-hydroxysuccinimide (HOSu, **4.28**) can be used in tandem with carbodiimide reagents to form an active ester which is less reactive than either the *O*-acylisourea or other active esters. The HOSu ester is stable enough to be isolated and stored at low temperatures. As this active ester has a reduced reactivity, it may be that this reagent can be used to selectively react with a primary amine in the presence of a hydroxy group, for example during the attachment of the activated 3-hydroxyhexanoic acid monomer to the growing peptide chain as it would avoid the potential problem of polymerisation.

Recently, a new additive known as Oxyma (**4.29**) has also been developed. Oxyma has an improved coupling efficiency to HOBt (**4.26**) and is at least equal to HOAt (**4.27**). It also has a remarkable ability to suppress racemisation. Also, significantly, it has a considerably lower risk of explosion (which is possible with HOBt **4.26** and HOAt **4.27**).[336] A uronium salt version of Oxyma (**4.29**) has been developed known as COMU (**4.20**), which was mentioned previously.

4.2.2.4 Synthetic strategy for solid-phase assembly of linear solonamides

In this synthetic strategy, PyOxim[337] (**4.29**) will be used as a coupling agent for the formation of the initial tetramer peptide. Problems with polymerisation may become apparent if PyOxim[338] is also used to couple the 3-hydroxyhexanoic acid residue due to the presence of the unprotected hydroxy group. Therefore, initially, DIC (**4.24**) and HOSu (**4.28**) will be used to assess if it is possible to couple this final residue without the need for protection of the hydroxy group.

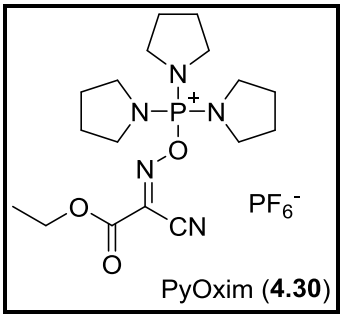


Figure 138: Structure of PyOxim (**4.30**)

4.2.3 Resin selection and Cleavage

Mild cleavage conditions are likely to reduce any possible side reactions during this important step. As Fmoc-SPPS will be used to synthesise the peptide chain, the resin linker must be stable under basic conditions. 2-Chlorotrityl-functionalised resin (**4.31**) is resistant to basic conditions and dilute trifluoroacetic acid (1% TFA) is often used for acidolytic release of the assemble peptide chain.[339] Even milder conditions can also be used, including the use of hexafluoroisopropanol or trifluoroethanol.[339] There are no special protecting group requirements in this synthetic strategy, therefore this resin seems to be suitable for the required purposes.

During cleavage of peptide tethered to 2-chlorotrityl resin, carbocations are generated. Therefore, the scavenger triisopropylsilane (TIPS, **4.32**) will be used to assure these reactive cations do not cause any problematic side reactions.

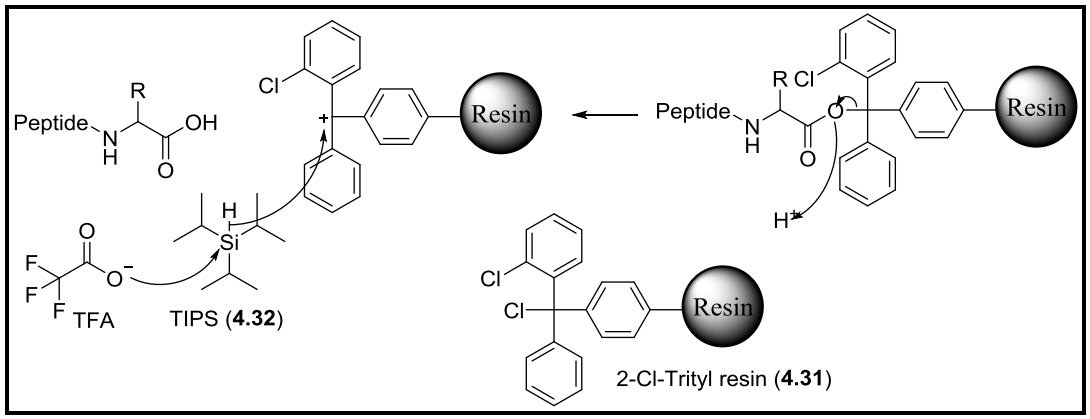


Figure 139: Structure of 2-chlorotrityl resin (**4.31**) and the mechanism for cleavage in acidic conditions

4.2.4 Cyclisation

Whole textbooks have been dedicated to reactions which form esters in various situations using a plethora of different reagents.[340] As this strategy will produce a linear peptide containing an alcohol functionality at the "N-terminal" and a carboxylic acid at the C-terminal, protocols using these functionalities for lactone formation are required.[341]

The simplest reaction protocol producing esters involved simply heating carboxylic acids in the presence of alcohols.[340] Addition of a base or acid catalyst can speed this process up considerably and also lowers the temperature required for the reaction.[342] Many researchers use this method routinely for simple esters. For some substrates, acid or base catalysis is inadequate. The reagents or products could be sensitive to extreme pH, the reaction may be sterically hindered or energetically unfavourable. This is almost always the case when forming macrocycles.[341] Thus, an activator of the carboxylic acid is employed. The principles of carboxylic acid activation are similar for esterification as to those previously discussed for the formation of amide bonds in solid-phase peptide synthesis. However, alcohol groups are considerably less nucleophilic than amines and therefore stronger activating groups would be required.

The use of carbodiimides represents one of the most versatile strategies for the production of difficult esters.[340] However, as with amide formation, the formation of *N*-acylurea side products still remains a problem[320] and an additive is required for the formation of an active ester. Many of the "additives" used in peptide synthesis for the formation of amide bonds do not activate the carboxylic acid sufficiently for attack by the weaker hydroxy nucleophile. However, PyBOP (**4.15**) was used for a macrolactonisation in the total synthesis of the *E. faecalis* AIP analgoue, GBAP (**1.19**).[199] In carbodiimide-mediated activations, *p*-aminopyridines are commonly used as acyl transfer agents.[343] The most commonly used of these is dimethylaminopyridine (DMAP, **4.33**). The use of DMAP (**4.33**) with DCC (**4.21**), DIC (**4.24**) or EDC (**4.25**) has previously been successfully employed during many macrolactonisations.[344] As this

strategy has achieved widespread success, it appears to be promising and will be initially employed for the macrocyclisation of the linear peptide **1.64**.

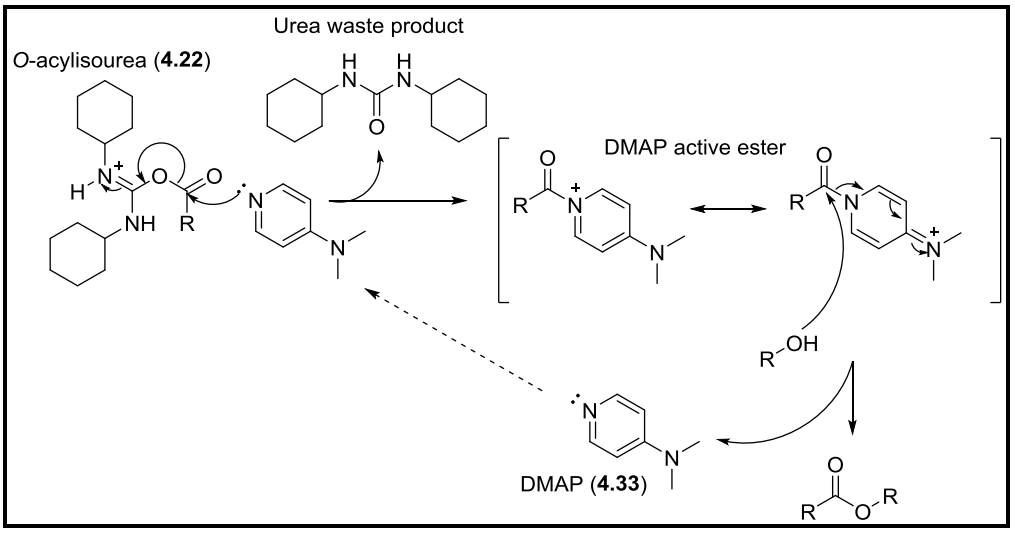


Figure 140: Mechanism of DCC/DMAP-mediated esterification

4.3 Initial synthesis of solonamide A using 3-(RS)-hydroxyhexanoic acid

Thus, the linear peptide chain was synthesised without significant problems using standard Fmoc-SPPS on 2-chlorotrityl resin. An overnight reaction with DIC (**4.24**) and HOSu (**4.28**) in DCM was employed to produce the linear resin-bound peptide **1.63**. Mass spectrometric analysis of test cleavages revealed no evidence of polymerisation due to the free hydroxy moiety. Complete resin cleavage was then achieved with 2% TFA in DCM affording the linear peptide **1.64** in an 85% yield. Finally, *N*'-methyl polystyrene-*N*-cyclohexylcarbodiimide (**4.34**) in the presence of catalytic amounts of DMAP (**4.33**) in $CHCl_3$ successfully cyclised the linear peptide over seven days, generating a mixture of the expected products, SolA (**1.21**), and the related epimer, epiSolA (**1.65**). HPLC purification of these epimers was problematic. Both epimers eluted with similar retention times and the low solubility of the final products also affected the yield. However, both SolA (**1.21**) and epiSolA (**1.65**) were isolated with a yield of 11% and 4% respectively.

The cyclisation step proceeded very slowly but proceeded to completion over seven days, when monitored by HPLC. It may be possible to find a reaction which proceeds at a faster rate. However, at this stage, the cyclisation functioned adequately and, until the fully stereoselective synthesis was implemented, there was no need to optimise this reaction further. Apart from problems with purification, this synthesis was reliable and high yielding. Furthermore, in the *P3::lux* bioreporter assay, both compounds showed promising activity (reported in Chapter 6 beginning on page 230) Therefore, it was considered that this synthetic strategy was acceptable.

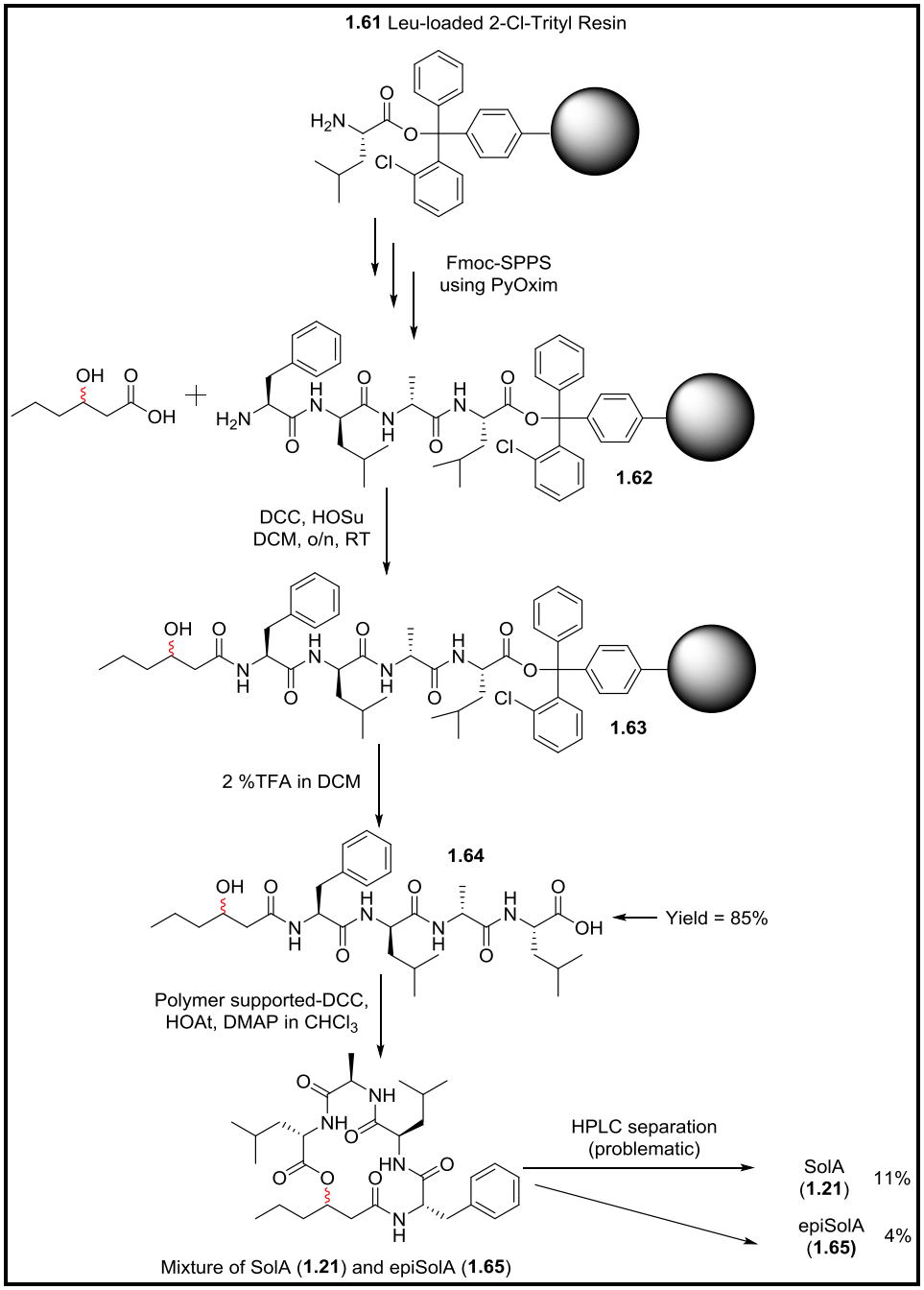


Figure 141: Initial synthesis of SolA (**1.21**) and epiSolA (**1.65**)

4.4 Synthetic strategy for the 3-(R)-hydroxy acids

An initial synthesis of the solonamides had been developed and both SolA (**1.21**) and epiSolA (**1.65**) showed promising activity against AgrC1. Therefore, the project moved on to the development of a stereoselective synthesis of the solonamides. Initially, a synthesis of 3-(*R*)-hydroxyhexanoic acid was required. Literature research revealed many strategies for the production of this monomer.[345] A promising synthetic strategy involved the chiral intermediate 4-substituted oxetan-2-one reported by Nelson *et al*.[346, 347] In, fact, a simple hydrolysis reaction of these 4-substituted oxetan-2-ones with aqueous lithium hydroxide would afford the required 3-(*R*)-hydroxy fatty acids.

4.5 Synthesis of 3-(R)-hydroxyhexanoic acid

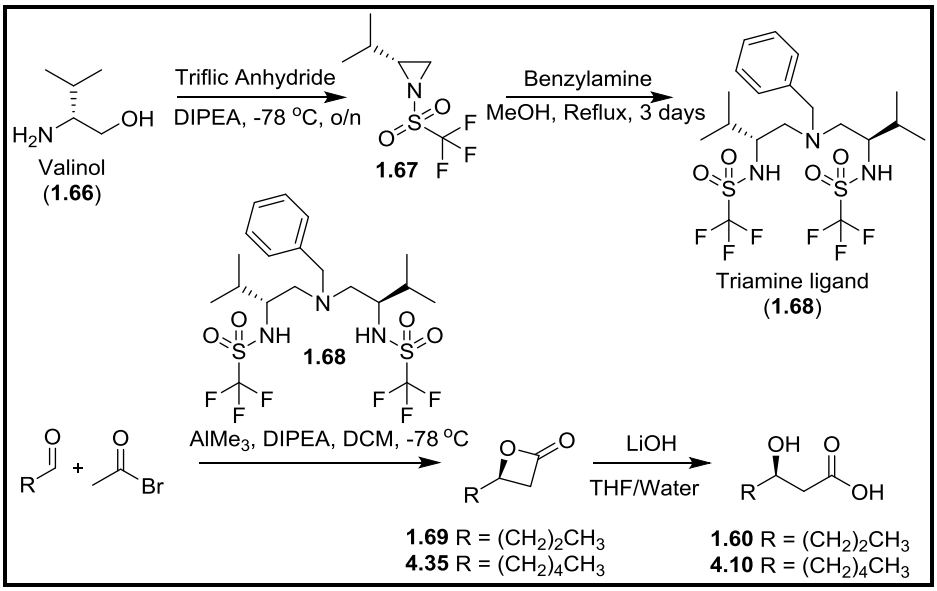


Figure 142: Synthesis of 3-hydroxyhexanoic acid (**1.60**) adapted from Nelson *et al.*[346]

4.5.1 Aziridine production

The principles behind the triamine ligand synthesis were originally reported by Cernerud *et al.*[348] and later developed for the production of chiral alcohols.[349] Chiral amino alcohols were considered to provide a wide variety of starting materials, allowing the production of a large number of C_3-symmetric tripodal tetraamines. These could then be deployed as useful ligands in a variety of applications. The chiral properties incorporated by the use of amino alcohols were considered to be useful as agents of selectivity in creating these ligands. Later developments by Nelson *et al.*[235, 346, 347] used valinol to produce a triamine ligand which imparted stereoselectivity to an aluminium mediated ketene-aldehyde cycloaddition. Therefore, maintenance of enantiomeric purity in these early stages is vital for the eventual production of 3-(*R*)-hydroxyhexanoic acid.

In the first instance the aziridine **1.67** is attained by nucleophilic substitution of triflic anhydride by both the amine and the alcohol of valinol (**1.66**). An intramolecular nucleophilic substitution ensues where the nitrogen attacks the carbon releasing the triflate leaving group and forming the aziridine **1.67** (Figure 143). This reaction was performed at -78 ^{0}C and produced a pale yellow oil. Initial thin layer chromatography with permanganate staining

showed a single spot after work up. However, mass spectroscopic and NMR analysis of the oil showed a strange mixture of products. When the oil was reanalysed by TLC, further spots were now evident. It was concluded that the product was unstable and therefore, the aziridine product was immediately used in the following reaction. Nevertheless, a sample was immediately dissolved in cold chloroform and ^{1}H-NMR was quickly performed to confirm their identity. The ^{1}H-NMR spectrum showed a distinctive doublet at 2.45 ppm and a multiplet at 1.65 ppm indicative of the aziridine moiety.

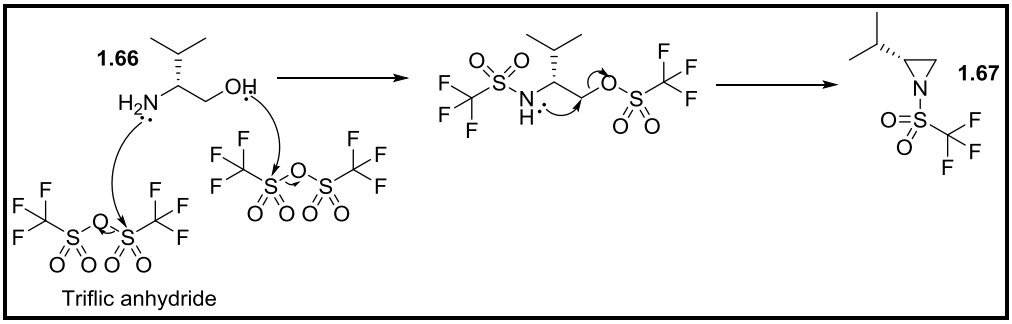


Figure 143: Mechanism of aziridine **1.67** production

4.5.2 Triamine ligand formation

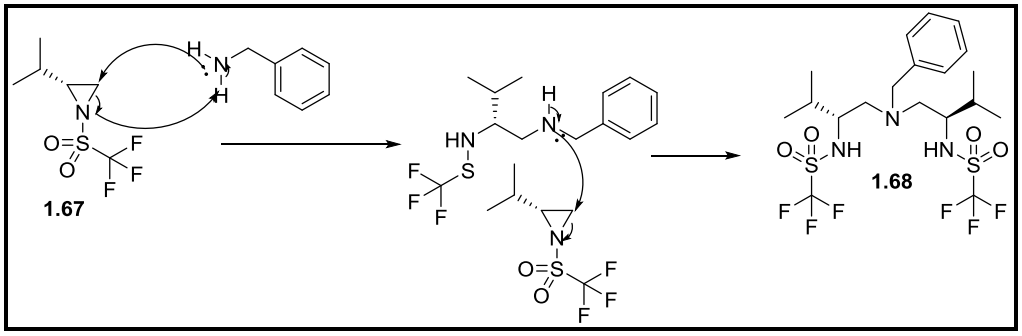


Figure 144: Mechanism for Triamine ligand **1.68** synthesis

As the aziridine is a strained three-membered ring with a significant electron withdrawing group on the nitrogen atom, these aziridines are vulnerable to nucleophilic addition (see Figure 144). The literature procedure for the formation of the triamine ligand required the addition of one equivalent of benzylamine to two equivalents of the aziridine **1.67** in DCM, followed by heating under reflux at 100 ^{0}C.[347] When initially attempting this synthesis using DCM, it was found that the solubility of the reagents and products was limited in this solvent. Furthermore, sample preparation for column chromatography was challenging. It was also found that trituration with hexane regularly failed if the

fraction isolated from column chromatography was impure. The use of MeOH as a solvent improved solubility and made sample preparation for the column considerably easier. Furthermore, this actually improved chromatographic separation. In fact, this was also the method originally used by Cernerud *et al*.[349]

4.5.3 Ketene-Aldehyde cycloaddition

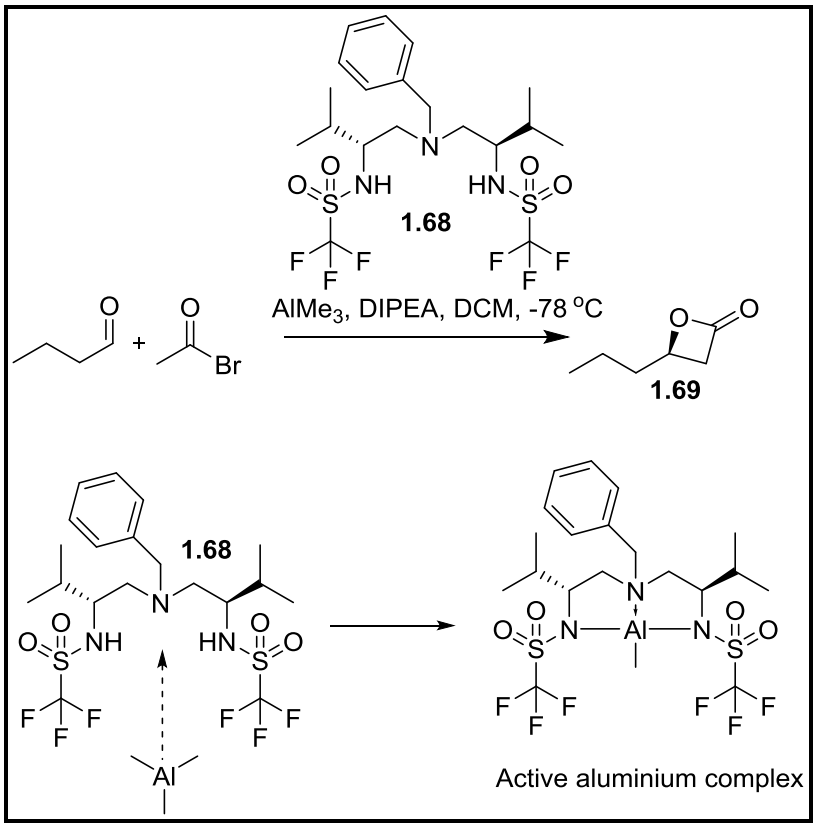


Figure 145: The ketene-aldehyde cycloaddition reaction and the formation of the active aluminium complex

During this reaction, the methods outlined in Nelson *et al*.[347] were followed. Trimethylaluminium and the triamine ligand **1.68** were mixed at room temperature under nitrogen to form the active aluminium complex. The mixture was then cooled to -78 ^{0}C. Acetyl bromide was very slowly added forming a ketene stabilised by the aluminium complex. Following the addition of the acetyl bromide, the butanal was then slowly added. The reaction was maintained at -78 ^{0}C overnight. During work up, the use of strong acids such as HCl resulted in the formation of some side-products. Therefore, 10% citric acid was used instead which resolved the problem. Nelson *et al.* purified the final product **1.69** by distillation. However, the team who were responsible for checking the protocol reported that the product degraded under these

conditions.[347] Therefore, the product was isolated using column chromatography with 1:9 EtOAc/Hex as eluent, as reported by the second team. This afforded the final product as an oil in 82% yield.

It was found that many of the oxetan-2-one products synthesised were not stable on storage. Therefore, instead of attempting to analyse the enantiomeric excess (*ee*) at this stage, the products were immediately used in the next reaction to produce 3-(*R*)-hydroxy acid moieties.

4.5.4 Hydrolysis reaction

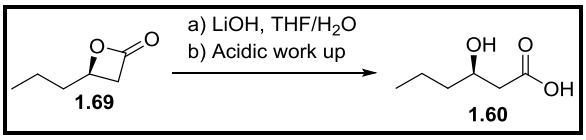


Figure 146: LiOH-mediated hydrolysis of oxetan-2-one **1.69** to produce product **1.60**

It was expected that the oxetan-2-one product **1.69** could be simply hydrolysed with LiOH to produce the required product **1.60**. Thus, the cyclic lactone **1.69** was dissolved in THF and LiOH was added. The reaction was stirred for 2 hours, and following a work-up procedure, the desired compound was obtained as a pale yellow oil in a quantitative yield. It was pleasing to discover upon NMR analysis that this did correspond to the product **1.60**. However, it still remained unclear as to the enantiomeric excess achieved by this synthesis. As a chiral column was unavailable, a different method for characterisation of the enantiomeric purity would need to be devised.

(1*R*,2*R*)-(−)-2-Amino-1-(4-nitrophenyl)-1,3-propanediol was reported to be a good resolving agent when reacted with gossypol (a natural phenolic aldehyde).[350] However, when coupled with racemic 3-hydroxyhexanoic acid using DCC and HOSu the products could not be separated by HPLC and the NMR showed a complex mixture. Therefore, this method could not be used for the determination of the *ee*. Moreover, derivatization with Mosher's acyl chloride produced a complex mixture.

Gratifyingly, coupling of the racemic 3-hydroxyhexanoic acid with phenylalanine methyl ester revealed two peaks with similar elution times in the HPLC analysis (Figure 148). Mass spectroscopy confirmed their identity as the

expected products **4.36** and **4.37**. Optimisation of the gradient could not completely separate the peaks. However, it was believed that the separation was sufficient to afford an estimate of the *ee* for the synthesised product **1.60** which was calculated to be 78% (Figure 148).

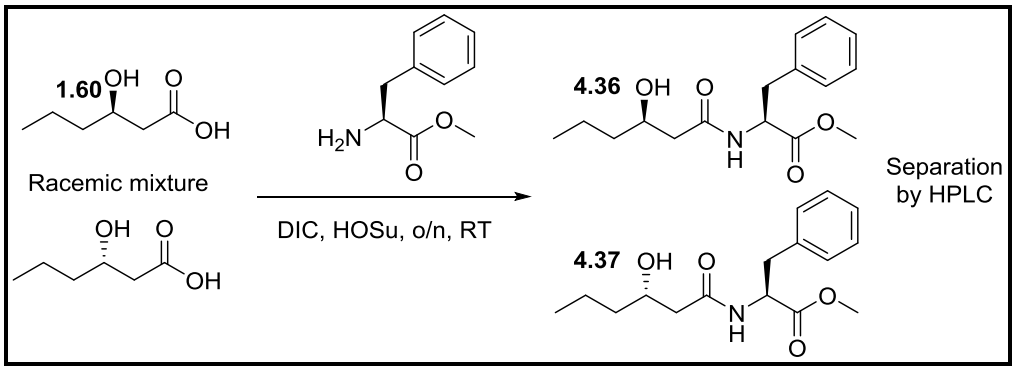
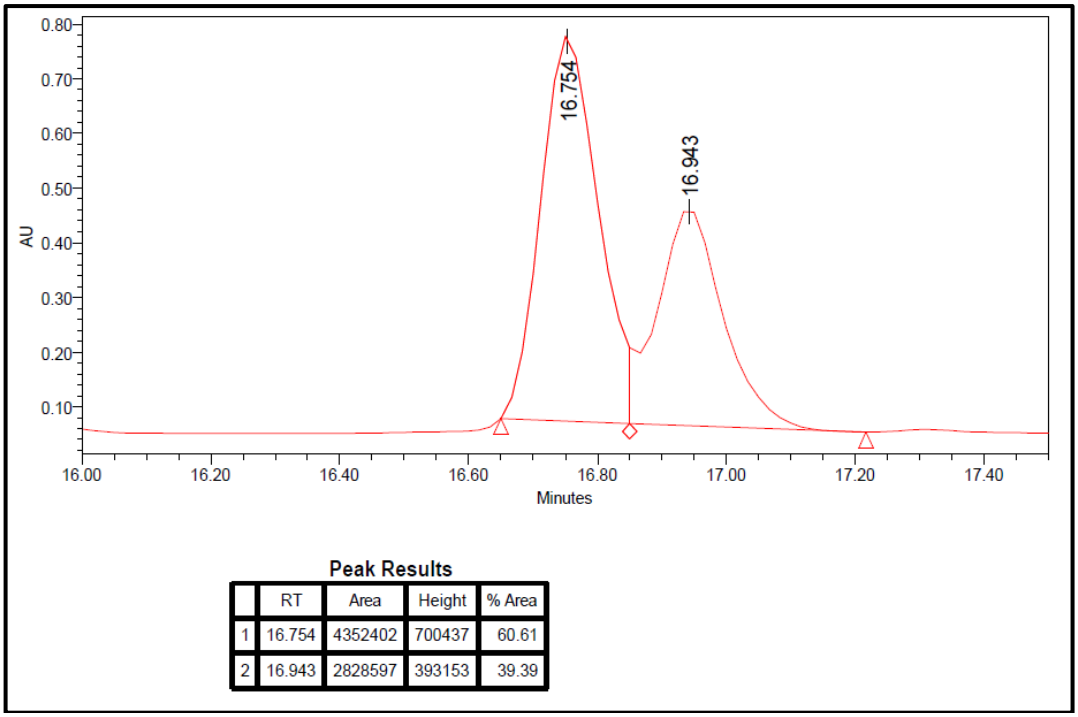


Figure 147: Scheme showing the derivatisation of a racemic 3-hydroxyhexanoic acid mixture to produce **4.36** and **4.37**

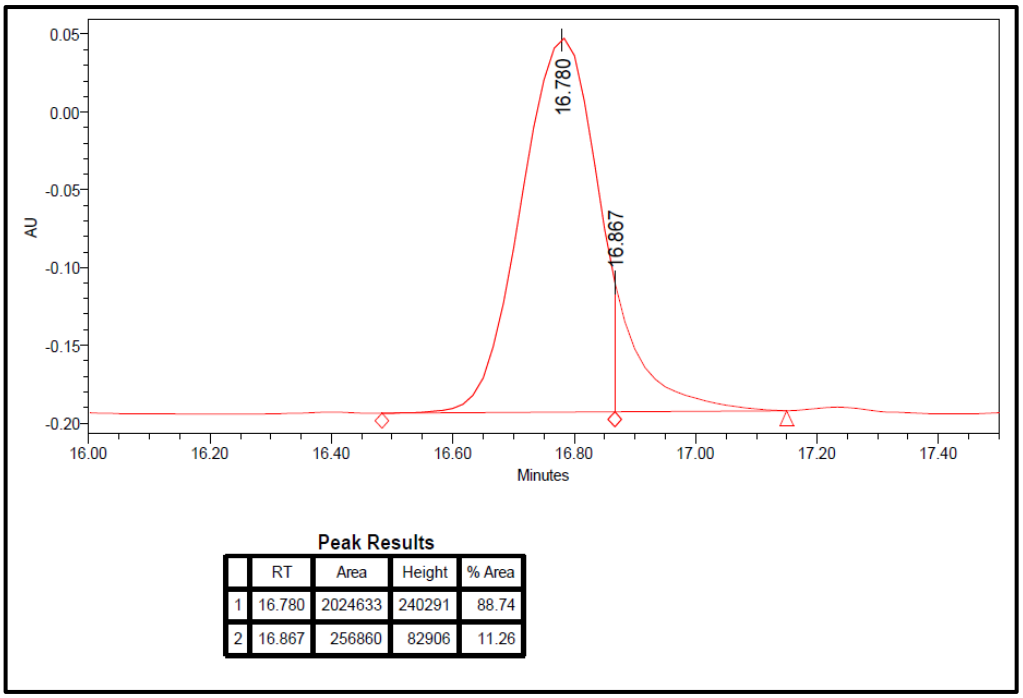
Thus, this synthetic method was employed to synthesise 3-(*R*)-hydroxyoctanoic acid (**4.10**) to produce SolB (**1.22**) and a further panel of 3-(*R*)-hydroxy acid analogues which were eventually incorporated into solonamide analogues in order to determine the SAR towards the AgrC receptor.



Peak Results

	RT	Area	Height	% Area
1	16.754	4352402	700437	60.61
2	16.943	2828597	393153	39.39

Figure 148: 3-(*R*/*S*)-hydroxy hexanoic acid was coupled to phenylalanine methyl ester using DIC and HOSu in $CHCl_3$. Analytical HPLC (20% B for 2 mins to 80% B over 20 mins) of the product showed good separation of diastereomers.



Peak Results

	RT	Area	Height	% Area
1	16.780	2024633	240291	88.74
2	16.867	256860	82906	11.26

Figure 149: 3-(*R*)-hydroxy hexanoic acid (**1.60**) was coupled to phenylalanine methyl ester using DIC and HOSu in $CHCl_3$. Analytical HPLC (20% B for 2 mins to 80% B over 20 mins) of the product (**4.36**) showed a high enantiomeric excess of the desired *R*-diastereomers.

4.6 Stereoselective synthesis of solonamide A and B

Having successfully produced the key building block 3-(*R*)-hydroxyhexanoic acid (**1.60**), the previously developed solonamide synthesis was used for stereoselective synthesis of SolA (**1.21**). As previously, Fmoc-SPPS produced the tetramer peptide without any problems. Coupling of the 3-(*R*)-hydroxyhexanoic acid (**1.60**) proceeded as expected. Acidolytic cleavage produced the expected crude linear peptide **1.64**. Finally, the macrolactonisation using the Steglich reaction produced the crude product, in yields similar to those reported earlier (Section 4.3).

However, HPLC purification of the crude synthesised product revealed a disappointing diastereomeric excess (*de*) of SolA (**1.21**) product. Specifically, purification afforded 10 mg of SolA; this represented a yield of 20%, which was an improvement on previous yields. However, 2 mg of epiSolA (**1.65**) was also produced. This represented a purified *de* of 67%. Furthermore, careful analysis of the original HPLC trace suggested an actual *de* in the crude mixture of closer to 20%.

As the *ee* of the 3-(*R*)-hydroxyhexanoic acid had been estimated at approximately 80% (which represented a conservative estimate as the peaks did not completely separate), it was initially unclear as to how this loss of stereoselectivity had occured. However, the desired compound was isolated and the method was successfully applied for the synthesis of other solonamide analogues.

4.7 Synthesis of solonamide analogues

Multiple solonamide analogues were produced using this synthesis. Initially, solonamide B was synthesised. The initial peptide assembly stage afforded approximately 120 mg of the linear peptide, which represented an improved yield of 99%. Cyclisation afforded nearly 60 mg of crude product which was also an improvement on the solonamide A synthesis. Analytical HPLC traces revealed a *de* of approximately 70%. However, purification *via* semi-preparative HPLC afforded 3 mg (2.6% yield) of SolB and 3.8 mg (3.3% yield) of epiSolB. It is believed that the analytical HPLC data represents a more accurate measure of the *de* of the crude mixture as some material is inevitably lost on collection of fractions to prevent contamination of either of the epimers. However, this loss of *de* during the isolation of each diastereomer was of further concern and necessitated continued work, both to discover the cause of the loss of stereoselectivity and, hopefully, rectify the problem. However, this synthesis was employed for the production of further analogues as there was sufficient data to identify each of the solonamide epimers (Figure 150-Figure 152). This synthesis also fortuitously allowed considerable data to be accrued on the SAR of the related solonamide epimers which would not have been available if this initial synthesis had been completely stereoselective.

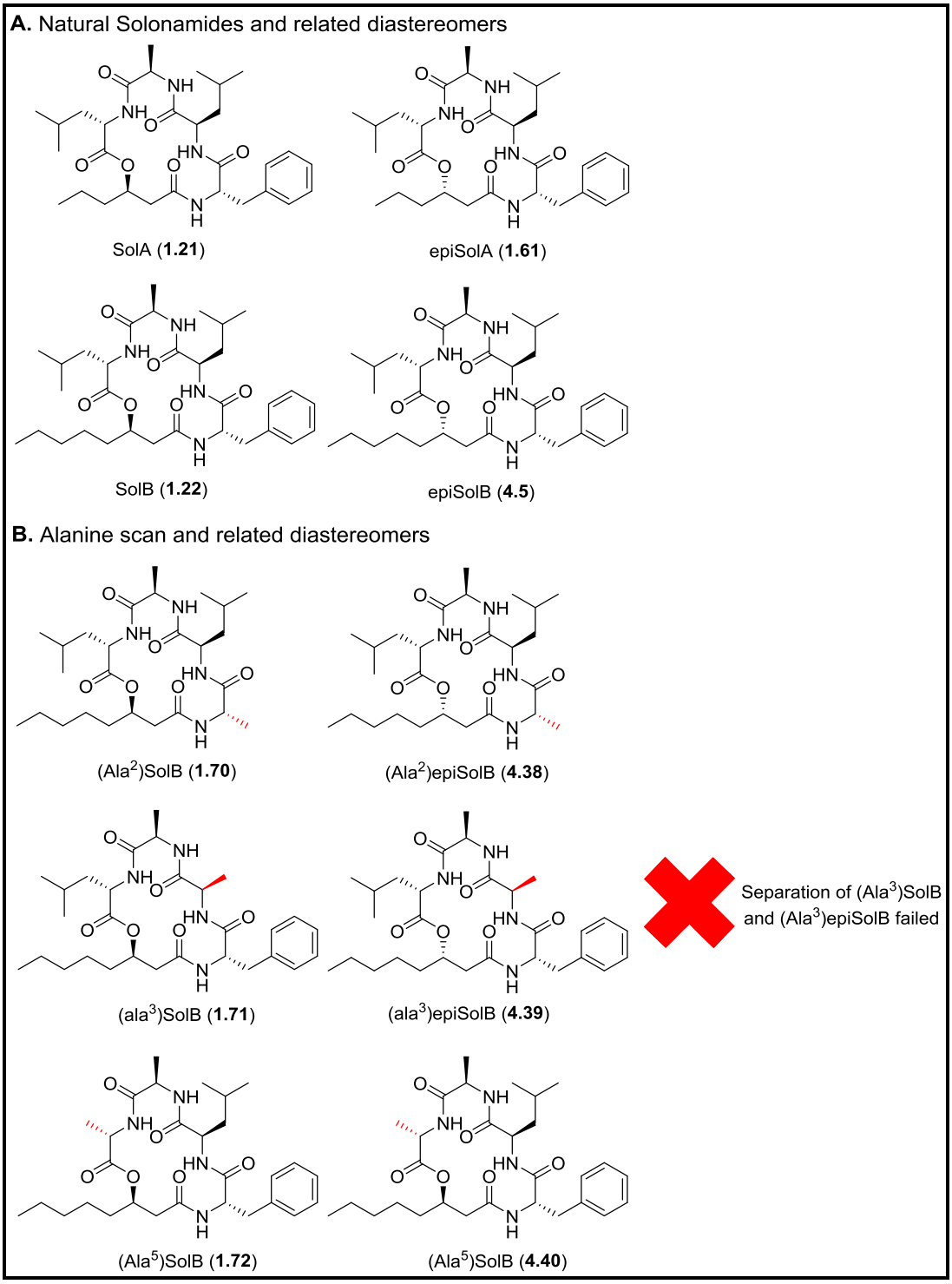


Figure 150: Diagram of the analogues produced using this synthesis including **A.** the natural products and related diastereomers and **B.** an alanine scan and related diastereomers. (ala^3)SolB (**1.71**) and (ala^3)epiSolB (**4.39**) could not be produced using this synthesis as the diastereomers eluted too closely on HPLC purification.

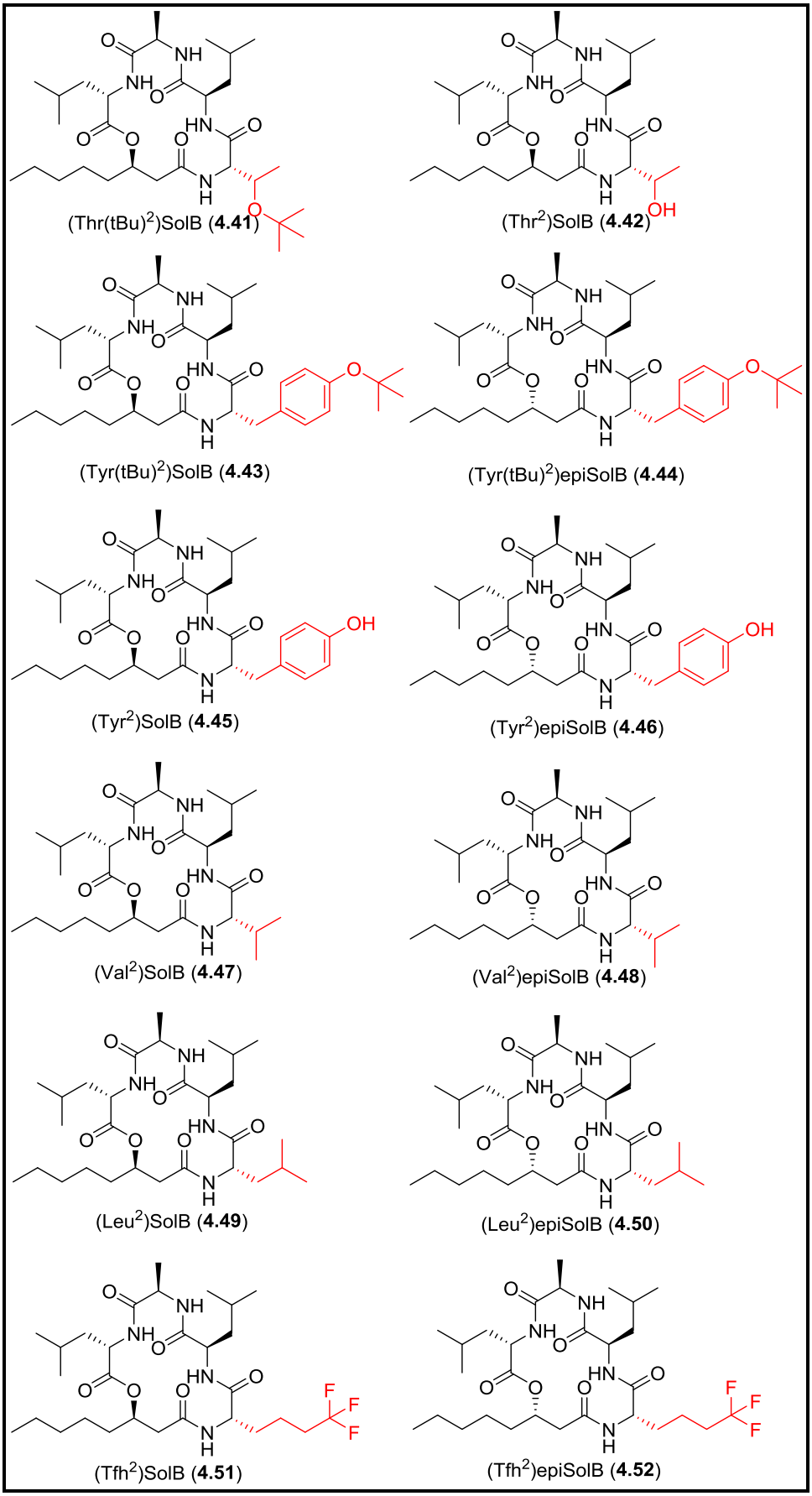


Figure 151: Diagram of the solonamide analogues produced by variation of Phe^2 residue

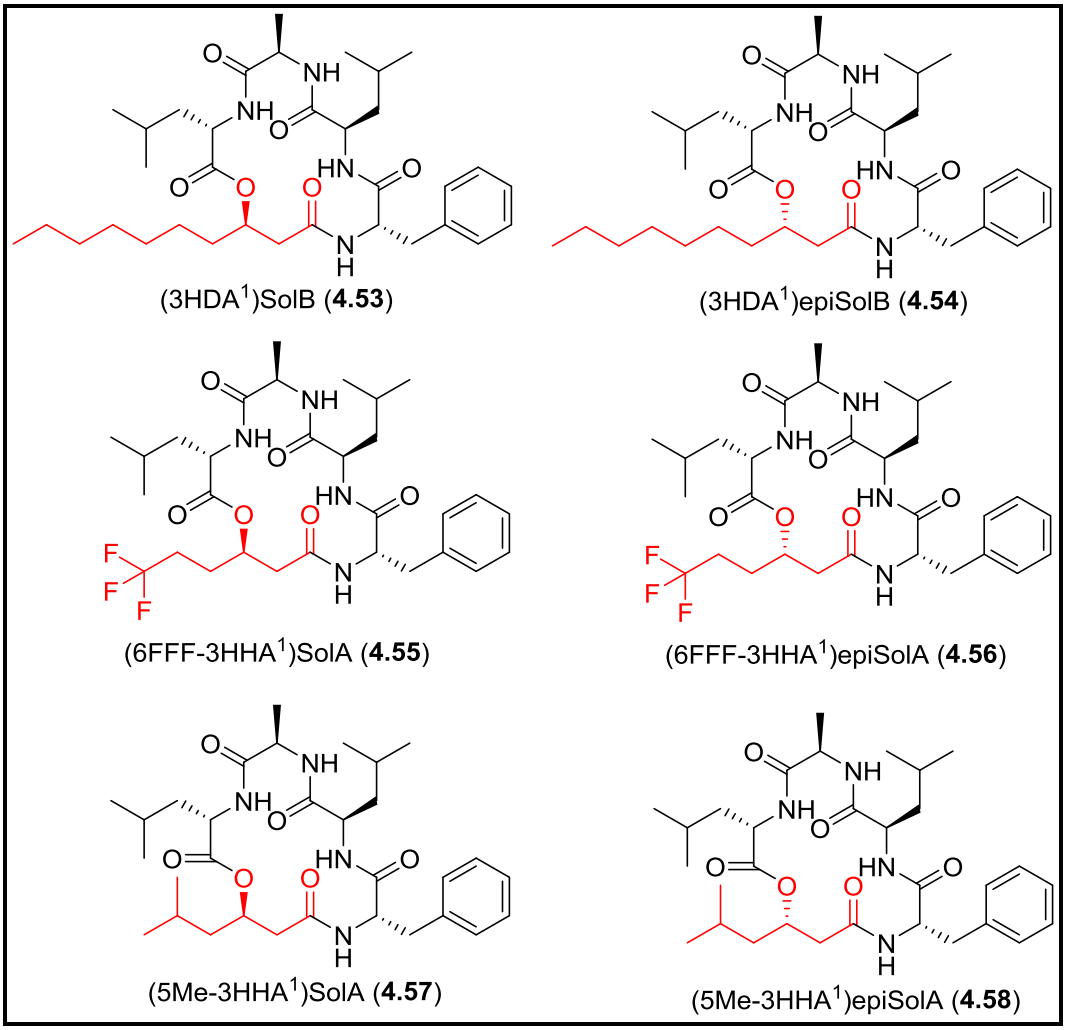


Figure 152: Diagram of the solonamide analogues produced by variation of the 3-(*R*)-hydroxyoctanoic acid residue.

4.7.1 Epimerisation of the (ala[3])SolB

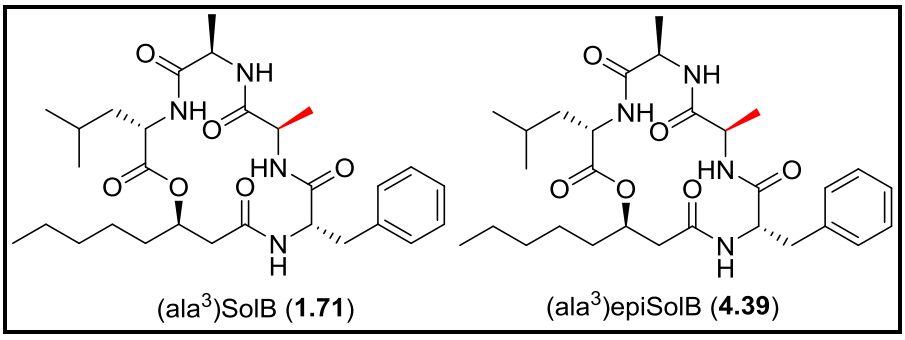


Figure 153: Structure of (ala[3])SolB (**1.71**) and the related diastereomer, (ala[3])epiSolB (**4.39**)

During the synthesis of solonamide analogues, one analogue was found to be particularly vulnerable to epimerisation; it was also challenging to separate by HPLC methods. The (ala[3])SolB (**1.71**) and its diastereomer (**4.39**) could not be effectively isolated by HPLC. Therefore, this was considered to be an ideal

candidate to investigate the loss of stereoselectivity and for attempts to develop an improved stereoselective synthesis. These issues are considered in the next chapter.

4.8 Conclusion

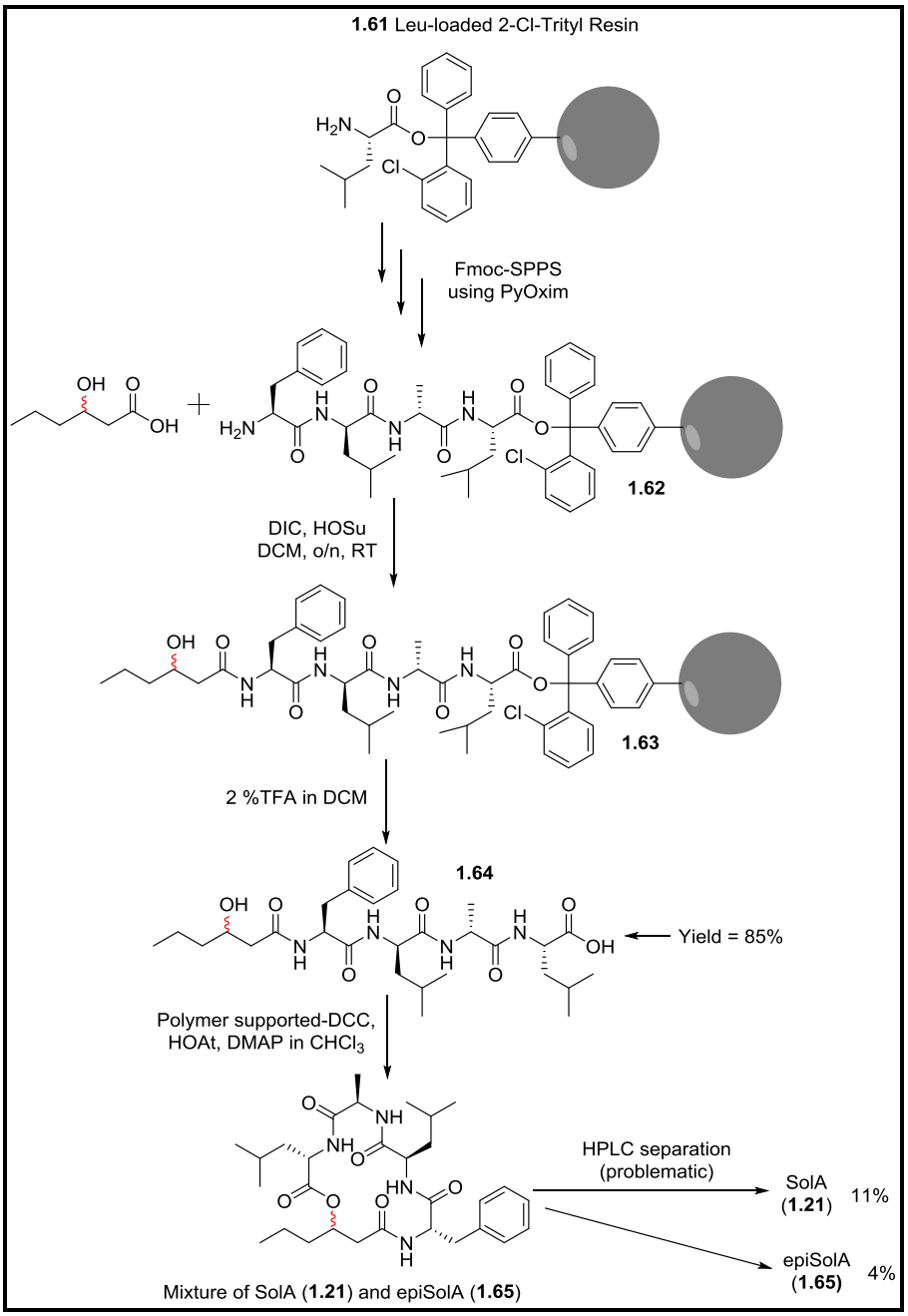


Figure 154: Initial synthesis of solonamide A (**1.21**) and epiSolA (**1.65**)

In this chapter, an initial racemic synthesis of solonamide A (**1.21**) was reported. Fmoc-SPPS using the usual protocols and commercially available Fmoc-protected amino acids produced resin-bound peptide **1.62**. This was followed by condensation with racemic 3-hydroxyhexanoic acid (**1.60**), activated using DIC and HOSu in DCM, to produce the linear resin-bound peptide **1.63**. TFA-mediated acidolytic cleavage proceeded to produce the linear

peptide **1.64** with a crude yield of 85%. Cyclisation of the linear peptide using polymer-bound carbodiimide **4.34** in the presence of DMAP (**4.33**) followed by HPLC purification afforded the final SolA (**1.21**) product in 11% yield. A related epimer, epiSolA (**1.65**), was also produced in a 4% yield as expected. This pilot synthesis afforded the product with a total cumulative yield of roughly 9% which compares favourably with the pilot synthesis of Kitir *et al*. which afforded the product with a cumulative yield of less than 5%.[318]

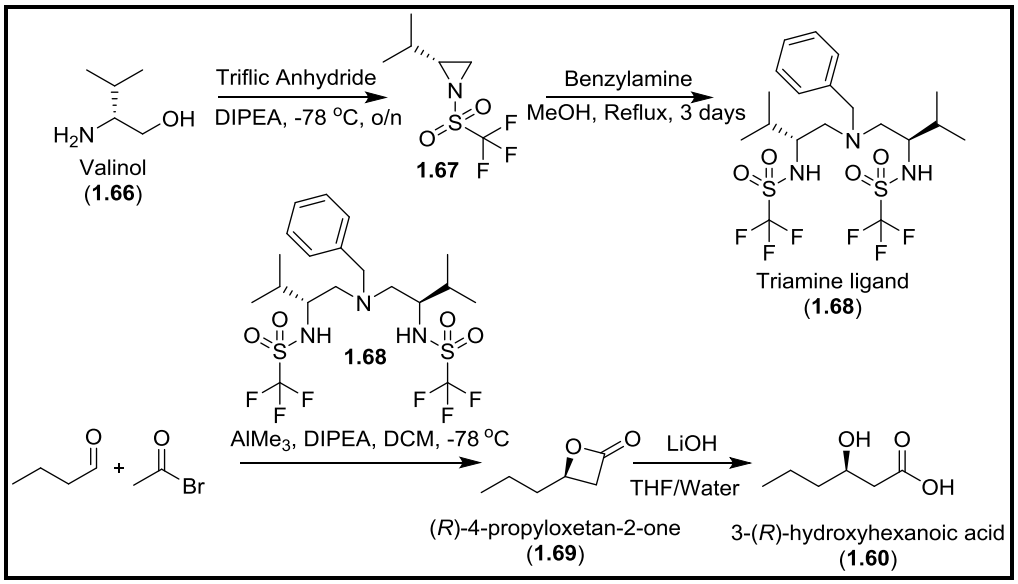


Figure 155: A synthesis of 3-hydroxyhexanoic acid (**1.60**) adapted from Nelson *et al*.[346]

Following the successful development of a convergent approach for total synthesis of SolA, the procedure of Nelson *et al.* was adapted to produce 3-(*R*)-hydroxyhexanoic acid (**1.60**), using a ketene-aldehyde cycloaddition assisted by a chiral aluminium-triamine ligand complex. A new method using phenylalanine methyl ester was used to derivatise a racemic 3-hydroxyhexanoic acid which was then used to determine the *ee* of the synthesised compound (**1.60**). The *ee* was found to be 78%.

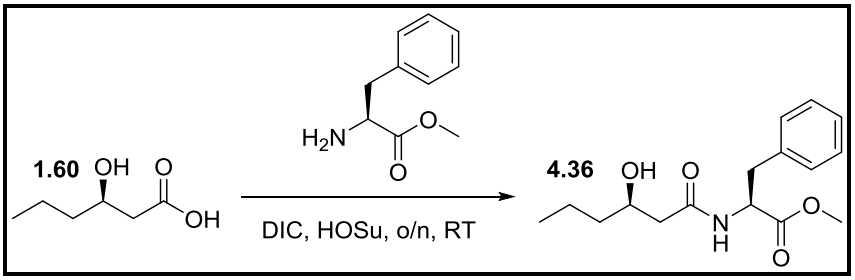


Figure 156: Scheme showing the derivatisation of 3-(*R*)-hydroxyhexanoic acid to produce **4.36**

Thus, the 3-hydroxy acid (**1.60**) proved to have good optical purity and was then employed for the synthesis of SolA. Unfortunately, stereopurity was reduced at some point during the solonamide synthesis, producing a *de* of 67% after HPLC purification in SolA (**1.21**). Although several solonamide analogues were subsequently synthesised and purified using this route, some analogues were more vulnerable to this reduction in stereopurity. Notably, (ala^3)SolB (**1.71**) and its related epimer were inseparable by HPLC and this analogue was therefore selected for development of an improved stereoselective synthesis.

Solonamide A (**1.21**), Solonamide B (**1.22**) and their related epimers and analogues will all be tested in *P3::lux* based bioreporter assays against AgrC1. This will allow full assessment of the structure activity relationship against the AgrC receptor. A full pharmacological assessment of the mode of binding and mode of action of the solonamides will also be executed. This is fully discussed in Chapter 6 beginning on page 230.

This synthesis is not satisfactory as the final *de* is below satisfactory levels. Furthermore, HPLC purification of these diastereomers is time consuming and material loss at this stage reduces the yield of the synthesis considerably. Therefore, work to improve this synthesis with a special focus on the maintenance of the stereopurity of the products is required. Discussion of the cause of the loss of stereopurity, strategies to improve the synthesis, and results of their implementation are detailed in the following chapter.

5 Developing an improved method for the synthesis of solonamides

This chapter focuses on the development of a robust method for the total stereoselective synthesis of the challenging analogue, (ala^3)SolB (**1.71**). This method was then applied for the synthesis of SolA and SolB as well as three further analogues.

Initially, the established synthesis outlined in Chapter 4 was analysed to reveal potential problematic reactions. Then, work developing the acidolytic cleavage conditions and experiments intended to improve the cyclisation protocol are detailed. Following the failure of these methods to produce an improved synthetic method, a new method was devised which utilises an alternative cyclisation site; this approach employs a macrolactamisation instead of macrolactonisation to form the macrocyclic structure. Finally, this new stereoselective synthesis is evaluated in comparison to the previously published synthesis of Kitir *et al.*[318] and the synthesis discussed in the previous chapter 4.

5.1 Introduction

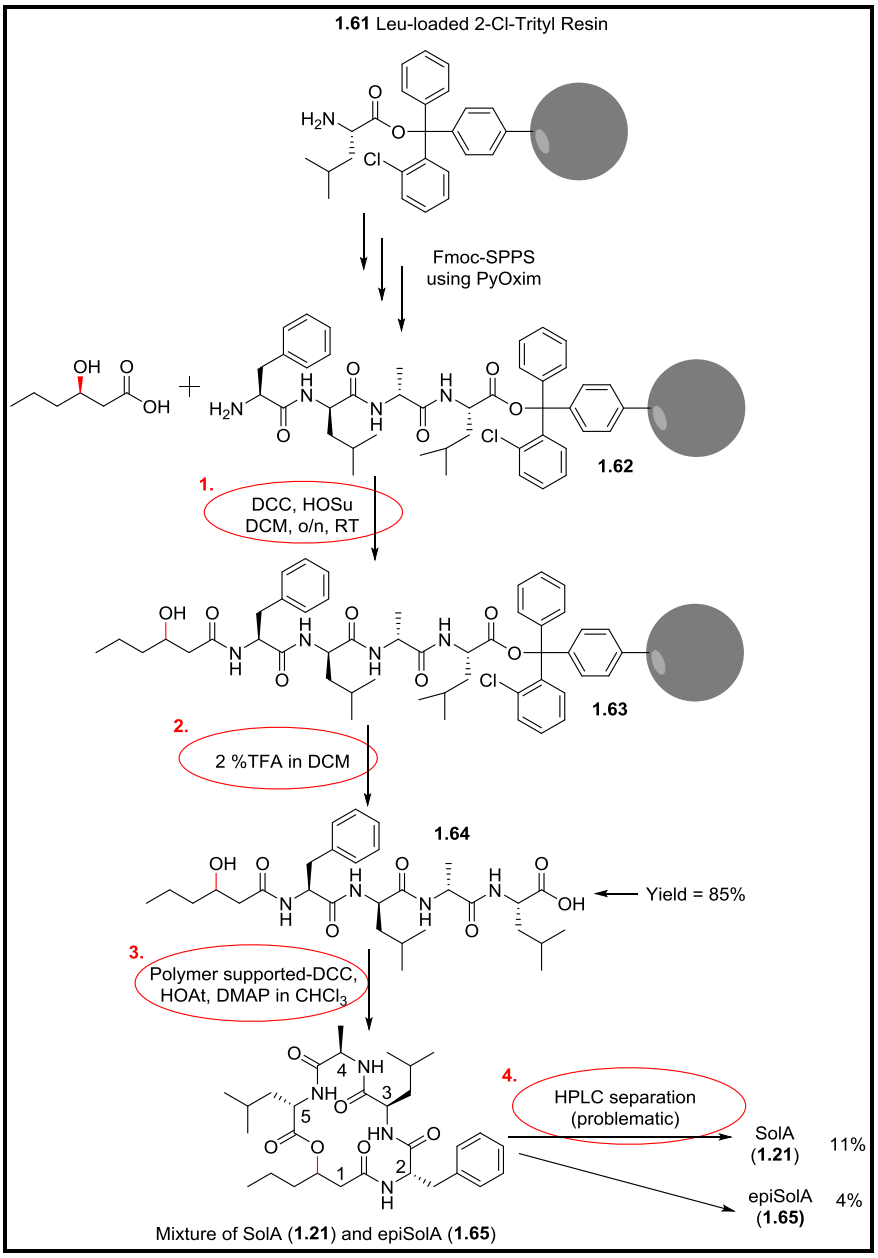


Figure 157: Initial synthesis of solonamide A (**1.21**) and epiSolA (**1.65**)

The loss of stereopurity could be produced during only four processes (see Figure 157). These four suspect protocols are:

1. coupling the 3-(*R*)-hydroxyhexanoic acid to the assembled peptide sequence
2. acidolytic cleavage of the peptide from the resin
3. macrolactonisation of the linear peptide
4. purification by HPLC

Two of these processes could be easily eliminated from this list. Assessment of the *ee* of the 3-(*R*)-hydroxyhexanoic acid monomer (**1.60**) had been executed using a DIC and HOSu mediated coupling with phenylalanine methyl ester producing the derivatised product **4.37** (see Figure 158). This was identical to the conditions used to initially couple the 3-(*R*)-hydroxyhexanoic acid (**1.60**) to the growing peptide producing **1.63**. Thus, this coupling was known to produce products with a high diastereomeric purity and could not be responsible for the loss of *de*.

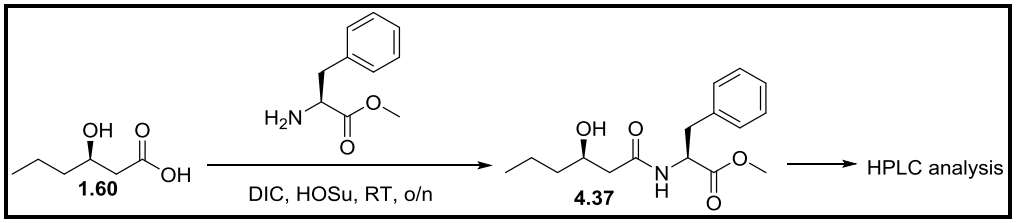


Figure 158: Scheme showing derivatisation and analysis of **1.60** which produced a product with a very high *de.*

The derivatisation of 3-(*R*)-hydroxyhexanoic acid with phenylalanine methyl ester, followed by HPLC analysis of the derivatisation product **4.37** which showed essentially a single diastereomer. Furthermore, it is highly unlikely that HPLC purification of the final macrocyclic peptide is responsible for the lost diastereomeric purity. Furthermore, if this was the case, repurification of NMR samples in DMSO-*d6* would have similarly lost diastereomeric purity which was not the case.

Moreover, under acidic conditions, loss of diasteromeric purity during peptide cleavage from the resin was highly unlikely. However, given that solubility of the linear peptide had occasionally been a problem during cleavage, it was decided to trial some further milder cleavage conditions to optimise this process (see Section 5.2).

Finally, the macrocyclisation step was considered and the details are outline in Sections **Error! Reference source not found.** and 5.3. This reaction lasts even days in the presence of the basic reagent, DMAP (**4.33**). It was considered that even trace amounts of water in the solvent in the presence of a strong basic reagent, such as DMAP (**4.33**), could potentially cause epimerisation of the 3-

hydroxy acid moiety. A reactive carbodiimide **4.34** is present and these reagents have been known to cause C-terminal epimerisation,[329] however, the epimerisation problem observed was at the 3-hydroxy position and not the C-terminal amino acid. Therefore, this reagent is unlikely to be causing these problems. In response to these potential problems, the isolated 3-(*R*)-hydroxyhexanoyl-*L*-phenylalanine methyl ester (**4.37**) would be exposed to DMAP (**4.33**) for a defined period and then resubjected to HPLC analysis. Loss of diastereomeric purity would prove that DMAP is likely to be responsible for the loss of *de* during the cyclisation reaction.

5.2 Alternative cleavage conditions

Many mild conditions are available for the removal of assembled peptides from 2-chlorotrityl resin. Four methods were selected in an attempt to resolve the occasional solubility problems on peptide cleavage from the resin, aiming to possibly improve the yield or the ease of the protocol. (ala^3)SolB (**1.71**) was used as the model system as previously discussed. The four conditions evaluated were as follows:

1. 0.5% TFA, 1% TIPS in DCM - wash through resin
2. 20% HFIP, 1% TIPS in DCM - 1 h incubation
3. 10% Acetic acid, 1% TIPS in DCM - 2 h incubation
4. 20% Trifluoroethanol, 1% TIPS in DCM - 2 h incubation

Condition 3 and condition 4 mildly increased the yield, however, on cyclisation the products were racemic with no observeable *de*. The reason(s) for this precipitous loss of *de* is unclear. In contrast, the original condition 1 had a marginally lower yield but displayed an average crude *de* of roughly 50%. Finally, use of cleavage mixture 1 followed by a small volume of isopropanol rinse of the spent resin afforded the linear product with a similar yield and maintained a *de* of roughly 50% upon cyclisation. Therefore, the use of this isopropanol wash following cleavage was employed in future syntheses of solonamide analogues. This allowed the initial synthesis of the linear peptides be achieved with near quantitative yields.

5.3 Effects of changing cyclisation reagents and conditions

Table 9: All conditions tested for the production of (ala[3])SolB (**1.71**). Conversion measured by HPLC.

Coupling agent	Additive	Acyl Transfer Reagent	Base	Result	Conversion
Polymer DCC (**4.34**)	HOBt	DMAP (**4.33**)	-	Loss of *de*	50%
Polymer DCC (**4.34**)	-	DMAP (**4.33**)	-	Loss of *de*	50%
Polymer DCC (**4.34**)	HOBt	-	-	No product	-
Polymer DCC (**4.34**)	HOBt	DMAP (**4.33**) (0.1 eqv)	-	-	~5%
DIC (**4.24**)	HOBt	PBu_3 (**5.1**)	-	Slow	15%
COMU (**4.20**)	-	-	Collidine	No product	-
COMU (**4.20**)	-	-	DIPEA	Trace	-
PyOxim (**4.30**)	-	-	DIPEA	No product	-
Mukaiyama Reagent (**5.2**)	-	-	$NaHCO_3$	No product	-
Mukaiyama Reagent (**5.2**)	-	-	DIPEA	No product	-
TBCR (**5.3**)	-	-	Collidine	Elimination	20%
TBCR (**5.3**)	-	-	DIPEA	Elimination	100%

Initially, as it had been discovered that DMAP (**4.33**) was likely to be causing the problems with epimerisation, the macrolactonisation reaction was attempted with polymer supported DCC (**4.34**) and HOBt (**4.26**) alone, with no additional DMAP (**4.33**). As expected, no product was produced.

Given that DMAP (**4.33**) acts as an acyl transfer catalyst and is recycled in the macrolactonisation reaction, it was considered that reducing the equivalents of DMAP (**4.33**) may reduce epimerisation while maintaining a broadly similar reaction rate. However, when the equivalents of DMAP (**4.33**) were reduced from 1 eq to 0.1 eq, the conversion of the starting material is very low over 1 week.

Some reports suggested that tributylphosphine (**5.1**) can act as an acyl transfer reagent in a manner similar to DMAP (**4.33**). However, when tributylphosphine (**5.1**) was employed in place of DMAP (**4.33**), only trace amounts of the product **1.63** was detected.

Following these failures, COMU (**4.20**) and PyOxim (**4.30**) were considered as coupling agents. COMU (**4.20**) has previously been used successfully in the formation of esters[351] and it was believed that it could possibly produce the

required product in this case. COMU (**4.20**) requires two equivalents of base to function; therefore, two reactions with different bases were attempted. COMU (**4.20**) in the presence of collidine did not produce any detectable product. COMU (**4.20**) in the presence of DIPEA only produced trace amounts of the product. PyOxim (**4.30**) also failed to produce any of product **1.63**.

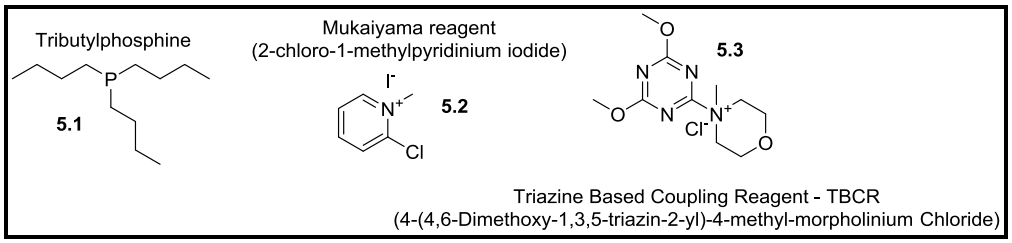


Figure 159: Structures of Tributyl phosphine (**5.1**), Mukaiyama reagent (**5.2**) and DMTMM (**5.3**)

It was clear that the active esters being produced by the above reactions are ineffective. Therefore, a group of reagents which produce "super active" esters was considered. Mukaiyama *et al.* first discovered that 2-chloro-1-methylpyridinium iodide (**5.2**) was an effective condensation reagent which could produce esters (Figure 160).[352]

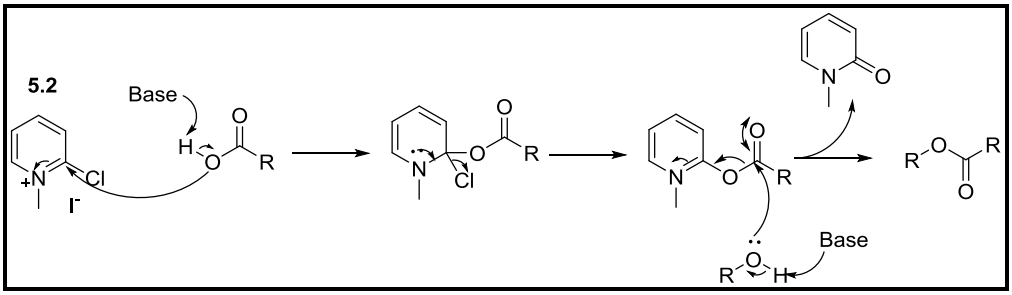


Figure 160: Mechanism for the formation of esters by the Mukaiyama reagent.

Exploiting this reaction mechanism also led to the development of triazine based coupling reagents. Initially, cyanuric chloride (**5.4**) was employed as a coupling reagent. It has actually been used successfully in the production of macrocyclic lactones.[353] However, the excessive reactivity of cyanuric chloride (**5.4**) can prove to be a problem when it is used with compounds with multiple functionalities.[334] More recently, while searching for a reagent with a reduced side reaction profile, CDMT (**5.5**) was successfully applied as a condensation reagent.[354] Further development of this reagent by Kunishima *et al.*[355]

incorporated the *N*-methylmorpholine moiety to afford a reagent which could be used easily in a one-pot reaction. This reagent is known as DMTMM (**5.6**).

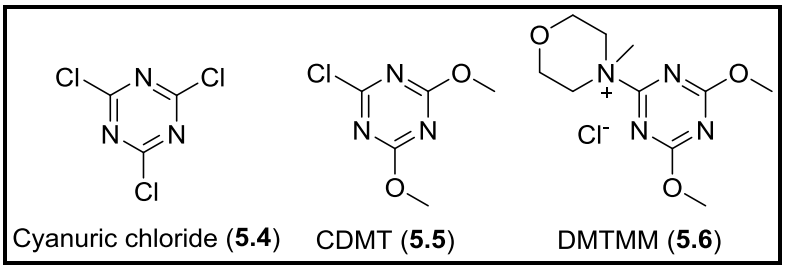


Figure 161: Structures of triazine based coupling reagents.

Protocols using both Mukaiyama reagent (**5.2**) and DMTMM (**5.6**) were employed in attempts to produce (ala[3])SolB (**1.71**) stereoselectively. However, the Mukaiyama reaction did not produce any detectable product. Strangely, DMTMM (**5.6**) produced a single product with a molecular weight of 683; this mass is 18 units less than the triazine-activated peptide As this reaction was on a pilot scale, insufficient material was available for further characterisation. It was hypothesised that this product was the active ester followed by a activation-dehydration reaction at the hydroxy group to produce product **5.7**.

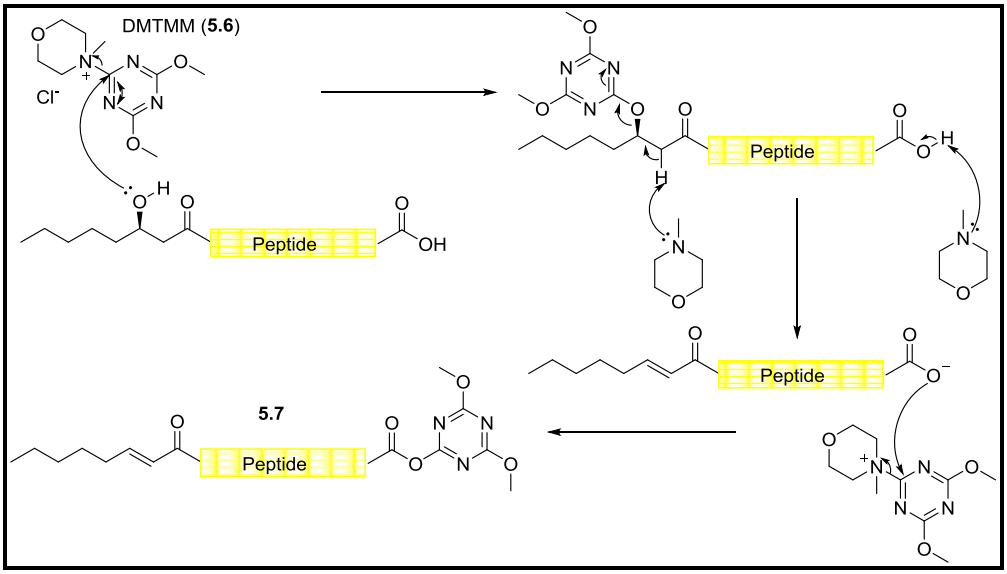


Figure 162: Potential mechanism for the formation of side product **5.7**

Further protocols for ester formation were still available for consideration at this juncture. For example, a Mitsunobu reaction could have been attempted. However, given the repeated failure to produce the product (ala[3])SolB (**1.71**) due to epimerisation or elimination at the 3-hydroxy position, it was considered

that the exposed 3-hydroxy group would continue to make this step problematic. Therefore, a change of strategy was required.

5.4 Alternative cyclisation strategy

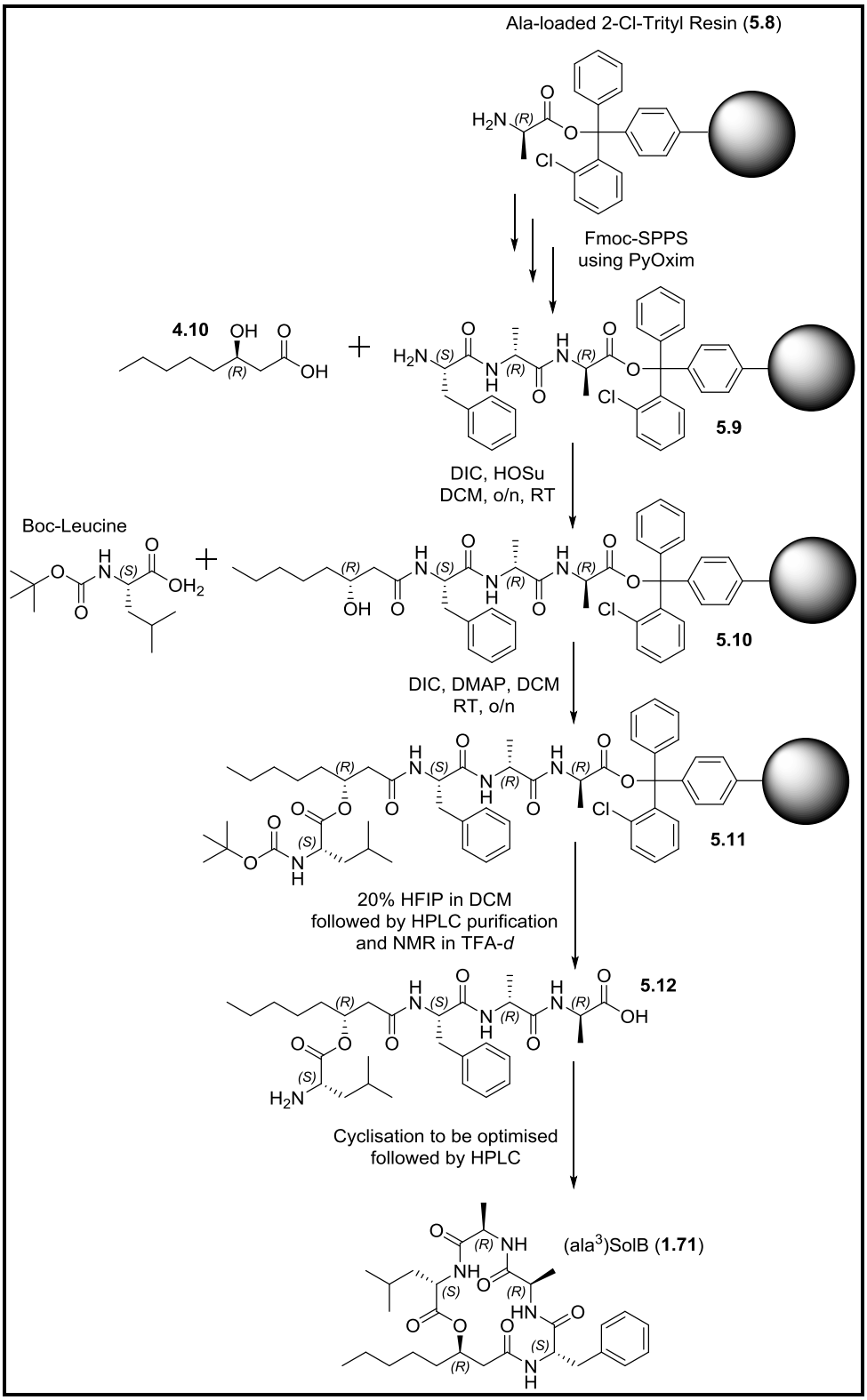


Figure 163: New strategy for the synthesis of (ala³)SolB (**1.71**)

Having evaluated several different protocols for a stereoselective macrolactonisation to afford the product (ala³)SolB (**1.71**) and being

unsuccessful in each attempt, an alteration of cyclisation strategy was considered (see Figure 163), which requires the assembly of a branched peptide. Following acidolytic release of the peptide, macrocyclisation will be mediated *via* an amide bond formation.

Macrolactamisation is known to be more favourable due to the increased nucleophilicity of the amine functionality. However, the formation of the ester bond remains a problem to be addressed. Thus, a three amino acid residue peptide would be assembled using standard Fmoc-SPPS protocols on 2-chlorotrityl resin. The original adapted DIC/HOSu coupling of 3-(*R*)-hydroxyoctanoic acid (**4.10**) would then be employed, followed by a single coupling reaction of Boc-Leucine. It was considered that by creating the ester bond while the peptide remained attached to the resin, a high concentration of reagents could be used thereby increasing the rate of reaction. It was hoped that this increase in rate during the ester formation would reduce the epimerisation which had occurred during the previous approach of applying a week long macrocyclisation reaction. It was also hoped that the following macrolactamisation could be achieved at a much higher rate than the macrolactonisation, thereby reducing the synthesis time for each new solonamide analogue.

5.4.1 Alternative esterification reagents and conditions

As the combination of DMAP (**4.33**) and DIC (**4.24**) had previously successfully formed ester bonds in this synthesis, it was decided that these conditions would be evaluated for the formation of the ester bond between the 3-hydroxy acid moiety and the Boc-Leucine, thus forming resin-bound depsipeptide **5.11**. Resin cleavage using 20% HFIP would afford the Boc-protected linear peptide **5.12**. This peptide could be analysed and purified by HPLC, it was considered that the large steric bulk of the Boc-protecting group was likely to aid in separation of diastereomers if epimerisation did occur.

Following HPLC purification, the peptide **5.12** would be dissolved in TFA-*d* for two purposes. TFA-*d* would easily deprotect the remaining Boc-protecting group, producing the required linear peptide **5.13** and the resulting mixture

could undergo NMR analysis. The β-proton of the 3-hydroxy moiety or the α-proton of the leucine would be most likely to indicate the optical purity of the linear peptide. It was anticipated that the purified and deprotected peptide (**5.13**) could then be easily cyclised through a macrolactamisation reaction.

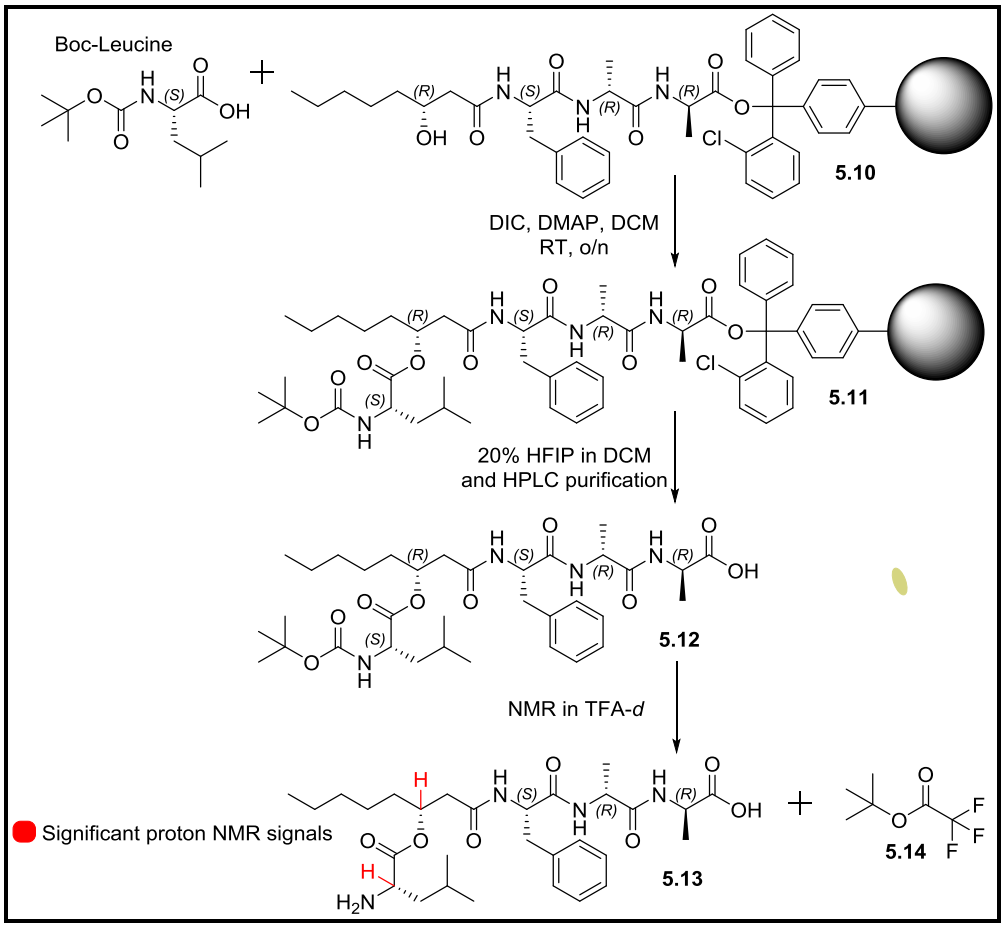


Figure 164: Coupling of Boc-Leucine to resin-bound peptide **5.10** to produce **5.11**. Resin cleavage to produce Boc-protected **5.12**. Followed by NMR in TFA-*d* producing **5.13** and volatile side product *tert*-butyl trifluoroacetate **5.14**

When this new protocol was attempted, mass spectrometric analysis of the linear peptide showed the presence of the expected product **5.12**. Gratifyingly, HPLC-MS analysis did not display the peaks splitting previously indicative of the presence of an epimer. ^{1}H-NMR performed on the purified fractions in TFA-*d* showed signals which were consistent with the presence of the linear peptide **5.13** (Figure 165). Importantly, the ^{1}H-NMR signals of the β-proton of the 3-hydroxy moiety or α-proton of the leucine signals did not show any peak splitting which would be expected if a diastereomeric mixture had been formed. It was believed that this was indicative that the coupling had successfully

yielded the linear peptide **5.13**. The only hurdle remaining to a full stereoselective synthesis of (ala[3])SolB (**1.71**) was the macrolactamisation.

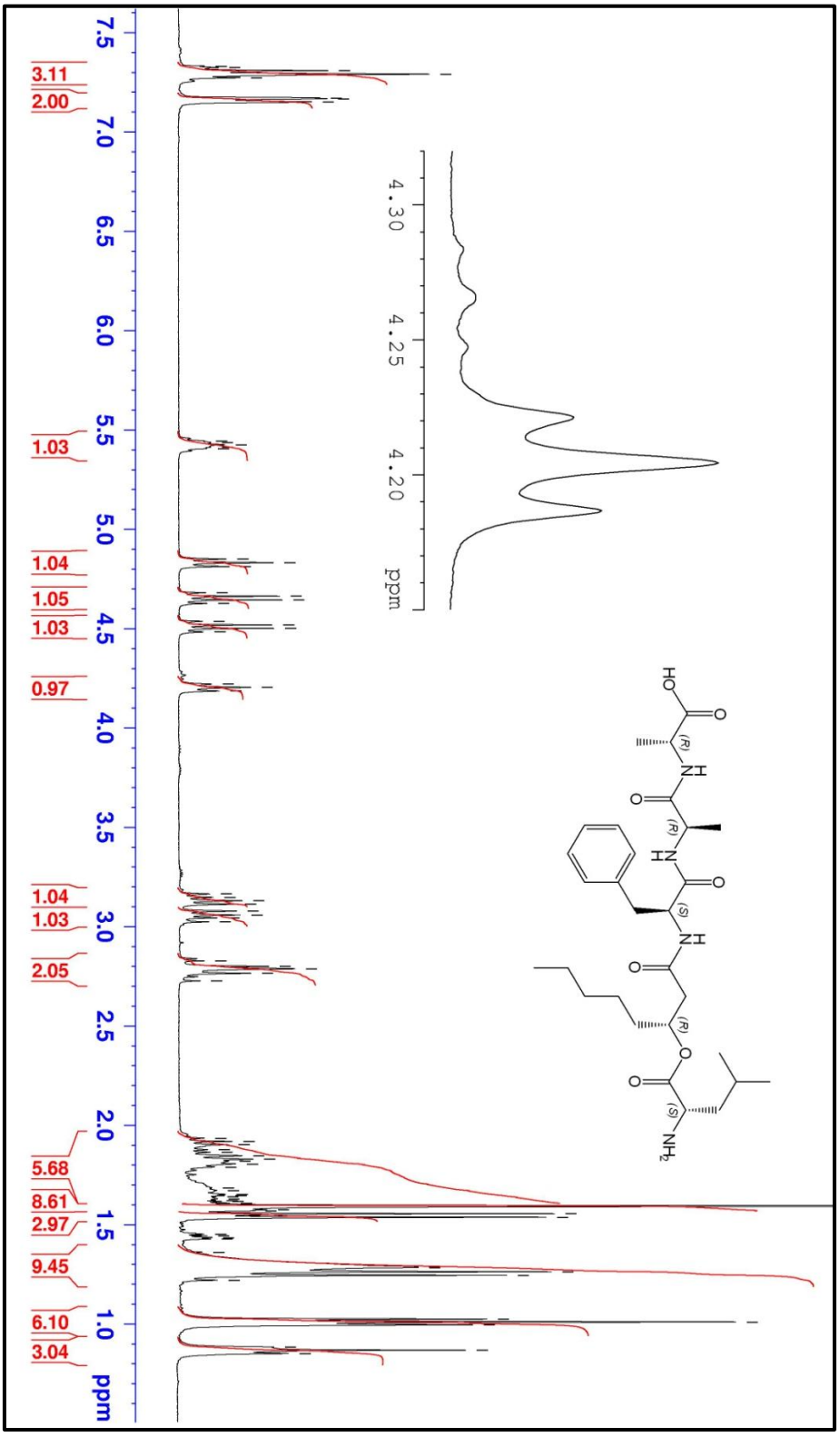


Figure 165: [1]H-NMR spectrum of **5.13**

5.4.2 Establishing the cyclisation

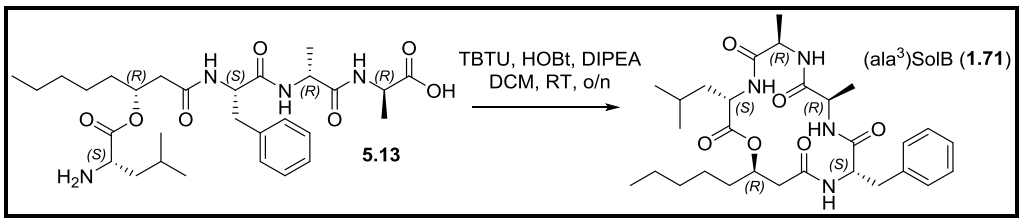


Figure 166: Scheme showing the planned macrolactamisation of **5.13** forming the product, (ala[3])SolB (**1.71**)

In this laboratory, a macrolactamisation had recently been achieved using TBTU (**4.18**) and HOBt (**4.26**) in the presence of DIPEA as a base. Therefore, a small sample of the linear peptide was exposed overnight to the presence of 4 eq of both TBTU (**4.18**) and HOBt (**4.26**) and 8 eq of DIPEA. Mass spectrometric analysis showed a peak consistent with the expected product (ala[3])SolB (**1.71**). HPLC analysis showed no presence of the starting material and the desired product peak was symmetrical with no proximal peaks suggesting that a diastereomer had not been formed to any significant extent. Encouraged by this, a larger scale experiment was performed. Similar results were found in both HPLC and mass spectrometric analysis. Purification of the product yielded an impressive 7.6 mg, with a yield of 46% and a cumulative yield of 7% for the entire synthesis. This was a significant improvement on all previous syntheses both in Chan's lab and elsewhere. NMR analysis was consistent with the structure of (ala[3])SolB (**1.71**).

In order to establish the reliability and robustness of this method, the protocol was applied for the synthesis of several other analogues including SolA (**1.21**) and SolB (**1.22**). These compounds (Figure 167) showed impressive *de* and cumulative yields. This demonstrates that the new synthetic strategy is reliable, high yielding, and widely applicable for the generation of solonamide analogues.

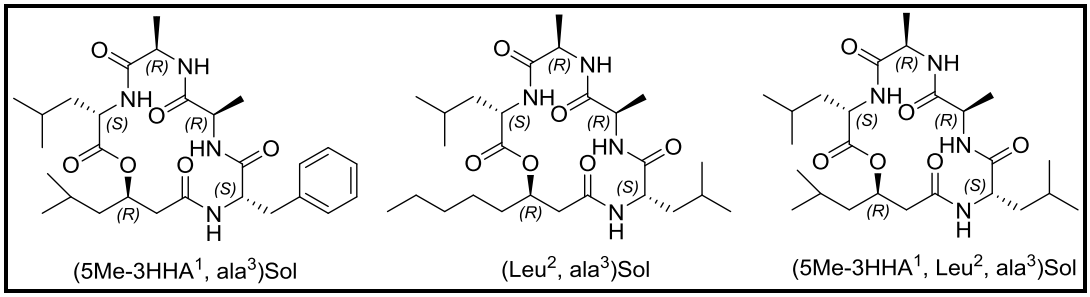


Figure 167: Diagram of further analogues using the newly developed alternative solonamide synthesis

5.5 Conclusion

Following the difficulties with stereoselectivity experienced with the synthesis described in the previous chapter, this chapter sought to develop a fully stereoselective synthesis of (ala^3)SolB (**1.71**) as a test compound.

Initial analysis and variation of the acidolytic cleavage protocol marginally improved the yield of the linear peptide. However, attempts to improve the macrolactonisation reaction so that it yielded a single diastereomer failed.

Following the failure, the synthesis was redesigned. The new synthetic strategy used a macrolactamisation, instead of the previous macrolactonisation, and required the development of a reaction to form an ester bond between Boc-Leucine and the peptide chain **5.10** on the resin. The use of DMAP (**4.33**), HOBt (**4.26**), and DIC (**4.24**) followed by deprotection with 20% HFIP in DCM afforded the linear peptide with a yield of 15%. The subsequent macrolactamisation reaction using TBTU (**4.18**), HOBt (**4.26**), and DIPEA proceeded without problems. HPLC purification yielded the single diastereomer (ala^3)SolB (**1.71**) with a good yield of 46%. The cumulative yield of this synthesis was 7%. Later syntheses producing further analogues increased the cumulative yield to 29%. The relatively high yield, short synthesis time and lack of side-products of this synthetic strategy make it a significant improvement over any previously known synthesis. It is foreseen that many solonamide analogues could be synthesised using this strategy to further expand the SAR of this interesting molecule.

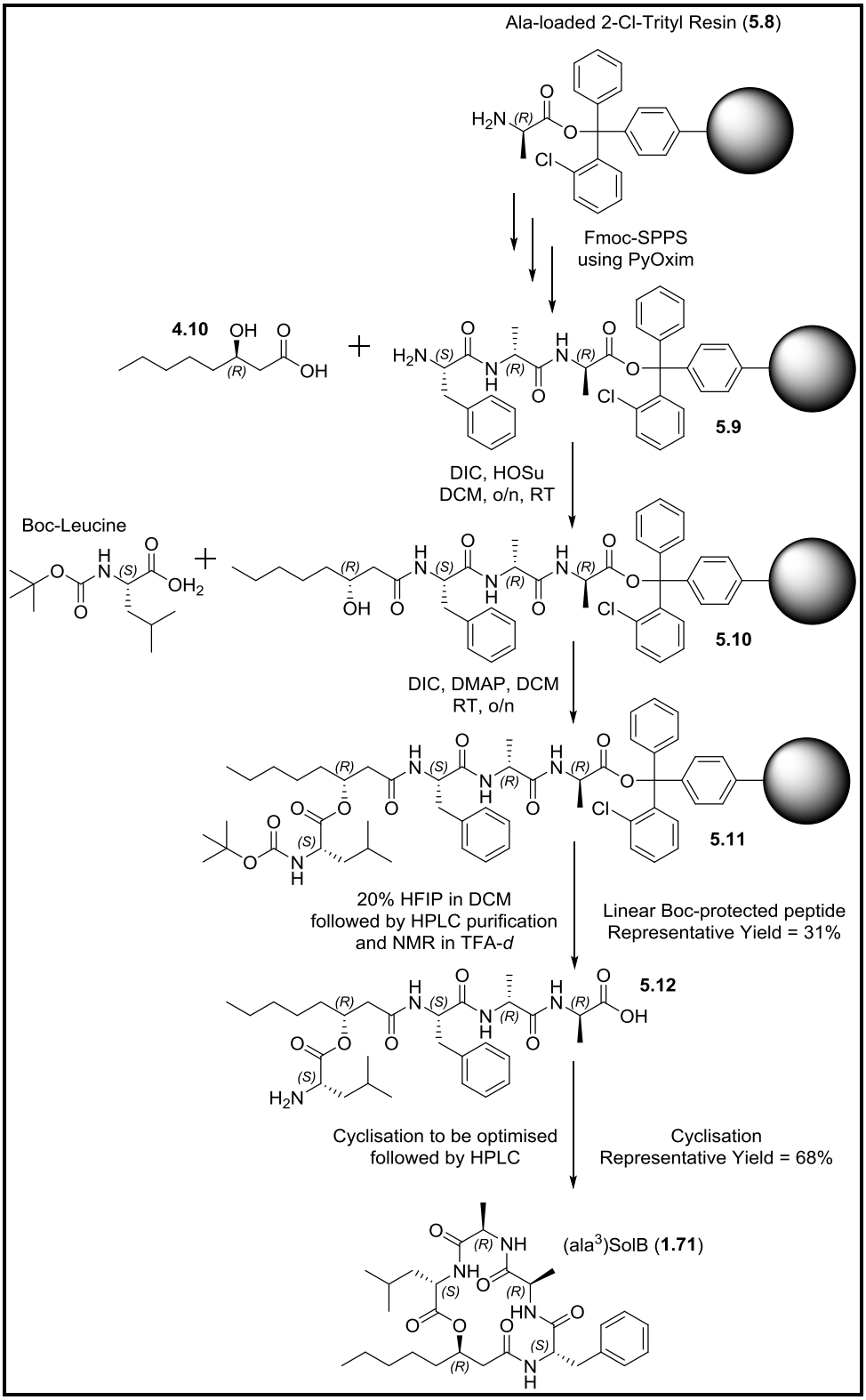


Figure 168: New strategy for the synthesis of (ala[3])SolB (**1.71**)

5.6 Future Work

Currently, this synthetic strategy employs a resin cleavage protocol followed by a deprotection reaction. It should be possible to combine these stages into a one-pot acidolytic deprotection and resin cleavage by using 50% TFA in DCM. However, the HPLC purification stage prior to macrolactamisation may also be unnecessary. If it is possible to use the crude peptide for the macrolactamisation without compromising yield or stereoselectivity, this would be a very beneficial modification. Further experiments are required to see if either of these changes could be useful.

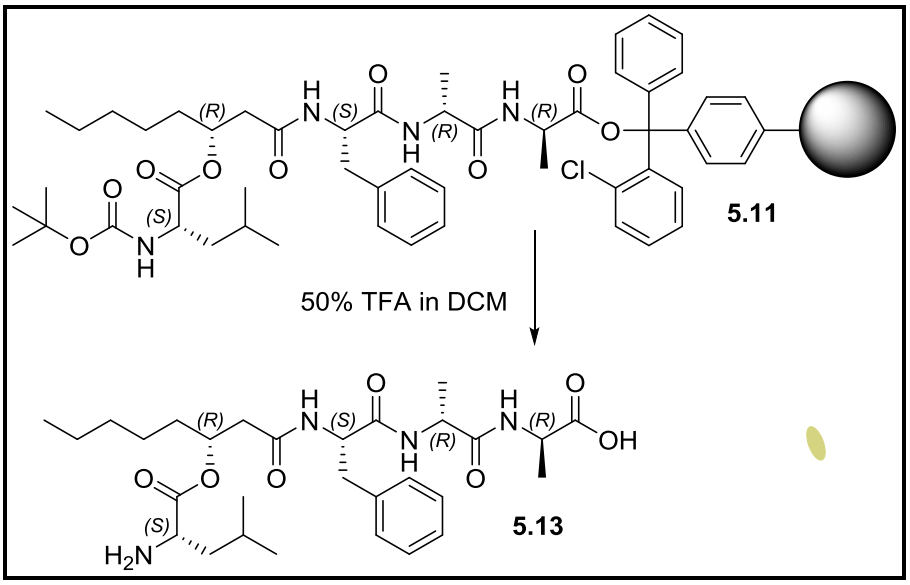


Figure 169: Modified single step resin cleavage and deprotection protocol transforming the resin-bound protected peptide **5.11** directly to the linear peptide **5.13**.

Immediate further work includes using this synthesis to produce solonamide analogues required in the elaboration of the SAR of the solonamides as described in the next chapter. Initially, amino acid residues can easily be substituted for any other naturally occurring amino acid or any other non-natural but commercially available amino acids. Furthermore, 3-hydroxy acid moieties other than 3-(*R*)-hydroxyhexanoic acid (**1.60**) and 3-(*R*)-hydroxyoctanoic acid (**4.10**) can be produced and incorporated into the molecule (see Figure 170).

When Nelson *et al*. initially developed the synthesis of the oxetan-2-ones, such as **4.35**, only simple 3-hydroxy acids could be synthesised.[346] However, they recently conducted further work which developed methods that allow the production of lactones with an α-substitution (see Figure 171).[235] Although synthesis of the second generation triamine ligand **5.26** is more complex, the protocol for the production of the chiral oxetan-2-ones could be adapted. These developments could still be employed to produce interesting new analogues of the solonamides (see Figure 171) allowing a more detailed analysis of the SAR of these 3-hydroxy acid moieties. The α-substitution could beneficial to improving the effectiveness of these compounds.

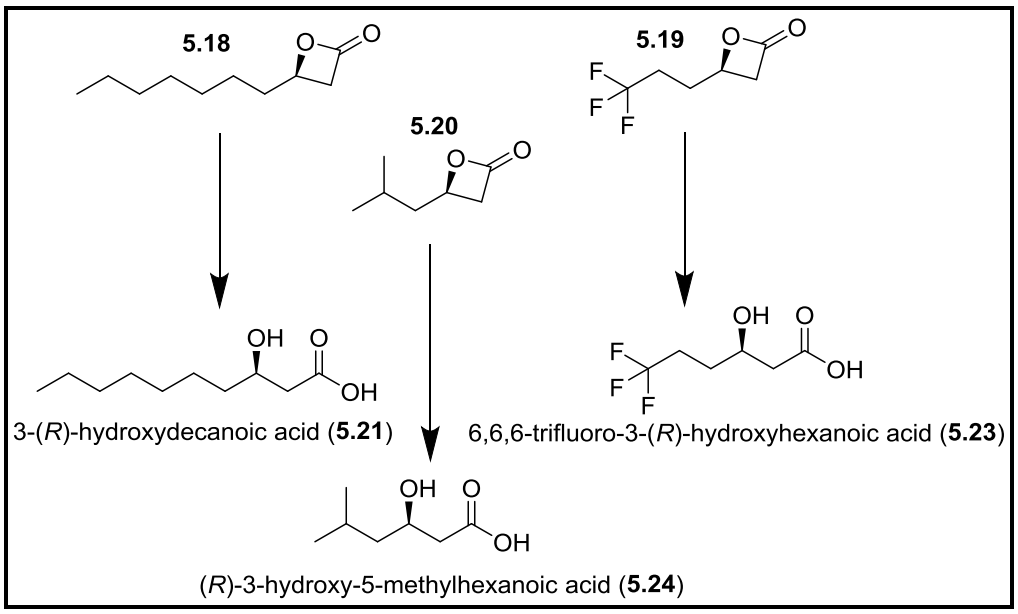


Figure 170: New 3-(*R*)-hydroxy acid moieties to be used to elucidate the structure activity relationship

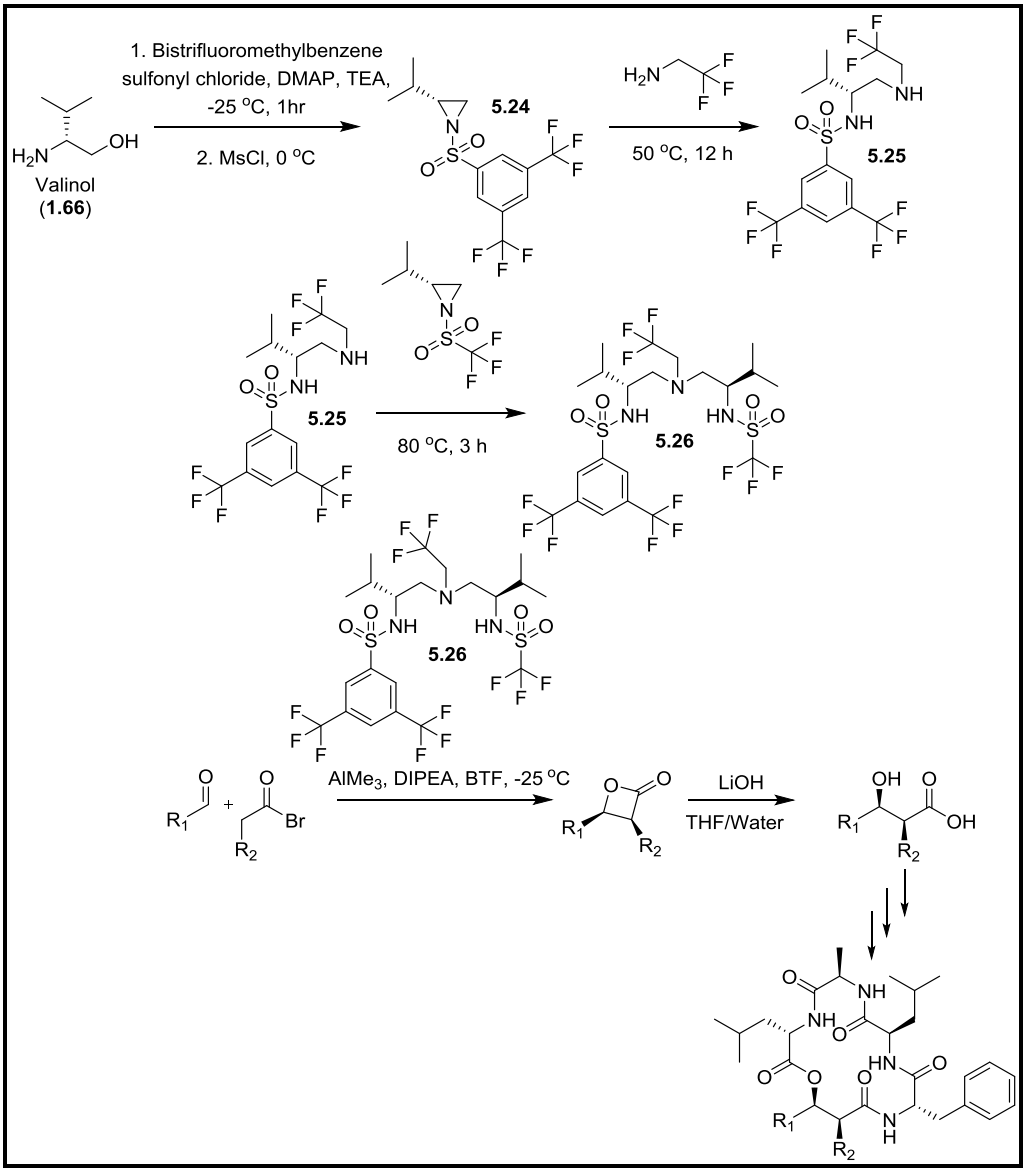


Figure 171: Developed synthesis of α-substituted 3-hydroxy acid compounds adapted from Nelson *et al.*[235]

6 Pharmacology of solonamide analogues

The aim of this chapter is to fully pharmacologically assess SolA (**1.21**) and SolB (**1.22**), and to develop a deeper understanding of their mode of binding and SAR.

Initially, the current state of research in the field is briefly discussed. There is then followed by a section discussing potential modes of binding and the methods used to analyse them. The full pharmacological analysis of SolA (**1.21**) and SolB (**1.22**) and the related epimers, epiSolA (**1.61**) and epiSolB (**4.5**) is then outlined including activation, inhibition, and Schild analysis at AgrC1 receptors in whole bacterial reporter assays. Phenotypic studies confirming this activity utilising Western blots and hemolysis assays are then reported. Finally, the SAR of the solonamide scaffold is elucidated using an alanine scan followed by variation of a selected residue and the 3-hydroxy acid moiety.

6.1 Introduction

At the time of writing, the inhibition of AgrC by the solonamides (Figure 172) has not been accurately quantified. IC_{50} data in respect to the solonamides have not been reported, and the only available data are qualitative assays showing reductions in virulence expression. This severely limits researchers ability to accurately evaluate the potential of these new compounds in comparison to existing inhibitors. Initial investigations by Mansson *et al*.[214] and Nielsen *et al*.[216] seem to indicate that inhibition can be accomplished by using 5 µg/ml (roughly 8.5 µM) of either SolA (**1.21**) or SolB (**1.22**). However, as in these assays spent culture medium containing AIP was used *in lieu* of synthetic agonist, the actual agonist concentration is unclear. Furthermore, the synthesis developed by Kitir *et al*.[318] has not been further extended to modify the solonamide scaffold and explore the SAR against AgrC.

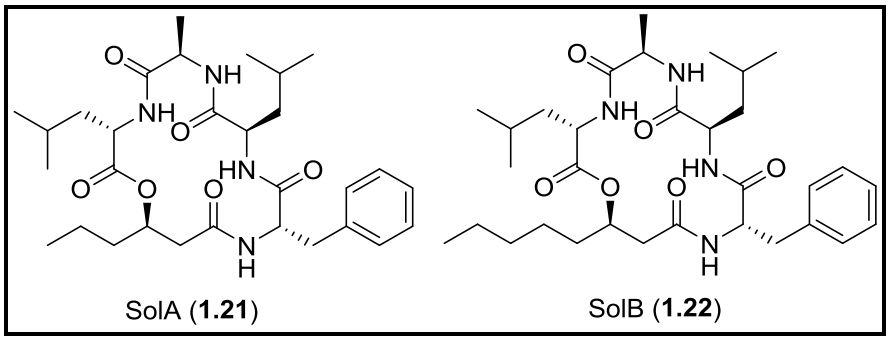


Figure 172: Structure of the natural product macrocyclic depsipeptides, SolA (**1.21**) and SolB (**1.22**)

Importantly, Nielsen *e al.* proposed that the mode of action of the solonamides is *via* competitive inhibition with the endogenous AIP ligands at the AgrC recognition site.[216] However, the assays conducted were not conclusive. The first assay used a zone of inhibition assay to demonstrate dose-dependence (see Figure 173). However, dose-dependent inhibition can be a feature of non-competitive and irreversible inhibitors. Thus, dose-dependence does not prove that the solonamides act as competitive inhibitors. A subsequent assay aiming to demonstrate that increased AIP concentrations cause reduced inhibition by the solonamides was carried out (Figure 174); however, even using 20% AIP-containing culture supernatant, full activity was not restored.

This could actually indicate either non-competitive or irreversible inhibition. Furthermore, even if full activity was restored by the cognate ligand, this would not exclude that the ligand in question could act as either a non-competitive or an irreversible inhibitor, which can also display this type of activity. Therefore, the mode of action of the solonamides still remains to be determined.

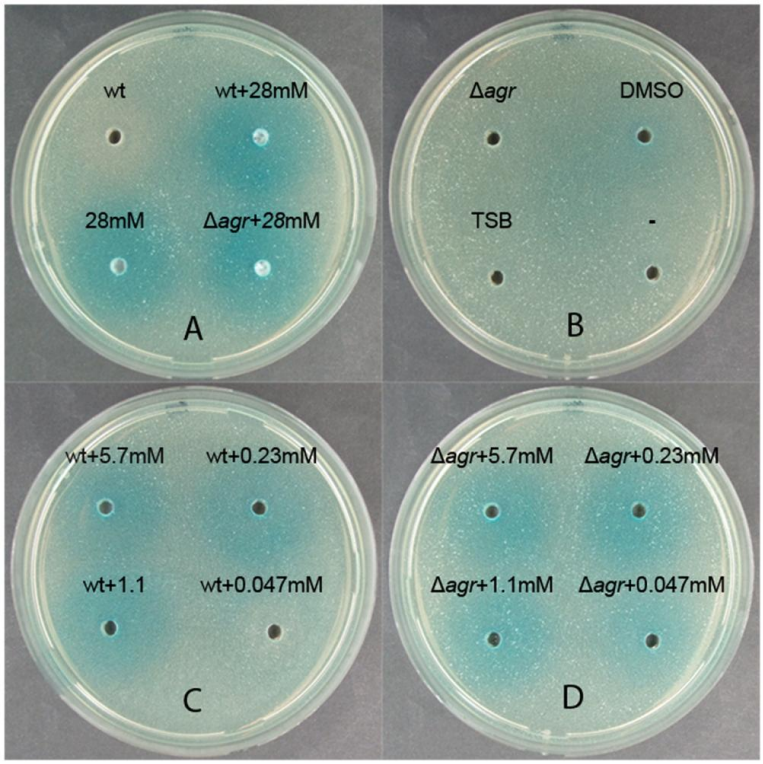


Figure 173: Zone of inhibition assay from Nielsen *et al.*[216] Agar plates covered with a *spa::lacZ S. aureus* bioreporter. DMSO (10 µl) with 0, 0.8, 4, 20, 100 and 500 µg SolB and supernatant (20 µl) of an overnight culture of 8325-4 (labelled as "wt") or RN6911, Δ*agr* mutant cells (labelled as "Δ*agr*") or TSB medium. No solonamide is present in (**B**) and solonamide B is present in the indicated concentrations in (**A**, **C**, **D**).

Thus, this chapter aims to fully assess the mode of action whilst quantifying the solonamide inhibition so that the compounds can be effectively compared with existing inhibitors. Following this full pharmacological assessment, the SAR against the AgrC receptors will be examined using multiple solonamide analogues.

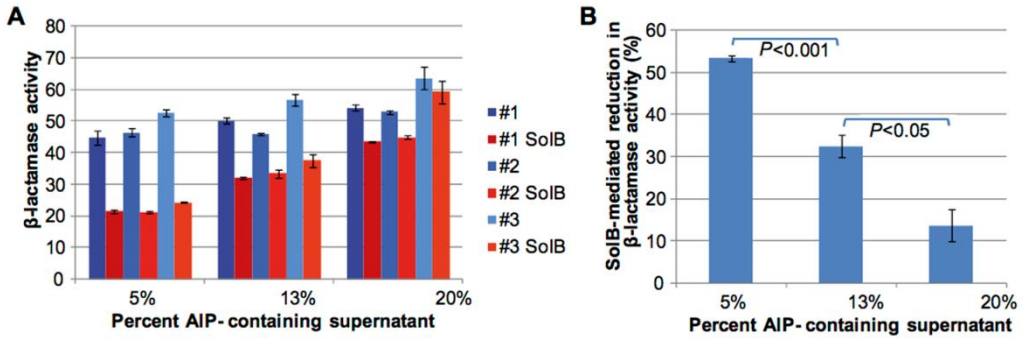


Figure 174: Varying AIP levels to assess competition between AIP and solonamide B by Nielsen *et al*.[216] Activity of SolB (5 µg/mL) on RNAIII expression was assessed in the presence of increasing concentrations of AIP in a *P3::blaZ* bioreporter strain. 30 min after SolB and AIP addition, β-lactamase activity was determined with and without SolB in triplicate (#1–#3). Bars represent mean average +/− SEM from triplicate activity measurements (**A**). Average inhibition caused by SolB at increasing AIP concentrations. Bars represent the mean (+/− SEM) reduction in β-lactamase activity observed in triplicate (**B**). *P*-values between AIP treatments were calculated by two-sided Student's t-test.

6.2 Mode of binding

Pharmacology has defined many different classes of compound which interact with membrane-bound receptors in specific ways. Antagonism generally falls into one of three categories: competitive inhibition, non-competitive inhibition, and uncompetitive inhibition. This section will explain each of these in detail to establish a background to the complete pharmacological analysis of the solonamides.

6.2.1 Competitive inhibition

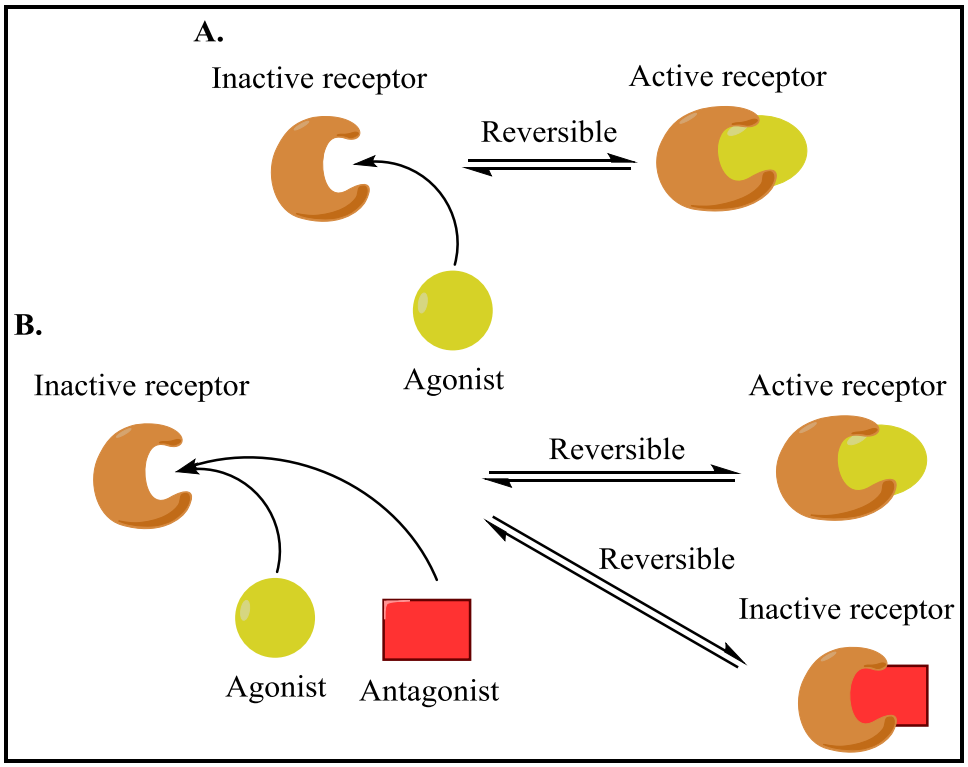


Figure 175: Diagram showing (**A**) agonism of the cognate receptor by the endogenous ligand and (**B**) competitive inhibition by an orthosteric antagonist.

For a receptor to be activated, a ligand must bind the recognition site known as the orthosteric site. A competitive inhibitor is a substance which also reversibly binds the receptor in such a manner that only the endogenous agonistic ligand or the inhibitor can be bound to the receptor at any given time (see Figure 175). Many competitive antagonists bind at the orthosteric site and, in this case, they are also orthosteric antagonists.

The first mathematical equation for the competitive binding of two ligands was derived by John Henry Gaddum in 1937.[356] For two compounds, A and B, competing for a recognition site, receptor occupancy by compound A can be written as:

$$p_A = \frac{c_A}{1 + c_A + c_B}$$

where $c_A = [A]/K_A$ and K_A is the equilibrium dissociation constant of A and $c_B = [B]/K_B$ with K_B representing the equilibrium dissociation constant of B.

However, this equation only described receptor occupancy, i.e. receptor binding, which could not easily be measured using the experimental tools of the day and is difficult to relate to measurable physiological responses. It was not until the work of Schild in 1947 that this could be employed to understand the physiological effects of a compound i.e. the response.[357] Before Schild, many attempts had been made to link the inhibition of a response, which had been caused by constant concentrations of an agonist, to the concentration of the antagonist causing the response inhibition. The widespread and common use of IC_{50} values is a relic of these investigations which is often still used today. However, instead of analysing the inhibition caused by the antagonist, Schild measured the proportion of agonist increase required to maintain a specific response in the presence of a constant concentration of antagonist. This is known as the dose-ratio and is now part of the well known Schild equation which is as follows:

$$r = 1 + \frac{[B]}{K_B}$$

where *r* is the dose-ratio, [B] is the concentration of the antagonist, and K_B is the equilibrium dissociation constant of the antagonist. Treating the problem in this manner allowed Schild to remove any reference to the concentration of the agonist from his equation.

If the equation is rearranged to the following form:

$$\log(r-1) = -\log(K_B) + \log([B])$$

It predicts that by increasing the concentration of the antagonist, B, that the curve produced by plotting log([A]) against response will be shifted to the right in a parallel fashion. This is because the only term in the equation affected by the concentration of the antagonist is $\log([B])$. The parameter K_B is predicted to be a physical constant defined by the interaction of the antagonist with the receptor. This constant can be calculated by using experimental values to discover the dose-ratio, r. Whereas the IC_{50} values extensively examined before Schild vary in response to the agonist used, the K_B is a specific property which describes only the relationship between the antagonist and the receptor. Therefore, this value is considerably more useful when attempting to compare the performance of antagonists using different agonists or in the presence of different concentrations of the same agonist.

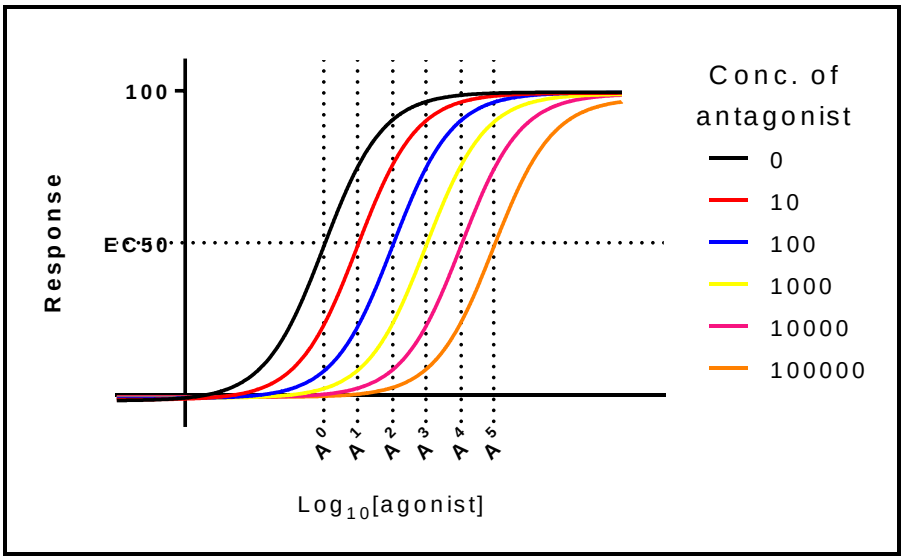


Figure 176: Example of the results expected for a competitive antagonist

The Schild equation is used to determine the mode of binding of an antagonist. Initially, an experiment to determine the EC_{50} of a system is performed. Following this initial experiment, further experiments are performed to establish the EC_{50} in the presence of increasing amounts of antagonist. If the antagonist is competitive, it should produce a graph similar to that seem in Figure 176.

Importantly, it should be noted that the maximal potential activation by the agonist remains constant across all concentrations of the antagonist. A competitive antagonist does not show any sign of saturation at any concentration, therefore theoretically the rightwards shift should continue *ad infinitum*. However, in reality, practical considerations such as solubility and aggregation can prevent this at high concentrations.

Once these results have been obtained, dose-ratios can be calculated allowing the construction of a Schild plot. The dose-ratio is calculated as follows:

$$r = A^x / A^0$$

where $A^0$is the concentration of the agonist required to cause a given level of response and A^x is the concentration required to give the same response in the presence of a given concentration of the antagonist.

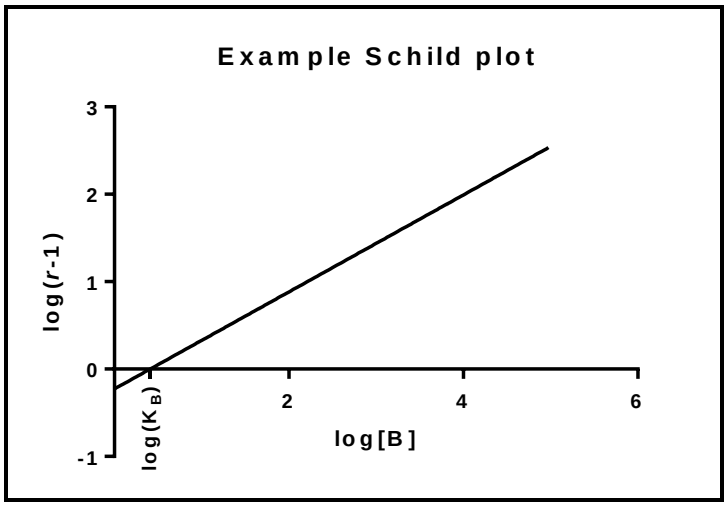


Figure 177: An example of a Schild plot. A linear plot with a gradient of 1 indicates a competitive antagonist. If this is the case, the abscissa intercept is log(K_B)

In a Schild plot, log(*r*-1) is plotted against -log([B]). The gradient of this graph can reveal the mode of binding of the antagonist. A competitive antagonist produces a linear regression with a gradient of 1. Non-competitive inhibitors are likely to produce curved graphs because as the concentration of a non-competitive inhibitor increases, increasingly more agonist is required to cause the same response. Heterogeneous systems often produce discontinuous trends.

Although K_B is more useful for comparison of competitive antagonists in different systems with different concentrations of agonist, full Schild analysis can require large amounts of precious synthetic inhibitor. Large amounts of data can also be required to accurately calculate the K_B with satisfactory statistical confidence; acquiring this data can be time consuming and labourious. Also, in the same system, using the same concentration of agonist, IC_{50} data is directly comparable and much easier to produce. Therefore, during this study, full Schild analysis will only be performed on strategic analogues while, generally, IC_{50} data will be used to compare compounds in the SAR studies.

There are three subtypes of competitive antagonist which are defined by their ability to agonise the receptor. A partial agonist can mildly activate the receptor at a reduced level to the endogenous agonist. An inverse agonist reduces the activation state of the receptor. Specifically, the inverse agonist binds to and stabilises the inactive state of the receptor. Hence, if a receptor has a basal level of activity, an inverse agonist reduces the level of activation of the receptor thereby reducing the response caused by the basal activity of the receptor. A silent antagonist is a compound which has no effect on the activity of the receptor. It bonds the orthosteric site, but does not affect the activity level of the receptor.

6.2.2 Non-competitive inhibition

Non-competitive inhibition is defined as a situation where the binding of the agonist to the receptor has no effect on the ability of the receptor to bind the antagonist. Any orthosteric inhibitor must bind at the orthosteric site i.e. the same site as the agonist. Therefore, the agonist must have an effect on the ability of the antagonist to bind the receptor as the two compounds cannot occupy the same space inside the orthosteric site. For this reason, non-competitive inhibitors always bind the receptor at a site other than the orthosteric site. These sites are generally known as allosteric sites. It should be noted that all non-competitive antagonists are, by definition, allosteric antagonists.

However, not all allosteric antagonists necessarily act as non-competitive inhibitors. For example, it is possible that binding of the agonist at the orthosteric site can change the receptor conformation in such a manner that the antagonist cannot bind its allosteric site. However, binding of the antagonist to its allosteric site of the unoccupied receptor could still prevent activation of the receptor by the agonist. This kind of mechanism would be a competitive inhibition. For example, an allosteric competitive inhibitor was recently discovered which inhibits the glucose-1-phosphate thymidylyltransferase of *P. auruginosa*.[358]

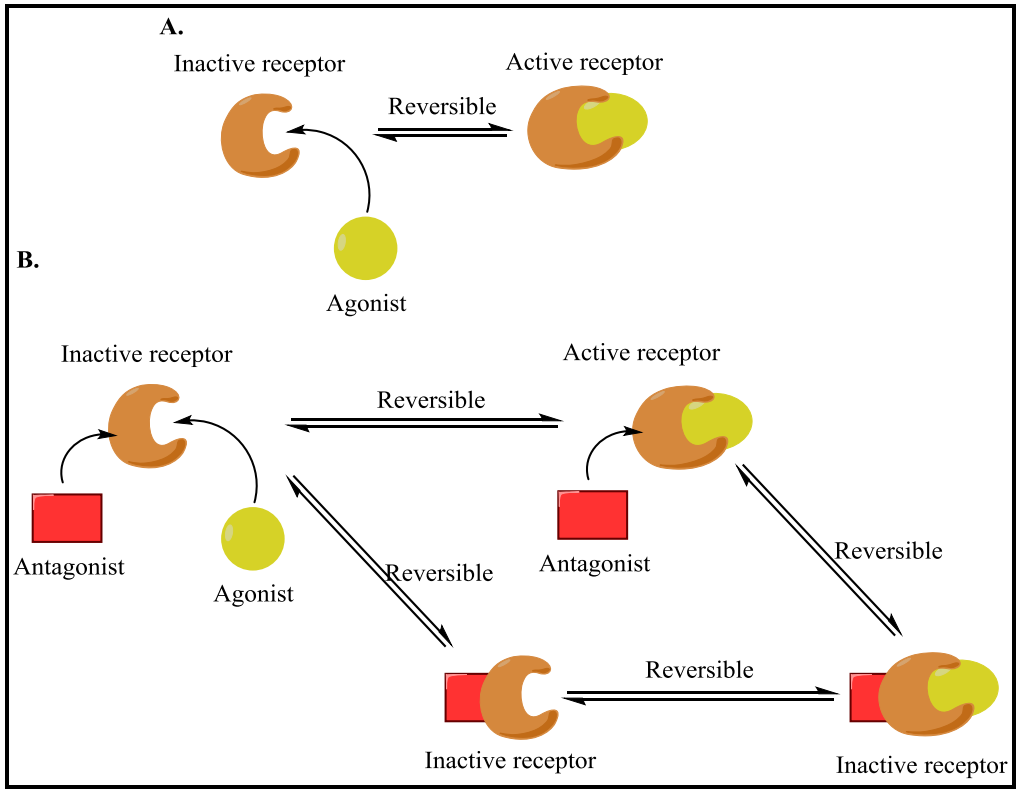


Figure 178: Diagram showing (**A**) agonism of the receptor by the endogenous ligand and (**B**) non-competitive inhibition by an allosteric antagonist.

Attempting to represent non-competitive inhibition mathematically is significantly more complex than the previously discussed models of competitive inhibition. This is because models of competitive inhibition only have to account for a single orthosteric binding site which can only interact with one of two possible compounds at any given time. In contrast, non-competitive inhibition by necessity involves multiple sites. Also, allosteric binding can cause multiple effects on the receptor. An allosteric antagonist can increase or decrease the

affinity of the endogenous agonist, it can also increase or decrease the ability of the bound agonist to activate the receptor; these antagonists are commonly referred to as positive or negative allosteric modulators, respectively. In the model of competitive antagonism previously discussed, the interaction of each competitive antagonist with a receptor could be described by a single term, K_B. However, as seen in the operational model of allosterism seen below, allosteric compounds must be compared using a large panel of mathematical terms.

In fact, the operational model of allosterism is as follows:

$$E = \frac{E_M(\tau_A[A](K_B + \alpha\beta[\mathrm{B}]) + \tau_B[B]K_B)^n}{([A]K_B + K_AK_B + K_A[B] + \alpha[\mathrm{A}][\mathrm{B}])^n + (\tau_A[A](K_B + \alpha\beta[\mathrm{B}]) + \tau_B[B]K_A)^n}$$

where E is the observed agonism of the system, E_M is the maximum possible agonism of the system, n is a constant which relates to the slope of the curves, [A] and [B] are the concentration of the agonist and antagonist respectively, τ_A and τ_B are the operational efficacies of the agonist and antagonist respectively (efficacy is a measure of the propensity to cause agonism), K_A and K_B are the dissociation constants of the agonist and antagonist respectively (dissociation constants are a measure of the affinity of a compound), α is the cooperativity factor which describes how the antagonist affects the ability of the receptor to bind the agonist, and β which is the cooperativity factor which describes how the antagonist affects the ability of the receptor to be agonised by the bound agonist.[359]

The only variables which are experimentally determined in this model are the concentration of the agonist, the concentration of the antagonist, the maximal possible agonism of the system, and the observed activation of the system. It is possible to determine dissociation constants using radioligand binding assays or other experiments. However, this requires the synthesis of 'hot' radioactive ligands, the isolation of the receptor in its biologically active conformation, and a relatively high affinity to overcome background non-specific binding effects. In the absence of these complex experiments, all of the other terms must be discovered by fitting experimental data from dose-

response curves to the mathematical model. To enable accurate prediction of all these variables, large amounts of data are required.

Once this large amount of data has been fitted to the model, the relation of an antagonist to a receptor-agonist complex is defined by the antagonist dissociation constant, operational efficacy, and both cooperativity factors. The agonist relationship to the system is also defined by both a dissociation constant and operational efficacy. The agonist effect is also modified by the terms related to the antagonist. As can be seen in this model, allosteric agonism and antagonism rely on multiple characteristics of both the agonist used and the nature of the antagonist. Therefore, given the large numbers of constants used to accurately describe these relationships, it is hard to make meaningful comparisons between compounds.

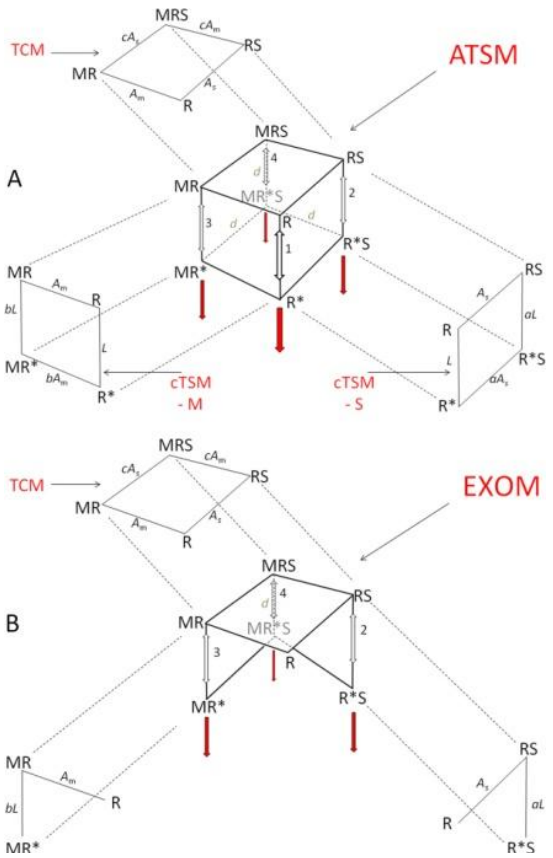


Figure 179: Diagram from Bindslev[360] showing reaction schemes of the Allosteric Two State Model (ATSM) and Extended Operational Model (EXOM). Both incorporate the Ternary Complex Model (TCM) while ATSM also incorporates the cyclic Two-State Model (cTSM). R represents the inactive receptor, R* is the receptor in an activated configuration, S is the substrate or agonist, and M represents the allosteric compound. The red arrows indicate receptor states which can cause a response.

The operational model of allosterism, discussed above, is one of several approaches used to model the effects of allosteric antagonists. The operational model observes that dose-response curves are commonly hyperbolic, and deduces that the relationship between receptor occupancy and observed effect must also be hyperbolic if the law of mass action can be applied at the receptor-agonist level.[361] However, it does not take into account the possibility that the unoccupied receptor may spontaneously adopt the active configuration and then more easily allow agonist binding (a process known as selection) as opposed to the more commonly discussed mechanism where the agonist binds the receptor thereby causing activation (known as induction).[360]

The extended two-state model of allosterism is a mechanistic model created by applying the two state model of agonism to the ternary complex model. In all of these kinds of model, there are multiple possible states of a receptor in a

system with an allostere and an agonist. The equilibrium between each state has an equilibrium constant and extracting these figures into an equation forms the model (see Figure 179). The extended two-state model of allosterism does take into account receptor activation by selection as well as induction.[360]

For example, the equation for the allosteric two-state model is as follows:

$$\frac{[R]_{active}}{[R]_{total}} = \frac{L(1 + \tau_\alpha K_A[\mathrm{A}] + \tau_\beta K_B[\mathrm{B}](1 + \tau_\alpha \alpha\beta K_A[\mathrm{A}]))}{1 + L + K_B[B](1 + \tau_\beta L) + K_A[A](1 + \tau_\alpha L + \alpha K_B[\mathrm{B}](1 + \tau_\alpha \tau_\beta \beta L))}$$

where the terms used in the equation represent the same measures as outlined previously for the operational model of allosterism (however, derived in a different manner), and L is the receptor isomerisation constant which is a measure of the propensity of the unoccupied receptor to spontaneously form the active conformation.

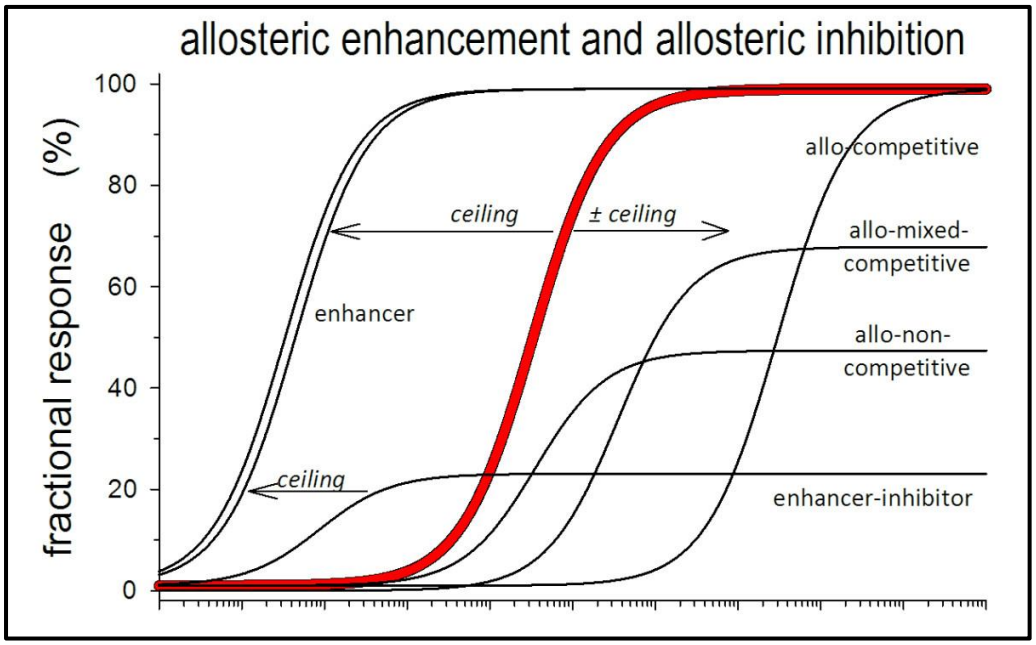


Figure 180: Diagram from Bindslev[360] showing some characteristic effects on dose response graphs when allosteric inhibitors are added.

Fitting data to either of these models with sufficient confidence can require large amounts of data and some luck when selecting the initial values for each term so that computer-simulated iterations converge on a useful model of the given system. However, some distinctive trends often indicate a non-competitive (and therefore an allosteric) antagonist without a complete mathematical description of the compound interactions with the receptor (see

Figure 180). For example, competitive antagonists cannot reduce maximal activation. Increasing EC_{50} values alongside reductions in maximal activation must indicate a non-competitive negative allosteric modulator.

6.2.3 Irreversible inhibition

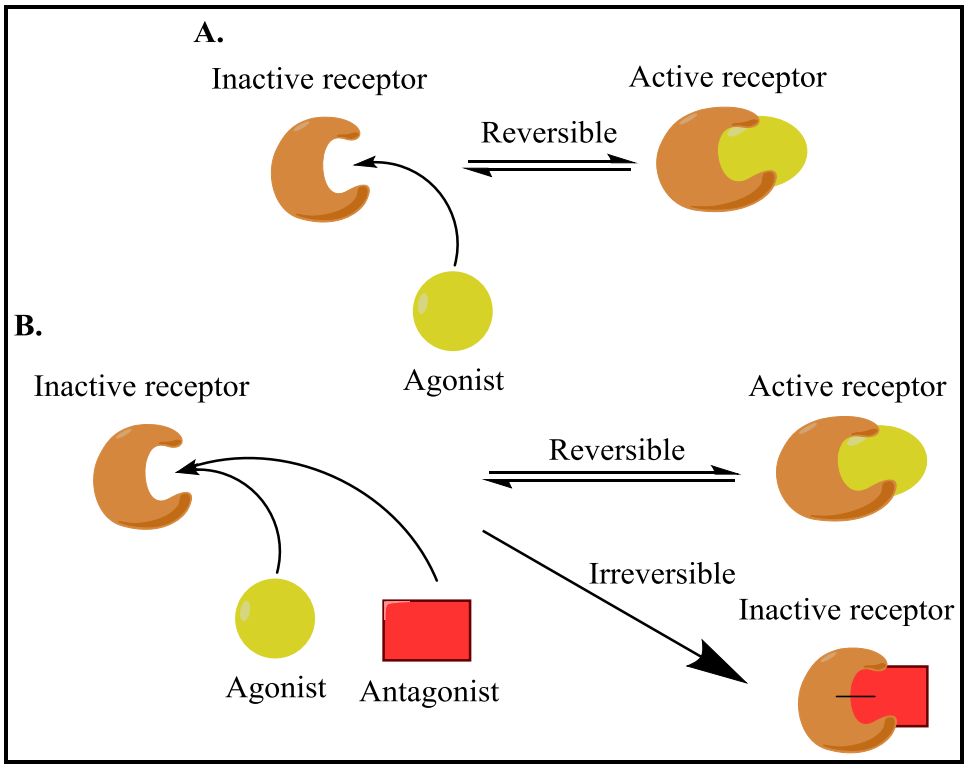


Figure 181: Diagram showing (**A**) agonism of the receptor by the endogenous ligand and (**B**) irreversible inhibition by an orthosteric antagonist.

Irreversible antagonists bind the receptor and have an exceptionally extended time bound to the receptor (Figure 181). This could be caused by covalent bonding to the receptor, or it could be caused by a change of the receptor conformation which makes release of the antagonist impossible. Often these inactivated receptors are internalised and recycled by the cell. This means that these inhibitors cannot be accurately characterised by IC_{50} readings as the inhibition of these compounds is often time-dependent as opposed to concentration-dependent. These compounds also do not fit the equations and models previously discussed. Phenoxybenzamine (an α-adrenergic receptor antagonist which can be used to treat some forms of hypertension and naloxazone (a μ-opioid receptor antagonist used to treat opiate overdose) are two examples of irreversible antagonists.

6.2.4 Uncompetitive inhibition

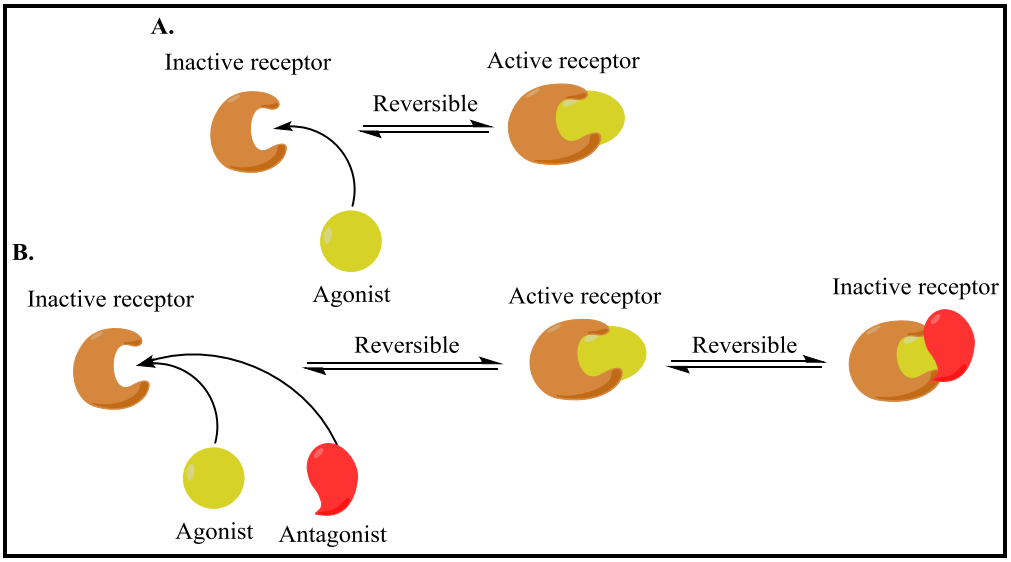


Figure 182: Diagram showing (**A**) agonism of the receptor by the endogenous ligand and (**B**) uncompetitive inhibition by an antagonist.

An uncompetitive antagonist requires the agonist to bind the orthosteric site before the antagonist can bind and inhibit the receptor (Figure 182). This produces unorthodox kinetic profiles. An identical amount of antagonist often produces a larger inhibitory effect in the presence of large amounts of agonist than in the presence of small amounts of agonist. An example of this kind of antagonist is memantine (an NMDA receptor antagonist occasionally used to treat Alzheimer's disease).[362]

6.3 Pharmacological assessment of solonamide A, B and their epimers

Historically, AgrC inhibitors have generally been characterised by reporting the IC_{50} in *P3::lux* or *P3::blaZ* based reporters.[309, 312, 315] To be able to effectively compare the solonamides with other previously discovered inhibitors, it was decided to characterise them using IC_{50} data from the *P3::lux* reporter previously discussed in Chapter 3 (beginning on page 109). A Schild analysis using this reported would also be employed to confirm the hypothesised competitive antagonism mode of action.

6.3.1 Confirmation of inhibition and IC_{50}s

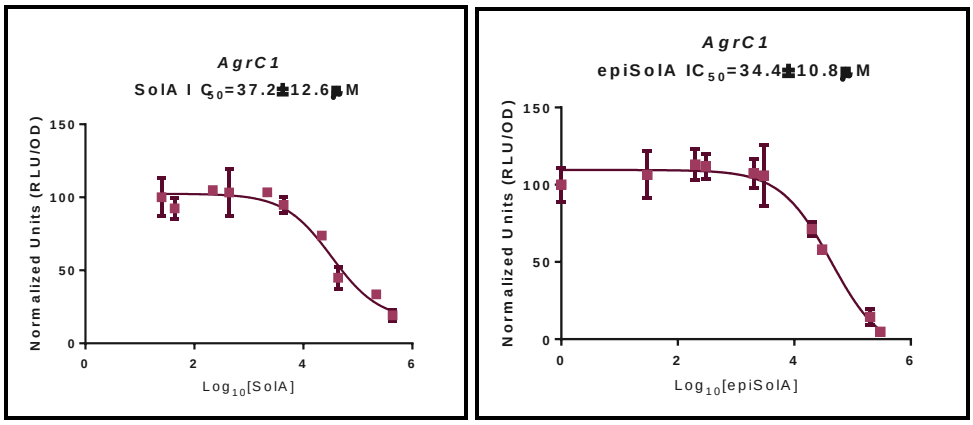


Figure 183: Dose-response curves generated for SolA (**1.21**) and epiSolA (**1.65**) using a *P3::lux* based reporter in the presence of 100 nM of AIP1.

Dose-response curves were created for both SolA (**1.21**) and epiSolA (**1.65**) in the *P3::lux*-based AgrC1 bioreporter assay. Triplicate experiments revealed an IC_{50} of 37.2 ± 12.6 μM for SolA (**1.21**) and 34.4 ± 10.8 μM for epiSolA (**1.65**) (representative graphs can be seen in Figure 183). In an identical system with the same agonist concentration, compared to the truncated AIP-based inhibitors, these solonamides are roughly 3-4 orders of magnitude less potent. These values are consistent with the concentrations required for inhibition in Nielsen *et al*. who indicated that a relatively high IC_{50} was likely.[216] Furthermore, because the truncated AIP-based inhibitors were developed through many years of study and structural refinement, and because they are modelled on the endogenous ligand, it is unsurprising that these unrelated natural products show a reduced potency. Further development may well

improve the IC_{50} dramatically if a similar amount of research is conducted on this scaffold.

It is interesting to note that epiSolA (**1.65**) produces curves where AgrC activation is reduced to basal levels. Conversely, SolA (**1.21**) produces curves where basal activity is not attained even at high concentrations (Figure 183). Given this disparity, it was decided that both compound would be tested to assess their agonistic properties against the AgrC1 receptor.

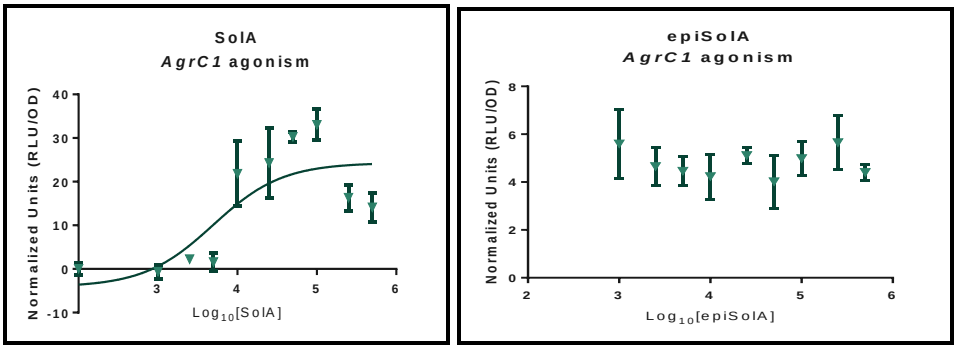


Figure 184: Dose-response curves generated for SolA (**1.21**) and epiSolA (**1.65**) using a *P3::lux* based reporter without the addition of AIP1 agonist.

Dose-response curves for the activation of *P3::lux*-based AgrC1 revealed that SolA (**1.21**) was a partial agonist showing approximately 30% of the maximal agonism caused by AIP1 (Figure 184). This agonism was reduced at high concentrations. Hence, it is possible that binding at both recognition sites of the receptor dimer could cause reduced agonism. Furthermore, EC_{50} data for partial agonists are heavily dependent on the compounds propensity to agonise the receptor. A stronger agonist could have a different EC_{50} than a weaker agonist with the same molecular affinity for the receptor. It was hoped that Schild analysis would reveal any effects due to heterogeneous inhibition.

Surprisingly, the non-natural analogue, epiSolA (**1.65**) did not display a similar agonism of AgrC1. Though both SolA (**1.21**) and epiSolA display a similar IC_{50}, this lack of agonism makes epiSolA (**1.65**) a better antagonist of the AgrC1 receptor. This effect also highlights the importance of the configuration of the 3-hydroxy acid moiety to the biological effect of the solonamides. As further epimers at this position were also synthesised, this could be further investigated in later analogues.

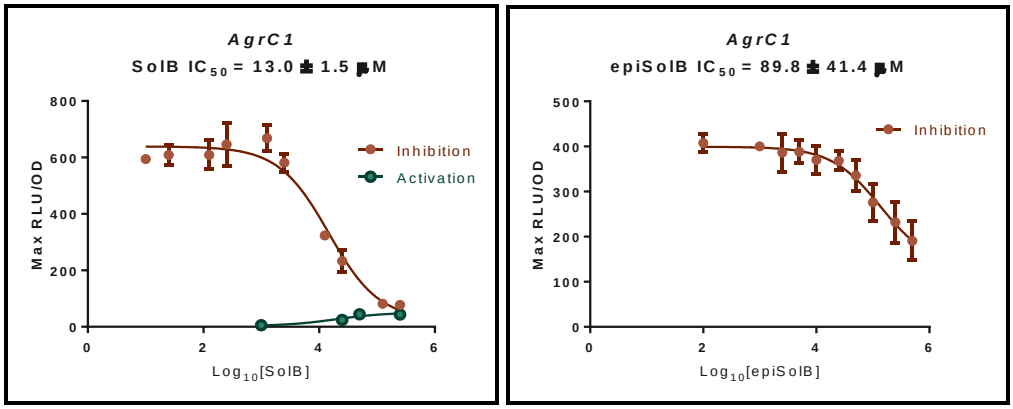


Figure 185: Dose-response curves generated for SolB (**1.22**) and epiSolB (**4.5**) using a *P3::lux* based reporter with 100nM of AIP1 and without the addition of AIP1.

Analogous experiments on SolB (**1.22**) revealed that this analogue possesses an improved IC_{50} of 13.0 ± 1.5 μM when compared to SolA (**1.21**). This corroborates the original observations of Mansson *et al.*[214] and Nielsen *et al.*[216] which suggested that SolB (**1.22**) is a better inhibitor than SolA (**1.21**). Furthermore, agonism by SolB (**1.22**) was reduced in comparison to SolA (**1.21**). This suggested that lengthening the alkyl chain of the 3-hydroxy acid moiety could both reduce the undesirable observed agonism and improve the IC_{50}. This is consistent with many reports that lipophilicity is important for inhibition of AgrC as longer alkyl chains are more lipophilic by nature.[313]

In contrast to the similar inhibitory activities displayed by SolA (**1.21**) and epiSolA (**1.65**), the epiSolB (**4.5**) diastereomer did not present the same activity as SolB (**1.22**); epiSolB (**4.5**) is only a low affinity partial antagonist with an IC_{50} of nearly 90 μM in comparison to the high affinity antagonist of SolB (**1.22**). It is possible that the similar inhibitory activities of SolA (**1.21**) and epiSolA (**1.65**) were accomplished with considerably different conformations. Perhaps the alkyl extension could change the conformation in epiSolB (**4.5**) without similar changes in SolB (**1.22**).

This is the first time IC_{50} data had been produced allowing quantification of the respective effects of each of the solonamides and comparison with other AgrC inhibitors.

6.3.2 Schild analysis

Following quantification of the solonamides inhibition at the AgrC1 receptor, the mode of binding was fully assessed by Schild analysis. Surprisingly, this revealed that the solonamides do not act as competitive antagonists as previously reported.[216] The solonamides are, in fact, non-competitive antagonists. Thus, they act as allosteric inhibitors which was a further surprise given the structural similarity of the solonamides and the native AIP ligands, which was discussed by Mansson *et al*. when the solonamide compounds were first discovered.[214] Given that both maximal activation and EC_{50} are affected, Bindslev *et al*. would refer to SolA and SolB as allo-mixed-competitive inhibitors, epiSolA would be an allo-competitive inhibitor (see Figure 180 on page 243 for graphical comparison).[360] Curve fitting using both the extended operational model of allosterism and the allosteric two-state model did not produce statistically reliable results. This could be due to potential effects of binding a dimeric receptor but could also be caused by a low quantity of data.

In fact, Schild analysis also revealed that epiSolA (**1.65**) operated in a very different way to both SolA (**1.21**) and SolB (**1.22**). EpiSolB (**4.5**) increased the EC_{50} values but did not reduce the maximal activation (E_{max}) caused by AIP1 at all. Therefore, binding of epiSolA (**1.65**) must cause a reduction in AIP1 affinity for the AgrC1 receptor thus functioning as a allo-competitive antagonist.[360] In sharp contrast, both SolA (**1.21**) and SolB (**1.22**) produced significant reductions in the E_{max} while also affecting the EC_{50}. This indicates that, on SolA or SolB binding the receptor, the affinity of AIP1 is reduced but also the propensity of AIP1 to activate the receptor is reduced. By definition, these inhibitors are negative allosteric modulators.

This is an exciting discovery as only one other class of negative allosteric modulators of the AgrC receptor are known, namely, the tetronic and tetramic acids. These were derived from an *N*-acyl-homoserine lactone quorum sensing compound originating in *P. aeruginosa* and are exemplified by 3-tetradecanoyltetronic acid.[223] However, these compounds are known to be toxic with an MIC only just above the IC_{50}s reported by Murray *et al*.[223] In contrast,

analysis of growth curves showed that the solonamides have no toxic effects even at very high concentrations. Therefore, these compounds are the first negative allosteric modulators which could be employed as pure anti-virulence compounds.

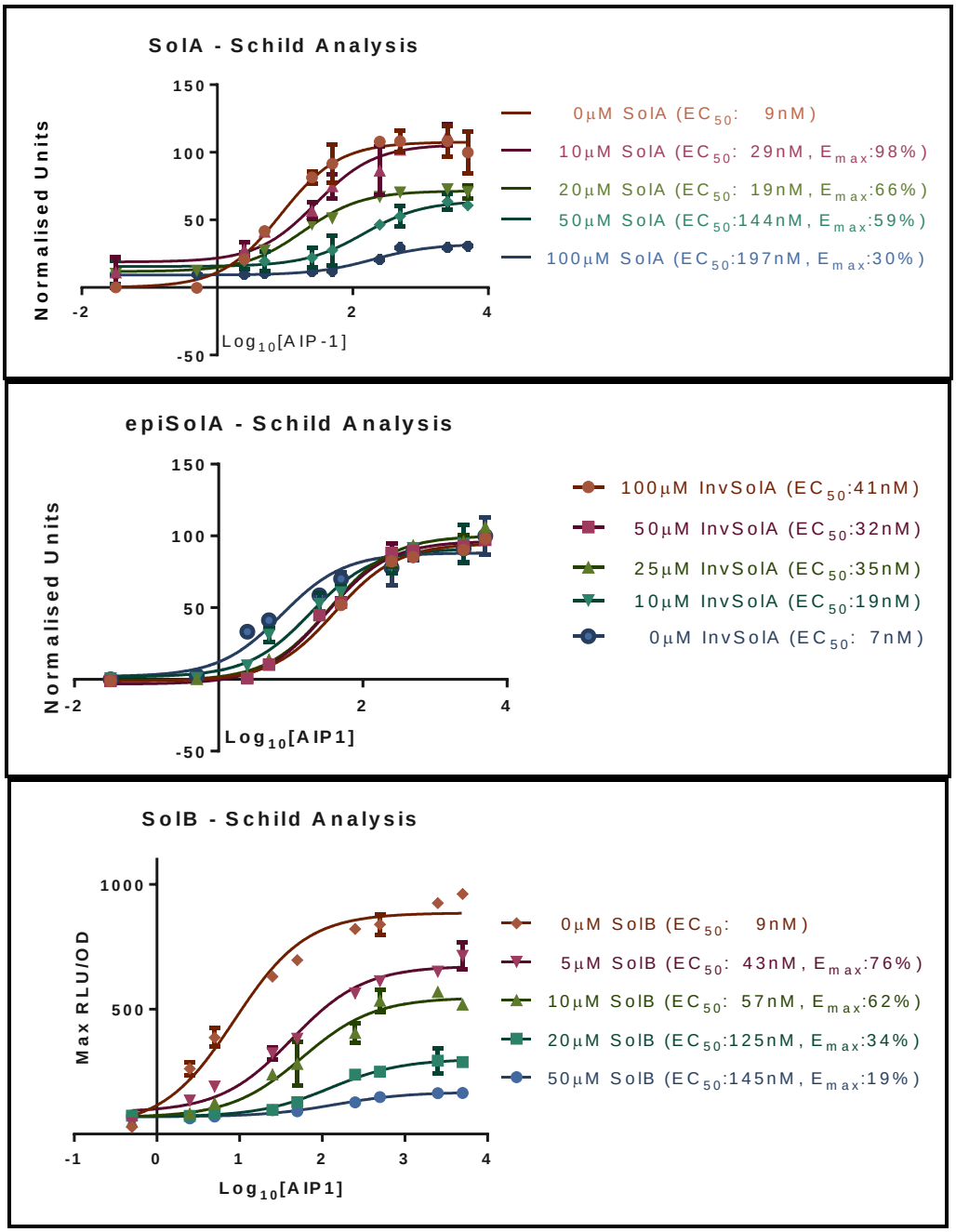


Figure 186: Schild analysis of SolA (**1.21**), epiSolA (**1.65**), and SolB (**1.22**).

6.3.3 Phenotypic studies

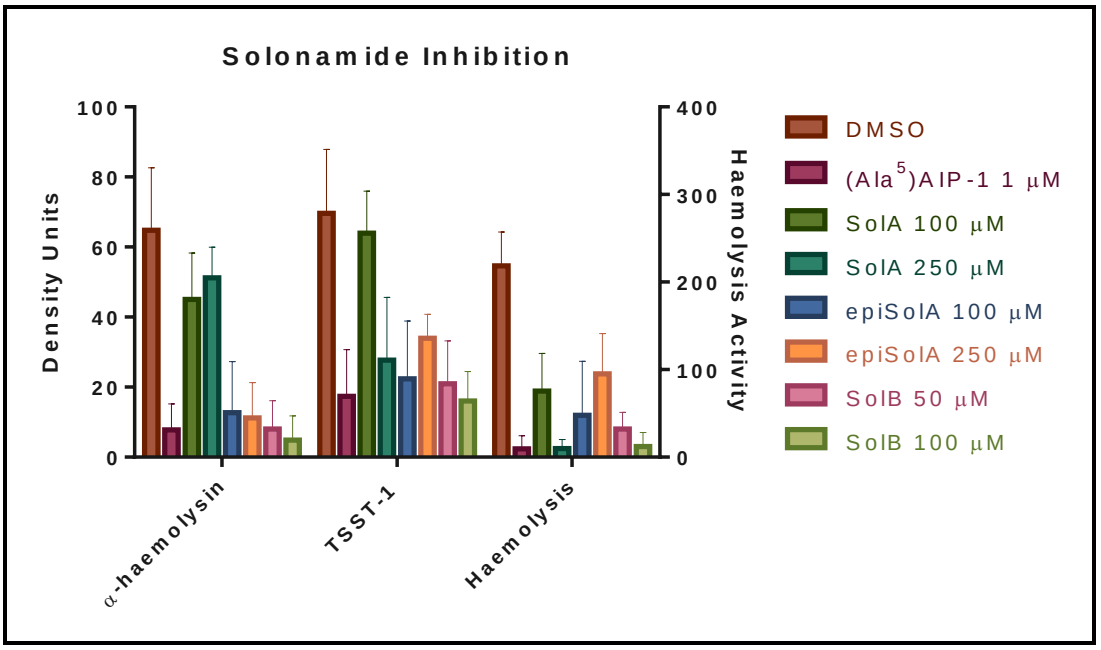


Figure 187: Graph showing the inhibition of erythrocyte hemolysis, and α-hemolysin and TSST-1 production by *S. aureus* KH1187A. Bars represent the standard deviation from triplicate repeats

Following the full pharmacological assessment of the mode of binding of both natural solonamides (**1.21** and **1.22**) and the related diastereomer, epiSolB (**1.65**), phenotypic studies were used to confirm the physiological effects of these negative allosteric modulators. Initially, the stability of the solonamides was confirmed using a HPLC assay. The compounds did not show any signs of breakdown when dissolved in water and stored at 37 ^{o}C over 24 hrs. EpiSolA (**1.65**), SolA (**1.21**) and SolB (**1.22**) were incubated with wild type *S. aureus* (KH1187A) over six hours. The culture supernatant was then isolated and subjected to Western blots for α-hemolysin and TSST-1. Hemolysis assays using defibrinated sheep blood were also used to determine the hemolytic activity of the bacterial supernatant after treatment with the solonamides. Both epiSolA (**1.65**) and SolB (**1.22**) significantly inhibited in all three assays producing activity which was similar to the known inhibitor, (Ala^5)AIP1 (**1.59**). However, SolA (**1.21**) did not display a similarly potent inhibition at high concentrations though similarly potent inhibition was observed in hemolysis assays. However, there was still a significant reduction in comparison to the untreated bacteria.

As SolB (**1.22**) possesses an improved IC_{50} and displays more potent inhibition in phenotypic assays, it was decided that SolB (**1.22**) would be the parent compound for the investigation of the structure activity relationship of the solonamides with the AgrC1 receptor.

6.4 Synthetic programme

Given that no previous investigations of the SAR of the solonamides had been undertaken, a systematic assessment of the contribution of each of the amino acid residues was required. Initially, an alanine scan would provide this information for each of the amino acid residues. A significant amino acid residue identified by the alanine scan will then be selected for further analysis of the SAR with AgrC1. The residue will be replaced with physicochemically similar residues and residues which differ significantly. The contribution of the 3-hydroxy acid moiety to the SAR would then be evaluated. Synthetic analogues of the 3-hydroxy acid building blocks will be used to produce further solonamide analogues. Biological evaluation of these compounds will elucidate the contribution of the 3-hydroxy acid moiety to the SAR. Finally, successful modifications from any of the alanine scan, selected amino acid variation or 3-hydroxy acid studies would be combined to form second generation compounds with the aim of creating more potent inhibitors of AgrC or ligands with improved lipophilic efficiency (LipE).

6.4.1.1 Alanine scan

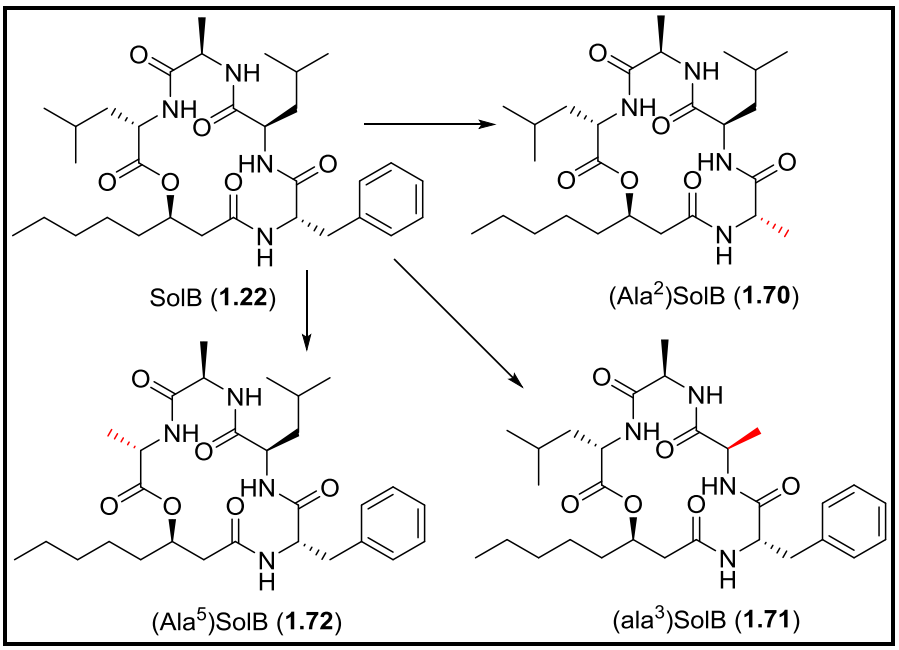


Figure 188: Diagram showing the planned alanine scan of SolB (**1.22**)

As four amino acid residues are present in SolB (**1.22**) and one is already an alanine residue, three analogues were required for a complete alanine scan. The

initial solonamide synthesis employing a macrolactonisation reaction was employed for the synthesis of these three compounds. (Ala[2])SolB (**1.70**) and (Ala[5])SolB (**1.72**) and the related epimers, (Ala[2])epiSolB (**4.38**) and (Ala[5])epiSolB (**4.40**) obtained as an enriched diastereomeric mixture and effectively separated by HPLC using this method (Chapter 4). However, (ala[3])SolB (**1.71**) could not be synthesised in this manner. Unfortunately, the synthesis produced a racemic mixture of (ala[3])SolB (**1.71**) and its epimer, (ala[3])epiSolB (**4.39**) which could not be effectively purified by HPLC as the diastereomers eluted without enough separation between the two compounds. The synthetic programme continued while efforts were made to stereoselectively synthesise (ala[3])SolB (**1.71**). Eventually, (ala[3])SolB (**1.71**) was produced *via* an alternative macrolactamisation strategy (detailed in Chapter 5) and used in the bioreporter assay. However, it was too late to influence our later synthetic decisions (for full details see Chapter 4 and 5 beginning on page 170 and 210 respectively).

6.4.1.2 3-hydroxy acid variation

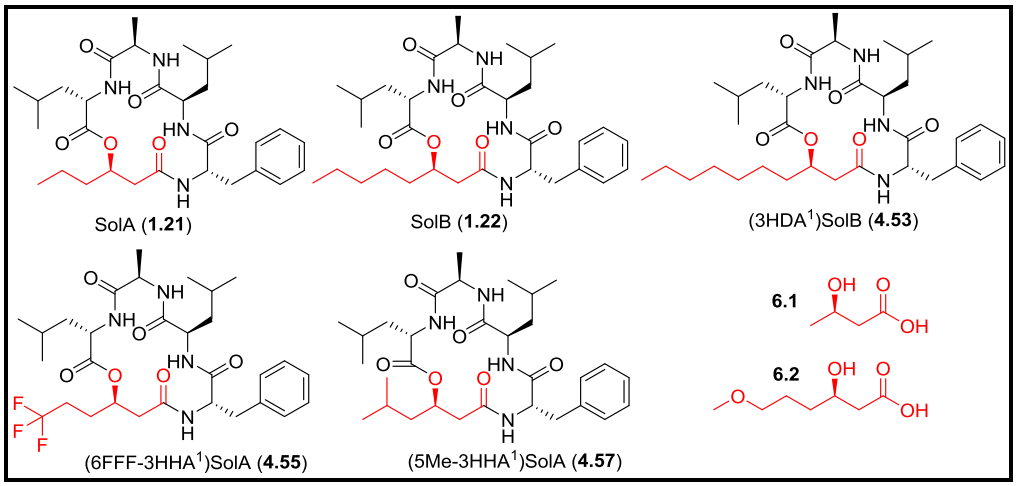


Figure 189: Scheme showing planned compounds to investigate the structure activity relationship of the 3-hydroxy acid moieties.

Initially, five further compounds were planned to analyse the structure activity relationship of the 3-hydroxy acid moieties. (3HDA[1])SolB (**4.53**) was intended to investigate the effect of further lengthening the alkyl tail. It was hypothesised that by further increasing tail length and lipophilicity, the solonamide compound would attain further improve affinity and antagonism characteristics. Trifluoromethyl groups, such as that present in (6FFF-

3HHA[1])SolA (**4.55**), can be incorporated to replace terminal methyl groups. They induce an increase in polarity in the alkyl chain which increases cLogP. Hopefully this modification will not also negatively affect the lipophilicity of the region. This group also introduces potential partners for hydrogen bonding interactions with the receptors amide backbone. Branched compounds such as (5Me-3HHA[1])SolA (**4.57**) can be a more efficient way of incorporating reduced lipophilicity into a compound maintaining the same molecular weight. A linear alkyl chain with the same number of carbons displays an increased LogP in comparison with a similar branched alkyl chain. Initially, two further compounds, **6.1** and **6.2** were planned; however, attempts to synthesise these monomers failed. The aldehyde precursor for compound **6.1** was very volatile and difficult to use. The failure to secure compound **6.2** was due to the ketene aldehyde cycloaddition yielding a complex mixture with no trace of the required product. Given the synthetic difficulties, production of these compounds was abandoned.

6.4.1.3 Variation of Phe[2] residue

Analysis of the activity profile of (Ala[2])SolB (**1.70**) and (Ala[5])SolB (**1.72**) revealed that alteration of the Leu[5] position severely reduced activity indicating that the Leu residue is likely to be important for solonamide binding or activity (see Section 6.5.2). The analogue (Ala[2])SolB maintained a significantly better activity profile indicating that it could be possible to vary this residue to achieve improvements in the pharmacology of the compound. These variations are illustrated in Figure 190.

Firstly, the most obvious change is the incorporation of tyrosine residue (**4.45**), this residue is very similar to the native phenylalanine residue while it contains a polar phenolic group. Using this analogue, the effects of increasing polarity at this position could be assessed. Given that the tyrosine residue would require protection, a *tert*-butyl group was selected for this purpose. This group would allow the isolation of the protected intermediate so that this analogue could also be analysed. This analogue (**4.43**) would conceal the polarity of the phenolic group while installing some considerable steric bulk.

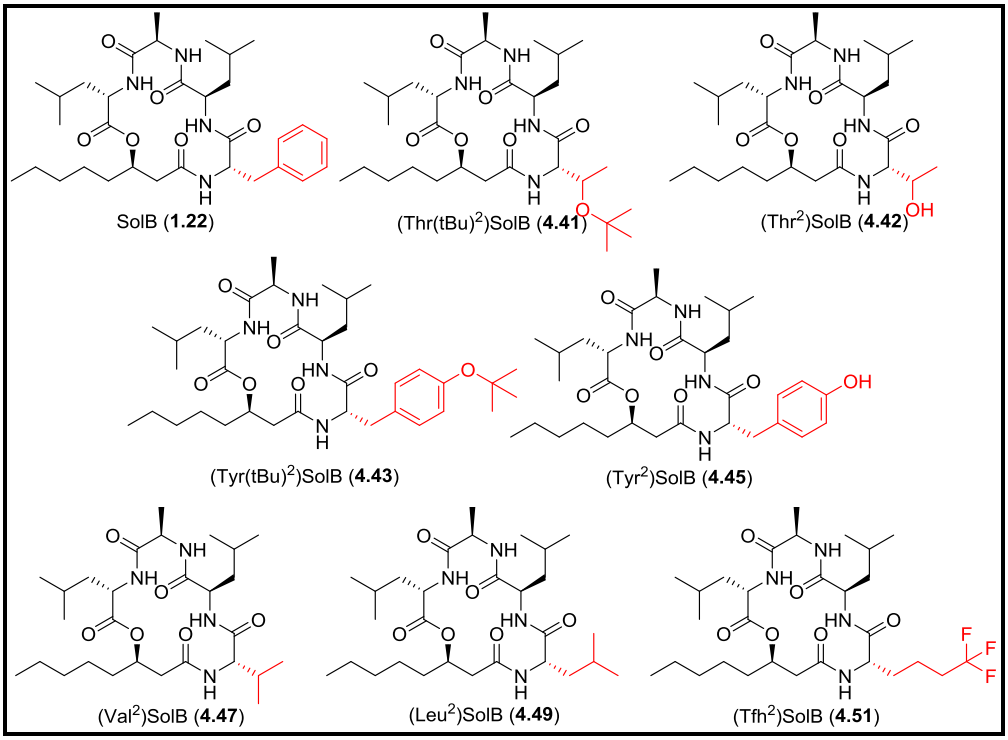


Figure 190: Diagram showing compounds produced which vary the original Phe[2] position of SolB (**1.22**).

Also, given the interesting affects caused by β-branched amino acid side-chains in the AIP based ligands, replacement of Phe[2] with the β-branched residues valine (**4.47**) and threonine (**4.42**) were proposed to assess whether similar patterns of activity would also be evident in the solonamides. Threonine was also interesting as the effects of polarity at this position could be assessed. Leucine variation (**4.49**) removed the aromatic functionality of Phe[2] while maintaining some of its steric bulk. It could also be used for comparison with valine and threonine analogues due to its lack of β-branching.

The non-natural trifluoromethylated amino acid (2*S*)-2-amino-6,6,6-trifluorohexanoic acid (Tfh) synthesised by Dr. Fabio Rui was also employed in this series of analogues. This analogue **4.51** would again possess increased polarity in the alkyl chain, increasing cLogP and introducing potential hydrogen bonding partners.

6.4.1.4 Second generation analogues

Once these analogues had all undergone biological testing and analysis, successful modifications would be combined in an effort to create a much more

potent solonamide compound. It is hoped additive effects would result in the identification of a much improved second generation analogue.

6.5 The Structure-Activity Relationship of solonamide analogues

Following the synthesis of this panel of solonamide analogues, *P3::lux* based AgrC1 bioreporter assays were performed to produce an IC_{50} for the purposes of comparing each of the analogues in this series.

6.5.1 3-hydroxy acid analogues

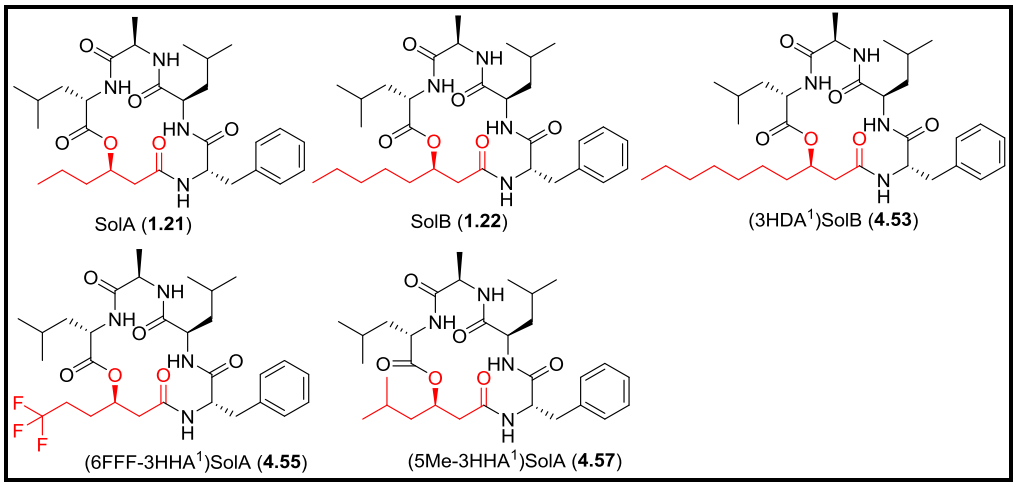


Figure 191: Scheme showing planned compounds investigating the structure activity relationship of the 3-hydroxy acid moieties.

Initially, it was hypothesised that lengthening the alkyl chain of SolB (**1.22**) would produce an improved compound in a similar manner to the improvement seen between SolA (**1.21**) and SolB (**1.22**). This led to the production of (3HDA[1])SolB (**4.53**). However, this analogue displayed minimal inhibition. The shape of the dose-response curve also did not seem to fit the usual rectangular hyperbola. Further testing revealed that, surprisingly, (3HDA[1])SolB (**4.53**) is a potent agonist of AgrC1. The EC_{50} is 320 nM in comparison to the roughly 10 nM of AIP1. This is very surprising as generally inhibition of the AgrC receptor is much more common than agonism. Changes to the native AIP ligands commonly produce inhibitors or inactive analogues. Furthermore, the parent compound, SolB (**1.22**) acts as a negative allosteric modulator meaning that this simple chemical modification dramatically alters the mode of action. Although allosteric agonists have been sporadically reported, they have not been widely accepted and are not currently recognised by the International Union of Pharmacology.[363] Given the structural similarity of the solonamides and the AIP endogenous ligands, it is also possible that this modification has allowed the

compound to bind the orthosteric site of the receptor in a similar manner to the AIP ligands. Further assays will be executed to establish whether this agonism is also present in AgrC2 and AgrC3.

Table 10: Structure activity relationship of the 3-hydroxy acid variation analogues.

Compound	#	Macrocyclic peptides	IC_{50} (AgrC1)
SolA	**1.21**	3(*R*)HHA*-Phe-*D*Leu-*D*Ala-Leu*	37.1±12.6[1(24%)]
epiSolA	**1.61**	3(*S*)HHA*-Phe-*D*Leu-*D*Ala-Leu*	34.4±10.8
SolB	**1.22**	3(*R*)HOA*-Phe-*D*Leu-*D*Ala-Leu*	13.0±1.5[1(15%)]
(5Me-3HHA[1])SolA	**4.57**	5Me3(*R*)HHA*- Phe-*D*Leu-*D*Ala-Leu*	11.3±6.8[1(20%)]
(5Me-3HHA[1])epiSolA	**4.58**	5Me3(*S*)HHA*- Phe-*D*Leu-*D*Ala-Leu*	No inhibition[1(43%)]
(3HDA[1])SolB	**4.53**	3(*R*)HDA*-Phe-*D*Leu-*D*Ala-Leu*	Agonism (78%) EC_{50}=320 nM
(3HDA[1])epiSolB	**4.54**	3(*S*)HDA*-Phe-*D*Leu-*D*Ala-Leu*	No activity
(6FFF-3HHA[1])SolA	**4.55**	6FFF3(*R*)HHA*-Phe-*D*Leu-*D*Ala-Leu*	53.4±5.4[1(43%)]
(6FFF-3HHA[1])epiSolA	**4.56**	6FFF3(*S*)HHA*-Phe-*D*Leu-*D*Ala-Leu*	No activity

3(*S*)HHA=3*S*-hydroxyhexanoic acid, 3(*R*)HOA=3*R*-hydroxyoctanoic acid, 5Me3(*S*)HHA= 5-methyl-3*S*-hydroxyhexanoic acid, 3(*R*)HDA= 3*R*-hydroxydecanoic acid, 6FFF3(*S*)HHA=6,6,6-triflouro-3*S*-hydroxyhexanoic acid.

[1(10%)] Partial agonism (10% activation compared with 100 nM AIP). [2(30%)] Partial antagonism (30% of full activity remaining), *lux* activity continues to be observed at high concentrations.

Modification of the 3-hydroxy acid moiety to the branched chain analogue (5Me-3HHA[1])SolA (**4.57**) produced marginal improvements in the IC_{50} in comparison to SolB (**1.22**). As this compound contains less carbon atoms in the alkyl tail and possesses a branched structure, the moiety is considerably less lipophilic. Interestingly, this alkyl chain has a close structural similarity to leucine which has commonly appeared in truncated AIP inhibitors. Given the improvement in IC_{50} this modification is likely to be incorporated into second generation analogues.

In contrast to the initial success of epiSolB (**1.65**), all of the diastereomers in this series were inactive. Given the observations that epiSolB (**1.65**) seems to operate in a very different way to both SolA (**1.21**) and SolB (**1.22**), it could be that this mechanism is much less tolerant of changes in the 3-hydroxy acid moiety than the mechanism observed in the other two analogues.

6.5.2 Alanine scan of SolB

Initially, (ala[3])SolB (**1.71**) was not available for analysis due to synthesis difficulties. Testing of (Ala[2])SolB (**1.70**) and (Ala[5])SolB (**1.72**) revealed that the Leu[5] position is vital for activity. Replacing the leucine residue for alanine

dramatically affects the IC_{50} of the compound reducing its potency by over an order of magnitude (Table 11). It was therefore considered that the Leu^5 is important for activity and its replacement would not be a good prospect for analysis of its SAR. Therefore, Phe^2 was selected for a more in depth analysis.

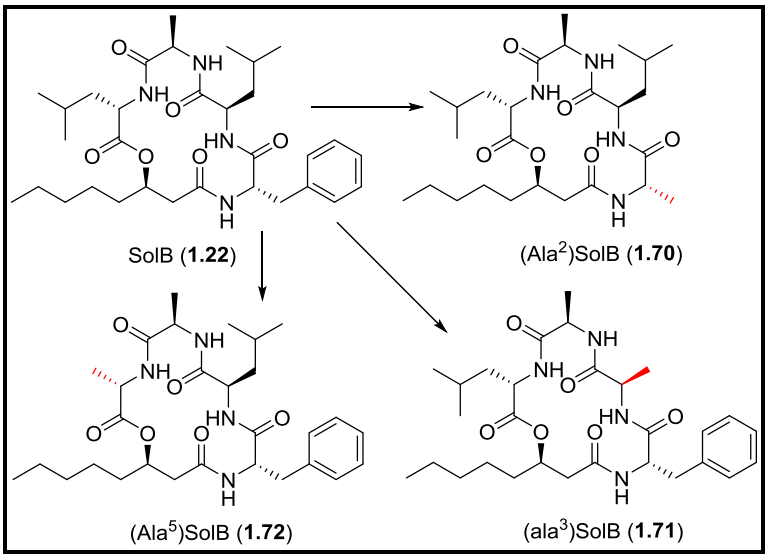


Figure 192: Diagram showing the planned alanine scan of SolB (**1.22**)

Initially, replacement of Phe^2 with alanine produced an analogue which was no longer a partial agonist. The IC_{50} was also only slightly affected. Therefore, this position was thought to be a promising position for variation to improve the EC_{50} while addressing the problem with the undesired partial agonism.

The two epimers (**4.38** and **4.40**) produced were, as previously, not very good inhibitors. This further highlights the importance of the configuration of the 3-hydroxy acid moiety and consequently the importance of a reliable stereoselective synthesis.

Once, (ala^3)SolB (**1.71**) was produced, it was tested and found to be a significantly improved antagonist. It was considered that, in future, this position may be a promising position for further SAR studies. However, variation of this position will not be a part of this study due to time constraints. The modification will be included in the second generation analogues in an attempt to produce more potent and drug-like solonamide compounds.

Table 11: Structure activity relationship of the 3-hydroxy acid variation analogues.

Compound	#	Macrocyclic peptides	LipE	IC_{50} (AgrC1)
SolA	**1.21**	3(*R*)HHA*-Phe-*D*Leu-*D*Ala-Leu*	-1.07	37.1±12.6[1(24%)]
epiSolA	**1.65**	3(*S*)HHA*-Phe-*D*Leu-*D*Ala-Leu*	-1.04	34.4±10.8
SolB	**1.22**	3(*R*)HOA*-Phe-*D*Leu-*D*Ala-Leu*	-1.67	13.0±1.5[1(15%)]
(Ala[2])SolB	**1.70**	3(*R*)HOA*-Ala-*D*Leu-*D*Ala-Leu*	-0.65	32.3±6.9
(Ala[2])epiSolB	**4.38**	3(*S*)HOA*-Ala-*D*Leu-*D*Ala-Leu*	-	Mild inhibition[2(60%)]
(ala[3])SolB	**1.71**	3(R)HOA*-Phe-*D*Ala-*D*Ala-Leu*	-0.05	8.9±1.5
(Ala[5])SolB	**1.72**	3(*R*)HOA*-Phe-*D*Leu-*D*Ala-Ala*	-1.30	159±14[1(14%)]
(Ala[5])epiSolB	**4.40**	3(*S*)HOA*-Phe-*D*Leu-*D*Ala-Ala*	-	No activity

3(*S*)HHA=3*S*-hydroxyhexanoic acid, 3(*R*)HOA=3*R*-hydroxyoctanoic acid.
[1(10%)] Partial agonism (10% activation compared with 100 nM AIP). [2(30%)] Partial antagonism (30% of full activity remaining), *lux* activity continues to be observed at high concentrations.

6.5.3 Variation of Phe[2] residue

Unfortunately, the loss of partial agonism observed in the (Ala[2])SolB (**1.70**) was not observed in any of the subsequent analogues (Figure 193) which are varied this position.

Replacement of phenylalanine with tyrosine (**4.45**) produced a completely inactive analogue indicating that polar phenolic group attached to the aromatic ring is unlikely to be well tolerated. However, the *tert*-butyl protected tyrosine analogue (**4.43**) was one of the most potent solonamide analogues yet tested (Table 12). The *tert*-butyl group is particularly bulky indicating that there must be considerable space available in the allosteric site for accommodation of this group. However, full antagonism was not observed. The protected analogue **4.43** is also particularly lipophilic so it negatively effects the LipE making this an undesirable modification.

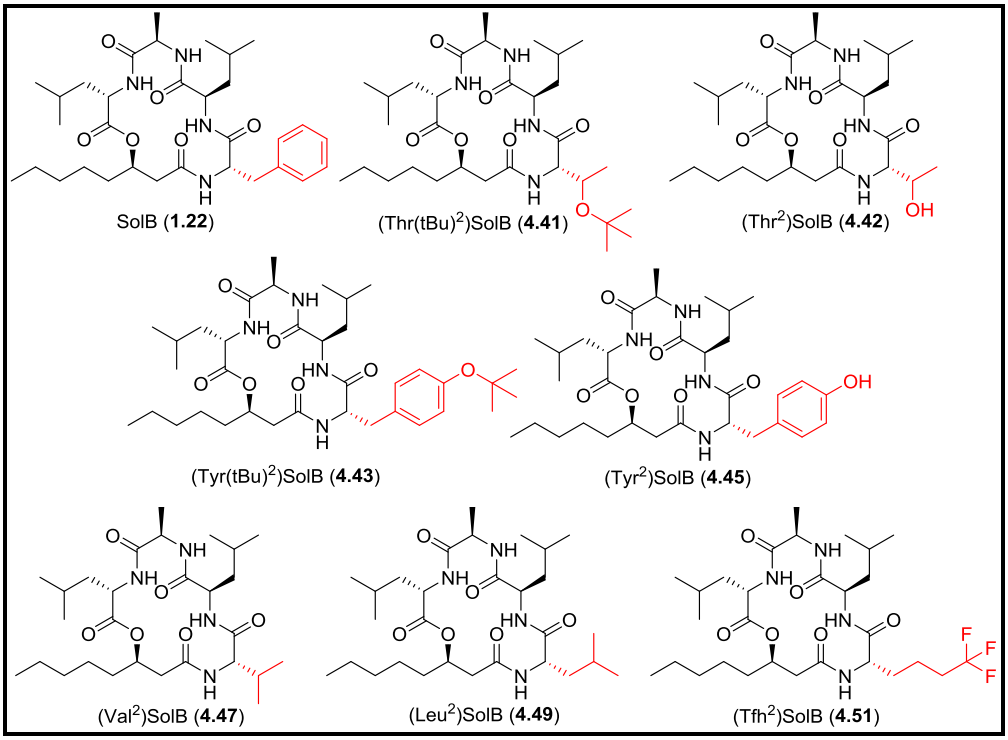


Figure 193: Diagram showing compounds produced which vary the original Phe² position of SolB (**1.22**).

Table 12: SAR of analogues produced by variation of Phe².

Compound	#	Macrocyclic peptides	LipE	IC_{50} (AgrC1)
SolA	**1.21**	3(*R*)HHA*-Phe-*D*Leu-*D*Ala-Leu*	-1.07	37.1±12.6[1(24%)]
epiSolA	**1.65**	3(*S*)HHA*-Phe-*D*Leu-*D*Ala-Leu*	-1.04	34.4±10.8
SolB	**1.22**	3(*R*)HOA*-Phe-*D*Leu-*D*Ala-Leu*	-1.67	13.0±1.5[1(15%)]
(Thr(tBu)²)SolB	**4.41**	3(R)HOA*-Thr(tBu)-DLeu-DAla-Leu*	-1.77	30.9±9.5[2(32%)]
(Thr²)SolB	**4.42**	3(R)HOA*-Thr-DLeu-DAla-Leu*	-0.37	86.5±7.4[2(28%)]
(Tyr(tBu)²)SolB	**4.43**	3(R)HOA*-Tyr(tBu)-DLeu-DAla-Leu*	-2.29	3.8±0.7[2(24%)]
(Tyr(tBu)²)epiSolB	**4.44**	3(S)HOA*-Tyr(tBu)-DLeu-DAla-Leu*	-	No activity
(Tyr²)SolB	**4.45**	3(R)HOA*-Tyr-DLeu-DAla-Leu*	-	No activity
(Tyr²)epiSolB	**4.46**	3(S)HOA*-Tyr-DLeu-DAla-Leu*	-	No activity
(Val²)SolB	**4.47**	3(R)HOA*-Val-DLeu-DAla-Leu*	-	No activity
(Val²)epiSolB	**4.48**	3(S)HOA*-Val-DLeu-DAla-Leu*	-1.94	73.7±11.6[2(37%)]
(Leu²)SolB	**4.49**	3(R)HOA*-Leu-DLeu-DAla-Leu*	-1.24	4.4±1.8[2(48%)]
(Leu²)epiSolB	**4.50**	3(S)HOA*-Leu-DLeu-DAla-Leu*	-2.11	32.3±10.7[2(49%)]
(Tfh²)SolB	**4.51**	3(R)HOA*-Tfh-DLeu-DAla-Leu*	-1.19	12.6±0.8[2(39%)]
(Tfh²)epiSolB	**4.52**	3(S)HOA*-Tfh-DLeu-DAla-Leu*	-	No activity

3(*S*)HHA=3*S*-hydroxyhexanoic acid, 3(*R*)HOA=3*R*-hydroxyoctanoic acid, Tfh=(*S*)-2-amino-6,6,6-trifluorohexanoic acid.

[1(10%)] Partial agonism (10% activation compared with 100 nM AIP). [2(30%)] Partial antagonism (30% of full activity remaining), *lux* activity continues to be observed at high concentrations.

Incorporation of threonine and valine replacing Phe² was not well tolerated. Interestingly, incorporation of *tert*-butyl-protecting group to the Thr² analogue improved affinity. This highlights the importance of lipophilicity for binding to

this receptor. It is possible that a serine or *tert*-butyl-protected serine may produce better results at this position due to the lack of β-branching.

In contrast, an improved activity profile for the leucine (**4.49**) and trifluoromethylated analogue (**4.51**) was observed. The leucine analogue (**4.49**) was particularly potent which given its reduced lipophilicity in comparison to phenylalanine was particularly encouraging. However, it also produced significant agonism of the AgrC1 receptor. It could be that the aromatic nature of the phenylalanine group is less likely to cause agonism than the leucine group. Unexpectedly, (Val^2)epiSolB (**4.48**) was more active than it diastereomer counterpart.

6.5.4 Second generation analogues

Table 13: Structure activity relationship of the second generation analogues.

Compound	#	Macrocyclic peptides	LipE	IC_{50} (AgrC1)
SolA	**1.21**	3(*R*)HHA*-Phe-*D*Leu-*D*Ala-Leu*	-1.07	37.1±12.6$^{1(24\%)}$
epiSolA	**1.65**	3(*S*)HHA*-Phe-*D*Leu-*D*Ala-Leu*	-1.04	34.4±10.8
SolB	**1.22**	3(*R*)HOA*-Phe-*D*Leu-*D*Ala-Leu*	-1.67	13.0±1.5$^{1(15\%)}$
(5Me-3HHA^1, ala^3)Sol	**5.15**	5Me3(*R*)HHA*-Phe-*D*Ala-*D*Ala-Leu*	0.12	27.6±3.2
(Leu^2, ala^3)Sol	**5.16**	3(*R*)HOA*-Leu-*D*Ala-*D*Ala-Leu*	-1.10	91.0±0.9
(5Me-3HHA^1, Leu^2, ala^3)Sol	**5.17**	5Me3(*R*)HHA*-Leu-*D*Ala-*D*Ala-Leu*	-	>500

Three modifications improved both potency and LipE, these were the use of the 3-(*R*)-hydroxy-5-methyl-hexanoic acid, the replacement of Leu^3 to alanine, and the replacement of Phe^2 to leucine. Therefore, a panel of analogues combining these modifications was produced using the newly developed stereoselective synthesis described in Chapter 5. All three were produced with an excellent *de* above 90%, validating the reliability and applicability of the new synthetic approach.

Compound **5.15** incorporating the alanine and 3-(*R*)-hydroxy-5-methylhexanoic acid modifications was less active than SolB (**1.22**). However, it was not a partial antagonist and its LipE was dramatically improved. Therefore, this compound could be a promising lead compound for future studies. Unfortunately, compound **5.16** which incorporated the Leu^2 and ala^3 modifications was significantly less active than the parent compound SolB (**1.22**). It is possible that by modifying two residues simultaneously the

macrocycle conformation changes in an unfavourable manner thus reducing the desired inhibitory properties. This hypothesis is further supported by the fact that compound **5.17**, which incorporates all of the three previously successful modifications, is completely inactive.

6.5.5 Phenotypic studies

Western blots were performed to assess the effectiveness of a small panel of compounds selected for either interest or effectiveness. As illustrated in Figure 194, (ala^3)SolB (**1.71**), (5Me-3HHA^1)SolA (**4.57**), and (Tyr(tBu)^2)SolB (**4.43**) all effectively reduced the secretion of α-hemolysin indicating their phenotypic effects are commensurate with the experimental results obtained using the bioreporter assay. As anticipated, the analogue (3HDA^1)SolB (**4.53**), which is an agonist of AgrC1 agonist, did not reduce α-hemolysin secretion.

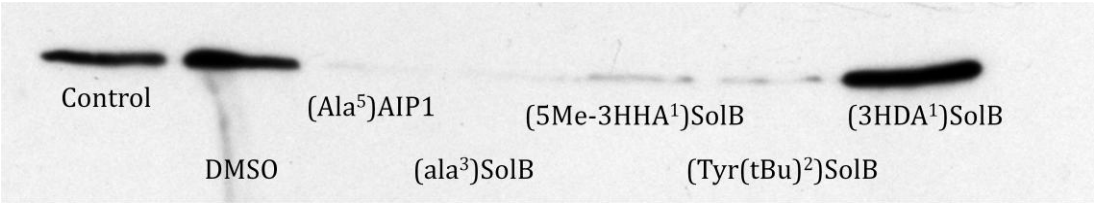


Figure 194: A western blot showing reduction of α-hemolysin production by solonamide analogues.

6.5.6 Complete structure activity relationship data plus additional data from AgrC2 and AgrC3 reporters

Table 14: Complete results table for all solonamide analogues tested

Compound	Macrocyclic peptides	LipE	IC_{50} (AgrC1)	IC_{50} (AgrC2)	IC_{50} (AgrC3)
AIP-1	H-Tyr-Ser-Thr-Cys*-Asp-Phe-Ile-Met*	-	-	50.8±11.8nM	22.3±5.6nM
SolA	3(*R*)HHA*-Phe-*D*Leu-*D*Ala-Leu*	-1.07	37.1±12.6[1(24%)]	91.0±1.0[2]	46.0±4.4
epiSolA	3(*S*)HHA*-Phe-*D*Leu-*D*Ala-Leu*	-1.04	34.4±10.8	126.1±31.3[2]	9.6±1.8[2]
SolB	3(*R*)HOA*-Phe-*D*Leu-*D*Ala-Leu*	-1.67	13.0±1.5[1(15%)]	6.2±0.8	4.5±0.1
epiSolB	3(*S*)HOA*-Phe-*D*Leu-*D*Ala-Leu*	-2.51	89.8±41.4[2(40%)]	>200	>200
(Ala²)SolB	3(*R*)HOA*-Ala-*D*Leu-*D*Ala-Leu*	-0.65	32.3±6.9	Not tested	Not tested
(Ala²)epiSolB	3(*S*)HOA*-Ala-*D*Leu-*D*Ala-Leu*	-	Mild inhibition[2(60%)]	Not tested	Not tested
(ala³)SolB	3(*R*)HOA*-Phe-*D*Ala-*D*Ala-Leu*	-0.05	8.9±1.5	Not tested	Not tested
(Ala⁵)SolB	3(*R*)HOA*-Phe-*D*Leu-*D*Ala-Ala*	-1.30	159±14[1(14%)]	Not tested	Not tested
(Ala⁵)epiSolB	3(*S*)HOA*-Phe-*D*Leu-*D*Ala-Ala*	-	No activity	Not tested	Not tested
(Thr(tBu)²)SolB	3(*R*)HOA*-Thr(tBu)-*D*Leu-*D*Ala-Leu*	-1.77	30.9±9.5[2(32%)]	Not tested	Not tested
(Thr²)SolB	3(*R*)HOA*-Thr-*D*Leu-*D*Ala-Leu*	-0.37	86.5±7.4[2(28%)]	Not tested	Not tested
(Tyr(tBu)²)SolB	3(*R*)HOA*-Tyr(tBu)-*D*Leu-*D*Ala-Leu*	-2.29	3.8±0.7[2(24%)]	Not tested	Not tested
(Tyr(tBu)²)epiSolB	3(*S*)HOA*-Tyr(tBu)-*D*Leu-*D*Ala-Leu*	-	No activity	Not tested	Not tested
(Tyr²)SolB	3(*R*)HOA*-Tyr-*D*Leu-*D*Ala-Leu*	-	No activity	Not tested	Not tested
(Tyr²)epiSolB	3(*S*)HOA*-Tyr-*D*Leu-*D*Ala-Leu*	-	No activity	Not tested	Not tested
(Val²)SolB	3(*R*)HOA*-Val-*D*Leu-*D*Ala-Leu*	-	No activity	Not tested	Not tested
(Val²)epiSolB	3(*S*)HOA*-Val-*D*Leu-*D*Ala-Leu*	-1.94	73.7±11.6[2(37%)]	Not tested	Not tested
(Leu²)SolB	3(*R*)HOA*-Leu-*D*Leu-*D*Ala-Leu*	-1.24	4.4±1.8[2(48%)]	Not tested	Not tested
(Leu²)epiSolB	3(*S*)HOA*-Leu-*D*Leu-*D*Ala-Leu*	-2.11	32.3±10.7[2(49%)]	Not tested	Not tested
(Tfh²)SolB	3(*R*)HOA*-Tfh-*D*Leu-*D*Ala-Leu*	-1.19	12.6±0.8[2(39%)]	Not tested	Not tested
(Tfh²)epiSolB	3(*S*)HOA*-Tfh-*D*Leu-*D*Ala-Leu*	-	No activity	Not tested	Not tested
(5Me-3HHA¹)SolA	5Me3(*R*)HHA*- Phe-*D*Leu-*D*Ala-Leu*	-0.95	11.3±6.8[1(20%)]	Not tested	Not tested
(5Me-3HHA¹)epiSolA	5Me3(*S*)HHA*- Phe-*D*Leu-*D*Ala-Leu*	-	No inhibition[1(43%)]	Not tested	Not tested
(3HDA¹)SolB	3(*R*)HDA*-Phe-*D*Leu-*D*Ala-Leu*	-2.32	Agonism (78%) EC_{50}=320nM	1.1±0.05[2 (33%)]	0.95±0.4
(3HDA¹)epiSolB	3(*S*)HDA*-Phe-*D*Leu-*D*Ala-Leu*	-	No activity	Not tested	Not tested
(6FFF-3HHA¹)SolA	6FFF3(*R*)HHA*-Phe-*D*Leu-*D*Ala-Leu*	-0.74	53.4±5.4[1(43%)]	Not tested	Not tested
(6FFF-3HHA¹)epiSolA	6FFF3(*S*)HHA*-Phe-*D*Leu-*D*Ala-Leu*	-	No activity	Not tested	Not tested
(5Me-3HHA¹, ala³)Sol	5Me3(*R*)HHA*-Phe-*D*Ala-*D*Ala-Leu*	0.12	27.6±3.2	Not tested	Not tested
(Leu², ala³)Sol	3(*R*)HOA*-Leu-*D*Ala-*D*Ala-Leu*	-1.10	91.0±0.9	Not tested	Not tested
(5Me-3HHA¹ Leu², ala³)Sol	5Me3(*R*)HHA*-Leu-*D*Ala-*D*Ala-Leu*	-	>500	Not tested	Not tested

3(*S*)HHA=3*S*-hydroxyhexanoic acid, 3(*R*)HOA=3*R*-hydroxyoctanoic acid, Tfh=(*S*)-2-amino-6,6,6-trifluorohexanoic acid, 5Me3(*S*)HHA= 5-methyl-3*S*-hydroxyhexanoic acid, 3(*R*)HDA= 3*R*-hydroxydecanoic acid, 6FFF3(*S*)HHA=6,6,6-triflouro-3*S*-hydroxyhexanoic acid.

[1(10%)] Partial agonism (10% activation compared with 100 nM AIP). [2(30%)] Partial antagonism (30% of full activity remaining), *lux* activity continues to be observed at high concentrations.

Interestingly, the agonistic activity caused by (3HDA[1])SolB (**4.53**) towards AgrC1 was not observed with AgrC2 and AgrC3. In fact, this compound inhibited these reporters quite effectively. This further supports the hypothesis that compound **4.53** is an orthosteric agonist in AgrC1, since its activity trend towards AgrC1, AgrC2 and AgrC3 are similar to the native ligand AIP1.

Testing the original SolA (**1.21**), SolB (**1.22**), epiSolA (**1.65**), and epiSolB (**4.5**) compounds in AgrC2 and AgrC3 revealed that epiSolB (**4.5**) is the least active compound in all three *agr* groups. SolB (**1.22**) is also a considerably more potent antagonist in these three group than the other compounds affirming its selection as the parent compound for the SAR studies.

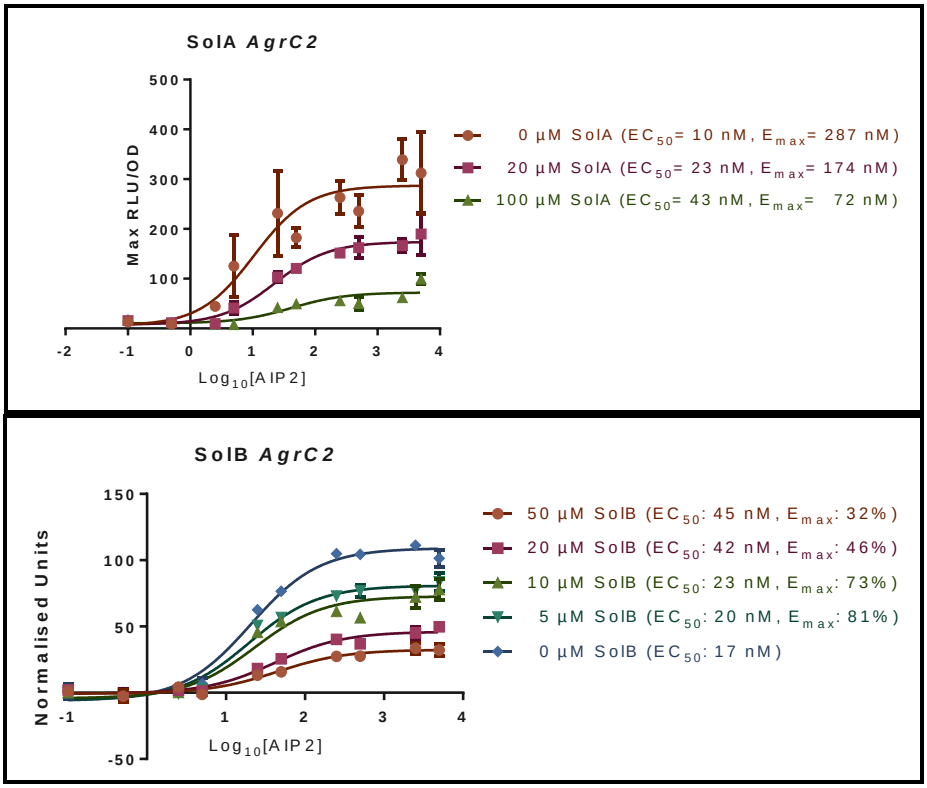


Figure 195: Schild analysis graphs in AgrC2 for SolA (**1.21**) and SolB (**1.22**)

No agonism was observed with any solonamide analogues in either the AgrC2 or AgrC3 reporters, suggesting that this partial agonism effect is specific to AgrC1. Given that the partial agonism effect was group specific, it could be possible that these compounds inhibit AgrC2 and AgrC3 *via* a different mode of binding. Therefore, Schild analysis for both SolA (**1.21**) and SolB (**1.22**) was also performed. These studies revealed that the solonamides still act as negative allosteric modulators in AgrC2 (Figure 195). This reveals that the allosteric site

is likely to be conserved across all the *agr* groups. The solonamides could therefore be employed as pan-group antivirulence agents.

6.6 Conclusions

During the course of the work described herein, the recently discovered natural product depsipeptides known as the solonamides are fully pharmacologically characterised. Their inhibitory activity has been quantified experimentally for the first time, with IC_{50} data for both natural products, SolA (**1.21**) and SolB (**1.22**), and their related epimers, epiSolA (**1.65**) and epiSolB (**4.5**). This allows comparison with the previously discovered and developed truncated AIP-based inhibitors. The solonamides are roughly 3-4 orders of magnitude less potent than the truncated AIP-based inhibitors.

Further assays revealed that the compounds are not competitive antagonists as originally assumed. Schild analysis revealed that these compounds actually act as non-competitive negative allosteric modulators of AgrC and not as competitive antagonists as previously asserted by Nielsen *et al*.[216] These are the first non-toxic allosteric inhibitors of AgrC to be discovered. Continuing this research in AgrC2 and AgrC3 revealed that the compounds also inhibit both of these receptors indicating that the allosteric site is likely to be conserved across multiple *agr* groups. Given the presence of *agr* analogues in several pathogenic organisms, it is also possible that these compounds may be able to exert pharmacological effects in these organisms.

Examination of the SAR of the solonamides with AgrC1 using an alanine scan revealed two promising positions, Phe^2 and leu^3, which could be modified to produce improved inhibitors. Replacement of leu^3 with alanine produced a more potent antagonist without the problematic partial agonism previously observed. Furthermore, analogues of Phe^2 revealed that a leucine residue at this position could improve the IC_{50} and also the LipE of the compound.

SAR studies included changes to the 3-hydroxy acid moieties. Having originally hypothesised that extending the alkyl chain of these moieties would improve activity, it was surprising to discover that by lengthening this chain to a decanoyl group, the analogue **4.53** became a potent agonist of AgrC1. Moreover, this compound showed potent antagonism of AgrC2 and AgrC3.

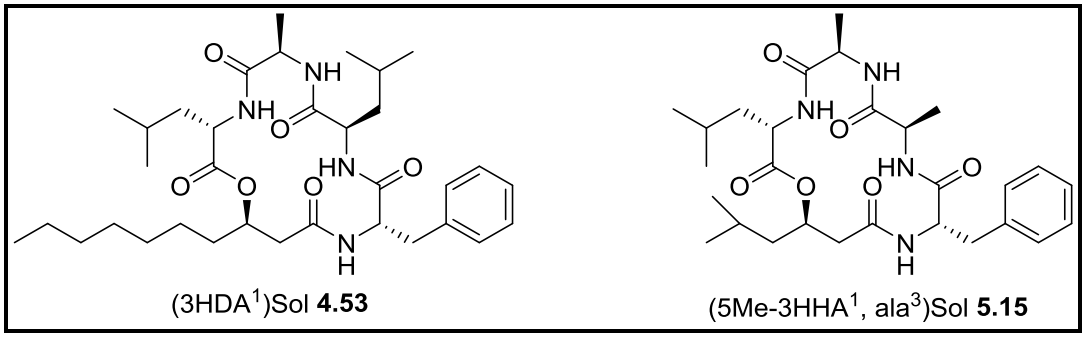


Figure 196: Structure of AgrC1 agonist, **4.53**, and negative allosteric modulator, **5.15**.

Modification of the 3-hydroxy acid moiety was also explored. A 5-methyl 3-hydroxy hexanoic acid did improve both the IC_{50} and the LipE of the compound. However, combining the successful modifications discovered did not lead to more potent solonamide compounds. However, a promising lead compound, (5Me-3HHA^1, ala^3)Sol (**5.15**), which maintained good antagonism with an improved LipE profile is a promising lead compound for further SAR studies.

6.7 Future Work

Further SAR studies could be used to develop more potent solonamide analogues. Variation of the leu[3] position could be an easy and promising strategy to pursue. Another option could be the evaluation of α-substituted 3-hydroxy acid moieties.

The solonamides are stable in culture media, however, it is unknown whether they are stable in more biologically relevant fluids such as blood plasma. Furthermore, there is no information as to the toxicity of these compounds against various mammalian cell lines. This would need to be established before any *in vivo* work could even be considered.

As the allosteric binding site is unknown, photolabelling techniques could be used to covalently bind the compound to the receptor, if an alkyne group were also incorporated into the solonamide compound a click reaction could be used to isolate the receptor-solonamide complex from cell lysate, trypsin digestion followed by mass spectrometric analysis could reveal at least a portion of the allosteric binding site.

NMR studies could be used to analyse the solution structures of the solonamide macrocycles and explore how they relate to biological activity.

Research into the solonamides is in its infancy, there remains considerable potential for further research and development of these unique and exciting compounds.

7 Conclusions and Future Work

The aim of this thesis was to develop more effective inhibitors of the staphylococcal *agr* quorum sensing system as potential anti-infective agents. In pursuit of this aim, three areas have been investigated: the role of the aureusimines in staphylococcal virulence, the SAR of truncated AIP-based compounds as AgrC inhibitors, and a full pharmacological assessment and SAR study of the solonamides as AgrC inhibitors.

During investigation of the aureusimines, the synthetic route reported in the literature[226] was found to be unreliable. Therefore, a new strategy was developed which replaced the unreliable DIBAL-H reduction of a methyl ester with a Swern oxidation of an alcohol to produce the required aldehyde **2.2**. Further investigation showed that this synthetic strategy required *O*-protection for aureusimine compounds containing phenol moieties. Thus, a tBu-protected tyrosinol (**1.38**) was employed for the synthesis of the required analogues.

The developed total synthesis was employed to produce tethered aureusimine analogues. These analogues were attached to a polymer support *via* a condensation reaction. The functionalised resin **2.46** was then used to attempt to determine the biological target of the aureusimines *via* affinity chromatography experiments.

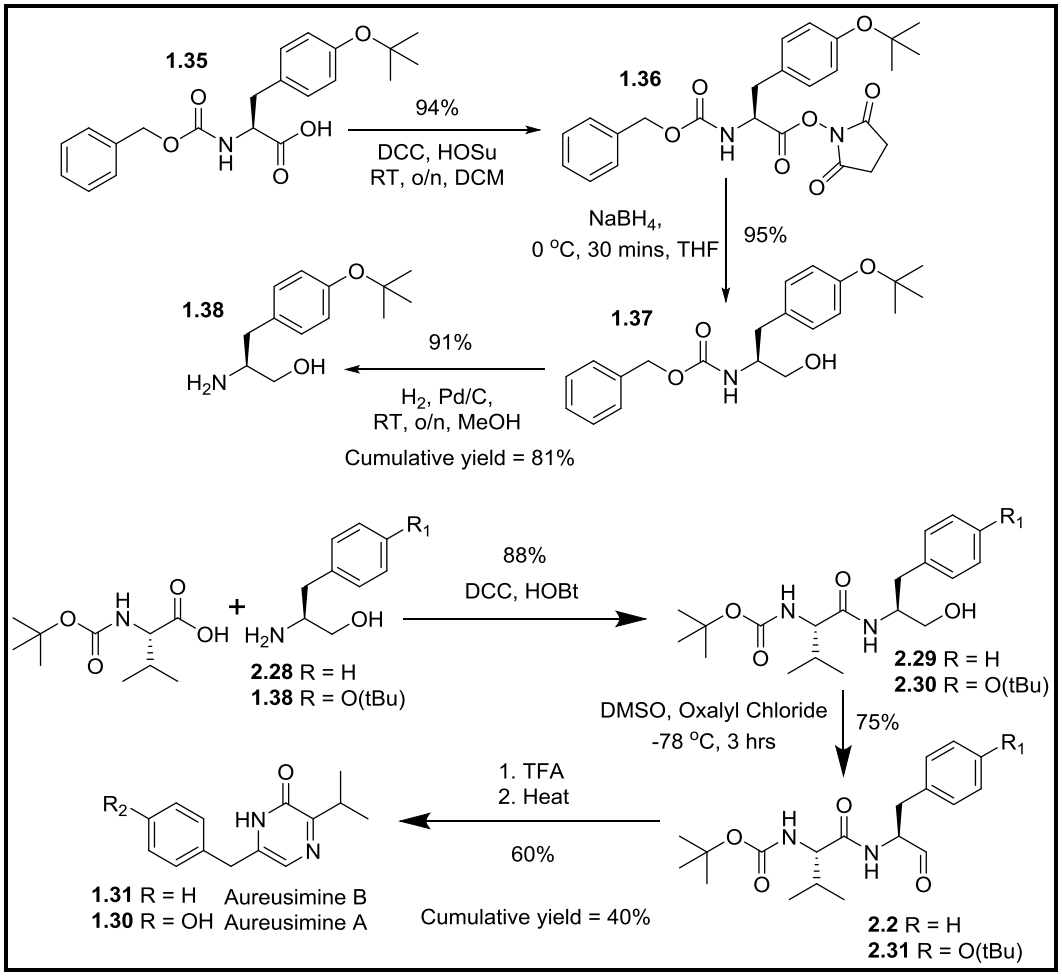


Figure 197: Total synthesis of both aureusimine A (**1.30**) and B (**1.31**)

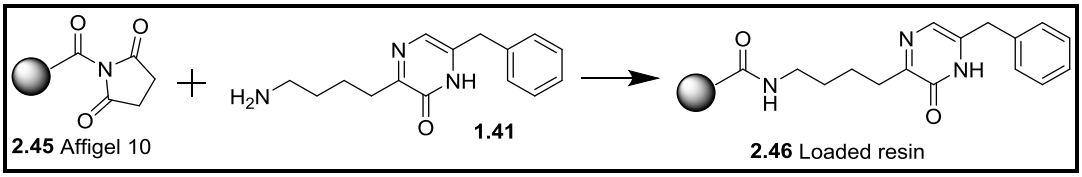


Figure 198: Condensation reaction to produce functionalised resin **2.46**

Affinity chromatography experiments identified a protein which preferentially binds the functionalised resin **2.46**. Trypsin digestion followed by mass spectrometric analysis revealed that this specific binding protein is elongation factor-G, part of the ribosomal complex. Given the high abundance of ribosomal proteins, they are often responsible for false positives in this type of experiment.[261] As a high amount of this protein was not isolated in these affinity chromatography experiments, it was considered that the elongation factor-G binding was unlikely to be highly specific.

Further biological assays revealed that the aureusimines only mildly inhibit the *agr* system at very high concentrations (>20 μM). Mild reductions of CCL-2

mediated chemotaxis of monocytes and staphylococcal biofilm formation were also discovered. These weak biological effects were not considered to be the main function of the aureusimines. However, these observations could be a starting point for the development of an aureusimine based inhibitor or further investigation of these complex phenomena.

Investigation of the SAR of the truncated AIP-based analogues revealed several potent cross-group inhibitors. The *N*-acetyl group was found to be important for activity as analogues lacking this group showed a dramatically reduced activity. Peptoid scanning revealed that most of the amide bond moieties are important for activity. The only analogue which maintained activity incorporated a peptoid modification of the Phe[3] residue. Variation of the amino acid residues revealed that modification of position 4 and 5 could produce highly potent inhibitors. Leu[4] modified compounds proved to be particularly successful. Notably, compound **3.23** (Figure 199) was a sub-nanomolar inhibitor of AgrC1 and also inhibited AgrC2, AgrC3 and AgrC4 in the low nanomolar range.

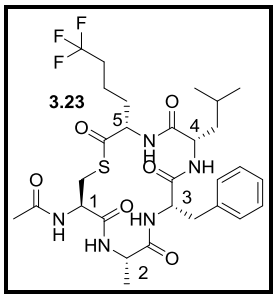


Figure 199: Compound **3.23** is a sub-nanomolar inhibitor of AgrC1 and a low nanomolar inhibitor of AgrC2, AgrC3 and AgrC4

A previously identified mutant receptor which is known to be resistant to (Ala[5])AIP1 inhibition was used to evaluate the potential of this panel of AIP-based analogues. Similar to (Ala[5])AIP1, many of the compounds tested herein were good-to-excellent agonists of this receptor. However, compound **3.23** acted as an effective inhibitor in the presence of potent agonists, such as AIP1. The IC_{50} was observed to be 2.4 nM.

Further analysis of these compounds using a partial constitutively active reporter showed that all the compounds tested eliminated activity of the

partially constitutive receptor at low concentrations, thus acting as inverse agonists. However, at higher concentrations (>25 μM), many of the compounds also caused significant agonism. From these results, it is difficult to infer any further insights into the binding and interaction of these analogues with the receptor. It is possible that the analogues interact with multiple sites on the receptor or that binding the recognition site of one member of the receptor dimer causes divergent effects. In contrast to other analogues, compound **3.23** caused only a very mild activation of the system(> 5%). Overall, compound **3.23** is very promising reagent. It is a potent inhibitor of all of the *agr* groups tested and its inhibition seems to be resistant to mutations introduced into the receptor.

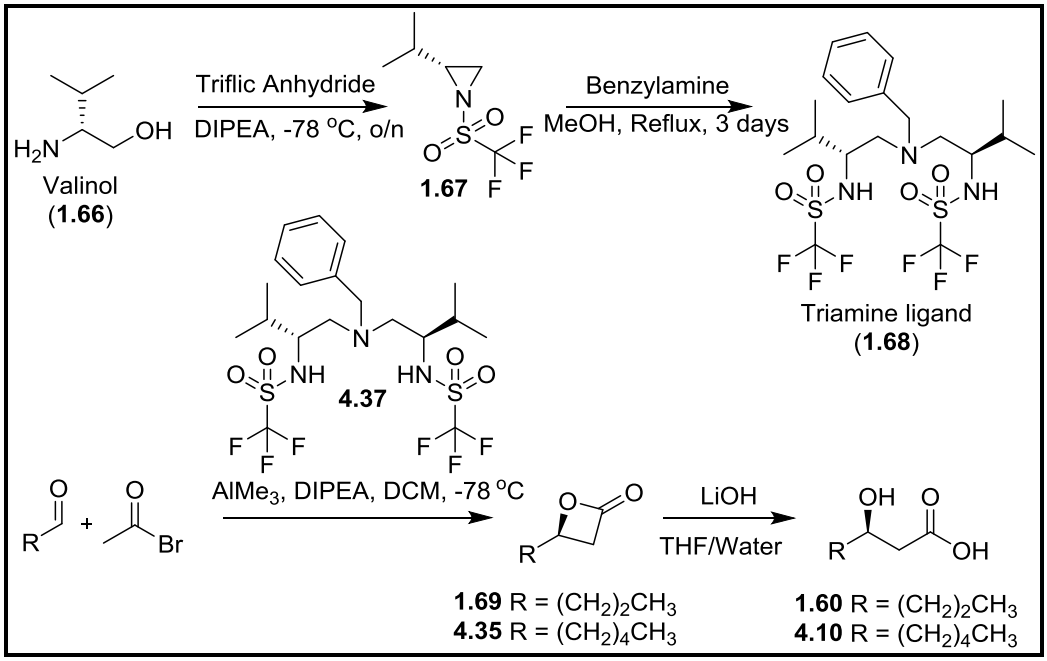


Figure 200: Scheme showing the stereoselective synthesis of the 3-hydroxy acid moieties adapted from Nelson *et al.*[347]

At the beginning of this research, a method for the synthesis of the natural depsipeptides, the solonamides, was not available. Later research by another group produced synthetic strategies with limited success; a non-stereoselective synthesis was developed and attempts to stereoselectively synthesise the solonamides produced multiple side products.[318] In this research, a fully stereoselective synthesis of the solonamides was developed and deployed to produce a wide range of analogues (Figure 200 and Figure 201).

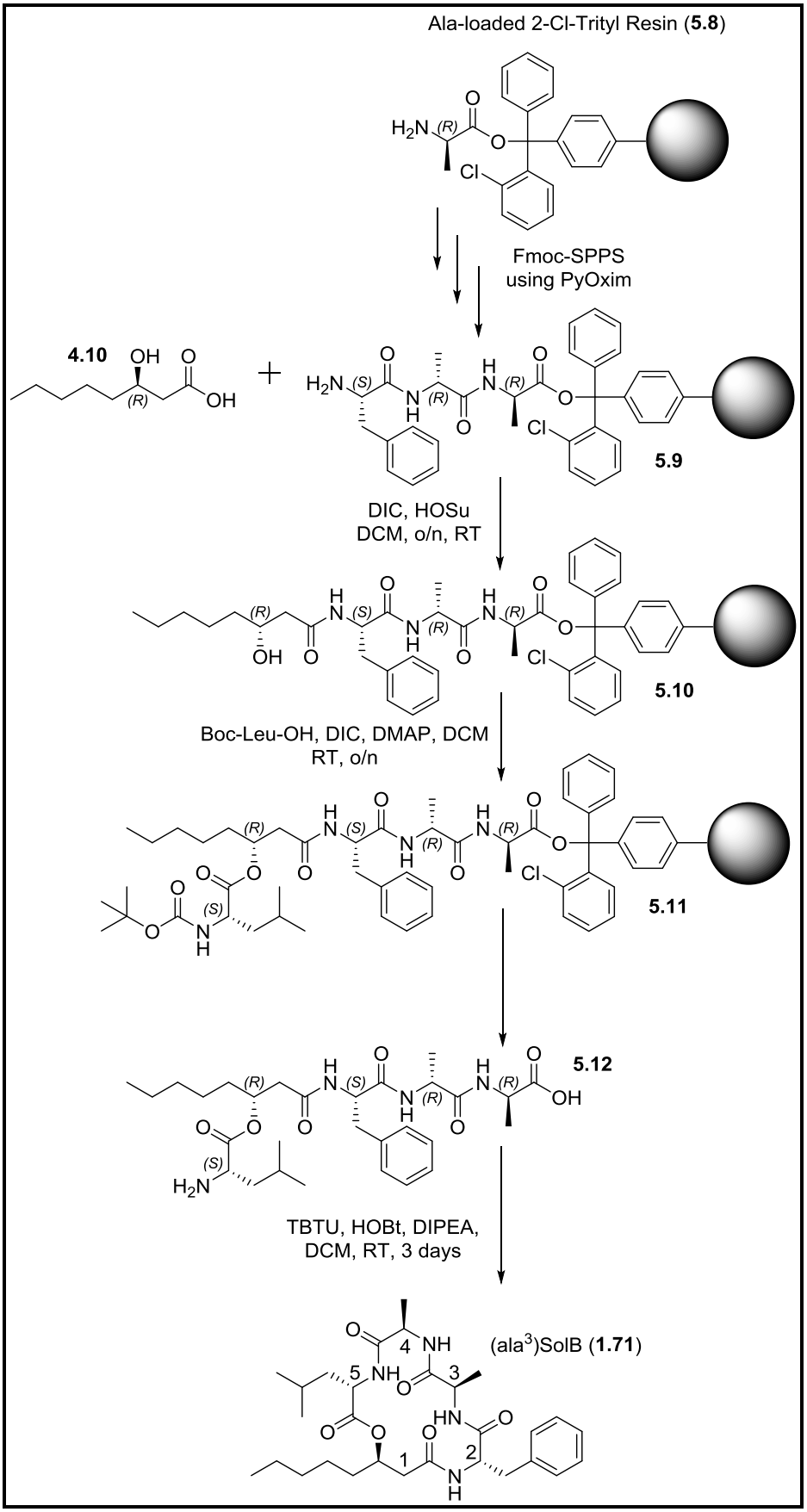


Figure 201: Stereoselective total synthesis of the challenging solonamide analogue, (ala^3)SolB (**1.71**).

Full pharmacological analysis of the natural products, solonamide A (**1.21**) and B (**1.22**) revealed that they do inhibit the *agr* system as reported.[214] However, they do not act as competitive inhibitors of AgrC as proposed previously.[216] Schild analysis revealed that the solonamides are non-competitive negative allosteric modulators of AgrC. These are the first non-toxic allosteric inhibitors of AgrC which have been discovered.

Detailed biological evaluation revealed that the solonamides inhibit AgrC2 and AgrC3 *via* an allosteric mode of action, SolB revealed an IC_{50} of 6.2 μM and 4.5 μM respectively. This was surprising as the allosteric site was not expected to be conserved across *agr* groups. Furthermore, the solonamides seem to inhibit these receptors more potently than the originally tested AgrC1 receptor.

The analogues produced *via* the stereoselective total synthesis helped to elaborate the SAR of the solonamide scaffold which had not previously been studied. Alanine scanning revealed that Leu^5 is important for the activity of the solonamides. In contrast, Phe^2 and leu^3 can be modified to produce improved inhibitors. Modification of the 3-hydroxy acid moiety can also marginally improve the physical properties of the solonamide analogues while maintaining potency. (5Me-3HHA^1)Sol (**4.57**) showed potent inhibition of AgrC1, with IC_{50} of 11.3 μM. Combinations of successful modifications at different locations did not result in additive gains although they did produce inhibitors with improve physical properties while maintaining inhibitory activity.

The solonamides are the first non-antibacterial cross-group allosteric inhibitors of the AgrC receptor. As such, they represent a promising scaffold for further research into the structure and function of the AgrC receptor and for further development of AgrC inhibitors.

7.1 Future work

7.1.1 Aureusimines

The aureusimine biosynthetic cluster genes represent roughly 0.5% of the *S. aureus* genome. However, the function of these non-ribosomal peptides is still a mystery. There are two methods which could be used to discover their function. Phenotypic testing in various conditions may eventually elucidate the function of the aureusimines. However, performing a panoply of different biological assays in an attempt to discover their biological function is not feasible. The incorporation of these compounds into high throughput screening panels may fortuitously reveal their biological purpose at some point in the future. This strategy also provides other benefits as the pyrazinone core of the aureusimine structure is a novel privileged structure. It may be that these compounds interact with other unrelated biological systems in new and useful ways, aiding development in other research areas.

A more targeted method for elucidation of the function of the aureusimines would be further development of the affinity chromatography investigations attempted in this research. Attachment to a solid support can be a barrier to effective discovery of high affinity binders.[364] Binding to target proteins is more favourable for chemical probes in solution. Therefore, chemical constructs with multiple functionalities can be deployed in solution to bind with potential targets. Following specific target binding to the aureusimine functionality in solution, a reactive functionality can covalently bond the probe to the protein of interest. A selectivity functionality can then be used to isolate the probe-protein complex. There are several methods are available for both the covalent binding of proteins of interest and isolation of probe-protein complexes from complex mixtures.[364] However, these functionalities must be attached to the aureusimine small molecules in multiple locations as the binding mode of the aureusimines is unknown. Multiple sites are potentially useful for the installation of the reactive and selectivity functions (Figure 202). It is possible that the aureusimines could act against host proteins, these probes could also be used with mammalian cell lysates to determine any possible host interactions.

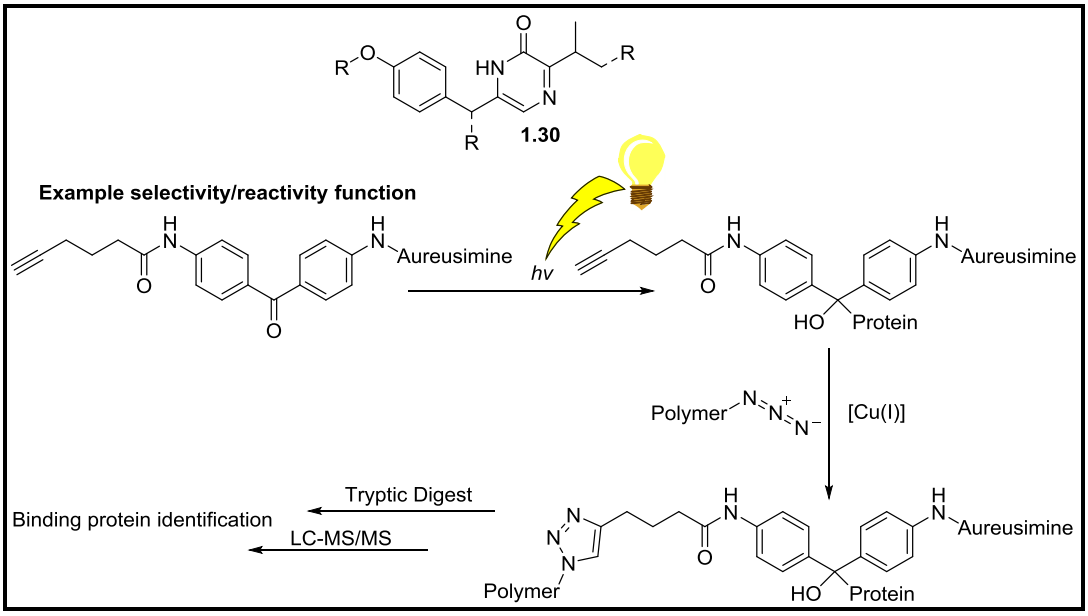


Figure 202: Potential sites for installation of reactivity and selectivity functionalities in aureusimine A (**1.30**) and an example of a possible selectivity/reactivity functionality and reaction scheme adapted Salisbury *et al.*[365]

7.1.2 AIP-based analogues

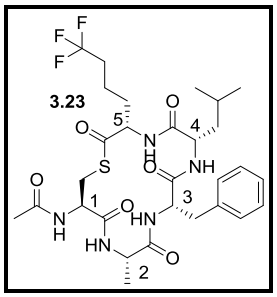


Figure 203: Compound **3.23** is a sub-nanomolar inhibitor of AgrC1 and a low nanomolar inhibitor of AgrC2, AgrC3 and AgrC4

Having developed a very potent cross-group inhibitor of the AgrC receptor in compound **3.23** and confirmed its biological activity using hemolysis assays and Western blots, its applicability in infection should be addressed. Previously, AIP2 (**1.15**) has been shown to protect mice from infection by *agr-I S. aureus* strains.[164] As **3.23** is structurally similar and its mechanism of action is identical to AIP2 (**1.15**), it is likely that a similar experiment would show similar results. However, this model demonstrates that abscess formation can be prevented if bacteria are co-administered with the inhibitor. However, in reality, bacterial infections are established before the infection is diagnosed and considerably before therapies can be administered. Therefore, a more robust and realistic model would allow the establishment of the infection before the administration

of the antagonist. As the original researchers found that *agr* expression is considerably upregulated during the staphylococcal exponential growth phase and then downregulated during the stationary phase of bacterial growth, it is possible that administration following establishment of an infection could be less effective due to the reduced importance of the *agr* system in the later stages of an infection.

To prepare for these kinds of *in vivo* experiments, several preliminary experiments are required. Initially, plasma stability should be assessed. It is possible that host biomolecules, e.g. proteins, in the bloodstream could sequester or breakdown the active compound **3.23**. Local delivery to the site of infection or more advanced drug delivery technologies could be employed to deliver the drug to the site of infection. Preliminary understanding of simple drug metabolism and pharmacokinetics is also vital to understanding the results of any *in vivo* experiments. Further experiments analysing stability and toxicology in several murine cell lines should also be performed. If breakdown of the active product is detected, further research may be required to establish the reason for breakdown and to develop a more stable analogue. If toxic effects are discovered, research into the mechanism of toxicity and further development of the active compound to remediate the toxicity may be required.

Findings in the *in vivo* AIP2 murine study by Wright *et al*.[164] revealed that the thiolactone moiety of AIP2 is unstable in physiological conditions. However, *agr* activation in the first 2-3 hrs of infection is vital to establishing an abscess. Thus, application of AIP2 alongside the infecting bacteria effectively eliminated early virulence factor production thereby preventing the establishment of a productive infection or abscess. The team also found that following a neutrophil-induced metabolic eclipse lasting for 2–3 days post infection, *agr* was reactivated. It is possible that *agr* inhibition at this time point may also reduce virulence expression and thereby aid in resolution of the infection by the host adaptive and innate immune systems. If this is the case, a stable AgrC inhibitor may be able to effectively treat the infection by administration following the full establishment of an infection.

Apart from *in vivo* research, there are also other areas still to be investigated. It is unclear how the trifluoromethyl moiety of **3.23** contributes to the potency of the compound. A further trifluoromethyl analogue with a shorter carbon side chain, **3.25**, did not display the same level of potency as **3.23**. It was hypothesised that the electron withdrawing properties of the trifluoromethyl group allow the residue to effectively mimic the endogenous methionine residue; however, this has not been proved. Furthermore, research on AIP-based inhibitors has often revealed that modifications which benefit the antagonistic properties of the compound, often do not produce additive benefits when combined in later generation compounds. A mechanistic understanding of how side-groups affect the macrocyclic structure of the AIP-based analogues and their activity would help significantly in understanding their mode of binding and in the design of more potent and stable analogues.

To this effect, NMR studies could be utilised to effectively model the structures of the truncated AIP-based analogues in solution. The magnitude of ROESY and NOESY NMR signals are proportional to the average distance between individual protons and can be converted to angstrom distances before being used in modeling software as distance constraints. The software can then produce many possible conformations based on the constraints. Individual analogues produce different constraints and therefore different combinations of possible conformations are calculated by the software. These conformations are representative of the conformations which can be accessed by the analogue. Analysis of the pattern of accessible conformations may reveal information about how individual modifications affect the overall macrocyclic structure. This information may in turn aid in the future design of AIP-based inhibitors.

7.1.3 Solonamides

Research into the solonamides is still in its infancy. The investigations detailed in this thesis have advanced the field, however, further questions remain to be answered. No *N*-methyl or peptoid scan of the solonamide scaffold has yet been performed. As the amide groups of a macrocycle are very important for its macrostructure and therefore its function, this would be an ideal place to begin. The robust synthesis presented in this research could easily

be adapted for the production of an *N*-methyl or peptoid library. Findings from this kind of study could result in the discovery of more potent solonamide analogues or facilitate the future design of improved solonamide-based inhibitors.

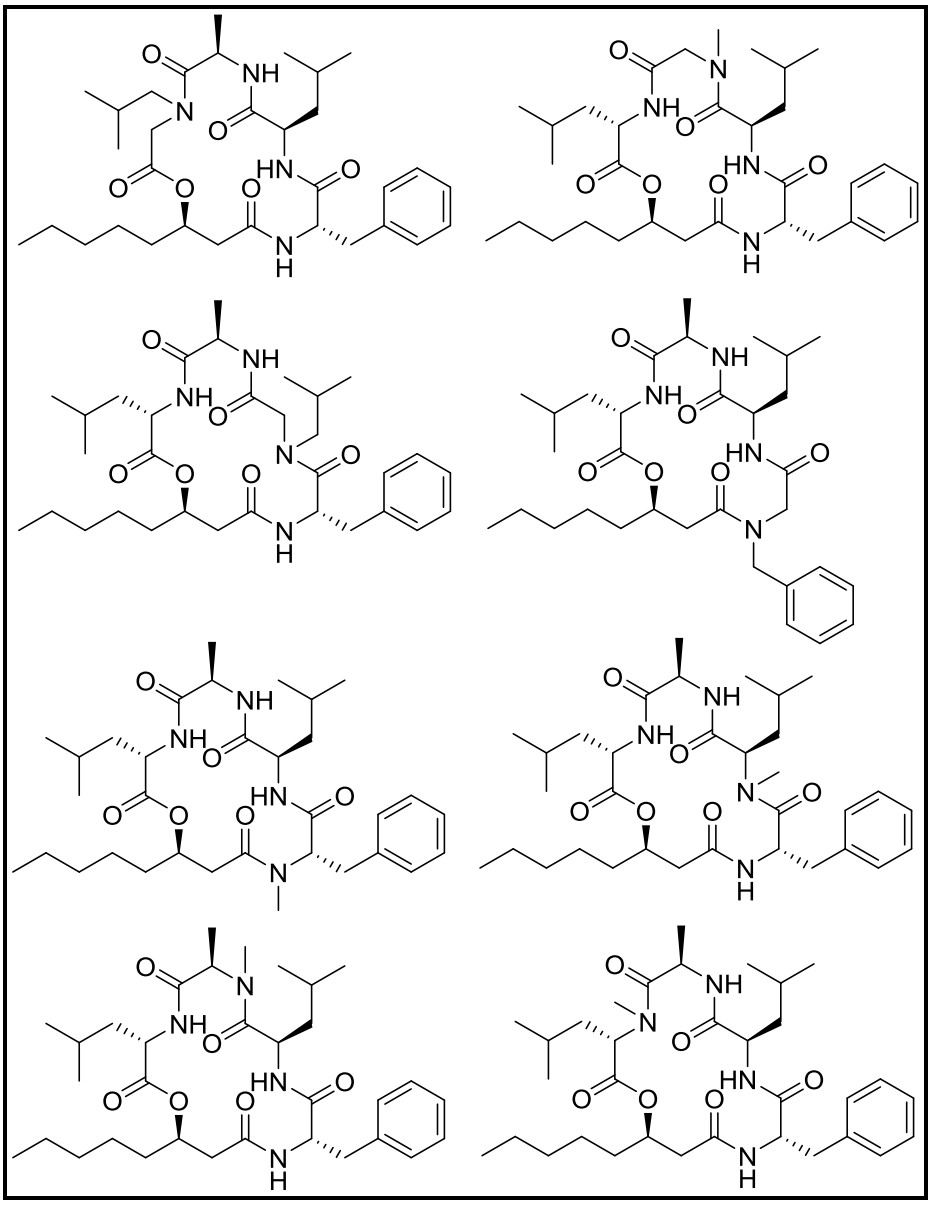


Figure 204: Proposed panel of analogues for a peptoid and *N*-methyl scan of the solonamides.

Although the non-competitive inhibition of the solonamide compounds has been established, nothing is known about the location or nature of the new putative allosteric site of AgrC. Given that the site seems to be conserved across *agr* groups, it would be very beneficial to elucidate its location and binding properties, so that more effective inhibitors can be designed. To this end,

photoaffinity labeling could be utilised to cause irreversible covalent bonding of the solonamides to the AgrC receptor. Isolation of this complex *via* a selectivity function, followed by trypsin digestion and LC-MS/MS analysis could reveal the location of the allosteric binding site and the nature of the local chemical environment.

The photoaffinity label, trifluoromethyldiazirine (Figure 205) which could be incorporated into the solonamide scaffold in place of Phe[2]. A selectivity function such as an alkyne functionality could also be incorporated into the 3-hydroxy acid moieties. An alkyne functionality would enable "click" reactions facilitating isolation of the solonamide receptor complex using azide-functionalised resins.

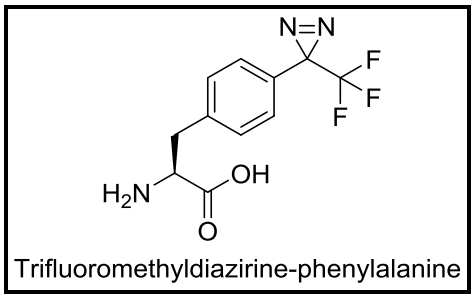


Figure 205: Trifluoromethyldiazirine moiety incorporated into the phenylalanine residue. This compound has been previously synthesised.[366]

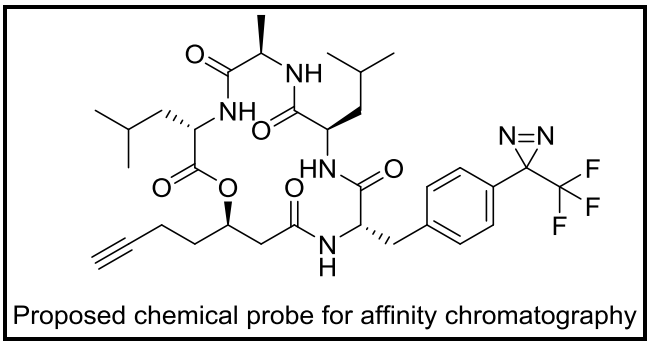


Figure 206: Structure of a chemical probe which could potentially be used to identify the allosteric binding site of the solonamides

Following isolation of the solonamide-receptor complex and trypsin digestion, the specific peptide fragment binding the solonamide could be identified. This would allow identification of the binding location of the Phe[2] residue. Computer modelling may then allow more advanced binding studies to elucidate the nature of the allosteric binding site and the mode of binding of the solonamides.

Finally, NMR studies similar to those proposed for the AIP-analogues may also help to elucidate the effects of individual modifications on the conformations which the solonamide scaffold can access. This, in turn, may help to rationalise the effects of individual chemical modifications on compound potency.

8 Experimental

Bacterial strain list

Table 15: All bacterial strains used in the course of this study

Strain	Description	Genotype	Source
Aureusimines			
	Wild Type strain	WT	[262]
	Aureusimine negative	ΔAusA	[262]
AIP analogues & solonamides			
ROJ48	AgrC *lux* reporter parent strain	RN4220 Δagr::*ErmB* p3agr-lux tet^R erm^R	[167, 231]
ROJ143	AgrC1 *lux* reporter	ROJ48 pSKermP2 *agrC1 agrA*	[167, 231]
EM28	AgrC2 *lux* reporter	ROJ48 pSKermP2 *agrC2 agrA*	Ewan Murray
ROJ154	AgrC3 *lux* reporter	ROJ48 pSKermP2 *agrC3 agrA*	[231]
ROJ145	AgrC4 *lux* reporter	ROJ48 pSKermP2 *agrC4 agrA*	[167, 231]
	A101T T104V AgrC1 *lux* reporter	ROJ48 pSKermP2 agrC1A101TT104V agrA	[167, 231]
	AgrC1 (S116K) *lux* constitutive reporter	ROJ48 pSKermP2 *agrC1S116K agrA*	J. Chamberlain, V. Steele

General chemistry

Chemicals and solvents were purchased from standard suppliers and used without further purification. All solvents were used as supplied (analytical, HPLC or peptide grade), without prior purification. Milli-Q water was used for chemical reactions. Deuterated solvents were purchased from Sigma Aldrich

and other commercial suppliers. Reactions were monitored by using TLC, analytical RP-HPLC, and MS.

TLC was performed on commercially available aluminium backed plates (Merck 60 F254), visualised under UV at 254 nm followed by staining with ninhydrin or $KMnO_4$. Mass spectra (ES-TOF) were recorded on a Waters 2795 separation module/Micromass LCTTM platform. Proton and Carbon-13 nuclear magnetic resonance spectra were recorded at 20 °C (unless otherwise stated) on a Bruker AV400 operating at 400.13 (^{1}H-NMR) and 100.62 (^{13}C-NMR) using WILMAD™ Economy 5 mm or Norell Select Series™ 3 mm NMR tubes. Chemical shifts (δ) are reported in parts per million (ppm), referenced to the solvent (^{1}H-NMR: $CDCl_3$ 7.26 ppm, $(CD_3)_2SO$ 2.50 ppm; ^{13}C-NMR: $CDCl_3$ 77.16, $(CD_3)_2SO$ 39.52). Coupling constants (J) are recorded in Hz and significant multiplicities described by singlet (s), doublet (d), doublet of doublets (dd), doublet of triplets (dt), triplet (t), quadruplet (q), broad (br), multiplet (m). Spectra were assigned where possible using appropriate COSY spectra.

RP-HPLC was performed using a Waters setup, comprised of two 510 pumps, a 486 detector and Millenium™ software. The systems outlined below were used for purification and to confirm purity unless otherwise stated.

Aureusimines (Chapter 2 and Section 8.1 of this experimental chapter)

Semipreparative HPLC was performed using a Chromolith®SemiPrep RP-18e 100-10 mm column (# Merck 1.52016.0001). A flow rate of 3 mL/min was used with solvent A: 0.06% TFA in water and solvent B: 0.06% TFA in CH_3CN:H_2O (90:10) with UV detection at 214 nm and 254 nm. Gradients are recorded for each individual compound. The analytical retention time are reported using a Phenomenex Onyx Monolithic reversed-phase C18 column (4.6 x 100 mm) with solvent A = 0.05% TFA in H_2O and solvent B = 0.05% TFA in 9:1 *v*:*v* CH_3CN:H_2O at a flow rate of 3.0 mL/min. Gradients are recorded for individual compounds where relevant. Purities of all compounds subsequently tested in biological systems were determined by RP-HPLC as being ≥95%.

Solonamides (Chapter 4 & 5, Section 8.3 & 8.4 of this experimental chapter)

Analytical RP-HPLC was performed using Phenomenex Onyx Monolithic reversed-phase C18 column (4.6 x 100 mm). Solvent A: 0.06% TFA in water and solvent B: 0.06% TFA in CH_3CN:H_2O (90:10), flow rate of 3.0 mL/min, run 20% for 1 mins followed by gradient 20-80 (%B), curve = 6, over 20 mins, and detection at 216 nm. Semi-preparative RP-HPLC was generally performed using a Waters 2525 binary gradient pump equipped with a water 2487 dual λ absorbance detector and a Kromasil 100-5-C8 10x150 SemiPrep column. Generally, a flow rate of 9 mL/min was used with solvent A: 0.06% TFA in water and solvent B: 0.06% TFA in CH_3CN:H_2O (90:10). run at 50% for 2mins followed gradient 50-100 (%B) over 20 mins, curve = 6, with UV detection at 214 nm and 254 nm.

In section 8.3.4, a Luna 5u C18(2) 100A (250 x 4.6 mm) reversed phase column was used for analytical RP-HPLC in place of the Phenomenex Onyx Monolithic column mentioned above.

8.1 Aureusimines

Semipreparative HPLC was performed in this section using a a Chromolith®SemiPrep RP-18e 100-10 mm column (# Merck 1.52016.0001). The analytical retention time of the final pure products are reported in this section using an analytical RP-HPLC method of 0 - 5 min 5% solvent B in solvent A, 5 – 20 min gradient of 5% to 50% solvent B in solvent A, 20 – 21 min 50% to 100% solvent B in solvent A, 21 – 24 min held at 100% B in solvent A, 24 – 25 min 100% to 5% solvent B in solvent A, 25 – 26 min held at 10% solvent B in solvent A (solvent A = 0.05% TFA in H_2O, solvent B = 0.05% TFA in 9:1 *v*:*v* CH_3CN:H_2O). Purities of all compounds subsequently tested in biological systems were determined by RP-HPLC as being ≥95%.

8.1.1 Literature synthesis of aureusimine A and B

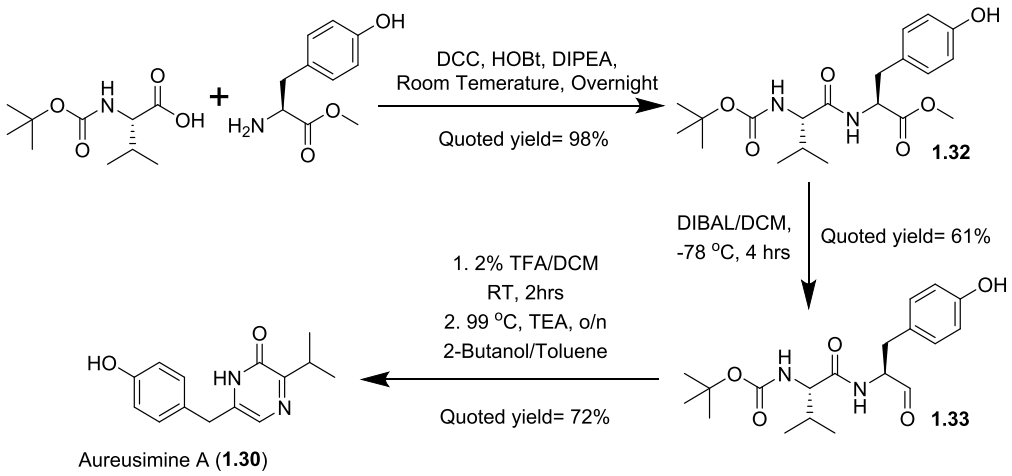
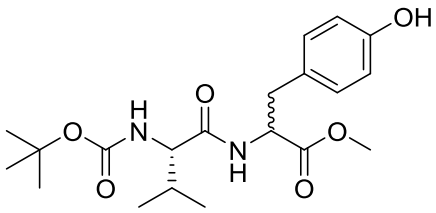


Figure 207: Original Synthesis of Aureusimine A[258]

Methyl (*tert*-butoxycarbonyl)-*L*-valyltyrosinate (**1.32**)[367]

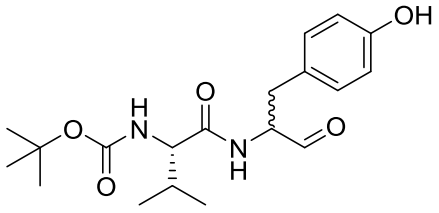


Boc-protected Valine (459 mg, 2.1 mmol) and Hydroxybenzotriazole (HOBt, 279 mg, 2.1 mmol) were dissolved in DCM (15 ml). DCC (626 mg, 3.0 mmol) was

added to the mixture at 0 °C and was then allowed to warm to room temperature. Tyrosine methyl ester hydrochloride (615 mg, 2.6 mmol) was dissolved in DCM (15 ml) with DIPEA (0.45 ml, 4.6 mmol). This mixture was added to the reaction mixture and it was stirred overnight. The reaction was filtered under gravity and the solvent was removed *in vacuo*. The crude product was dissolved in EtOAc (30 ml) and was washed with 10% Citric Acid (10 ml x 2), 10% $KHCO_3$ solution (10 ml x 2) and brine (20 ml x 2). The organic layer was dried with Na_2SO_4 and evaporated. The resulting oil was triturated with diethyl ether (Et_2O) to furnish the title compound **1.32** in good yield (773 mg, 2.0 mmol, 93%) as a yellow foam.

Boc-Val-Tyr-OMe (**1.32**) TLC R_f= 0.44 (1:1 EtOAc/Hex); MS^+ (ES-TOF): m/z calcd: 395.2308 $[M+H]^+$; found: 395.2345; ^{1}H-NMR (400 MHz, $CDCl_3$) δ (mixture of diastereomers) 6.95-6.92 (m, 2H), 6.74-6.69 (m, 2H), 6.54 (dd, *J* = 7.9 Hz, 0.5H), 6.44 (d, *J* = 7.9 Hz, 0.5H), 5.13-4.98 (m, 1H), 4.88-4.80 (m, 1H), 4.01-3.93 (m, 0.5H), 3.91-3.83 (m, 0.5H), 3.72 (s, 3H), 3.09-2.96 (m, 2H), 2.19-2.06 (m, 1H), 1.45 (d, *J* = 3.7 Hz, 9H), 0.94-0.78 (m, 6H), phenol proton absent. Consistent with the literature[367]

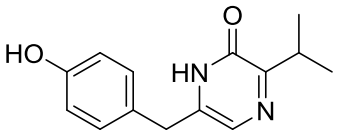
tert-Butyl ((*2S*)-1-((1-(4-hydroxyphenyl)-3-oxopropan-2-yl)amino)-3-methyl-1-oxobutan-2-yl)carbamate (**1.33**)



Boc-Val-Tyr-OMe (**1.32**, 242 mg, 0.6 mmol) was dissolved in dry DCM (5 ml) and cooled to -78 °C under a nitrogen atmosphere whilst stirring. DIBAL-H (1.5 ml, 1.5 mmol) in Hex was added slowly. The reaction was maintained at -78 °C for 5 hours when the reaction was quenched by the addition of EtOAc (5 ml). After 30 mins, saturated potassium tartrate solution (5 ml) was added and the mixture was stirred for a further 30 minutes. The reaction was then allowed to warm to room temperature. The organic layer was isolated and the aqueous

layer was extracted with DCM (15 ml). The combined organic layers were then washed with brine (20 ml x 2), dried with Na_2SO_4, filtered under gravity and evaporated. This resulted in a mixture of product **1.33** and starting material **1.32**. The yield ranged from negligible to 52% with an average of 12% as measured by the relation between the aldehyde and methyl ester peaks in the NMR spectrum at 9.60 ppm and 3.57 ppm respectively.

6-(4-hydroxybenzyl)-3-isopropylpyrazin-2(1H)-one (Aureusimine A, **1.30**)



Compound could not be produced using this synthesis.

8.1.2 Adapted oxidative synthesis of aureusimine A and B

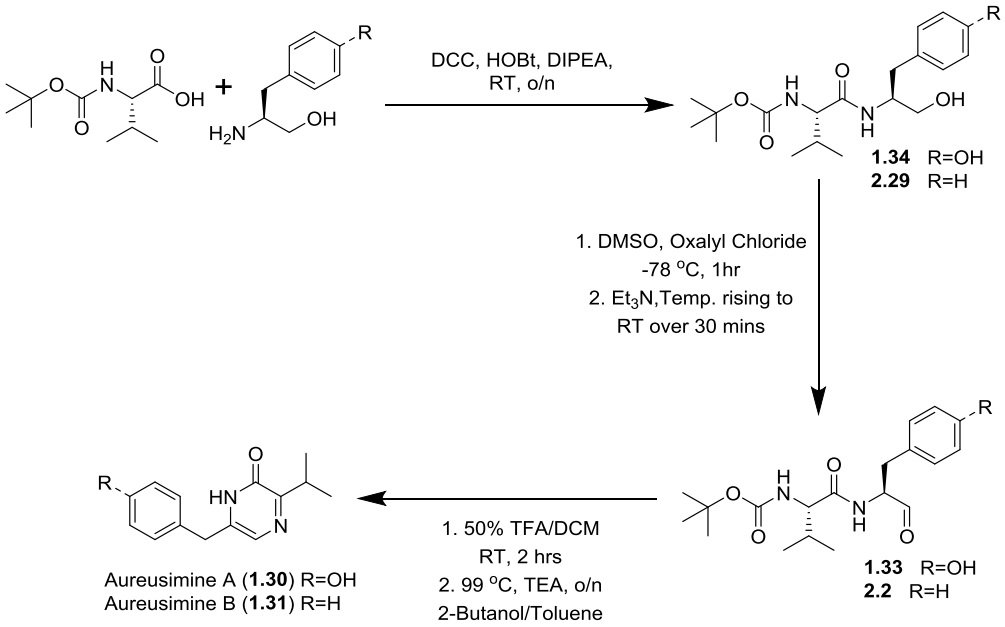
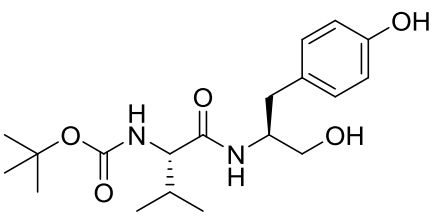


Figure 208: Alternative aureusimine synthesis using Swern Oxidation

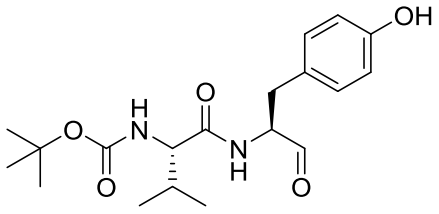
tert-Butyl ((*S*)-1-(((*S*)-1-hydroxy-3-(4-hydroxyphenyl)propan-2-yl)amino)-3-methyl-1-oxobutan-2-yl)carbamate (**1.34**)



Boc-Val-OH (854 mg, 3.9 mmol) and HOBt (535 mg, 3.9 mmol) were dissolved in 2:1 MeCN/DCM (20 mL). DCC (1.07 g, 5.2 mmol) was added to the mixture at 0 ^{o}C and was then allowed to warm to room temperature. Tyrosinol.HCl (963 mg, 4.7 mmol) was then dissolved in 2:1 MeCN/DCM (20 mL) with DIPEA (1.36 ml, 7.82 mmol) and this mixture was added to the activation mixture and stirred overnight. The reaction was filtered under gravity and the solvent was removed *in vacuo*. The crude product was dissolved in EtOAc (40 ml) and was washed with 10% Citric Acid (30 ml x 2), 10% $KHCO_3$ solution (30 ml x 1) and brine (30 ml x 1). The organic layer was then dried with Na_2SO_4, filtered and evaporated. The resulting oil was triturated with Et_2O, blown under nitrogen for 2 hours and dried *in vacuo* overnight to furnish the title product Boc-Val-Tyr-ol (**1.34,** 1.4802g, 86%) as a yellow foam.

Boc-Val-Tyr-ol (**1.34**) TLC R_f = 0.34 (3:1 EtOAc/Hex); MS^+ (ES-TOF): m/z calcd: 367.2217 $[M+H]^+$; found: 367.1935; ^{1}H-NMR (400 MHz, $CDCl_3$) δ 7.0 (d, *J* = 8.5 Hz, 2H, Tyr-ArH), 6.73 (d, *J* = 8.5 Hz, 2H, Tyr-ArH), 6.53 (d, *J* = 8.1 Hz, 1-H, Tyr-NH), 5.14 (d, *J* = 8.1, 1H, Val-NH), 4.17-4.07 (m, 1H, Tyr-C_αH), 3.86-3.79 (m, 1H, Val-C_αH), 3.62 (dd, *J* = 3.7 Hz, 11.2 Hz, 1H, Tyr-OH), 3.52 (dd, *J* = 4.9 Hz, 11.1 Hz, 1H, Tyr-C**H$_2$**OH), 2.82-2.67 (m, 2H, Tyr-C_βH), 2.12-2.01 (m, 1H, Val-C_βH), 1.44 (s, 9H, tBu-H), 0.90 (d, *J* = 6.8 Hz, 3H, Val-C_γH), 0.84 (d, *J* = 5.7 Hz, 3H, Val-C_γH), alcohol and phenol proton absent.

tert-Butyl ((*S*)-1-(((*S*)-1-(4-hydroxyphenyl)-3-oxopropan-2-yl)amino)-3-methyl-1-oxobutan-2-yl)carbamate (**1.33**)



Method 1. Swern Oxidation - Boc-Val-Tyr-ol (**1.34**, 445 mg, 1.2 mmol) was dissolved in DCM (6 ml) and the reaction vessel was flushed with nitrogen and cooled to -78 ^{o}C in an acetone/dry ice bath. DMSO (1 ml, 14.1mmol) was added to DCM (10 ml) in a separate vessel under a nitrogen atmosphere at -78 ^{o}C.

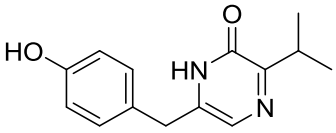
Oxalyl Chloride solution (2 M in DCM, 0.7 ml, 1.4 mmol) was added slowly, the mixture was then stirred for ten minutes. The previously prepared solution of **1.34** was then added. The solution was stirred at -78 ^{o}C for 1 hour. Triethylamine (Et_3N, 0.4 ml, 5.8 mmol) was added and the solution was maintained at -78 ^{o}C for a further three hours. It was then quenched by the addition of pH 4 citrate buffer (10 ml) and allowed to warm to room temperature. Water (20 ml) and DCM (10 ml) were added to the mixture and the organic layer was separated, dried with Na_2SO_4, filtered and evaporated. The residue was dissolved in EtOAc (30 ml) which was washed with 10% Citric Acid solution (20 ml x 2), 10% $KHCO_3$ solution (20 ml x 2), and brine (20 ml x 2). It was dried with Na_2SO_4, filtered and evaporated. TLC, MS and NMR revealed a complex mixture including a major mass peak at 465.2044 which is assumed to be a meththiomethyl ether side product **2.22** which formed due to a side reaction at the phenol functionality.

Method 2. Parikh Doering Oxidation -Sulfur dioxide-pyridine complex (0.78 g, 4.9 mmol) was dissolved in DMSO. Boc-Val-Tyr-ol (**1.34**, 0.6 g, 1.5 mmol) was dissolved in DCM/DMSO mixture (10 mL/2 mL) with DIPEA (1.7 mL, 9.8 mmol). After 15 min, the sulfur dioxide-pyridine complex mixture was added to the solution of alcohol **1.34** over 20 min. A pH4 citrate buffer was used to quench the reaction. Aqueous work up followed by mass spectroscopic analysis revealed the presence of a suspected meththiomethylether side product **2.22**.

Method 3. IBX oxidation - 2-iodobenzoic acid (1.78 g, 7.2 mmol) was added to a solution of potassium peroxymonosulfate (2.86 g, 9.2 mmol) in water (30 mL). The mixture was heated to 100 ^{o}C over 20 mins and stirred at this temperature for 4 hrs. The suspension was cooled to 5 ^{o}C and slowly stirred for 1.5 hrs. The mixture was filtered and the filtrate was washed with water and acetone. This was allowed to dry overnight at room temperature furnishing a white crystalline powder of IBX (**2.18**, 1.97 g, 7.2 mmol, 99% yield). Boc-Val-Tyr-ol (**1.34,** 0.6 g, 1.2 mmol) was dissolved in EtOAc (30 mL) and IBX (**2.18**, 1.6 g, 5.7 mmol) was added. The mixture was stirred under reflux for 6 hrs, filtered under gravity and the filtrate was evaporated. The product was triturated with Et_2O. ^{1}H-NMR experiments did not reveal the presence of an

aldehyde peak. Analysis by mass spectroscopy revealed that the starting material (**1.33**, $[M + H]^+$ = 367.2608) and the suspected *o*-quinone (**2.24**, $[M + H]^+$ = 379.2628) were present.

Aureusimine A (**1.30**)



Compound could not be produced using this synthesis.

8.1.3 Protected synthesis

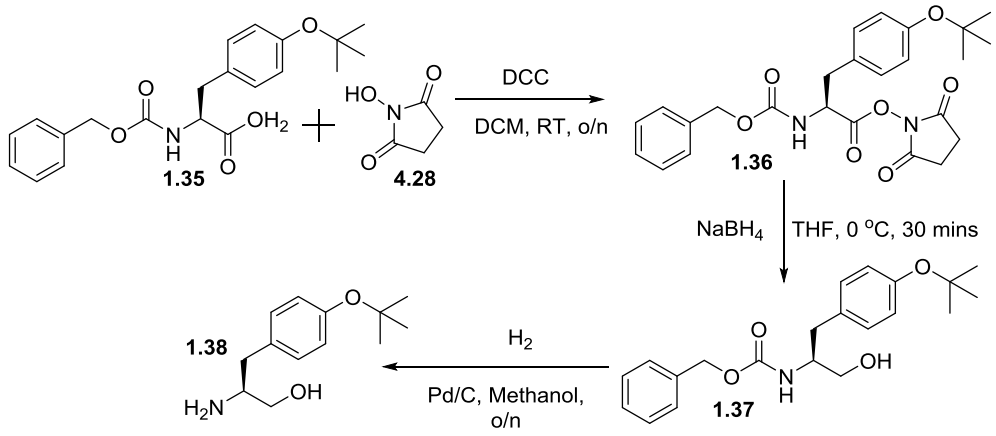
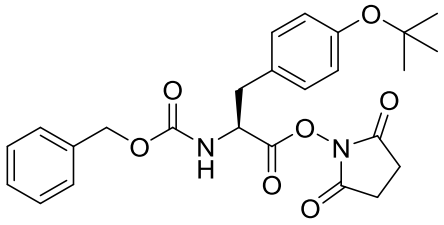


Figure 209: tert-butyl protected tyrosinol synthesis

2,5-dioxopyrrolidin-1-yl (*S*)-2-(((benzyloxy)carbonyl)amino)-3-(4-(*tert*-butoxy)phenyl)propanoate (**1.36**)

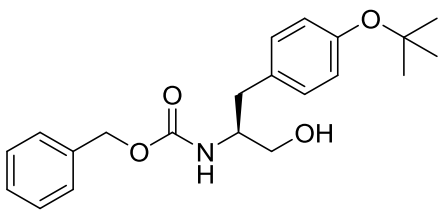


Z-Tyr(tBu)-OH·DCHA (**1.35**, 2.30 g, 4.2 mmol) was dissolved in EtOAc (30 ml). This was then washed with pH4 Citrate buffer (0.5 M, 20 ml x 2), dried with Na_2SO_4, filtered and evaporated. The residue was then dried by blowing with nitrogen and weighed to assure no loss of starting material. The residue was redissolved in tetrahydofuran (THF, 20 ml) and *N*-hydroxysuccinimide (**4.28**,

430 mg, 3.6 mmol) was added. The solution was then cooled to 5 °C and DCC (**4.21**, 851 mg, 7.2 mmol) was added. The mixture was allowed to warm to room temperature and was stirred overnight. The reaction was then filtered under gravity; 2 ml of the 20 ml solution was taken for purification and characterization. The remainder was evaporated yielding a crude red solid (1.48 g, 3.2 mmol, yield = 94%). The sample was purified by column chromatography (3:1 EtOAc/Hex). The fraction found at R_f 0.18 was evaporated affording 0.11 g (0.2 mmol, yield = 63%) of pale yellow solid.

Z-Tyr(tBu)-OSu (**1.36**) TLC R_f= 0.18 (3:1 EtOAc/Hex); MS^+ (ES-TOF): m/z calcd: 469.1930 $[M+H]^+$; found: 469.1967; ^{1}H-NMR (400 MHz, $CDCl_3$) δ 7.35-7.23 (m, 5H, Cbz-ArH), 7.13 (d, *J* = 8.3 Hz, 2H, Tyr-ArH), 6.88 (d, *J* = 8.5 Hz, 2H, Tyr-ArH), 5.43 (d, *J* = 8.6 Hz, 1H, Tyr-NH), 5.04 (dd, *J* = 12.2 Hz, 15.8 Hz, 2H, Cbz-H), 4.99-4.90 (m, 1H, Tyr-C_αH), 3.25 (dd, *J* = 5.6 Hz, 14.3 Hz, 1H, Tyr-C_βH), 3.12 (dd, *J* = 6.8 Hz, 14.3 Hz, 1H, Tyr-C_βH), 2.12 (s, 4H, Su-H), 1.30 (s, 9H, tBu-H).

Benzyl (*S*)-(1-(4-(*tert*-butoxy)phenyl)-3-hydroxypropan-2-yl)carbamate (**1.37**)[368]

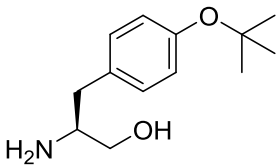


Z-Tyr(tBu)-OSu (**1.36**, 1.48 g, 3.2 mmol) was dissolved in THF (40 ml) and cooled to 0 °C. $NaBH_4$ (227 mg, 6.0 mmol) was dissolved in water (6 ml) and added to the solution. The mixture was stirred at 0 °C for 40 mins and monitored by TLC (3:1 EtOAc/Hex). Once the reaction was complete, EtOAc (80 ml) and brine (40 ml) was added to the mixture and it was acidified with pH4 citrate buffer (1 M, 20 ml). The organic layer was isolated and the aqueous layer was further extracted with EtOAc (10 ml x 2). The combined organic layers were washed with brine (20 ml), dried with Na_2SO_4, filtered and evaporated. The residue was dissolved in 3:1 EtOAc/Hex and passed through a silica pad.

The solvent was again evaporated affording the title compound (1.07 g, 3.0 mmol, yield = 95%) as a yellow-brown oil.

Z-Tyr(tBu)-ol (**1.37**) TLC R_f = 0.70 (3:1 EtOAc/Hex); MS^+ (ES-TOF): m/z calcd: 358.1974 $[M+H]^+$; found: 358.1704; ^{1}H-NMR (400 MHz, $CDCl_3$) δ 7.37-7.27 (m, 5H, Cbz-ArH), 7.08 (d, *J* = 7.9 Hz, 2H, Tyr-ArH), 6.90 (d, *J* = 8.3 Hz, 2H, Tyr-ArH), 5.13 (d, *J* = 6.2 Hz, 1H, Tyr-NH), 5.06 (s, 2H, Cbz-H), 3.96-3.81 (m, 1H, Tyr-C_αH), 3.64 (dd, *J* = 2.9 Hz, 10.8 Hz, 1H, Tyr-C**H$_2$**OH), 3.53 (dd, *J* = 4.5 Hz, 10.7 Hz, 1H, Tyr-C**H$_2$**OH), 2.80 (d, *J* = 6.9 Hz, 2H, Tyr-C_βH), 2.73-2.44 (br, 1H, Tyr-CH_2O**H**), 1.36-1.24 (m, 9H, tBu-H). Consistent with the literature[368]

(*S*)-2-amino-3-(4-(*tert*-butoxy)phenyl)propan-1-ol (**1.38**)[369]



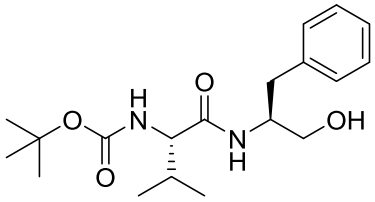
CAUTION: PALLADIUM ON CARBON (Pd/C) CAN IGNITE IN AIR! Z-Tyr(tBu)-ol (**1.37**, 985 mg, 2.8 mmol) was dissolved in MeOH (25 ml) in a two necked round bottomed flask. Pd/C (115 mg) was weighed into a vial. Deionised water (2 ml) was immediately added and the suspension was added to the reaction vessel and gently stirred. The vessel was sealed and a nitrogen atmosphere was established. The gas flow was stopped and the mixture was degassed *in vacuo*, before restarting the flow of nitrogen several times. A hydrogen atmosphere was then created and the mixture was similarly degassed several times. The mixture was left under a hydrogen atmosphere stirring at room temperature overnight. The mixture was then carefully filtered through celite assuring that it was always covered by solvent; the Pd/C waste was discarded appropriately. The filtrate was dried with Na_2SO_4, filtered, and evaporated affording the title compound as a pale yellow foam (561 mg, 2.5 mmol, yield = 91%);

Tyr(tBu)-ol (**1.38**) MS^+ (ES-TOF): m/z calcd: 224.1606 $[M+H]^+$; found: 224.1594; ^{1}H-NMR (400 MHz, $CDCl_3$) δ 7.14 (d, *J* = 7.8 Hz, 2H, Tyr-ArH), 6.90 (d, *J* = 7.8 Hz, 2H, Tyr-ArH), 3.48-3.38 (m, 1H, Tyr-NH_2), 3.33-3.23 (m, 1H, Tyr-NH_2), 3.17-3.04 (m, 1H, Tyr-$C_\beta H_1$), 2.77-2.60 (m, 2H, Tyr-$C_\beta H_2$, Tyr-OH), 2.53-

2.49 (m, 1H, Tyr-C_αH), 2.42 (q, *J* = 13.1 Hz, 2H, Tyr-C**H₂**OH) 1.27 (s, 9H, tBu-H). Consistent with literature.[369]

8.1.3.1 Aureusimine B synthesis

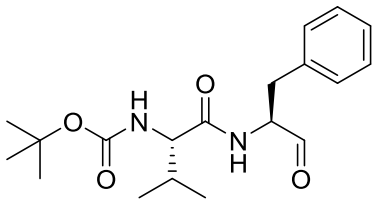
tert-Butyl ((*S*)-1-(((*S*)-1-hydroxy-3-phenylpropan-2-yl)amino)-3-methyl-1-oxobutan-2-yl)carbamate (**2.29**)[370]



Boc-Valine (931 mg, 4.2 mmol) and HOBt (552 mg, 4.2 mmol) was dissolved in DCM (20 ml). DCC (1.05 g, 5.1 mmol) was added to the mixture at 0 °C and was then allowed to warm to room temperature. Phenylalaninol·HCl (769 mg, 5.1 mmol) was then dissolved in DCM (20 ml) with DIPEA (0.86 ml, 5.1 mmol) and this mixture was added to the reaction and stirred overnight. The reaction was filtered under gravity and the solvent was removed *in vacuo*. The crude product was dissolved in EtOAc (40 ml) and was washed with 10% Citric Acid (30 ml x 2), 10% $KHCO_3$ solution (30 ml x 1) and brine (30 ml x 1). The organic layer was then dried with Na_2SO_4, filtered and evaporated. The resulting oil was triturated with Et_2O, blown under nitrogen for 2 hours and dried *in vacuo* overnight to furnish the product as a yellow foam (1.30 g, 3.7 mmol, yield = 88%).

Boc-Val-Phe-ol (**2.29**) TLC R_f= 0.60 (3:1 EtOAc/Hex); MS^+ (ES-TOF): m/z calcd: 351.2239 $[M+H]^+$; found: 351.2359; ^{1}H-NMR (400 MHz, $CDCl_3$) δ 7.34-7.18 (m, 5H, Phe-ArH), 6.25 (d, *J* = 7.7 Hz, 1H, Phe-NH), 4.99-4.87 (m, 1H, Val-NH), 4.24-4.15 (m, 1H, Phe-C_αH), 3.83 (dd, *J* = 5.9 Hz, 7.9 Hz, 1H, Val-C_αH), 3.69 (dd, *J* = 3.5 Hz, 11.1 Hz, 1H, Phe-C**H₂**OH), 3.57 (dd, *J* = 4.9 Hz, 11.1 Hz, 1H, Phe-C**H₂**OH), 2.95-2.80 (m, 2H, Phe-C_βH), 2.77-2.64 (m, 1H, Phe-OH), 2.16-2.06 (m, 1H, Val-C_βH), 1.44 (s, 9H, tBu-H), 0.91 (d, *J* = 6.8 Hz, 3H, Val-C_γH), 0.82 (d, *J* = 5.2 Hz, 3H, Val-C_γH). Consistent with literature.[370]

tert-butyl ((*S*)-3-methyl-1-oxo-1-(((*S*)-1-oxo-3-phenylpropan-2-yl)amino)butan-2-yl)carbamate (**2.2**)[370]



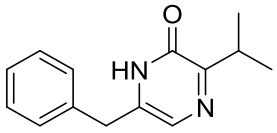
Method 1: Swern Oxidation - DMSO (0.5 ml, 3.3 mmol) was added to dry DCM (5 ml) under an inert atmosphere. Oxalyl Chloride in DCM (2 M, 1.2 ml, 2.4 mmol) was then added slowly at -78 ^{o}C. The mixture was then stirred for 15 mins. Boc-Val-Phe-ol (**2.29**, 578 mg, 1.65 mmol) was dissolved in dry DCM (15 ml) under a nitrogen atmosphere and was slowly added to the reaction which was maintained at -78 ^{o}C. The reaction was stirred for 1 hour, then Et_3N (1.1 ml, 8.1 mmol) was added and it was allowed to warm to room temperature over 30 minutes. pH4 citric acid buffer (1 M, 5 ml) was added to quench the reaction. The organic layer was then evaporated and the residue dissolved in EtOAc (30 ml). This was washed with pH4 citric acid buffer (1 M, 20 ml x 2), 10% $KHCO_3$ solution (20 ml x 2) and brine (20 ml x 2). The organic layer was then dried with Na_2SO_4, filtered, evaporated and triturated with Et_2O. The waxy solid was then blown with nitrogen for 2 hours and dried *in vacuo* overnight to give the product as a yellow solid (429 mg, 1.23 mmol, Yield = 75%).

Boc-Val-Phe-al (**2.2**) TLC R_f = 0.87 (3:1 EtOAc/Hex); MS^+ (ES-TOF): m/z calcd: 349.2083 $[M+H]^+$; found: 349.2052; ^{1}H-NMR (400 MHz, $CDCl_3$) δ 9.60 (s, 1H, Tyr-al), 7.33-7.13 (m, 5H, Phe-ArH), 6.52 (d, *J* = 6.4 Hz, 1H, Phe-NH), 4.98 (d, *J* = 7.9 Hz, 1H, Val-NH), 4.77-4.65 (m, 1H, Phe-C_αH), 3.99-3.89 (m, 1H, Val-C_αH), 3.24-3.08 (m, 2H, Phe-C_βH), 2.18-2.03 (m, 1H, Val-C_βH), 1.43 (s, 9H, tBu-H), 0.97-0.77 (m, 6H, Val-C_γH). Consistent with literature.[370]

Method 2: IBX Oxidation - Boc-Val-Phe-ol (**2.29**, 430 mg, 1.3 mmol) was dissolved in EtOAc (25 ml). 2-iodobenzoic acid (1.13 g, 3.9 mmol) was added to the solution. The mixture was refluxed overnight with vigorous stirring. The reaction was cooled to room temperature and filtered through a medium porosity sintered glass funnel. The solid was washed with EtOAc and Acetone

and the combined filtrate was evaporated. MS indicated that this yielded a mixture of starting material and product. NMR also indicated some IBX type impurities and racemisation of the phenylalanine.

6-benzyl-3-isopropylpyrazin-2(1H)-one (Aureusimine B, **1.31**)[240]



Boc-Val-Phe-al (**2.2**, 308 mg, 1.06 mmol) was dissolved in DCM (5 ml) to which TFA (5 ml) was added. The reaction was stirred at room temperature for 2 hours and monitored by TLC. Once the reaction was complete, the solvent was evaporated and the crude product was dissolved in 4:1 2-butanol/toluene (10 ml). Et_3N (140 µl) was added and the solution was heated at 99 ^oC overnight. The solvent was evaporated leaving the product as a yellow solid (146 mg, 0.64 mmol, yield = 60%). This solid was purified by HPLC (20% MeCN/80% water to 80% MeCN/20% water over 20 mins) eluting at 5.83 mins.

AusB (**1.31**) MS^+ (ES-TOF): m/z calcd: 229.1296 $[M+H]^+$; found: 229.1283; Analytical RP-HPLC Onyx Monolithic C18 100 × 4.6 mm, 20% for 1 min increasing to 80% B in 20 min, t_R 4.41 min; ^{1}H-NMR (400 MHz, $CDCl_3$) δ 12.85 (br, 1H, ArNH), 7.39-7.18 (m, 6H, ArH), 3.83 (s, 2H, Ph-C**H$_2$**-Ar), 3.50-3.36 (m, 1H, C**H**$(CH_3)_2$), 1.25 (d, J = 6.8 Hz, 6H, CH(C**H$_3$**)$_2$). ^{13}C-NMR (125 MHz, $CDCl_3$) δ 162.2, 158.2, 137.4, 136.3, 130.0, 129.4, 128.2, 122.3, 37.4, 30.8, 19.8.Consistent with literature.[240]

8.1.3.2 AusA synthesis

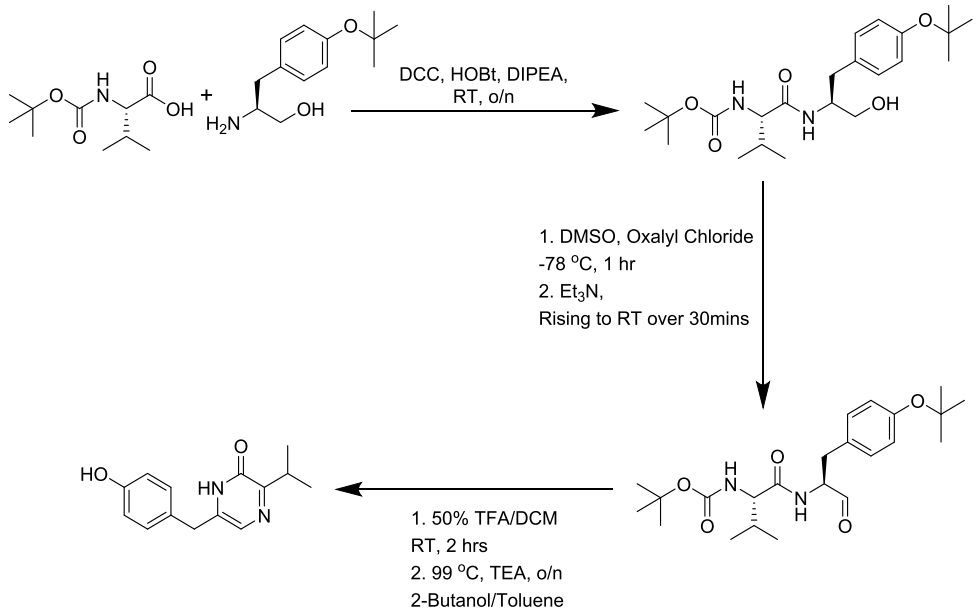
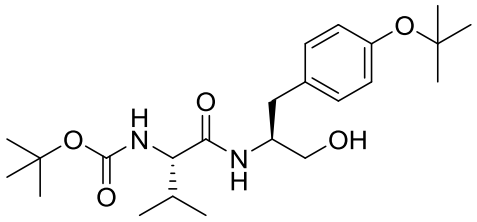


Figure 210: Synthesis of aureusimine A using tBu-protected tyrosinol

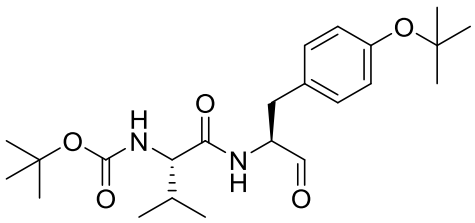
tert-Butyl ((*S*)-1-(((*S*)-1-(4-(*tert*-butoxy)phenyl)-3-hydroxypropan-2-yl)amino)-3-methyl-1-oxobutan-2-yl)carbamate (**2.30**)



Boc-Valine (319 mg, 1.5 mmol) and HOBt (208 mg, 1.5 mmol) were dissolved in DCM (20 ml). DCC (374 mg, 1.8 mmol) was added to the mixture at 0 °C and it was then allowed to warm to room temperature. Tyr(tBu)-ol (**1.38**, 404 mg, 1.8 mmol) was dissolved in DCM (20 ml) with DIPEA (0.26 ml, 1.8 mmol) and this mixture was added to the reaction and stirred overnight. The reaction was filtered under gravity and the solvent was removed *in vacuo*. The crude product was dissolved in EtOAc (40 ml) and was washed with 10% Citric Acid (30 ml x 2), 10% $KHCO_3$ solution (30 ml x 1) and brine (30 ml x 1). The organic layer was then dried with Na_2SO_4, filtered and evaporated. The resulting oil was triturated with Et_2O, blown under nitrogen for 2 hours and dried *in vacuo* overnight to furnish the title product as a yellow foam (565 mg, 1.3 mmol, yield = 91%).

Boc-Val-Tyr(tBu)-ol (**2.30**) TLC R_f= 0.56 (3:1 EtOAc/Hex); MS^+ (ES-TOF): m/z calcd: 423.2814 $[M+H]^+$; found: 423.2733; ^{1}H-NMR (400 MHz, $CDCl_3$) δ 7.09 (d, *J* = 8.4 Hz, 2H, Tyr-ArH), 6.88 (d, *J* = 8.4 Hz, 2H, Tyr-ArH), 6.54 (d, *J* = 8.0 Hz, 1H, Tyr-NH), 5.10 (d, *J* = 8.1 Hz, 1H, Val-NH), 4.19-4.06 (m, 1H, Tyr-C_αH), 3.83 (dd, *J* = 6.4 Hz, 7.9 Hz, 1H, Val-C_αH), 3.66-3.59 (m, 1H, C**H$_2$**OH), 3.58-3.50 (m, 1H, C**H$_2$**OH), 3.30 (t, *J* = 5.1 Hz, 1H, CH_2O**H**), 2.88-2.74 (m, 2H, Tyr-C_βH), 2.28-2.19 (m, 1H,), 2.11-2.01 (m, 1H, Val-C_βH), 1.43 (s, 9H, tBu-H), 1.29 (s, 9H, tBu-H), 0.88 (d, *J* = 6.8 Hz, 3H, Val-C_γH), 0.81 (d, *J* = 6.2 Hz, 3H, Val-C_γH).

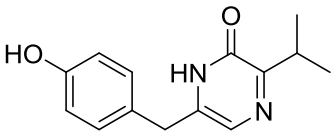
tert-Butyl ((*S*)-1-(((*S*)-1-(4-(tert-butoxy)phenyl)-3-oxopropan-2-yl)amino)-3-methyl-1-oxobutan-2-yl)carbamate (**2.31**)



DMSO (1.0 ml, 14.1 mmol) was added to dry DCM (15 ml) under an inert atmosphere. Oxalyl Chloride in DCM (2 M, 1.5 ml, 2.6 mmol) was then added slowly at -78 ^{o}C. The mixture was then stirred for 15 mins. Boc-Val-Tyr(tBu)-ol (**2.30**, 554 mg, 1.3 mmol) was dissolved in dry DCM (10 ml) under a nitrogen atmosphere and was slowly added to the activation mixture which was maintained at -78 ^{o}C. The reaction was stirred for 1 hour, then Et_3N (0.9 ml, 6.5 mmol) was added and it was maintained at -78 ^{o}C for 5 hours. pH4 citric acid buffer (1 M, 10 ml) was added to quench the reaction and the reaction was allowed to warm to room temperature. The organic layer was then evaporated and the residue dissolved in EtOAc (30 ml). This was washed with pH4 citric acid buffer (1 M, 20 ml x 2), 10% $KHCO_3$ solution (20 ml x 2) and brine (20 ml x 2). The organic layer was then dried with Na_2SO_4, filtered, evaporated and triturated with Et_2O. The waxy solid was then blown with nitrogen for 2 hours and dried *in vacuo* overnight to afford the product as a yellow solid (463 mg, 1.1 mmol, Yield = 84%).

Boc-Val-Tyr(tBu)-al (**2.31**) MS^+ (ES-TOF): m/z calcd: 421.2658 $[M+H]^+$; found: 421.2482; ^{1}H-NMR (400 MHz, $CDCl_3$) δ 9.57 (s, 1H, $CH_2C\mathbf{H}O$), 7.04 (d, *J* = 8.4 Hz, 2H, Tyr-ArH), 6.89 (d, *J* = 8.5 Hz, Tyr-ArH), 6.68 (d, *J* = 6.3 Hz, 1H, Tyr-NH), 5.11-5.01 (m, 1H, Val-NH), 4.73-4.58 (m, 1H, Tyr-C_αH) 3.98-3.88 (m, 1H, Val-C_αH), 3.45 (q, *J* = 7.0 Hz, 2H, $C\mathbf{H_2}CHO$), 3.07 (d, *J* = 6.4 Hz, 2H, Tyr-C_βH), 2.14-2.01 (m, 1H, Val-C_βH), 1.42 (s, 9H, tBu-H), 1.30 (s, 9H, tBu-H), 0.90 (d, *J* = 6.8 Hz, 3H, Val-C_γH), 0.81 (d, *J* = 6.9 Hz, 3H, Val-C_γH).

Aureusimine A (**1.30**)[371]

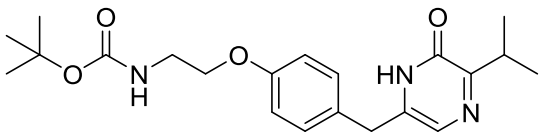


Boc-Val-Tyr(tBu)-al (**2.31**, 418 mg, 1.0 mmol) was dissolved in DCM (15 ml) to which TFA (15 ml) was added. The reaction was stirred at room temperature for 1 hour and monitored by TLC. Once the reaction was complete, the solvent was evaporated and the crude product was dissolved in 4:1 2-butanol/toluene (20 ml). Et_3N (400 µl) was added and the solution was heated at 99 ^oC overnight. The solvent was evaporated producing a crude yellow solid (261 mg). This solid was purified by HPLC (20% MeCN/80% water to 35% MeCN/65% water over 10 mins) eluting at 3.58 mins. The resulting solution was blown with nitrogen for 1 hour and then freeze dried producing a light fine yellow powder (72 mg, 0.3 mmol, yield = 30%) of pure aureusimine A.

AusA (**1.30**) MS^+ (ES-TOF): m/z calcd: 245.1245 $[M+H]^+$; found: 245.1254; ^{1}H-NMR (400 MHz, $CDCl_3$) δ 7.53 (s, 1H, PhO**H**), 7.14 (d, J = 8.5 Hz, 2H, Ar-PhH), 6.98 (br, 2H, Ar-NH, Ar-CH)6.81 (d, *J* = 8.5 Hz, 2H, Ar-PhH), 3.84 (s, 2H, Ph-$C\mathbf{H_2}$-Ar), 3.42 (m, 1H, $C\mathbf{H}(CH_3)_2$), 1.25 (d, *J* = 6.8 Hz, 6H, $CH(C\mathbf{H_3})_2$); ^{13}C-NMR (125 MHz, $CDCl_3$) δ 155.5, 130.6, 126.7, 124.8, 116.2, 77.4, 77.0 36.0, 30.4, 20.0. Consistent with literature.[371]

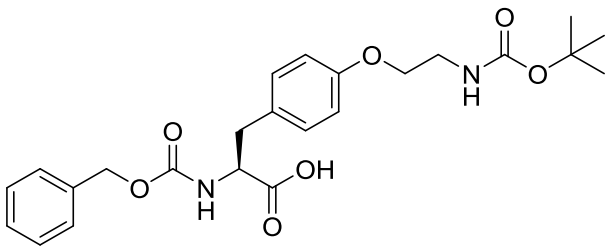
8.1.4 Affinity chromatography - synthesis of tethered aureusimine

tert-Butyl (2-(4-((5-isopropyl-6-oxo-1,6-dihydropyrazin-2-yl)methyl)phenoxy)ethyl)carbamate (**2.32**)



AusA (**1.30**, 20 mg, 85 μM) was dissolved in acetone (2 mL) and K_2CO_3 (25 mg, 170 μM) was added. The mixture was heated to reflux for 1 hr then Boc-amino-ethyl bromide (95 mg, 425 μM) was added and the mixture was stirred over the weekend. Mass spectroscopic analysis of the mixture revealed the presence of significant amounts of starting material and small amounts of product. Therefore, further Boc-amino-ethyl bromide (100 mg, 430 μM) was added and stirred overnight. Further mass spectroscopic analysis of the mixture still showed the presence of starting material **1.30**. Therefore, further Boc-amino-ethyl bromide (100 mg, 430 μM) was added and stirred overnight. The mixture was evaporated and analysed by HPLC. Three significant peaks corresponding to the desired product **2.32**, the starting material **1.30**, and a dual addition product **2.33** were observed, only trace amounts were isolated. This method was considered unsuitable for the synthesis of AusP (**2.35**).

(*S*)-2-(((Benzyloxy)carbonyl)amino)-3-(4-(2-((*tert*-butoxycarbonyl)amino)ethoxy)phenyl)propanoic acid (**2.35**)



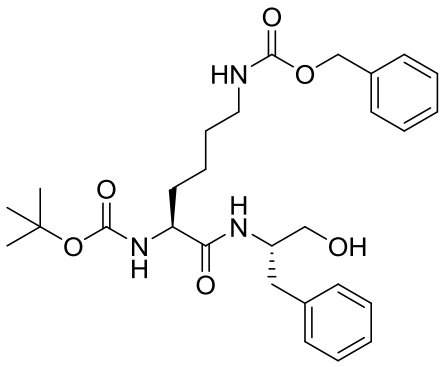
Z-Tyr-OH (**2.34**, 1.4 g, 4.5 mmol) was dissolved in DMF (10 mL) and treated with NaH (0.21 g, 8.9 mmol) for 1 hr. Boc-amino-ethyl bromide (1 g, 4.5 mmol) was added and the mixture was stirred for 16 hrs. The solvent was evaporated

and the residue was dissolved in water. This was acidified to pH 3 and extracted with EtOAc. The organic layer was dried with Na_2SO_4, filtered and evaporated. Column chromatography (97:3:1 $CHCl_3$/MeOH/AcOH) afforded a mixture of the starting material **2.34** and product **2.35**. This reaction was considered unsuitable due to low yields.

Z-Tyr-OH (**2.34**, 1.55 g, 4.9 mmol) was dissolved in THF (10 mL) and K_2CO_3 (1.85 g, 13.4 mmol) was added. The mixture was heated to 50 °C for 15 min. Boc-amino-ethyl bromide (1 g, 4.5 mmol) was added and the mixture was stirred for overnight. The solvent was evaporated and the residue was dissolved in water. This was acidified to pH 3 and extracted with EtOAc. The organic layer was dried with Na_2SO_4, filtered and evaporated. Only the starting material could be detected in the residue.

Z-Tyr-OH (**2.34**, 1.24 g, 3.9 mmol) was dissolved in THF (20 mL) and TEA (2 mL, 14.3 mmol) was added. The mixture was heated to 80 °C. Boc-amino-ethyl bromide (0.8 g, 3.6 mmol) was added and the mixture was stirred over the weekend. The solvent was evaporated and the residue was dissolved in water. This was acidified to pH 3 and extracted with EtOAc. The organic layer was dried with Na_2SO_4, filtered and evaporated. The residue contained the product **2.35**, the deprotected product, and residual TEA. At this point, this strategy was abandoned.

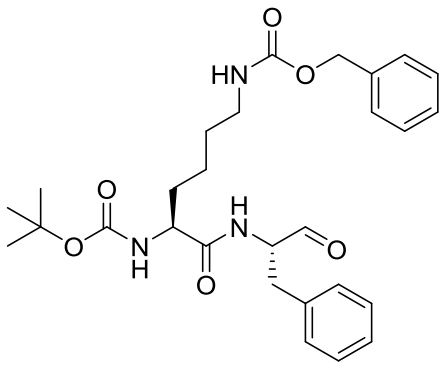
Benzyl *tert*-butyl ((*S*)-6-(((*S*)-1-hydroxy-3-phenylpropan-2-yl)amino)-6-oxohexane-1,5-diyl)dicarbamate (**2.37**)



Procedure as for **2.29** above. The reaction yielded 2.18 g of the title compound (77% yield) as a pale yellow oil.

Boc-Lys(Cbz)-Phe-ol (**2.37**) TLC R_f= 0.56 (3:1 EtOAc/Hex); MS^+ (ES-TOF): m/z calcd: 514.2872 $[M+H]^+$; found: 514.2495; ^{1}H-NMR (400 MHz, $CDCl_3$) δ 7.38-7.24 (m, 7H, ArH), 7.23-7.17 (m, 3H, ArH), 6.46 (d, *J* = 8.1 Hz, 1H, Phe-NH), 5.28 (d, *J* = 6.6 Hz, 1H, Lys-NH), 5.08 (dd, *J* = 12.6 Hz, 15.0 Hz, 2H, Cbz-C**H$_2$**), 5.04-4.98 (m, 1H, Cbz-NH), 4.22-4.12 (m, 1H, Lys-C_αH), 4.04-3.93 (m, 1H, Phe-C_αH), 3.65 (dd, *J* = 3.5 Hz, 11.3 Hz, 1H, Phe-C_βH), 3.50 (dd, *J* = 4.7 Hz, 11.1 Hz, 1H, Phe-C_βH), 3.15 (q, *J* = 6.2 Hz, 2H, Lys-C_εH), 2.91-2.79 (m, 2H, CHC**H$_2$**OH), 1.80-1.66 (m, 1H, Lys-C_βH), 1.65-1.53 (m, 1H, Lys-C_βH), 1.52-1.44 (m, 2H, Lys-C_δH), 1.43 (s, 9H, tBu-H), 1.33-1.25 (m, 2H, Lys-C_γH), alcohol proton missing.

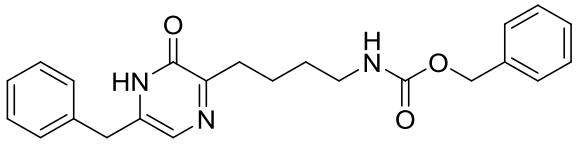
Benzyl *tert*-butyl ((*S*)-6-oxo-6-(((*S*)-1-oxo-3-phenylpropan-2-yl)amino)hexane-1,5-diyl)dicarbamate (**2.39**)



Procedure as for **2.2** above. The reaction yielded 1.57 g of the title compound (88% yield) as a pale yellow oil.

Boc-Lys(Cbz)-Phe-al (**2.39**) TLC R_f= 0.71 (3:1 EtOAc/Hex); MS^+ (ES-TOF): m/z calcd: 512.2716 $[M+H]^+$; found: 512.2709; ^{1}H-NMR (400 MHz, $CDCl_3$) δ 9.53 (s, 1H, C**H**O), 7.35-7.10 (m, 10H, ArH), 7.08-6.97 (m, 1H, Phe-NH), 5.40-5.29 (m, 1H, Lys-NH), 5.27-5.13 (m, 1H, Cbz-NH), 5.11-5.00 (m, 2H, Cbz-C**H$_2$**), 4.66-4.52 (m, 1H, Phe-C_αH), 4.16-4.00 (m, 1H, Lys-C_αH), 3.21-3.08 (m, 3H, Lys-C_εH, Phe-C_βH), 3.04 (dd, *J* = 7.1 Hz 14.1 Hz, 1H, Phe-C_βH), 1.81-1.62 (m, 2H, Lys-C_δH), 1.61-1.51 (m, 2H, Lys-C_βH), 1.40 (s, 9H, tBu-H), 1.34-1.26 (m, 2H, Lys-C_γH).

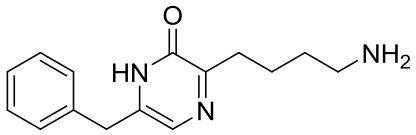
Benzyl (4-(5-benzyl-3-oxo-3,4-dihydropyrazin-2-yl)butyl)carbamate (AusK(Z), **2.41**)



Procedure as for **1.31** above. The reaction yielded 0.35 g of the title compound (33% yield) as a pale yellow powder.

AusK(Z) (**2.41**) MS^+ (ES-TOF): m/z calcd: 392.1929 $[M+H]^+$; found: 392.1978; ^{1}H-NMR (400 MHz, $(CD_3)_2SO$) δ 7.40-7.20 (m, 11H, ArH), 7.13-7.00 (m, 1H, Cbz-NH), 6.55 (br, 1H, Ar-NH), 4.99 (s, 2H, Ar-CH_2), 3.74 (s, 2H, Ar-CH_2), 3.00 (q, 2H, *J* = 6.99 Hz, $CH_2C\mathbf{H_2}NH$), 2.62-2.54 (m, 2H, $C\mathbf{H_2}(CH_2)_3NH$), 1.62-1.51 (m, 2H, $C\mathbf{H_2}(CH_2)_2NH$), 1.48-1.36 (m, 2H, $C\mathbf{H_2}CH_2NH$).

3-(4-aminobutyl)-6-benzylpyrazin-2(1H)-one (AusK, **1.41**)



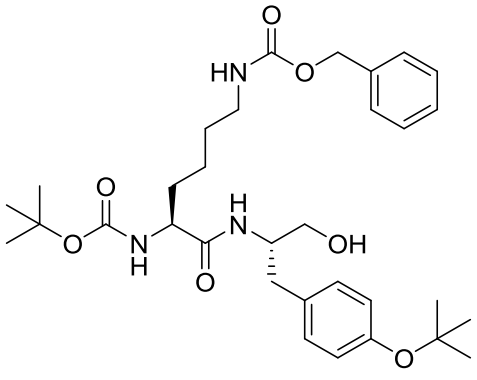
Method 1 Catalytic Hydrogenation - AusK(Z) (**2.41**, 0.183 g, 0.47 mmol) was dissolved in THF (10 mL). Palladium on carbon was added and the mixture was sealed under nitrogen. The mixture was degassed several times before the atmosphere was exchanged for hydrogen. The mixture was degassed a further two times. The mixture was then left stirring overnight. The suspension was then filtered through diatomaceous earth and the filtrate was evaporated. Mass spectrometric analysis revealed the presence of a product with a mass of 261.1980 corresponding to the deprotected and hydrogenated product **2.43**.

Method 2 Strong acid - 3 equal portions of AusK(Z) (**2.41**, 0.183 g, 0.47 mmol) were dissolved in MeCN (10 mL). Strong acids were added (10 mL - 50% TFA in DCM/4M HCl in water/4M HCl in anhydrous dioxane) and the mixtures were stirred overnight. The TFA and aqueous HCl mixtures were evaporated

under a stream of nitrogen then lyophilised. Mess spectrometric analysis revealed significant amounts of the starting material still present which was further confirmed by NMR. The organic HCl reaction produced a suspension of white crystals which were separated from the mixture by filtration. Mass spectrometric analysis showed a mixture of two mass ions of 240.6456 and 258.7302 representing an unknown compound and the product respectively. HPLC could not separate these mass ions. A small sample of the crystals were dissolved in DCM (500 µL) and acetic anhydride (20 µL) and DIPEA (20 µL) were added. The mixture was stirred for 1 hr and then mass spectrometric analysis showed a single mass peak of 299.8214 corresponding to the acetylated product **2.44**.

AusK (**1.41**) MS^+ (ES-TOF): m/z calcd: 258.1562 $[M+H]^+$; found: 258.7302; Analytical RP-HPLC Onyx Monolithic C18 100 × 4.6 mm, 2% for 10 min increasing to 15% B in 10 min, t_R 17.84 min; ^{1}H-NMR (400 MHz, $(CD_3)_2SO$) δ 7.34-7.28 (m, 2H, ArH), 7.28-7.24 (m, 1H, ArH), 7.24-7.20 (m, 2H, ArH), 7.18 (s, 1H, ArH), 3.87 (s, 2H, Ar-CH_2), 2.96-2.88 (m, 2H, C**H$_2$**NH), 2.71-2.64 (m, 2H, C**H$_2$**$(CH_2)_3$NH), 1.66-1.58 (m, 4H, C**H$_2$**C**H$_2$**CH_2NH), Ar-NH proton missing.

Benzyl *tert*-butyl ((*S*)-6-(((*S*)-1-(4-(tert-butoxy)phenyl)-3-hydroxypropan-2-yl)amino)-6-oxohexane-1,5-diyl)dicarbamate (**2.38**)

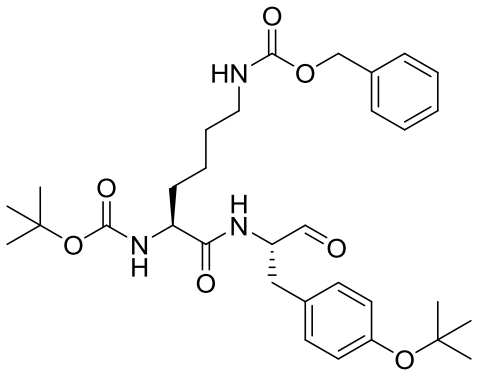


Procedure as for **2.37** above. The reaction yielded 0.18 g of the title compound (89% yield) as a white waxy solid.

Boc-Lys(Cbz)-Tyr(tBu)-ol (**2.38**) TLC R_f= 0.56 (3:1 EtOAc/Hex); MS^+ (ES-TOF): m/z calcd: 586.3448 $[M+H]^+$; found: 586.3878; ^{1}H-NMR (400 MHz, $CDCl_3$)

δ 7.37-7.27 (m, 5H, ArH), 7.12-7.03 (m, 2H, ArH), 6.91-6.86 (m, 2H, ArH), 6.45 (d, *J* = 7.9 Hz, 1H, Tyr-NH), 5.27 (d, *J* = 6.4 Hz, 1H, Lys-NH), 5.18-5.02 (m, 3H, Cbz-NH, Cbz-CH_2), 4.18-4.08 (m, 1H, Tyr-C_αH), 4.02-3.91 (m, 1H, Lys-C_αH), 3.65 (dd, *J* = 3.3 Hz, 11.2 Hz, 1H, Tyr-C_βH), 3.53-3.41 (m, 1H, Tyr-C_βH), 3.20-3.07 (m, 2H, Lys-C_εH), 2.86-2.73 (m, 2H, C**H**$_2$OH), 1.76-1.55 (m, 2H, Lys-C_βH), 1.51-1.45 (m, 2H, Lys-C_δH), 1.43 (s, 9H, tBu-H), 1.31 (s, 9H, tBu-H), 1.30-1.23 (m, 2H, Lys-C_γH), alcohol proton missing.

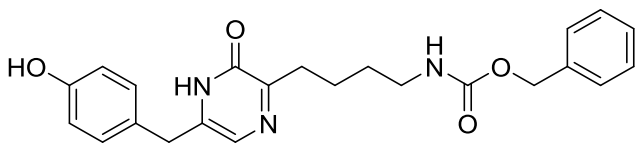
Benzyl *tert*-butyl ((*S*)-6-(((*S*)-1-(4-(*tert*-butoxy)phenyl)-3-oxopropan-2-yl)amino)-6-oxohexane-1,5-diyl)dicarbamate (**2.40**)



Procedure as for **2.39** above. The reaction yielded 0.458 g of the title compound (86% yield) as a pale yellow oil.

Boc-Lys(Cbz)-Tyr(tBu)-al (**2.40**) MS^+ (ES-TOF): m/z calcd: 584.3291 $[M+H]^+$; found: 584.4066; ^{1}H-NMR (400 MHz, $CDCl_3$) δ 9.56 (s, 1H), 7.38-7.27 (m, 5H), 7.11-7.01 (m, 2H), 6.92-6.84 (m, 2H), 6.82 (d, *J* = 6.3 Hz, 1H), 5.21-4.98 (m, 4H), 4.68-4.59 (m, 1H), 4.15-4.01 (m, 1H), 3.51-3.40 (m, 1H), 3.23-2.99 (m, 4H), 1.63-1.53 (m, 2H), 1.52-1.45 (m, 2H), 1.42 (s, 9H), 1.31 (s, 9H).

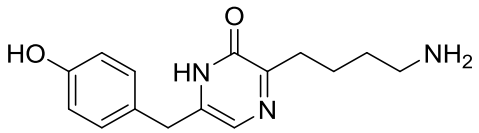
Benzyl (4-(5-(4-hydroxybenzyl)-3-oxo-3,4-dihydropyrazin-2-yl)butyl)carbamate (AusTK(Z), **2.42**)



Procedure as for **2.41** above. A small sample was purified for characterisation and the rest of the crude product was used in the deprotection below.

AusTK(Z) (**2.42**) MS^+ (ES-TOF): m/z calcd: 408.1879 $[M+H]^+$; found: 408.0739; ^{1}H-NMR (400 MHz, $(CD_3)_2SO$) δ 7.40-7.26 (m, 5H, Cbz-ArH), 7.08 (d, *J* = 8.5 Hz, 2H, Ph-ArH), 7.02-6.98 (m, 1H, ArH), 6.69 (d, *J* = 8.4 Hz, 2H, Ph-ArH), 4.99 (s, 2H, Ar-C**H$_2$**-Ar), 3.65-3.57 (m, 2H, Cbz-C**H$_2$**), 3.38 (br s, 2H, Ar-NH, Cbz-NH), 3.03-2.95 (m, 2H, C**H$_2$**NH), 2.60-2.53 (m, 2H, C**H$_2$**$(CH_2)_3$NH), 1.56-1.49 (m, 2H, C**H$_2$**$(CH_2)_2$NH), 1.46-1.35 (m, 2H, C**H$_2$**CH_2NH), missing phenol.

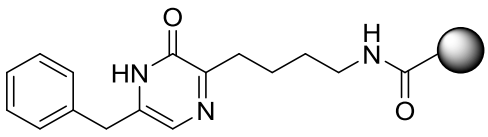
3-(4-aminobutyl)-6-(4-hydroxybenzyl)pyrazin-2(1H)-one (AusTK, **1.40**)



Procedure as for **1.41** above. The reaction yielded 10.9 mg of the title compound as white crystals.

AusTK (**1.40**) MS^+ (ES-TOF): m/z calcd: 274.1511 $[M+H]^+$; found: 274.1950; Analytical RP-HPLC Onyx Monolithic C18 100 × 4.6 mm, 2% for 10 min increasing to 50% B in 15 min, t_R 15.06 min; ^{1}H-NMR (400 MHz, $(CD_3)_2SO$) δ 7.13 (s, 1H, ArH), 7.07 (d, *J* = 8.6 Hz, 2H, ArH), 6.76 (d, *J* = 8.6 Hz, 2H, ArH), 3.74 (s, 2H, Cbz-CH_2), 2.97-2.88 (m, 2H, C**H$_2$**NH), 2.69-2.60 (m, 2H, C**H$_2$**$(CH_2)_3$NH), 1.65-1.56 (m, 4H, C**H$_2$**C**H$_2$**CH_2NH), Ar-NH, amine and phenol missing; ^{13}C-NMR (125 MHz, $CDCl_3$) δ 136.5, 135.1, 133.5, 120.3, 106.4, 99.0, 94.5, 45.4, 25.5, 17.9, 13.5, 9.5, 5.1.

AusK Resin (**2.46**)



Affigel 10 (**2.45**, 3 mL) was added to a buchner funnel and the supernatant was drained. The gel was washed with cold isopropanol (20 mL). The gel was

transferred to a reaction vessel, AusK (**1.41**, 15 mg, 0.05 mmol) and DIPEA (9 µL, 0.05 mmol) were added. Analytical HPLC was immediately performed on the supernatant. The reaction was stirred for 4 hours and ethanolamine (5 µL, 0.07 mmol) was added to cap unreacted sites. After 1 hour, analytical HPLC showed that 71% of AusK had been loaded onto the resin indicating a resin loading of 83%. A similar process to that detailed above was used to prepare a blank control resin by loading ethanolamine alone.

8.1.5 Biology

8.1.5.1 Agr assays

The experimental procedure was identical to the process detailed in Section 8.2.3.

8.1.5.2 Affinity Chromatography

Two portions (2 mL) of an overnight culture of *S. aureus* strain Newman was pelleted, resuspended in PBS (1 mL), pelleted again, and resuspended in a further portion of PBS (1 mL). This was added to BHI (300 mL) and grown for 4 hrs at 37 ^{o}C. The bacteria was centrifuged at 4200 rpm for 5 mins and the supernatant was removed. PBS (10 mL), lysostaphin (5 mg/ml, 90 µL) and protease inhibitors were added to the pellets. 4 portions (5 mL each) of this mixture was incubated at 37 ^{o}C for 1 hr with 250 rpm agitation. The mixture was centrifuged at 10,000 rpm for 15 min at 4 ^{o}C. The supernatant was stored at -80 ^{o}C. The pellet was incubated with Triton for 1, 4, or 16 hrs. The AusK-resin (50 mg) and blank control resin (50 mg) were then incubated with supernatant (1.5 mL) or pellet mixture (1.5 mL) for 1hr, 4 hr, and 16 hr. Each resin mixture was then pelleted, and washed with Tris.HCl (50 mM), NaCl (1M), CHAPS (0.125 mM), EDTA (0.25 mM) mixture at pH8. The mixture was further pelleted and washed with Tris.HCl (50 mM), NaCl (1M) mixture at pH8. The mixture was pelleted once more and washed with Tris.HCl (50 mM), NaCl (100 mM) mixture at pH8. Finally, the pellet was incubated in SDS-PAGE sample buffer for either 100 ^{o}C for 5 min or 37 ^{o}C for 30 min. The samples were analysed using standard SDS-PAGE techniques.

8.1.5.3 Swarming

Dr. Eric Pollitt performed the experiments, the protocol is similar to those experiments reported in his thesis.[372]

8.1.5.4 Persistence

S. aureus strain Newman was grown overnight in TSB medium. The culture was diluted 1 in 100 into 20 mL of TSB. After 2 hr incubation at 37 ^{o}C, add ciprofloxacin (final concentration of 15 ug/ml) to 5 mL of the culture. A portion (1 mL) of original culture is used to determine initial colony forming units. Further portions (1 mL) are used to determine remaining colony forming units at later time points. The sample (1 mL) is pelleted and resuspended in fresh medium. The culture is serially diluted 100 µL in 900 µL. For each dilution, 100 µL is grown on agar plates. Counting the colonies and multiplying by the dilution factor determines the colony forming units (performed by Daniel Dyer).

8.1.5.5 Biofilm

S. aureus strain Newman was grown in chelated RPMI-1640 and 2% glucose supplemented TSB overnight. The cultures were then diluted to an OD_{595} of 0.1 in the relevant media. The culture was then inoculated into triplicate wells of a 12-well microtitre plate, and supplemented with either DMSO (control), aureusimine A (**1.21**) or aureusimine B (**1.22**). After 24 hrs, the wells were carefully washed with phosphate-buffered saline and adherent bacteria were stained with 1% safranin. Biofilm formation was assessed using OD_{490}measurements. Method originally developed by Dr. Alan Cockayne.[298, 299]

8.1.5.6 CCL-2 mediated chemotaxis

Performed by Dr. Alex Hudson in accordance with the original publication by Saleki *et al*.[303]

8.2 Pharmacology of AIP analogues

8.2.1 Bacterial strains and culture conditions

Bacteria were routinely grown in Brain and Heart Infusion (BHI) medium, which was prepared at 37 g/l, and on BHI agar plates at 37 ^{o}C. (Oxoid Agar was used at 1.5% w/v). Both were autoclaved before use as per the manufacturer's instructions. Chloramphenicol (CML) solutions were prepared at 10 mg/ml in 100% EtOH and stored at -20 ^{o}C. AIP-1, 2, 3, 4 and analogue stock solutions were prepared at 1 mM in DMSO and stored at -20 ^{o}C. All strains were derived from RN4220. The strains and plasmids used as reporter organisms were previously reported[167] apart from the AgrC2 and AgrC1 (S116K) reporters which were constructed in a similar manner as below.

Primers (Forward Primer [Bam HI]: 5'-CGTAGGATCCCATATGGAAACAATAAACAACTTAGC 168 nucleotides downstream from annotated gene, Reverse Primer [Hind III]: 5'-CGTAAAGCTTTTATTTTTTTTTAACGTTTCTCACCG) were used to amplify *agrCA* from the group 2 strain Mu50 utilising the restriction enzymes shown. CA insert was cut and ligated into PskermP2[167] and transformed into ROJ48 to make the AgrC2 reporter, EM28. The insert was sequenced at the University of Nottingham sequencing facility.

Mutation of *agrC1* on pAgrC1agrA was achieved using the Phusion Site-Directed Mutagenesis Kit (New England Biolabs). pAgrC1agrA was amplified using a mutation specific forward primer (Forward Primer: 5′-*AAATTTTTTGTAGTTTATGTGACTATTAG, Reverse Primer: 5′-*AGGGAATATTACAAATATACTATCAG). PCR product was ligated and electroporated into *E. coli* TOP10 cells. Plasmid was extracted using QIAprep Spin Miniprep Kit (Qiagen), transformed into ROJ48 to make the AgrC1 (S116K) constitutive reporter, and the desired mutation was confirmed by Sanger sequencing (Source BioScience).

8.2.2 Construction of agrP3::lux bioreporter strains

The parent *S. aureus* bioreporter strain was created by substituting the complete *agrBDCA* locus in RN4220 with *ermB*, the erythromycin resistance gene. An *agrP3: :luxABCDE* promoter fusion was integrated as a single cross generating ROJ48 as previously reported.[167] For AIP assays, plasmids pAgrC1A, pAgrC2A, pAgrC3A, pAgrC4A, pAgrC1A101TT104VA, and pAgrC1S116KA were electroporated into ROJ48 to cause a response to AIP1, 2, 3, and 4. The AgrCA plasmids are based on pSK5630 with the agrP2 promoter (containing AgrC and A) and an *ermB* cassette added. AgrC1, 3, 4, and AgrC1 (A101TT104V) reporter strains were previously reported.[167, 231] The AgrC2 and AgrC1 (S116K) reporters are new constructs created in a similar manner to the previous reporters.

8.2.3 AIP/AgrC bioluminescent reporter assay

BHI agar plates were prepared containing CML (10 μg/ml). The AIP-bioreporter strain (stock stored at -80 ^{o}C) was streaked onto the plates and incubated overnight at 37 ^{o}C. A single colony was then grown overnight at 37 ^{o}C in BHI medium at 200 rpm with supplementary CML (10 μg/mL). A portion of the overnight culture (10 μL) was added to fresh medium (5 mL) supplemented with CML (10 μg/mL) and incubated for 5 hours at 37 ^{o}C. A portion of the culture (1 in 20, final volume 200 μL) was added to 96-well mictrotitre plates containing AIP1, 2, 3, or 4 (giving a final concentration of 100 nM, 100 nM, 400 nM, and 100 nM respectively), a dilution series of the AIP analogue, and BHI medium. Each analogue concentration was measured independently in three separate wells. The plates were then incubated in a TECAN® infinite F200 Pro, OD_{492} and relative light units were measured every 15 mins for 24 hours. The peak Relative Light Units/Optical Density (Max RLU/OD) value and Log_{10}[Concentration of inhibitor] for each well was calculated in Excel (Microsoft Corp.) and was exported to Prism6 (GraphPad, San Diego, CA). Prism6 analysed the data and produced a best fit sigmoidal dose-response curve. EC_{50} and IC_{50} values were then extracted from the curve. Each EC_{50} and IC_{50} value (and the standard deviation) was calculated from an average of three independent experiments.

8.2.4 Hemolysis assays and western blots

Strain KH1187A was grown overnight in BHI medium at 37 °C. Cells (1 ml) were washed three times in PBS before being diluted (1 in 200) into fresh BHI with/without the compound at the stated concentration. Cells were grown for 6 hrs at 37 °C. After 6 hours, cells (1 mL) were pelleted and the supernatant removed. Supernatant (200 µL) was removed for use in the hemolysis assay.

Trichloroacetic acid (200 µL) was added to the 800 µl of remaining supernatant and incubated on ice for 15 mins. Precipitated protein was pelleted and the pellet washed twice with ice cold acetone before suspension in 200 µl lameli buffer. The samples were loaded onto SDS-PAGE gels to perform standard gel electrophoresis. Standard western blot methods were then utilised.

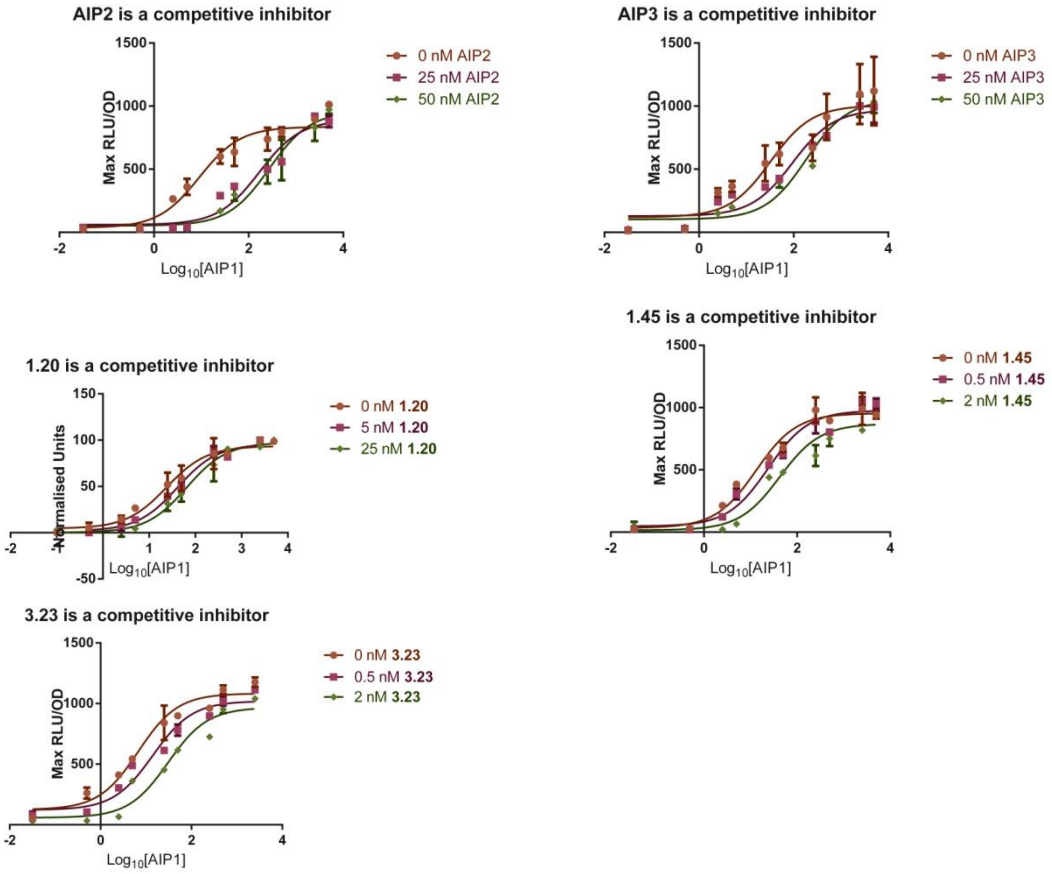
For detection of α-hemolysin, a 1 in 3000 dilution of monoclonal anti-hla antibody (created in house) was used followed by Protein A-HRP conjugate (Sigma) diluted 1 in 4000. For detection of Toxic Shock Syndrome Toxin-1, a 1 in 3000 dilution of polyclonal anti-tsst antibody (created in house) was used followed by Protein A-HRP conjugate (Sigma) diluted 1 in 4000. Visualisation was with ECL HRP substrate from GE healthcare.

For assessing the hemolytic activity, supernatant (20 µL x3) was added to 965 µl of PBS and 15 µl of defibrinated rabbit red blood cells. The mixture was incubated at 37 °C for 15 mins and pelleted. Absorbance at 543 nm of supernatants measured. One unit of hemolysin activity is defined as the amount which causes an increase in OD_{543} of 0.5 per min due to erythrocyte lysis per OD_{600} unit of original culture.[373]

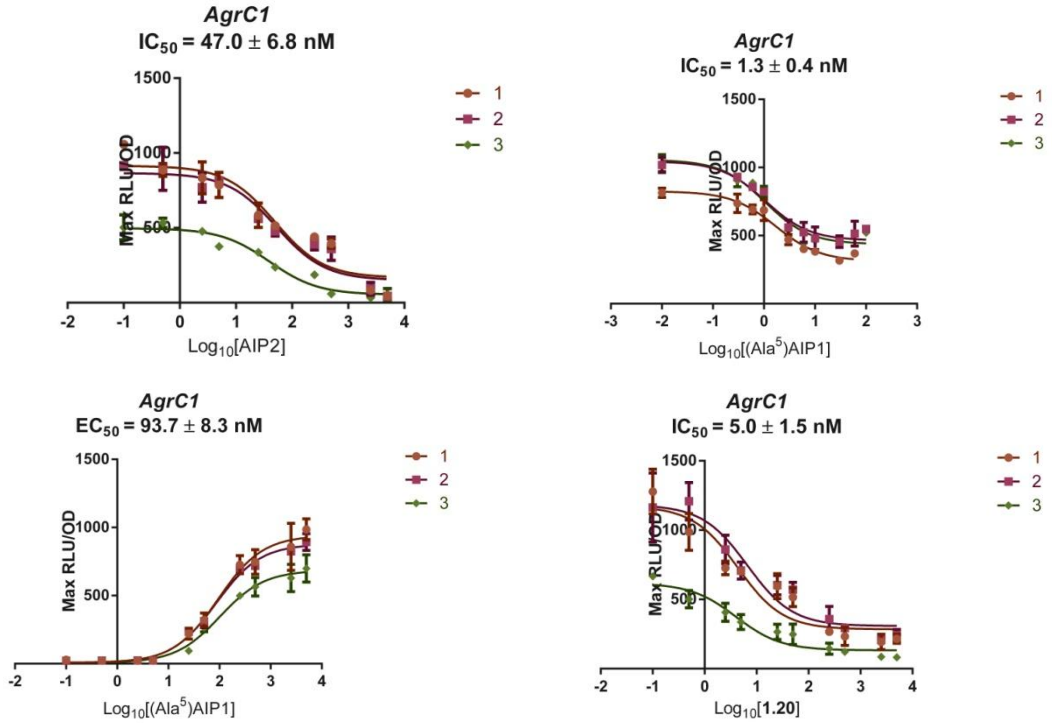
8.2.5 AgrC/AIP bioluminescent reporter assay graphs

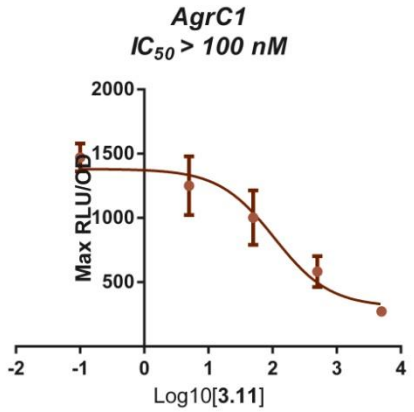
All of the graphs produced by Prism 6 (Graph Pad, San Diego, CA) confirming modes of inhibition and calculating EC_{50} and IC_{50} data for the structure-activity relationship of the AIP analogues are recorded below.

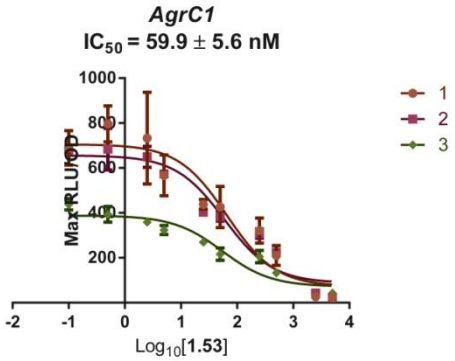
8.2.5.1 AgrC1 Competition assays

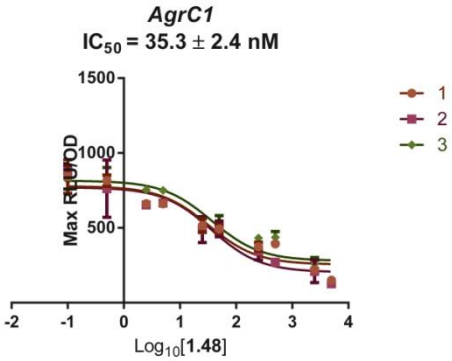


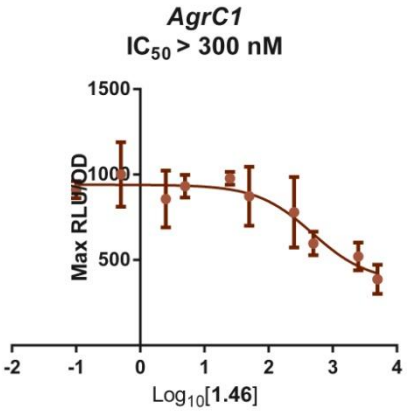
8.2.5.2 AgrC1

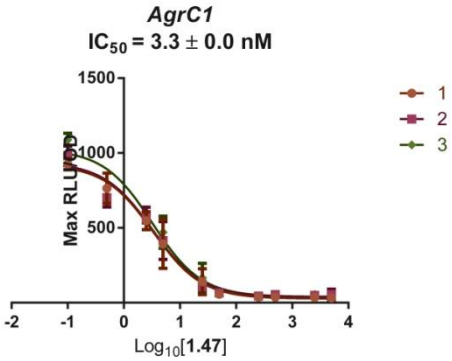


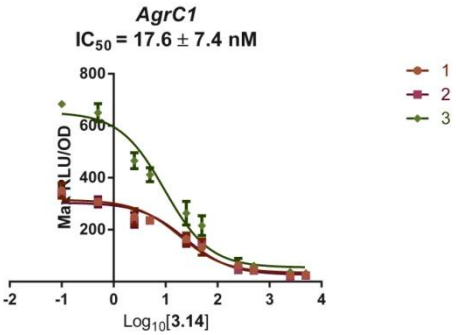

AgrC1
IC50 > 100 nM
Max RLU/OD
Log10[3.11]

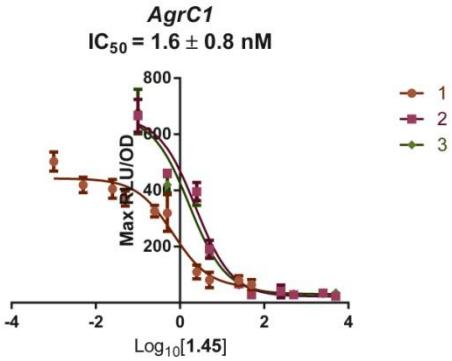

AgrC1
IC50 = 59.9 ± 5.6 nM
Max RLU/OD
Log10[1.53]
1
2
3

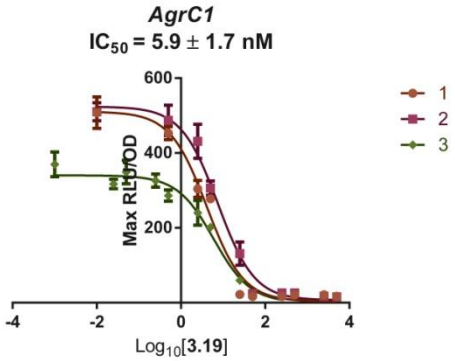

AgrC1
IC50 = 35.3 ± 2.4 nM
Max RLU/OD
Log10[1.48]
1
2
3

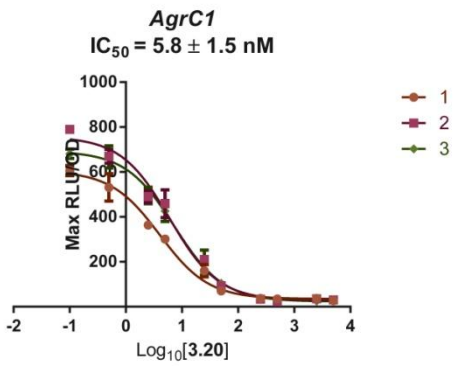

AgrC1
IC50 > 300 nM
Max RLU/OD
Log10[1.46]

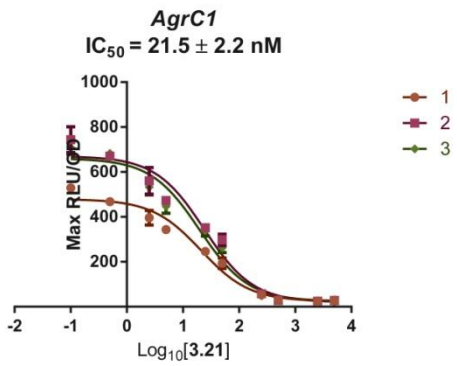

AgrC1
IC50 = 3.3 ± 0.0 nM
Max RLU/OD
Log10[1.47]
1
2
3

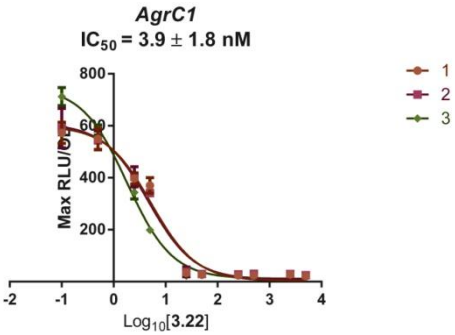

AgrC1
IC50 = 17.6 ± 7.4 nM
Max RLU/OD
Log10[3.14]
1
2
3

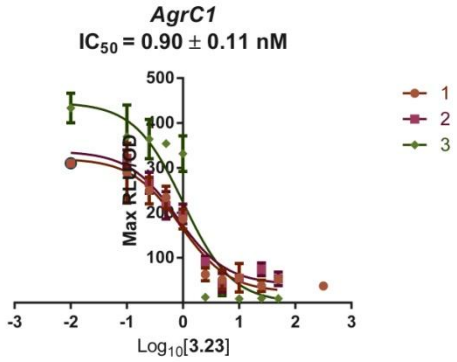

AgrC1
IC50 = 1.6 ± 0.8 nM
Max RLU/OD
Log10[1.45]
1
2
3

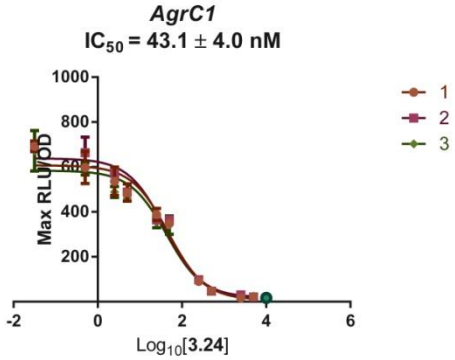

AgrC1
IC50 = 5.9 ± 1.7 nM
Max RLU/OD
Log10[3.19]
1
2
3

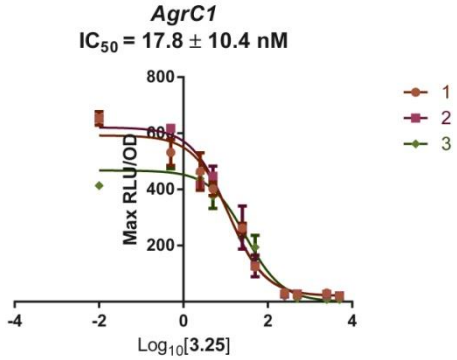

AgrC1
IC50 = 5.8 ± 1.5 nM
Max RLU/OD
Log10[3.20]
1
2
3

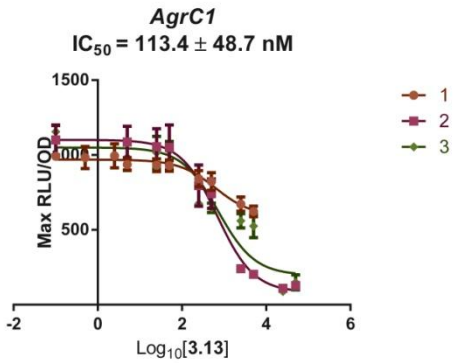

AgrC1
IC50 = 21.5 ± 2.2 nM
Max RLU/OD
Log10[3.21]
1
2
3

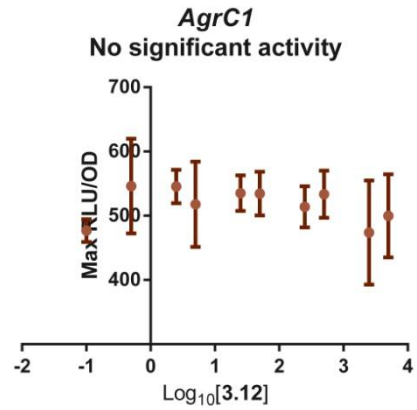

AgrC1
IC50 = 3.9 ± 1.8 nM
Max RLU/OD
Log10[3.22]
1
2
3

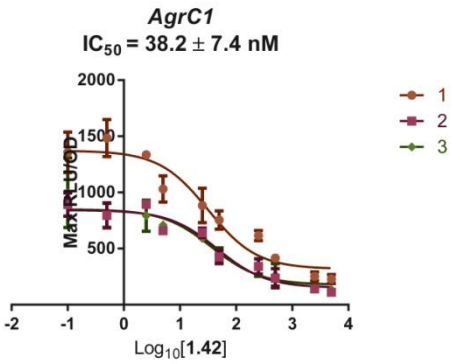

AgrC1
IC50 = 0.90 ± 0.11 nM
Max RLU/OD
Log10[3.23]
1
2
3

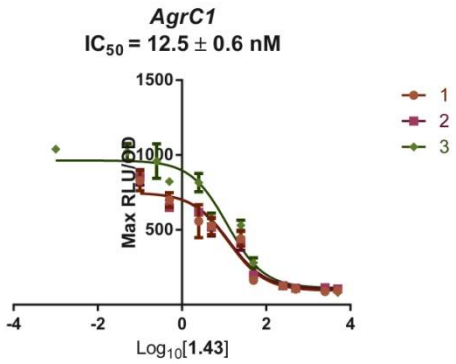

AgrC1
IC50 = 43.1 ± 4.0 nM
Max RLU/OD
Log10[3.24]
1
2
3

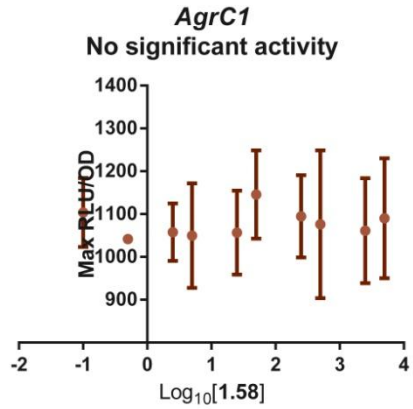

AgrC1
IC50 = 17.8 ± 10.4 nM
Max RLU/OD
Log10[3.25]
1
2
3

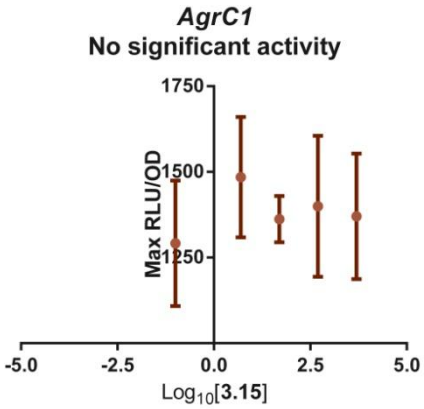

AgrC1
IC50 = 113.4 ± 48.7 nM
Max RLU/OD
Log10[3.13]
1
2
3

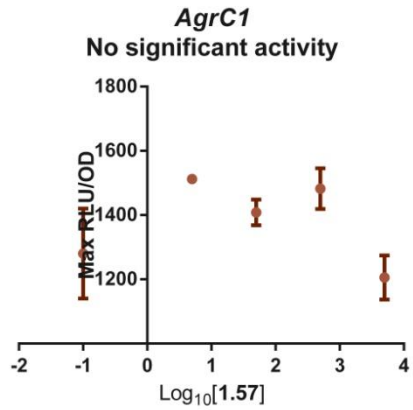

AgrC1
No significant activity
Max RLU/OD
Log10[3.12]

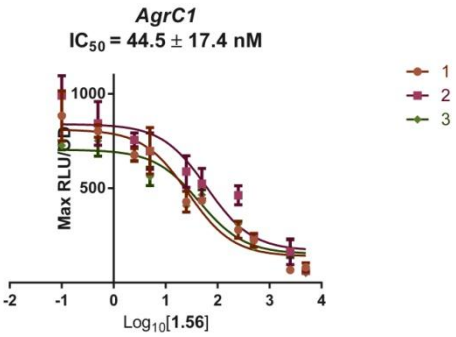

AgrC1
IC50 = 38.2 ± 7.4 nM
Max RLU/OD
Log10[1.42]
1
2
3

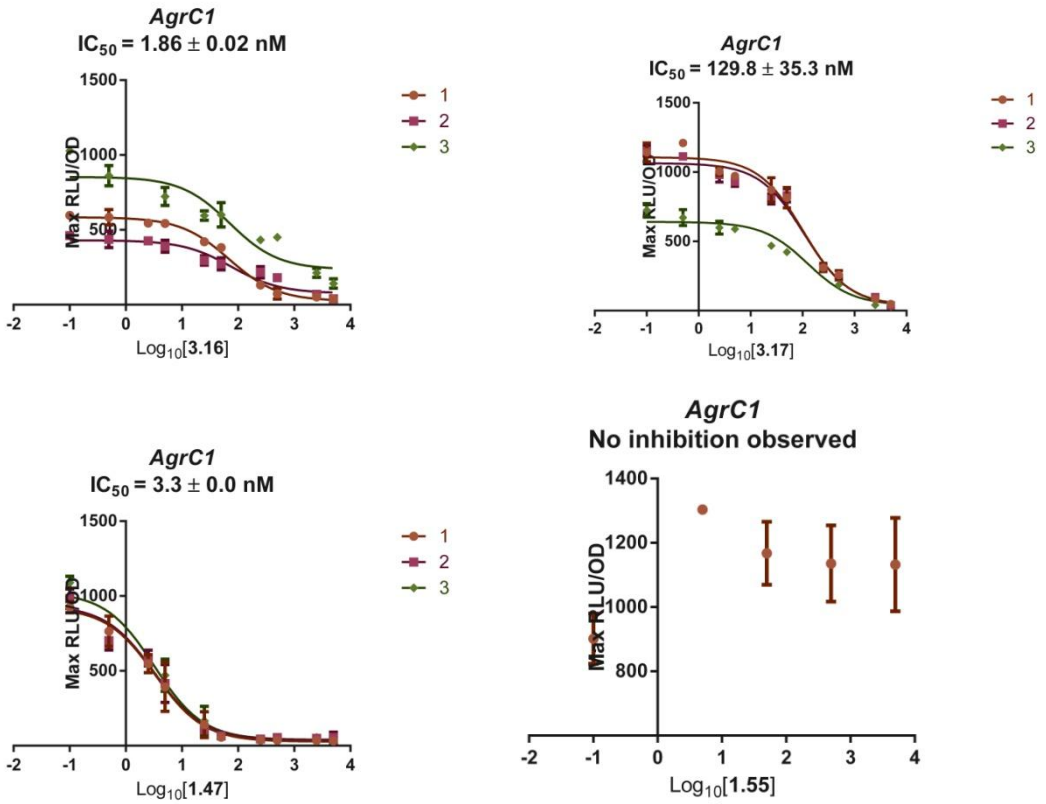

AgrC1
IC50 = 12.5 ± 0.6 nM
Max RLU/OD
Log10[1.43]
1
2
3


AgrC1
No significant activity
Max RLU/OD
Log10[1.58]

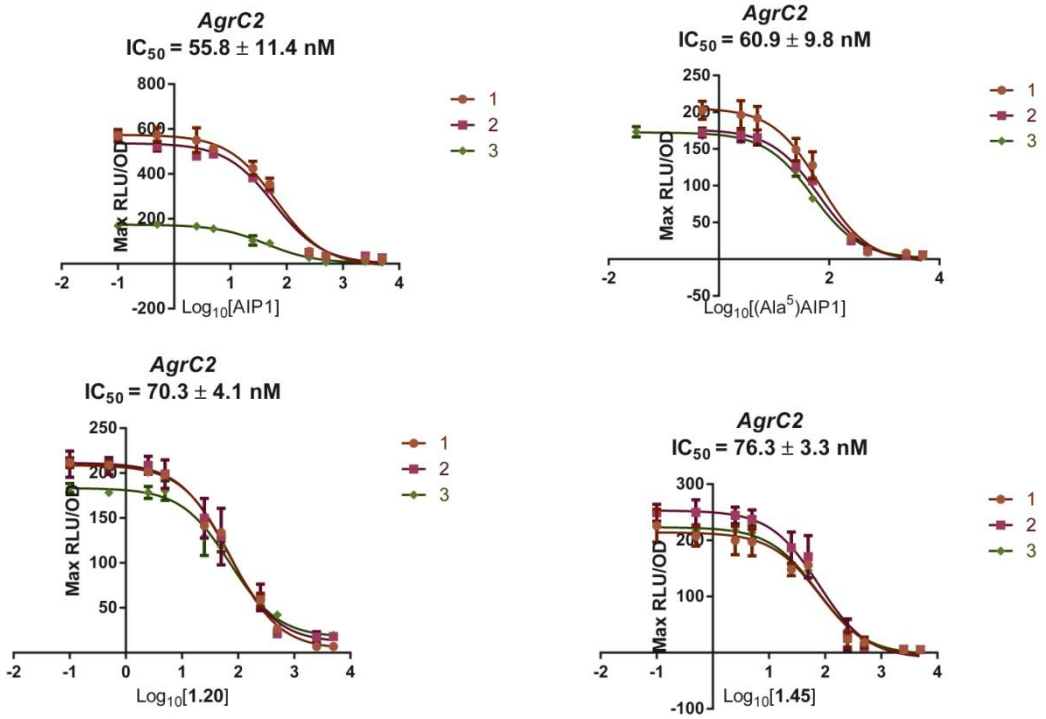

AgrC1
No significant activity
Max RLU/OD
Log10[3.15]

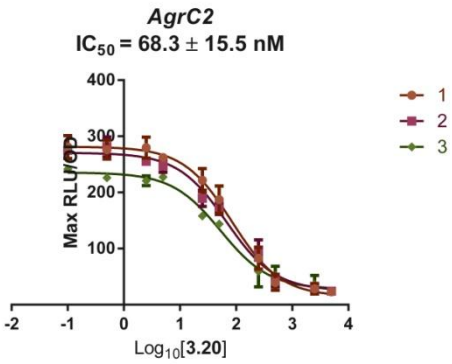

AgrC1
No significant activity
Max RLU/OD
Log10[1.57]

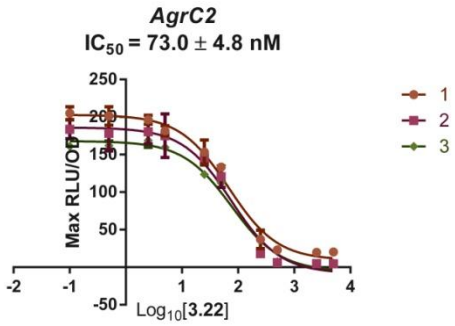

AgrC1
IC50 = 44.5 ± 17.4 nM
Max RLU/OD
Log10[1.56]
1
2
3

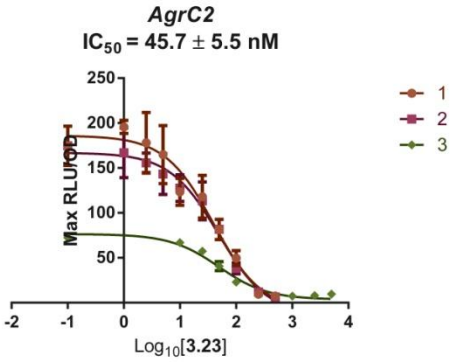

AgrC1
IC50 = 1.86 ± 0.02 nM
Max RLU/OD
Log10[3.16]
AgrC1
IC50 = 129.8 ± 35.3 nM
Max RLU/OD
Log10[3.17]
AgrC1
IC50 = 3.3 ± 0.0 nM
Max RLU/OD
Log10[1.47]
AgrC1
No inhibition observed
Max RLU/OD
Log10[1.55]
1
2
3

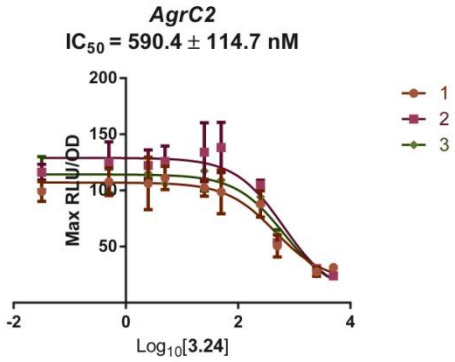
8.2.5.3 AgrC2

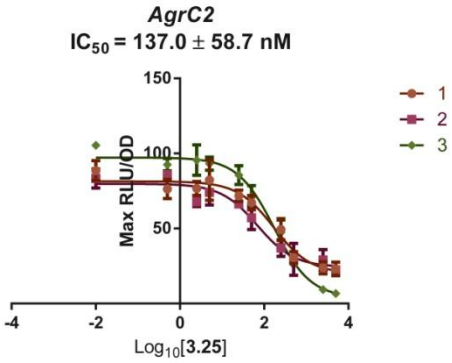

AgrC2
IC50 = 55.8 ± 11.4 nM
Max RLU/OD
Log10[AIP1]
AgrC2
IC50 = 60.9 ± 9.8 nM
Max RLU/OD
Log10[(Ala5)AIP1]
AgrC2
IC50 = 70.3 ± 4.1 nM
Max RLU/OD
Log10[1.20]
AgrC2
IC50 = 76.3 ± 3.3 nM
Max RLU/OD
Log10[1.45]
1
2
3

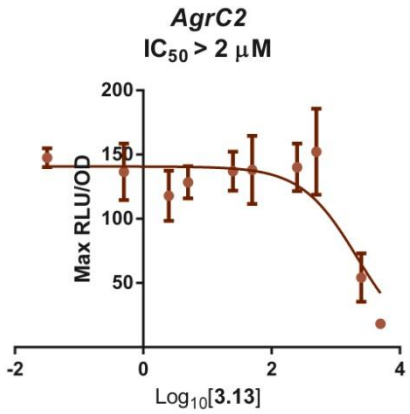

AgrC2
IC50 = 68.3 ± 15.5 nM
Max RLU/OD
Log10[3.20]
1
2
3

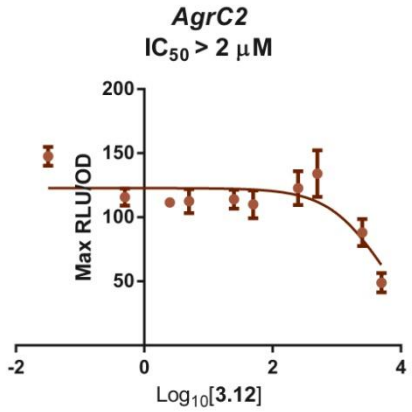

AgrC2
IC50 = 73.0 ± 4.8 nM
Max RLU/OD
Log10[3.22]
1
2
3

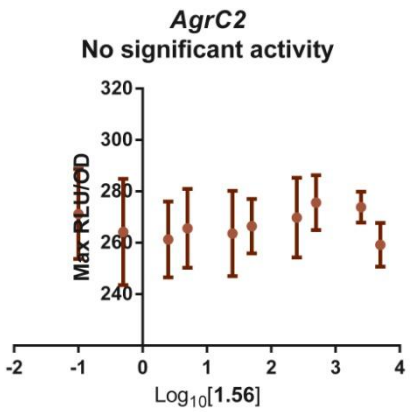

AgrC2
IC50 = 45.7 ± 5.5 nM
Max RLU/OD
Log10[3.23]
1
2
3

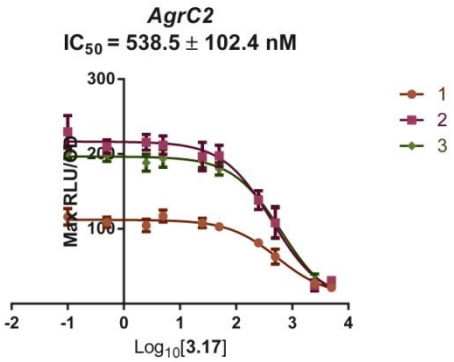

AgrC2
IC50 = 590.4 ± 114.7 nM
Max RLU/OD
Log10[3.24]
1
2
3


AgrC2
IC50 = 137.0 ± 58.7 nM
Max RLU/OD
Log10[3.25]
1
2
3

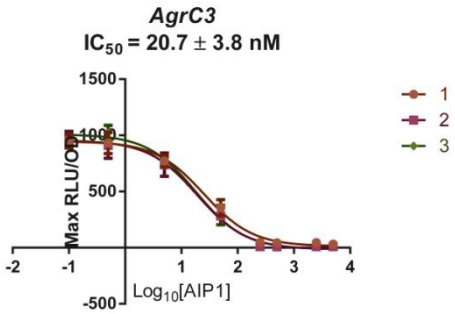

AgrC2
IC50 > 2 µM
Max RLU/OD
Log10[3.13]

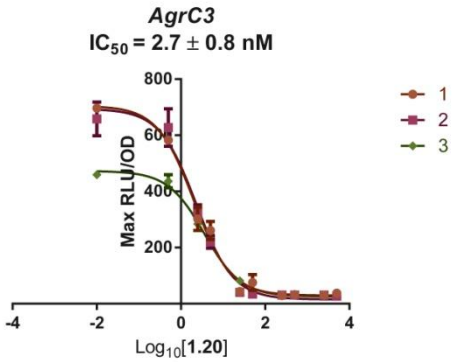

AgrC2
IC50 > 2 μM
Max RLU/OD
Log10[3.12]

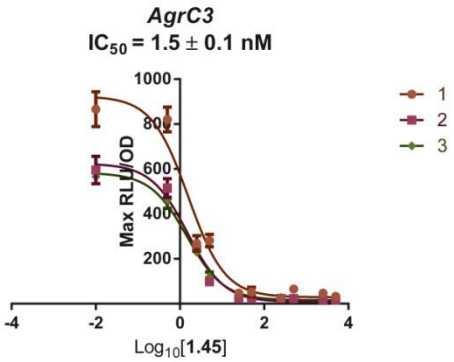

AgrC2
No significant activity
Max RLU/OD
Log10[1.56]

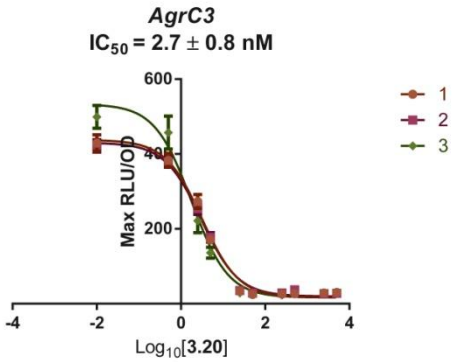

AgrC2
IC50 = 538.5 ± 102.4 nM
Max RLU/OD
Log10[3.17]
1
2
3

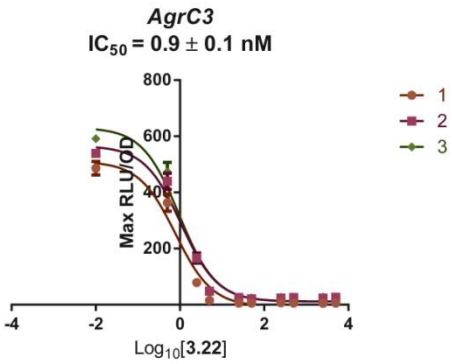
8.2.5.4 AgrC3

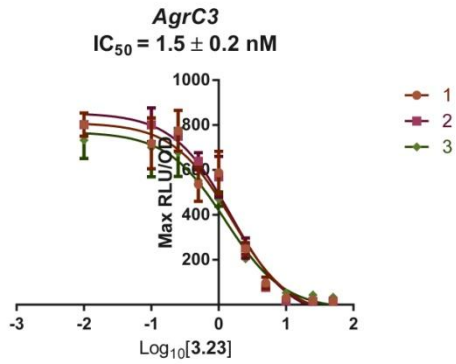

AgrC3
IC50 = 20.7 ± 3.8 nM
Max RLU/OD
Log10[AIP1]
1
2
3

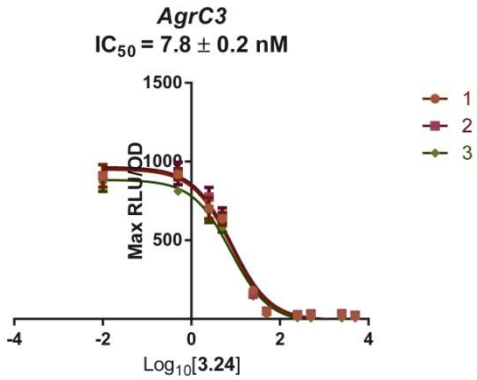

AgrC3
IC50 = 2.7 ± 0.8 nM
Max RLU/OD
Log10[1.20]
1
2
3

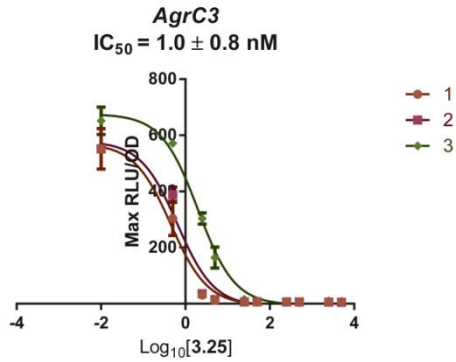

AgrC3
IC50 = 1.5 ± 0.1 nM
Max RLU/OD
Log10[1.45]
1
2
3

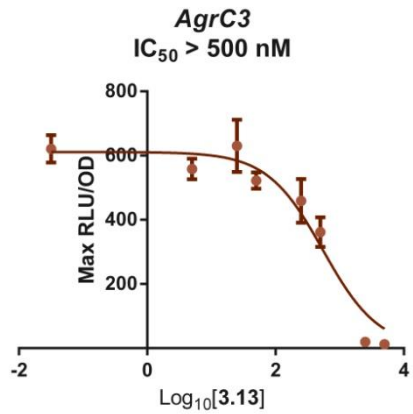

AgrC3
IC50 = 2.7 ± 0.8 nM
Max RLU/OD
Log10[3.20]
1
2
3

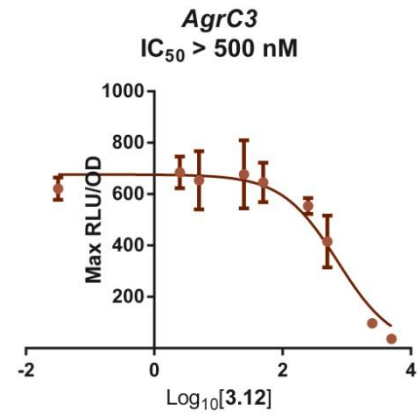

AgrC3
IC50 = 0.9 ± 0.1 nM
Max RLU/OD
Log10[3.22]
1
2
3

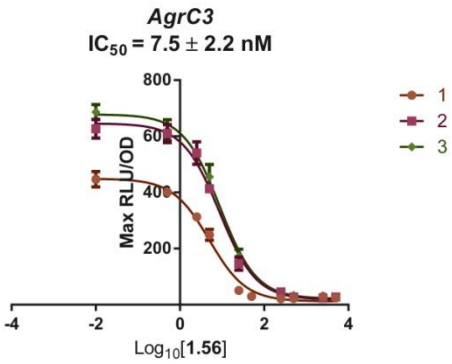

AgrC3
IC50 = 1.5 ± 0.2 nM
Max RLU/OD
Log10[3.23]
1
2
3

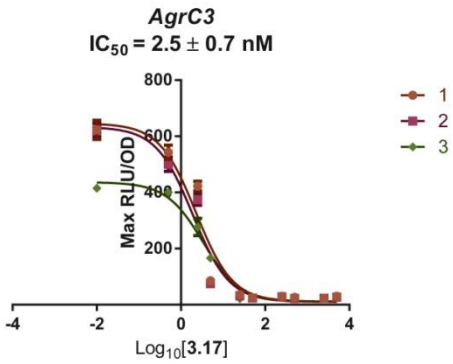

AgrC3
IC50 = 7.8 ± 0.2 nM
Max RLU/OD
Log10[3.24]
1
2
3


AgrC3
IC50 = 1.0 ± 0.8 nM
Max RLU/OD
Log10[3.25]
1
2
3

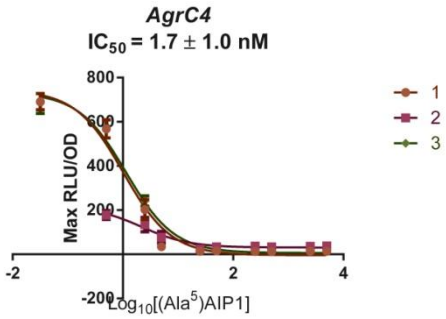

AgrC3
IC50 > 500 nM
Max RLU/OD
Log10[3.13]

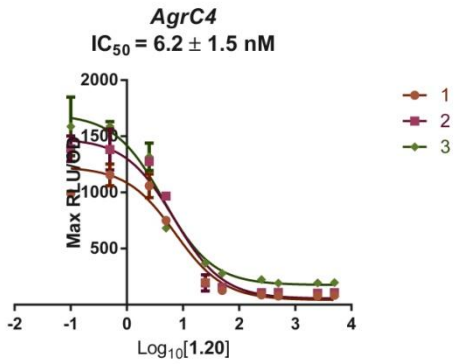

AgrC3
IC50 > 500 nM
Max RLU/OD
Log10[3.12]

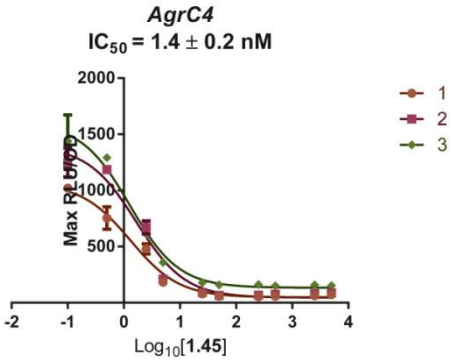

AgrC3
IC50 = 7.5 ± 2.2 nM
Max RLU/OD
Log10[1.56]
1
2
3

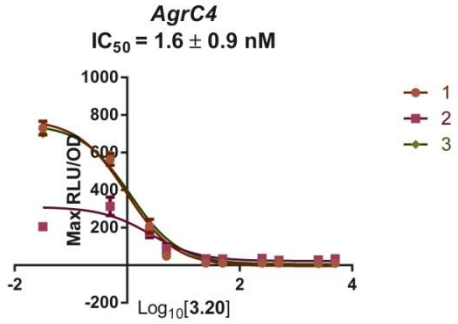

AgrC3
IC50 = 2.5 ± 0.7 nM
Max RLU/OD
Log10[3.17]
1
2
3

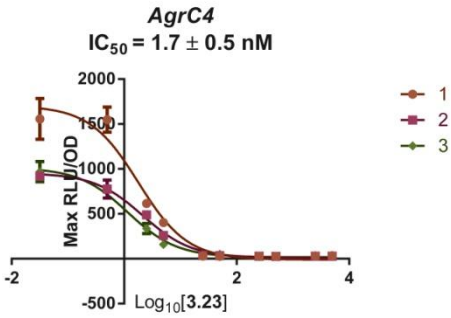
8.2.5.5 AgrC4

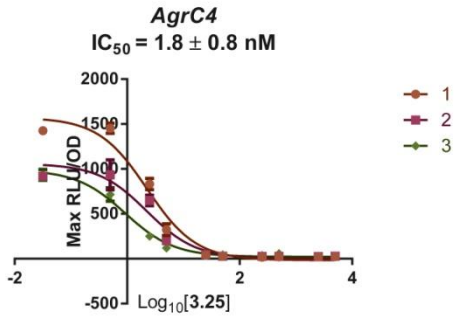

AgrC4
IC50 = 1.7 ± 1.0 nM
Max RLU/OD
Log10[(Ala5)AIP1]
1
2
3

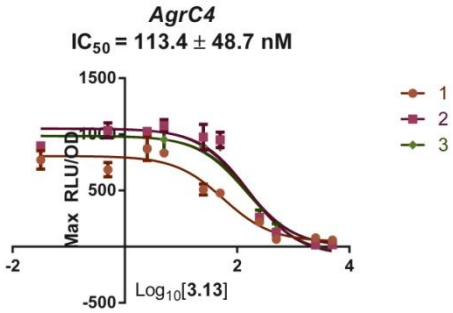

AgrC4
IC50 = 6.2 ± 1.5 nM
Max RLU/OD
Log10[1.20]
1
2
3

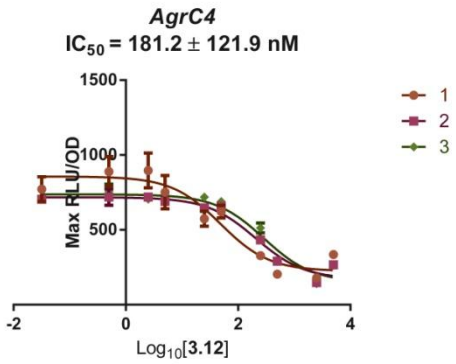

AgrC4
IC50 = 1.4 ± 0.2 nM
Max RLU/OD
Log10[1.45]
1
2
3

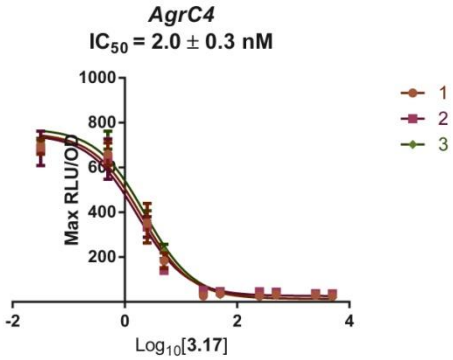

AgrC4
IC50 = 1.6 ± 0.9 nM
Max RLU/OD
Log10[3.20]
1
2
3


AgrC4
IC50 = 1.7 ± 0.5 nM
Max RLU/OD
Log10[3.23]
1
2
3

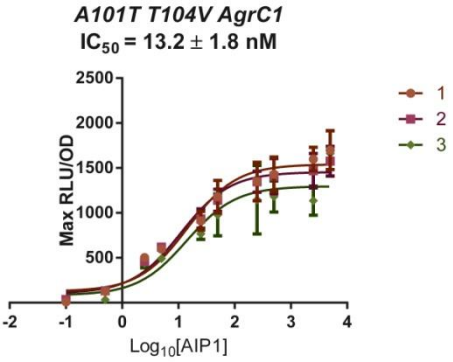

AgrC4
IC50 = 1.8 ± 0.8 nM
Max RLU/OD
Log10[3.25]
1
2
3

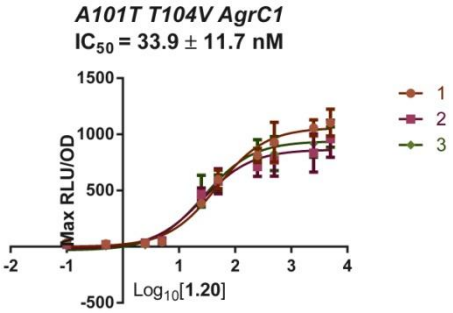


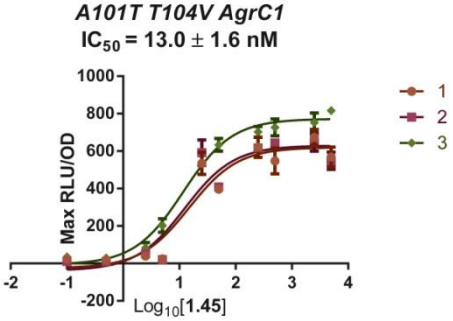


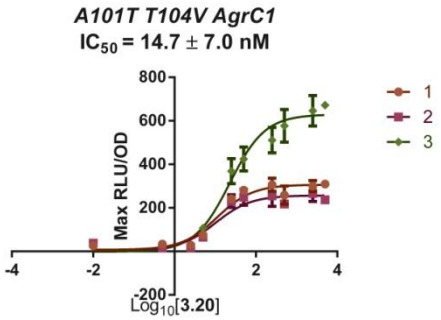


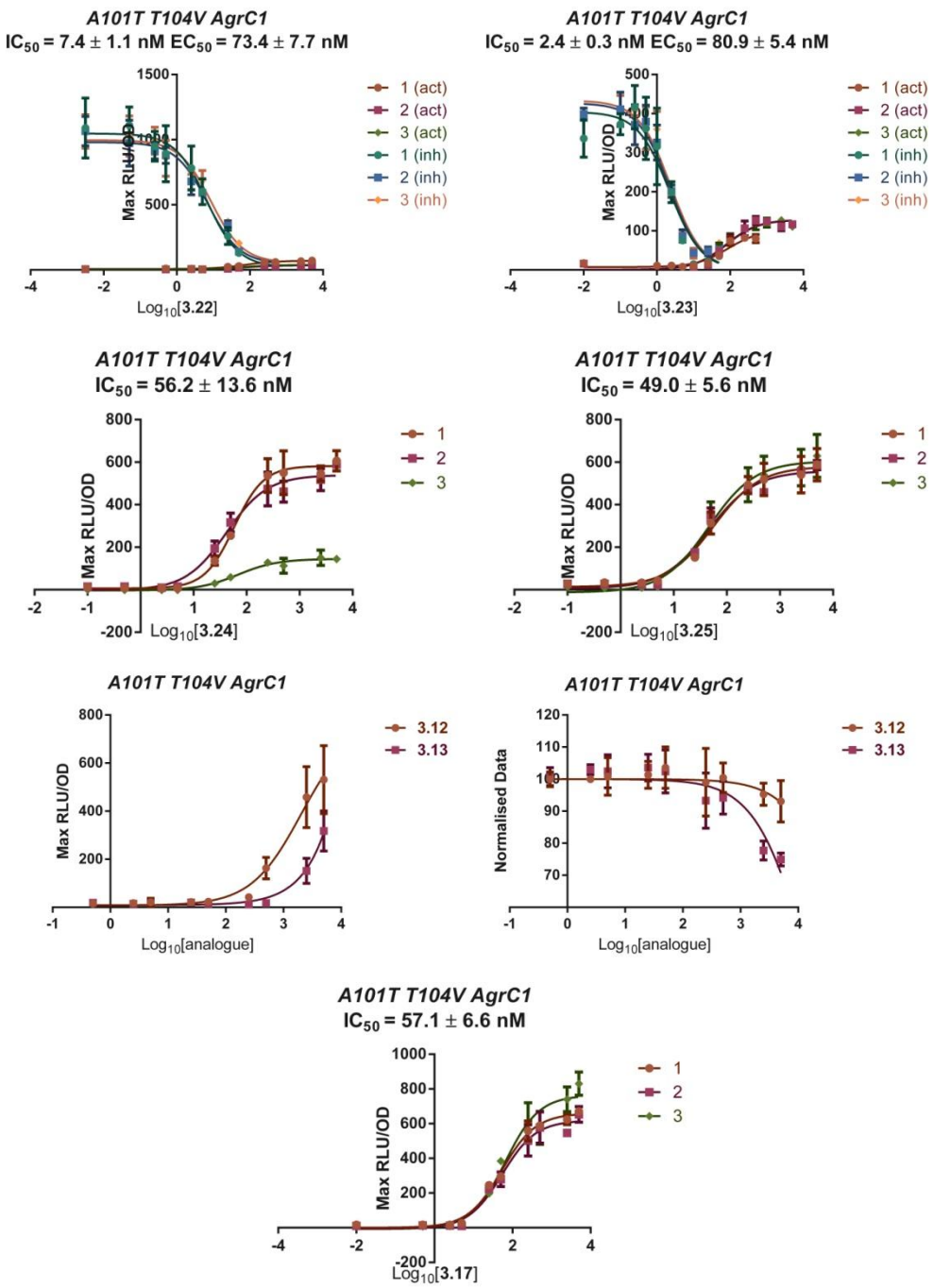
8.2.5.6 A101T, T104V AgrC1



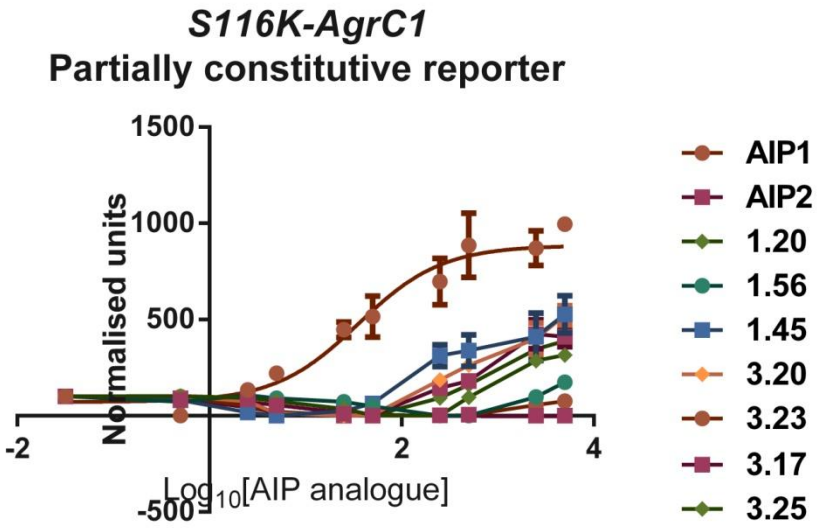








8.2.5.7 S116K AgrC1


S116K-AgrC1
Partially constitutive reporter
Normalised units
1500
1000
500
-500
-2
2
4
Log10[AIP analogue]
AIP1
AIP2
1.20
1.56
1.45
3.20
3.23
3.17
3.25

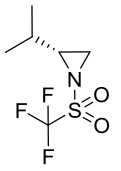
8.3 Total synthesis of the solonamides

8.3.1 Standard UV Fmoc quantification

Loaded resin (10 mg) was stirred with 20% piperidine in DMF (3 mL) for 2 hours. Supernatant (150 µL) was transferred to a quartz cuvette with further 20% piperidine in DMF (2.85 mL). A reference cuvette containing 20% piperidine in DMF (3 mL) was used to tare the UV spectrophotometer. Absorbance measured at 290 nm and used to calculate the resin loading.

8.3.2 Synthesis of triamine ligand

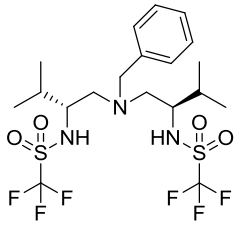
(*R*)-*N*-Triflouromethylsulfonyl-2-isopropylaziridine (**1.67**)



A mixture of *D*-valinol (**1.66**, 1.11 g, 10.8 mmol) and triethylamine (3.01 mL, 21.6 mmol) in dry $CHCl_3$ (25 mL) was cooled to -78 ^oC. Triflyl anhydride was added (1 M in $CHCl_3$, 23.8 mL) dropwise over 20 mins. The reaction mixture was maintained at -78 ^oC and stirred overnight. The cold solution was diluted with cold $CHCl_3$ (25 mL) and was washed sequentially with cold 10% citric acid (2x25 mL), cold sat. $NaHCO_3$ (2x25 mL), and brine (1x25 mL). The organic phase was dried with Na_2SO_4, filtered and the solvent removed *in vacuo* to afford a volatile brown oil (2.29 g, 97.7%) with a yield of 82% when adjusted for remaining solvent quantified by ^1H-NMR. The product was used in the next reaction without further purification as it has low stability.

Aziridine (**1.67**) ^1H-NMR (400 MHz, $CDCl_3$) δ 2.88 (td, *J* = 6.8 Hz, 5.1 Hz, 1H), 2.83 (d, *J* = 7.0 Hz, 1H), 2.44 (d, *J* = 5.1 Hz, 1H), 1.63 (m, 1H), 1.03 (d, *J* = 7.3 Hz, 3H), 1.01 (d, *J* = 6.8 Hz, 3H).

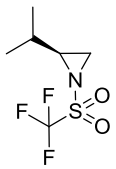
(2*R*,6*R*)-4-Benzyl-1,7-bis(triflouromethylsulfonyl)-2,6-diisopropyl-1,4,7-triazaheptane (**1.68**)



To a stirred solution of benzylamine (419 μL, 3.84 mmol) in MeOH (25 mL) was added aziridine **1.67** (1 g, 4.61 mmol). The reaction mixture was heated to reflux under nitrogen. After 4 hours, further aziridine (1 g, 4.61 mmol) was added and the solution was refluxed under nitrogen for 3 days. The solvent was evaporated *in vacuo* and the residue was separated by column chromatography (1:9 EtOAc/Hex) to give 1.90 g of pale yellow oily solid (91.3% yield). This was further purified by trituration with hexane (5 mL) yielding 1.22 g of the product **1.68** as a fine white powder (58.5% yield).

Triamine ligand (**1.68**) TLC R_f = 0.85 (3:1 EtOAc/Hex); mp 105-106 °C; MS^+ (ES-TOF): m/z calcd: 542.15372 $[M+H]^+$; found: 542.1494; $[\alpha]_D^{20}$ = +58.1 ° (c 1.6, MeOH); ^{1}H-NMR (400 MHz, $CDCl_3$) δ 7.43-7.23 (m, 5H, ArH), 5.53-5.17 (br s, 2H, NH), 3.94 (d, *J* = 12.9 Hz, 1H, Ar-C**H$_2$**-N), 3.64-3.54 (m, 2H, C**H**CH$(CH_3)_2$), 3.41 (d, *J* = 13.4 Hz, 1H, Ar-C**H$_2$**-N), 2.67 (dd, *J* = 11.7 Hz, 8.3 Hz, 2H, R_2NC**H$_2$**CH), 2.51 (dd, *J* = 13.4 Hz, 4.2 Hz, 2H, R_2NC**H$_2$**CH), 2.03-1.90 (m, 2H, C**H**$(CH_3)_2$), 0.87 (d, *J* = 6.7 Hz, 6H, CH(C**H$_3$**$)_2$), 0.83 (d, *J* = 7.1 Hz, 6H, CH(C**H$_3$**$)_2$); ^{13}C-NMR (100 MHz, $CDCl_3$) δ 137.2, 129.8, 128.9, 127.9, 119.5 (J_{CF} = 321 Hz), 58.78, 58.74, 55.6, 30.0, 18.2, 17.5.

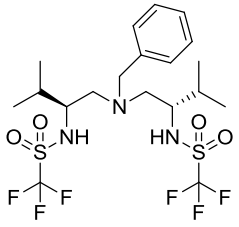
(*S*)-*N*-Triflouromethylsulfonyl-2-isopropylaziridine (**1.67*S***)[349]



Procedure as for **1.67** above. The reaction yielded 3.24 g of the title compound (93% yield) as a pale yellow oil. The product was used in the next reaction without further purification as it has low stability.

Aziridine (**1.67*S***) ^{1}H-NMR (400 MHz, $CDCl_3$) δ 2.90 (td, *J* = 6.9 Hz, 4.9 Hz, 1H), 2.85 (d, *J* = 7.2 Hz, 1H), 2.45 (d, *J* = 4.9 Hz, 1H), 1.64 (m, 1H), 1.05 (d, *J* = 6.8 Hz, 3H), 1.02 (d, *J* = 6.9 Hz, 3H). Consistent with literature.[349]

(2*S*,6*S*)-4-Benzyl-1,7-bis(triflouromethylsulfonyl)-2,6-diisopropyl-1,4,7-triazaheptane (**1.68*S***)[349]

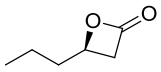


Procedure as for **1.68** above. The reaction yielded 1.54 g of the title compound (**1.68*S*** - 72% yield) as a white powder.

Triamine Ligand (**1.68*S***) TLC R_f = 0.84 (3:1 EtOAc/Hex); mp 104-106 °C; MS^+ (ES-TOF): m/z calcd: 542.15372 $[M+H]^+$; found: 542.1936; $[\alpha]_D^{20}$ = +58.3 ° (c 1.6, MeOH); ^{1}H-NMR (400 MHz, $CDCl_3$) δ 7.38-7.25 (m, 5H, ArH), 5.88-4.83 (br s, 2H, NH), 3.91 (d, *J* = 13.2 Hz, 1H, Ar-C**H$_2$**-N), 3.63-3.55 (m, 2H, C**H**CH$(CH_3)_2$), 3.42 (d, *J* = 13.2 Hz, 1H, Ar-C**H$_2$**-N), 2.66 (dd, *J* = 13.4 Hz, 8.3 Hz, 2H, R_2NC**H$_2$**CH), 2.51 (dd, *J* = 13.6 Hz, 5.6 Hz, 2H, R_2NC**H$_2$**CH), 2.05-1.91 (m, 2H, C**H**$(CH_3)_2$), 0.88 (d, *J* = 6.7 Hz, 6H, CH(C**H$_3$**)$_2$), 0.82 (d, *J* = 7.2 Hz, 6H, CH(C**H$_3$**)$_2$); ^{13}C-NMR (100 MHz, $CDCl_3$) δ 137.1, 129.7, 128.6, 127.7, 119.5 (J_{CF} = 321 Hz), 58.64, 58.58, 55.4, 29.8, 18.1, 17.3. Consistent with literature.[349]

8.3.3 Stereoselective synthesis of β-hydroxy acids

(4*R*)-4-(2-propyl)-oxetan-2-one (**1.69**)[374]

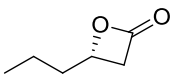


To a stirred solution of triamine **1.68** (1.00 g, 1.85 mmol) in dry $CHCl_3$ (30 mL) under nitrogen was added trimethylaluminium (1 M in heptane, 1.85 mL) (CAUTION: methane gas evolution). The reaction mixture was stirred for 2 hours at room temperature before being cooled to -78 °C. Diisopropylethylamine (5.5 mL, 31.57 mmol) was added followed by acetyl

bromide (2.6 mL, 35.10 mmol) which was added dropwise over 20 mins. Butanal (1.7 mL, 18.50 mmol) was then added slowly and the mixture was allowed to stir overnight at -78 ^{o}C. The reaction mixture was diluted with cold $CHCl_3$ (20 mL)and was washed consecutively with 10% citric acid (2x50 mL), sat. $NaHCO_3$ solution (2x50 mL), and brine (1x50 mL). After each washing, the aqueous phase was extracted with a single portion of Et_2O (50 mL). Once washing was complete, the organic and ethereal extract were combined, dried with Na_2SO_4, and evaporated *in vacuo* (room temperature, low vacuum). The residue was purified by column chromatography (1:9 EtOAc/Hex) yielding 1.72 g of a colourless oil (81.5% yield).

R-propyloxetan-2-one (**1.69**) TLC R_f= 0.35 (1:4 EtOAc/Hex); ^{1}H-NMR (400 MHz, $CDCl_3$) δ 4.54-4.46 (m, 1H, $C_\beta H$), 3.50 (dd, *J* = 16.2 Hz, 5.8 Hz, 1H, $C_\alpha H$), 3.04 (dd, *J* = 16.2 Hz, 4.4 Hz, 1H, $C_\alpha H$), 1.90-1.78 (m, 1H, $C_\gamma H$), 1.76-1.66 (m, 1H, $C_\gamma H$), 1.55-1.33 (m, 2H, $C_\delta H$), 0.96 (t, *J* = 7.4 Hz, 3H, $C_\varepsilon H$); ^{13}C-NMR (100 MHz, $CDCl_3$) δ 168.4, 71.1, 42.9, 36.7, 18.3, 13.7. Consistent with literature.[374]

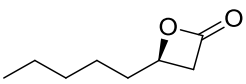
(4*S*)-4-(2-propyl)-oxetan-2-one (**1.69*S***)



Procedure as for **1.69** above. The reaction yielded 1.03 g of the title compound (**1.69*S*** - 69% yield) as a colourless oil.

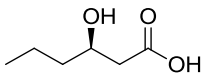
S-propyloxetan-2-one (**1.69*S***) TLC R_f= 0.36 (1:4 EtOAc/Hex); ^{1}H-NMR (400 MHz, $CDCl_3$) δ 4.56-4.46 (m, 1H, $C_\beta H$), 3.50 (dd, *J* = 16.3, 5.8 Hz, 1H, $C_\alpha H$), 3.05 (dd, *J* = 16.3 Hz, 4.3 Hz, 1H, $C_\alpha H$), 1.91-1.80 (m, 1H, $C_\gamma H$), 1.77-1.67 (m, 1H, $C_\gamma H$), 1.55-1.37 (m, 2H, $C_\delta H$), 0.98 (t, *J* = 7.4 Hz, 3H, $C_\varepsilon H$); ^{13}C-NMR (100 MHz, $CDCl_3$) δ 168.5, 71.3, 43.0, 36.8, 18.4, 13.8.

(4*R*)-4-(2-pentyl)-oxetan-2-one (**4.35**)[375]



R-pentoxetan-2-one (**4.35**) Procedure as for **1.69** above. Produced colourless oil (1.30 g, 68.0% yield). TLC R_f= 0.296 (1:9 EtOAc/Hex); ^{1}H-NMR (400 MHz, $CDCl_3$) δ 4.54-4.44 (m, 1H, $C_\beta H$), 3.48 (dd, *J* = 16.3 Hz, 5.8 Hz, 1H, $C_\alpha H$), 3.03 (dd, *J* = 16.3 Hz, 4.2 Hz, 1H, $C_\alpha H$), 1.90-1.78 (m, 1H, $C_\gamma H$), 1.76-1.65 (m, 1H, $C_\gamma H$), 1.47-1.19 (m, 6H, $C_\delta H$, $C_\varepsilon H$, $C_\zeta H$), 0.87 (t, *J* = 6.8 Hz, 3H, $C_\eta H$); ^{13}C-NMR (100 MHz, $CDCl_3$) δ 163.57, 71.47, 42.97, 34.74, 31.40, 24.67, 22.55, 13.99. Consistent with literature.[375]

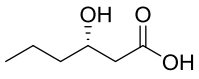
(*R*)-3-hydroxyhexanoic acid (**1.60**)[376]



Cyclic lactone (**1.69**, 163 mg, 1.4 mmol) was dissolved in THF (3 mL) and LiOH (1 M, 3 mL) was added. The reaction was stirred for 2 hours and then blown with nitrogen to remove THF. The mixture was diluted with brine (10 mL) and acidified with sat. $KHSO_4$ (10 mL). The product was extracted with EtOAc (20 mLx2), dried with Na_2SO_4, filtered and evaporated to furnish a pale yellow oil (190.5 mg, quantitative yield).

3-*R*-OH-Hex Acid (**1.60**) TLC R_f= 0.33 (1:1 EtOAc/Hex); MS$^-$ (ES-TOF): m/z calcd: 131.07137 [M-H]$^-$; found: 131.0747; $[\alpha]_D^{20}$ = -2.2 ^{o} (c 3, MeOH); ^{1}H-NMR (400 MHz, $CDCl_3$) δ 4.07-3.97 (m, 1H, $C_\beta H$), 2.49 (dd, *J* = 16.1 Hz, 3.5 Hz, 1H, $C_\alpha H$), 2.41 (dd, *J* = 16.3 Hz, 8.8 Hz, 1H, $C_\alpha H$), 1.61-1.25 (m, 4H, $C_\gamma H$, $C_\delta H$), 0.88 (t, *J* = 6.8 Hz, 3H, $C_\varepsilon H$); ^{13}C-NMR (100 MHz, $CDCl_3$) δ 177.2, 68.1, 41.3, 38.6, 18.7, 14.0. Consistent with literature.[376]

(*S*)-3-hydroxyhexanoic acid (**1.60*S***)[376]

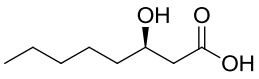


Procedure as for **1.60** above. The reaction yielded 0.50 g of the title compound (98% yield) as a colourless oil.

3-*S*-OH-Hex Acid (**1.60*S***) TLC R_f= 0.31 (1:1 EtOAc/Hex); MS$^-$ (ES-TOF): m/z calcd: 131.07137 [M-H]$^-$; found: 130.4014; $[\alpha]_D^{20}$ = +2.2 ^{o} (c 3, MeOH); ^{1}H-NMR

(400 MHz, $CDCl_3$) δ 4.08-4.01 (m, 1H, $C_\beta H$), 2.57 (dd, *J* = 16.5 Hz, 3.2 Hz, 1H, $C_\alpha H$), 2.47 (dd, *J* = 16.5 Hz, 8.9 Hz, 1H, $C_\alpha H$), 1.59-1.31 (m, 4H, $C_\gamma H$, $C_\delta H$), 0.94 (t, *J* = 7.1 Hz, 3H, $C_\varepsilon H$); ^{13}C-NMR (100 MHz, $CDCl_3$) δ 177.8, 67.9, 41.2, 38.7, 18.8, 14.0. Consistent with literature.[376]

(*R*)-3-hydroxyoctanoic acid (**4.10**)[318]

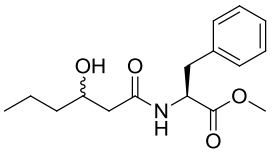


Cyclic lactone (**4.35**, 73 mg, 0.5 mmol) was treated using the procedure for **1.60** above. Produced a colourless oil (90 mg, quantitative yield).

3-*R*-OH-Oct Acid (**4.10**) TLC R_f= 0.19 (30:70 EtOAc/Hex); $[\alpha]_D^{20}$ = +32.0 ^{o} (c 3, MeOH); ^{1}H-NMR (400 MHz, $CDCl_3$) δ 4.02-3.94 (m, 1H, $C_\beta H$), 2.46 (dd, *J* = 15.6 Hz, 4.7Hz, 1H, $C_\alpha H$), 2.38 (dd, *J* = 15.5Hz, 8.1Hz, 1H, $C_\alpha H$), 1.52-1.23 (m, 8H, $C_\gamma H$, $C_\delta H$, $C_\varepsilon H$, $C_\zeta H$), 0.86 (t, *J* = 6.9 Hz, 3H, $C_\eta H$); ^{13}C-NMR (100 MHz, $CDCl_3$) δ 177.62, 68.28, 41.23, 36.55, 31.77, 25.23, 22.68, 14.11. Consistent with literature.[318]

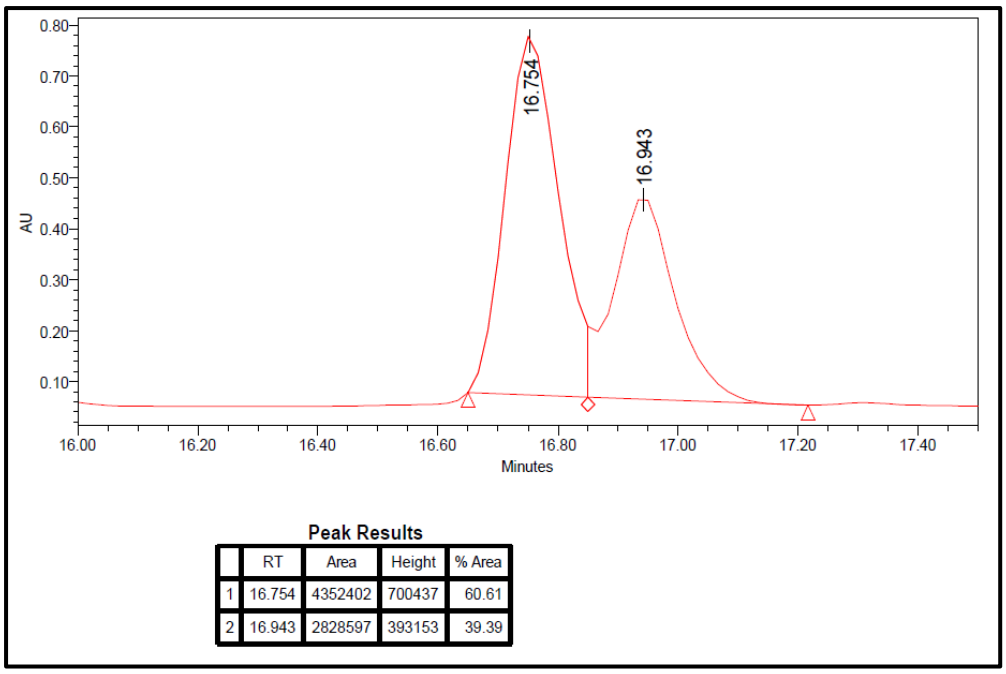
8.3.4 Derivatisation to determine ee

(*S*)-methyl 2-(3-hydroxyhexanamido)-3-phenylpropanoate (Mixture of **4.36** and **4.37**)



L-Phenylalanine methylester hydrochloride (103 mg, 0.58 mmol) was dissolved in sat. $NaHCO_3$ (10 mL) and extracted into EtOAc (30 mL). The organic portion was washed with brine, dried with Na_2SO_4, filtered and evaporated *in vacuo*. The residue was then redissolved in $CHCl_3$ (10 mL). Commercially available 3-hydroxyhexanoic acid (38 mg, 0.29 mmol) was dissolved in $CHCl_3$ (5 mL) and *N*-hydroxysuccinimide (HOSu, 46 mg, 0.38 mmol) and diisopropylcarbodiimide (DIC, 65 µL, 0.42 mmol) was added to the stirred solution. The *L*-phenylalanine methylester solution was then added to the reaction vessel and allowed to stir at room temperature overnight. The $CHCl_3$

was evaporated and the residue was redissolved with MeCN (1 mL) and a portion (100 μL) was analysed by HPLC for comparison with the enantiomerically enriched derivatisation of **1.56** and **1.56*S*** (below).

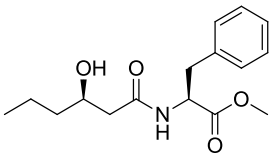


Peak Results

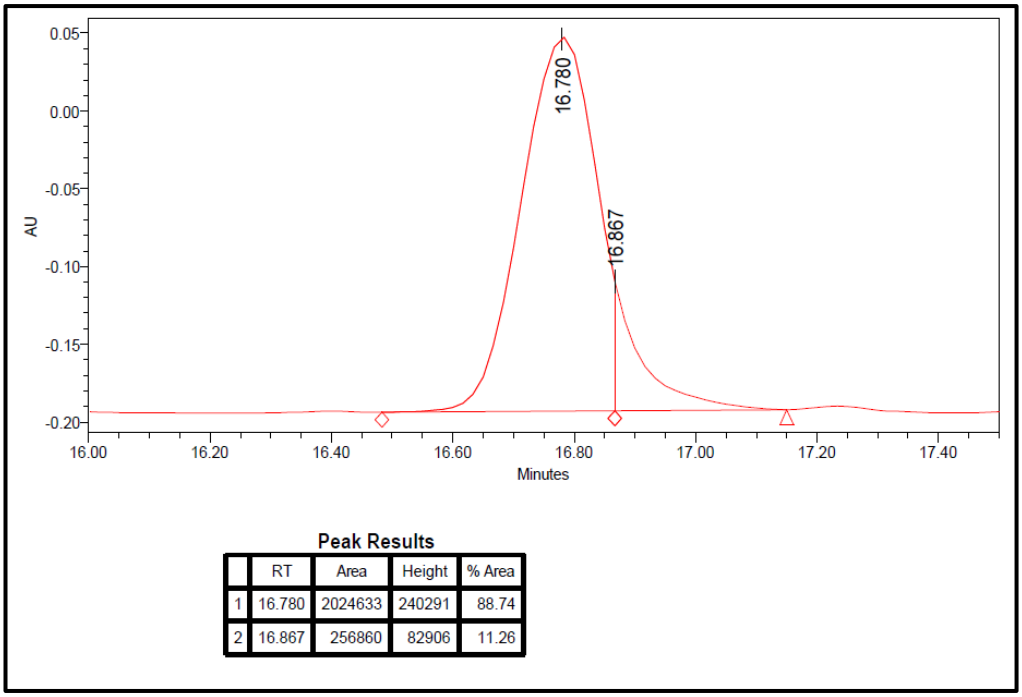
	RT	Area	Height	% Area
1	16.754	4352402	700437	60.61
2	16.943	2828597	393153	39.39

Figure 211: 3-(*R*/*S*)-hydroxy hexanoic acid was coupled to phenylalanine methyl ester using DIC and HOSu in $CHCl_3$. Analytical HPLC (20% B for 2 mins to 80% B over 20 mins) of the product showed good separation of enantiomers.

(*S*)-methyl 2-((*R*)-3-hydroxyhexanamido)-3-phenylpropanoate (**4.36**)



L-Phenylalanine methylester hydrochloride was prepared as above. Enantiomerically enriched compound **1.60** (38 mg, 0.29 mmol) was treated as the 3-hydroxyhexanoic acid above. The $CHCl_3$ was evaporated and the residue was redissolved with MeCN (1 mL) and a portion (100 µL) was analysed by HPLC and compared with the HPLC trace of the derivatised commercial 3-hydroxyhexanoic acid (above) to prove an enantiomeric excess of the (*R*) isomer in the original compound (**1.60**, *ee* ≈ 77%).

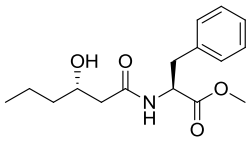


Peak Results

	RT	Area	Height	% Area
1	16.780	2024633	240291	88.74
2	16.867	256860	82906	11.26

Figure 212: 3-(*R*)-hydroxy hexanoic acid (**1.60**) was coupled to phenylalanine methyl ester using DIC and HOSu in $CHCl_3$. Analytical HPLC (20% B for 2 mins to 80% B over 20 mins) of the product (**4.36**) showed a high enantiomeric excess of the desired *R*-enantiomer.

(*S*)-methyl 2-((*S*)-3-hydroxyhexanamido)-3-phenylpropanoate (**4.37**)



L-Phenylalanine methylester hydrochloride was prepared as above. Enantiomerically enriched compound **1.60*S*** (29 mg, 0.25 mmol) was treated as the 3-hydroxyhexanoic acid above. The $CHCl_3$ was evaporated and the residue was redissolved with MeCN (1 mL) and a portion (100 µL) was analysed by HPLC and compared with the HPLC trace of the derivatised commercial 3-hydroxyhexanoic acid (above) to prove an enantiomeric excess of the (*S*) isomer in the original compound (**1.60*S***, ee ≈ 88%).

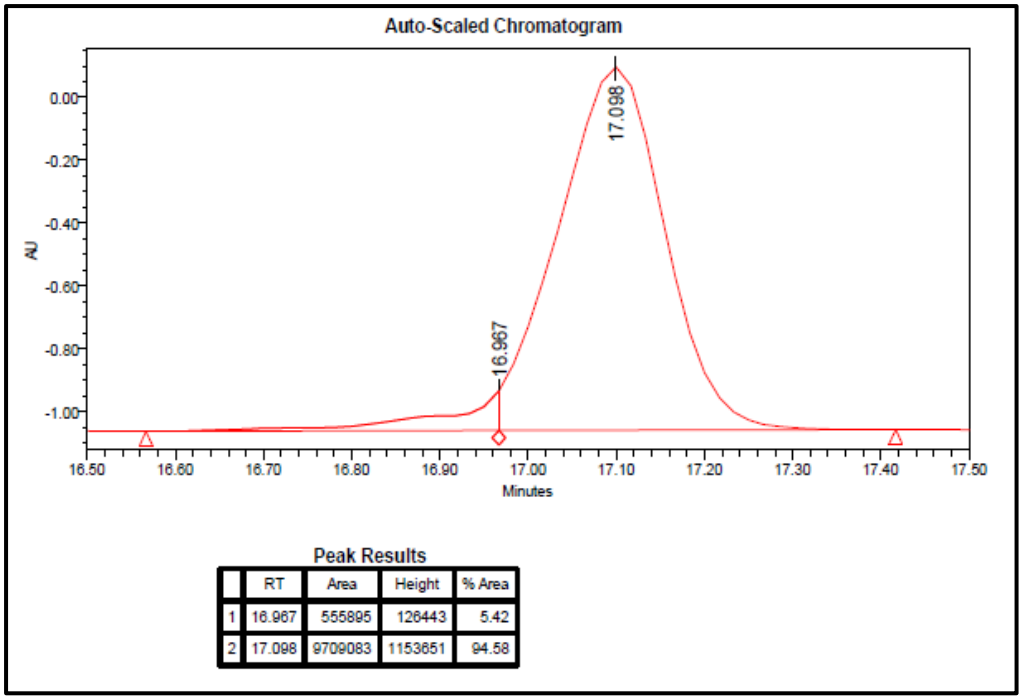
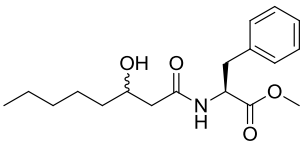
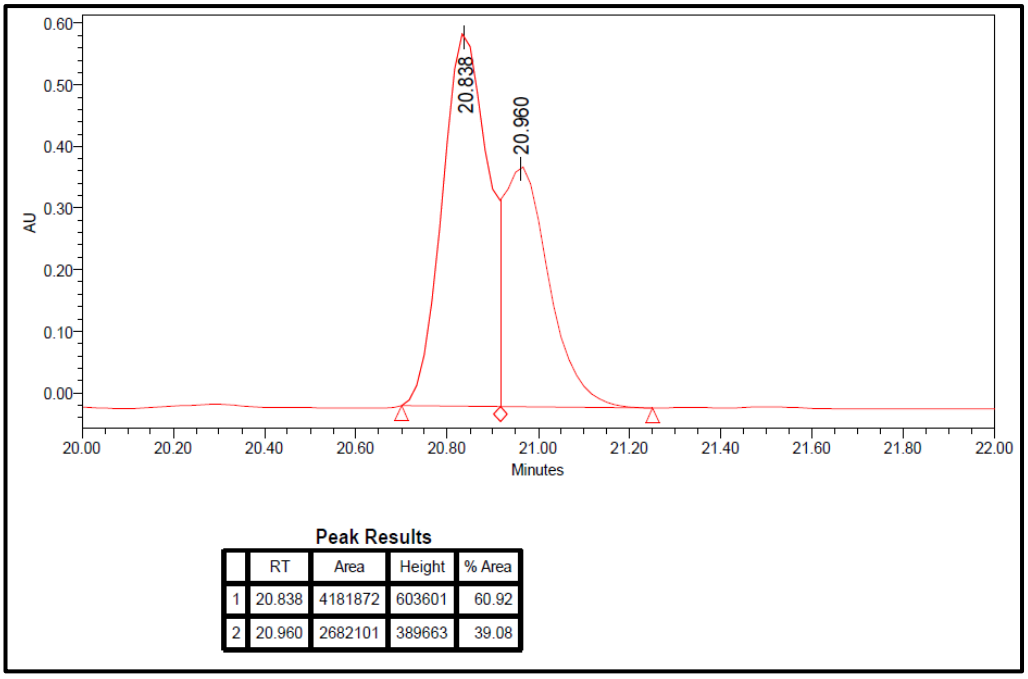


Figure 213: 3-(*S*)-hydroxy hexanoic acid (**1.60*S***) was coupled to phenylalanine methyl ester using DIC and HOSu in $CHCl_3$. Analytical HPLC (20% B for 2 mins to 80% B over 20 mins) of the product (**4.37**) showed a high enantiomeric excess of the desired *S*-enantiomer.

(*S*)-methyl 2-(3-hydroxyoctanamido)-3-phenylpropanoate



Commercially available 3-hydroxyoctanoic acid (59 mg, 0.35 mmol) was derivatised using the same procedure as for 3-hydroxyhexanoic acid above. Analytical HPLC was used for comparison with the enantiomerically enriched derivatisation of compound **4.10** (below).

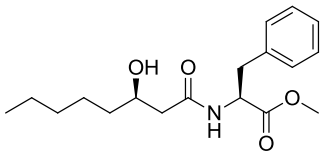


Peak Results

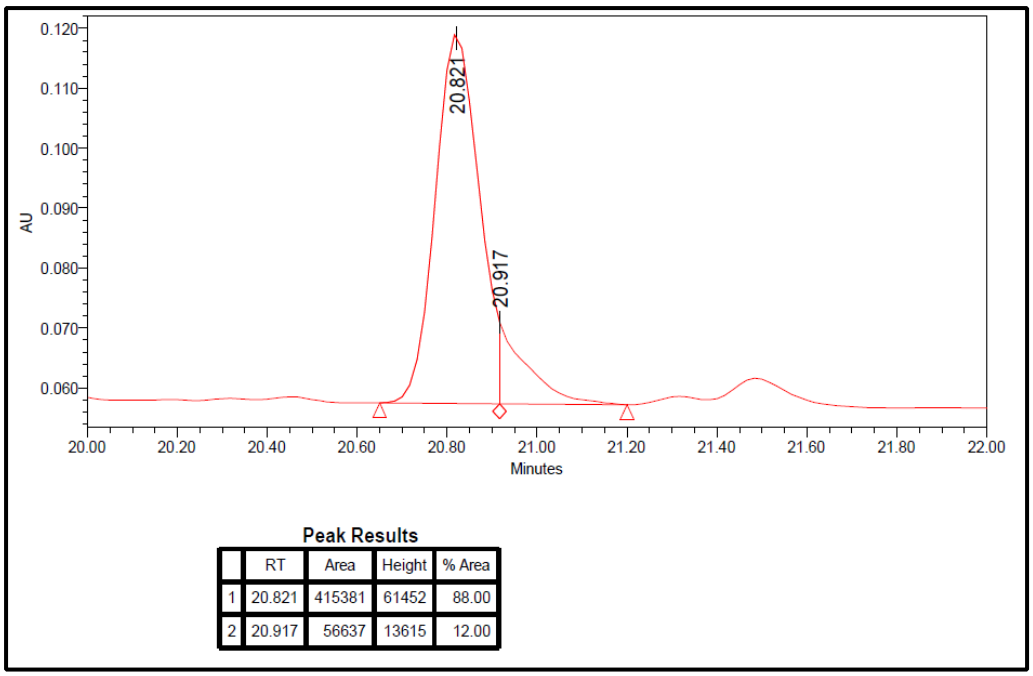
	RT	Area	Height	% Area
1	20.838	4181872	603601	60.92
2	20.960	2682101	389663	39.08

Figure 214: 3-(*R*/*S*)-hydroxy octanoic acid was coupled to phenylalanine methyl ester using DIC and HOSu in $CHCl_3$. Analytical HPLC (20% B for 2 mins to 80% B over 20 mins) of the product showed good separation of enantiomers.

(*S*)-methyl 2-((*R*)-3-hydroxyoctanamido)-3-phenylpropanoate



Compound **4.10** (66 mg, 0.41 mmol) was derivatised using the same procedure as for compound **1.60** above. Analytical HPLC was compared with the HPLC trace of the derivatised commercial 3-hydroxyoctanoic acid (above) to prove an enantiomeric excess of the (*R*) isomer in the original compound (**4.10**, *ee* ≈ 76.0%).



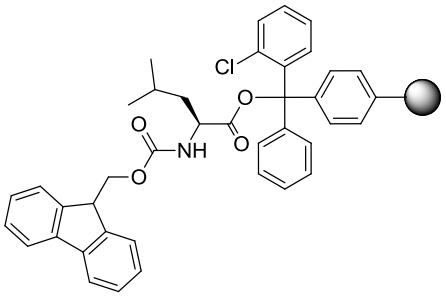
Peak Results

	RT	Area	Height	% Area
1	20.821	415381	61452	88.00
2	20.917	56637	13615	12.00

Figure 215: 3-(*R*)-hydroxy octanoic acid (**4.10**) was coupled to phenylalanine methyl ester using DIC and HOSu in $CHCl_3$. Analytical HPLC (20% B for 2 mins to 80% B over 20 mins) of the product showed a high enantiomeric excess of the desired *R*-enantiomer.

8.3.5 Preparation of Fmoc-Leu-2ClTrt Resin

Fmoc-Leucine 2-chlorotrityl-resin (**1.61**)

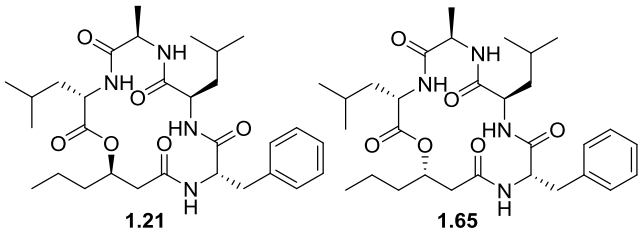


2-Chlorotritylchloride resin (100-200 mesh), 1% DVB (**4.31**, 0.6605 g, loading=1.22 mmol/g) (Merck Chemicals Ltd. Lot S6264017 127) was swelled in dry $CHCl_3$ (2 mL) overnight prior to the addition of 1.2 eq. of Fmoc-Leu-OH (0.3393 g, 0.96 mmol), and 2 eq. of DIPEA (278.8 µL, 1.6 mmol). The resulting suspension was stirred at room temperature for 3 hours. An excess of MeOH (1.5 mL) and DIPEA (250 µL) was then added. After a further 15 mins of gentle stirring, the resin was filtered and washed with DMF (2×5 mL), $CHCl_3$ (2×5 mL), and hexane (2×5 mL). The resin was dried overnight under high vacuum and

standard UV Fmoc quantification revealed a resin loading of 0.89 mmol/g (loading = 100%).

8.3.6 Initial synthesis of solonamide depsipeptides

General Method A - Solonamide A and epimer Solonamide A (SolA, **1.21**, and epiSolA, **1.65**)[214]



Fmoc-Leu-2-Chlorotritylchloride resin (**1.61**, 227.8 mg, 0.2 mmol, loading = 0.89 mmol/g) was placed in an Omnifit™ BenchMark™ column assembly and swelled with 1:1 DMF/$CHCl_3$ (2.5 mL) overnight. Utilising a NovaSyn® manual peptide synthesizer (flow rate: 2.8 mL/min), the resin was washed with DMF, Fmoc-deprotection was achieved using a flow of 20% piperidine in DMF, and a further DMF wash was effected. The column was drained and a solution of Fmoc-D-Ala-OH (251.0 mg, 0.8 mmol), PyOxim (423.6 mg, 0.8 mmol), and DIPEA (279 µL, 1.6 mmol) in DMF (2 mL) was added. The column was intermittently agitated at room temperature for 3.5 hours after which the resin was washed (DMF 2.8 mL/min), Fmoc-deprotected (20% piperidine in DMF, 2.8 mL/min), and washed (DMF 2.8 mL/min). The linear peptide sequence was prepared *via* subsequent rounds of acylation (as expanded above) utilising Fmoc-D-Leu-OH (283.8 mg, 0.8 mmol) and then Fmoc-Phe-OH (315.5 mg, 0.8 mmol). Each acylation was achieved using a solution of 4.0 eq. PyOxim (422 mg, 0.8 mmol) and 8.0 eq. DIPEA (279 µL, 1.6 mmol) in DMF (2 mL) at room temperature over 3 hours followed by a wash-deprotection-wash cycle. A final coupling was achieved with 3-hydroxy-hexanoic acid (commercial racemic mixture, 106 mg, 0.8 mmol), DIC (141 µL, 0.9 mmol), and HOSu (80.9 mg, 0.8 mmol). The column was intermittently agitated at room temperature overnight after which the resin was washed with DMF (2.8 mL/min). The column was drained and the resin was washed with DMF (2 × 5.0 mL), $CHCl_3$ (2 × 5.0 mL), and Hexane (2 × 5.0 mL) and dried *in vacuo*.

Cleavage of the linear peptide (**1.64**) from resin **1.63** was achieved by washing the resin with a TFA cocktail (2 x 5 mL, 2% TFA and 2% TIPS in $CHCl_3$). The solvent was removed *in vacuo*, the residual crude material was then redissolved in acetonitrile (1.5 mL) to which water (4 mL) was added. Volatiles were removed by blowing with nitrogen for 1 hour and the compound was lyophilized producing a fluffy white solid (**1.64**, 97.8 mg, 85% yield).

A suspension of the crude linear peptide (**1.64**, 31 mg, 53.1 μmol), HOAt (8.7 mg, 63.7 μmol), N'-methyl polystyrene-N-cyclohexylcarbodiimide (0.115 g, 0.265 mmol, loading 2.3 mmol/g) (Merck Chemicals Ltd. # 8.55029), DMAP (10.5 mg, 52 μmol) and CH_3Cl (45 mL) was stirred under an atmosphere of nitrogen for 7 days. After this period the solution was filtered and concentrated *in vacuo*. The residual crude material was triturated with ice-cold ether (5 mL) to furnish an off-white solid which was purified *via* semi-preparative RP-HPLC to afford SolA (**1.20**, 3.1 mg, 10.5%) and its diastereomer, epiSolA (**1.65**, 1.2 mg, 4.0%)

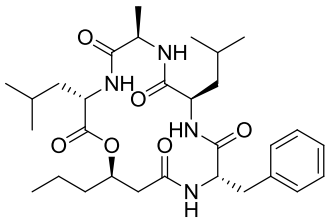
SolA (**1.20**) MS^+ (ES-TOF): m/z calcd: 559.3451 $[M+H]^+$; found: 559.3477; Analytical RP-HPLC Onyx Monolithic C18 100 × 4.6 mm, 20% for 2 min increasing to 80% B in 20 min, t_R 12.56 min; $[\alpha]_D^{20}$ = +13.9 ^{o} (c 0.3, MeOH); ^{1}H-NMR (400 MHz, $(CD_3)_2SO$) δ 8.65 (d, *J* = 5.7 Hz, 1H, Leu-NH), 8.61 (d, *J* = 3.1 Hz, 1H, Phe-NH), 7.47 (d, *J* = 9.0 Hz, 1H, Ala-NH), 7.30-7.16 (m, 5H, ArH), 7.05 (d, *J* = 9.0 Hz, 1H, Leu-NH), 5.19-5.11 (m, 1H, 3HHA-C_βH), 4.47 (dt, *J* = 4.1 Hz, 10.1 Hz, 1H, Leu-C_αH), 4.26 (ddd, *J* = 3.3 Hz, 6.1 Hz, 9.7 Hz, 1H, Phe-C_αH), 4.22-4.12 (m, 1H, Ala-C_αH), 3.60-3.52 (m, 1H, Leu-C_αH), 2.94 (dd, *J* = 6.0 Hz, 13.2 Hz, 1H, Phe-C_βH), 2.73 (dd, *J* = 10.0 Hz, 13.2 Hz, 1H, Phe-C_βH), 2.67 (dd, *J* = 3.7 Hz, 13.6 Hz, 1H, 3HHA-C_αH), 2.11 (dd, *J* = 10.4 Hz, 13.4 Hz, 1H, 3HHA-C_αH), 1.62 (m, 1H, Leu-$C_\beta H_1$), 1.61 (m, 1H, 3HHA-C_γH), 1.53 (m, 1H, Leu-$C_\beta H_2$), 1.53 (m, 1H, Leu-C_γH), 1.46 (m, 1H, 3HHA-C_γH), 1.33 (m, 2H, Leu-C_βH), 1.30 (d, *J* = 7.4 Hz, 3H, Ala-C_βH), 1.23 (m, 2H, 3HHA-C_δH), 0.99 (m, 1H, Leu-C_γH), 0.87 (d, *J* = 6.3 Hz, 3H, Leu-C_δH), 0.86 (t, *J* = 7.4 Hz, 3H, 3HHA-C_εH), 0.82 (d, *J* = 6.4 Hz, 3H, Leu-C_δH), 0.69 (d, *J* = 6.6 Hz, 3H, Leu-C_δH), 0.52 (d, *J* = 6.5 Hz, 3H, Leu-C_δH); ^{13}C-NMR (125 MHz, $(CD_3)_2SO$) δ 174.45, 171.71, 171.13, 171.04, 170.61, 136.33, 129.02, 128.20, 126.49, 72.04, 55.90, 52.94, 48.89, 48.09, 40.77, 40.11, 38.80, 36.32, 36.31,

24.00, 23.53, 23.25, 23.19, 21.33, 20.67, 17.76, 16.63, 13.83. Consistent with literature.[214]

epiSolA (**1.65**) MS^+ (ES-TOF): m/z calcd: 559.3451 $[M+H]^+$; found: 559.3431; Analytical RP-HPLC Onyx Monolithic C18 100 × 4.6 mm, 20% for 2 min increasing to 80% B in 20 min, t_R 12.01 min; $[\alpha]_D^{20}$ = +34.0 ^{o} (c 0.3, MeOH); ^{1}H-NMR (400 MHz, $(CD_3)_2SO$) δ 8.47 (d, *J* = 5.2 Hz, 1H, Phe-NH), 8.41 (d, *J* = 7.2 Hz, 1H, Leu-NH), 7.42 (d, *J* = 9.0 Hz, 1H, Ala-NH), 7.37 (d, *J* = 6.6 Hz, 1H, Leu-NH), 7.30-7.14 (m, 5H, ArH), 4.93-4.84 (m, 1H, 3HHA-C_βH), 4.37-4.28 (m, 1H, Phe-C_αH), 4.27-4.19 (m, 1H, Ala-C_αH), 3.83 (m, 1H, Leu-C_αH), 3.82 (m, 1H, Leu-C_αH), 2.89 (dd, *J* = 6.8 Hz, 13.4 Hz, 1H, Phe-C_βH), 2.79 (dd, *J* = 9.1 Hz, 13.1 Hz, 1H, Phe-C_βH), 2.60 (dd, *J* = 4.4 Hz, 14.6 Hz, 1H, 3HHA-C_αH), 2.25 (dd, *J* = 6.1 Hz, 14.5 Hz, 1H, 3HHA-C_αH), 1.91 (dd, *J* = 7.6 Hz, 8.7 Hz, 1H, Leu-$C_\beta H_1$), 1.81-1.69 (m, 1H, 3HHA-C_γH), 1.60-1.45 (m, 2H, 3HHA-C_γH, Leu-C_γH), 1.52 (dd, *J* = 7.6 Hz, 13.6 Hz, 1H, Leu-$C_\beta H_2$), 1.40-1.29 (m, 2H, Leu-C_βH), 1.27 (m, 1H, 3HHA-$C_\delta H_1$), 1.25 (d, *J* = 7.3 Hz, 3H, Ala-C_βH), 1.18 (m, 1H, 3HHA-$C_\delta H_2$), 1.00-0.91 (m, 1H, Leu-C_γH), 0.87 (d, *J* = 6.2 Hz, 3H, Leu-C_δH), 0.84 (d, *J* = 6.2 Hz, 3H, Leu-C_δH), 0.84 (t, *J* = 7.4 Hz, 3H, 3HHA-C_εH), 0.70 (d, *J* = 6.6 Hz, 3H, Leu-C_δH), 0.58 (d, *J* = 6.4 Hz, 3H, Leu-C_δH); ^{13}C-NMR (125 MHz, $(CD_3)_2SO$) δ 172.6, 171.9, 171.4, 170.3, 170.2, 136.7, 129.1, 128.2, 126.4, 71.1, 55.5, 53.3, 52.0, 48.3, 38.5, 38.3, 36.7, 35.4, 24.6, 23.5, 23.1, 22.5, 21.8, 20.8, 17.8, 17.0, 13.7.

8.3.7 Stereoselective synthesis of solonamide depsipeptides

SolA (**1.21**)[214]



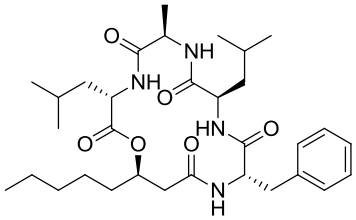
Initial resin preparation and peptide couplings were similar to those reported in Method A above. The final coupling was performed similar to Method A but using (*R*)-3-hydroxy-hexanoic acid (**1.60**, 106.4 mg, 0.8 mmol).

Cleavage of the linear peptide from the resin and lyophilisation were executed as in Method A producing a fluffy pale yellow solid (77 mg, 67% yield).

Further processes were performed as described in Method A furnishing an off-white solid (58.3 mg, quantitative crude yield) which was purified *via* semi-preparative RP-HPLC to afford pure SolA (**1.21**, 10.0 mg, 20% yield) and epiSolA (**1.65**, 2.0 mg, 4%).

Analytical data were confirmed to be identical to those found above.

Solonamide B (SolB, **1.22**)[214]



Initial resin preparation and peptide couplings were similar to those reported in Method A above. The final coupling was performed similar to Method A but using (*R*)-3-hydroxy-octanoic acid (**4.10**, 42 mg, 0.26 mmol).mL). Cleavage of the linear peptide from the resin and lyophilisation were executed as in Method A producing a white fluffy powder (116.6 mg, 99.4%).

Further processes were performed as described in Method A furnishing a yellow solid (58.2 mg, 51% crude yield) which was purified *via* semi-preparative RP-HPLC to afford pure SolB (**1.22**, 3.0 mg, 2.6%) and epiSolB (**4.5**, 3.8 mg, 3.3%).

SolB (**1.22**) MS^+ (ES-TOF): m/z calcd: 587.37639 $[M+H]^+$; found: 587.3768; Analytical RP-HPLC Onyx Monolithic C18 100 × 4.6 mm, 20% for 2 min increasing to 80% B in 20 min, t_R 14.77 min; $[\alpha]_D^{20}$ = +38.9 ^{o} (c 0.3, MeOH); ^{1}H-NMR (400 MHz, $(CD_3)_2SO$) δ 8.66 (d, *J* = 5.8 Hz, 1H, Leu-NH), 8.61 (d, *J* = 3.1 Hz, 1H, Phe-NH), 7.49 (d, *J* = 9.2 Hz, 1H, Ala-NH), 7.30-7.17 (m, 5H, ArH), 7.06 (d, *J* = 9.6 Hz, 1H, Leu-NH), 5.18-5.10 (m, 1H, 3HOA-C_βH), 4.47 (dt, *J* = 4.4 Hz, 10.1 Hz, 1H, Leu-C_αH), 4.30-4.23 (m, 1H, Phe-C_αH), 4.22-4.14 (m, 1H, Ala-C_αH), 3.60-3.54 (m, 1H, Leu-C_αH), 2.96 (dd, *J* = 6.2 Hz, 13.2 Hz, 1H, Phe-$C_\beta H_1$), 2.74 (dd, *J* = 10.1

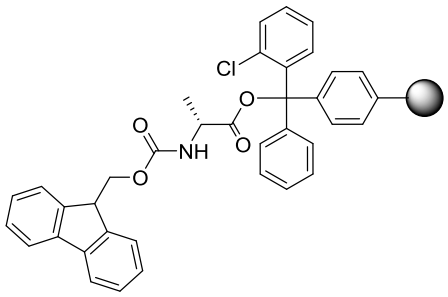
Hz, 13.2 Hz, 1H, Phe-$C_\beta H_2$), 2.69 (dd, *J* = 3.7 Hz, 13.6 Hz, 1H, 3HOA-$C_\alpha H_1$), 2.11 (dd, *J* = 9.9 Hz, 13.4 Hz, 1H, 3HOA-$C_\alpha H_2$), 1.69-1.17 (m, 16H, Ala-$C_\beta H$, 3HOA-$C_\gamma H$, 3HOA-$C_\delta H$, 3HOA-$C_\varepsilon H$, 3HOA-$C_\zeta H$, Leu^1-$C_\beta H$, Leu^2-$C_\beta H$, Leu-$C_\gamma H$), 0.99 (m, 1H, Leu-$C_\gamma H$), 0.87 (d, *J* = 6.6 Hz, 3H, Leu-$C_\delta H$), 0.86 (t, *J* = 6.8 Hz, 3H, 3HOA-$C_\eta H$), 0.83 (d, *J* = 6.5 Hz, 3H, Leu-$C_\delta H$), 0.71 (d, *J* = 6.5 Hz, 3H, Leu-$C_\delta H$), 0.54 (d, *J* = 6.5 Hz, 3H, Leu-$C_\delta H$); ^{13}C-NMR (125 MHz, $(CD_3)_2SO$) δ 174.49, 171.71, 171.11, 171.04, 170.62, 136.32, 129.01, 128.20, 126.48, 72.32, 55.88, 52.93, 48.90, 48.08, 40.74, 40.10, 38.80, 36.32, 34.05, 31.03, 24.08, 24.00, 23.53, 23.22, 23.19, 21.92, 21.33, 20.67, 16.64, 13.84. Consistent with literature.[214]

epiSolB (**4.5**) MS^+ (ES-TOF): m/z calcd: 587.37639 $[M+H]^+$; found: 587.3768; Analytical RP-HPLC Onyx Monolithic C18 100 × 4.6 mm, 20% for 2 min increasing to 80% B in 20 min, t_R 14.58 min; $[\alpha]_D^{20}$ = +91.1 ^{o} (c 0.3, MeOH); ^{1}H-NMR (400 MHz, $(CD_3)_2SO$) δ 8.48 (d, *J* = 5.2 Hz, 1H, Phe-NH), 8.41 (d, *J* = 7.1 Hz, 1H, Leu-NH), 7.43 (d, *J* = 9.1 Hz, 1H, Ala-NH), 7.38 (d, *J* = 6.5 Hz, 1H, Leu-NH), 7.30-7.15 (m, 5H, ArH), 4.91-4.85 (m, 1H, 3HOA-$C_\beta H$), 4.35-4.29 (m, 1H, Phe-$C_\alpha H$), 4.26-4.21 (m, 1H, Ala-$C_\alpha H$), 3.87-3.81 (m, 1H+1H, Leu^1-$C_\alpha H$, Leu^2-$C_\alpha H$), 2.90 (dd, *J* = 7.0 Hz, 13.1 Hz, 1H, Phe-$C_\beta H$), 2.80 (dd, *J* = 8.9 Hz, 13.1 Hz, 1H, Phe-$C_\beta H$), 2.61 (dd, *J* = 4.5 Hz, 14.4 Hz, 1H, 3HOA-$C_\alpha H_1$), 2.26 (dd, *J* = 6.4 Hz, 14.4 Hz, 1H, 3HOA-$C_\alpha H_2$), 1.91 (dd, *J* = 7.3 Hz, 8.9 Hz, 1H, Leu^1-$C_\beta H_1$), 1.77-1.70 (m, 1H, 3HOA-$C_\gamma H_1$), 1.70-1.15 (m, 14H, Ala-$C_\beta H$, 3HOA-$C_\gamma H_2$, 3HOA-$C_\delta H$, 3HOA-$C_\varepsilon H$, 3HOA-$C_\zeta H$, Leu^1-$C_\beta H_2$, Leu^2-$C_\beta H$, Leu-$C_\gamma H$), 1.03-0.91 (m, 1H, Leu-$C_\gamma H$), 0.88 (d, *J* = 6.1 Hz, 3H, Leu-$C_\delta H$), 0.85 (d, *J* = 6.0 Hz, 3H, Leu-$C_\delta H$), 0.82 (t, *J* = 6.8 Hz, 3H, 3HOA-$C_\eta H$), 0.71 (d, *J* = 6.6 Hz, 3H, Leu-$C_\delta H$), 0.59 (d, *J* = 6.4 Hz, 3H, Leu-$C_\delta H$). Further amounts of epiSolB were synthesised using the racemic 3-hydroxyhexanoic acid in Method A detailed above.

8.4 Developing an improved solonamide synthesis

8.4.1 Preparation of Fmoc-*D*-Ala-2ClTrt Resin

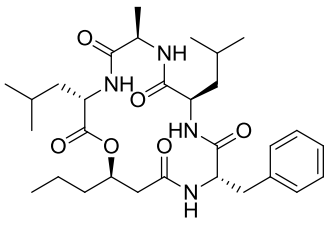
Fmoc-*D*-Alanine 2-chlorotrityl-resin (**5.8**)



2-Chlorotritylchloride resin (100-200 mesh), 1% DVB (**4.31**, 1.22 g, loading=1.22 mmol/g) (Merck Chemicals Ltd. Lot S6264017 127) was swelled in dry $CHCl_3$ (2 mL) overnight prior to the addition of 1.2 eq. of Fmoc-*D*-Ala-OH (582 mg, 1.8 mmol), and 2 eq. of DIPEA (523 µL, 3.0 mmol). The resulting suspension was stirred at room temperature for 3 hours. An excess of MeOH (2 mL) and DIPEA (500 µL) was then added. After a further 15 mins of gentle stirring, the resin was filtered and washed with DMF (2×5 mL), $CHCl_3$ (2×5 mL), and hexane (2×5 mL). The resin was dried overnight under high vacuum affording 1.43 g of the loaded resin **5.8.** Standard UV Fmoc quantification revealed a resin loading of 0.89 mmol/g (loading = 100%).

8.4.2 Stereoselective synthesis of solonamide depsipeptides

General Method B - SolA (**1.21**)[319]



Fmoc-*D*-Ala-2-Chlorotritylchloride resin (**5.8**, 113.0 mg, 0.1 mmol, loading = 0.89 mmol/g) was placed in an Omnifit™ BenchMark™ column assembly and swelled with 1:1 DCM (2.5 mL) overnight. Utilising a NovaSyn® manual peptide

synthesizer (flow rate: 2.8 mL/min), the resin was washed with DMF, Fmoc-deprotection was achieved using a flow of 20% piperidine in DMF, and a further DMF wash was effected. The column was drained and a solution of Fmoc-D-Leu-OH (144.0 mg, 0.4 mmol), PyOxim (230.0 mg, 0.4 mmol), and DIPEA (140 μL, 0.8 mmol) in DMF (1 mL) was added. The column was intermittently agitated at room temperature for 3.5 hours after which the resin was washed (DMF 2.8 mL/min), Fmoc-deprotected (20% piperidine in DMF, 2.8 mL/min), and washed (DMF 2.8 mL/min). The linear peptide sequence underwent a subsequent round of acylation (as expanded above) utilising Fmoc-Phe-OH (154.0 mg, 0.4 mmol). The coupling of the 3-hydroxyhexanoic acid (**1.60**, 54.0 mg, 0.4 mmol), DIC (120 μL, 0.45 mmol), and HOSu (42.0 mg, 0.4 mmol). The column was intermittently agitated at room temperature overnight after which the resin was washed with DMF (2.8 mL/min). The column was drained and the resin was washed with DMF (2 × 5.0 mL), $CHCl_3$ (2 × 5.0 mL), and Hexane (2 × 5.0 mL) and dried *in vacuo*. The resin was added to anhydrous DCM containing Boc-Leu-OH (100.0 mg, 0.4 mmol) and DIC (31.3 μL, 0.2 mmol). DMAP (7.0 mg, 0.05 mmol) was added and the mixture was stirred overnight. The mixture was filtered and washed with DCM (2 × 5.0 mL), and Hexane (2 × 5.0 mL) to isolate the resin-bound linear sequence.

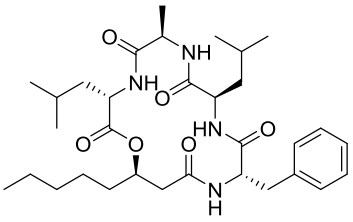
Cleavage of the linear peptide from the resin was achieved by washing the resin with a TFA cocktail (2 x 5 mL, 1% TFA and 1% TIPS in $CHCl_3$). The solvent was removed *in vacuo*, the residual crude material was then purified *via* semi-preparative RP-HPLC and the compound was lyophilized producing the linear Boc-protected peptide as a fluffy white solid. Deuterated TFA was used to perform NMR thereby assessing the purity of the linear intermediate and concurrently deprotecting the Boc group. The sample was then blown with nitrogen to remove TFA-d and redissolved in MeCN/water before lyophilisation afforded the highly pure linear peptide as a white fluffy powder (8.5 mg, 15% yield).

The highly pure linear peptide (8.5 mg, 14.7 μmol), HOAt (8.0 mg, 59.0 μmol), TBTU (18.9 mg, 59.0 μmol), DIPEA (20.6 μL, 0.12 mmol) and DCM (40 mL) were stirred overnight. After this period the solution was concentrated *in*

vacuo. The residual crude material was purified *via* semi-preparative RP-HPLC to afford SolA (**1.21**, 4.0 mg, 49.0%, 95% *dr*)

Analytical data were confirmed to be identical to those found above.

SolB (**1.22**, Method B)

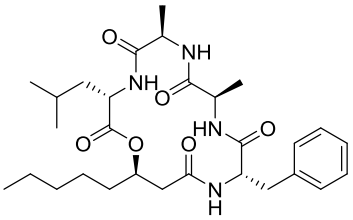


Initial resin preparation and peptide couplings were similar to those reported in Method B above. (*R*)-3-hydroxy-octanoic acid (**4.10**, 67 mg, 0.4 mmol) was used in place of (*R*)-3-hydroxy-hexanoic acid. Cleavage of the linear peptide from the resin, lyophilisation, NMR, and Boc-deprotection were executed as in Method B producing a white fluffy powder (12.2 mg, 20%).

Further processes were performed as described in Method B furnishing a yellow solid which was purified *via* semi-preparative RP-HPLC to afford pure SolB (**1.22**, 5.4 mg, 46%).

Analytical data were confirmed to be identical to those found above.

(ala^3)SolB (**1.71**, Method B)



Initial resin preparation and peptide couplings were similar to those reported in Method B above on a 0.2mmol scale. (*R*)-3-hydroxy-octanoic acid (**4.10**, 125.3 mg, 0.8 mmol) was used in place of (*R*)-3-hydroxy-hexanoic acid. The resin was washed with DMF (2 × 5.0 mL), $CHCl_3$ (2 × 5.0 mL), and Hexane (2 × 5.0 mL) and dried *in vacuo*. The resin was then split into three equal

portions. Coupling of Boc-L-Leu-OH (92.5 mg, 0.4 mmol) was attempted with: COMU (216 mg, 0.5 mmol) and DIPEA (174.2 µL, 1.0 mmol); TBTU (185 mg, 0.5 mmol) and DBU (149.8 µL, 1.0 mmol); and DIC (31.3 µL, 0.2 mmol) and DMAP (16 mg, 0.1 mmol). Only DIC and DMAP produced the required product **5.12**.

Cleavage of the linear peptide **5.12** from the resin **5.11**, HPLC purification, and lyophilisation produced the Boc-protected linear peptide as previously outlined. ^{1}H-NMR in TFA-*d* allowed both analysis and full deprotection of the peptide producing peptide **5.13** (17.1 mg, 46%)**.** This peptide was not fully isolated and characterised before it was used in the following reaction.

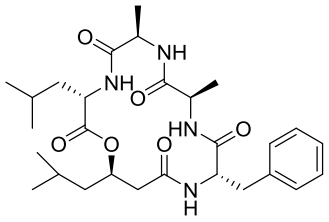
Linear (ala^{3})SolB (**5.13**) ^{1}H-NMR (400 MHz, $(CD_3)_2SO$) δ 7.34-7.24 (m, 3H, Ar-H), 7.19-7.13 (m, 2H, Ar-H), 5.47-5.37 (m, 1H, 3HOA^{1}-C$_\beta$H), 4.83 (t, *J* = 7.56 Hz, 1H, Phe-C$_\alpha$H), 4.65 (q, *J*=7.31 Hz, 1H, Ala^{b}-C$_\alpha$H), 4.51 (q, *J*=7.14 Hz, 1H, Ala^{b}-C$_\alpha$H), 4.20 (t, *J*=6.92 Hz, 1H, Leu-C$_\alpha$H), 3.14 (dd, *J*=13.68 Hz, 7.12 Hz, 1H, Phe-C$_\beta$H), 2.85-2.71 (m, 2H, 3HOA^{1}-C$_\alpha$H), 1.97-1.61 (m, 6H, 3HOA^{1}-C$_\gamma$H, Leu-C$_\beta$H, Leu-C$_\gamma$H), 1.59 (s, 9H, tBu-H), 1.55 (d, *J*=7.32 Hz, 3H, Ala^{a}-C$_\beta$H), 1.39-1.20 (m, 9H, Ala^{b}-C$_\beta$H, 3HHA^{1}-C$_\delta$H, 3HOA^{1}-C$_\varepsilon$H, 3HOA^{1}-C$_\zeta$H), 1.01 (t, *J*=5.86 Hz, 6H, Leu-C$_\delta$H$_1$, Leu-C$_\delta$H$_2$), 0.87 (t, *J*=12.92 Hz, 3H, 3HOA^{1}-C$_\eta$H).

Further processes were performed as described in Method B furnishing a yellow solid which was purified *via* semi-preparative RP-HPLC to afford pure (ala^{3})SolB (**1.71**, 7.6 mg, 46%).

(ala^{3})SolB (**1.71**) MS^{+} (ES-TOF): m/z calcd: 545.3294 $[M+H]^{+}$; found: 545.3497; Analytical RP-HPLC Onyx Monolithic C18 100 × 4.6 mm, 20% for 2 min increasing to 80% B in 20 min, t_R 11.72 min; $[\alpha]_D^{20}$ = +9.72 ^{o} (c 0.3, MeOH); ^{1}H-NMR (400 MHz, $(CD_3)_2SO$) δ 8.85 (d, J = 5.2 Hz, 1H, Ala^{a}-NH), 8.52 (d, J = 3.8 Hz, 1H, Phe-NH), 7.35 (d, J = 8.9 Hz, 1H, Ala^{b}-NH), 7.33-7.19 (m, 5H, Ar-H), 7.16 (d, *J* = 9.6 Hz, 1H, Leu-NH), 5.16-5.06 (m, 1H, 3HOA^{1}-C$_\beta$H), 4.46 (dt, *J* = 4.4 Hz, 10.1 Hz, 1H, Leu-C$_\alpha$H), 4.25 (dt, *J* = 3.7 Hz, 7.5 Hz, 1H, Phe-C$_\alpha$H), 4.19 (td, *J* = 7.6 Hz, 15.9 Hz, 1H, Ala^{b}-C$_\alpha$H), 3.82-3.73 (m, 1H, Ala^{a}-C$_\alpha$H), 2.88 (dd, *J* = 8.1 Hz, 13.8 Hz, 1H, Phe-C$_\beta$H$_1$), 2.81 (dd, *J* = 7.3 Hz, 13.8 Hz, 1H, Phe-C$_\beta$H$_2$), 2.66 (dd, *J* = 4.0 Hz, 13.6 Hz, 1H, 3HOA^{1}-C$_\alpha$H$_1$), 2.11 (dd, *J* = 9.5 Hz, 13.6 Hz, 1H, 3HOA^{1}-C$_\alpha$H$_2$),

1.74-1.39 (m, 5H, Leu-$C_\beta H$, Leu-$C_\gamma H$, 3HOA^1-$C_\gamma H$), 1.34 (d, *J*= 7.4 Hz, 3H, Ala^b-$C_\beta H$), 1.30-1.16 (m, 6H, 3HHA^1-$C_\delta H$, 3HOA^1-$C_\varepsilon H$, 3HOA^1-$C_\zeta H$), 1.13 (d, *J*= 7.4 Hz, 3H, Ala^a-$C_\beta H$), 0.90-0.79 (m, 9H, Leu-$C_\delta H$, 3HOA^1-$C_\eta H$); ^{13}C-NMR (125 MHz, $(CD_3)_2SO$) δ 174.43, 171.75, 171.16, 171.07, 170.66, 136.90, 128.98, 128.12, 126.51, 72.16, 55.78, 50.17, 49.06, 48.13, 40.32, 35.98, 33.92, 31.01, 24.05, 23.98, 23.21, 21.89, 21.28, 16.63, 16.03, 13.80.

(5Me-3HHA^1, ala^3)Sol (**5.15**, Method B)



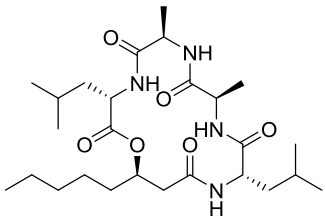
Initial resin preparation and peptide couplings were similar to those reported in Method B above. (*R*)-3-hydroxy-5-methylhexanoic acid (**5.23**, 52 mg, 0.4 mmol) was used in place of (*R*)-3-hydroxy-hexanoic acid. Cleavage of the linear peptide from the resin, lyophilisation, NMR, and Boc-deprotection were executed as in Method B producing a white fluffy powder (16.8 mg, 31%).

Further processes were performed as described in Method A furnishing a yellow solid which was purified *via* semi-preparative RP-HPLC to afford pure 1-(5Me-3HHA^1, ala^3)Sol (**5.15**, 6.1 mg, 38%).

(5Me-3HHA^1, ala^3)Sol (**5.15**) MS^+ (ES-TOF): m/z calcd: 531.3138 $[M+H]^+$; found: 531.3547; Analytical RP-HPLC Onyx Monolithic C18 100 × 4.6 mm, 20% for 2 min increasing to 80% B in 20 min, t_R 10.34 min; $[\alpha]_D^{20}$ = +12.78^o (c 0.3, MeOH); ^{1}H-NMR (400 MHz, $(CD_3)_2SO$) δ 8.85 (d, *J* = 5.1 Hz, 1H, Ala-NH), 8.55 (d, *J* = 4.0 Hz, 1H, Phe-NH), 7.35-7.20 (m, 6H, Ala-NH, Ar-H), 7.16 (d, *J* = 9.6 Hz, 1H, Leu-NH), 5.23-5.14 (m, 1H, 5Me3HHA^1-$C_\beta H$), 4.44 (dt, *J* = 5.1 Hz, 9.8 Hz, 1H, Leu-$C_\alpha H$), 4.25 (dt, *J* = 4.0 Hz, 7.6 Hz, 1H, Phe-$C_\alpha H$), 4.19 (td, *J* = 7.3 Hz, 15.9 Hz, 1H, Ala-$C_\alpha H$), 3.78 (td, *J* = 7.4 Hz, 12.5 Hz, 1H, Ala-$C_\alpha H$), 2.90 (dd, *J* = 8.0 Hz, 13.8 Hz, 1H, Phe-$C_\beta H_1$), 2.82 (dd, *J* = 7.3 Hz, 13.7 Hz, 1H, Phe-$C_\beta H_2$), 2.68 (dd, *J* = 4.5 Hz, 13.7 Hz, 1H, 5Me3HHA^1-$C_\alpha H_1$), 2.11 (dd, *J* = 8.8 Hz, 13.8 Hz, 1H, 5Me3HHA^1-$C_\alpha H_1$), 1.73-1.57 (m, 3H, Leu^5-$C_\beta H$, 5Me3HHA^1-$C_\gamma H_1$), 1.57-1.42 (m, 2H, Leu-$C_\gamma H$,

5Me3HHA^{1}-C$_{\delta}$H), 1.34 (d, *J*= 7.4 Hz, 3H, Ala-C$_{\beta}$H), 1.31-1.21 (m, 1H, 3HHA^{1}-C$_{\gamma}$H$_2$), 1.13 (d, *J* = 7.5 Hz, 3H, Ala-C$_{\beta}$H), 0.92-0.78 (m, 12H, Leu-C$_{\delta}$H, 3HHA^{1}-C$_{\varepsilon}$H); ^{13}C-NMR (125 MHz, (CD$_3$)$_2$SO) δ 174.46, 171.75, 171.23, 170.97, 170.45, 136.94, 128.98, 128.12, 126.50, 70.37, 55.77, 50.20, 49.13, 48.10, 43.42, 40.58, 39.19, 36.01, 24.00, 23.81, 23.21, 22.76, 22.32, 21.24, 16.68, 16.03.

(Leu^{2}, ala^{3})Sol (**5.16**, Method B)



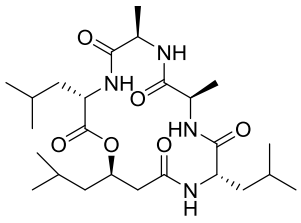
Initial resin preparation and peptide couplings were similar to those reported in Method B above. (*R*)-3-hydroxy-octanoic acid (**4.10**, 70.8 mg, 0.4 mmol) was used in place of (*R*)-3-hydroxy-hexanoic acid. Cleavage of the linear peptide from the resin, lyophilisation, NMR, and Boc-deprotection were executed as in Method B producing a white fluffy powder (4.4 mg, 8.3%).

Further processes were performed as described in Method A furnishing a yellow solid which was purified *via* semi-preparative RP-HPLC to afford pure (Leu^{2}, ala^{3})Sol (**5.16**, 2.87 mg, 68%).

(Leu^{2}, ala^{3})Sol (**5.16**) MS^{+} (ES-TOF): m/z calcd: 511.3451 [M+H]$^{+}$; found: 511.4052; Analytical RP-HPLC Onyx Monolithic C18 100 × 4.6 mm, 20% for 2 min increasing to 80% B in 20 min, t_R 11.58 min; ^{1}H-NMR (400 MHz, (CD$_3$)$_2$SO) δ 9.10 (d, *J* = 5.3 Hz, 1H, Ala^{b}-NH), 8.31 (d, *J* = 3.8 Hz, 1H, Leu^{a}-NH), 7.44 (d, *J* = 9.1 Hz, 1H, Ala^{a}-NH), 7.15 (d, *J* = 9.9 Hz, 1H, Leu^{b}-NH), 5.16-5.07 (m, 1H, 3HOA^{1}-C$_{\beta}$H), 4.44 (dt, *J* = 4.2 Hz, 15.2 Hz, 1H, Leu^{b}-C$_{\alpha}$H), 4.20 (td, *J* = 7.4 Hz, 16.1 Hz, 1H, Ala^{a}-C$_{\alpha}$H), 4.07-4.00 (m, 1H, Leu^{a}-C$_{\alpha}$H), 3.89 (td, *J* = 7.5 Hz, 12.7 Hz, 1H, Ala^{b}-C$_{\alpha}$H), 2.68 (dd, *J* = 3.9 Hz, 13.4 Hz, 1H, 3HOA^{1}-C$_{\alpha}$H$_1$), 2.10 (dd, *J* = 10.1 Hz, 13.6 Hz, 1H, 3HOA^{1}-C$_{\alpha}$H$_2$), 1.72-1.56 (m, 3H, Leu^{b}-C$_{\beta}$H$_1$, 3HOA^{1}-C$_{\gamma}$H$_1$, Leu$^{a/b}$-C$_{\gamma}$H), 1.56-1.40 (m, 4H, Leu^{a}-C$_{\beta}$H$_2$, Leu^{b}-C$_{\beta}$H$_2$, 3HOA^{1}-C$_{\gamma}$H$_2$, Leu$^{a/b}$-C$_{\gamma}$H), 1.36 (d, *J*= 7.4 Hz, 3H, Ala^{a}-C$_{\beta}$H), 1.30 (d, *J*= 7.4 Hz, 3H, Ala^{b}-C$_{\beta}$H), 1.29-1.14 (m, 7H, Leu^{a}-C$_{\beta}$H$_1$, 3HOA^{1}-C$_{\delta}$H, 3HOA^{1}-C$_{\varepsilon}$H, 3HOA^{1}-C$_{\zeta}$H), 0.93 (d, *J*= 6.6 Hz, 3H, Leu$^{a/b}$-C$_{\delta}$H), 0.91-

0.78 (m, 12H, Leu$^{a/b}$-C$_\delta$H, Leu$^{a/b}$-C$_\delta$H, Leu$^{a/b}$-C$_\delta$H, 3HOA^1-C$_\eta$H); ^{13}C-NMR (125 MHz, (CD$_3$)$_2$SO) δ 175.34, 171.91, 171.12, 171.08, 170.75, 140.90, 72.24, 58.08, 52.67, 50.33, 48.91, 48.16, 37.38, 34.01, 31.01, 24.04, 23.97, 23.92, 23.22, 22.60, 21.89, 21.75, 21.25, 16.57, 16.34, 13.80.

(5Me-3HHA^1, Leu^2, ala^3)Sol (**5.17**, Method B)



Initial resin preparation and peptide couplings were similar to those reported in Method B above. (*R*)-3-hydroxy-5-methylhexanoic acid (**5.23**, 61.0 mg, 0.4 mmol) was used in place of (*R*)-3-hydroxy-hexanoic acid. Cleavage of the linear peptide from the resin, lyophilisation, NMR, and Boc-deprotection were executed as in Method B producing a white fluffy powder (9.9 mg, 19.2%).

Further processes were performed as described in Method A furnishing a yellow solid which was purified *via* semi-preparative RP-HPLC to afford pure 1-(5Me-3HHA^1, Leu^2, ala^3)Sol (**5.17**, 4.87 mg, 51%).

(5Me-3HHA^1, Leu^2, ala^3)Sol (**5.17**) MS$^+$ (ES-TOF): m/z calcd: 497.3294 [M+H]$^+$; found: 497.4018; Analytical RP-HPLC Onyx Monolithic C18 100 × 4.6 mm, 20% for 2 min increasing to 80% B in 20 min, t_R 9.77 min; $[\alpha]_D^{20}$ =-5.00^o (c 0.3, MeOH); ^{1}H-NMR (400 MHz, (CD$_3$)$_2$SO) δ 9.10 (d, *J* = 5.3 Hz, 1H, Ala^a-NH), 8.34 (d, *J* = 3.5 Hz, 1H, Leu^a-NH), 7.42 (d, *J* = 9.1 Hz, 1H, Ala^b-NH), 7.14 (d, *J* = 9.6 Hz, 1H, Leu^b-NH), 5.24-5.14 (m, 1H, 5Me3HHA^1-C$_\beta$H), 4.42 (dt, *J* = 4.4 Hz, 15.2 Hz, 1H, Leu^b-C$_\alpha$H), 4.20 (td, *J* = 7.4 Hz, 16.1 Hz, 1H, Ala^b-C$_\alpha$H), 4.08-4.00 (m, 1H, Leu^a-C$_\alpha$H), 3.90 (td, *J* = 7.4 Hz, 12.7 Hz, 1H, Ala^a-C$_\alpha$H), 2.69 (dd, *J* = 4.2 Hz, 13.7 Hz, 1H, 5Me3HHA^1-C$_\alpha$H$_1$), 2.11 (dd, *J* = 9.5 Hz, 13.7 Hz, 1H, 5Me3HHA^1-C$_\alpha$H$_2$), 1.73-1.55 (m, 3H, 5Me3HHA^1-C$_\gamma$H$_1$, Leu$^{a/b}$-C$_\gamma$H, Leu^a-C$_\beta$H$_1$), 1.57-1.42 (m, 4H, Leu^b-C$_\beta$H, Leu$^{a/b}$-C$_\gamma$H, Leu^a-C$_\beta$H$_2$), 1.36 (d, *J*= 7.4 Hz, 3H, Ala^b-C$_\beta$H), 1.35-1.32(m, 1H, 5Me3HHA^1-C$_\delta$H), 1.30 (d, *J*= 7.4 Hz, 3H, Ala^a-C$_\beta$H), 1.29-1.21 (m, 1H, 5Me3HHA^1-C$_\gamma$H$_2$), 0.93 (d, *J* = 6.6 Hz, 3H, Leu$^{a/b}$-C$_\delta$H/5Me3HHA^1-C$_\varepsilon$H), 0.90-0.86

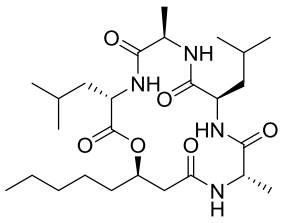
(m, 9H, Leu$^{a/b}$-C_δH/5Me3HHA^1-C_εH), 0.84 (d, *J* = 6.5 Hz, 3H, Leu$^{a/b}$-C_δH/5Me3HHA^1-C_εH), 0.81 (d, *J* = 6.4 Hz, 3H, Leu$^{a/b}$-C_δH/5Me3HHA^1-C_εH); ^{13}C-NMR (125 MHz, $(CD_3)_2SO$) δ 175.37, 171.92, 171.19, 170.97, 170.55, 140.91, 70.48, 58.08, 52.68, 50.36, 48.98, 48.13, 40.93, 37.38, 23.98, 23.94, 23.84, 23.21,22.74, 22.58, 22.43, 21.79, 21.22, 16.62, 16.34.

8.5 Pharmacology of the solonamides

8.5.1 Synthesis of solonamide analogues

8.5.1.1 Alanine scan

(Ala[2])SolB (**1.70**- Method A)



Initial resin preparation and peptide couplings were similar to those reported in Method A above. The final coupling was performed similar to Method A but using (*R*)-3-hydroxy-octanoic acid (**4.10**, 151 mg, 0.8 mmol). Cleavage of the linear peptide from the resin and lyophilisation were executed as in Method A producing a white fluffy powder (78.6 mg, 74%).

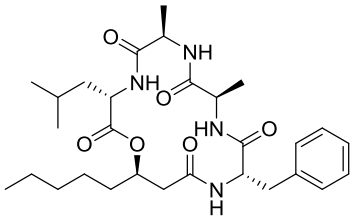
Further processes were performed as described in Method A furnishing a yellow solid which was purified *via* semi-preparative RP-HPLC to afford pure (Ala[2])SolB (**1.70**, 6.5 mg, 9%) and (Ala[2])epiSolB (**4.38**, 4.6 mg, 6%).

(Ala[2])SolB (**1.70**) MS^+ (ES-TOF): m/z calcd: 511.3451 $[M+H]^+$; found: 511.3481; Analytical RP-HPLC Onyx Monolithic C18 100 × 4.6 mm, 20% for 2 min increasing to 80% B in 20 min, t_R 11.05 min; $[\alpha]_D^{20}$ = -0.7 ^{o} (c 0.3, MeOH); ^{1}H-NMR (400 MHz, $(CD_3)_2SO$) δ 8.95 (d, *J* = 5.4 Hz, 1H, Leu^a-NH), 8.50 (d, *J* = 3.3 Hz, 1H, Ala^a-NH), 7.47 (d, *J* = 8.8 Hz, 1H, Ala^b-NH), 7.12 (d, *J* = 9.9 Hz, 1H, Leu^b-NH), 5.12-5.03 (m, 1H, 3HOA^1-C$_\beta$H), 4.46 (dt, *J* = 4.4 Hz, 10.0 Hz, 1H, Leu^b-C$_\alpha$H), 4.20 (m, 1H, Ala^b-C$_\alpha$H), 4.08 (dq, 1H, *J* = 3.6 Hz, 7.0 Hz, Ala^a-C$_\alpha$H), 3.83-3.76 (m, 1H, Leu^a-C$_\alpha$H), 2.66 (dd, *J* = 3.7 Hz, 13.4 Hz, 1H, 3HOA^1-C$_\alpha$H$_1$), 2.10 (dd, *J* = 10.4 Hz, 13.5 Hz, 1H, 3HOA^1-C$_\alpha$H$_2$), 1.83-1.70 (m, 1H, Leu^b-C$_\gamma$H), 1.70-1.40 (m, 7H, Leu^a-C$_\beta$H, Leu^a-C$_\gamma$H, Leu^b-C$_\beta$H 3HOA^1-C$_\gamma$H), 1.36 (d, *J* = 7.4 Hz, 3H, Ala^b-C$_\beta$H) 1.31-1.12 (m, 9H, Ala^a-C$_\beta$H, 3HOA^1-C$_\delta$H, 3HOA^1-C$_\varepsilon$H, 3HOA^1-C$_\zeta$H), 0.91 (d, *J* = 6.6 Hz, 3H, Leu^b-C$_\delta$H$_1$), 0.89-0.79 (m, 12H, 3HOA^1- C$_\eta$H, Leu^a-C$_\delta$H, Leu^b-C$_\delta$H$_2$); ^{13}C-NMR (125

MHz, $(CD_3)_2SO$) δ 176.67, 172.50, 172.10, 171.52, 171.03, 72.86, 58.62, 53.71, 50.03, 49.34, 48.72, 41.17, 37.95, 34.54, 31.57, 24.89, 24.55, 24.40, 23.71, 23.43, 22.39, 21.81, 21.32, 17.08, 1654, 14.30.

(Ala^2)epiSolB (**4.38**) MS^+ (ES-TOF): m/z calcd: 511.3417 $[M+H]^+$; found: 511.3226; Analytical RP-HPLC Onyx Monolithic C18 100 × 4.6 mm, 20% for 2 min increasing to 80% B in 20 min, t_R 10.98 min; $[\alpha]_D^{20}$ = +7.6 ^{o} (c 0.3, MeOH); ^{1}H-NMR (400 MHz, $(CD_3)_2SO$) δ 8.61 (d, *J* = 7.0 Hz, 1H, Leu^a-NH), 8.38 (d, *J* = 4.7 Hz, 1H, Ala^a-NH), 7.47 (d, *J* = 9.1 Hz, 1H, Ala^b-NH), 7.36 (d, *J* = 6.4 Hz, 1H, Leu^b-NH), 4.90-4.82 (m, 1H, 3HOA^1-C$_\beta$H), 4.25 (td, *J* = 7.3 Hz, 16.0 Hz, 1H, Ala-C$_\alpha$H), 4.11 (td, *J* = 6.9 Hz, 11.7 Hz, 1H, Ala^a-C$_\alpha$H), 4.01-3.93 (m, 1H, Leu^a-C$_\alpha$H), 3.84 (td, *J* = 6.6 Hz, 7.8 Hz, 1H, Leu^b-C$_\alpha$H), 2.60 (dd, *J* = 4.1 Hz, 14.2 Hz, 1H, 3HOA^1-C$_\alpha$H$_1$), 2.27 (dd, *J* = 6.8 Hz, 14.2 Hz, 1H, 3HOA^1-C$_\alpha$H$_2$), 1.95-1.84 (m, 1H, Leu^b-C$_\beta$H$_1$), 1.78-1.63 (m, 2H, Leu^a-C$_\gamma$H, 3HOA^1-C$_\gamma$H$_1$), 1.63-1.44 (m, 5H, Leu^a-C$_\beta$H, Leu^b-C$_\beta$H$_2$, Leu^b-C$_\gamma$H, 3HOA^1-C$_\gamma$H$_2$), 1.33-1.14 (m, 12H, Ala^a-C$_\beta$H, Ala^b-C$_\beta$H, 3HOA^1-C$_\delta$H, 3HOA^1-C$_\varepsilon$H, 3HOA^1-C$_\zeta$H), 0.93-0.78 (m, 15H, Leu$^{a/b}$-C$_\delta$H/3HOA^1- C$_\eta$H); ^{13}C-NMR (125 MHz, $(CD_3)_2SO$) δ 174.13, 171.78, 171.37, 170.22, 169.96, 71.51, 53.32, 52.18, 49.24, 48.68, 38.71, 38.37, 33.32, 30.98, 24.68, 24.45, 24.04, 22.92, 22.31, 21.97, 20.95, 17.11, 16.58, 13.81.

(ala^3)SolB (**1.71**- Method A)

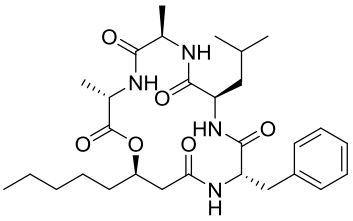


Initial resin preparation and peptide couplings were similar to those reported in Method A above. The final coupling was performed similar to Method A but using (*R*)-3-hydroxy-octanoic acid (**4.10**, 137 mg, 0.8 mmol). Cleavage of the linear peptide from the resin and lyophilisation were executed as in Method A producing a white fluffy powder (76.5 mg, 68%).

Further processes were performed as described in Method A furnishing a yellow solid. Purification *via* semi-preparative RP-HPLC was attempted but the

diastereomers, (ala^3)SolB (**1.71**) and (ala^3)epiSolB (**4.39**), could not be separated.

(Ala^5)SolB (**1.72**- Method A)



Initial resin preparation and peptide couplings were similar to those reported in Method A above. The final coupling was performed similar to Method A but using (*R*)-3-hydroxy-octanoic acid (**4.10**, 143 mg, 0.8 mmol) Cleavage of the linear peptide from the resin and lyophilisation were executed as in Method A producing a white fluffy powder (107.4 mg, 95%).

Further processes were performed as described in Method A furnishing a yellow solid which was purified *via* semi-preparative RP-HPLC to afford pure (Ala^5)SolB (**1.72**, 8.9 mg, 9%) and (Ala^5)epiSolB (**4.40**, 5.9 mg, 6%).

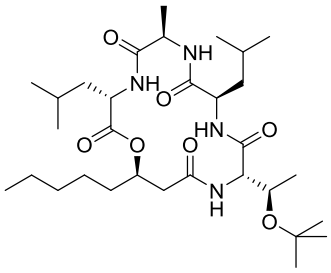
(Ala^5)SolB (**1.72**) MS$^+$ (ES-TOF): m/z calcd: 545.3294 $[M+H]^+$; found: 545.3304; Analytical RP-HPLC Onyx Monolithic C18 100 × 4.6 mm, 20% for 2 min increasing to 80% B in 20 min, t_R 11.41 min; $[\alpha]_D^{20}$ = +18.8 ^{o} (c 0.3, MeOH); ^{1}H-NMR (400 MHz, $(CD_3)_2SO$) δ 8.66-8.60 (m, 2H, Leu-NH, Phe-NH), 7.49 (d, *J* = 9.0 Hz, 1H, Ala^a-NH), 7.30-7.15 (m, 6H, Ala^b-NH, Ar-H), 5.20-5.09 (m, 1H, 3HOA^1-C$_\beta$H), 4.59-4.49 (m, 1H, Ala^b-C$_\alpha$H), 4.29-4.22 (m, 1H, Phe-C$_\alpha$H), 4.18 (td, *J* = 7.4 Hz, 16.2 Hz, 1H, Ala^a-C$_\alpha$H), 3.61-3.53 (m, 1H, Leu-C$_\alpha$H), 2.97 (dd, *J* = 5.8 Hz, 13.3 Hz, 1H, Phe-C$_\beta$H$_1$), 2.73 (dd, *J* = 10.1 Hz, 13.1 Hz, 1H, Phe-C$_\beta$H$_2$), 2.70 (dd, *J* = 3.9 Hz, 13.3 Hz, 1H, 3HOA^1-C$_\alpha$H$_1$), 2.12 (dd, *J* = 10.4 Hz, 13.5 Hz, 1H, 3HOA^1-C$_\alpha$H$_2$), 1.71-1.58 (m, 1H, 3HOA^1-C$_\gamma$H$_1$), 1.53-1.42 (m, 1H, 3HOA^1-C$_\gamma$H$_2$), 1.42-1.17 (m, 14H, Ala^a-C$_\beta$H, Ala^b-C$_\beta$H, Leu-C$_\beta$H, 3HOA^1-C$_\delta$H, 3HOA^1-C$_\varepsilon$H, 3HOA^1-C$_\zeta$H), 1.02-0.90 (m, 1H, Leu-C$_\gamma$H), 0.86 (t, *J* = 6.7 Hz, 3H, 3HOA^1- C$_\eta$H), 0.71 (d, *J* = 6.6 Hz, 3H, Leu-C$_\delta$H), 0.53 (d, *J* = 6.4 Hz, 3H, Leu-C$_\delta$H); ^{13}C-NMR (125 MHz, $(CD_3)_2SO$) δ 174.45, 171.69, 171.20, 170.83, 170.65, 136.25, 129.03, 128.20, 126.50, 72.46,

55.94, 52.94, 48.12, 46.15, 40.81, 38.79, 36.35, 34.14, 31.05, 24.08, 23.50, 23.18, 21.93, 20.67, 16.75, 16.70, 13.86.

(Ala^5)epiSolB (**4.40**) MS$^+$ (ES-TOF): m/z calcd: 545.3294 $[M+H]^+$; found: 545.3327; Analytical RP-HPLC Onyx Monolithic C18 100 × 4.6 mm, 20% for 2 min increasing to 80% B in 20 min, t_R 11.32 min; $[\alpha]_D^{20}$ = +30.6 ^{o} (c 0.3, MeOH); ^{1}H-NMR (400 MHz, $(CD_3)_2SO$) δ 8.47 (d, *J* = 6.8 Hz, 1H, Leu-NH), 8.43 (d, *J* = 5.4 Hz, 1H, Phe-NH), 7.50 (d, *J* = 8.9 Hz, 1H, Ala^a-NH), 7.42 (d, *J* = 6.3 Hz, 1H, Ala^b-NH), 7.30-7.16 (m, 5H, Ar-H), 4.94-4.85 (m, 1H, 3HOA^1-C$_\beta$H), 4.36 (td, *J* = 6.4 Hz, 8.5 Hz, 1H, Phe-C$_\alpha$H), 4.20 (td, *J* = 7.2 Hz, 15.9 Hz, 1H, Ala^a-C$_\alpha$H), 3.95-3.86 (m, 1H, Ala^b-C$_\alpha$H), 3.85-3.77 (m, 1H, Leu-C$_\alpha$H), 2.89 (dd, *J* = 7.0 Hz, 13.3 Hz, 1H, Phe-C$_\beta$H$_1$), 2.80 (dd, *J* = 8.9 Hz, 13.3 Hz, 1H, Phe-C$_\beta$H$_2$), 2.61 (dd, *J* = 4.8 Hz, 14.4 Hz, 1H, 3HOA^1-C$_\alpha$H$_1$), 2.25 (dd, *J* = 5.8 Hz, 14.2 Hz, 1H, 3HOA^1-C$_\alpha$H$_2$), 1.79-1.68 (m, 1H, 3HOA^1-C$_\gamma$H$_1$), 1.62-1.50 (m, 1H, 3HOA^1-C$_\gamma$H$_2$), 1.42-1.31 (m, 5H, Ala^b-C$_\beta$H, Leu-C$_\beta$H), 1.31-1.09 (m, 9H, Ala^a-C$_\beta$H, 3HOA^1-C$_\delta$H, 3HOA^1-C$_\varepsilon$H, 3HOA^1-C$_\zeta$H), 1.07-0.93 (m, 1H, Leu-C$_\gamma$H), 0.85 (t, *J* = 6.9 Hz, 3H, 3HOA^1- C$_\eta$H), 1.73 (d, *J* = 6.6 Hz, 3H, Leu-C$_\delta$H), 0.61 (d, *J* = 6.5 Hz, 3H, Leu-C$_\delta$H); ^{13}C-NMR (125 MHz, $(CD_3)_2SO$) δ 173.35, 172.52, 171.93, 171.15, 170.50, 137.21, 129.55, 128.61, 126.89, 71.84, 55.76, 52.75, 50.66, 48.70, 38.88, 37.32, 33.67, 31.47, 24.67, 24.04, 23.53, 22.39, 21.39, 17.24, 17.16, 16.40, 14.31.

8.5.1.2 Variation of Phe^2 analogues

(Thr(tBu)^2)SolB (**4.41**- Method A)



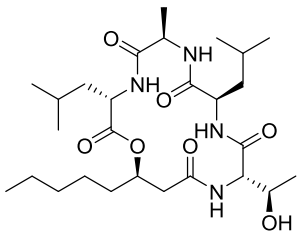
Initial resin preparation and peptide couplings were similar to those reported in Method A above. The final coupling was performed similar to Method A but using (*R*)-3-hydroxy-octanoic acid (**4.10**, 129 mg, 0.8 mmol)

Cleavage of the linear peptide from the resin and lyophilisation were executed as in Method A producing a white fluffy powder (69.2 mg, 56%).

Further processes were performed as described in Method A furnishing a yellow solid which was purified *via* semi-preparative RP-HPLC to afford pure (Thr(tBu)^2)SolB (**4.41**, 9.5 mg, 14%). (Thr(tBu)^2)epiSolB was only isolated in trace amounts.

(Thr(tBu)^2)SolB (**4.41**) MS$^+$ (ES-TOF): m/z calcd: 597.4183 $[M+H]^+$; found: 597.4193; Analytical RP-HPLC Onyx Monolithic C18 100 × 4.6 mm, 20% for 2 min increasing to 80% B in 20 min, t_R 15.25 min; ^{1}H-NMR (400 MHz, $(CD_3)_2SO$) δ 8.69 (d, *J* = 5.2 Hz, 1H, Leu^a-NH), 7.90 (d, *J* = 4.0 Hz, 1H, Thr-NH), 7.50 (d, *J* = 8.8 Hz, 1H, Ala-NH), 7.28 (d, *J* = 9.6 Hz, 1H, Leu^b-NH), 5.07-4.99 (m, 1H, 3HOA^1-C_βH), 4.46-4.37 (m, 1H, Leu^b-C_αH), 4.19 (td, *J* = 7.5 Hz, 15.9 Hz, 1H, Ala-C_αH), 4.07 (t, 1H, *J* = 4.4 Hz, Thr-C_αH), 3.85-3.75 (m, 2H, Thr-C_βH, Leu^a-C_αH), 2.78 (dd, *J* = 4.0 Hz, 13.5 Hz, 1H, 3HOA^1-$C_\alpha H_1$), 2.12 (dd, *J* = 8.9 Hz, 13.5 Hz, 1H, 3HOA^1-$C_\alpha H_2$), 1.87-1.74 (m, 1H, Leu^a-C_γH), 1.71-1.41 (m, 7H, Leu^a-C_βH, Leu^b-C_βH, Leu^b-C_γH, 3HOA^1-C_γH), 1.33 (d, *J* = 7.4 Hz, 3H, Ala-C_βH) 1.29-1.17 (m, 6H, 3HOA^1-C_δH, 3HOA^1-C_εH, 3HOA^1-C_ζH), 1.14 (s, 9H, tBu-CH), 1.07 (d, *J* = 6.2 Hz, 3H, Thr-C_γH), 0.91 (d, *J* = 6.6 Hz, 3H, Leu^a-$C_\delta H_1$), 0.88-0.78 (m, 12H, Leu^a-$C_\delta H_2$, Leu^b-C_δH, 3HOA^1- C_ηH); ^{13}C-NMR (125 MHz, $(CD_3)_2SO$) δ 172.68, 171.79, 171.15, 170.98, 170.42, 161.63, 151.27, 73.74, 72.10, 66.12, 58.77, 53.43, 49.21, 48.19, 40.40, 33.82, 31.00, 27.70, 24.18, 24.10, 23.93, 23.24, 23.14, 21.92, 21.32, 20.41, 18.95, 16.69, 13.82.

(Thr^2)SolB (**4.42**- Method A)

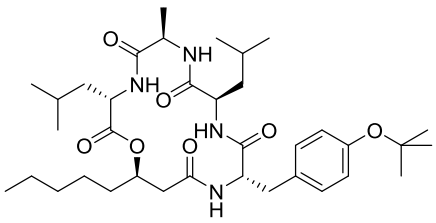


(Thr(tBu)^2)SolB (**4.41**, 5.4 mg) was dissolved in TFA. After 16 hours, the TFA was evaporated *in vacuo*. The residue was dissolved and then the solvent was evaporated using toluene, hexane and Et_2O to remove traces of TFA. The

residue was then dissolved in MeCN/H_2O and lyophilised affording the final product, (Thr^2)SolB (**4.42**), as a fluffy white powder (4.2 mg, 86%)

(Thr^2)SolB (**4.42**) MS^+ (ES-TOF): m/z calcd: 541.3557 $[M+H]^+$; found: 541.3839; Analytical RP-HPLC Onyx Monolithic C18 100 × 4.6 mm, 20% for 2 min increasing to 80% B in 20 min, t_R 9.70 min; $[\alpha]_D^{20}$ = -3.5 ^{o} (c 0.3, MeOH); ^{1}H-NMR (400 MHz, $(CD_3)_2SO$) δ 9.06 (d, *J* = 5.6 Hz, 1H, Leu^a-NH), 8.33 (d, *J* = 2.6 Hz, 1H, Thr-NH), 7.63 (d, *J* = 8.8 Hz, 1H, Ala-NH), 7.07 (d, *J* = 9.7 Hz, 1H, Leu^b-NH), 5.16-5.07 (m, 1H, 3HOA^1-C$_\beta$H), 4.46 (dt, *J* = 4.3 Hz, 10.1 Hz, 1H, Leu^b-C$_\alpha$H), 4.21 (td, *J* = 7.4 Hz, 16.2 Hz, 1H, Ala-C$_\alpha$H), 3.87-3.78 (m, 2H, Thr-C$_\alpha$H, Leu^a-C$_\alpha$H), 3.65 (td, *J* = 6.4 Hz, 15.0 Hz, 1H, Thr-C$_\beta$H), 2.77 (dd, *J* = 3.6 Hz, 13.3 Hz, 1H, 3HOA^1-C$_\alpha$H$_1$), 2.08 (dd, *J* = 10.5 Hz, 13.5 Hz, 1H, 3HOA^1-C$_\alpha$H$_2$), 1.81-1.69 (m, 1H, Leu^a-C$_\gamma$H), 1.67-1.39 (m, 7H, Leu^a-C$_\beta$H, Leu^b-C$_\beta$H, Leu^b-C$_\gamma$H, 3HOA^1-C$_\gamma$H), 1.35 (d, *J* = 7.4 Hz, 3H, Ala-C$_\beta$H), 1.32-1.15 (m, 6H, 3HOA^1-C$_\delta$H, 3HOA^1-C$_\varepsilon$H, 3HOA^1-C$_\zeta$H), 1.06 (d, *J* = 6.2 Hz, 3H, Thr-C$_\gamma$H), 0.91 (d, *J* = 6.6 Hz, 3H, Leu^a-C$_\delta$H$_1$), 0.88-0.77 (m, 12H, Leu^a-C$_\delta$H$_2$, Leu^b-C$_\delta$H, 3HOA^1- C$_\eta$H); ^{13}C-NMR (125 MHz, $(CD_3)_2SO$) δ 173.64, 171.68, 171.04, 171.02, 170.85, 161.64, 157.80, 72.67, 65.39, 61.88, 53.12, 48.81, 48.17, 40.96, 34.14, 31.06, 24.19, 24.04, 23.95, 23.23, 23.19, 21.93, 21.34, 20.28, 19.99, 16.64, 13.84.

(Tyr(tBu)^2)SolB (**4.43**- Method A)



Initial resin preparation and peptide couplings were similar to those reported in Method A above. The final coupling was performed similar to Method A but using (*R*)-3-hydroxy-octanoic acid (**4.10**, 127 mg, 0.8 mmol) Cleavage of the linear peptide from the resin and lyophilisation were executed as in Method A producing a white fluffy powder (79.1 mg, 58%).

Further processes were performed as described in Method A furnishing a yellow solid which was purified *via* semi-preparative RP-HPLC to afford pure

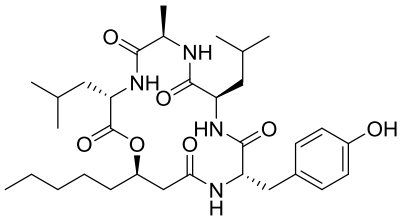
(Tyr(tBu)^2)SolB (**4.43**, 31.7 mg, 41%) and (Tyr(tBu)^2)epiSolB (**4.44**, 9.3 mg, 12%).

(Tyr(tBu)^2)SolB (**4.43**) MS$^+$ (ES-TOF): m/z calcd: 659.4339 [M+H]$^+$; found: 659.3524; Analytical RP-HPLC Onyx Monolithic C18 100 × 4.6 mm, 20% for 2 min increasing to 80% B in 20 min, t_R 15.92 min; $[\alpha]_D^{20}$ = +7.5 ^{o} (c 0.3, MeOH); ^{1}H-NMR (400 MHz, $(CD_3)_2SO$) δ 8.71 (d, *J* = 5.6 Hz, 1H, Leu^a-NH), 8.57 (d, *J* = 3.2 Hz, 1H, Tyr-NH), 7.51 (d, *J* = 8.8 Hz, 1H, Ala-NH), 7.11 (d, *J* = 8.5 Hz, 2H, Ar-H), 7.07 (d, *J* = 9.7 Hz, 1H, Leu^b-NH), 6.86 (d, *J* = 8.4 Hz, Ar-H), 5.19-5.09 (m, 1H, 3HOA^1-C_βH), 4.48 (dt, *J* = 4.2 Hz, 10.0 Hz, Ala-C_αH), 4.26-4.14 (m, 2H, Tyr-C_αH, Leu^b-C_αH), 3.68-3.60 (m, 1H, Leu^a-C_αH), 2.89 (dd, *J* = 5.9 Hz, 13.6 Hz, 1H, Tyr-$C_\beta H_1$), 2.72 (dd, *J* = 9.8 Hz, 13.6 Hz, 1H, Tyr-$C_\beta H_2$), 2.69 (dd, *J* = 3.8 Hz, 13.6 Hz, 1H, 3HOA^1-$C_\alpha H_1$), 2.11 (dd, *J* = 10.2 Hz, 13.7 Hz, 1H, 3HOA^1-$C_\alpha H_2$), 1.71-1.59 (m, 2H, Leu$^{a/b}$-C_γH, 3HOA^1-$C_\gamma H_1$), 1.58-1.36 (m, 5H, Leu^a-C_βH, Leu^b-C_βH, 3HOA^1-$C_\gamma H_1$), 1.34 (d, *J* = 7.3 Hz, 3H, Ala-C_βH), 1.28 (s, 9H, tBu-CH), 1.27-1.13 (m, 7H, Leu$^{a/b}$-C_γH, 3HOA^1-C_δH, 3HOA^1-C_εH, 3HOA^1-C_ζH), 0.92-0.78 (m, 9H, Leu$^{a/b}$-C_δH, 3HOA^1- C_ηH), 0.74 (d, *J* = 6.6 Hz, 3H, Leu$^{a/b}$-$C_\delta H_1$), 0.62 (d, *J* = 6.4 Hz, 3H, Leu$^{a/b}$-$C_\delta H_2$); ^{13}C-NMR (125 MHz, $(CD_3)_2SO$) δ 174.58, 171.71, 171.11, 171.04, 170.59, 161.63, 153.80, 130.83, 129.55, 123.21, 77.53, 72.29, 55.90, 53.01, 48.90, 48.10, 43.44, 40.79, 35.69, 34.05, 31.02, 28.53, 24.06, 24.00, 23.72, 23.21, 23.10, 21.92, 21.32, 20.58, 16.61, 13.83.

(Tyr(tBu)^2)epiSolB (**4.44**) MS$^+$ (ES-TOF): m/z calcd: 659.4339 [M+H]$^+$; found: 659.3456; Analytical RP-HPLC Onyx Monolithic C18 100 × 4.6 mm, 20% for 2 min increasing to 80% B in 20 min, t_R 15.80 min; $[\alpha]_D^{20}$ = +24.3 ^{o} (c 0.3, MeOH); ^{1}H-NMR (400 MHz, $(CD_3)_2SO$) δ 8.45 (d, *J* = 6.0 Hz, 2H, Leu^a-NH, Tyr-NH), 7.44 (d, *J* = 9.1 Hz, 1H, Ala-NH), 7.38 (d, *J* = 6.5 Hz, 1H, Leu^b-NH), 7.11 (d, *J* = 8.5 Hz, 2H, Ar-H), 6.85 (d, *J* = 8.6 Hz, 2H, Ar-H), 4.92-4.83 (m, 1H, 3HOA^1-C_βH), 4.33-4.18 (m, 2H, Ala-C_αH, Tyr-C_αH), 3.93-3.80 (m, 2H, Leu^a-C_αH, Leu^b-C_αH), 2.83 (dd, *J* = 6.8 Hz, 13.6 Hz, 1H, Tyr-$C_\beta H_1$), 2.77 (dd, *J* = 9.0 Hz, 13.5 Hz, 1H, Tyr-$C_\beta H_2$), 2.61 (dd, *J* = 4.3, 14.5 Hz, 1H, 3HOA^1-$C_\alpha H_1$), 2.26 (dd, *J* = 6.4 Hz, 14.6 Hz, 1H, 3HOA^1-$C_\alpha H_2$), 1.92 (td, *J* = 9.2 Hz, 16.8 Hz, 1H, Leu^a-$C_\beta H_1$), 1.80-1.68 (m, 1H, 3HOA^1-$C_\gamma H_1$), 1.64-1.49 (m, 2H, 3HOA^1-$C_\gamma H_2$, Leu^a-$C_\beta H_2$), 1.45-1.08 (m, 21H, Ala-

$C_\beta H$, 3HOA^1-$C_\delta H$, 3HOA^1-$C_\varepsilon H$, 3HOA^1-$C_\zeta H$, Leu^a-$C_\gamma H$, Leu^b-$C_\beta H$, tBu-CH), 0.92-0.83 (m, 9H, 3HOA^1- $C_\eta H$, Leu^a-$C_\delta H_1$, Leu^a-$C_\delta H_2$), 0.75 (d, *J* = 6.6Hz, 3H, Leu^b-$C_\delta H_1$), 0.65 (d, *J* = 6.5 Hz, 3H, Leu^b-$C_\delta H_2$); ^{13}C-NMR (125 MHz, $(CD_3)_2SO$) δ 182.34, 171.87, 171.43, 170.26, 170.15, 161.63, 153.73, 131.21, 129.58, 123.21, 77.53, 55.52, 53.26, 52.06, 48.37, 38.52, 37.40, 36.08, 33.09, 30.98, 28.53, 27.06, 24.64, 24.12, 23.72, 23.05, 22.44, 21.93, 21.87, 20.78, 17.04, 13.81.

(Tyr^2)SolB (**4.45**- Method A)

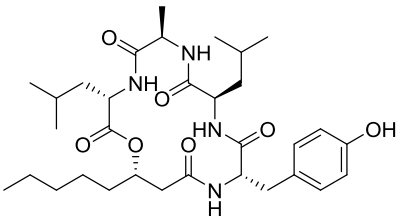


(Tyr(tBu)^2)SolB (**4.43**, 12.4 mg) was dissolved in TFA. After 16 hours, the TFA was evaporated *in vacuo*. The residue was dissolved and then the solvent was evaporated using toluene, hexane and Et_2O to remove traces of TFA. The residue was then dissolved in MeCN/H_2O and lyophilised affording the final product, (Tyr^2)SolB (**4.45**), as a fluffy white powder (11.3 mg, quantitative yield)

(Tyr^2)SolB (**4.45**) MS$^+$ (ES-TOF): m/z calcd: 603.3713 $[M+H]^+$; found: 603.3384; Analytical RP-HPLC Onyx Monolithic C18 100 × 4.6 mm, 20% for 2 min increasing to 80% B in 20 min, t_R 11.67 min; $[\alpha]_D^{20}$ = +7.5 ^{o} (c 0.3, MeOH); ^{1}H-NMR (400 MHz, $(CD_3)_2SO$) δ 9.18 (s, 1H, Ar-OH), 8.58 (d, *J* = 5.6 Hz, 1H, Leu^a-NH), 8.54 (d, *J* = 3.2 Hz, 1H, Tyr-NH), 7.50 (d, *J* = 9.1 Hz, 1H, Ala-NH), 7.07 (d, *J* = 9.7 Hz, 1H, Leu^b-NH), 6.97 (d, *J* = 8.5 Hz, 2H, Ar-H), 6.64 (d, *J* = 8.6 Hz, 2H, Ar-H), 5.17-5.08 (m, 1H, 3HOA^1-$C_\beta H$), 4.46 (dt, *J* = 4.3 Hz, 15.0 Hz, 1H, Leu^b -$C_\alpha H$), 4.24-4.13 (m, 2H, Tyr-$C_\alpha H$, Ala-$C_\alpha H$), 3.62-3.53 (m, 1H, Leu^a-$C_\alpha H$), 2.83 (dd, *J* = 6.2 Hz, 13.6 Hz, 1H, Tyr-$C_\beta H_1$), 2.68 (dd, *J* = 3.8 Hz, 13.5 Hz, 1H, 3HOA^1-$C_\alpha H_1$), 2.62 (dd, *J* = 10.2 Hz, 13.3 Hz, 1H, Tyr-$C_\beta H_2$), 2.10 (dd, *J* = 10.5 Hz, 13.7 Hz, 1H, 3HOA^1-$C_\alpha H_2$), 1.71-1.58 (m, 2H, Leu^b-$C_\beta H_1$, 3HOA^1-$C_\gamma H_1$), 1.57-1.35 (m, 4H, Leu^a-$C_\beta H_1$, Leu^b-$C_\beta H_2$, Leu^b-$C_\gamma H$, 3HOA^1-$C_\gamma H_2$), 1.33 (d, *J* = 7.4 Hz, 3H, Ala-$C_\beta H$), 1.31-1.15 (m, 7H, Leu^a-$C_\beta H_2$, 3HOA^1-$C_\delta H$, 3HOA^1-$C_\varepsilon H$, 3HOA^1-$C_\zeta H$), 1.13-1.00 (m, 1H, Leu^a-

$C_\gamma H$), 0.91-0.79 (m, 9H, Leu^b-$C_\delta H$, 3HOA^1- $C_\eta H$), 0.74 (d, *J* = 6.6 Hz, 3H, Leu^a-$C_\delta H_1$), 0.58 (d, *J* = 6.4 Hz, 3H, Leu^a-$C_\delta H_2$); ^{13}C-NMR (125 MHz, $(CD_3)_2SO$) δ 174.56, 171.77, 171.12, 171.02, 170.54, 156.11, 129.87, 126.19, 114.92, 72.32, 56.21, 52.91, 48.89, 48.06, 40.74, 39.20, 35.57, 34.06, 31.02, 24.06, 24.00, 23.61, 23.21, 21.91, 21.34, 20.46, 16.63, 13.83.

(Tyr^2)epiSolB (**4.46**- Method A)

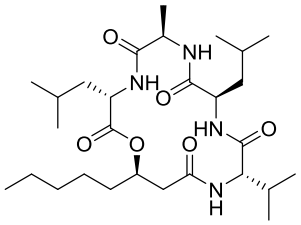


(Tyr(tBu)^2)epiSolB (**4.44**, 2.9 mg) was dissolved in TFA. After 16 hours, the TFA was evaporated *in vacuo*. The residue was dissolved and then the solvent was evaporated using toluene, hexane and Et_2O to remove traces of TFA. The residue was then dissolved in MeCN/H_2O and lyophilised affording the final product, 2thr-SolB, as a fluffy white powder (2.6 mg, quantitative yield)

(Tyr^2)epiSolB (**4.46**) MS$^+$ (ES-TOF): m/z calcd: 603.3713 $[M+H]^+$; found: 603.3424; Analytical RP-HPLC Onyx Monolithic C18 100 × 4.6 mm, 20% for 2 min increasing to 80% B in 20 min, t_R 11.68 min; $[\alpha]_D^{20}$ = +26.11 ^{o} (c 0.3, MeOH); ^{1}H-NMR (400 MHz, $(CD_3)_2SO$) δ 9.18 (s, 1H, Ar-OH), 8.42 (d, *J* = 5.0 Hz, 1H, Tyr-NH), 8.35 (d, *J* = 7.2 Hz, 1H, Leu^a-NH), 7.41 (d, *J* = 9.0 Hz, 1H, Ala-NH), 7.37 (d, *J* = 6.3 Hz, 1H, Leu^b-NH), 6.98 (d, *J* = 8.6 Hz, 2H, Ar-H), 6.64 (d, *J* = 8.6 Hz, 2H, Ar-H), 4.91-4.83 (m, 1H, 3HOA^1-$C_\beta H$), 4.29-4.17 (m, 2H, Ala-$C_\alpha H$, Tyr-$C_\alpha H$), 3.87-3.78 (m, 2H, Leu^a-$C_\alpha H$, Leu^b-$C_\alpha H$), 2.78 (d, *J* = 6.6 Hz, 13.4 Hz, 1H, Tyr-$C_\beta H_1$), 2.68 (dd, *J* = 9.3 Hz, 13.5 Hz, 1H, Tyr-$C_\beta H_2$), 2.61 (dd, *J* = 4.4 Hz, 14.3 Hz, 1H, 3HOA^1-$C_\alpha H_1$), 2.26 (dd, *J* = 6.3 Hz, 14.3 Hz, 1H, 3HOA^1-$C_\alpha H_2$), 1.92 (td, *J* = 9.0 Hz, 16.7 Hz, 1H, Leu^b-$C_\beta H_1$), 1.79-1.67 (m, 1H, 3HOA^1-$C_\gamma H_1$), 1.65-1.45 (m, 3H, 3HOA^1-$C_\gamma H_2$, Leu^b-$C_\beta H_2$, Leu^b-$C_\gamma H$), 1.43-1.13 (m, 11H, Leu^a-$C_\beta H$, Ala-$C_\beta H$, 3HOA^1-$C_\delta H$, 3HOA^1-$C_\varepsilon H$, 3HOA^1-$C_\zeta H$), 1.06-0.94 (m, 1H, Leu^a-$C_\gamma H$), 0.91-0.82 (m, 9H, 3HOA^1- $C_\eta H$, Leu^b-$C_\delta H_1$, Leu^b-$C_\delta H_2$), 0.74 (d, *J* = 6.6Hz, 3H, Leu^a-$C_\delta H_1$), 0.62 (d, *J* = 6.4 Hz, 3H, Leu^a-$C_\delta H_2$); ^{13}C-NMR (125 MHz, $(CD_3)_2SO$) δ 172.71, 171.88, 171.85, 171.45, 170.17,

156.06, 129.94, 126.53, 114.88, 71.40, 55.86, 53.30, 51.99, 48.37, 38.54, 38.31, 37.40, 35.93, 33.20, 30.98, 27.03, 24.66, 24.09, 23.55, 23.14, 22.41, 21.93, 20.71, 17.07, 13.80.

(Val^{2})SolB (**4.47**- Method A)



Initial resin preparation and peptide couplings were similar to those reported in Method A above. The final coupling was performed similar to Method A but using (*R*)-3-hydroxy-octanoic acid (**4.10**, 136 mg, 0.8 mmol) Cleavage of the linear peptide from the resin and lyophilisation were executed as in Method A producing a white fluffy powder (68.9 mg, 62%).

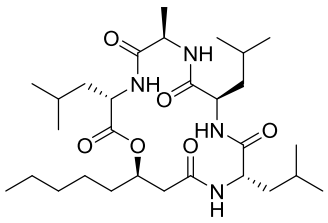
Further processes were performed as described in Method A furnishing a yellow solid which was purified *via* semi-preparative RP-HPLC to afford pure (Val^{2})SolB (**4.47**, 28.0 mg, 42%) and (Val^{2})epiSolB (**4.48**, 4.6 mg, 7%).

(Val^{2})SolB (**4.47**) MS^{+} (ES-TOF): m/z calcd: 539.3764 $[M+H]^{+}$; found: 539.4097; Analytical RP-HPLC Onyx Monolithic C18 100 × 4.6 mm, 20% for 2 min increasing to 80% B in 20 min, t_R 12.96 min; $[\alpha]_D^{20}$ = +2.8 ^{o} (c 0.3, MeOH); ^{1}H-NMR (400 MHz, $(CD_3)_2SO$) δ 8.94 (d, *J* = 6.1 Hz, 1H, Leu^{a}-NH), 8.30 (d, *J* = 3.8 Hz, 1H, Val-NH), 7.50 (d, *J* = 9.1 Hz, 1H, Ala-NH), 7.09 (d, *J* = 9.7 Hz, 1H, Leu^{b}-NH), 5.19-5.09 (m, 1H, 3HOA^{1}-C$_{\beta}$H), 4.45 (dt, *J* = 4.3 Hz, 10.1 Hz, 1H, Leu^{b}-C$_{\alpha}$H), 4.21 (td, *J* = 7.4 Hz, 16.1 Hz, 1H, Ala-C$_{\alpha}$H), 3.88-3.79 (m, 1H, Leu^{a}-C$_{\alpha}$H), 3.72 (dd, *J* = 3.9 Hz, 8.9 Hz, 1H, Val-C$_{\alpha}$H), 2.71 (dd, *J* = 3.9 Hz, 13.5 Hz, 1H, 3HOA^{1}-C$_{\alpha}$H$_1$), 2.11 (dd, *J* = 10.0 Hz, 13.5 Hz, 1H, 3HOA^{1}-C$_{\alpha}$H$_2$), 1.85-1.70 (m, 2H, Leu-C$_{\gamma}$H, Val-C$_{\beta}$H), 1.70-1.56 (m, 3H, 3HOA^{1}-C$_{\gamma}$H$_1$, Leu^{a}-C$_{\beta}$H$_1$, Leu^{b}-C$_{\beta}$H$_1$), 1.56-1.40 (m, 4H, 3HOA^{1}-C$_{\gamma}$H$_2$, Leu-C$_{\gamma}$H, Leu^{a}-C$_{\beta}$H$_2$, Leu^{b}-C$_{\beta}$H$_2$), 1.35 (d, *J*= 7.4 Hz, 3H, Ala-C$_{\beta}$H), 1.31-1.12 (m, 6H, 3HOA^{1}-C$_{\delta}$H, 3HOA^{1}-C$_{\varepsilon}$H, 3HOA^{1}-C$_{\zeta}$H), 1.00 (d, *J*= 6.6 Hz, 3H, Val-C$_{\gamma}$H$_1$), 0.91 (d, *J* = 6.6 Hz, 3H, Val-C$_{\gamma}$H$_2$), 0.88-0.78 (m, 15H, Leu$^{a\&b}$-C$_{\delta}$H, 3HOA^{1}- C$_{\eta}$H); ^{13}C-NMR (125 MHz, $(CD_3)_2SO$) δ 174.72, 171.73, 171.15, 171.02,

170.85, 72.22, 60.75, 52.91, 48.96, 48.18, 40.66, 38.81, 34.07, 31.07, 28.37, 24.12, 24.07, 23.97, 23.21, 21.92, 21.30, 20.18, 20.11, 18.73, 16.57, 13.83.

(Val^{2})epiSolB (**4.48**) MS^{+} (ES-TOF): m/z calcd: 539.3764 [M+H]$^{+}$; found: 539.4097; Analytical RP-HPLC Onyx Monolithic C18 100 × 4.6 mm, 20% for 2 min increasing to 80% B in 20 min, t_R 12.73 min; $[\alpha]_D^{20}$ = +44.0 ^{o} (c 0.3, MeOH); ^{1}H-NMR (400 MHz, $(CD_3)_2SO$) δ 8.67 (d, *J* = 6.9 Hz, 1H, Leu^{a}-NH), 8.22 (d, *J* = 5.8 Hz, 1H, Val-NH), 7.44 (d, *J* = 9.1 Hz, 1H, Ala-NH), 7.39 (d, *J* = 6.6 Hz, 1H, Leu^{b}-NH), 4.91-4.83 (m, 1H, 3HOA^{1}-C$_{\beta}$H), 4.27 (td, *J* = 7.3 Hz, 16.2 Hz, 1H, Ala-C$_{\alpha}$H), 4.06-3.98 (m, 1H, Leu^{a}-C$_{\alpha}$H), 3.86-3.76 (m, 2H, Leu^{b}-C$_{\alpha}$H, Val-C$_{\alpha}$H), 2.66 (dd, *J* = 4.3 Hz, 14.4 Hz, 1H, 3HOA^{1}-C$_{\alpha}$H$_1$), 2.27 (dd, *J* = 5.7 Hz, 14.4 Hz, 1H, 3HOA^{1}-C$_{\alpha}$H$_2$), 1.92 (td, *J* = 9.0 Hz, 16.5 Hz, 1H, Leu^{b}-C$_{\beta}$H$_1$), 1.87-1.62 (m, 4H, Val-C$_{\beta}$H, 3HOA^{1}-C$_{\gamma}$H$_1$, Leu^{a}-C$_{\gamma}$H, Leu^{b}-C$_{\gamma}$H), 1.62-1.49 (m, 4H, Leu^{a}-C$_{\beta}$H, Leu^{b}-C$_{\beta}$H$_2$, 3HOA^{1}-C$_{\gamma}$H$_2$), 1.33-1.12 (m, 9H, Ala-C$_{\beta}$H, 3HOA^{1}-C$_{\delta}$H, 3HOA^{1}-C$_{\varepsilon}$H, 3HOA^{1}-C$_{\zeta}$H), 0.94 (d, *J* = 6.6 Hz, 3H, Val-C$_{\gamma}$H$_1$), 0.72-0.98 (m, 18H, Leu$^{a\&b}$-C$_{\delta}$H, Val-C$_{\gamma}$H$_2$, 3HOA^{1}- C$_{\eta}$H); ^{13}C-NMR (125 MHz, $(CD_3)_2SO$) δ 173.06, 171.87, 171.45, 170.33, 170.29, 71.30, 60.18, 58.10, 53.21, 52.08, 48.27, 33.01, 31.01, 28.79, 24.62, 24.16, 23.19, 22.49, 21.94, 21.80, 20.39, 19.66, 18.84, 16.95, 16.69, 13.81.

(Leu^{2})SolB (**4.49**- Method A)



Initial resin preparation and peptide couplings were similar to those reported in Method A above. The final coupling was performed similar to Method A but using (*R*)-3-hydroxy-octanoic acid (**4.10**, 126 mg, 0.8 mmol) Cleavage of the linear peptide from the resin and lyophilisation were executed as in Method A producing a white fluffy powder (67.7 mg, 59%).

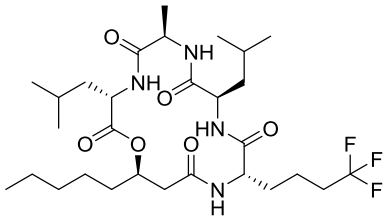
Further processes were performed as described in Method A furnishing a yellow solid which was purified *via* semi-preparative RP-HPLC to afford pure (Leu^{2})SolB (**4.49**, 12.5 mg, 19%) and (Leu^{2})epiSolB (**4.50**, 7.4 mg, 11%).

(Leu^2)SolB (**4.49**) MS$^+$ (ES-TOF): m/z calcd: 553.3920 [M+H]$^+$; found: 553.4168; Analytical RP-HPLC Onyx Monolithic C18 100 × 4.6 mm, 20% for 2 min increasing to 80% B in 20 min, t_R 14.85 min; $[\alpha]_D^{20}$ = -0.3 ^{o} (c 0.3, MeOH); ^{1}H-NMR (400 MHz, $(CD_3)_2SO$) δ 9.08 (d, *J* = 5.9 Hz, 1H, Leu^a-NH), 8.35 (d, *J* = 3.3 Hz, 1H, Leu^b-NH), 7.51 (d, *J* = 8.8 Hz, 1H, Ala-NH), 7.06 (d, *J* = 9.9 Hz, 1H, Leu^c-NH), 5.16-5.06 (m, 1H, 3HOA^1-C$_\beta$H), 4.46 (dt, *J* = 4.3 Hz, 10.1 Hz, 1H, Leu^c-C$_\alpha$H), 4.21 (td, *J* = 7.4 Hz, 16.2 Hz, 1H, Ala-C$_\alpha$H), 4.05 (dt, *J* = 3.4 Hz, 7.6 Hz, 1H, Leu^b-C$_\alpha$H), 3.85-3.76 (m, 1H, Leu^a-C$_\alpha$H), 2.67 (dd, *J* = 3.8 Hz, 13.5 Hz, 1H, 3HOA^1-C$_\alpha$H$_1$), 2.10 (dd, *J* = 10.4 Hz, 13.5 Hz, 1H, 3HOA^1-C$_\alpha$H$_2$), 1.80-1.69 (m, 1H, Leu^a-C$_\gamma$H), 1.69-1.38 (m, 10H, Leu^a-C$_\beta$H, Leu^b-C$_\beta$H, Leu^c-C$_\beta$H, Leu^b-C$_\gamma$H, Leu^b-C$_\gamma$H, 3HOA^1-C$_\gamma$H,), 1.36 (d, *J*= 7.4 Hz, 3H, Ala-C$_\beta$H), 1.31-1.13 (m, 6H, 3HOA^1-C$_\delta$H, 3HOA^1-C$_\varepsilon$H, 3HOA^1-C$_\zeta$H), 0.93 (d, *J*= 6.5 Hz, 3H, Leu$^{b/c}$-C$_\delta$H), 0.90 (d, *J* = 6.6 Hz, 3H, Leu^a-C$_\delta$H$_1$), 0.89-0.77 (m, 15H, Leu^a-C$_\delta$H$_2$, Leu$^{b/c}$-C$_\delta$H, 3HOA^1- C$_\eta$H); ^{13}C-NMR (125 MHz, $(CD_3)_2SO$) δ 175.56, 171.73, 171.08, 171.03, 170.78, 72.32, 53.11, 52.81, 48.86, 48.16, 40.73, 38.73, 34.06, 31.02, 24.27, 24.13, 24.06, 23.96, 23.22, 23.10, 22.43, 22.08, 21.92, 21.31, 20.34, 16.59, 13.82.

(Leu^2)epiSolB (**4.50**) MS$^+$ (ES-TOF): m/z calcd: 553.3920 [M+H]$^+$; found: 553.4087; Analytical RP-HPLC Onyx Monolithic C18 100 × 4.6 mm, 20% for 2 min increasing to 80% B in 20 min, t_R 14.41 min; $[\alpha]_D^{20}$ = +7.5 ^{o} (c 0.3, MeOH); ^{1}H-NMR (400 MHz, $(CD_3)_2SO$) δ 8.77 (d, *J* = 7.2 Hz, 1H, Leu^a-NH), 8.27 (d, *J* = 5.2 Hz, 1H, Leu^b-NH), 7.46 (d, *J* = 9.0 Hz, 1H, Ala-NH), 7.36 (d, *J* = 6.4 Hz, 1H, Leu^c-NH), 4.90-4.82 (m, 1H, 3HOA^1-C$_\beta$H), 4.27 (td, *J* = 7.1 Hz, 16.2 Hz, 1H, Ala-C$_\alpha$H), 4.10 (dt, *J* = 5.3 Hz, 7.6 Hz, 1H, Leu^b-C$_\alpha$H), 4.04-3.95 (m, 1H, Leu^a-C$_\alpha$H), 3.81 (td, *J* = 6.3 Hz, 8.7 Hz, 1H, Leu^c-C$_\alpha$H), 2.61 (dd, *J* = 4.5 Hz, 14.3 Hz, 1H, 3HOA^1-C$_\alpha$H$_1$), 2.26 (dd, *J* = 6.3 Hz, 14.3 Hz, 1H, 3HOA^1-C$_\alpha$H$_2$), 1.93 (td, *J* = 9.2 Hz, 16.1 Hz, 1H, Leu^c-C$_\beta$H$_1$), 1.80-1.69 (m, 1H, 3HOA^1-C$_\gamma$H$_1$), 1.69-1.61 (m, 1H, Leu$^{a/b/c}$-C$_\gamma$H), 1.61-1.47 (m, 6H, Leu^a-C$_\beta$H, Leu^c-C$_\beta$H$_2$, 3HOA^1-C$_\gamma$H$_2$, Leu$^{a/b/c}$-C$_\gamma$H, , Leu$^{a/b/c}$-C$_\gamma$H), 1.41 (t, *J* = 7.2 Hz, 2H, Leu^b-C$_\beta$H), 1.29 (d, *J* = 7.2 Hz, 3H, Ala-C$_\beta$H), 1.27-1.13 (m, 6H, 3HOA^1-C$_\delta$H, 3HOA^1-C$_\varepsilon$H, 3HOA^1-C$_\zeta$H), 0.95-0.82 (m, 18H, Leu-C$_\delta$H, 3HOA^1-C$_\eta$H), 0.80 (d, *J* = 6.4 Hz, 3H, Leu-C$_\delta$H); ^{13}C-NMR (125 MHz, $(CD_3)_2SO$) δ 173.72, 171.85, 171.43, 170.35, 170.23, 161.63, 71.39, 53.32, 52.38, 52.16, 48.38, 38.45,

38.31, 33.14, 30.99, 30.68, 24.64, 24.30, 24.16, 24.09, 23.09, 22.43, 22.35, 22.25, 21.94, 21.84, 20.58, 17.01, 13.81.

(Tfh^2)SolB (**4.51**- Method A)



Initial resin preparation and peptide couplings were similar to those reported in Method A above. The final coupling was performed similar to Method A but using (*R*)-3-hydroxy-octanoic acid (**4.10**, 124 mg, 0.8 mmol) Cleavage of the linear peptide from the resin and lyophilisation were executed as in Method A producing a white fluffy powder (92.9 mg, 74%).

Further processes were performed as described in Method A furnishing a yellow solid which was purified *via* semi-preparative RP-HPLC to afford pure (Tfh^2)SolB (**4.51**, 6.5 mg, 7%) and (Tfh^2)epiSolB (**4.52**, 7.8 mg, 9%).

(Tfh^2)SolB (**4.51**) MS$^+$ (ES-TOF): m/z calcd: 607.3638 $[M+H]^+$; found: 607.3293; Analytical RP-HPLC Onyx Monolithic C18 100 × 4.6 mm, 20% for 2 min increasing to 80% B in 20 min, t_R 14.52 min; $[\alpha]_D^{20}$ = -14.0 ^{o} (c 0.3, MeOH); ^{1}H-NMR (400 MHz, $(CD_3)_2SO$) δ 9.05 (d, *J* = 5.7 Hz, 1H, Tfh-NH), 8.50 (d, *J* = 3.3 Hz, 1H, Leu^a-NH), 7.51 (d, *J* = 9.1 Hz, 1H, Ala-NH), 7.06 (d, *J* = 9.6 Hz, 1H, Leu^b-NH), 5.15-5.05 (m, 1H, 3HOA^1-C$_\beta$H), 4.45 (dt, *J* = 4.3 Hz, 15.2 Hz, 1H, Leu^b-C$_\alpha$H), 4.22 (td, *J* = 7.4 Hz, 16.2 Hz, 1H, Ala-C$_\alpha$H), 4.04-3.96 (m, 1H, Leu^a-C$_\alpha$H), 3.87-3.79 (m, 1H, Tfh-C$_\alpha$H), 2.68 (dd, *J* = 3.8 Hz, 13.5 Hz, 1H, 3HOA^1-C$_\alpha$H$_1$), 2.41-2.24 (m, 2H, Tfh-C$_\delta$H), 2.11 (dd, *J*= 10.4 Hz, 13.5 Hz, 1H, 3HOA^1-C$_\alpha$H$_2$), 1.80-1.69 (m, 1H, Leu^b-C$_\gamma$H), 1.69-1.38 (m, 11H, 3HOA^1-C$_\gamma$H, Tfh-C$_\beta$H, Tfh-C$_\gamma$H, Leu^a-C$_\beta$H, Leu^b-C$_\beta$H, Leu^a-C$_\gamma$H), 1.36 (d, *J* = 7.4 Hz, 3H, Ala- C$_\beta$H), 1.31-1.13 (m, 6H, 3HOA^1-C$_\delta$H, 3HOA^1-C$_\varepsilon$H, 3HOA^1-C$_\zeta$H), 0.90 (d, *J* = 6.6 Hz, 3H, Leu^b-C$_\delta$H$_1$), 0.88-0.77 (m, 12H, 3HOA^1- C$_\eta$H, Leu^a-C$_\delta$H, Leu^b-C$_\delta$H$_2$); ^{13}C-NMR (125 MHz, $(CD_3)_2SO$) δ 175.06, 171.54, 171.01, 170.98, 170.69, 161.61, 72.31, 58.08, 54.06, 53.05, 48.85, 48.17,

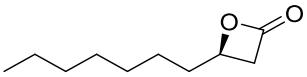
40.66, 38.67, 37.38, 34.03, 30.99, 28.71, 24.15, 24.04, 23.93, 23.19, 23.11, 21.89, 21.31, 20.15, 16.58, 13.80.

(Tfh^{2})epiSolB (**4.52**) MS^{+} (ES-TOF): m/z calcd: 607.3638 [M+H]$^{+}$; found: 607.3367; Analytical RP-HPLC Onyx Monolithic C18 100 × 4.6 mm, 20% for 2 min increasing to 80% B in 20 min, t_R 14.48 min; $[\alpha]_D^{20}$ = +60.0 ^{o} (c 0.3, MeOH); ^{1}H-NMR (400 MHz, $(CD_3)_2SO$) δ 8.72 (d, *J* = 7.1 Hz, 1H, Tfh-NH), 8.37 (d, *J* = 5.1 Hz, 1H, Leu^{a}-NH), 7.51 (d, *J* = 8.8 Hz, 1H, Ala-NH), 7.38 (d, *J* = 6.6 Hz, 1H, Leu^{b}-NH), 4.90-4.82 (m, 1H, 3HOA^{1}-C$_\beta$H), 4.27 (td, *J* = 7.2 Hz, 16.1 Hz, 1H, Ala-C$_\alpha$H), 4.11-3.97 (m, 2H, Leu^{a}-C$_\alpha$H, Tfh-C$_\alpha$H), 3.84 (td, *J* = 6.4 Hz, 8.5 Hz, 1H, Leu^{b}-C$_\alpha$H), 2.61 (dd, *J* = 4.2 Hz, 14.4 Hz, 1H, 3HOA^{1}-C$_\alpha$H$_1$), 2.40-2.20 (m, 3H, 3HOA^{1}-C$_\alpha$H$_2$, Tfh-C$_\delta$H), 1.90 (td, *J* = 9.0 Hz, 16.6 Hz, 1H, Leu^{b}-C$_\beta$H$_1$), 1.79-1.34 (m, 11H, Leu^{a}-C$_\beta$H, Leu^{b}-C$_\beta$H$_2$, Leu^{a}-C$_\gamma$H, Leu^{b}-C$_\gamma$H Tfh-C$_\beta$H, Tfh-C$_\gamma$H, 3HOA^{1}-C$_\gamma$H), 1.33-1.13 (m, 9H, Ala-C$_\beta$H, 3HOA^{1}-C$_\delta$H, 3HOA^{1}-C$_\varepsilon$H, 3HOA^{1}-C$_\zeta$H), 0.94-0.82 (m, 12H, Leu$^{a/b}$-C$_\delta$H, 3HOA^{1}-C$_\eta$H). 0.80 (d, *J*= 6.6 Hz, 3H, Leu$^{a/b}$-C$_\delta$H); ^{13}C-NMR (125 MHz, $(CD_3)_2SO$) δ 173.05, 171.73, 171.30, 170.29, 170.14, 71.40, 53.51, 53.25, 52.09, 48.45, 39.02, 38.56, 38.30, 37.38, 33.11, 30.99, 30.97, 29.24, 24.62, 24.20, 24.08, 23.08, 22.38, 21.91, 21.86, 20.39, 18.02 (q, J_{CF} = 3.8 Hz), 17.03, 13.78.

8.5.1.3 β-hydroxy acid analogues

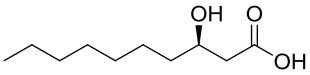
8.5.1.3.1 β-hydroxy acid synthesis

(4*R*)-4-(2-heptyl)-oxetan-2-one (**5.18**)[377]



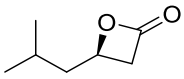
Procedure as for **4.35** above (Section 8.3.3). Produced colourless oil (589.1 mg, 63% yield). TLC R_f= 0.212 (1:10 EtOAc/Hex); ^{1}H-NMR (400 MHz, $CDCl_3$) δ 4.55-4.46 (m, 1H, C$_\beta$H), 3.50 (dd, *J* = 5.8 Hz, 16.3 Hz, 1H, C$_\alpha$H$_1$), 3.05 (dd, *J* = 4.3 Hz, 16.2 Hz, 1H, C$_\alpha$H$_2$), 1.92-1.81 (m, 1H, C$_\gamma$H$_1$), 1.80-1.68 (m, 1H, C$_\gamma$H$_2$), 1.51-1.22 (m, 10H, C$_\delta$H, C$_\varepsilon$H, C$_\zeta$H, C$_\eta$H, C$_\theta$H), 0.88 (t, *J* = 6.7 Hz, 3H, C$_\iota$H); ^{13}C-NMR (100 MHz, $CDCl_3$) δ 168.50, 71.45, 43.03, 34.83, 31.81, 29.25, 29.21, 25.03, 22.73, 14.19. Consistent with literature.[377]

(*R*)-3-hydroxydecanoic acid (**5.21**)[378]



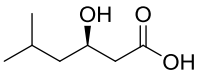
Cyclic lactone (**5.18**, 589 mg, 0.35 mmol) was treated using the procedure for **1.60** above (Section 8.3.3). Produced a colourless oil (613 mg, 94% yield). $[\alpha]_D^{20}$ = +33.8 ^{o} (c 3, MeOH); ^{1}H-NMR (400 MHz, $CDCl_3$) δ 4.07-3.98 (m, 1H, $C_\beta H$), 2.55 (dd, J = 3.1 Hz, 16.4 Hz, 1H, $C_\alpha H_1$), 2.45 (dd, J = 8.9 Hz, 16.4 Hz, 1H, $C_\alpha H_2$), 1.61-1.18 (m, 12H, $C_\gamma H$, $C_\delta H$, $C_\varepsilon H$, $C_\zeta H$, $C_\eta H$, $C_\theta H$), 0.87 (t, J = 7.1 Hz, 3H, $C_\iota H$); ^{13}C-NMR (100 MHz, $CDCl_3$) δ 177.76, 60.30, 41.25, 36.58, 31.91, 29.56, 29.33, 25.57, 22.76, 14.19. Consistent with literature.[378]

(4*R*)-isobutyl-oxetan-2-one (**5.20**)[374]



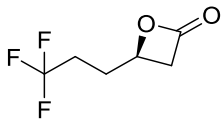
Procedure as for **4.35** above (Section 8.3.3). Produced colourless oil (549 mg, 93% yield). TLC R_f= 0.179 (1:9 EtOAc/Hex); ^{1}H-NMR (400 MHz, $CDCl_3$) δ 4.61-4.54 (m, 1H, $C_\beta H$), 3.53 (dd, *J* = 5.8 Hz, 16.2 Hz, 1H, $C\alpha H_1$), 3.05 (dd, *J* = 4.3 Hz, 16.2 Hz, 1H, $C\alpha H_2$), 1.87-1.72 (m, 2H, $C_\gamma H$), 1.64-1.53 (m, 1H, $C_\delta H$), 0.97 (d, *J* = 6.6 Hz, 6H, $C_\varepsilon H$); ^{13}C-NMR (100 MHz, $CDCl_3$) δ 168.48, 70.36, 43.77, 43.61, 25.52, 22.89, 22.32. Consistent with literature.[374]

(*R*)-3-hydroxy-5methylhexanoic acid (**5.23**)[379]



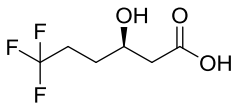
Cyclic lactone (**5.20**, 221 mg, 1.7 mmol) was treated using the procedure for **1.60** above (Section 8.3.3). Produced a colourless oil (252 mg, quantitative yield). $[\alpha]_D^{20}$ = +45.3 ^{o} (c 3, MeOH); ^{1}H-NMR (400 MHz, $CDCl_3$) δ 4.16-4.07 (m, 1H, $C_\beta H$), 2.56 (dd, *J* = 3.2 Hz, 16.6 Hz, 1H, $C_\alpha H_1$), 2.46 (dd, *J* = 8.8 Hz, 16.7 Hz, 1H, $C_\alpha H_2$), 2.10-1.73 (m, 2H, $C_\gamma H$), 1.56-1.46 (m, 1H, $C_\delta H$), 1.27-1.18 (m, 1H, $C_\delta H$), 0.93 (d, *J* = 6.8 Hz, 6H); ^{13}C-NMR (100 MHz, $CDCl_3$) δ 176.63, 66.11, 45.58, 41.31, 24.46, 23.21, 21.98. Consistent with literature.[379]

(4*R*)-(3,3,3-trifluoropropyl)-oxetan-2-one (**5.19**)



Procedure as for **4.35** above (Section 8.3.3). Produced colourless oil (481 mg, 90% yield). TLC R_f = 0.194 (1:9 EtOAc/Hex); ^{1}H-NMR (400 MHz, $CDCl_3$) δ 4.60-4.51 (m, 1H, $C_\beta H$), 3.60 (dd, *J* = 5.8 Hz, 16.4 Hz, 1H, $C\alpha H_1$), 3.13 (dd, *J* = 4.3 Hz, 16.4 Hz, 1H, $C\alpha H_2$), 2.41-2.04 (m, 4H, $C_\gamma H$, $C_\delta H$); ^{13}C-NMR (100 MHz, $CDCl_3$) δ 167.09, 126.5 (q, J_{CF} = 276 Hz), 69.32, 43.33, 30.02 (q, J_{CF} = 30 Hz), 27.79 (q, J_{CF} = 3 Hz).

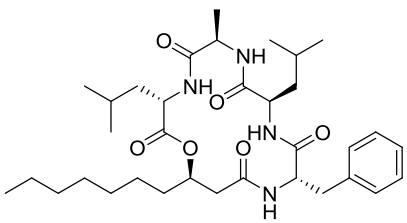
(*R*)-6,6,6-trifluoro-3-hydroxy-hexanoic acid (**5.22**)



Cyclic lactone (**5.19**, 416 mg, 2.5 mmol) was treated using the procedure for **1.60** above (Section 8.3.3). Produced a colourless oil (412 mg, 90% yield). $[\alpha]_D^{20}$ = +20.0 ^{o} (c 3, MeOH); ^{1}H-NMR (400 MHz, $CDCl_3$) δ 4.10-4.03 (m, 1H, $C_\beta H$), 2.60 (dd, *J* = 3.3 Hz, 17.1 Hz, 1H, $C_\alpha H_1$), 2.52 (dd, *J* = 8.7 Hz, 17.1 Hz, 1H, $C_\alpha H_2$), 2.46-2.28 (m, 1H, $C_\delta H_1$), 2.28-2.12 (m, 1H, $C_\delta H_2$), 1.80-1.68 (m, 2H, $C_\gamma H$). ^{13}C-NMR (100 MHz, $CDCl_3$) δ 177.36, 127.26 (q, J_{CF} = 276 Hz), 66.48, 41.05, 30.21 (q, J_{CF} = 29 Hz), 28.75 (q, J_{CF} = 3 Hz).

8.5.1.3.2 Synthesis of β-hydroxy acid analogues

(3HDA^1)Sol (**4.53**- Method A)



Initial resin preparation and peptide couplings were similar to those reported in Method A above. The final coupling was performed similar to

Method A but using (*R*)-3-hydroxy-decanoic acid (**5.21**, 158 mg, 0.8 mmol) Cleavage of the linear peptide from the resin and lyophilisation were executed as in Method A producing a white fluffy powder (74.0 mg, 59%).

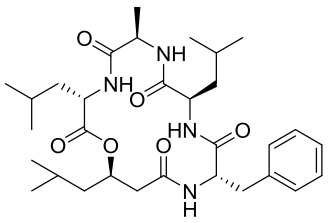
Further processes were performed as described in Method A furnishing a yellow solid which was purified *via* semi-preparative RP-HPLC to afford pure (3HDA^1)Sol (**4.53**, 4.8 mg, 7%) and (3HDA^1)epiSol (**4.54**, 4.1 mg, 6%).

(3HDA^1)Sol (**4.53**) MS$^+$ (ES-TOF): m/z calcd: 615.4077 $[M+H]^+$; found: 615.4139; Analytical RP-HPLC Onyx Monolithic C18 100 × 4.6 mm, 20% for 2 min increasing to 80% B in 20 min, t_R 16.18 min; $[\alpha]_D^{20}$ = +13.89 ^{o} (c 0.3, MeOH); ^{1}H-NMR (400 MHz, $(CD_3)_2SO$) δ 8.65 (d, *J* = 5.6 Hz, 1H, Leu^a-NH), 8.60 (d, *J* = 3.2 Hz, 1H, Phe-NH), 7.49 (d, *J* = 9.1 Hz, 1H, Ala-NH), 7.30-7.17 (m, 5H, Ar-H), 7.06 (d, *J* = 9.6 Hz, 1H, Leu^b-NH), 5.19-5.09 (m, 1H, 3HDA^1-C$_\beta$H), 4.46 (dt, *J* = 4.3 Hz, 15.1 Hz, 1H, Leu^b-C$_\alpha$H), 4.31- 4.23 (m, 1H, Phe-C$_\alpha$H), 4.19 (td, *J* = 7.5 Hz, 16.3 Hz, 1H, Ala-C$_\alpha$H), 3.61-3.53 (m, 1H, Leu^a-C$_\alpha$H), 2.96 (dd, *J* = 6.1 Hz, 13.3 Hz, 1H, Phe-C$_\beta$H$_1$), 2.74 (dd, *J* =10.0 Hz, 13.3 Hz, 1H, Phe-C$_\beta$H$_2$), 2.69 (dd, *J* =3.8 Hz, 13.6 Hz, 1H, 3HDA^1-C$_\alpha$H$_1$), 2.11 (dd, *J* = 10.3 Hz, 13.5 Hz, 1H, 3HDA^1-C$_\alpha$H$_2$), 1.71-1.58 (m, 2H, Leu^b-C$_\beta$H$_1$, 3HDA^1-C$_\gamma$H$_1$), 1.59- 1.43 (m, 3H, Leu^a-C$_\beta$H, Leu^b-C$_\beta$H$_2$, 3HDA^1-C$_\gamma$H$_2$), 1.43-1.18 (m, 15H, Ala-C$_\beta$H, Leu^b-C$_\gamma$H, 3HDA^1-C$_\delta$H, 3HDA^1-C$_\varepsilon$H, 3HDA^1-C$_\zeta$H, 3HDA^1-C$_\eta$H, 3HDA^1-C$_\theta$H), 1.06-0.95 (m, 1H, Leu^a-C$_\gamma$H), 0.91-0.80 (m, 9H, Leu^b-C$_\delta$H, 3HDA^1- C$_\iota$H), 0.71 (d, *J* = 6.7 Hz, 3H, Leu^a-C$_\delta$H$_1$), 0.54 (d, *J* = 6.5 Hz, 3H, Leu^a-C$_\delta$H$_2$); ^{13}C-NMR (125 MHz, $(CD_3)_2SO$) δ 174.42, 171.70, 171.10, 171.02, 170.60, 161.63, 136.32, 129.01, 128.19, 126.48, 72.30, 55.87, 52.92, 48.91, 48.08, 40.73, 37.39, 36.32, 34.07, 31.15, 28.78, 28.52, 24.40, 24.00, 23.53, 23.20, 23.16, 22.05, 21.33, 20.66, 16.62, 13.93.

(3HDA^1)epiSol (**4.54**) MS$^+$ (ES-TOF): m/z calcd: 615.4077 $[M+H]^+$; found: 615.3928; Analytical RP-HPLC Onyx Monolithic C18 100 × 4.6 mm, 20% for 2 min increasing to 80% B in 20 min, t_R 14.97 min; $[\alpha]_D^{20}$ = +26.1 ^{o} (c 0.3, MeOH); ^{1}H-NMR (400 MHz, $(CD_3)_2SO$) δ 8.48 (d, *J* = 5.1 Hz, 1H, Phe-NH), 8.40 (d, *J* = 7.2 Hz, 1H, Leu^a-NH), 7.43 (d, *J* = 9.1 Hz, 1H, Ala-NH), 7.38 (d, *J* = 6.5 Hz, 1H, Leu^b-NH), 7.31-7.15 (m, 5H, Ar-H), 4.92-4.83 (m, 1H, 3HDA^1-C$_\beta$H), 4.36- 4.28 (m, 1H, Phe-C$_\alpha$H), 4.24 (td, *J* = 7.3 Hz, 16.2 Hz, 1H, Ala-C$_\alpha$H), 3.89- 3.79 (m, 2H, Leu^a-C$_\alpha$H,

Leu^{b}-C$_{\alpha}$H), 2.90 (dd, *J* = 6.7 Hz, 13.3 Hz, 1H, Phe-C$_{\beta}$H$_1$), 2.80 (dd, *J* = 9.2 Hz, 13.2 Hz, 1H, Phe-C$_{\beta}$H$_2$), 2.61 (dd, *J* = 4.4 Hz, 14.4 Hz, 1H, 3HDA^{1}-C$_{\alpha}$H$_1$), 2.26 (dd, *J* = 6.3 Hz, 14.4 Hz, 1H, 3HDA^{1}-C$_{\alpha}$H$_2$), 1.91 (td, *J* = 8.9 Hz, 16.5 Hz, 1H, Leu^{b}-C$_{\beta}$H$_1$), 1.79- 1.66 (m, 1H, 3HDA^{1}-C$_{\gamma}$H$_1$), 1.62-1.47 (m, 3H, Leu^{b}-C$_{\beta}$H$_2$, Leu^{b}-C$_{\gamma}$H, 3HDA^{1}-C$_{\gamma}$H$_2$), 1.42- 1.09 (m, 15H, Ala-C$_{\beta}$H, Leu^{a}-C$_{\beta}$H, 3HDA^{1}-C$_{\delta}$H, 3HDA^{1}-C$_{\varepsilon}$H, 3HDA^{1}-C$_{\zeta}$H, 3HDA^{1}-C$_{\eta}$H, 3HDA^{1}-C$_{\theta}$H), 1.02- 0.91 (m, 1H, Leu^{a}-C$_{\gamma}$H), 0.91- 0.80 (m, 9H, Leu^{b}-C$_{\delta}$H, 3HDA^{1}- C$_{\iota}$H), 0.71 (d, *J* = 6.6 Hz, 3H, Leu^{a}-C$_{\delta}$H$_1$), 0.59 (d, *J* = 6.4 Hz, 3H, Leu^{a}-C$_{\delta}$H$_2$); ^{13}C-NMR (125 MHz, (CD$_3$)$_2$SO) δ 172.53, 171.85, 171.41, 170.20, 161.63, 136.66, 129.08, 128.15, 126.42, 71.38, 55.49, 53.26, 51.98, 48.40, 38.57, 38.32, 37.40, 36.70, 33.18, 31.12, 28.72, 28.54, 24.65, 24.45, 23.49, 23.11, 22.42, 22.05, 21.91, 21.82, 17.06, 13.91.

(5Me-3HHA^{1})Sol (**4.57**- Method A)



Initial resin preparation and peptide couplings were similar to those reported in Method A above. The final coupling was performed similar to Method A but using (*R*)-3-hydroxy-5-methyl-hexanoic acid (**5.23**, 117 mg, 0.8 mmol) Cleavage of the linear peptide from the resin and lyophilisation were executed as in Method A producing a white fluffy powder (40.0 mg, 34%).

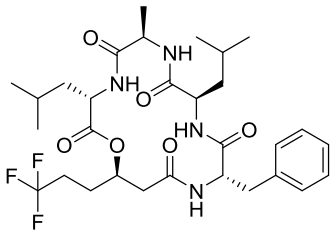
Further processes were performed as described in Method A furnishing a yellow solid which was purified *via* semi-preparative RP-HPLC to afford pure (5Me-3HHA^{1})Sol (**4.57**, 5.6 mg, 15%) and (5Me-3HHA^{1})epiSol (**4.58**, 4.0 mg, 10%).

(5Me-3HHA^{1})Sol (**4.57**) MS^{+} (ES-TOF): m/z calcd: 573.3607 [M+H]$^{+}$; found: 573.3742; Analytical RP-HPLC Onyx Monolithic C18 100 × 4.6 mm, 20% for 2 min increasing to 80% B in 20 min, t_R 12.87 min; $[\alpha]_D^{20}$ = +8.3 ^{o} (c 0.3, MeOH); ^{1}H-NMR (400 MHz, (CD$_3$)$_2$SO) δ 8.69-8.60 (m, 2H, Leu^{a}-NH, Phe-NH), 7.47 (d, *J* = 9.0 Hz, 1H, Ala-NH), 7.31-7.17 (m, 5H, Ar-H), 7.06 (d, *J* = 9.7 Hz, 1H, Leu^{b}-NH),

5.27-5.17 (m, 1H, 5Me3HHA^{1}-C$_{\beta}$H), 4.46 (dt, *J* = 4.4 Hz, 10.1 Hz, 1H, Leu^{b}-C$_{\alpha}$H), 4.31-4.24 (m, 1H, Phe-C$_{\alpha}$H), 4.19 (td, *J* = 7.3 Hz, 16.1 Hz, 1H, Ala-C$_{\alpha}$H), 3.61-3.53 (m, 1H, Leu^{a}-C$_{\alpha}$H), 2.97 (dd, *J* = 6.1 Hz, 13.3 Hz, 1H, Phe-C$_{\beta}$H$_{1}$), 2.75 (dd, *J* = 10.4 Hz, 13.7 Hz, 1H, Phe-C$_{\beta}$H$_{2}$), 2.71 (dd, *J* = 3.9 Hz, 13.8 Hz, 1H, 5Me3HHA^{1}-C$_{\alpha}$H$_{1}$), 2.12 (dd, *J* = 9.6 Hz, 13.7 Hz, 1H, 5Me3HHA^{1}-C$_{\alpha}$H$_{2}$), 1.70-1.45 (m, 5H, 5Me3HHA^{1}-C$_{\gamma}$H$_{1}$, 5Me3HHA^{1}-C$_{\delta}$H, Leu^{b}-C$_{\beta}$H, Leu^{b}-C$_{\gamma}$H), 1.44-1.21 (m, 6H, Ala-C$_{\beta}$H, 5Me3HHA^{1}-C$_{\gamma}$H$_{2}$, Leu^{a}-C$_{\beta}$H), 1.07-0.96 (m, 1H, Leu^{a}-C$_{\gamma}$H), 0.93-0.85 (m, 9H, Leu^{b}-C$_{\delta}$H, 5Me3HHA^{1}-C$_{\varepsilon}$H$_{1}$), 0.83 (d, *J* = 6.5 Hz, 3H, 5Me3HHA^{1}-C$_{\varepsilon}$H$_{2}$), 0.72 (d, *J* = 6.6 Hz, 3H, Leu^{a}-C$_{\delta}$H$_{1}$), 0.54 (d, *J* = 6.5 Hz, 3H, Leu^{a}-C$_{\delta}$H$_{2}$); ^{13}C-NMR (125 MHz, (CD$_{3}$)$_{2}$SO) δ 174.46, 171.71, 171.16, 170.92, 170.42, 151.27, 136.35, 129.01, 128.19, 126.48, 70.57, 55.89, 52.95, 48.97, 48.05, 43.63, 41.09, 38.81, 36.35, 24.01, 23.88, 23.53, 23.21, 23.16, 22.76, 22.44, 21.31, 20.68, 16.67.

(5Me-3HHA^{1})epiSol (**4.58**) MS^{+} (ES-TOF): m/z calcd: 573.3607 [M+H]$^{+}$; found: 573.3616; Analytical RP-HPLC Onyx Monolithic C18 100 × 4.6 mm, 20% for 2 min increasing to 80% B in 20 min, t_{R} 12.40 min; $[\alpha]_{D}^{20}$ = +22.8 ^{o} (c 0.3, MeOH); ^{1}H-NMR (400 MHz, (CD$_{3}$)$_{2}$SO) δ 8.48 (d, *J* = 5.3 Hz, 1H, Phe-NH), 8.43 (d, *J* = 7.1 Hz, 1H, Leu^{a}-NH), 7.42 (d, *J* = 4.3 Hz, 1H, Ala-NH), 7.40 (d, *J* = 1.4 Hz, 1H, Leu^{b}-NH), 7.30-7.17 (m, 5H, Ar-H), 5.02-4.93 (m, 1H, 5Me3HHA^{1}-C$_{\beta}$H), 4.38-4.30 (m, 1H, Phe-C$_{\alpha}$H), 4.24 (td, *J* = 7.3 Hz, 16.2 Hz, 1H, Ala-C$_{\alpha}$H), 3.88- 3.79 (m, 2H, Leu^{a}-C$_{\alpha}$H, Leu^{b}-C$_{\alpha}$H), 2.90 (dd, *J* = 6.8 Hz, 13.3 Hz, 1H, Phe-C$_{\beta}$H$_{1}$), 2.80 (dd, *J* = 9.2 Hz, 13.3 Hz, 1H, Phe-C$_{\beta}$H$_{2}$), 2.64 (dd, *J* = 4.7 Hz, 14.7 Hz, 1H, 5Me3HHA^{1}-C$_{\alpha}$H$_{1}$), 2.24 (dd, *J* = 5.3 Hz, 14.6 Hz, 1H, 5Me3HHA^{1}-C$_{\alpha}$H$_{2}$), 1.93 (td, *J* = 9.2 Hz, 16.8 Hz, 1H, Leu^{a}-C$_{\beta}$H$_{1}$), 1.84- 1.74 (m, 1H, 5Me3HHA^{1}-C$_{\gamma}$H$_{1}$), 1.64-1.46 (m, 3H, Leu^{a}-C$_{\beta}$H$_{2}$, Leu^{a}-C$_{\gamma}$H, 5Me3HHA^{1}-C$_{\delta}$H), 1.42- 1.18 (m, 6H, Ala-C$_{\beta}$H, 5Me3HHA^{1}-C$_{\gamma}$H$_{2}$, Leu^{b}-C$_{\beta}$H), 1.03- 0.92 (m, 1H, Leu^{b}-C$_{\gamma}$H), 0.88 (d, *J* = 6.2 Hz, 3H, 5Me3HHA^{1}-C$_{\varepsilon}$H$_{1}$), 0.87- 0.83 (m, 9H, 5Me3HHA^{1}-C$_{\varepsilon}$H$_{2}$, Leu^{a}-C$_{\delta}$H), 0.71 (d, *J* = 6.7 Hz, 3H, Leu^{b}-C$_{\delta}$H$_{1}$), 0.60 (d, *J* = 6.4 Hz, 3H, Leu^{b}-C$_{\delta}$H$_{2}$); ^{13}C-NMR (125 MHz, (CD$_{3}$)$_{2}$SO) δ 172.71, 171.91, 171.38, 170.34, 170.02, 161.62, 136.67, 129.08, 128.14, 126.41, 69.47, 55.42, 53.19, 52.08, 48.21, 42.30, 38.48, 38.33, 36.71, 24.62, 23.64, 23.50, 23.12, 22.80, 22.54, 21.92, 21.76, 20.82, 17.05.

(6FFF-3HHA^{1})Sol (**4.55**- Method A)



Initial resin preparation and peptide couplings were similar to those reported in Method A above. The final coupling was performed similar to Method A but using (*R*)-3-hydroxy-6,6,6-trifluoro-hexanoic acid (**5.5.22**, 123 mg, 0.8 mmol) Cleavage of the linear peptide from the resin and lyophilisation were executed as in Method A producing a white fluffy powder (93.8 mg, 74%).

Further processes were performed as described in Method A furnishing a yellow solid which was purified *via* semi-preparative RP-HPLC to afford pure (6FFF-3HHA^1)Sol (**4.55**, 28.4 mg, 31%) and (6FFF-3HHA^1)epiSol (**4.56**, 12.2 mg, 13%).

(6FFF-3HHA^1)Sol (**4.55**) MS$^+$ (ES-TOF): m/z calcd: 613.3168 $[M+H]^+$; found: 613.2690; Analytical RP-HPLC Onyx Monolithic C18 100 × 4.6 mm, 20% for 2 min increasing to 80% B in 20 min, t_R 13.15 min; $[\alpha]_D^{20}$ = +12.2 ^{o} (c 0.3, MeOH); ^{1}H-NMR (400 MHz, $(CD_3)_2SO$) δ 8.70 (d, *J* = 5.7 Hz, 1H, Leu^a-NH), 8.59 (d, *J* = 4.0 Hz, 1H, Phe-NH), 7.34 (d, *J* = 9.0 Hz, 1H, Ala-NH), 7.31-7.17 (m, 5H, Ar-H), 7.05 (d, *J* = 9.5 Hz, 1H, Leu^b-NH), 5.19-5.09 (m, 1H, 6FFF3HHA^1-C$_\beta$H), 4.50 (dt, *J* = 5.5 Hz, 9.5 Hz, 1H, Leu^b-C$_\alpha$H), 4.35-4.27 (m, 1H, Phe-C$_\alpha$H), 4.22 (td, *J* = 7.3 Hz, 16.3 Hz, 1H, Ala-C$_\alpha$H), 3.65-3.56 (m, 1H, Leu^a-C$_\alpha$H), 2.94 (dd, *J* = 6.6 Hz, 13.5 Hz, 1H, Phe-C$_\beta$H$_1$), 2.80-2.69 (m, 2H, Phe-C$_\beta$H$_2$, 6FFF3HHA^1-C$_\alpha$H$_1$), 2.34-2.08 (m, 3H, 6FFF3HHA^1-C$_\alpha$H$_2$, 6FFF3HHA^1-C$_\delta$H), 2.08-1.95 (m, 1H, 6FFF3HHA^1-C$_\gamma$H$_1$), 1.84-1.72 (m, 1H, 6FFF3HHA^1-C$_\gamma$H$_2$), 1.69-1.47 (m, 3H, Leu^b-C$_\gamma$H, Leu^b-C$_\beta$H), 1.47-1.34 (m, 2H, Leu^a-C$_\beta$H), 1.32 (d, *J* = 7.3 Hz, 3H, Ala-C$_\beta$H), 1.12-1.00 (m, 1H, Leu^a-C$_\gamma$H), 0.89 (d, *J* = 6.6 Hz, 3H, Leu^b-C$_\delta$H), 0.84 (d, *J* = 6.4 Hz, 3H, Leu^b-C$_\delta$H), 0.73 (d, *J* = 6.6 Hz, 3H, Leu^a-C$_\delta$H), 0.57 (d, *J* = 6.4 Hz, 3H, Leu^a-C$_\delta$H); ^{13}C-NMR (125 MHz, $(CD_3)_2SO$) δ 174.46, 171.60, 171.58, 171.16, 170.10, 136.40, 129.01, 128.20, 126.51, 70.45, 55.71, 53.00, 49.35, 47.93, 40.19, 38.85, 36.40, 28.92 (q, J_{CF} = 28.5 Hz), 26.30 (q, J_{CF} = 2.8 Hz), 24.07, 23.60, 23.23, 23.14, 21.24, 20.73, 16.59.

(6FFF-3HHA^1)epiSol (**4.56**) MS^+ (ES-TOF): m/z calcd: 613.3168 $[M+H]^+$; found: 613.2814; Analytical RP-HPLC Onyx Monolithic C18 100 × 4.6 mm, 20% for 2 min increasing to 80% B in 20 min, t_R 13.01 min; $[\alpha]_D^{20}$ = +26.1 ^{o} (c 0.3, MeOH); ^{1}H-NMR (400 MHz, $(CD_3)_2SO$) δ 8.56 (d, *J* = 6.5 Hz, 1H, Leu^a-NH), 8.45 (d, *J* = 6.0 Hz, 1H, Phe-NH), 7.49 (d, *J* = 6.8 Hz, 1H, Leu^b-NH), 7.31-7.16 (m, 6H, Ala-NH, Ar-H), 5.00-4.91 (m, 1H, 6FFF3HHA^1-C_βH), 4.45- 4.37 (m, 1H, Phe-C_αH), 4.29 (td, *J* = 7.1 Hz, 16.3 Hz, 1H, Ala-C_αH), 3.86- 3.73 (m, 2H, Leu^a-C_αH, Leu^b-C_αH), 2.88 (dd, *J* = 7.1 Hz, 13.4 Hz, 1H, Phe-$C_\beta H_1$), 2.81 (dd, *J* = 8.8 Hz, 13.4 Hz, 1H, Phe-$C_\beta H_2$), 2.66 (dd, *J* = 5.7 Hz, 15.0 Hz, 1H, 6FFF3HHA^1-$C_\alpha H_1$), 2.33 (dd, *J* = 3.1 Hz, 14.9 Hz, 1H, 6FFF3HHA^1-$C_\alpha H_2$), 2.31-2.05 (m, 3H, 6FFF3HHA^1-C_γH, 6FFF3HHA^1-$C_\delta H_1$), 2.04-1.92 (m, 1H, Leu^b-$C_\beta H_1$), 1.86-1.74 (m, 1H, 6FFF3HHA^1-$C_\delta H_2$), 1.65-1.50 (m, 2H, Leu^b-$C_\beta H_2$, Leu^b-C_γH), 1.42-1.34 (m, 2H, Leu^a-C_βH), 1.23 (d, *J* = 7.2 Hz, 3H, Ala-C_βH), 1.11- 1.02 (m, 1H, Leu^a-C_γH), 0.88 (d, *J* = 6.3 Hz, 3H, Leu^b-C_δH), 0.86 (d, *J* = 6.2 Hz, 3H, Leu^b-C_δH), 0.74 (d, *J* = 6.6 Hz, 3H, Leu^a-C_δH), 0.62 (d, *J* = 6.4 Hz, 3H, Leu^a-C_δH); ^{13}C-NMR (125 MHz, $(CD_3)_2SO$) δ 173.27, 172.36, 171.38, 170.53, 169.59, 136.71, 129.06, 128.16, 126.43, 69.29, 55.10, 52.89, 52.43, 47.56, 39.00, 37.66, 37.56, 36.76, 24.56, 23.60, 23.09, 22.80, 21.46, 20.87, 16.38.

8.5.1.4 Second generation compounds

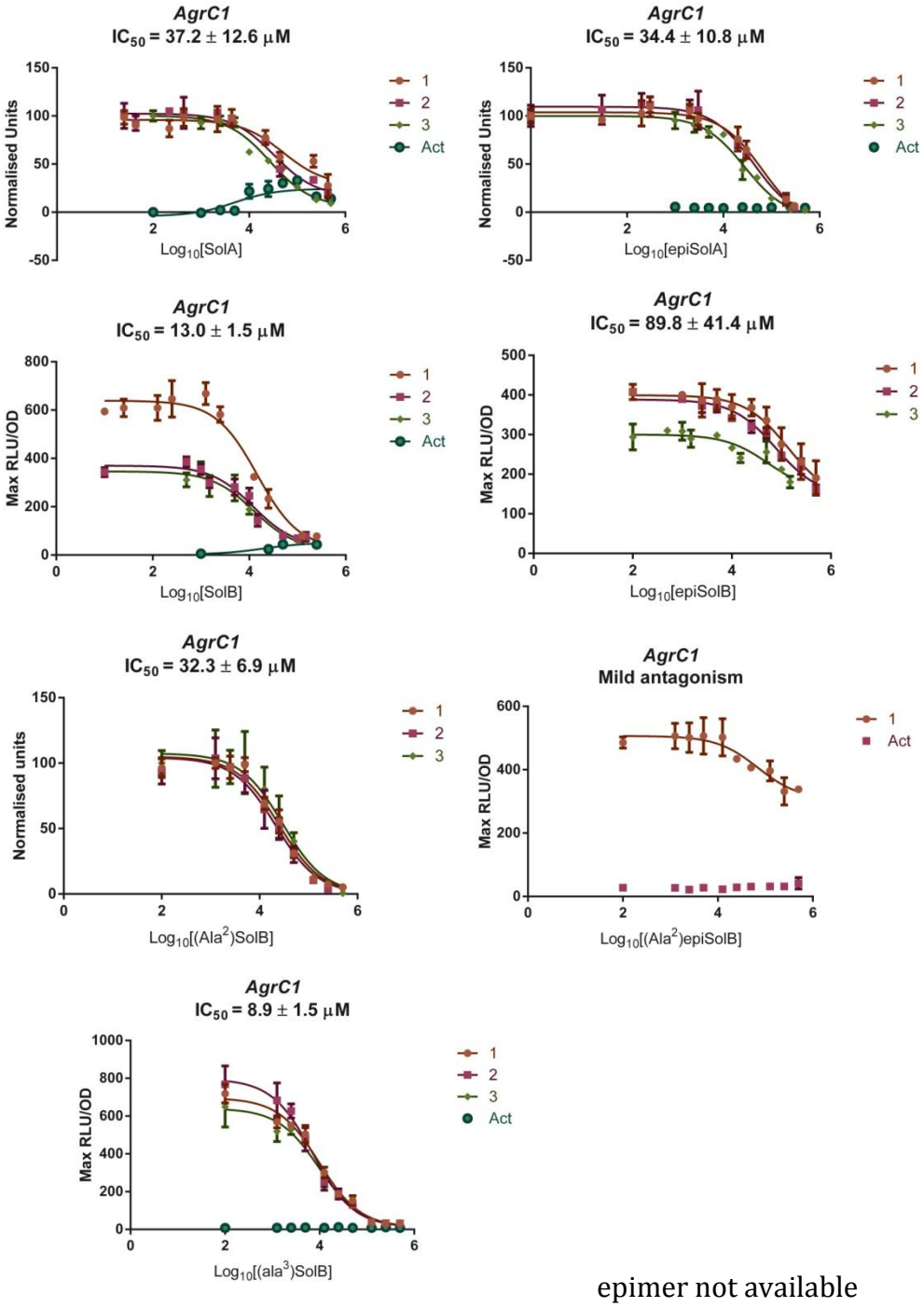
Synthesis details and analytical data are in Section 8.4.2 above.

8.5.2 Biological Assessment

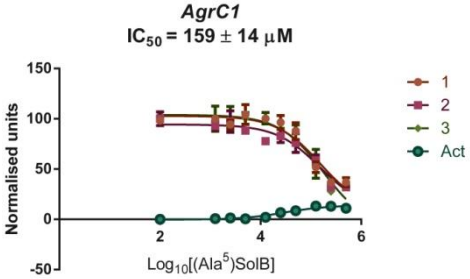
Hemolysis assays and western blots were performed as in Section 8.2.4.

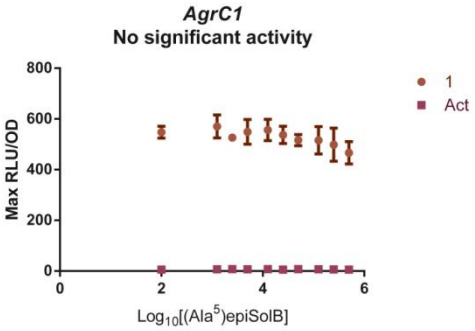
Bioluminescent reporter assays were performed as in Section 8.2.3. Data was processed with Excel (Microsoft Corp.) and IC_{50} and EC_{50} curves were calculated using Prism 6 (Graph Pad, San Diego, CA). All graphs are recorded below.

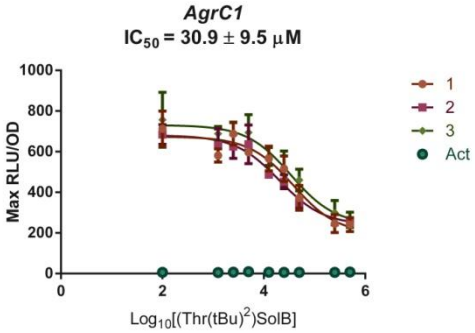
8.5.2.1 AgrC1 bioassays



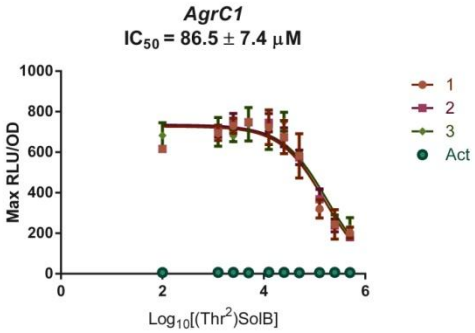
epimer not available



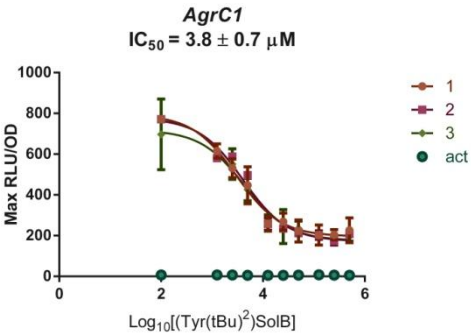


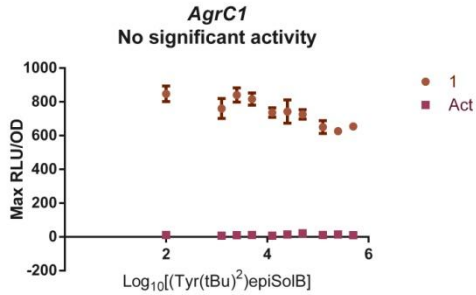


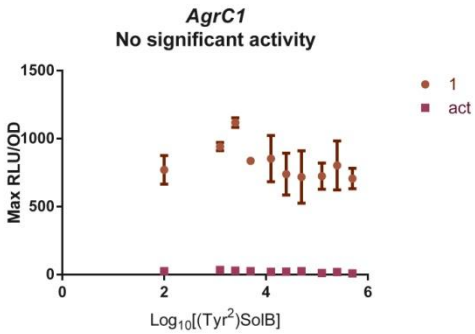
epimer not available

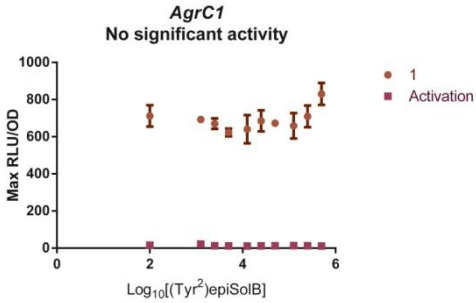


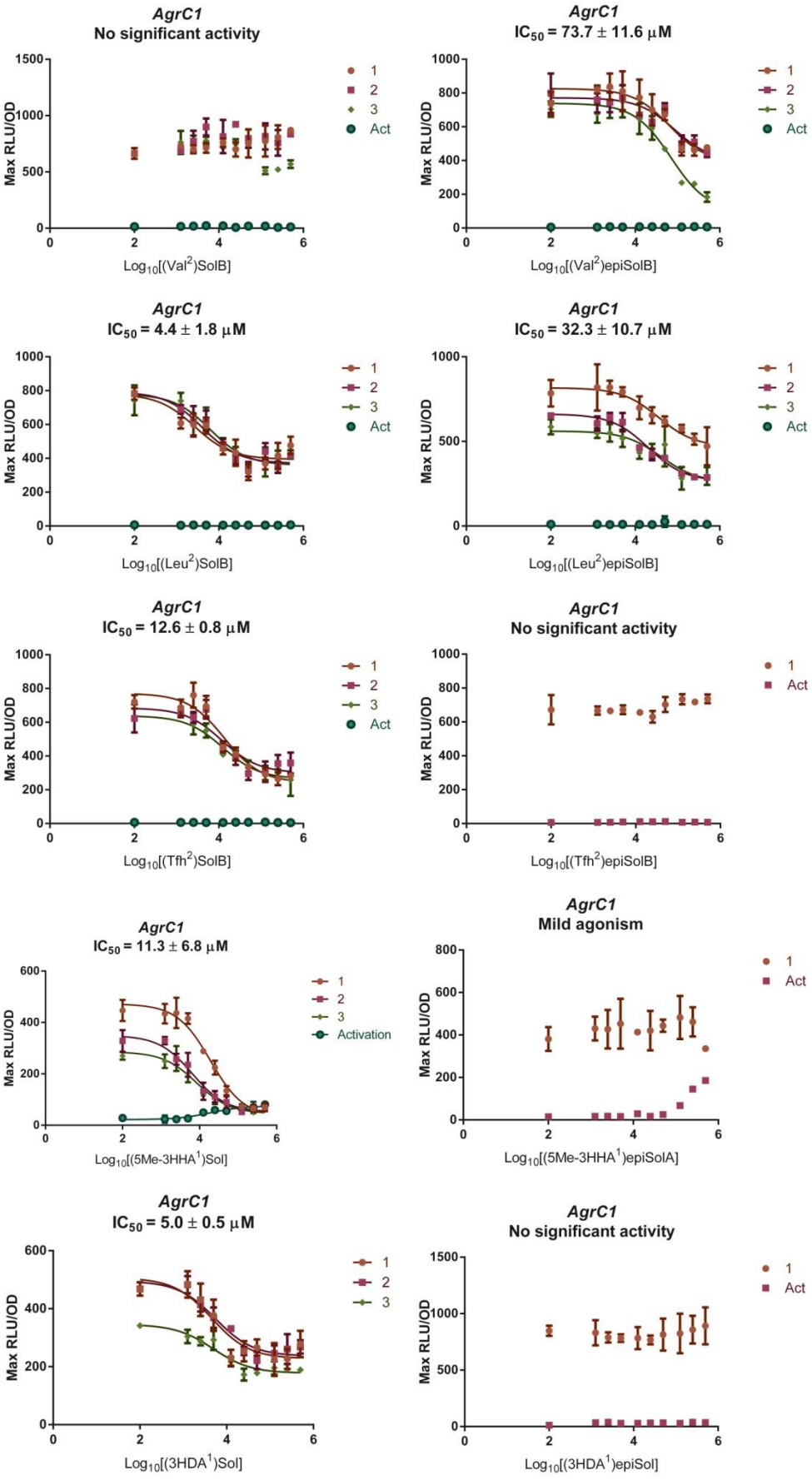
epimer not available

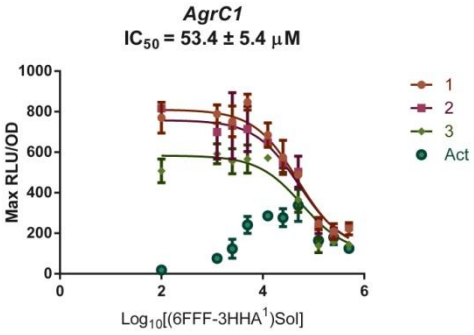


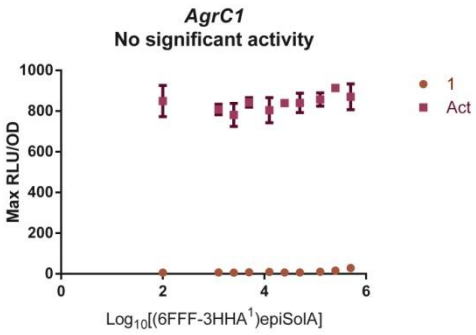


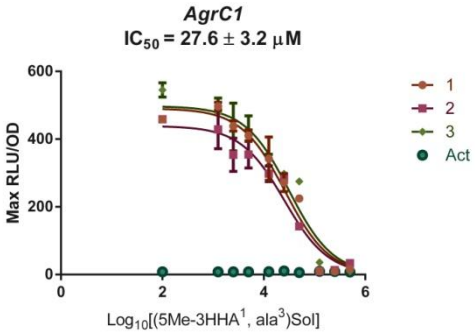




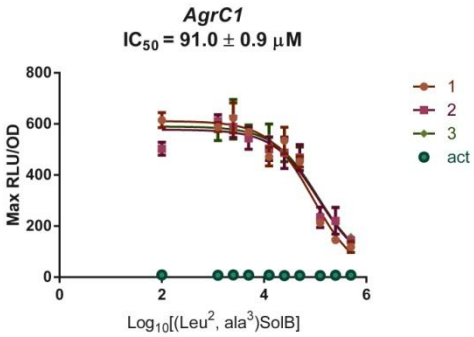

AgrC1
No significant activity
Max RLU/OD
Log10[(Val2)SolB]
1
2
3
Act
AgrC1
IC50 = 73.7 ± 11.6 μM
Log10[(Val2)epiSolB]
AgrC1
IC50 = 4.4 ± 1.8 μM
Log10[(Leu2)SolB]
AgrC1
IC50 = 32.3 ± 10.7 μM
Log10[(Leu2)epiSolB]
AgrC1
IC50 = 12.6 ± 0.8 μM
Log10[(Tfh2)SolB]
AgrC1
No significant activity
Log10[(Tfh2)epiSolB]
AgrC1
IC50 = 11.3 ± 6.8 μM
Activation
Log10[(5Me-3HHA1)Sol]
AgrC1
Mild agonism
Log10[(5Me-3HHA1)epiSolA]
AgrC1
IC50 = 5.0 ± 0.5 μM
Log10[(3HDA1)Sol]
AgrC1
No significant activity
Log10[(3HDA1)epiSol]



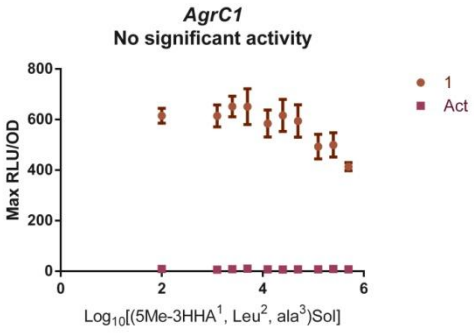




epimer not available

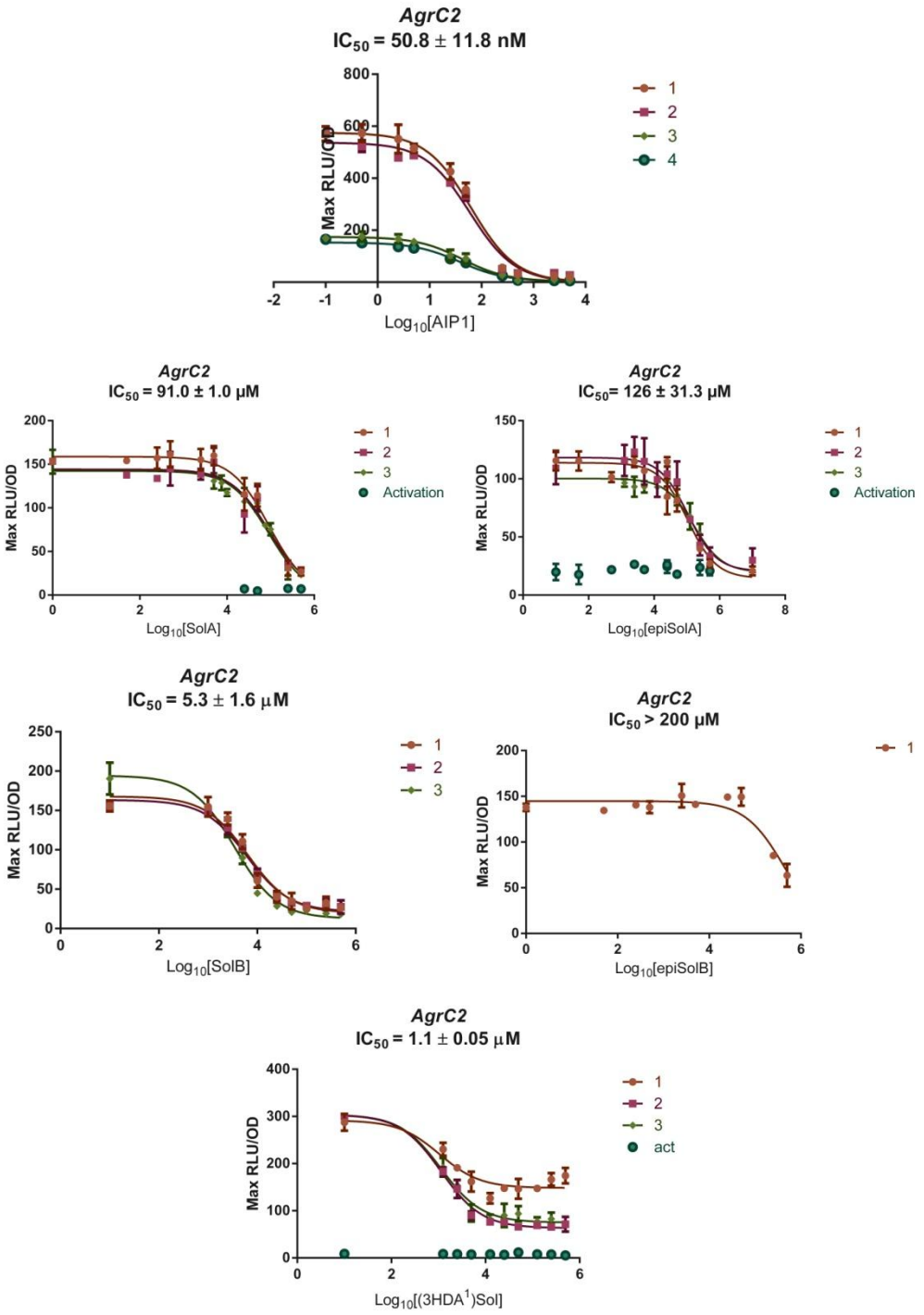


epimer not available

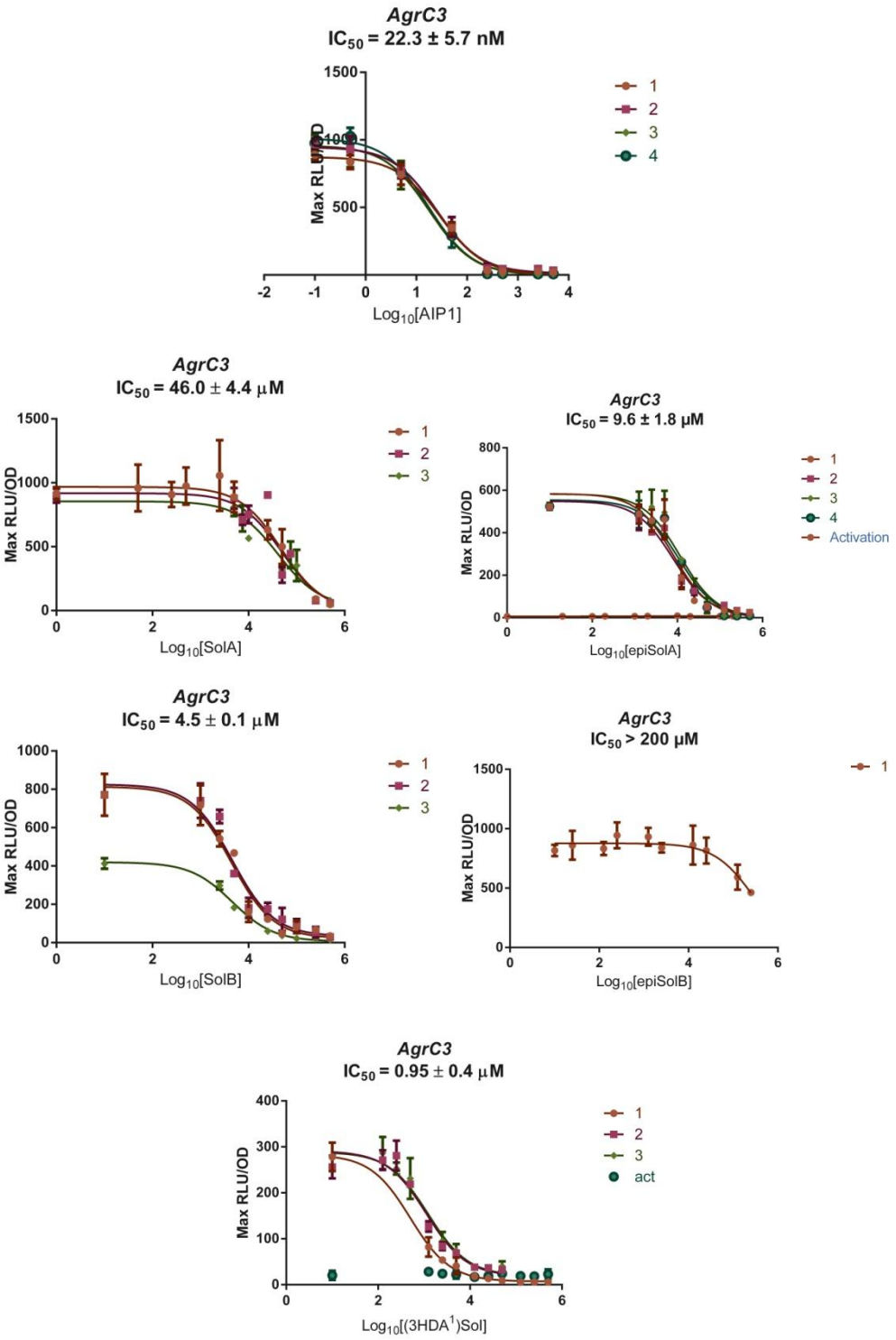


epimer not available

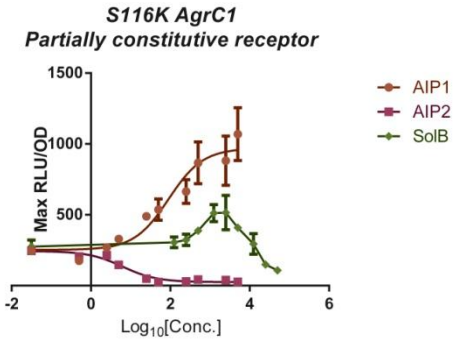
8.5.2.2 AgrC2 bioassays



8.5.2.3 AgrC3 bioassays



8.5.2.4 S116K AgrC bioassays



8.5.3 Temperature dependant NMR

Proton nuclear magnetic resonance spectra were recorded at 298, 301, 304, 307, and 310 K on a Bruker AV400 operating at 400.13 (^{1}H-NMR) using Norell Select Series™ 3 mm NMR tubes. Chemical shifts (δ) are reported in parts per million (ppm), referenced to the solvent ($(CD_3)_2SO$: 2.50 ppm). Coupling constants (J) are recorded in Hz and significant multiplicities described by singlet (s), doublet (d), doublet of doublets (dd), doublet of triplets (dt), triplet (t), quadruplet (q), broad (br), multiplet (m). Amide chemical shifts were plotted on a scatter graph using Excel (Microsoft Corp.). Temperature coefficient was calculated as the gradient of the line of best fit and is quoted in ppm/K. A temperature coefficient less than $2x10^{-3}$ ppm/K is considered to be indicative of solvent shielded amide and above $3x10^{-3}$ ppm/K is considered to be a solvent exposed amide.

8.5.4 Stability testing

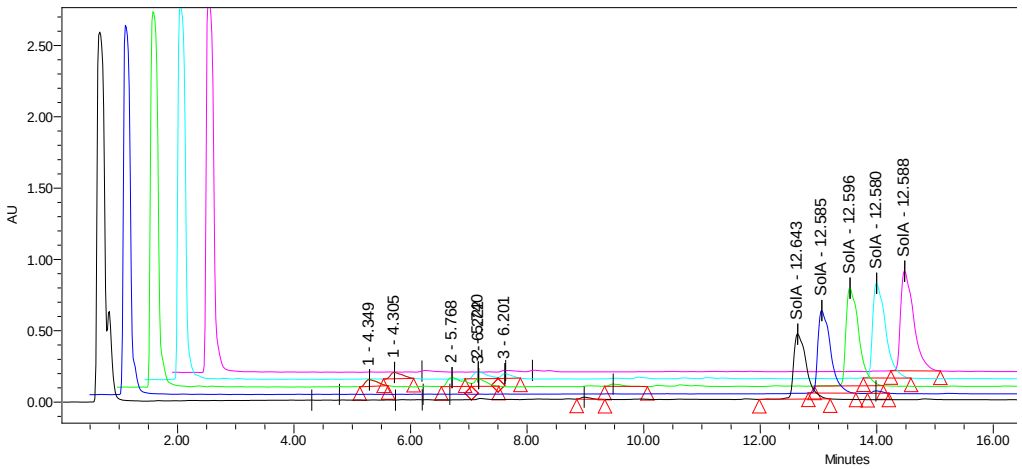


Figure 216: Overlay of HPLC traces of SolA (**1.21**) at different time points stored at 37°C in 2% DMSO/H_2O. Traces bottom to top: 0hr, 1hr, 3hrs, 6hrs, 24hrs. HPLC

Gradient: 20% B for 2mins to 80% B over 25mins. Solvent A (100% H_2O, 0.06% TFA). Solvent B (90% MeCN, 10% H_2O, 0.06% TFA). No significant change over time observed.

9 References

1. Kashket, E. R., Proton motive force in growing *Streptococcus lactis* and *Staphylococcus aureus* cells under aerobic and anaerobic conditions. *J Bacteriol* **1981,** *146* (1), 369-376.

2. Berry, S.; Morton, S.; Atatoa Carr, P.; Marks, E.; Ritchie, S.; Upton, A.; Williamson, D.; Grant, C., Colonisation with *Staphylococcus aureus* and *Streptococcus pyogenes* in New Zealand preschool children. *New Zeal Med J* **2015,** *128* (1410), 60-7.

3. Rao, G. G.; Michalczyk, P.; Nayeem, N.; Walker, G.; Wigmore, L., Prevalence and risk factors for meticillin-resistant *Staphylococcus aureus* in adult emergency admissions - a case for screening all patients? *J Hosp Infect* **2007,** *66* (1), 15-21.

4. Carrier, M.; Marchand, R.; Auger, P.; Hebert, Y.; Pellerin, M.; Perrault, L. P.; Cartier, R.; Bouchard, D.; Poirier, N.; Page, P., Methicillin-resistant *Staphylococcus aureus* infection in a cardiac surgical unit. *J Thorac Cardiov Sur* **2002,** *123* (1), 40-44.

5. Naves, K. S. C.; da Trindade, N. V.; Gontijo, P. P., Methicillin-resistant *Staphylococcus aureus* bloodstream infection: risk factors and clinical outcome in non-intensive-care units. *Rev Soc Bras Med Trop* **2012,** *45* (2), 189-193.

6. Garcia-Garrote, F.; Cercenado, E.; Marin, M.; Bal, M.; Trincado, P.; Corredoira, J.; Ballesteros, C.; Pita, J.; Alonso, P.; Vindel, A. Methicillin-resistant *Staphylococcus aureus* carrying the mecC gene: emergence in Spain and report of a fatal case of bacteraemia. *J Antimicrob Chemoth* **2014,** *69* (1), 45-50.

7. Miyazaki, S.; Matsumoto, Y.; Sekimizu, K.; Kaito, C., Evaluation of *Staphylococcus aureus* virulence factors using a silkworm model. *Fems Microbiol Lett* **2012,** *326* (2), 116-124.

8. Boyce, T.; Murray, E.; Holmes, A., What are the drivers of the UK media coverage of meticillin-resistant *Staphylococcus aureus*, the inter-relationships and relative influences? *J Hosp Infect* **2009,** *73* (4), 400-407.

9. Norrby, R.; Powell, M.; Aronsson, B.; Bonnet, D. L.; Lutsar, I.; Bocsan, I. S.; Cars, O.; Giamarellou, H.; Gyssens, I. C. *The bacterial challenge: time to react. A call to narrow the gap between multidrug-resistant bacteria in the EU and the development of new antibacterial agents.*; European Centre for Disease Prevention and Control, European Medicines Agency: Stockholm, 2007.

10. Tassa, E.; Corsini, V.; Gourdol, A.; Juchno, P.; Krazewska, K.; Marcu, M.; Flander, A. O.; Vasileva, K.; Marchetti, E. *Demography Report 2010*; European Commission: Luxembourg, 2011; p 33.

11. *Staphylococcus aureus*: guidance, data and analysis England, P. H., Ed. 2014.

12. Morse, A. *Emergency admissions to hospital: managing the demand*; National Audit Office: London, 2013; p 24.

13. Network, N. H. S., National and state healthcare associated infections progress report. Control, C. f. D., Ed. Atlanta, 2013.

14. *Fast Facts on US Hospitals*; American Hospitals Association: Chicago, 2014.

15. Gould, I. M., VRSA-doomsday superbug or damp squib? *Lancet Infect Dis* **2010,** *10* (12), 816-818.

16. Alsterholm, M.; Flytstrom, I.; Bergbrant, I. M.; Faergemann, J., Fusidic acid-resistant *Staphylococcus aureus* in impetigo contagiosa and secondarily infected atopic dermatitis. *Act Derm-Venereol* **2010,** *90* (1), 52-57.

17. Capdevila, O.; Grau, I.; Vadillo, M.; Cisnal, M.; Pallares, R., Bacteremic pneumococcal cellulitis compared with bacteremic cellulitis caused by *Staphylococcus aureus* and *Streptococcus pyogenes*. *Eur J Clin Microbiol* **2003,** *22* (6), 337-341.

18. Kalinka, J.; Hachmeister, M.; Geraci, J.; Sordelli, D.; Hansen, U.; Niemann, S.; Oetermann, S.; Peters, G.; Loffler, B.; Tuchscherr, L., *Staphylococcus aureus* isolates from chronic osteomyelitis are characterized by high host cell invasion and intracellular adaptation, but still induce inflammation. *Int J Med Microbiol* **2014,** *304* (8), 1038-1049.

19. N'Guyen, Y.; Baumard, S.; Vernet-Garnier, V.; Batalla, A. S.; de Champs, C.; Jaussaud, R.; Strady, C., Coagulase-negative *Staphylococcus* bacteraemia accounts for one third of *Staphylococcus* bacteraemia in a French university hospital. *Scand J Infect Dis* **2012,** *44* (2), 79-85.

20. Sherwood, M.; Smith, D.; Crisel, R.; Veledar, E.; Lerakis, S., *Staphylococcus aureus* endocarditis: The Grady Memorial Hospital experience. *Am J Med Sci* **2006,** *331* (2), 84-87.

21. Chi, C. Y.; Wang, S. M.; Lin, H. C.; Liu, C. C., A clinical and microbiological comparison of *Staphylococcus aureus* toxic shock and scalded skin syndromes in children. *Clin Infect Dis* **2006,** *42* (2), 181-185.

22. Brizzio, A. A.; Tedeschi, F. A.; Zalazar, F. E., Multiplex PCR strategy for the simultaneous identification of *Staphylococcus aureus* and detection of staphylococcal enterotoxins in isolates from food poisoning outbreaks. *Biomed* **2013,** *33* (1), 122-127.

23. Wertheim, H. F. L.; Vos, M. C.; Ott, A.; van Belkum, A.; Voss, A.; Kluytmans, J.; van Keulen, P. H. J.; Vandenbroucke-Grauls, C.; Meester, M. H. M.; Verbrugh, H. A., Risk and outcome of nosocomial Staphylococcus aureus bacteraemia in nasal carriers versus non-carriers. *Lancet* **2004,** *364* (9435), 703-705.

24. Ahmed, E. F.; Gad, G. F. M.; Abdalla, A. M.; Hasaneen, A. M.; Abdelwahab, S. F., Prevalence of Methicillin resistant *Staphylococcus aureus* among Egyptian patients after surgical interventions. *Surg Infect* **2014,** *15* (4), 404-411.

25. Miller, L. G.; Perdreau-Remington, F.; Rieg, G.; Mehdi, S.; Perlroth, J.; Bayer, A. S.; Tang, A. W.; Phung, T. O.; Spellberg, B., Necrotizing fasciitis caused by community-associated methicillin-resistant *Staphylococcus aureus* in Los Angeles. *New Engl J Med* **2005,** *352* (14), 1445-1453.

26. Feng, C. H.; Chuang, S. S., The diabetic foot with necrotizing fascitis-epidemiology, etiologies and treatment. *Wound Repair Regen* **2009,** *17* (2), A51-A51.

27. Smuszkiewicz, P.; Trojanowska, I.; Tomczak, H., Late diagnosed necrotizing fasciitis as a cause of multiorgan dysfunction syndrome: A case report. *Cases j* **2008,** *1* (1), 125.

28. Schuchat, A.; Broome, C. V., Toxic shock syndrome and tampons. *Epidemiol Rev* **1991,** *13*, 99-112.

29. Kazakova, S. V.; Hageman, J. C.; Matava, M.; Srinivasan, A.; Phelan, L.; Garfinkel, B.; Boo, T.; McAllister, S.; Anderson, J.; Jensen, B.; Dodson, D.; Lonsway, D.; McDougal, L. K.; Arduino, M.; Fraser, V. J.; Killgore, G.; Tenover, F. C.; Cody, S.; Jernigan, D. B., A clone of methicillin-resistant *Staphylococcus aureus* among professional football players. *New Engl J Med* **2005,** *352* (5), 468-475.

30. Campbell, K. M.; Vaughn, A. F.; Russell, K. L.; Smith, B.; Jimenez, D. L.; Barrozo, C. P.; Minarcik, J. R.; Crum, N. F.; Ryan, M. A. K., Risk factors for community-associated methicillin-resistant *Staphylococcus aureus* infections in an outbreak of disease among military trainees in San Diego, California, in 2002. *J Clin Microbiol* **2004,** *42* (9), 4050-4053.

31. Coronado, F.; Nicholas, J. A.; Wallace, B. J.; Kohlerschmidt, D. J.; Musser, K.; Schoonmaker-Bopp, D. J.; Zimmerman, S. M.; Boller, A. R.; Jernigan, D. B.; Kacica, M. A., Community-associated methicillin-resistant *Staphylococcus aureus* skin infections in a religious community. *Epidemiol Infect* **2007,** *135* (3), 492-501.

32. Gonzalez, B. E.; Martinez-Aguilar, G.; Hulten, K. G.; Hammerman, W. A.; Coss-Bu, J.; Avalos-Mishaan, A.; Mason, E. O.; Kaplan, S. L., Severe staphylococcal sepsis in adolescents in the era of community-acquired methicillin-resistant *Staphylococcus aureus*. *Pediatrics* **2005,** *115* (3), 642-648.

33. Otto, M., Community-associated MRSA: What makes them special? *Int J Med Microbiol* **2013,** *303* (6-7), 324-330.

34. Fridkin, S. K.; Hageman, J. C.; Morrison, M.; Sanza, L. T.; Como-Sabetti, K.; Jernigan, J. A.; Harriman, K.; Harrison, L. H.; Lynfield, R.; Farley, M. M., Methicillin-resistant *staphylococcus aureus* disease in three communities. *New Engl J Med* **2005,** *352* (14), 1436-1444.

35. Hiramatsu, K.; Cui, L.; Kuroda, M.; Ito, T., The emergence and evolution of methicillin-resistant *Staphylococcus aureus*. *Trends Microbiol* **2001,** *9* (10), 486-493.

36. a) Daum, R. S.; Ito, T.; Hiramatsu, K.; Hussain, F.; Mongkolrattanothai, K.; Jamklang, M.; Boyle-Wang, S., A novel methicillin-resistance cassette in community- acquired methicillin-resistant *Staphylococcus aureus* isolates of diverse genetic backgrounds. *J Infect Dis* **2002,** *186* (9), 1344-1347; b) Lee, S. M.; Ender, M.; Adhikari, R.; Smith, J. A. B.; Berger-Bachi, B.; Cook, G. M., Fitness cost of staphylococcal cassette chromosome mec in methicillin-resistant *Staphylococcus aureus* by way of continuous culture. *Antimicrob Agents Ch* **2007,** *51* (4), 1497-1499.

37. Diep, B. A.; Chambers, H. F.; Graber, C. J.; Szumowski, J. D.; Miller, G.; Han, L. L.; Chen, J. H.; Lin, F.; Lin, J.; Phan, T. H.; Carleton, H. A.; McDougal, L. K.; Tenover, F. C.; Cohen, D. E.; Mayer, K. H.; Sensabaugh, G. F.; Perdreau-Remington, F., Emergence of multidrug-resistant, community-associated, methicillin-resistant *Staphylococcus aureus* clone USA300 in men who have sex with men. *Ann Intern Med* **2008,** *148* (4), 249-257.

38. Cheung, G. Y. C.; Wang, R.; Khan, B. A.; Sturdevant, D. E.; Otto, M., Role of the accessory gene regulator *agr* in community-associated methicillin-resistant *Staphylococcus aureus* pathogenesis. *Infect Immun* **2011,** *79* (5), 1927-1935.

39. Voyich, J. A.; Braughton, K. R.; Sturdevant, D. E.; Whitney, A. R.; Said-Salim, B.; Porcella, S. F.; Long, R. D.; Dorward, D. W.; Gardner, D. J.; Kreiswirth, B. N.; Musser, J. M.; DeLeo, F. R., Insights into mechanisms used by *Staphylococcus aureus* to avoid destruction by human neutrophils. *J Immunol* **2005,** *175* (6), 3907-3919.

40. Li, M.; Diep, B. A.; Villaruz, A. E.; Braughton, K. R.; Jiang, X. F.; Deleo, F. R.; Chambers, H. F.; Lu, Y.; Otto, M., Evolution of virulence in epidemic community-associated methicillin-resistant *Staphylococcus aureus*. *P Natl Acad Sci USA* **2009,** *106* (14), 5883-5888.

41. Diep, B. A.; Chan, L.; Tattevin, P.; Kajikawa, O.; Martin, T. R.; Basuino, L.; Mai, T. T.; Marbach, H.; Braughton, K. R.; Whitney, A. R.; Gardner, D. J.; Fan, X. M.; Tseng, C. W.; Liu, G. Y.; Badiou, C.; Etienne, J.; Lina, G.; Matthay, M. A.; Deleo, F. R.; Chambers, H. F., Polymorphonuclear leukocytes mediate *Staphylococcus aureus* Panton-Valentine leukocidin-induced lung inflammation and injury. *P Natl Acad Sci USA* **2010,** *107* (12), 5587-5592.

42. von Eiff, C.; Becker, K.; Machka, K.; Stammer, H.; Peters, G.; Study, G., Nasal carriage as a source of *Staphylococcus aureus* bacteremia. *New Engl J Med* **2001,** *344* (1), 11-16.

43. Diep, B. A.; Gill, S. R.; Chang, R. F.; Phan, T. H.; Chen, J. H.; Davidson, M. G.; Lin, F.; Lin, J.; Carleton, H. A.; Mongodin, E. F.; Sensabaugh, G. F.; Perdreau-Remington, F., Complete genome sequence of USA300, an epidemic clone of community-acquired meticillin-resistant *Staphylococcus aureus*. *Lancet* **2006,** *367* (9512), 731-739.

44. Diep, B. A.; Otto, M., The role of virulence determinants in community-associated MRSA pathogenesis. *Trends Microbiol* **2008,** *16* (8), 361-369.

45. Ranotkar, S.; Kumar, P.; Zutshi, S.; Prashanth, K. S.; Bezbaruah, B.; Anand, J.; Lahkar, M., Vancomycin-resistant enterococci: Troublemaker of the 21st century. *J Global Antimicrob Res* **2014,** *2* (4), 205-212.

46. Dheda, K.; Gumbo, T.; Gandhi, N. R.; Murray, M.; Theron, G.; Udwadia, Z.; Migliori, G. B.; Warren, R., Global control of tuberculosis: from extensively drug-resistant to untreatable tuberculosis. *Lancet Resp Med* **2014,** *2* (4), 321-338.

47. Slimings, C.; Riley, T. V., Antibiotics and hospital-acquired *Clostridium difficile* infection: update of systematic review and meta-analysis. *J Antimicrob Ch* **2014,** *69* (4), 881-891.

48. Bonesso, M. F.; Marques, S. A.; Cunha, M., Community-acquired methicillin-resistant *Staphylococcus aureus*: molecular background, virulence, and relevance for public health. *J Venom Anim Toxins* **2011,** *17* (4), 378-386.

49. Hamilton-Miller, J. M., Vancomycin-resistant *Staphylococcus aureus*: A real and present danger? *Infection* **2002,** *30* (3), 118-124.

50. Pehrsson, E. C.; Forsberg, K. J.; Gibson, M. K.; Ahmadi, S.; Dantas, G., Novel resistance functions uncovered using functional metagenomic investigations of resistance reservoirs. *Front Microbiol* **2013,** *4*, 11.

51. Theuretzbacher, U., Accelerating resistance, inadequate antibacterial drug pipelines and international responses. *Int J Antimicrob Agents* **2012,** *39* (4), 295-299.

52. Zou, Y. M.; Ma, Y.; Liu, J. H.; Shi, J.; Fan, T.; Shan, Y. Y.; Yao, H. P.; Dong, Y. L., Trends and correlation of antibacterial usage and bacterial resistance: time series analysis for antibacterial stewardship in a Chinese teaching hospital (2009-2013). *Eur J Clin Microbiol* **2015,** *34* (4), 795-803.

53. Poole, K., Multidrug efflux pumps and antimicrobial resistance in *Pseudomonas aeruginosa* and related organisms. *J Mol Microbiol Biot* **2001,** *3* (2), 255-263.

54. a) Fernandez, L.; Hancock, R. E. W., Adaptive and mutational resistance: role of porins and efflux pumps in drug resistance. *Clin Microbiol Rev* **2012,** *25* (4), 661; b) Nikaido, H., Multidrug resistance in bacteria. *Annu Rev Biochem*, **2009,**. *78* 119-146; c) Wright, G. D., Molecular mechanisms of antibiotic resistance. *Chem Comm* **2011,** *47* (14), 4055-4061.

55. Brown, A. G., Clavulanic acid, a novel beta-lactamase inhibitor--a case study in drug discovery and development. *Drug des deliv* **1986,** *1* (1), 1-21.

56. Christ, W., Pharmacological properties of cephalosporins. *Infection* **1991,** *19*, S244-S252.

57. Endimiani, A.; Perez, F.; Bonomo, R. A., Cefepime: a reappraisal in an era of increasing antimicrobial resistance. *Expert Rev Anti Infect Ther* **2008,** *6* (6), 805-824.

58. Bradford, P. A., Extended-spectrum beta-lactamases in the 21st century: characterization, epidemiology, and detection of this important resistance threat. *Clin Microbiol Rev* **2001,** *14* (4), 933-951.

59. Andersen, J. L.; He, G. X.; Kakarla, P.; Ranjana, K. C.; Kumar, S.; Lakra, W. S.; Mukherjee, M. M.; Ranaweera, I.; Shrestha, U.; Tran, T.; Varela, M. F., Multidrug efflux pumps from Enterobacteriaceae, *Vibrio cholerae* and *Staphylococcus aureus* bacterial food pathogens. *Int J Environ Res Publ Health* **2015,** *12* (2), 1487-1547.

60. Tennent, J. M.; Lyon, B. R.; Midgley, M.; Jones, I. G.; Purewal, A. S.; Skurray, R. A., Physical and biochemical characterization of the *qaca* gene encoding antiseptic and disinfectant resistance in *Staphylococcus aureus*. *J Gen Microbiol* **1989,** *135*, 1-10.

61. Brown, M. H.; Skurray, R. A., Staphylococcal multidrug efflux protein QacA. *J Mol Microbiol Biot* **2001,** *3* (2), 163-170.

62. Paulsen, I. T.; Brown, M. H.; Littlejohn, T. G.; Mitchell, B. A.; Skurray, R. A., Multidrug resistance proteins QacA and QacB from *Staphylococcus aureus*: membrane topology and identification of residues involved in substrate specificity. *P Natl Acad Sci USA* **1996,** *93* (8), 3630-3635.

63. Ho, C. M.; Li, C. Y.; Ho, M. W.; Lin, C. Y.; Liu, S. H.; Lu, J. J., High rate of qacA- and qacB-positive methicillin-resistant *Staphylococcus aureus* isolates from chlorhexidine-Impregnated catheter-related bloodstream infections. *Antimicrob Agents Ch* **2012,** *56* (11), 5693-5697.

64. Otter, J. A.; Patel, A.; Cliff, P. R.; Halligan, E. P.; Tosas, O.; Edgeworth, J. D., Selection for qacA carriage in CC22, but not CC30, methicillin-resistant *Staphylococcus aureus* bloodstream infection isolates during a successful institutional infection control programme. *J Antimicrob Chemoth* **2013,** *68* (5), 992-999.

65. Shamsudin, M. N.; Alreshidi, M. A.; Hamat, R. A.; Alshrari, A. S.; Atshan, S. S.; Neela, V., High prevalence of qacA/B carriage among clinical isolates of meticillin-resistant *Staphylococcus aureus* in Malaysia. *J Hosp Infect* **2012,** *81* (3), 206-208.

66. Ubukata, K.; Itohyamashita, N.; Konno, M., Cloning and expression of the *norA* gene for fluoroquinolone resistance in *Staphylococcus aureus*. *Antimicrob Agents Ch* **1989,** *33* (9), 1535-1539.

67. Neyfakh, A. A.; Borsch, C. M.; Kaatz, G. W., Fluoroquinolone resistance protein NorA of *Staphylococcus aureus* is a multidrug efflux transporter. *Antimicrob Agents Ch* **1993,** *37* (1), 128-129.

68. Kaatz, G. W.; Seo, S. M.; Ruble, C. A., Efflux-mediated fluoroquinolone resistance in *Staphylococcus aureus*. *Antimicrob Agents Ch* **1993,** *37* (5), 1086-1094.

69. Ng, E. Y. W.; Trucksis, M.; Hooper, D. C., Quinolone resistance mediated by NorA - physiological characterization and relationship to FlqB, a quinolone resistance locus on the Staphylococcus aureus chromosome. *Antimicrob Agents Ch* **1994,** *38* (6), 1345-1355.

70. Kaatz, G. W.; Thyagarajan, R. V.; Seo, S. M., Effect of promoter region mutations and mgrA overexpression on transcription of norA, which encodes a *Staphylococcus aureus* multidrug efflux transporter. *Antimicrob Agents Ch* **2005,** *49* (1), 161-169.

71. Holler, J. G.; Christensen, S. B.; Slotved, H. C.; Rasmussen, H. B.; Guzman, A.; Olsen, C. E.; Petersen, B.; Molgaard, P., Novel inhibitory activity of the *Staphylococcus aureus* NorA efflux pump by a kaempferol rhamnoside isolated from *Persea lingue*. *J Antimicrob Chemoth* **2012,** *67* (5), 1138-1144.

72. Pieroni, M.; Dimovska, M.; Brincat, J. P.; Sabatini, S.; Carosati, E.; Massari, S.; Kaatz, G. W.; Fravolini, A., From 6-aminoquinolone antibacterials to 6-amino-7-thiopyranopyridinylquinolone ethyl esters as inhibitors of *Staphylococcus aureus* multidrug efflux pumps. *J Med Chem* **2010,** *53* (11), 4466-4480.

73. Kalia, N. P.; Mahajan, P.; Mehra, R.; Nargotra, A.; Sharma, J. P.; Koul, S.; Khan, I. A., Capsaicin, a novel inhibitor of the NorA efflux pump, reduces the intracellular invasion of *Staphylococcus aureus*. *J Antimicrob Chemoth* **2012,** *67* (10), 2401-2408.

74. Holler, J. G.; Slotved, H. C.; Molgaard, P.; Olsen, C. E.; Christensen, S. B., Chalcone inhibitors of the NorA efflux pump in *Staphylococcus aureus* whole cells and enriched everted membrane vesicles. *Bioorgan Med Chem* **2012,** *20* (14), 4514-4521.

75. German, N.; Wei, P.; Kaatz, G. W.; Kerns, R. J., Synthesis and evaluation of fluoroquinolone derivatives as substrate-based inhibitors of bacterial efflux pumps. *Eur J Med Chem* **2008,** *43* (11), 2453-2463.

76. Vidaillac, C.; Guillon, J.; Arpin, C.; Forfar-Bares, I.; Ba, B. B.; Grellet, J.; Moreau, S.; Caignard, D. H.; Jarry, C.; Quentin, C., Synthesis of omeprazole analogues and evaluation of these as potential inhibitors of the multidrug efflux pump NorA of *Staphylococcus aureus*. *Antimicrob Agents Ch* **2007,** *51* (3), 831-838.

77. Stavri, M.; Piddock, L. J. V.; Gibbons, S., Bacterial efflux pump inhibitors from natural sources. *J Antimicrob Chemoth* **2007,** *59* (6), 1247-1260.

78. Aygul, A., The Importance of Efflux Systems in Antibiotic Resistance and Efflux Pump Inhibitors in the Management of Resistance. *Mikrobiyol Bul* **2015,** *49* (2), 278-291.

79. Kaki, R.; Elligsen, M.; Walker, S.; Simor, A.; Palmay, L.; Daneman, N., Impact of antimicrobial stewardship in critical care: a systematic review. *J Antimicrob Chemoth* **2011,** *66* (6), 1223-1230.

80. Chang, Q. Z.; Wang, W. K.; Regev-Yochay, G.; Lipsitch, M.; Hanage, W. P., Antibiotics in agriculture and the risk to human health: how worried should we be? *Evol Appl* **2015,** *8* (3), 240-247.

81. Novick, R. P., Autoinduction and signal transduction in the regulation of staphylococcal virulence. *Mol Microbiol* **2003,** *48* (6), 1429-1449.

82. a) Hashimoto, M.; Tawaratsumida, K.; Kariya, H.; Kiyohara, A.; Suda, Y.; Krikae, F.; Kirikae, T.; Gotz, F., Not lipoteichoic acid but lipoproteins appear to be the dominant immunobiologically active compounds in *Staphylococcus aureus*. *J Immunol* **2006,** *177* (5), 3162-3169; b) Fournier, B.; Philpott, D. J., Recognition of *Staphylococcus aureus* by the innate immune system. *Clin Microbiol Rev* **2005,** *18* (3), 521.

83. a) Pisetsky, D. S., The role of nuclear macromolecules in innate immunity. *Proc Am Thorac Soc* **2007,** *4* (3), 258-62; b) Cavassani, K. A.; Ishii, M.; Wen, H. T.; Schaller, M. A.; Lincoln, P. M.; Lukacs, N. W.; Hogaboam, C. M.; Kunkel, S. L., TLR3 is an endogenous sensor of tissue necrosis during acute inflammatory events. *J Exp Med* **2008,** *205* (11), 2609-2621.

84. Scheibner, K. A.; Lutz, M. A.; Boodoo, S.; Fenton, M. J.; Powell, J. D.; Horton, M. R., Hyaluronan fragments act as an endogenous danger signal by engaging TLR2. *J Immunol* **2006,** *177* (2), 1272-1281.

85. Hair, P. S.; Wagner, S. M.; Friederich, P. T.; Drake, R. R.; Nyalwidhe, J. O.; Cunnion, K. M., Complement regulator C4BP binds to *Staphylococcus aureus* and decreases opsonization. *Mol Immunol* **2012,** *50* (4), 253-261.

86. Cunnion, K. M.; Zhang, H. M.; Frank, M. M., Availability of complement bound to *Staphylococcus aureus* to interact with membrane complement receptors influences efficiency of phagocytosis. *Infect Immun* **2003,** *71* (2), 656-662.

87. Zimin Yu, I.; Red'Kin, A. P., The role of antibody complement and protein A in the opsonization and phagocytosis of *Staphylococcus aureus*. *Immunologiya* **1987,** (3), 62-66.

88. Hair, P. S.; Ward, M. D.; Semmes, O. J.; Foster, T. J.; Cunnion, K. M., *Staphylococcus aureus* clumping factor A binds to complement regulator factor I and increases factor I cleavage of C3b. *J Infect Dis* **2008,** *198* (1), 125-133.

89. Cawdery, M.; Foster, W. D.; Hawgood, B. C.; Taylor, C., Role of coagulase in defence of *Staphylococcus aureus* against phagocytosis. *Brit J Exp Pathol* **1969,** *50* (4), 408.

90. Kubica, M.; Guzik, K.; Koziel, J.; Zarebski, M.; Richter, W.; Gajkowska, B.; Golda, A.; Maciag-Gudowska, A.; Brix, K.; Shaw, L.; Foster, T.; Potempa, J., A potential new pathway for *Staphylococcus aureus* dissemination: the silent survival of *S. aureus* phagocytosed by human monocyte-derived macrophages. *PloS One* **2008,** *3* (1), 16.

91. de Haas, C. J. C.; Veldkamp, K. E.; Peschel, A.; Weerkamp, F.; Van Wamel, W. J. B.; Heezius, E.; Poppelier, M.; Van Kessel, K. P. M.; van Strijp, J. A. G., Chemotaxis

inhibitory protein of *Staphylococcus aureus*, a bacterial antiinflammatory agent. *J Exp Med* **2004,** *199* (5), 687-695.

92. Chavakis, T.; Hussain, M.; Kanse, S. M.; Peters, G.; Bretzel, R. G.; Flock, J. I.; Herrmann, M.; Preissner, K. T., *Staphylococcus aureus* extracellular adherence protein serves as anti-inflammatory factor by inhibiting the recruitment of host leukocytes. *Nat Med* **2002,** *8* (7), 687-693.

93. Surewaard, B. G. J.; de Haas, C. J. C.; Vervoort, F.; Rigby, K. M.; DeLeo, F. R.; Otto, M.; van Strijp, J. A. G.; Nijland, R., Staphylococcal alpha-phenol soluble modulins contribute to neutrophil lysis after phagocytosis. *Cell Microbiol* **2013,** *15* (8), 1427-1437.

94. DuMont, A. L.; Yoong, P.; Surewaard, B. G. J.; Benson, M. A.; Nijland, R.; van Strijp, J. A. G.; Torres, V. J., *Staphylococcus aureus* elaborates Leukocidin AB to mediate escape from within human neutrophils. *Infect Immun* **2013,** *81* (5), 1830-1841.

95. Foster, T. J., Immune evasion by Staphylococci. *Nat Rev Microbiol* **2005,** *3* (12), 948-958.

96. Sieprawska-Lupa, M.; Mydel, P.; Krawczyk, K.; Wojcik, K.; Puklo, M.; Lupa, B.; Suder, P.; Silberring, J.; Reed, M.; Pohl, J.; Shafer, W.; McAleese, F.; Foster, T.; Travis, J.; Potempa, J., Degradation of human antimicrobial peptide LL-37 by *Staphylococcus aureus*-derived proteinases. *Antimicrob Agents Chemoth* **2004,** *48* (12), 4673-4679.

97. Jin, T.; Bokarewa, M.; Foster, T.; Mitchell, J.; Higgins, J.; Tarkowski, A., *Staphylococcus aureus* resists human defensins by production of staphylokinase, a novel bacterial evasion mechanism. *J Immunol* **2004,** *172* (2), 1169-1176.

98. Peschel, A.; Jack, R. W.; Otto, M.; Collins, L. V.; Staubitz, P.; Nicholson, G.; Kalbacher, H.; Nieuwenhuizen, W. F.; Jung, G.; Tarkowski, A.; van Kessel, K. P. M.; van Strijp, J. A. G., *Staphylococcus aureus* resistance to human defensins and evasion of neutrophil killing via the novel virulence factor MprF is based on modification of membrane lipids with L-lysine. *J Exp Med* **2001,** *193* (9), 1067-1076.

99. Collins, L. V.; Kristian, S. A.; Weidenmaier, C.; Faigle, M.; van Kessel, K. P. M.; van Strijp, J. A. G.; Gotz, F.; Neumeister, B.; Peschel, A., *Staphylococcus aureus* strains lacking *D*-alanine modifications of teichoic acids are highly susceptible to human neutrophil killing and are virulence attenuated in mice. *J Infect Dis* **2002,** *186* (2), 214-219.

100. Hammer, N. D.; Skaar, E. P., Molecular mechanisms of *Staphylococcus aureus* iron acquisition. *Annu Rev Microbiol,* **2011** *65*, 129-147.

101. Cassat, J. E.; Skaar, E. P., Metal ion acquisition in *Staphylococcus aureus*: overcoming nutritional immunity. *Semin Immunopathol* **2012,** *34* (2), 215-235.

102. Beasley, F. C.; Vines, E. D.; Grigg, J. C.; Zheng, Q.; Liu, S. Y.; Lajoie, G. A.; Murphy, M. E. P.; Heinrichs, D. E., Characterization of staphyloferrin A biosynthetic and transport mutants in *Staphylococcus aureus*. *Molecular Microbiology* **2009,** *72* (4), 947-963.

103. Diarra, M. S.; Rouille, B.; Lacasse, P., Characterization of *Staphylococcus aureus* that are defective for iron acquisition and assimilation. *Abstr Gen Meet Am Soc Microbiol* **2003,** *103*, B-322.

104. Wright, J. A.; Nair, S. P., The lipoprotein components of the Isd and Hts transport systems are dispensable for acquisition of heme by *Staphylococcus aureus*. *Fems Microbiol Lett* **2012,** *329* (2), 177-185.

105. Leonov, V. V.; Kosterina, V. V.; Varnitsina, V. V.; Timokhina, T. K.; Kurlovich, N. A., Iron-Dependent Synthesis of Hemolysins by *Staphylococcus aureus*. *B Exp Biol Med* **2012,** *153* (1), 41-43.

106. a) Llewelyn, M.; Cohen, J., Superantigens: microbial agents that corrupt immunity. *Lancet Infect Dis* **2002,** *2* (3), 156-162; b) Lee, L. Y.; Miyamoto, Y. J.; McIntyre, B. W.; Hook, M.; McCrea, K. W.; McDevitt, D.; Brown, E. L., The *Staphylococcus aureus* Map protein is an immunomodulator that interferes with T cell-mediated responses. *J Clin Invest* **2002,** *110* (10), 1461-1471.

107. Goodyear, C. S.; Silverman, G. J., Staphylococcal toxin induced preferential and prolonged in vivo deletion of innate-like B lymphocytes. *Proc Natl Acad Sci USA* **2004,** *101* (31), 11392-11397.

108. Becker, K.; Kriegeskorte, A.; Sunderkotter, C.; Loffler, B.; von Eiff, C., Persistent and recurrent skin and soft tissue infections by *Staphylococcus aureus*. Impact of the small colony-variant phenotype and of Panton-Valentine leukocidin-positive *S. aureus* isolates. *Hautarzt* **2014,** *65* (1), 15-25.

109. Folettit, D.; Strop, P.; Shaughnessy, L.; Hasa-Moreno, A.; Casas, M. G.; Russell, M.; Bee, C.; Wu, S.; Pham, A.; Zeng, Z. L.; Pons, J.; Rajpal, A.; Shelton, D., Mechanism of action and *in vivo* efficacy of a human-derived antibody against *Staphylococcus aureus* alpha-hemolysin. *J Mol Biol* **2013,** *425* (10), 1641-1654.

110. Tripathi, A.; Schofield, M. M.; Chlipala, G. E.; Schultz, P. J.; Yim, I.; Newmister, S. A.; Nusca, T. D.; Scaglione, J. B.; Hanna, P. C.; Tamayo-Castillo, G.; Sherman, D. H., Baulamycins A and B, broad-spectrum antibiotics identified as inhibitors of siderophore biosynthesis in *Staphylococcus aureus* and *Bacillus anthracis*. *J Am Chem Soc* **2014,** *136* (4), 1579-1586.

111. Thammavongsa, V.; Rauch, S.; Kim, H. K.; Missiakas, D. M.; Schneewind, O., Protein A-neutralizing monoclonal antibody protects neonatal mice against *Staphylococcus aureus*. *Vaccine* **2015,** *33* (4), 523-526.

112. Bassler, B. L.; Losick, R., Bacterially speaking. *Cell* **2006,** *125* (2), 237-246.

113. Miyashiro, T.; Ruby, E. G., Shedding light on bioluminescence regulation in *Vibrio fischeri*. *Mol Microbiol* **2012,** *84* (5), 795-806.

114. Daniels, R.; Vanderleyden, J.; Michiels, J., Quorum sensing and swarming migration in bacteria. *Fems Microbiol Rev* **2004,** *28* (3), 261-289.

115. Lee, J.; Wu, J.; Deng, Y.; Wang, J.; Wang, C.; Wang, J.; Chang, C.; Dong, Y.; Williams, P.; Zhang, L.-H., A cell-cell communication signal integrates quorum sensing and stress response. *Nat chem bio* **2013,** *9* (6), 406.

116. Ranall, M. V.; Butler, M. S.; Blaskovich, M. A.; Cooper, M. A., Resolving biofilm infections: current therapy and drug discovery strategies. *Curr Drug Targets* **2012,** *13* (11), 1375-1385.

117. Laverty, G.; Gorman, S. P.; Gilmore, B. F., Biomolecular mechanisms of staphylococcal biofilm formation. *Future Microbiol* **2013,** *8* (4), 509-524.

118. Struss, A. K.; Nunes, A.; Waalen, J.; Lowery, C. A.; Pullanikat, P.; Denery, J. R.; Conrad, D. J.; Kaufmann, G. F.; Janda, K. D., Toward implementation of quorum sensing autoinducers as biomarkers for infectious disease states. *Anal Chem* **2013,** *85* (6), 3355-3362.

119. Cotar, A. I.; Ionescu, B.; Pelinescu, D.; Voidarou, C.; Lazar, V.; Bezirtzoglou, E.; Chifiriuc, M. C., Current solutions for the interception of quorum sensing in *Staphylococcus aureus*. *Curr Org Chem* **2013,** *17* (2), 97-104.

120. Rutherford, S. T.; Bassler, B. L., Bacterial quorum sensing: its role in virulence and possibilities for its control. *Cold Spring Harb Perspect Med* **2012,** *2* (11), 25.

121. Li, Z.; Nair, S. K., Quorum sensing: how bacteria can coordinate activity and synchronize their response to external signals? *Protein Sci* **2012,** *21* (10), 1403-1417.

122. West, S. A.; Winzer, K.; Gardner, A.; Diggle, S. P., Quorum sensing and the confusion about diffusion. *Trends Microbiol* **2012,** *20* (12), 586-594.

123. Thoendel, M.; Horswill, A. R., Identification of *Staphylococcus aureus* AgrD residues required for autoinducing peptide biosynthesis. *J Biol Chem* **2009,** *284* (33), 21828-21838.

124. Lyon, G. J.; Wright, J. S.; Muir, T. W.; Novick, R. P., Key determinants of receptor activation in the agr autoinducing peptides of *Staphylococcus aureus*. *Biochem* **2002,** *41* (31), 10095-10104.

125. Cisar, E. A.; Geisinger, E.; Muir, T. W.; Novick, R. P., Symmetric signalling within asymmetric dimers of the Staphylococcus aureus receptor histidine kinase AgrC. *Mol Microbiol* **2009,** *74* (1), 44-57.

126. Lina, G.; Jarraud, S.; Ji, G. Y.; Greenland, T.; Pedraza, A.; Etienne, J.; Novick, R. P.; Vandenesch, F., Transmembrane topology and histidine protein kinase activity of AgrC, the agr signal receptor in *Staphylococcus aureus*. *Mol Microbiol* **1998,** *28* (3), 655-662.

127. Koenig, R. L.; Ray, J. L.; Maleki, S. J.; Smeltzer, M. S.; Hurlburt, B. K., *Staphylococcus aureus* AgrA binding to the RNAIII-agr regulatory region. *J Bacteriol* **2004,** *186* (22), 7549-7555.

128. Cheung, A. L.; Projan, S. J., Cloning and sequencing of *sarA* of Staphylococcus aureus, a gene required for the expression of agr. *J Bacteriol* **1994,** *176* (13), 4168-4172.

129. Queck, S. Y.; Jameson-Lee, M.; Villaruz, A. E.; Bach, T. H. L.; Khan, B. A.; Sturdevant, D. E.; Ricklefs, S. M.; Li, M.; Otto, M., RNAIII-independent target gene control by the *agr* quorum-sensing system: insight into the evolution of virulence regulation in *Staphylococcus aureus*. *Mol Cell* **2008,** *32* (1), 150-158.

130. Novick, R. P.; Projan, S. J.; Kornblum, J.; Ross, H. F.; Ji, G.; Kreiswirth, B.; Vandenesch, F.; Moghazeh, S., The *agr* P2 operon - an autocatalytic sensory transduction system in *Staphylococcus aureus*. *Mol Gen Genet* **1995,** *248* (4), 446-458.

131. Janzon, L.; Lofdahl, S.; Arvidson, S., Identification and nucleotide sequence of the delta-lysin gene, *hld*, adjacent to the accessory gene regulator (*agr*) of Staphylococcus aureus. *Mol Gen Genet* **1989,** *219* (3), 480-485.

132. Tseng, C.; Zhang, S.; Stewart, G. C., Agr control of enterotoxin D gene expression in *Staphylococcus aureus*. *Abstr Gen Meet Am Soc Microbiol* **2003,** *103*, B-068.

133. Regassa, L. B.; Couch, J. L.; Betley, M. J., Steady state staphylococcal Enterotoxin type C messenger-RNA is affected by a product of the accessory gene regulator and by glucose. *Infect Immun* **1991,** *59* (3), 955-962.

134. Sheehan, B. J.; Foster, T. J.; Dorman, C. J.; Park, S.; Stewart, G., Osmotic and growth-phase dependent regulation of the *eta* gene of Staphylococcus aureus - a role for DNA supercoiling. *Mol Gen Genet* **1992,** *232* (1), 49-57.

135. Recsei, P.; Kreiswirth, B.; Oreilly, M.; Schlievert, P.; Gruss, A.; Novick, R. P., Regulation of exoprotein gene expression in *Staphylococcus aureus* by *agr*. *Mol Gen Genet* **1986,** *202* (1), 58-61.

136. Bronner, S.; Stoessel, P.; Gravet, A.; Monteil, H.; Prevost, G., Variable expressions of *Staphylococcus aureus* bicomponent leucotoxins semiquantified by competitive reverse transcription-PCR. *Appl Environ Microbiol* **2000,** *66* (9), 3931-3938.

137. Daugherty, S.; Low, M. G., Cloning, expression, and mutagenesis of phosphatidylinositol-specific phospholipase-C from *Staphylococcus aureus* - a potential staphylococcal virulence factor. *Infect Immun* **1993,** *61* (12), 5078-5089.

138. Chamberlain, N. R.; Imanoel, B., Genetic regulation of fatty acid modifying enzyme from *Staphylococcus aureus*. *J Med Microbiol* **1996,** *44* (2), 125-129.

139. Reed, S. B.; Wesson, C. A.; Liou, L. E.; Trumble, W. R.; Schlievert, P. M.; Bohach, G. A.; Bayles, K. W., Molecular characterization of a novel *Staphylococcus aureus* serine protease operon. *Infect Immun* **2001,** *69* (3), 1521-1527.

140. Shaw, L.; Golonka, E.; Potempa, J.; Foster, S. J., The role and regulation of the extracellular proteases of *Staphylococcus aureus*. *Microbiol SGM* **2004,** *150*, 217-228.

141. Sun, F.; Liang, H. H.; Kong, X. Q.; Xie, S.; Cho, H.; Deng, X.; Ji, Q. J.; Zhang, H. Y.; Alvarez, S.; Hicks, L. M.; Bae, T.; Luo, C.; Jiang, H. L.; He, C., Quorum-sensing *agr* mediates bacterial oxidation response via an intramolecular disulfide redox switch in the response regulator AgrA. *Proc Natl Acad Sci USA* **2012,** *109* (23), 9095-9100.

142. Joo, H. S.; Chan, J. L.; Cheung, G. Y. C.; Otto, M., Subinhibitory concentrations of protein synthesis-inhibiting antibiotics promote increased expression of the *agr* virulence regulator and production of phenol-soluble modulin cytolysins in community-associated methicillin-resistant *Staphylococcus aureus*. *Antimicrob Agents Ch* **2010,** *54* (11), 4942-4944.

143. Rooijakkers, S. H. M.; Ruyken, M.; van Roon, J.; van Kessel, K. P. M.; van Strijp, J. A. G.; van Wamel, W. J. B., Early expression of SCIN and CHIPS drives instant immune evasion by Staphylococcus aureus. *Cell Microbiol* **2006,** *8* (8), 1282-1293.

144. Liu, Y.; Mu, C. H.; Ying, X. M.; Li, W. J.; Wu, N.; Dong, J.; Gao, Y. P.; Shao, N. S.; Fan, M.; Yang, G. A., RNAIII activates map expression by forming an RNA-RNA complex in *Staphylococcus aureus*. *FEBS Lett* **2011,** *585* (6), 899-905.

145. Geissmann, T.; Chevalier, C.; Cros, M.-J.; Boisset, S.; Fechter, P.; Noirot, C.; Schrenzel, J.; Francois, P.; Vandenesch, F.; Gaspin, C.; Romby, P., A search for small noncoding RNAs in *Staphylococcus aureus* reveals a conserved sequence motif for regulation. *Nucleic Acids Res* **2009,** *37* (21), 7239-7257.

146. Xue, T.; You, Y. B.; Shang, F.; Sun, B. L., Rot and Agr system modulate fibrinogen-binding ability mainly by regulating clfB expression in *Staphylococcus aureus* NCTC8325. *Med Microbiol Immunol* **2012,** *201* (1), 81-92.

147. Dassy, B.; Hogan, T.; Foster, T. J.; Fournier, J. M., Involvement of the accessory gene regulator in expression of type-5 capsular polysaccharide by *Staphylococcus aureus*. *J Gen Microbiol* **1993,** *139*, 1301-1306.

148. Luong, T.; Sau, S.; Gomez, M.; Lee, J. C.; Lee, C. Y., Regulation of *Staphylococcus aureus* capsular polysaccharide expression by *agr* and *sarA*. *Infect Immun* **2002,** *70* (2), 444-450.

149. SaraviaOtten, P.; Muller, H. P.; Arvidson, S., Transcription of *Staphylococcus aureus* fibronectin binding protein genes is negatively regulated by *agr* and an *agr*-independent mechanism. *J Bacteriol* **1997,** *179* (17), 5259-5263.

150. Wolz, C.; McDevitt, D.; Poster, T. J.; Cheung, A. L., Influence of *agr* on fibrinogen binding in *Staphylococcus aureus* Newman. *Infect Immun* **1996,** *64* (8), 3142-3147.

151. Pantrangi, M.; Singh, V. K.; Wolz, C.; Shukla, S. K., Staphylococcal superantigen-like genes, *ssl5* and *ssl8*, are positively regulated by *sae* and negatively by *agr* in the Newman strain. *Fems Microbiol Lett* **2010,** *308* (2), 175-184.

152. Boisset, S.; Geissmann, T.; Huntzinger, E.; Fechter, P.; Bendridi, N.; Possedko, M.; Chevalier, C.; Helfer, A. C.; Benito, Y.; Jacquier, A.; Gaspin, C.; Vandenesch, F.; Romby, P., *Staphylococcus aureus* RNAIII coordinately represses the synthesis of

virulence factors and the transcription regulator Rot by an antisense mechanism. *Genes Dev* **2007,** *21* (11), 1353-1366.

153. Naimi, T. S.; LeDell, K. H.; Como-Sabetti, K.; Borchardt, S. M.; Boxrud, D. J.; Etienne, J.; Johnson, S. K.; Vandenesch, F.; Fridkin, S.; O'Boyle, C.; Danila, R. N.; Lynfield, R., Comparison of community- and health care-associated methicillin-resistant Staphylococcus aureus infection. *Jama-J Am Med Assoc* **2003,** *290* (22), 2976-2984.

154. Strommenger, B.; Cuny, C.; Werner, G.; Witte, W., Obvious lack of association between dynamics of epidemic methicillin-resistant *Staphylococcus aureus* in Central Europe and *agr* specificity groups. *Eur J Clin Microbiol* **2004,** *23* (1), 15-19.

155. Tsuji, B. T.; Rybak, M. J.; Cheung, C. M.; Amjad, M.; Kaatz, G. W., Community- and health care-associated methicillin-resistant *Staphylococcus aureus*: a comparison of molecular epidemiology and antimicrobial activities of various agents. *Diagn Micr Infect Dis* **2007,** *58* (1), 41-47.

156. van Leeuwen, W.; van Nieuwenhuizen, W.; Gijzen, C.; Verbrugh, H.; van Belkum, A., Population studies of methicillin-resistant and -sensitive *Staphylococcus aureus* strains reveal a lack of variability in the *agrD* gene, encoding a staphylococcal autoinducer peptide. *J Bacteriol* **2000,** *182* (20), 5721-5729.

157. McDowell, P.; Affas, Z.; Reynolds, C.; Holden, M. T. G.; Wood, S. J.; Saint, S.; Cockayne, A.; Hill, P. J.; Dodd, C. E. R.; Bycroft, B. W.; Chan, W. C.; Williams, P., Structure, activity and evolution of the group I thiolactone peptide quorum-sensing system of *Staphylococcus aureus*. *Mol Microbiol* **2001,** *41* (2), 503-512.

158. Dufour, P.; Jarraud, S.; Vandenesch, F.; Greenland, T.; Novick, R. P.; Bes, M.; Etienne, J.; Lina, G., High genetic variability of the *agr* locus in *Staphylococcus* species. *J Bacteriol* **2002,** *184* (4), 1180-1186.

159. Ji, G. Y.; Beavis, R.; Novick, R. P., Bacterial interference caused by autoinducing peptide variants. *Science* **1997,** *276* (5321), 2027-2030.

160. a) Ji, G. Y.; Beavis, R. C.; Novick, R. P., Cell density control of staphylococcal virulence mediated by an octapeptide pheromone. *Proc Natl Acad Sci USA* **1995,** *92* (26), 12055-12059; b) Kavanaugh, J. S.; Thoendel, M.; Horswill, A. R., A role for type I signal peptidase in *Staphylococcus aureus* quorum sensing. *Mol Microbiol* **2007,** *65* (3), 780-798.

161. Rothfork, J. M.; Timmins, G. S.; Harris, M. N.; Chen, X.; Lusis, A. J.; Otto, M.; Cheung, A. L.; Gresham, H. D., Inactivation of a bacterial virulence pheromone by phagocyte-derived oxidants: New role for the NADPH oxidase in host defense. *Proc Natl Acad Sci USA* **2004,** *101* (38), 13867-13872.

162. Mayville, P.; Ji, G. Y.; Beavis, R.; Yang, H. M.; Goger, M.; Novick, R. P.; Muir, T. W., Structure-activity analysis of synthetic autoinducing thiolactone peptides from *Staphylococcus aureus* responsible for virulence. *Proc Natl Acad Sci USA* **1999,** *96* (4), 1218-1223.

163. Fleming, V.; Feil, E.; Sewell, A. K.; Day, N.; Buckling, A.; Massey, R. C., Agr interference between clinical *Staphylococcus aureus* strains in an insect model of virulence. *J Bacteriol* **2006,** *188* (21), 7686-7688.

164. Wright, J. S.; Jin, R.; Novick, R. P., Transient interference with staphylococcal quorum sensing blocks abscess formation. *Proc Natl Acad Sci USA* **2005,** *102* (5), 1691-1696.

165. Tal-Gan, Y.; Stacy, D. M.; Foegen, M. K.; Koenig, D. W.; Blackwell, H. E., Highly potent inhibitors of quorum sensing in *Staphylococcus aureus* revealed through a systematic synthetic study of the group-III autoinducing peptide. *J Am Chem Soc* **2013,** *135* (21), 7869-82.

166. Wang, B. Y.; Zhao, A. S.; Novick, R. P.; Muir, T. W., Activation and inhibition of the receptor histidine kinase AgrC occurs through opposite helical transduction motions. *Mol Cell* **2014,** *53* (6), 929-940.

167. Jensen, R. O.; Winzer, K.; Clarke, S. R.; Chan, W. C.; Williams, P., Differential recognition of *Staphylococcus aureus* quorum-sensing signals depends on both extracellular loops 1 and 2 of the transmembrane sensor AgrC. *J Mol Biol* **2008,** *381* (2), 300-309.

168. Geisinger, E.; George, E. A.; Muir, T. W.; Novick, R. P., Identification of ligand specificity determinants in AgrC, the *Staphylococcus aureus* quorum-sensing receptor. *J Biol Chem* **2008,** *283* (14), 8930-8938.

169. Chen, L. C.; Tsou, L. T.; Chen, F. J., Ligand-receptor recognition for activation of quorum sensing in *Staphylococcus aureus*. *J Microbiol* **2009,** *47* (5), 572-581.

170. Rowe, S. E.; Mahon, V.; Smith, S. G.; O'Gara, J. P., A novel role for SarX in *Staphylococcus epidermidis* biofilm regulation. *Microbiol-SGM* **2011,** *157*, 1042-1049.

171. a) Yao, Y. F.; Vuong, C.; Kocianova, S.; Villaruz, A. E.; Lai, Y. P.; Sturdevant, D. E.; Otto, M., Characterization of the *Staphylococcus epidermidis* accessory-gene regulator response: quorum-sensing regulation of resistance to human innate host defense. *J Infect Dis* **2006,** *193* (6), 941-948; b) Batzilla, C. F.; Rachid, S.; Engelmann, S.; Hecker, M.; Hacker, J.; Ziebuhr, W., Impact of the accessory gene regulatory system on extracellular proteins, codY expression and amino acid metabolism in *Staphylococcus epidermidis*. *Proteomics* **2006,** *6* (12), 3602-3613.

172. Wang, R.; Khan, B. A.; Cheung, G. Y. C.; Bach, T. H. L.; Jameson-Lee, M.; Kong, K. F.; Queck, S. Y.; Otto, M., *Staphylococcus epidermidis* surfactant peptides promote biofilm maturation and dissemination of biofilm-associated infection in mice. *J Clin Invest* **2011,** *121* (1), 238-248.

173. Otto, M.; Echner, H.; Voelter, W.; Gotz, F., Pheromone cross-inhibition between *Staphylococcus aureus* and *Staphylococcus epidermidis*. *Infect Immun* **2001,** *69* (3), 1957-1960.

174. Dell'Acqua, G.; Giacometti, A.; Cirioni, O.; Ghiselli, R.; Saba, V.; Scalise, G.; Gov, Y.; Balaban, N., Suppression of drug-resistant staphylococcal infections by the quorum-sensing inhibitor RNAIII-inhibiting peptide. *J Infect Dis* **2004,** *190* (2), 318-320.

175. Heilbronner, S.; Holden, M. T. G.; van Tonder, A.; Geoghegan, J. A.; Foster, T. J.; Parkhill, J.; Bentley, S. D., Genome sequence of *Staphylococcus lugdunensis* N920143 allows identification of putative colonization and virulence factors. *FEMS Microbiol Lett* **2011,** *322* (1), 60-67.

176. Vandenesch, F.; Storrs, M. J.; Poitevin-Later, F.; Etienne, J.; Courvalin, P.; Fleurette, J., Delta-like haemolysin produced by *Staphylococcus lugdunensis*. *FEMS microbiol lett* **1991,** *62* (1), 65-8.

177. Vandenesch, F.; Projan, S. J.; Kreiswirth, B.; Etienne, J.; Novick, R. P., Agr-related sequences in Staphylococcus-lugdunensis. FEMS *Microbiol Lett* **1993,** *111* (1), 115-122.

178. Gray, B.; Hall, P.; Gresham, H., Targeting agr- and agr-Like quorum sensing systems for development of common therapeutics to treat multiple Gram-positive bacterial infections. *Sensors* **2013,** *13* (4), 5130-5166.

179. Sakinc, T.; Kulczak, P.; Henne, K.; Gatermann, S. G., Cloning of an *agr* homologue of *Staphylococcus saprophyticus*. *FEMS Microbiol Lett* **2004,** *237* (1), 157-161.

180. Bannoehr, J.; Ben Zakour, N. L.; Waller, A. S.; Guardabassi, L.; Thoday, K. L.; van den Broek, A. H. M.; Fitzgerald, J. R., Population genetic structure of the *Staphylococcus intermedius* group: insights into *agr* diversification and the emergence of methicillin-resistant strains. *J Bacteriol* **2007,** *189* (23), 8685-8692.

181. Ji, G. Y.; Pei, W. H.; Zhang, L. S.; Qiu, R. D.; Lin, J. Q.; Benito, Y.; Lina, G.; Novick, R. P., *Staphylococcus intermedius* produces a functional *agr* autoinducing peptide containing a cyclic lactone. *J Bacteriol* **2005,** *187* (9), 3139-3150.

182. Monot, M.; Boursaux-Eude, C.; Thibonnier, M.; Vallenet, D.; Moszer, I.; Medigue, C.; Martin-Verstraete, I.; Dupuy, B., Reannotation of the genome sequence of *Clostridium difficile* strain 630. *J Med Microbiol* **2011,** *60* (8), 1193-1199.

183. Cooksley, C. M.; Davis, I. J.; Winzer, K.; Chan, W. C.; Peck, M. W.; Minton, N. P., Regulation of neurotoxin production and sporulation by a putative agrBD signaling system in proteolytic *Clostridium botulinum*. *Appl Environ Microbiol* **2010,** *76* (13), 4448-4460.

184. Li, J. H.; Chen, J. M.; Vidal, J. E.; McClane, B. A., The *agr*-like quorum-sensing System regulates sporulation and production of enterotoxin and beta2 toxin by *Clostridium perfringens* type A non-food-borne human gastrointestinal disease strain F5603. *Infect Immun* **2011,** *79* (6), 2451-2459.

185. Ohtani, K.; Yuan, Y.; Hassan, S.; Wang, R.; Wang, Y.; Shimizu, T., Virulence gene regulation by the *agr* System in *Clostridium perfringens*. *J Bacteriol* **2009,** *191* (12), 3919-3927.

186. Chen, J. M.; Rood, J. I.; McClane, B. A., Epsilon-toxin production by *Clostridium perfringens* type D strain CN3718 is dependent upon the *agr* operon but not the VirS/VirR two-component regulatory system. *Mbio* **2011,** *2* (6), 11.

187. Chen, J. M.; McClane, B. A., Role of the *agr*-like quorum-sensing system in regulating toxin production by *Clostridium perfringens* type B Strains CN1793 and CN1795. *Infect Immun* **2012,** *80* (9), 3008-3017.

188. Vidal, J. E.; Ma, M. L.; Saputo, J.; Garcia, J.; Uzal, F. A.; McClane, B. A., Evidence that the *agr*-like quorum sensing system regulates the toxin production, cytotoxicity and pathogenicity of *Clostridium perfringens* type C isolate CN3685. *Mol Microbiol* **2012,** *83* (1), 179-194.

189. Ohtani, K.; Hirakawa, H.; Tashiro, K.; Yoshizawa, S.; Kuhara, S.; Shimizu, T., Identification of a two-component VirR/VirS regulon in *Clostridium perfringens*. *Anaerobe* **2010,** *16* (3), 258-264.

190. Ma, M. L.; Li, J. H.; McClane, B. A., Structure-function analysis of peptide signaling in the *Clostridium perfringens agr*-like quorum sensing system. *J Bacteriol* **2015,** *197* (10), 1807-1818.

191. Darkoh, C.; DuPont, H. L.; Norris, S. J.; Kaplan, H. B., Toxin synthesis by *Clostridium difficile* is regulated through quorum signaling. *Mbio* **2015,** *6* (2), 10.

192. Pinkston, K. L.; Gao, P.; Diaz-Garcia, D.; Sillanpaa, J.; Nallapareddy, S. R.; Murray, B. E.; Harvey, B. R., The Fsr quorum-sensing system of *Enterococcus faecalis* modulates surface display of the collagen-binding MSCRAMM Ace through regulation of gelE. *J Bacteriol* **2011,** *193* (17), 4317-4325.

193. Engelbert, M.; Mylonakis, E.; Ausubel, F. M.; Calderwood, S. B.; Gilmore, M. S., Contribution of gelatinase, serine protease, and *fsr* to the pathogenesis of *Enterococcus faecalis* endophthalmitis. *Infect Immun* **2004,** *72* (6), 3628-3633.

194. a) Bourgogne, A.; Hilsenbeck, S. G.; Dunny, G. M.; Murray, B. E., Comparison of OG1RF and an isogenic fsrB deletion mutant by transcriptional analysis: the *Fsr* system of *Enterococcus faecalis* is more than the activator of gelatinase and serine protease. *J Bacteriol* **2006,** *188* (8), 2875-2884; b) Teixeira, N.; Santos, S.; Marujo, P.; Yokohata, R.; Iyer, V. S.; Nakayama, J.; Hancock, L. E.; Serror, P.; Lopes, M. D. S., The incongruent gelatinase genotype and phenotype in *Enterococcus faecalis* are due to shutting off the ability to respond to the gelatinase biosynthesis-activating pheromone quorum-sensing signal. *Microbiol-SGM* **2012,** *158*, 519-528; c) Bourgogne, A.; Thomson, L. C.; Murray, B. E., Bicarbonate enhances expression of the endocarditis and biofilm associated pilus locus, ebpR-ebpABC, in *Enterococcus faecalis*. *BMC Microbiol* **2010,** *10*, 13.

195. Qin, X.; Singh, K. V.; Weinstock, G. M.; Murray, B. E., Effects of *Enterococcus faecalis fsr* genes on production of gelatinase and a serine protease and virulence. *Infect Immun* **2000,** *68* (5), 2579-2586.

196. Nakayama, J.; Kariyama, R.; Kumon, H., Description of a 23.9-kilobase chromosomal deletion containing a region encoding *fsr* genes which mainly determines the

gelatinase-negative phenotype of clinical isolates of *Enterococcus faecalis* in urine. *Appl Environ Microbiol* **2002,** *68* (6), 3152-3155.

197. Nakayama, J.; Chen, S. M.; Oyama, N.; Nishiguchi, K.; Azab, E. A.; Tanaka, E.; Kariyama, R.; Sonomoto, K., Revised model for *Enterococcus faecalis fsr* quorum-sensing system: the small open reading frame fsrD encodes the gelatinase biosynthesis-activating pheromone propeptide corresponding to staphylococcal AgrD. *J Bacteriol* **2006,** *188* (23), 8321-8326.

198. Shankar, J.; Walker, R. G.; Ward, D.; Horsburgh, M. J., The *Enterococcus faecalis* exoproteome: identification and temporal regulation by Fsr. *PloS One* **2012,** *7* (3), 9.

199. Nakayama, J.; Cao, Y.; Horii, T.; Sakuda, S.; Nagasawa, H., Chemical synthesis and biological activity of the gelatinase biosynthesis-activating pheromone of *Enterococcus faecalis* and its analogs. *Biosci Biotech Bioch* **2001,** *65* (10), 2322-2325.

200. Nishiguchi, K.; Nagata, K.; Tanokura, M.; Sonomoto, K.; Nakayama, J., Structure-activity relationship of gelatinase biosynthesis-activating pheromone of *Enterococcus faecalis*. *J Bacteriol* **2009,** *191* (2), 641-650.

201. Nakayama, J.; Yokohata, R.; Sato, M.; Suzuki, T.; Matsufuji, T.; Nishiguchi, K.; Kawai, T.; Yamanaka, Y.; Nagata, K.; Tanokura, M.; Sonomoto, K., Development of a peptide antagonist against *fsr* quorum sensing of *Enterococcus faecalis*. *ACS Chem Biol* **2013,** *8* (4), 804-811.

202. Rieu, A.; Weidmann, S.; Garmyn, D.; Piveteau, P.; Guzzo, J., *Agr* system of *Listeria monocytogenes* EGD-e: role in adherence and differential expression pattern. *Appl Environ Microbiol* **2007,** *73* (19), 6125-6133.

203. Riedel, C. U.; Monk, I. R.; Casey, P. G.; Waidmann, M. S.; Gahan, C. G. M.; Hill, C., AgrD-dependent quorum sensing affects biofilm formation, invasion, virulence and global gene expression profiles in *Listeria monocytogenes*. *Mol Microbiol* **2009,** *71* (5), 1177-1189.

204. Autret, N.; Raynaud, C.; Dubail, I.; Berche, P.; Charbit, A., Identification of the *agr* locus of *Listeria monocytogenes*: role in bacterial virulence. *Infect Immun* **2003,** *71* (8), 4463-4471.

205. Williams, T.; Bauer, S.; Beier, D.; Kuhn, M., Construction and characterization of *Listeria monocytogenes* mutants with in-frame deletions in the response regulator genes identified in the genome sequence. *Infect Immun* **2005,** *73* (5), 3152-3159.

206. Garmyn, D.; Gal, L.; Briandet, R.; Guilbaud, M.; Lemaitre, J. P.; Hartmann, A.; Piveteau, P., Evidence of autoinduction heterogeneity *via* expression of the *agr* system of *Listeria monocytogenes* at the single-cell level. *Appl Environ Microbiol* **2011,** *77* (17), 6286-6289.

207. a) Balaban, N.; Goldkorn, T.; Nhan, R. T.; Dang, L. B.; Scott, S.; Ridgley, R. M.; Rasooly, A.; Wright, S. C.; Larrick, J. W.; Rasooly, R.; Carlson, J. R., Autoinducer of virulence as a target for vaccine and therapy against *Staphylococcus aureus*. *Science*

1998, *280* (5362), 438-440; b) Balaban, N.; Novick, R. P., Translation of RNAIII, the *Staphylococcus aureus agr* regulatory RNA molecule, can be activated by a 3'-end deletion. *FEMS Microbiol Lett* **1995,** *133* (1-2), 155-161.

208. a) Shaw, L. N.; Jonsson, I. M.; Singh, V. K.; Tarkowski, A.; Stewart, G. C., Inactivation of traP has no effect on the *agr* quorum-sensing system or virulence of *Staphylococcus aureus*. *Infect Immun* **2007,** *75* (9), 4519-4527; b) Tsang, L. H.; Daily, S. T.; Weiss, E. C.; Smeltzer, M. S., Mutation of traP in *Staphylococcus aureus* has no impact on expression of agr or biofilm formation. *Infect Immun* **2007,** *75* (9), 4528-4533.

209. Adhikari, R. P.; Arvidson, S.; Novick, R. P., A nonsense mutation in *agrA* accounts for the defect in *agr* expression and the avirulence of *Staphylococcus aureus* 8325-4 traP :: kan. *Infect Immun* **2007,** *75* (9), 4534-4540.

210. a) Ribeiro, P. D.; Ribeiro, O. D.; Marcolan, A. M.; Medina-Acosta, E., Treatment efficacy of the lead RNAIII-inhibiting peptide YSPWTNF-NH2 in acquired *Staphylococcus aureus* sepsis: a histopathological assessment. *Peptides* **2003,** *24* (11), 1829-1836; b) Balaban, N.; Cirioni, O.; Giacometti, A.; Ghiselli, R.; Braunstein, J. B.; Silvestri, C.; Mocchegiani, F.; Saba, V.; Scalise, G., Treatment of *Staphylococcus aureus* biofilm infection by the quorum-sensing inhibitor RIP. *Antimicrob Agents Ch* **2007,** *51* (6), 2226-2229; c) Simonetti, O.; Cirioni, O.; Ghiselli, R.; Goteri, G.; Scalise, A.; Orlando, F.; Silvestri, C.; Riva, A.; Saba, V.; Madanahany, K. D.; Offidani, A.; Balaban, N.; Scalise, G.; Giacometti, A., RNAIII-inhibiting peptide enhances healing of wounds infected with methicillin-resistant Staphylococcus aureus. *Antimicrob Agents Ch* **2008,** *52* (6), 2205-2211.

211. Yu, L. Q.; Wang, N.; Ma, J. Z.; Tong, C. Y.; Song, B. F.; Chi, J. Q.; Ma, G. D.; Zhu, Z. B.; Cui, Y. D., Improved protective efficacy of a chimeric *Staphylococcus aureus* vaccine candidate iron-regulated surface determinant B ((N126-P361))-target of RNAIII activating protein in mice. *Microbiol Immunol* **2013,** *57* (12), 857-864.

212. Kiran, M. D.; Adikesavan, N. V.; Cirioni, O.; Giacometti, A.; Silvestri, C.; Scalise, G.; Ghiselli, R.; Saba, V.; Orlando, F.; Shoham, M.; Balaban, N., Discovery of a quorum-sensing inhibitor of drug-resistant staphylococcal infections by structure-based virtual screening. *Mol Pharmacol* **2008,** *73* (5), 1578-1586.

213. Lyon, G. J.; Mayville, P.; Muir, T. W.; Novick, R. P., Rational design of a global inhibitor of the virulence response in *Staphylococcus aureus*, based in part on localization of the site of inhibition to the receptor-histidine kinase, AgrC. *Proc Natl Acad Sci USA* **2000,** *97* (24), 13330-13335.

214. Mansson, M.; Nielsen, A.; Kjaerulff, L.; Gotfredsen, C. H.; Wietz, M.; Ingmer, H.; Gram, L.; Larsen, T. O., Inhibition of virulence gene expression in *Staphylococcus aureus* by novel depsipeptides from a marine photobacterium. *Mar Drugs* **2011,** *9* (12), 2537-2552.

215. Geisinger, E.; Muir, T. W.; Novick, R. P., Agr receptor mutants reveal distinct modes of inhibition by staphylococcal autoinducing peptides. *Proc Natl Acad Sci USA* **2009,** *106* (4), 1216-1221.

216. Nielsen, A.; Mansson, M.; Bojer, M. S.; Gram, L.; Larsen, T. O.; Novick, R. P.; Frees, D.; Frokiaer, H.; Ingmer, H., Solonamide B inhibits quorum sensing and reduces *Staphylococcus aureus* mediated killing of human neutrophils. *PloS One* **2014,** *9* (1), 10.

217. Park, J.; Jagasia, R.; Kaufmann, G. F.; Mathison, J. C.; Ruiz, D. I.; Moss, J. A.; Meijler, M. M.; Ulevitch, R. J.; Janda, K. D., Infection control by antibody disruption of bacterial quorum sensing signaling. *Chem Biol* **2007,** *14* (10), 1119-1127.

218. Kirchdoerfer, R. N.; Garner, A. L.; Flack, C. E.; Mee, J. M.; Horswill, A. R.; Janda, K. D.; Kaufmann, G. F.; Wilson, I. A., Structural basis for ligand recognition and discrimination of a quorum-quenching antibody. *J Biol Chem* **2011,** *286* (19), 17351-17358.

219. Nakayama, J.; Uemura, Y.; Nishiguchi, K.; Yoshimura, N.; Igarashi, Y.; Sonomoto, K., Ambuic acid inhibits the biosynthesis of cyclic peptide quormones in Gram-positive bacteria. *Antimicrob Agents Ch* **2009,** *53* (2), 580-586.

220. Qazi, S.; Middleton, B.; Muharram, S. H.; Cockayne, A.; Hill, P.; O'Shea, P.; Chhabra, S. R.; Camara, M.; Williams, P., *N*-acylhomoserine lactones antagonize virulence gene expression and quorum sensing in *Staphylococcus aureus*. *Infect Immun* **2006,** *74* (2), 910-919.

221. Schobert, R.; Schlenk, A., Tetramic and tetronic acids: An update on new derivatives and biological aspects. *Bioorg Med Chem* **2008,** *16* (8), 4203-4221.

222. Lowery, C. A.; Park, J.; Gloeckner, C.; Meijler, M. M.; Mueller, R. S.; Boshoff, H. I.; Ulrich, R. L.; Barry, C. E.; Bartlett, D. H.; Kravchenko, V. V.; Kaufmann, G. F.; Janda, K. D., Defining the mode of action of tetramic acid antibacterials derived from *Pseudomonas aeruginosa* quorum sensing signals. *J Am Chem Soc* **2009,** *131* (40), 14473-14479.

223. Murray, E. J.; Crowley, R. C.; Truman, A.; Clarke, S. R.; Cottam, J. A.; Jadhav, G. P.; Steele, V. R.; O'Shea, P.; Lindholm, C.; Cockayne, A.; Chhabra, S. R.; Chan, W. C.; Williams, P., Targeting *Staphylococcus aureus* quorum sensing with nonpeptidic small molecule inhibitors. *J Med Chem* **2014,** *57* (6), 2813-2819.

224. Desouky, S. E.; Shojima, A.; Singh, R. P.; Matsufuji, T.; Igarashi, Y.; Suzuki, T.; Yamagaki, T.; Okubo, K.-I.; Ohtani, K.; Sonomoto, K.; Nakayama, J., Cyclodepsipeptides produced by actinomycetes inhibit cyclic-peptide-mediated quorum sensing in Gram-positive bacteria. *FEMS microbiol lett* **2015,** *362* (14).

225. Wyatt, M.; Wang, W.; Roux, C.; Beasley, F.; Heinrichs, D.; Dunman, P.; Magarvey, N., *Staphylococcus aureus* nonribosomal peptide secondary metabolites regulate virulence. *Science* **2010,** *329* (5989), 294-296.

226. Zeng, Y. B.; Li, Q. S.; Hanzlik, R. P.; Aube, J., Synthesis of a small library of diketopiperazines as potential inhibitors of calpain. *Bioorg Med Chem Lett* **2005,** *15* (12), 3034-3038.

227. Bruckner, R., *Organic Mechanisms: Reactions, Stereochemistry and Synthesis*. 3rd ed.; Springer: Berlin, 2007.

228. Song, J. I.; An, D. K., New method for synthesis of aldehydes from esters by sodium diisobutyl-t-butoxyaluminum hydride. *Chem Lett* **2007,** *36* (7), 886-887.

229. Stockman, R. Dibal reduction of an amino acid derived methyl ester. http://cssp.chemspider.com/161 (accessed 27th August).

230. Detzer, N. Development of peptide amino alcohols as cyclin A groove inhibitors. University of Nottingham, Nottingham, 2005.

231. Jensen, R. O. Functional analysis of the group specific interactions between AIP and AgrC in *Staphylococcus aureus* University of Nottingham, Nottingham, 2009.

232. Hage, D. S.; Anguizola, J. A.; Bi, C.; Li, R.; Matsuda, R.; Papastavros, E.; Pfaunmiller, E.; Vargas, J.; Zheng, X. W., Pharmaceutical and biomedical applications of affinity chromatography: Recent trends and developments. *J Pharm Biomed Anal* **2012,** *69*, 93-105.

233. Affinity Chromatography: Methods and Protocols, Second Edition. *Affinity Chromatography: Methods and Protocols, Second Edition* **2008,** *421*.

234. a) Neises, B.; Steglich, W., Esterification of carboxylic acids with dicyclohexylcarbodiimide / 4-dimethylaminopyridine : tert-butylethylfumarate. *Org Synth* **1985,** *63*, 183; b) Neises, B.; Steglich, W., Simple Method for the Esterification of Carboxylic Acids. *Angew Chem Int Ed Engl* **1978,** *17* (7), 522-524; c) Ziegler, F. E.; Berger, G. D., Mild method for the esterification of fatty acids. *Synth Commun* **1979,** *9* (6), 539-543; d) Gilon, C.; Klausner, Y.; Hassner, A., Novel method for the facile synthesis of depsipeptides. *Tetrahedron Lett* **1979,** (40), 3811-3814.

235. Nelson, S. G.; Zhu, C.; Shen, X. Q., Catalytic asymmetric acyl halide-aldehyde cyclocondensation reactions of substituted ketenes. *J Am Chem Soc* **2004,** *126* (1), 14-15.

236. Yim, G.; Wang, H. M. H.; Davies, J., Antibiotics as signalling molecules. *Phil Trans R Soc B* **2007,** *362* (1483), 1195-1200.

237. Byford, M. F.; Baldwin, J. E.; Shiau, C. Y.; Schofield, C. J., The mechanism of ACV synthetase. *Chem Rev* **1997,** *97* (7), 2631-2649.

238. Fischbach, M. A.; Walsh, C. T., Assembly-line enzymology for polyketide and nonribosomal peptide antibiotics: Logic, machinery, and mechanisms. *Chem Rev* **2006,** *106* (8), 3468-3496.

239. a) Lautru, S.; Deeth, R. J.; Bailey, L. M.; Challis, G. L., Discovery of a new peptide natural product by *Streptomyces coelicolor* genome mining. *Nat Chem Biol* **2005,** *1* (5), 265-269; b) Challis, G. L., Genome mining for novel natural product discovery. *J Med Chem* **2008,** *51* (9), 2618-2628.

240. Alvarez, M. E.; White, C. B.; Gregory, J.; Kydd, G. C.; Harris, A.; Sun, H. H.; Gillum, A. M.; Cooper, R., Phevalin, a new calpain inhibitor, from a *Streptomyces sp*. *J Antibiot* **1995,** *48* (10), 1165-1167.

241. Harding, K. E.; May, L. M.; Dick, K. F., Selective oxidation of allylic alcohols with chromic acid. *J Org Chem* **1975,** *40* (11), 1664-1665.

242. Poos, G. I.; Arth, G. E.; Beyler, R. E.; Sarett, L. H., Approaches to the total synthesis of adrenal steroids .5. 4b-methyl-7- ethylenedioxy-1,2,3,4,4aα,4b,5,6,7,8,10,10a β-dodecahydrophenanthrene-4 β-ol-1-one and related tricyclic derivatives. *J Am Chem Soc* **1953,** *75* (2), 422-429.

243. Cornforth, R. H.; Popjak, G.; Cornforth, J. W., Preparation of *R*- and *S*-mevalonolactones. *Tetrahedron* **1962,** *18* (DEC), 1351.

244. Corey, E. J.; Suggs, J. W., Pyridinium chlorochromate - efficient reagent for oxidation of primary and secondary alcohols to cabonyl-compounds. *Tetrahedron Lett* **1975,** (31), 2647-2650.

245. Kozikowski, A. P.; Ishida, H.; Chen, Y. Y., New synthesis and some selected reactions of the potential ergot alkaloid precursor indole-4-carboxyaldehyde. *J Org Chem* **1980,** *45* (16), 3350-3352.

246. d'Acunzo, F.; Galli, C.; Masci, B., Oxidation of phenols by laccase and laccase-mediator systems - solubility and steric issues. *Eur J Biochem* **2002,** *269* (21), 5330-5335.

247. Aliaga, C.; Juarez-Ruiz, J. M.; Scaiano, J. C.; Aspee, A., Hydrogen-transfer reactions from phenols to TEMPO prefluorescent probes in micellar systems. *Org Lett* **2008,** *10* (11), 2147-2150.

248. Griffith, W. P.; Ley, S. V.; Whitcombe, G. P.; White, A. D., Preparation and use of tetra-normal-butylammonium per-ruthenate (TBAP reagent) and tetra-normal-propylammonium per-ruthenate (TPAP reagent) as new catalytic oxidants for alcohols. *J Chem Soc Chem Comm* **1987,** (21), 1625-1627.

249. Katoh, T.; Itoh, E.; Yoshino, T.; Terashima, S., Total synthesis of an enantiomeric pair of FR900482 .1. Synthetic and end-game strategies. *Tetrahedron* **1997,** *53* (30), 10229-10238.

250. Tatsuta, K.; Takano, S.; Sato, T.; Nakano, S., The first total synthesis of a macrocyclic anti-protozoan, LL-Z1640-2. *Chem Lett* **2001,** (2), 172-173.

251. Meyer, S. D.; Schreiber, S. L., Acceleration of the Dess-Martin oxidation by water. *J Org Chem* **1994,** *59* (24), 7549-7552.

252. More, J. D.; Finney, N. S., A simple and advantageous protocol for the oxidation of alcohols with, o-iodoxybenzoic acid (IBX). *Org Lett* **2002,** *4* (17), 3001-3003.

253. Burdon, M. G.; Moffatt, J. G., Acid-catalysed reactions of phenols with dimethly sulfoxide and dicyclohexylcarbodiimide. *J Am Chem Soc* **1965**, *87* (20), 4656

254. Sato, K.; Inoue, S.; Ozawa, K.; Tazaki, M., Selective ortho-methylthiomethylation of phenols with dimethyl sulphoxide and thionyl chloride. J Chem Soc, Perkin Trans 1 **1984**, 2715-2719.

255. Katayama, S.; Watanabe, T.; Yamauchi, M., Convenient synthesis of 2,4-cyclohexadien-1-ones by regioselecctive methylthiomethylation of phenols. *Chem Pharm Bull* **1993**, *41* (3), 439-444.

256. Parikh, J. R.; Doering, W. v. E., Sulfur trioxide in the oxidation of alcohols by dimethyl sulfoxide. *J Am Chem Soc* **1967,** *89* (21), 5505-5507.

257. Magdziak, D.; Rodriguez, A. A.; Van De Water, R. W.; Pettus, T. R. R., Regioselective oxidation of phenols to o-quinones with o-iodoxybenzoic acid (IBX). *Org Lett* **2002,** *4* (2), 285-288.

258. Sun, F.; Cho, H.; Jeong, D.; Li, C.; He, C.; Bae, T., Aureusimines in *Staphylococcus aureus* are not in virulence. *PloS One* **2010,** *5* (12).

259. Wuts, P.; Greene, T., *Protective Groups in Organic Synthesis*. 4th ed.; Wiley-Blackwell: 2006.

260. Dehbi, M.; Moeck, G.; Arhin, F. F.; Bauda, P.; Bergeron, D.; Kwan, T.; Liu, J.; McCarty, J.; Dubow, M.; Pelletier, J., Inhibition of transcription in *Staphylococcus aureus* by a primary sigma factor-binding polypeptide from phage G1. *J Bacteriol* **2009,** *191* (12), 3763-3771.

261. Pardo, M.; Choudhary, F. S., Assignment of protein interactions from affinity purification/mass spectrometry data. *J Proteome Res* **2012,** *11* (3), 1462-1474.

262. Bae, T.; Banger, A. K.; Wallace, A.; Glass, E. M.; Aslund, F.; Schneewind, O.; Missiakas, D. M., *Staphylocloccus aureus* virulence genes identified by *bursa aurealis* mutagenesis and nematode killing. *Proc Natl Acad Sci USA* **2004,** *101* (33), 12312-12317.

263. Kaito, C.; Sekimizu, K., Colony spreading in *Staphylococcus aureus*. *J Bacteriol* **2007,** *189* (6), 2553-2557.

264. Tsompanidou, E.; Denham, E. L.; Becher, D.; de Jong, A.; Buist, G.; van Oosten, M.; Manson, W. L.; Back, J. W.; van Dijl, J. M.; Dreisbach, A., Distinct roles of phenol-soluble modulins in spreading of *Staphylococcus aureus* on wet surfaces. *Appl Environ Microbiol* **2013,** *79* (3), 886-895.

265. Tsompanidou, E.; Sibbald, M.; Chlebowicz, M. A.; Dreisbach, A.; Back, J. W.; van Dijl, J. M.; Buist, G.; Denham, E. L., Requirement of the *agr* locus for colony spreading of *Staphylococcus aureus*. *J Bacteriol* **2011,** *193* (5), 1267-1272.

266. Mandell, G. L.; Bennett, J. E.; Dolin, R., *Mandell, Douglas, and Bennett's Principles and Practice of Infectious Diseases*. 7th ed.; Churchill Livingstone: Philadelphia, 2009; p 4320.

267. Proctor, R. A.; Kahl, B.; von Eiff, C.; Vaudaux, P. E.; Lew, D. P.; Peters, G., Staphylococcal small colony variants have novel mechanisms for antibiotic resistance. *Clin Infect Dis* **1998,** *27*, S68-S74.

268. Proctor, R. A.; Vesga, O.; Otten, M. F.; Koo, S. P.; Yeaman, M. R.; Sahl, H. G.; Bayer, A. S., *Staphylococcus aureus* small colony variants cause persistent and resistant infections. *Chemotherapy* **1996,** *42*, 47-52.

269. Kahl, B. C., Small colony variants (SCVs) of *Staphylococcus aureus* - a bacterial survival strategy. *Infect Genet Evol* **2014,** *21*, 515-522.

270. von Eiff, C.; Lubritz, G.; Heese, C.; Peters, G.; Becker, K., Effect of trimethoprim-sulfamethoxazole prophylaxis in AIDS patients on the formation of the small colony variant phenotype of *Staphylococcus aureus*. *Diagn Microbiol Infect Dis* **2004,** *48* (3), 191-194.

271. Schaaff, F.; Bierbaum, G.; Baumert, N.; Bartmann, P.; Sahl, H. G., Mutations are involved in emergence of aminoglycoside-induced small colony variants of *Staphylococcus aureus*. *Int J Med Microbiol* **2003,** *293* (6), 427-435.

272. Lannergard, J.; Cao, S.; Norstrom, T.; Delgado, A.; Gustafson, J. E.; Hughes, D., Genetic complexity of fusidic acid-resistant small colony variants in *Staphylococcus aureus*. *PloS One* **2011,** *6* (11), 9.

273. Pan, X. S.; Hamlyn, P. J.; Talens-Visconti, R.; Alovero, F. L.; Manzo, R. H.; Fisher, L. M., Small-colony mutants of *Staphylococcus aureus* allow selection of gyrase-mediated resistance to dual-target fluoroquinolones. *Antimicrob Agents Ch* **2002,** *46* (8), 2498-2506.

274. Bayston, R.; Ashraf, W.; Smith, T., Triclosan resistance in methicillin-resistant *Staphylococcus aureus* expressed as small colony variants: a novel mode of evasion of susceptibility to antiseptics. *J Antimicrob Chemoth* **2007,** *59* (5), 848-853.

275. Lannergard, J.; von Eiff, C.; Sander, G.; Cordes, T.; Seggewiss, J.; Peters, G.; Proctor, R. A.; Becker, K.; Hughes, D., Identification of the genetic basis for clinical menadione-auxotrophic small-colony variant isolates of *Staphylococcus aureus*. *Antimicrob Agents Ch* **2008,** *52* (11), 4017-4022.

276. von Eiff, C.; Heilmann, C.; Proctor, R. A.; Woltz, C.; Peters, G.; Gotz, F., A site-directed *Staphylococcus aureus* hemB mutant is a small-colony variant which persists intracellularly. *J Bacteriol* **1997,** *179* (15), 4706-4712.

277. Besier, S.; Ludwig, A.; Ohlsen, K.; Brade, V.; Wichelhaus, T. A., Molecular analysis of the thymidine-auxotrophic small colony variant phenotype of *Staphylococcus aureus*. *Int J Med Microbiol* **2007,** *297* (4), 217-225.

278. Singh, R.; Ray, P.; Das, A.; Sharma, M., Role of persisters and small-colony variants in antibiotic resistance of planktonic and biofilm-associated *Staphylococcus aureus*: an *in vitro* study. *J Med Microbiol* **2009,** *58* (8), 1067-1073.

279. Brouillette, E.; Martinez, A.; Boyll, B. J.; Allen, N. E.; Malouin, F., Persistence of a *Staphylococcus aureus* small-colony variant under antibiotic pressure *in vivo*. *FEMS Immunol Med Microbiol* **2004,** *41* (1), 35-41.

280. Costerton, J. W.; Stewart, P. S.; Greenberg, E. P., Bacterial biofilms: a common cause of persistent infections. *Science* **1999,** *284* (5418), 1318-1322.

281. O'Gara, J. P., *Ica* and beyond: biofilm mechanisms and regulation in *Staphylococcus epidermidis* and *Staphylococcus aureus*. *FEMS Microbiol Lett* **2007,** *270* (2), 179-188.

282. Lister, J. L.; Horswill, A. R., *Staphylococcus aureus* biofilms: recent developments in biofilm dispersal. *Front Cell Infect Microbiol* **2014,** *4*, 9.

283. Foster, T. J.; Hook, M., Surface protein adhesins of *Staphylococcus aureus*. *Trends Microbiol* **1998,** *6* (12), 484-488.

284. Goetz, F., *Staphylococcus* and biofilms. *Mol Microbiol* **2002,** *43* (6), 1367-1378.

285. Cramton, S. E.; Gerke, C.; Schnell, N. F.; Nichols, W. W.; Gotz, F., The intercellular adhesion (*ica*) locus is present in *Staphylococcus aureus* and is required for biofilm formation. *Infect Immun* **1999,** *67* (10), 5427-5433.

286. Maira-Litran, T.; Kropec, A.; Abeygunawardana, C.; Joyce, J.; Mark, G.; Goldmann, D. A.; Pier, G. B., Immunochemical properties of the staphylococcal poly-N-acetylglucosamine surface polysaccharide. *Infect Immun* **2002,** *70* (8), 4433-4440.

287. Mack, D.; Fischer, W.; Krokotsch, A.; Leopold, K.; Hartmann, R.; Egge, H.; Laufs, R., The intercellular adhesin involved in biofilm accumulation of *Staphylococcus epidermidis* is a linear beta-1,6-linked glucosaminoglycan: Purification and structural analysis. *J Bacteriol* **1996,** *178* (1), 175-183.

288. Fitzpatrick, F.; Humphreys, H.; O'Gara, J. P., Environmental regulation of biofilm development in methicillin-resistant and methicillin-susceptible *Staphylococcus aureus* clinical isolates. *J Hosp Infect* **2006,** *62* (1), 120-122.

289. Fluckiger, U.; Ulrich, M.; Steinhuber, A.; Doring, G.; Mack, D.; Landmann, R.; Goerke, C.; Wolz, C., Biofilm formation, *icaADBC* transcription, and polysaccharide intercellular adhesin synthesis by staphylococci in a device-related infection model. *Infect Immun* **2005,** *73* (3), 1811-1819.

290. Conlon, K. M.; Humphreys, H.; O'Gara, J. P., *IcaR* encodes a transcriptional repressor involved in environmental regulation of *ica* operon expression and biofilm formation in *Staphylococcus epidermidis*. *J Bacteriol* **2002,** *184* (16), 4400-4408.

291. You, Y. B.; Xue, T.; Cao, L. Y.; Zhao, L. P.; Sun, H. P.; Sim, B. L., *Staphylococcus aureus* glucose-induced biofilm accessory proteins, GbaAB, influence biofilm formation in a PIA-dependent manner. *Int J Med Microbiol* **2014,** *304* (5-6), 603-612.

292. Tu Quoc, P. H.; Genevaux, P.; Pajunen, M.; Savilahti, H.; Georgopoulos, C.; Schrenzel, J.; Kelley, W. L., Isolation and characterization of biofilm formation-defective mutants of *Staphylococcus aureus*. *Infect immun* **2007,** *75* (3), 1079-88.

293. O'Neill, E.; Pozzi, C.; Houston, P.; Smyth, D.; Humphreys, H.; Robinson, D. A.; O'Gara, J. P., Association between methicillin susceptibility and biofilm regulation in *Staphylococcus aureus* isolates from device-related infections. *J Clin Microbiol* **2007,** *45* (5), 1379-1388.

294. Toledo-Arana, A.; Merino, N.; Vergara-Irigaray, M.; Dearbouille, M.; Penades, J. R.; Lasa, H., *Staphylococcus aureus* develops an alternative, *ica*-independent biofilm in the absence of the arlRS two-component system. *J Bacteriol* **2005,** *187* (15), 5318-5329.

295. Beenken, K. E.; Blevins, J. S.; Smeltzer, M. S., Mutation of *sarA* in *Staphylococcus aureus* limits biofilm formation. *Infect Immun* **2003,** *71* (7), 4206-4211.

296. Coelho, L. R.; Souza, R. R.; Ferreira, F. A.; Guimaraes, M. A.; Ferreira-Carvalho, B. T.; Figueiredo, A. M. S., *Agr* RNAIII divergently regulates glucose-induced biofilm formation in clinical isolates of *Staphylococcus aureus*. *Microbiol-SGM* **2008,** *154*, 3480-3490.

297. Yarwood, J. M.; Bartels, D. J.; Volper, E. M.; Greenberg, E. P., Quorum sensing in *Staphylococcus aureus* biofilms. *J Bacteriol* **2004,** *186* (6), 1838-1850.

298. Johnson, M.; Cockayne, A.; Williams, P. H.; Morrissey, J. A., Iron-responsive regulation of biofilm formation in *Staphylococcus aureus* involves fur-dependent and fur-independent mechanisms. *J Bacteriol* **2005,** *187* (23), 8211-8215.

299. Johnson, M.; Cockayne, A.; Morrissey, J. A., Iron-regulated biofilm formation in *Staphylococcus aureus* Newman requires *ica* and the secreted protein Emp. *Infect Immun* **2008,** *76* (4), 1756-1765.

300. Seidl, K.; Goerke, C.; Woiz, C.; Mack, D.; Berger-Baechi, B.; Bischoff, M., *Staphylococcus aureus* CcpA affects biofilm formation. *Infect Immun* **2008,** *76* (5), 2044-2050.

301. Dawson, J.; Miltz, W.; Mir, A. K.; Wiessner, C., Targeting monocyte chemoattractant protein-1 signalling in disease. *Exper Opin Ther Tar* **2003,** *7* (1), 35-48.

302. Klausmeyer, P.; Howard, O. M. Z.; Shipley, S. M.; McCoud, T. G., An inhibitor of CCL2-induced chemotaxis from the fungus *Leptoxyphium sp*. *J Nat Prod* **2009,** *72* (8), 1369-1372.

303. Saleki, M.; Colgin, N.; Kirby, J. A.; Cobb, S. L.; Ali, S., Evaluation of two cyclic di-peptides as inhibitors of CCL2 induced chemotaxis. *Medchemcomm* **2013,** *4* (5), 860-864.

304. a) Kim, J.; Kim, H.; Park, S. B., Privileged structures: efficient chemical "navigators" toward unexplored biologically relevant chemical spaces. *J Am Chem Soc* **2014,** *136* (42), 14629-14638; b) Mai, A. H.; Pawar, S.; De Borggraeve, W. M., Synthesis of 1-

benzyloxypyrazin-2(1H)-one derivatives. *Tetrahedron Lett* **2014,** *55* (33), 4664-4666.

305. Landi, F.; Johansson, C. M.; Campopiano, D. J.; Hulme, A. N., Synthesis and application of a new cleavable linker for "click"-based affinity chromatography. *Org Biomol Chem* **2010,** *8* (1), 56-59.

306. Liebeke, M.; Lalk, M., *Staphylococcus aureus* metabolic response to changing environmental conditions - A metabolomics perspective. *Int J Med Microbiol* **2014,** *304* (3-4), 222-229.

307. Lyon, G. J.; Wright, J. S.; Christopoulos, A.; Novick, R. P.; Muir, T. W., Reversible and specific extracellular antagonism of receptor-histidine kinase signaling. *J Biol Chem* **2002,** *277* (8), 6247-6253.

308. Scott, R. J.; Lian, L. Y.; Muharram, S. H.; Cockayne, A.; Wood, S. J.; Bycroft, B. W.; Williams, P.; Chan, W. C., Side-chain-to-tail thiolactone peptide inhibitors of the staphylococcal quorum-sensing system. *Bioorg Med Chem Lett* **2003,** *13* (15), 2449-2453.

309. George, E. A.; Novick, R. P.; Muir, T. W., Cyclic peptide inhibitors of staphylococcal virulence prepared by Fmoc-based thiolactone peptide synthesis. *J Am Chem Soc* **2008,** *130* (14), 4914-4924.

310. Snyder, J. P., Probable unimportance of intramolecular hydrogen-bonds for determining the secondary structure of cyclic hexapeptides - Roseotoxin-B. *J Am Chem Soc* **1984,** *106* (8), 2393-2400.

311. Laufer, B.; Frank, A. O.; Chatterjee, J.; Neubauer, T.; Mas-Moruno, C.; Kummerlowe, G.; Kessler, H., The impact of amino acid side chain mutations in conformational design of peptides and proteins. *Chem Eur J* **2010,** *16* (18), 5385-5390.

312. Tal-Gan, Y.; Stacy, D. M.; Foegen, M. K.; Koenig, D. W.; Blackwell, H. E., Highly potent inhibitors of quorum sensing in *Staphylococcus aureus* revealed through a systematic synthetic study of the group-III autoinducing peptide. *J Am Chem Soc* **2013,** *135* (21), 7869-7882.

313. Tal-Gan, Y.; Ivancic, M.; Cornilescu, G.; Cornilescu, C. C.; Blackwell, H. E., Structural characterization of native autoinducing peptides and abiotic analogues reveals key features essential for activation and inhibition of an AgrC quorum sensing receptor in *Staphylococcus aureus*. *J Am Chem Soc* **2013,** *135* (49), 18436-18444.

314. Tal-Gan, Y.; Stacy, D. M.; Blackwell, H. E., N-Methyl and peptoid scans of an autoinducing peptide reveal new structural features required for inhibition and activation of AgrC quorum sensing receptors in *Staphylococcus aureus*. *Chem Comm* **2014,** *50* (23), 3000-3003.

315. Johnson, J. G.; Wang, B. Y.; Debelouchina, G. T.; Novick, R. P.; Muir, T. W., Increasing AIP macrocycle size reveals key features of *agr* activation in *Staphylococcus aureus*. *Chembiochem* **2015,** *16* (7), 1093-1100.

316. Fowler, S. A.; Blackwell, H. E., Structure-function relationships in peptoids: recent advances toward deciphering the structural requirements for biological function. *Org Biomol Chem* **2009,** *7* (8), 1508-1524.

317. Tomlinson, G., Inhibition of radioligand binding to receptors - a competitive business. *Trends Pharmacol Sci* **1988,** *9* (5), 159-162.

318. Kitir, B.; Baldry, M.; Ingmer, H.; Olsen, C. A., Total synthesis and structural validation of cyclodepsipeptides solonamide A and B. *Tetrahedron* **2014,** *70* (42), 7721-7732.

319. Nielsen, A.; Nielsen, K. F.; Frees, D.; Larsen, T. O.; Ingmer, H., Method for screening compounds that influence virulence gene expression in *Staphylococcus aureus*. *Antimicrob Agents Ch* **2010,** *54* (1), 509-512.

320. Boden, E. P.; Keck, G. E., Proton-transfer steps in Steglich esterification - a very practical new method for macrolactonization. *J Org Chem* **1985,** *50* (13), 2394-2395.

321. Merrifield, R. B., Solid phase peptide synthesis. I. the synthesis of a tetrapeptide. *J Am Chem Soc* **1963,** *85* (14), 2149-2154.

322. Harris, P. W. R.; Brimble, M. A., Chemical synthesis of a polypeptide backbone derived from the primary sequence of the cancer protein NY-ESO-1 enabled by kinetically controlled ligation and pseudoprolines. *Biopolymers* **2015,** *104* (2), 116-127.

323. a) Sakakiba.S; Shimonis.Y; Kishida, Y.; Okada, M.; Sugihara, H., Use of anhydrous hydrogen fluoride in peptide synthesis .I. behaviour of various protective groups in anhydrous hydrogen fluoride. *Bull Chem Soc Jap* **1967,** *40* (9), 2164; b) Sakakiba.S; Kishida, Y.; Nishizaw.R; Shimonis.Y, Use of anhydous hydrogen fluoride in peptide synthesis .2. procedures for synthesis of simple peptides. *Bull Chem Soc Jap* **1968,** *41* (2), 438; c) Sakakiba.S; Nakamizo, N.; Kishida, Y.; Yoshimur.S, Use of anhydous hydrogen fluoride in peptide synthesis .3. synthesis of bradykinin. *Bull Chem Soc Jap* **1968,** *41* (6), 1477.

324. Muttenthaler, M.; Albericio, F.; Dawson, P. E., Methods, setup and safe handling for anhydrous hydrogen fluoride cleavage in Boc solid-phase peptide synthesis. *Nat Prot* **2015,** *10* (7), 1067-1083.

325. Amblard, M.; Fehrentz, J. A.; Martinez, J.; Subra, G., Methods and Protocols of modern solid phase peptide synthesis. *Mol Biotech* **2006,** *33* (3), 239-254.

326. Schnolzer, M.; Alewood, P.; Jones, A.; Alewood, D.; Kent, S. B. H., *In situ* neutralization in Boc-chemistry solid phase peptide synthesis - rapid, high yield assembly of difficult sequences. *Int J Peptide Res Therap* **2007,** *13* (1-2), 31-44.

327. Medini, K.; Harris, P. W. R.; Hards, K.; Dingley, A. J.; Cook, G. M.; Brimble, M. A., Chemical synthesis of a pore-forming antimicrobial protein, caenopore-5, by using native chemical ligation at a Glu-Cys Site. *Chembiochem* **2015,** *16* (2), 328-336.

328. Rovero, P.; Quartara, L.; Fabbri, G., Solid-phase synthesis of neurokinin A antagonists - comparison of the Boc and Fmoc methods. *Int J Peptide Prot Res* **1991,** *37* (2), 140-144.

329. Al-Warhi, T. I.; Al-Hazimi, H. M. A.; El-Faham, A., Recent development in peptide coupling reagents. *J Saudi Chem Soc* **2012,** *16* (2), 97-116.

330. Carpino, L. A.; Elfaham, A.; Minor, C. A.; Albericio, F., Advantageous applications of azabenzotriazole (triazolopyridine)-based coupling reagents to solid-phase peptide-synthesis. *J Chem Soc Chem Comm* **1994,** (2), 201-203.

331. Story, S. C.; Aldrich, J. V., Side-product formation during cyclization with HBTU on a solid support. *Int J Peptide Prot Res* **1994,** *43* (3), 292-296.

332. El-Faham, A.; Funosas, R. S.; Prohens, R.; Albericio, F., COMU: A safer and more effective replacement for benzotriazole-based uronium coupling reagents. *Chem Eur J* **2009,** *15* (37), 9404-9416.

333. Iwasawa, T.; Wash, P.; Gibson, C.; Rebek, J., Reaction of an introverted carboxylic acid with carbodiimide. *Tetrahedron* **2007,** *63* (28), 6506-6511.

334. Kaminski, Z. J., Triazine-based condensing reagents. *Biopolymers* **2000,** *55* (2), 140-164.

335. Carpino, L. A.; Elfaham, A.; Albericio, F., Efficiency in peptide coupling - 1-hydroxy-7-azabenzotriazole VS 3,4-dihydro-3-hydroxy-4-oxo-1,2,3-benzotriazine. *J Org Chem* **1995,** *60* (11), 3561-3564.

336. Subiros-Funosas, R.; Prohens, R.; Barbas, R.; El-Faham, A.; Albericio, F., Oxyma: an efficient additive for peptide synthesis to replace the benzotriazole-based HOBt and HOAt with a lower risk of explosion. *Chem Eur J* **2009,** *15* (37), 9394-9403.

337. Hoffmann, F.; Jager, L.; Griehl, C., Synthesis and chemical constitution of diphenoxyphosphoryl derivatives and phosphonium salts as coupling reagents for peptide segment condensation. *Phosphorus Sulfur Silicon Relat Elem* **2003**, *178* (2), 299-309.

338. Subiros-Funosas, R.; El-Faham, A.; Albericio, F., PyOxP and PyOxB: the Oxyma-based novel family of phosphonium salts. *Org Biomol Chem* **2010**, *8* (16), 3665-3673.

339. Barlos, K.; Chatzi, O.; Gatos, D.; Stavropoulos, G., 2-Chlorotrityl chloride resin - studies on anchoring of Fmoc-amino acids and peptide cleavage. *Int J Peptide Prot Res* **1991,** *37* (6), 513-520.

340. Otera, J., Esterification: Methods, Reactions, and Applications. 2nd ed.; Nishikido, J., Ed. Wiley-VCH Verlag GmbH & Co. KGaA: Weinheim, Germany, 2010.

341. Parenty, A.; Moreau, X.; Campagne, J. M., Macrolactonizations in the total synthesis of natural products. *Chem Rev* **2006,** *106* (3), 911-939.

342. Shimizu, M.; Ishii, K.; Fujisawa, T., Facile synthesis of beta-hydroxy-gamma-varelolactone via the ring opening reaction of beta-trichloromethyl-beta-propiolactone with ester enolates. *Chem Lett* **1997,** (8), 765-766.

343. Zhao, H. W.; Hua, W. T., Synthesis and characterization of pyridine-based polyamido-polyester optically active macrocycles and enantiomeric recognition for D- and L-amino acid methyl ester hydrochloride. *J Org Chem* **2000,** *65* (10), 2933-2938.

344. a)Paterson, I.; Yeung, K. S.; Ward, R. A.; Smith, J. D.; Cumming, J. G.; Lamboley, S., The total synthesis of swinholide-A .4. synthesis of swinholide-A and isoswinholide-A from the protected monomeric seco acid, pre-swinholide-A. *Tetrahedron* **1995,** *51* (34), 9467-9486; b) Evans, D. A.; Kaldor, S. W.; Jones, T. K.; Clardy, J.; Stout, T. J., Total synthesis of the macrolide antibiotic cytovaricin. *J Am Chem Soc* **1990,** *112* (19), 7001-7031; c) Ireland, R. E.; Thaisrivongs, S.; Dussault, P. H., An approach to the total synthesis of aplysiatoxin. *J Am Chem Soc* **1988,** *110* (17), 5768-5779.

345. Spengler, J.; Albericio, F., Asymmetric synthesis of alpha-unsubstituted beta-hydroxy acids. *Curr Org Synth* **2008,** *5* (2), 151-161.

346. Nelson, S. G.; Peelen, T. J.; Wan, Z. H., Catalytic asymmetric acyl halide-aldehyde cyclocondensations. A strategy for enantioselective catalyzed cross aldol reactions. *J Am Chem Soc* **1999,** *121* (41), 9742-9743.

347. Nelson, S.; Mills, P., Asymmetric Acyl Halide-Aldehyde Cyclocondensation Reaction [(4S)-4-(2-Phenylethyl)-2-oxetanone]. *Org Synth* **2005,** *82*, 170-178.

348. Cernerud, M.; Adolfsson, H.; Moberg, C., C-3-symmetric tripodal tetra-amines - preparation from chiral amino alcohols via aziridines. *Tetrahedron-Asymmetr* **1997,** *8* (15), 2655-2662.

349. Cernerud, M.; Skrinning, A.; Bergere, I.; Moberg, C., Bis(ethylsulfonamide)amines via nucleophilic ring-opening of chiral aziridines. Application to Ti-mediated addition of diethylzinc to benzaldehyde. *Tetrahedron-Asymmetr* **1997,** *8* (20), 3437-3441.

350. Zheng, D. K.; Meng, J. K.; Si, Y. K.; Ma, S. Y.; Huang, L., Studies on the resolution of racemic gossypol IV. use of threo-levo-1-P nitrophenyl-1 3-dihydroxy-2-propylamine or threo-dextro-1-P nitrophenyl-1 3-dihydroxy-2-propylamine as the resolving agent. *Yao xue Xue bao* **1990,** *25* (6), 430-434.

351. Twibanire, J. D. K.; Grindley, T. B., Efficient and controllably selective preparation of esters using uronium-based coupling agents. *Org Lett* **2011,** *13* (12), 2988-2991.

352. Mukaiyama, T.; Usui, M.; Shimada, E.; Saigo, K., A convenient method for the synthesis of carboxylic esters. *Chem Lett* **1975,** *4* (10), 1045-1048.

353. Venkataraman, K.; Wagle, D. R., Cyanuric chloride, a useful reagent for macrocyclic lactonization. *Tetrahedron Lett* **1980,** *21* (19), 1893-1896.

354. Kaminski, Z. J.; Leplawy, M. T., One-step synthesis of 5-acylamino-2,2-dialkyl-4-oxo-1,3-dioxanes - a cyclic system enabling simultaneous protection of hydroxyl and carboxyl functions in alpha hydroxymethyl-alpha-amino acids. *Synthesis-Stuttgart* **1986,** (8), 649-651.

355. Kunishima, M.; Kawachi, C.; Morita, J.; Terao, K.; Iwasaki, F.; Tani, S., 4-(4,6-dimethoxy-1,3,5-triazin-2-yl)-4-methyl-morpholinium chloride: An efficient condensing agent leading to the formation of amides and esters. *Tetrahedron* **1999,** *55* (46), 13159-13170.

356. Gaddum, J. H., The quantitative effects of antagonistic drugs. *J. Physiol.* **1937,** *89*, 7P-9P.

357. a) Schild, H. O., PA, A new scale for the measurement of drug antagonism. *Br J Pharmacol* **1947,** *2* (3), 189-206; b) Schild, H. O., Pax and competitive drug antagonism. *Br J Pharmacol* **1949,** *4* (3), 277-280; c) Schild, H. O., Drug antagonism and Pax. *Pharmacol Rev* **1957,** *9* (2), 242-246; d) Arunlakshana, O.; Schild, H. O., Some quantitative uses of drug antagonists. *Br J Pharmacol* **1959,** *14* (1), 48-58.

358. Alphey, M. S.; Pirrie, L.; Torrie, L. S.; Boulkeroua, W. A.; Gardiner, M.; Sarkar, A.; Maringer, M.; Oehlmann, W.; Brenk, R.; Scherman, M. S.; McNeil, M.; Rejzek, M.; Field, R. A.; Singh, M.; Gray, D.; Westwood, N. J.; Naismith, J. H., Allosteric competitive inhibitors of the glucose-1-phosphate thymidylyltransferase (RmlA) from *Pseudomonas aeruginosa*. *ACS Chem Biol* **2013,** *8* (2), 387-396.

359. Giraldo, J., Operational models of allosteric modulation: caution is needed. *Trends Pharmacol Sci* **2015,** *36* (1), 1-2.

360. Bindslev, N., Allosteric transition: a comparison of two models. *BMC Pharmacol Toxicol* **2013,** *14*, 12.

361. Black, J. W.; Leff, P., Operational models of pharmacological agonism. *Proc R Soc Ser B* **1983,** *220* (1219), 141-162.

362. Parsons, C. G.; Stoffler, A.; Danysz, W., Memantine: a NMDA receptor antagonist that improves memory by restoration of homeostasis in the glutarnatergic system - too little activation is bad, too much is even worse. *Neuropharmacology* **2007,** *53* (6), 699-723.

363. Schwartz, T. W.; Holst, B., Allosteric enhancers, allosteric agonists and ago-allosteric modulators: where do they bind and how do they act? *TrendsPharmacol Sci* **2007,** *28* (8), 366-373.

364. Lenz, T.; Fischer, J. J.; Dreger, M., Probing small molecule-protein interactions: A new perspective for functional proteomics. *J Proteomics* **2011,** *75* (1), 100-115.

365. Salisbury, C. M.; Cravatt, B. F., Activity-based probes for proteomic profiling of histone deacetylase complexes. *Proc Natl Acad Sci USA* **2007,** *104* (4), 1171-1176.

366. Fishwick, C. W. G.; Sanderson, J. M.; Findlay, J. B. C., An efficient route to *S-N*-(9-fluorenylmethoxycarbonyl)-4'-(1-azi-2,2,2-trifluoroethyl)phenylal anine. *Tetrahedron Lett* **1994,** *35* (26), 4611-4614.

367. Tsuboi, S.; Nakabayashi, K.; Matsumoto, Y.; Teno, N.; Tsuda, Y.; Okada, Y.; Nagamatsu, Y.; Yamamoto, J., Amino-acids and peptides .28. Synthesis of peptide-fragments related to eglin-C and studies on the relationship between their structure and effects on human-leukocyte elastase, cathepsin-G and alpha-chymotrypsin. *Chem Pharm Bull* **1990**, *38* (9), 2369-2376.

368. Douat-Casassus, C.; Pulka, K.; Claudon, P.; Guichard, G., Microwave-enhanced solid-phase synthesis of *N,N'*-linked aliphatic oligoureas and related hybrids. *Org Lett* **2012**, *14* (12), 3130-3133.

369. Page, P.; Bradley, M.; Walters, I.; Teague, S., Solid-phase synthesis of tyrosine peptide aldehydes. Analogues of (S)-MAPI. *J Org Chem* **1999**, *64* (3), 794-799.

370. Kammermeier, B.; Beck, G.; Holla, W.; Jacobi, D.; Napierski, B.; Jendralla, H., Vanadium(II)- and niobium(III)-induced, diastereoselective pinacol coupling of peptide aldehydes to give a C-2-symmetrical HIV protease inhibitor. *Chem Eur J* **1996**, *2* (3), 307-315.

371. Zimmermann, M.; Fischbach, M. A., A Family of pyrazinone natural products from a conserved nonribosomal peptide synthetase in *Staphylococcus aureus*. *Chem Bio* **2010**, *17* (9), 925-930.

372. Pollitt, E. J. G. Evolutionary and ecological considerations of social behaviours in Staphylococcus aureus. University of Nottingham, Nottingham, 2013.

373. Chan, P. F.; Foster, S. J., Role of SarA in virulence determinant production and environmental signal transduction in Staphylococcus aureus. *J Bacteriol* **1998,** *180* (23), 6232-6241.

374. Nelson, S. G.; Spencer, K. L., Sequential acyl halide-aldehyde cyclocondensation and enzymatic resolution as a route to enantiomerically enriched beta-lactones. *J Org Chem* **2000**, *65* (4), 1227-1230.

375. Gnanadesikan, V.; Corey, E. J., Enantioselective beta-lactone formation from ketene and aldehydes catalyzed by a chiral oxazaborolidine. *Org Lett* **2006**, *8* (21), 4943-4945.

376. Yan, T. H.; Hung, A. W.; Lee, H. C.; Chang, C. S.; Liu, W. H., Asymmetric aldol-type reactions of acetate imide enolates. *J Org Chem* **1995**, *60* (11), 3301-3306.

377. Kull, T.; Peters, R., Practical enantioselective synthesis of beta-lactones catalyzed by aluminum bissulfonamide complexes. *Adv Synth Catal* **2007**, *349* (10), 1647-1652.

378. Kodai, T.; Nakatani, T.; Noda, N., The absolute configurations of hydroxy fatty acids from the royal Jelly of honeybees (*Apis mellifera*). *Lipids* **2011**, *46* (3), 263-270.

379. Wang, Z.; Zhao, C. L.; Pierce, M. E.; Fortunak, J. M., Enantioselective synthesis of beta-hydroxy carboxylic acids: direct conversion of beta-oxocarboxylic acids to enantiomerically enriched beta-hydroxy carboxylic acids via neighboring group control. *Tetrahedron-Asymmetr* **1999**, *10* (2), 225-228.